Forschungsbericht 2012-02

The DLR Project
Wetter & Fliegen

Thomas Gerz, Carsten Schwarz
(Editoren, Projektleiter)

Deutsches Zentrum für Luft- und Raumfahrt
Oberpfaffenhofen, Braunschweig,
Göttingen und Hamburg

DLR
Deutsches Zentrum
für Luft- und Raumfahrt e.V.
in der Helmholtz-Gemeinschaft

Herausgeber Deutsches Zentrum
für Luft- und Raumfahrt e.V.
Bibliotheks- und
Informationswesen
D-51170 Köln
Porz-Wahnheide
Linder Höhe
D-51147 Köln

Telefon (0 22 03) 6 01- 44 44
Telefax (0 22 03) 6 01- 47 47

ISSN 1434-8454

Flugzeug, Flughafen, Wirbelschleppe, Gewitter, Winterwetter,
Detektion, Verfolgung, Charakterisierung, Prognose, Abmilderung, Vermeidung,
operationelle Konzepte, Kosten-Nutzen-Analyse,
Expertensysteme für Luftverkehrsführung und Cockpit, Pilotenassistenzsysteme
(Veröffentlicht in englischer Sprache)

DLR Forschungszentren Oberpfaffenhofen, Braunschweig, Göttingen und Hamburg
Thomas Gerz, Carsten Schwarz (Editoren, Projektleiter)

Das DLR-Projekt Wetter & Fliegen

DLR-Forschungsbericht 2012-02, 2012, 280 Seiten, 210 Bilder, 25 Tabellen, 389 Literaturstellen, 43,00 € zzgl. MwSt.

Dieser Bericht beinhaltet die wesentlichen Ergebnisse des vierjährigen DLR-Projekts Wetter & Fliegen. Beteiligte DLR Institute und Einrichtungen waren die Institute für Physik der Atmosphäre, Flugsystemtechnik, Flugführung, Robotik und Mechatronik, Aerodynamik und Strömungstechnik, Lufttransportsysteme sowie DLR Flugexperimente und Systemhaus Technik. Ziel war es, zur Sicherheit und Effizienz des zukünftigen Lufttransportsystems beizutragen durch

- Entwicklung von Wetter- und Wirbelschleppen-Expertensystemen sowie operationellen Konzepten für die Luftverkehrsführung am Flughafen und
- Erforschen neuer Sensoren und Entwickeln von automatischen Flugsteuerungs- und innovativen Cockpit-Informationstechnologien für Flugzeuge.

Vertiefende Erkenntnisse wurden erzielt hinsichtlich der Physik der Wirbelschleppe, der Auswirkungen auf in Wirbelschleppen einfliegende Flugzeuge und Staffelungsprognosen, sowie der Detektion, Verfolgung und Vorhersage von Wetterphänomenen wie Gewitter, Schneefall und Vereisungsbedingungen am Flughafen. Neue operationelle Konzepte für Luftverkehrsführung und Flugzeugsysteme wurden entwickelt und die Expertensysteme wurden technologisch und ökonomisch bewertet. Prototypen wurden bis zu verschiedenen Reifegraden entwickelt und mit Mensch-Maschine-Schnittstellen in Simulation und realer Umgebung getestet und bewertet. Aufbauend auf diesen Ergebnissen werden die Aktivitäten im Rahmen des DLR-Vorhabens Wetteroptimierter Luftverkehr fortgeführt.

aircraft, airport, wake vortex, thunderstorm, wintry weather,
detection, tracking, characterisation, prediction, alleviation, avoidance,
concept of operation, cost-benefit analysis,
expert systems for air traffic management and flight crew, pilot assistance systems

DLR Research Centres Oberpfaffenhofen, Braunschweig, Göttingen, and Hamburg
Thomas Gerz, Carsten Schwarz (Editors and Project Coordinators)

The DLR Project Wetter & Fliegen (Weather & Flying)

DLR-Forschungsbericht 2012-02, 2012, 280 pages, 210 figures., 25 tables., 389 references., 43.00 € plus VAT

This report compiles major results of the 4-year DLR Project Wetter & Fliegen. Contributing DLR institutes and facilities were the Institutes of Atmospheric Physics, Flight Systems, Flight Guidance, Robotics and Mechatronics, Aerodynamics and Flow Technology, Air Transportation Systems as well as DLR Flight Experiments and Systemhaus Technik. The aim was to contribute to safety and efficiency of tomorrow's air transportation by

- developing weather and wake vortex expert systems along with operational concepts for the air traffic management and control at airports and
- researching new sensors and delivering automated flight control and innovative flight crew information technologies for the aircraft.

Deeper insights were gained into wake vortex physics, the consequences for wake-encountering aircraft and separation prediction, as well as the detection, tracking and prediction of adverse weather phenomena like thunderstorms and snow and icing conditions. New operational concepts for air traffic control and tools for flight systems have been developed and the expert systems have been assessed from a technological and economical perspective. Prototype systems have been matured towards different levels of technology readiness and have been tested and evaluated with human-in-the-loop simulations and in field campaigns in real environments. Building on these achievements the work will be continued in the forthcoming DLR Project Weather Optimised Air Traffic.

Forschungsbericht 2012-02

The DLR Project
Wetter & Fliegen

Thomas Gerz, Carsten Schwarz
(Editoren, Projektleiter)

Deutsches Zentrum für Luft- und Raumfahrt
Oberpfaffenhofen, Braunschweig,
Göttingen und Hamburg

280 Seiten
210 Bilder
25 Tabellen
389 Literaturstellen

Deutsches Zentrum
für Luft- und Raumfahrt e.V.
in der Helmholtz-Gemeinschaft

The DLR Project

WETTER & FLIEGEN

January 2008 - December 2011

Aerodrome Information and Management Systems for Wake Vortices, Thunderstorms and Wintry Weather Conditions

Systems to Control and Monitor Aircraft Performance and to Inform the Flight Deck about Gusts, Wake Vortices and Thunderstorms

Final Report

Involved Institutes and Facilities	**Atmospheric Physics** **Flight Systems** **Flight Guidance** **Robotics and Mechatronics** **Aerodynamics and Flow Technology** **Air Transportation Systems** **Flight Experiments** **Systemhaus Technik**
Edited by	**Dr. Thomas Gerz, Atmospheric Physics** **Carsten Schwarz, Flight Systems**
Issued	**February 2012**

This report compiles major results of the 4-year DLR Project *Wetter & Fliegen (Weather & Flying)*. The editors and all contributors thank the Board of DLR, its Programme Management and the Directors of the Institutes for their long-lasting support to run such a big project. Special thanks go to Dr. Brigitte Brunner and Dr. Ulrich Herrmann for providing us the necessary financial ressources.

aircraft, airport, wake vortex, thunderstorm, wintry weather,
detection, tracking, characterisation, prediction, alleviation, avoidance,
concept of operation, cost-benefit analysis,
expert systems for air traffic management and flight crew, pilot assistance systems

The DLR Project Wetter & Fliegen (Weather & Flying)

This report compiles major results of the 4-year DLR Project Wetter & Fliegen. Contributing DLR institutes and facilities were the Institutes of Atmospheric Physics, Flight Systems, Flight Guidance, Robotics and Mechatronics, Aerodynamics and Flow Technology, Air Transportation Systems as well as DLR Flight Experiments and Systemhaus Technik. The aim was to contribute to safety and efficiency of tomorrow's air transportation by

- developing weather and wake vortex expert systems along with operational concepts for the air traffic management and control at airports and
- researching new sensors and delivering automated flight control and innovative flight crew information technologies for the aircraft.

Deeper insights were gained into wake vortex physics, the consequences for wake-encountering aircraft and separation prediction, as well as the detection, tracking and prediction of adverse weather phenomena like thunderstorms and snow and icing conditions. New operational concepts for air traffic control and tools for flight systems have been developed and the expert systems have been assessed from a technological and economical perspective. Prototype systems have been matured towards different levels of technology readiness and have been tested and evaluated with human-in-the-loop simulations and in field campaigns in real environments. Building on these achievements the work will be continued in the forthcoming DLR Project Weather Optimised Air Traffic.

Flugzeug, Flughafen, Wirbelschleppe, Gewitter, Winterwetter,
Detektion, Verfolgung, Charakterisierung, Prognose, Abmilderung, Vermeidung,
operationelle Konzepte, Kosten-Nutzen-Analyse,
Expertensysteme für Luftverkehrsführung und Cockpit, Pilotenassistenzsysteme

Das DLR-Projekt Wetter & Fliegen

Dieser Bericht beinhaltet die wesentlichen Ergebnisse des vierjährigen DLR-Projekts Wetter & Fliegen. Beteiligte DLR Institute und Einrichtungen waren die Institute für Physik der Atmosphäre, Flugsystemtechnik, Flugführung, Robotik und Mechatronik, Aerodynamik und Strömungstechnik, Lufttransportsysteme sowie DLR Flugexperimente und Systemhaus Technik. Ziel war es, zur Sicherheit und Effizienz des zukünftigen Lufttransportsystems beizutragen durch

- Entwicklung von Wetter- und Wirbelschleppen-Expertensystemen sowie operationellen Konzepten für die Luftverkehrsführung am Flughafen und
- Erforschen neuer Sensoren und Entwickeln von automatischen Flugsteuerungs- und innovativen Cockpit-Informationstechnologien für Flugzeuge.

Vertiefende Erkenntnisse wurden erzielt hinsichtlich der Physik der Wirbelschleppe, der Auswirkungen auf in Wirbelschleppen einfliegende Flugzeuge und Staffelungsprognosen, sowie der Detektion, Verfolgung und Vorhersage von Wetterphänomenen wie Gewitter, Schneefall und Vereisungsbedingungen am Flughafen. Neue operationelle Konzepte für Luftverkehrsführung und Flugzeugsysteme wurden entwickelt und die Expertensysteme wurden technologisch und ökonomisch bewertet. Prototypen wurden bis zu verschiedenen Reifegraden entwickelt und mit Mensch-Maschine-Schnittstellen in Simulation und realer Umgebung getestet und bewertet. Aufbauend auf diesen Ergebnissen werden die Aktivitäten im Rahmen des DLR-Vorhabens Wetteroptimierter Luftverkehr fortgeführt.

1. Introduction

The impact of the atmosphere on aviation is threefold: safety, economic efficiency and ecologic sustainability of aviation depend – sometimes crucially, sometimes marginally – on the state and the motion of the air masses through which an aircraft flies. The Vision 2020 (GoP 2001), the Advisory Council for Aeronautics Research in Europe, ACARE, and follow-on initiatives like Flight Path 2050 set ambitious goals to increase safety and punctuality in aviation. The goals have to be met under all weather conditions, "flying safely in all weather, aircraft are running on schedule 99% of the time". However, weather is not a technical problem which can totally be controlled: "we cannot control it but we need to learn to live with the elements and steadily eliminate the service disruption that they may cause". The stakeholders have to bear in mind that weather, from its nature, is difficult and only within limits to predict.

Adverse weather is hardly the single source for accidents in aviation but it is very often a contributing factor. Between 1995 and 2004 weather was the primary cause in 13% of all aircraft losses (Boeing 2005); in 33% of all accidents between 2004 and 2007 weather was involved as a primary or secondary cause (NTSB 2007). Aircraft "wake turbulence" (an imprecise terminology for two coherent counter-rotating vortices shed by the aircraft) is a safety topic of high global relevance for aviation. Aircraft wake vortex encounters were the most frequent reasons for loss of control of jet aircraft between 1987 and 1995 (Aviation Week 2002).

Weather is, on the other hand, the largest single source for delays and inconveniences in air traffic over the USA (FAA 2007) as well as over Europe (Theusner and Röhner 2006). Airport hubs and flight corridors which operate close to their capacity limits will be disrupted already by small weather events leading to nevertheless high costs and delays. Adverse weather was responsible for 40-50% of all flight delays in Europe already in 2006. Today, in November 2011 almost 56% of all delays were due to adverse weather at the airports in Europe. More specifically, weather was the main reason for delays at the airport of Munich, Germany, in more than 80% of all delay cases in 2011. Also in the USA, adverse weather is the primary reason for disruptions in the air transport system. For example, up to 90% of all delays in the US American airspace during the summer months are due to thunderstorm activity (Leighton 2006).

All phases of flight are exposed to weather but the flights in the vicinity of an airport, the so-called terminal manoeuvring area, are mainly hindered by adverse weather conditions. Now, aviation is one of a few business sectors with large annual growth rates – the number of flights in Europe increased about 13% from 2003 to 2010, with a peak of 20% between 2003 to 2008 (EUROCONTROL, 2011). Since growth in aviation means basically a growing number of scheduled flights and not so much a growth in the infrastructure – the number of delays increased by 83% from 2003 to 2008 (DFS, 2011), aviation will become even more vulnerable to weather in the future. To mitigate the potential hazard of encountering wake vortices, minimum separation distances are prescribed for different flight phases. These separation standards, however, limit capacity. The foreseen high increase in air traffic amplifies the capacity and safety problems also with regard to aircraft wake vortices, especially for major European airports.

The Eurocontrol Performance Review Commission reports that the year 2010 was marked by a number of exceptional events for aviation in Europe. Besides industrial actions (e.g. strikes) and the volcanic ash cloud from Iceland also unusually severe weather conditions occurred. Each event had a significant impact on traffic growth, the level of delays and the flight efficiency. For example, approximately 26,000 flights were cancelled in Europe in 2010 due to strikes and alike (that is as much as the total air traffic on one average day in 2010 in Europe) but some 45,000 flights were cancelled due to bad weather conditions. Air transport punctuality in 2010 was the worst recorded since 2001 (24.2% of flights delayed more than 15 minutes). Again the main reasons were industrial actions and weather-related delays (mostly snow and freezing conditions in winter 2009 and December 2010). Interesting though, the volcanic ash cloud in April/May 2010 had only a limited impact on punctuality, as the majority of the flights were cancelled. (EUROCONTROL, 2011).

The Eurocontrol study further exemplifies that the weather phenomena that have the largest impact on the delays in the European air traffic flow management are thunderstorms and snow/ice, followed by low visibility/ceiling and wind, see Figure 1. This ranking is about constant throughout the years.

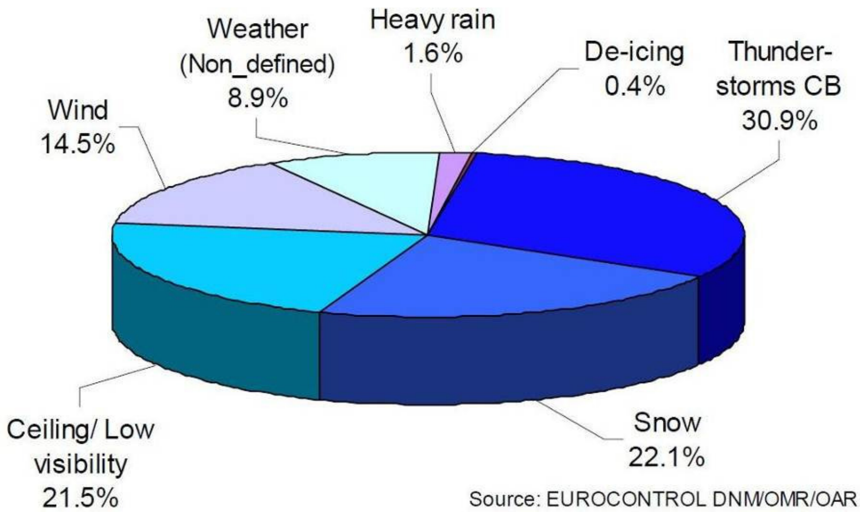

Figure 1: Impact of weather phenomena on delays in the European air traffic flow management (from Eurocontrol 2011, Figure 8-10).

These numbers and trends indicate that there is a clear need for improved weather information that help all air space users to plan well in advance to mitigate the weather impact. The present meteorological services for aviation like aerodrome forecasts (TAF), trend-type landing forecast (TREND), aerodrome warnings or, for aircraft en-route, standard and warning information for airmen (AIRMET/SIGMET) do not meet the needs of today's aircraft operators and air space users since they are not specific enough, not covering all phases of flight and not containing important parameters.

There is a growing community in aviation who believes that the disrupting impact of adverse weather on aviation can be mitigated by using and integrating dedicated and tailored observations and forecasts of weather. Not only reacting on an event that happens already but anticipating the weather to come and taking measures proactively is the growing common sense among the stakeholders. A reduction of weather-induced costs by 40% and more seems feasible. With regard to aircraft wake vortices, Hemm et al. (1999) expect a reduction of costs by 15 Mio US-$ per year with an installed wake vortex advisory systems at a large hub.

The DLR Project "Wetter & Fliegen" ("Weather & Flying") has taken the Vision 2020 slogans as guidelines for its 4 years work programme. To develop weather expert systems for airports, air navigation safety providers, air space users, and airplane manufactures is the overarching intention of our work.

1.1 Aircraft Wake Vortices

Aircraft wake vortices are an inevitable consequence of the lift generation of a flying aircraft and poses a potential risk for other aircraft when encountering the wake. Therefore, minimum separation distances are prescribed in order to ensure safe operations. The current separation distances, however, are considered to be overly conservative in many cases. Hence, the safety issue beomes a capacity issue, too. Wake vortex is an aviation topic of high global importance. It is of relevance in the context of increasing airport congestion and the increasing diversity of aircraft types like the recent enter into service of very large transport aircraft on one side and the advent of very light jets on the other side. For future ATM concepts, e.g. reduced aircraft separation based on higher navigation performance, the safety and capacity aspects imposed by wake vortices have to be addressed on a national, European and international level.

Extensive research and development activities have been conducted on this topic over the last years and decades. Science and technological development have been successful in understanding the wake vortex topic and is now in a phase which progresses towards implementation. New technologies are emerging like wake prediction tools, onboard advisory systems or wake vortex detection sensors (e.g. Lidar or Radar), for which integration has to be evaluated and benefits have to be analysed. Operational wake separation concepts like weather dependant dynamic aircraft spacing are proposed which require feedback by users and stakeholders and a risk and safety analysis.

The research activities comprise topics such as

- wake vortex physics, formation and evolution of wakes under different flight and environmental conditions,
- wake vortex encounter mechanics, flight dynamics aspects and resulting safety issues,
- feasibility of reducing separation distances under specific conditions, such as cross-wind.

These activities have greatly improved the understanding of the whole chain from generation of the wakes at the aircraft via its influence on the encountering aircraft to the operational impacts. In Europe, first local operational improvements have been introduced already or are underway which make use of this knowledge (e.g. WIDAO at Paris CDG airport, A380 wake vortex separation assessment). In the US a similar trend to operational solutions can be observed (closely spaced parallel runways FAA order 7110.65 (diagonal separation 1.5 nm), departure/ arrival crosswind concepts (WTMD/WTMA), B747-8 wake vortex separation assessment). The recent joint Eurocontrol/FAA RECAT Phase I proposal is going a first step towards a re-categorisation of all aircraft classes with respect to wake vortex risk by proposing a new class layout providing capacity benefits while keeping the same level of safety.

1.2 Air Traffic Management and Meteorology

The future air traffic management (ATM), as envisaged by the European and US-American modernisation programmes SESAR and NextGen, will focus on a trajectory planning in space and time (four-dimensional, 4d) to facilitate a dynamic airspace management. Effective planning and management are mandatory to deliver the flexibility to airspace users of choosing their optimum business trajectory. Conflicts between flight trajectories must be recognised and solved quickly, especially in congested airspace, by analysing and assessing a huge amount of data from very different types and sources as aircraft performances, trajectory profiles, aeronautical and geographical data, to name but a few. Further, also the operational environment of demand and capacity, state of use and constraints of airports and airspaces must be considered at the same time.

To run a 4d trajectory management operationally and efficiently it is perspicuous that the meteorological information (MET) along trajectories, at destinations and alternates and so on is provided adequately and in a timely manner. Especially information on adverse weather must be tailored to the user’s needs, easy to understand, self-explaining and clear in its message. MET is an essential component of the ATM workflow, therefore, it must be commonly shared and integrated in the operating procedures of the stakeholder to allow collaborative decisions. MET has to become an integral part of the Aeronautical Information Management (AIM) concept. AIM in turn is the ATM component of the System Wide Information Management (SWIM) as envisaged by the programmes SESAR and NextGen. Essential elements for Aeronautical Information Management read (see also EANPG 2004):

- a sufficiently dense weather observation network, weather diagnosis, short-term forecasting ("nowcasting") of adverse or disruptive weather, and highly resolved probabilistic weather forecasts;
- the translation of the disruptive weather in aviation constraints ("no-fly" areas) and the conversion of these constraints to the impact on aviation (demand versus reduced capacity);
- the integration of tailored and timely MET and its impact in the operational processes for collaborative and dynamic decision making;
- the development of "net-centric" procedures (where each aerodrome and each aircraft are considered as "nodes") to allow broad situational awareness based on an effective information management for the aircraft, the air traffic control and management, the airline operating centres and the airports.

1.3 Aircraft and Atmosphere

Atmospheric conditions may hinder a flight, reduce the passengers comfort, adversely affect aircraft behaviour and reduce the controllability of an aircraft. They further may impose additional loads on the airframe, or even jeopardise the safety of a flight. Such conditions may occur at all flight levels everywhere in the atmosphere. The disturbances always require additional control activities and increase the workload of the flight crew which may also negatively impact the safety. Thunderstorms are top-ranked by pilots as a weather situation compromising the flight safety since many hazards can come together in such an event. Strong turbulence and wind shear lead to accelerations of the aircraft which can result in loss of flight altitude or a rotation of the aircraft; turbulence also gives rise to vibrations of the airframe and wings such that an engine may fall off. Icing, i.e. cloud and rain droplets which freeze on the cold body of the aircraft, can block sensors and flight control devices resulting in false speed indications and reduced maneuverability. A lightning stroke, although of no harm to crew and passengers, may destroy electric circuits. Hail and heavy precipitation can destroy the cockpit window and the radar dome or result in an engine flame-out. Other hazardous phenomena linked to weather are wake vortices, volcanic ash and sand storms. See Hauf et al. (2004) for more details.

The information for pilots about such adverse weather today is, if at all, based on significant weather charts and alike. This information is handed to the pilots before the flight when they check the aircraft for take-off. Such services, however, don't give the necessary, tailored and reliable information required for a particular flight and often are outdated when needed. Significant weather charts, for example, are deduced from coarse numerical weather forecasting models many hours ahead. Moreover, neither do sensors exist today to recognise phenomena like clear-air turbulence or wake vortices from on-board an aircraft, nor are aircraft flight control mechanisms dedicated to mitigate respective encounters.

Hence, what is required today and even more in the light of a coming dynamic airspace management, where autonomous flights get an increasing share, is not only a modern ATM system but also an adequately equipped aircraft which

- recognises hazardous situations caused by atmospheric phenomena,
- informs pilots and crew in an appropriate way and suggesting alternative routing, and
- is capable to mitigate encountered atmospheric disruptions automatically by control mechanisms.

Thereby, the information will have to originate from both on-board data as well as data up-linked from ground systems.

1.4 The DLR Project Wetter & Fliegen

The Deutsches Zentrum für Luft- und Raumfahrt – German Aerospace Center – (DLR) has the capacity and expertise to accept that challenge and, therefore, initiated the major interdisciplinary Project "Wetter & Fliegen" (Weather & Flying). The Project was running from January 2008 to December 2011. Its goal was to contribute to safety and efficiency of tomorrow's air transportation system by

- developing weather information expert systems along with operational concepts for ATM on one hand and
- researching new sensors and delivering automated flight control and innovative flight crew information technologies for the aircraft on the other hand.

These two strands of work are outlined in Figure 2.

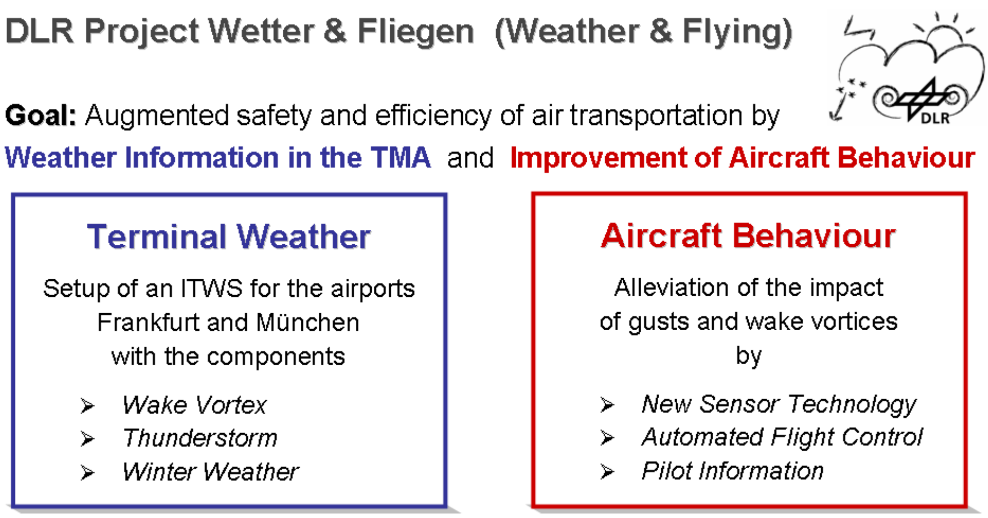

Figure 2. Outline of the DLR project Wetter & Fliegen.

Terminal/Airport Weather

Three weather information expert systems for the Terminal Manoeuvring Area (TMA) of an airport have been developed to improve the detection, tracking, and prediction of weather phenomena adversely affecting airport operations, namely

- wake vortex,
- deep convection (thunderstorms, hail, wind), and
- wintry weather conditions.

The idea is to concatenate all observation and prediction data available in the TMA, to produce tailored products according to the stakeholders' needs and to deliver simple but accurate and unambiguous output. This approach is pre-requisite to guarantee that all involved partners possess the same information as a basis for their collaborative tactical as well as strategic decision making from minutes up to one day in advance.

In-line with working on the meteorological expert systems, also new corresponding operational concepts have been developed. The expert systems have been tested at the second most frequented German airport Munich, and the value-added chain has been assessed technologically as well as monetarily.

Aircraft Behaviour

To improve the behaviour of the aircraft when confronted with turbulence, wake vortices, and thunderstorms, two modes of on-board systems have been developed, namely

- automated flight control and evasion-manoeuvre methods, and
- enhanced flight surveillance concepts including most recent weather information for crews.

Also, feasibility studies have been performed for

- new on-board sensor technologies to detect hazardous wake vortices ahead of the aircraft.

An integrated flight control system has been developed, to improve flight characteristics, and reduce (work) loads on pilot, passengers and aircraft in extreme atmospheric motions. Moreover, to support pilot decision making, tactical avoidance manoeuvres have been developed. The requirements for forward-looking on-board sensors to detect such hazards have been specified and the feasibility to produce the novel sensors has been elaborated. To increase the situational awareness of the flight crew new pilot displays and assistance tools have conceptually be derived and developed in order to uplink the necessary data to the cockpit and display them together with data from on-board systems. The developed procedures and systems have been tested in flight simulators and during flight tests and assessed by pilots.

1.5 Outline of the Report

The activities performed and the results achieved follow the two strands *Airport Terminal Weather* and *Aircraft Behaviour*. The chapters of this report reflect roughly the structure of the project.

Chapter 2 – Wake and Weather Information Systems for Aerodromes – covers DLR's further developed wake vortex advisory system as well as new meteorological information concepts and systems for thunderstorms and wintry weather conditions affecting the aerodrome area.

Chapter 3 – Risk and Economic Assessments – introduces attempts to translate the developed advisory and information system for aircraft wake vortices and thunderstorms into business cases and investment returns. It further presents a tool to simulate realistic wake vortex scenarios in an aerodrome environment for risk assessments.

Chapter 4 – Advanced Flight Control Systems for Atmospheric Disturbance Mitigation – focuses on new sensors and control concepts to first detect and identify and then control and mitigate encounters of the aircraft with wake vortices or hazardous atmospheric disturbances.

Chapter 5 – Flight Systems to Increase Situational Awareness and Avoid Hazards – briefs the reader on warning and information systems in the cockpit to raise the flight crew's attention and awareness regarding wake vortices or thunderstorms ahead of the aircraft in order to avoid the hazard.

Chapter 6 – Wake Vortex Physics and Encounter Consequences – presents new physical insight in the behaviour and dynamics of aircraft wake vortices. Results from flight tests and simulations pave the way for encounter severity assessment metrics which are necessary for the ongoing international attempt to re-categorise the wake vortex separation standards and to assess new (large) aircraft types.

Chapter 7 – Concluding Remarks and Future Activities – summarises the work and gives an outlook on DLR's research activities of the coming years in national, European and international contexts.

References

Aviation Week 2002, August 26, p. 50.

Boeing 2005: Statistical Summary of Commercial Jet Airplane Accidents - Worldwide Operations, Boe-ing Commercial Airplanes - Aviation Safety, May 2005

DFS 2011: Air Traffic Flow and Capacity Management, 4th Workshop on MET Support to ATM, 1-3 February 2011, Brussels

EANPG: MET Strategy in supporting the CNS/ATM concept for the EU Region, 2004. EANPG METG Project Team on MET, Attachment to METG/14 – WP/11.

EUROCONTROL 2004: Challenges to Growth 2004 Report; European Air Traffic Management Pro-gramme, 01.12.2004, 58 pp.

EUROCONTROL Performance Review Commission 2011: Performance Review Report 2010, http://www. eurocon-trol.int/prc/public/standard_page/doc_prr.html.

FAA 2007: Report of the Weather-ATM Integration Working Group; Research, Engineering and Devel-opment Advisory Commit-tee, Federal Aviation Administration, October 2007.

GoP 2001: European Aeronautics: A Vision for 2020 - Meeting society's needs and winning global lead-ership. Report of the Group of Personalities, European Commission January 2001, 26pp.

Hauf T., Leykauf H., Schumann U. (eds.) 2004: Luftverkehr und Wetter, Statuspapier. DLR-Mitteilungen 2004-02, 57 pp.

Hemm, R., Shapiro, G., Lee, D.A., Gribko, J., Glaser, B., 1999: Benefit Estimates of Terminal Area Productivity Program Technol-ogies. NASA/CR-1999-208989, p. 144.

ICAO 2005: ICAO Global Air Traffic Management Operational Concept; 1st edition 2005, Doc 9854, AN/458, §§ 2.9.17-19.

Leighton, Q., 2006: Modeling and Simulation Needs for Next Generation Air Transportation System Re-seach. AIAA Modeling and Simulation Technologies Conference and Exhibit, 21-24 August 2006, Key-stone, Colorado, AIAA 2006-6109, p 1-8.

NTSB 2007: Query for weather related accidents between 2004 and 2007 via http://www.ntsb.gov/ntsb/query.asp

Theusner & Röhner 2006: Weather Hazards, Weather Impact Areas and Evaluation Methods. D 2.1-1 Report of the FLYSAFE Project.

2. Wake and Weather Information Systems for Aerodromes

2.1 Prediction of Dynamic Pairwise Wake Vortex Separations for Approach and Landing

Frank Holzäpfel[1] , Klaus Dengler[1], Thomas Gerz[1], Carsten Schwarz[2]
[1] *Institute of Atmospheric Physics,* [2]*Institute of Flight Systems*

Design and performance of the Wake Vortex Prediction and Monitoring System WSVBS are described. The WSVBS has been developed to tactically increase airport capacity for approach and landing on single runways as well as closely-spaced parallel runways. It is thought to dynamically adjust aircraft separations dependent on weather conditions and the resulting wake vortex behavior without compromis>ing safety. Dedicated meteorological instrumentation and short-term numerical terminal weather prediction provide the input to the prediction of wake-vortex behavior and respective safety areas. LIDAR monitors the correctness of WSVBS predictions in the most critical gates at low altitude. The WSVBS is integrated in the arrival manager AMAN of DLR. Performance tests of the WSVBS have been accomplished at Frankfurt airport in winter 2006/07 and at Munich Airport in summer 2010. Aircraft separations for landings on single runways have been compared employing the concepts of either heavy-medium weight class combinations or dynamic pairwise separations where individual aircraft type pairings are considered. For the very conservative baseline setup of the WSVBS the potential capacity gains of dynamic pairwise operations for single runways appear to be very small. On the other hand, the consideration of individual aircraft types and their respective wake characteristics may almost double the fraction of time when radar separation could be applied.

Introduction

Aircraft trailing vortices may pose a potential risk to following aircraft. The empirically motivated separation standards between consecutive aircraft which were introduced in the 1970s still apply. These aircraft separations limit the capacity of congested airports in a rapidly growing aeronautical environment. The most likely growth scenario within a Eurocontrol study (Euurocontrol 2008) indicates that in the year 2030 airport capacity will lag demand by some 2.3 million IFR flights. This is opposed by an estimate of annual savings of US $ 15 million per year and airport that could be achieved by the introduction of a wake-vortex advisory system (Hemm et al. 1999). A survey on wake-vortex advisory systems and modifications of procedures that are meant to increase airport capacity is available in Elsenaar et al. 2006.

DLR has developed the Wake Vortex Prediction and Monitoring System (WirbelSchleppen-Vorhersage- und -BeobachtungsSystem WSVBS, Gerz et al. 2005, Gerz et al. 2009, Holzäpfel et al. 2009-1) to tactically increase airport capacity for approach and landing. The WSVBS is thought to dynamically adjust aircraft separations dependent on weather conditions and the resulting wake vortex behavior without compromising safety. For this purpose it predicts wake vortex transport and decay and the resulting safety areas along the glide slope from final approach fix to threshold. The design of the WSVBS for closely-spaced parallel runways systems has been described in detail in Holzäpfel et al. 2009-1. During a performance test at Frankfurt airport in winter 06/07 capacity-improving wake-vortex separation concepts of operation could have been used in 75% of the time and continuously applied for at least several tens of minutes (Gerz et al. 2009). It was found that the system ran stable and the predicted minimum separation times were totally confirmed by Lidar measurements of wake vortex transport. From fast-time simulations the eventual capacity gain for Frankfurt was estimated to be 3% taking into account the real traffic mix and operational constraints in the period of one month.

Initially, the system has been particularly adapted to the closely-spaced parallel runway system of Frankfurt airport. Meanwhile the WSVBS has been further developed to predict dynamic pairwise separations for landings on single runways. The concept of dynamic pairwise separations corresponds to the favoured procedure foreseen in the final development stage of NextGen (Lang 2010, FAA 2011) and SESAR (SESAR 2010, Steen et al. 2010). The elements of the WSVBS are generic and can well be adjusted to other runway systems and airport locations.

This paper, which has been presented previously (Holzäpfel et al. 2011) describes the design of the WSVBS with all its components and their interaction and the extension of the WSVBS to the prediction of dynamic and time-based separations for individual aircraft type pairings landing on single runways. The performance of the dynamic pairwise separations setup is analysed employing data gathered during a three-month measurement campaign at Frankfurt Airport in winter 2006/07 and another three-month measurement campaign accomplished at Munich Airport in summer 2010. The baseline setup of the WSVBS for dynamic pairwise separations is compared to a number of alternative setups. This analysis evaluates which capacity gain could be achieved theoretically with the dynamic pairwise separations concept and how much this theoretical maximum is reduced by conservative uncertainty allowances of the components of the WSVBS that consider statistical variations of aircraft flight tracks, meteorological parameters, wake vortex behavior, and resulting safety areas.

System Overview and Topology

Figure 1 delineates the components of the WSVBS and their interplay. The bottleneck of runway systems prevails in ground proximity because there stalling or rebounding wake vortices may not descend below the flight corridor. Therefore, in that domain the best wake prediction skill is required which here is achieved based on measurements of meteorological conditions with a SODAR/RASS system and an ultrasonic anemometer (USA).

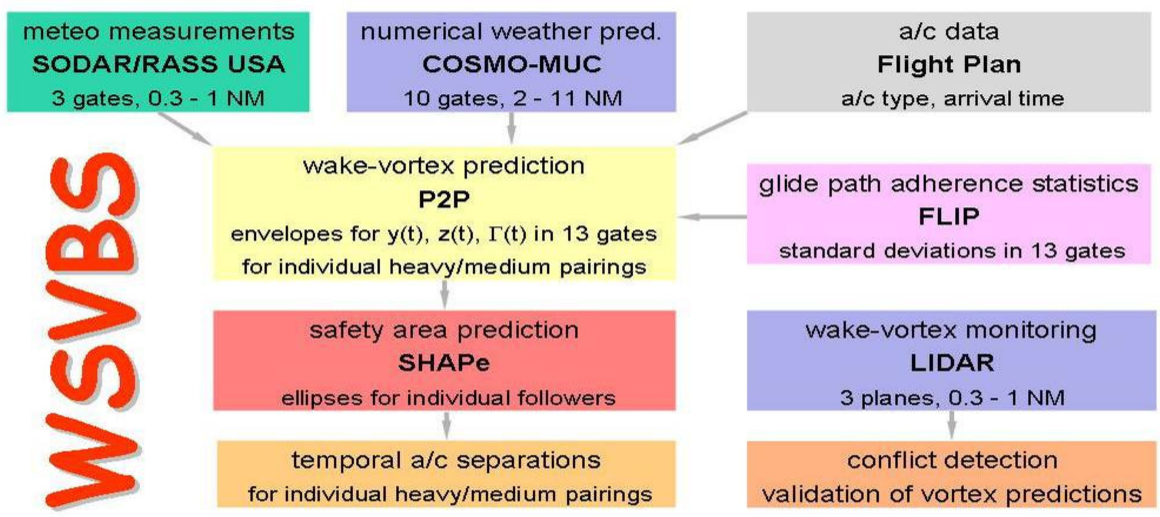

Figure 1. Flowchart of the WSVBS.

Because it is not possible to cover the whole glide slope with such instrumentation, the meteorological conditions in the remaining area are predicted with a numerical weather prediction system (COSMO-MUC) leading to wake predictions with increased uncertainty bounds. Based on glide path adherence statistics (FLIP) the probabilistic wake vortex model P2P predicts upper and lower bounds for position and strength of vortices generated by heavy aircraft. These bounds are expanded by the safety area around a vortex that must be avoided by follower aircraft for safe and undisturbed flight (SHAPe). Wake vortex and safety area predictions can be conducted optionally based upon either weight class combinations (heavy/medium) or individual aircraft type pairings according to the flight plan. The instant when the safety areas do not overlap with the flight corridor define the temporal separation between an individual aircraft pairing. The LIDAR monitors the correctness of WSVBS predictions in the most critical gates at low altitude. The components of the WSVBS will be described in detail later, together with their respective references.

The WSBVS concept requires that all aircraft are established on the glide slope at the final approach fix (FAF) which is situated 11 NM before the touchdown zone (TDZ). The wake-vortex evolution is predicted within 13 gates along the final approach. In ground proximity the gate separation of 1 NM is reduced to 1/3 NM to properly resolve the interaction of wake vortices with the ground. Figure 2 delineates the runway with the employed geodetic coordinate system and the gates 10 -13 next to the ground.

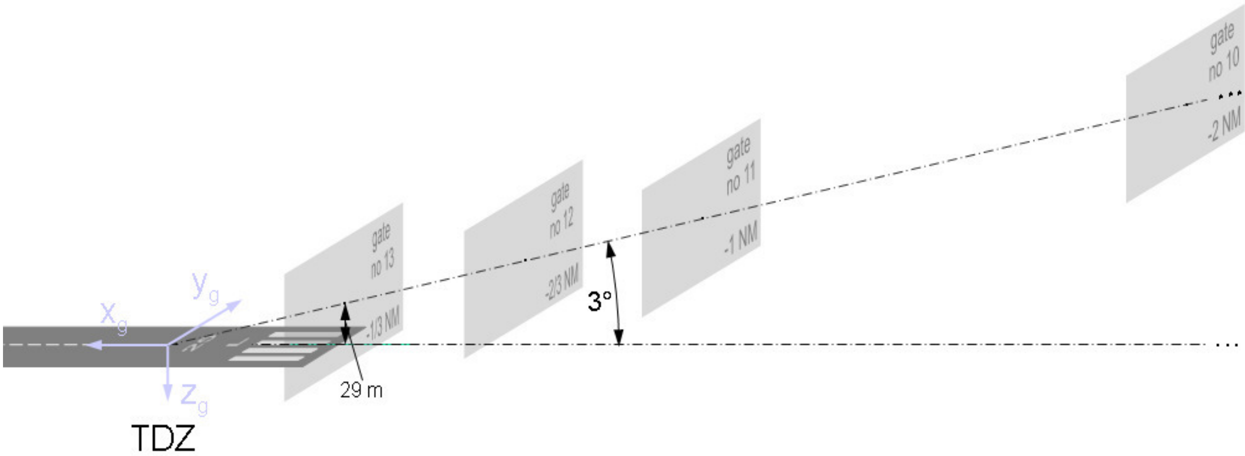

Figure 2. Zoom on gates 10 to 13.

System Components

It is planned to adjust the different system components to consistent probability levels such that the WSVBS will meet accepted risk probabilities as a whole. Since a comprehensive risk assessment of the WSVBS is still pending, we currently employ by default 95.4% probabilities (two standard deviations, 2σ, for Gaussian distributions) as a basis for the probabilistic components of the WSVBS. In the following the components delineated in the flowchart of Figure 1 are described in detail.

Meteorological Data

For prediction of wake-vortex behavior along the final approach path meteorological conditions with good accuracy must be provided for the complete considered airspace with a forecast horizon of 1 hour. A combination of measurements (employing the persistence assumption) and numerical weather predictions accounts for the required temporal and spatial coverage.

For approach and landing the largest probability to encounter wake vortices prevails at altitudes below 300 ft (Critchly & Foot 1991, Holzäpfel et al. 2009-2, Elsenaar et al. 2006). There, stalling or rebounding vortices may not clear the flight corridor vertically and weak crosswinds may be compensated by vortex-induced lateral transport which may prevent the vortices to quit laterally. Since vortex decay close to the ground is not very sensible to meteorological conditions (Holzäpfel & Steen 2007), the most important mechanism that may allow for reduced aircraft separations is lateral transport of wake vortices by crosswind.

Frech & Holzäpfel (2008) demonstrates that the best wake-vortex prediction skill of lateral transport in ground proximity is achieved employing SODAR wind measurement data. Only if it is assumed that the measured wind would persist longer than about one hour, the lateral vortex transport predicted with input

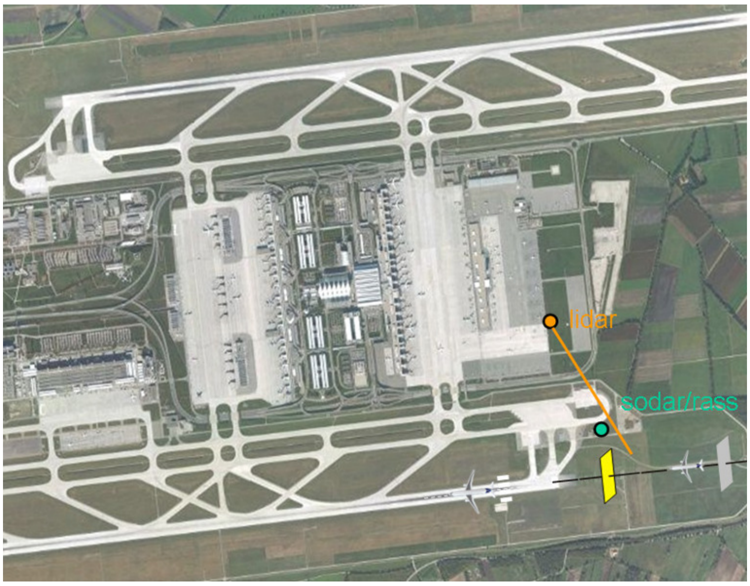

Figure 3. Sketch of instrumentation set-up at Munich Airport.

from numerical weather prediction would yield on average superior results. Because it is not feasible to cover the complete final approach path with instrumentation we employ SODAR/RASS data for wake prediction in the bottleneck at low altitudes (gates 11 – 13) whereas for the less critical area aloft (gates 1 – 10) we use COSMO-MUC data which yields minor wake prediction skill.

Figure 3 shows runway 26L of Munich airport with the locations of the employed sensors and the two lowest gates for the prediction of wake vortex behavior. Close to the lowest gate (yellow) a METEK SODAR with a RASS extension provides 10-minute averages of vertical profiles of the three wind components, vertical fluctuation velocity, and virtual temperature with a vertical resolution of 20 m. The SODAR/RASS system is complemented by an ultrasonic anemometer (USA) mounted on a 10 m mast. Eddy dissipation rate (EDR) profiles are derived from vertical fluctuation velocity and the vertical wind gradient employing a simplified budget equation (Frech 2004). A spectral analysis of the longitudinal velocity measured by the sonic is used to estimate EDR by fitting the -5/3 slope in the inertial sub-range of the velocity frequency spectrum.

For the area which was not covered by measurements (the more remote 10 gates from 2 to 11 NM) numerical weather predictions were conducted with the model COSMO-MUC (Dengler et al. 2009, see Section 2.5).

Approach Corridor Dimensions

For the definition of approach corridor dimensions we employ as baseline the glide path adherence statistics of the FLIP study (Frauenkron et al. 2001), an investigation of the navigational performance of ILS (Instrument Landing System) approaches at Frankfurt airport. FLIP provides statistics of 35,691 tracks of precision approaches on Frankfurt ILS of runways 25L/R. It does not differentiate between manual and automatic approaches. The study indicates that the measured flight path deviations are much smaller than specified by ICAO localizer and glide slope tolerances. The employed corridor dimensions decrease monotonically when approaching the runways and are kept constant within a distance of 2 NM from TDZ (see Figure 4).

Investigations of arrival flight track data at the airports St. Louis (Hall & Soares 2008), Atlanta (3,394 approaches, Zhang et al. 2009), and Chicago (1,112 approaches, Zhang et al. 2009) indicate that the lateral aircraft deviations below a distance of 2 NM from TDZ are significantly smaller than assumed in the FLIP study (see Figure 4). Therefore, we alternatively apply a fit to the to the lateral RMS deviations found in the studies of Hall & Soares and Zhang et al. which is effective at distances from the TDZ below 3.3 NM and retain the FLIP statistics for larger distances:

$$\sigma_{y,fit} = 2.76\,\mathrm{m} + 3.85\,\mathrm{m/NM} \cdot x[\mathrm{NM}]; \quad x < 3.3\,\mathrm{NM}$$
$$\sigma_{y,FLIP} = 11.5\,\mathrm{m} + 1.23\,\mathrm{m/NM} \cdot x[\mathrm{NM}]; \quad x \geq 3.3\,\mathrm{NM}$$

The approach corridors in the different gates consist of ellipses (see green ellipse in Figure 7). Vertical and horizontal semi axes of these ellipses correspond to two standard deviations derived from glide path adherence statistics, respectively. For Gaussian distributions two standard deviations (2σ) correspond to a probability of 95.4% that an aircraft does not leave the corridor in one dimension (either laterally or vertically). For ellipsoidal corridors this probability reduces to 86.5% assuming statistical independence of lateral and vertical positions.

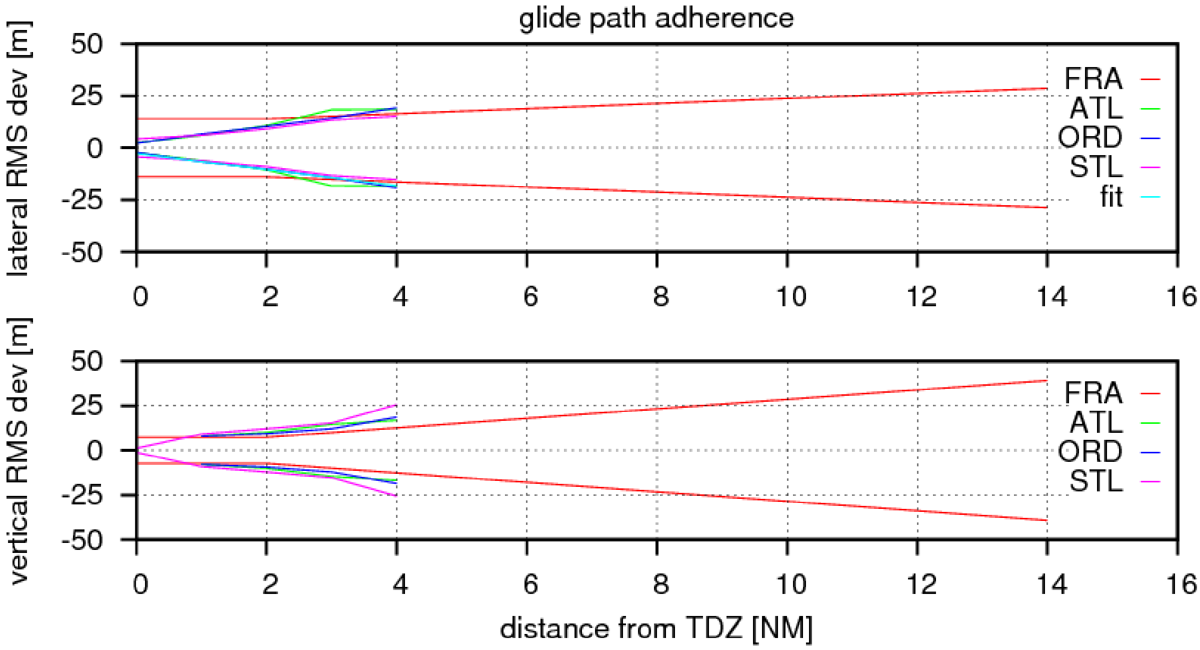

Figure 4. Lateral and vertical RMS deviations of aircraft from the glide path at the airports FRA, ATL, ORD, and STL.

Representation of Aircraft Types

The latest version of the WSVBS also predicts conservative separations for individual aircraft pairings as it is foreseen in the final development stages of NextGen and SESAR. This approach requires that the approaching aircraft types are known. During the Munich campaign the WSVBS provided predictions for all heavy leader and medium follower aircraft types that were scheduled to land within the same five minute interval according to the flight plan. So far the WSVBS may predict separations between the following individual heavy leader aircraft types (aircraft designators according to ICAO): A306, A310, A332, A333, A343, A346, B744, B762, B763, B764, B772, B773, B77W, IL96, MD11 and the medium follower aircraft types A319, A320, A321, AT43, AT45, AT72, B462 , B463, B712, B733, B734, B735, B736, B737, B738, B752, B753, CRJ1, CRJ2, CRJ7, CRJ9, D328, DH8D, E145, E170, E190, F100, F70, MD82, MD83, RJ1H, RJ85, SB20, SF34.

For each generator aircraft type the envelopes for wake vortex behavior are predicted assuming a maximum and a minimum initial circulation value that could occur during approach and landing. The minimum circulation assumes an aircraft weight corresponding to the operational empty weight (OEW) plus the fuel weight for one hour of flight plus the weight of 10% of the maximum amount of passengers combined with the flight speed at the final approach fix (FAF) of about 200 kts (103 m/s). The maximum circulation is based upon maximum landing weight (MLW) and a landing speed of 70 m/s (136 kts).

In order to keep the system as simple as possible and, thus, to minimize additional workload for controllers, the WSVBS may alternatively consider aircraft weight class combinations. The relevant combinations are heavy followed by heavy (HH) and heavy followed by medium (HM) aircraft. Conservative measures for initial circulation, wing span, and final approach speed as function of the maximum take-off weight are taken to characterize the classes (Holzäpfel et al. 2009-1).

Wake-Vortex Prediction

Wake-vortex prediction is conducted with the Probabilistic Two-Phase wake-vortex decay model (P2P) which is described in detail in Holzäpfel (2003). Applications, assessments and further developments are reported in Frech & Holzäpfel 2008, Holzäpfel & Robins 2004, Holzäpfel 2006, and Holzäpfel & Steen 2007. P2P considers all effects of the leading order impact parameters: aircraft configuration (span, weight, velocity, and trajectory), wind (cross and head components), wind shear, turbulence, temperature stratification, and ground proximity. P2P has been validated against data of over 10,000 cases gathered in two US and six European measurement campaigns.

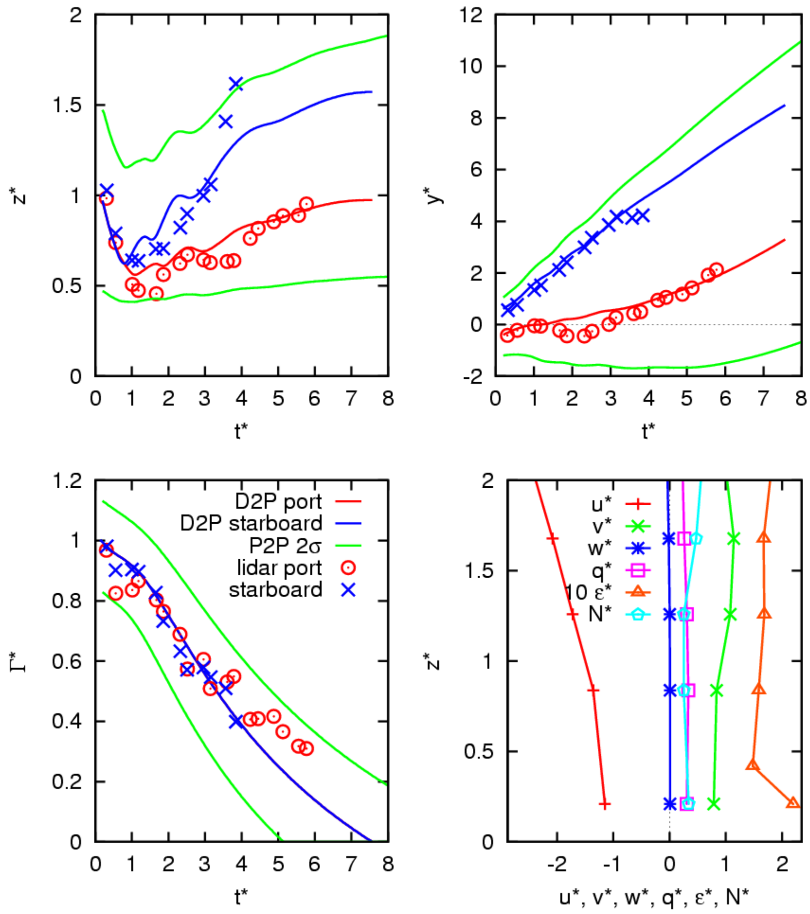

Figure 5. Evolution of normalized vertical and lateral positions and circulation of wake vortices in ground proximity. Measurements by lidar (symbols) and predictions with the P2P wake vortex model (lines). Red and blue lines denote deterministic behavior; green lines are probabilistic envelopes (95.4%). Right below vertical profiles of measured meteorological parameters. Normalizations based on initial values of vortex spacing, circulation, and time needed to descend one vortex spacing.

Precise deterministic wake vortex predictions are not feasible operationally. Primarily, it is the nature of turbulence that deforms and transports the vortices in a stochastic way and leads to considerable spatiotemporal variations of vortex position and strength. Moreover, the variability of environmental conditions must be taken into account. Therefore, the output of P2P consists of confidence intervals for vortex position and strength. Figure 5 illustrates asymmetric vortex rebound characteristics caused by crosswind in ground proximity.

For the time being, the confidence intervals for y, z, and Γ are adjusted by default to 2σ-probabilities. The respective uncertainty allowances are achieved by a training procedure which employs statistics of measured and predicted wake vortex behavior (Holzäpfel 2006). Note that the training procedure implicitly considers the quality of the meteorological input data. As a consequence, uncertainty allowances of wake-vortex predictions based on the high-quality SODAR/RASS measurements in the lowest three gates are smaller than uncertainty allowances applied to wake-predictions at higher altitudes which are based on COSMO-MUC input.

Safety-Area Prediction

Once the potential positions of the wake vortices at each gate are known, safe distances between wake vortex core positions and the follower aircraft need to be assigned. The Simplified Hazard Area (SHA) concept (Hahn et al. 2004, Schwarz & Hahn 2006) predicts distances which guarantee safe and undisturbed operations. The SHA-concept assumes that for encounters during approach and landing the vortex induced rolling moment constitutes the dominant effect and can be used to define a safety area representing the entire aircraft reaction. Then encounter severity can be characterized by a single parameter, the required Roll Control Ratio, RCR_{req}, which relates the wake vortex induced rolling moment to the maximum available roll control power.

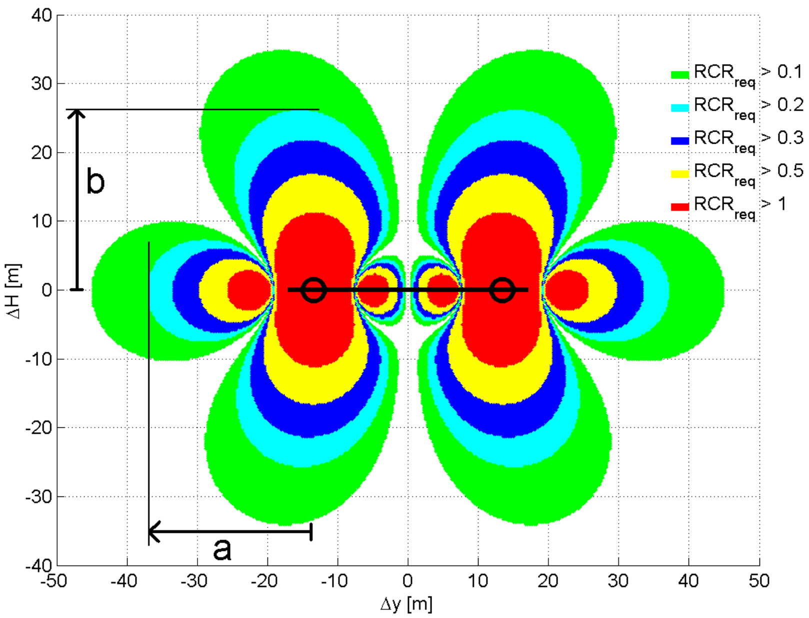

Figure 6. Roll control power required to compensate wake-vortex induced rolling moments. Horizontal and vertical allowances a and b for $RCR_{req} < 0.2$.

In Figure 6 the red areas with $RCR_{req} > 1$ denote regions where the roll control capability of the encountering aircraft is exceeded. Full flight simulator investigations (Schwarz & Hahn 2006) yield acceptable results for manual control for a value of $RCR_{req} = 0.2$. Results from real flight tests, using DLR's fly-by-wire in-flight simulator ATTAS, support this conclusion (Schwarz & Hahn 2005). In Figure 6 the lines a and b denote the resulting distances between vortex centres and follower aircraft for $RCR_{req} < 0.2$ which are added to the wake vortex envelopes.

As for wake vortex prediction either individual wake vortex and follower aircraft pairings are considered or wake vortex envelopes representing the heavy category combined with the follower categories medium or heavy. In order to represent the follower aircraft weight classes heavy and medium all relevant aircraft parameters (wing span, wing area, airspeed, lift gradient, maximum roll control power, and taper ratio) are conservatively combined to mimic the worst case scenarios. The values of the worst case parameter combinations are again derived from envelopes of aircraft parameters as function of MTOW, similarly as it was described for the wake vortex predictor before. This method of using MTOW based aircraft parameters for the determination of simplified hazard areas is called SHAPe (Simplified Hazard Area Prediction, Hahn et al. 2004).

System Integration

Here we describe how the above introduced components are combined for the prediction of adapted aircraft separations. First components within a single gate are considered. Then it is explained how the minimum temporal aircraft separations are derived from the predictions within all the gates. Finally, the temporal prediction cycle which defines parameters like update rate and prediction horizon is sketched.

Figure 7 illustrates the process seen in flight direction in control gate 11 for a heavy leader aircraft and a vortex age of 100 s. The different ellipses are defined by the respective sums of vertical and horizontal probabilistic allowances of the components approach corridor, vortex area prediction, and safety area prediction. Note that horizontal and vertical dimensions in Figure 7 are in scale. The dark blue corridor of possible vortex positions indicates that superimposed to vortex descent a southerly cross-wind advects the wake away from runway 26L.

Because the lateral vortex position can only be predicted less precisely (uncertainty and variability of crosswind) than vertical position, the aspect ratio of the vortex area ellipse exceeds a value of eight. Out of ground effect this aspect ratio is much smaller because there uncertainties regarding vortex descent are increased (Holzäpfel & Steen 2007). Safety area margins for large and small follower aircraft are added to the vortex corridors, resulting in overall safety areas to be avoided. One important aspect is that the safety corridors are not static but move depending on wake transport. Further, they grow due to vortex spreading and shrink according to wake decay.

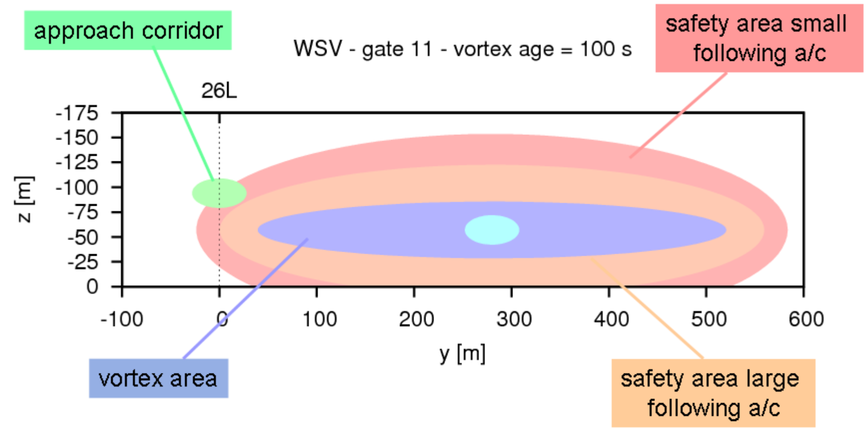

Figure 7. Ellipses denoting approach corridor dimensions, vortex areas, and safety areas in gate 11 for a vortex age of 100 s and runway 26L.

For aircraft pairings on approach to the same runway, the time interval between the passage of the generator aircraft through a gate and the time when a safety area does no longer overlap with the approach corridor (gate obstruction time) determines the minimum temporal separation for that gate. For a closely-spaced parallel runway system, the question is whether the safety areas reach the neighboring approach corridor within the prediction horizons or not. Our example in Figure 7 illustrates that after 100 s the safety area for a large following aircraft has just left the approach corridor, yet the gate is blocked for a small follower aircraft, because the respective safety corridor still overlaps with the approach corridor.

One prediction sequence comprises 13 gates along the glide path. The cases with maximum vortex ages with conflicts (gate obstruction times) define minimum aircraft separation times, MST. For dynamic pairwise landings on a single runway the predicted MST have the following format:

31-Aug-2010 Tue 1345 A343 AT72 81
31-Aug-2010 Tue 1320 A332 B738 89
31-Aug-2010 Tue 1320 A332 D328 96
31-Aug-2010 Tue 1320 A332 A320 89

Date, scheduled landing time, leader aircraft type, follower aircraft type, and predicted aircraft separation time in seconds. In the time frame from 13:20 to 13:25 a heavy A332 and three medium follower aircraft types are scheduled to land such that three individual separation times are suggested. Every 10 minutes new SODAR/RASS and COSMO-MUC data are available. When new weather data is available WSVBS predictions are initiated. The predictions are available 20 min prior to landing. The predictions could also be provided for longer lead times at the expense that the uncertainty allowances of the wake vortex corridors in gates 11-13 driven by SODAR/RASS meteorological input data would need to be increased. Wake-vortex monitoring is used to identify potential erroneous predictions of the WSVBS. For this purpose DLR's 2 µm pulsed Doppler LIDAR is operated in vertical scan mode with elevations between -0.5° to 6° to detect and track the vortices alternately in the lowest and most critical gate (see Figure 3).

Performance and Improved Capacity

The baseline setup of the WSVBS for pairwise dynamic separations is compared to a number of alternative setups listed in Table 1. This analysis may contribute to set the scene for a discussion which capacity gain could be achieved theoretically with the pairwise dynamic separations concept and how much this theoretical maximum is reduced by conservative uncertainty allowances of the components of the

WSVBS that consider statistical variations of aircraft flight path, meteorological parameters, wake vortex behavior, and resulting safety areas.

The analysis is based on the field campaign data gathered from 23 June 2010 to 8 September 2010 at Munich airport. In that time frame WSVBS predictions for 7300 landings of individual leading heavy aircraft and medium type follower aircraft on runway 26L have been conducted. The investigated scenarios are listed in Table 1. Setup 1 denotes the baseline scenario of the WSVBS where the uncertainty allowances of the approach corridor dimensions and probabilistic wake vortex predictions are set to 2σ (95.4%). Setup 2 neglects the safety area (SHAPe) and herewith investigates the contribution of the safety area on the potential capacity gain. Setup 3 assumes long-lived vortices (llv) by delaying the onset of rapid vortex decay by one time unit $t_0 = b_0 / w_o$ where b_0 denotes the initial wake vortex separation and w_0 the initial wake vortex descent speed. Setups 4 and 5 assume perfect (deterministic) wake vortex prediction capabilities where the uncertainty allowances of wake vortex behavior can be neglected without or with safety areas, respectively. These scenarios can also be considered as a reference for the potential capacity gain that could be achieved if the real wake vortex behavior would be perfectly known. Setups 1 – 5 always assume the same approach corridor dimensions. Setups 6 and 7 now consistently vary the uncertainty allowances of all probabilistic components between 1σ (68.3%) and 3σ (99.7%). These setups may provide an indication of the bandwidth of reasonable uncertainty allowances. Finally, setup 8 corresponds to the baseline setup 1 but employs the reduced lateral the flight corridor width (rw) at distances below 3.3 NM to the TDZ (gates 9 -13).

Table 1. Survey on investigated scenarios.

setup	1	2	3	4	5	6	7	8
approach corridor	2σ	2σ	2σ	2σ	2σ	1σ	3σ	2σ rw
wake-vortex prediction	2σ	2σ	2σ llv	0σ	0σ	1σ	3σ	2σ
safety area	yes	no	yes	no	yes	yes	yes	yes

Table 2 lists the average minimum separation times (MST) in which pairwise separations for landings on single runways could have been reduced either below ICAO separation (125 s) or radar separation (70 s) and their respective frequency of use. For the standard setup of the WSVBS in only 1.1% (4.0%) of the time the aircraft separations could have been reduced below radar (ICAO) separation. Setup 2 indicates that the consideration of a safety area around the vortex centers, which guarantees safe and undisturbed flight, noticeably reduces the potential capacity gain. However, even with neglected safety areas the frequency of use of 2.6% for radar separation still is small. The comparison of setups 1 and 3 indicates that the increased lifetimes of the vortices in setup 3 have only a minor effect on the frequency of use of the WSVBS because mainly vortex transport out of the approach corridor (and not vortex decay) enables reduced separations.

Table 2. Minimum separation times (MST) and frequency of use for different scenarios.

setup	1		2		3		4		5		6		7		8	
MST below [s]	70	125	70	125	70	125	70	125	70	125	70	125	70	125	70	125
average MST [s]	59	87	53	80	60	87	50	82	52	93	53	87	-	-	56	83
frequency of use [%]	1.1	4.0	2.6	6.7	1.0	3.8	16.2	49.3	6.2	38.1	7.4	34.1	0.0	0.0	1.6	4.7

Notably, even deterministic wake vortex predictions and the neglect of safety areas in setup 4 only allow for 16.2% (49.3%) reductions of aircraft separations below radar (ICAO) separation. This is that at radar separation the vortices have not left the approach corridor in at least one of the considered gates in more than 80% of the cases. Setup 5 employs deterministic wake vortex prediction and considers the safety areas. So even if the meteorological input data and the resulting wake vortex predictions would be perfect, reductions of aircraft separations below radar (ICAO) separation could safely be achieved only in 6.2% (38.1%).

Setup 6, employing 1σ-uncertainty allowances for both aircraft and wake corridors, indicates that also the approach corridor dimensions play an important role. The fraction of time for radar separations or less is with 7.4% even slightly higher than the 6.2% achieved with deterministic wake vortex predictions combined with 2σ-approach corridor dimensions (setup 5). On the other hand, setup 7 employing 3σ-uncertainty allowances is obviously far too conservative. Setup 7 would allow in only one case out of 7300 to reduce aircraft separations to 128 s. Finally, setup 8 confirms the relatively large impact of the flight corridor dimensions on the achievable reductions of aircraft separations: the reduced lateral flight corridor widths in the lowest gates may increase the fraction of radar separation by almost 50% compared to the baseline setup 1.

Figure 8 delineates the history of arrivals for which dynamic pairwise aircraft separations could have been reduced either below ICAO separation (125 s) or radar separation (70 s) for the baseline case (setup 1, above) and the deterministic wake vortex predictions without safety areas (setup 4, below). Additionally, predicted aircraft separations below 180 s are shown. The small fraction of 7% of the arrivals in which aircraft separations could have been reduced below 180 s indicates one more time that the baseline setup 1 of the WSVBS is designed very conservatively. In contrast, for the non-conservative setup 4 the fraction of arrivals with reduced separations and the respective durations are significantly higher.

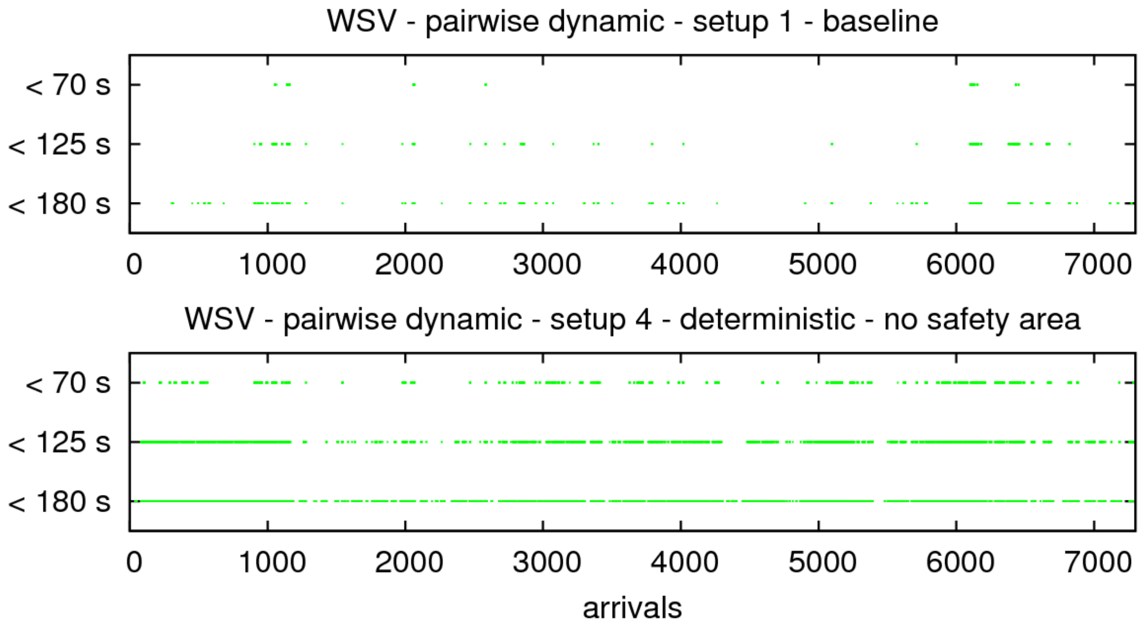

Figure 8. History of potential usage of dynamic pairwise separations for the 7300 arrivals during the Munich campaign.

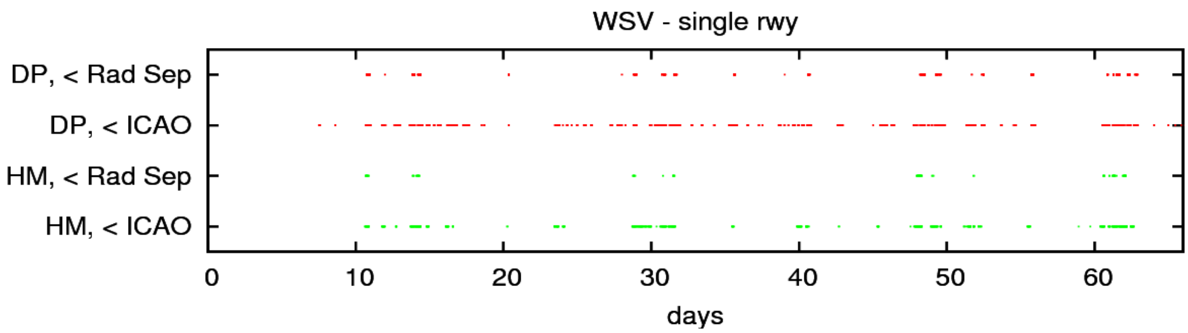

Figure 9. History of potential usage of ICAO separations or radar separations for heavy/medium aircraft weight class combinations (HM, green) or dynamic pairwise separations (DP, red) during the 66 days of the Frankfurt campaign. (From Gerz et al. 2009.)

A comparison of the potential benefits of dynamic pairwise separations and heavy/medium aircraft weight class based separations has been conducted employing the weather data gathered during the demonstration campaign of the WSVBS at Frankfurt airport in the year 06/07 (see Figure 9). For this purpose the Frankfurt traffic mix of a single representative day has been used. The fraction of time for radar separations is almost doubled from 1.5% for heavy/medium pairings to 2.8% for dynamic pairwise separations. For the latter aircraft separations could have been reduced below the ICAO standards in 10.6% of the time. During the Munich campaign dynamic pairwise separations reduced below the ICAO standards could have been applied only in 4.0% of the arrivals (see Table 2). This comparison indicates that the Frankfurt trial benefited from the strong wind periods occurring during January and February 2007. This highlights that the capacity gains found in this study strongly depend on the weather conditions prevailing during the respective measurement campaign and may differ significantly for other periods of the year and/or other airport locations.

For the interested reader Figure 10 reveals which gates impede reduced aircraft separations for the setups 1, 4, 6, and 8. In the baseline case (setup 1) gate 13 (the one closest to the runway threshold where aircraft fly at 29 m above ground) hinders WSVBS operations in 41%. In 57% gates 11 – 13 where the wake vortex predictions are driven by SODAR/RASS measurements limit reduced separations. On one hand, this is further evidence for the bottleneck close to the ground. On the other hand, this also means that only in 43% of the landings improved numerical weather prediction could increase the usage period of the WSVBS.

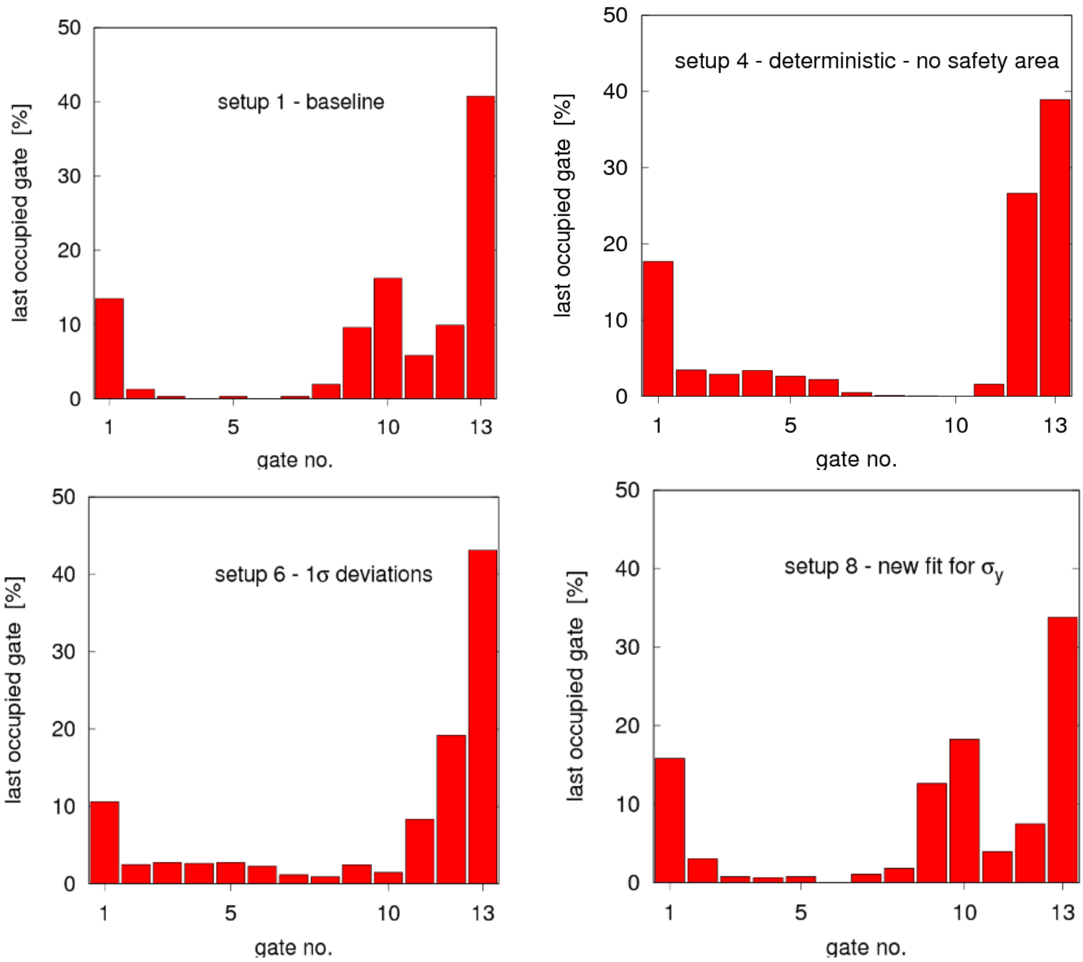

Figure 10. Last gates impeding reduced aircraft separations for four different system setups.

Interestingly though, gate 1 (the farthest-out gate at 1077 m height) blocks reduced separations in almost 14% of the cases. This is attributed to the fact that the first approach corridor features the largest dimensions. Further, gate 10 impedes reduced separations in 16% of the time. At this gate two effects appear decisive. First, it is the lowest gate employing numerical cross-wind predictions, which lead to larger uncertainty allowances of vortex position compared with predictions using actual wind measurements. Second, the aircraft vortices are shed at 190 m height where ground effect still contributes to the lateral wake vortex transport for the aircraft with the largest wing spans.

Furthermore, Figure 10 indicates that reduced uncertainty allowances for wake vortex prediction further increase the dominance of the gates 11 - 13 in ground proximity (setup 4 – deterministic: 67%, setup 6 - 1σ deviations: 71%). On the other hand, gate 10 becomes non-relevant. In contrast, the reduced lateral flight corridor dimensions in setup 8 diminish the blocking effect of the lowest gates 11 – 13 from 57% in the baseline case to 45%. It has also been investigated whether the wake vortex predictions initialized with a maximum or a minimum circulation value (see above) block the gates for longer times. It appears that both wake vortex prediction runs are of similar importance. Interestingly, the wake predictions based on the minimum circulation block the gates slightly more frequently which probably can be attributed to the reduced wake vortex descent speed in the gates out of ground effect.

Figure 11 demonstrates the principle of operation of the WSVBS (setup 1) and variations of it (setups 2, 4) for a case with strong crosswind where extremely short aircraft separations between a leading B762 and a following A321 have been predicted. Figure 11 right below shows vertical profiles of wind and potential temperature indicating excellent agreement between the measured (SoRa) and predicted (COSMO) wind profiles. The crosswind (green) rises from 7.0 m/s at 10 m height to a maximum of 17 m/s at 450 m height. Also due to the veering of the wind with height (Ekman spiral) the crosswind then decreases again to 6.0 m/s at the highest gate at 1077 m above ground. Due to this particular wind profile either gate 1 and/or gate 13 are cleared at last from wake vortices or safety areas. For the baseline setup the WSVBS predicts that the safety areas (Figure 11, top right, blue) have left the flight corridor (dashed lines) laterally in gate 1 already at only 37 s. For probabilistic wake vortex prediction and neglect of the safety areas (setup 2, P2P, red) this time reduces to 30 s and it is further reduced to 17 s for deterministic wake vortex predictions without safety areas (setup 4, D2P, green). The three plots on the left side indicate that for all considered setups neither vortex descent nor vortex decay would allow for the achieved short separations.

In order to further assess the benefits of dynamic pairwise separations compared to weight class based separations we evaluate the sensitivity of the predicted separations on the aircraft type combinations. The results recapitulated here only for the baseline case are similar for the other setups. For a given heavy leader aircraft at a given environmental situation the separation times of the different medium follower aircraft landing within the five minutes increment of the flight plan vary only slightly. On average this variation amounts to 6 s. Little surprising, maximum variations reaching up to about 40 s may occur when a heavy leader aircraft (e.g. B744) is followed either by a relatively heavy medium type aircraft (e.g. A321, MTOW = 83 t) or a relatively light medium type aircraft (e.g. DH8D, MTOW = 29 t). For the same follower aircraft and different heavy leader aircraft at a given environmental situation the separation times vary stronger. On average this separation time difference amounts to 13 s where maximum variations may reach up to about 60 s. An example for this are leading B77W (MTOW = 352 t) and A310 (MTOW = 150 t) followed by a SB20 (MTOW = 23 t).

From the high percentage of cases in which the wake vortices have not left the flight corridor (setups 4 and 5 employing deterministic wake vortex predictions) one may conclude that even under ICAO separations it is daily practice that approaching aircraft fly close to not fully decayed wake vortices. This finding is also corroborated by long-term lidar measurements of wake vortices at Charles de Gaulle airport. There it was found that in 3% of the cases the vortices were at least as close as 25 m to following landing aircraft within one gate close to the threshold (Treve 2011). The observations at Charles de Gaulle airport imply that a non-negligible number of landing aircraft could theoretically encounter the wake vortex core regions where the exerted rolling moments have maximum strength. This raises the question which mechanisms secure the safety of current operations and which mechanisms allow pilots even to land at radar separation under VFR conditions. It is not likely that the pilots are always successful at flying upwind and/or above the vortices in particular close to the threshold.

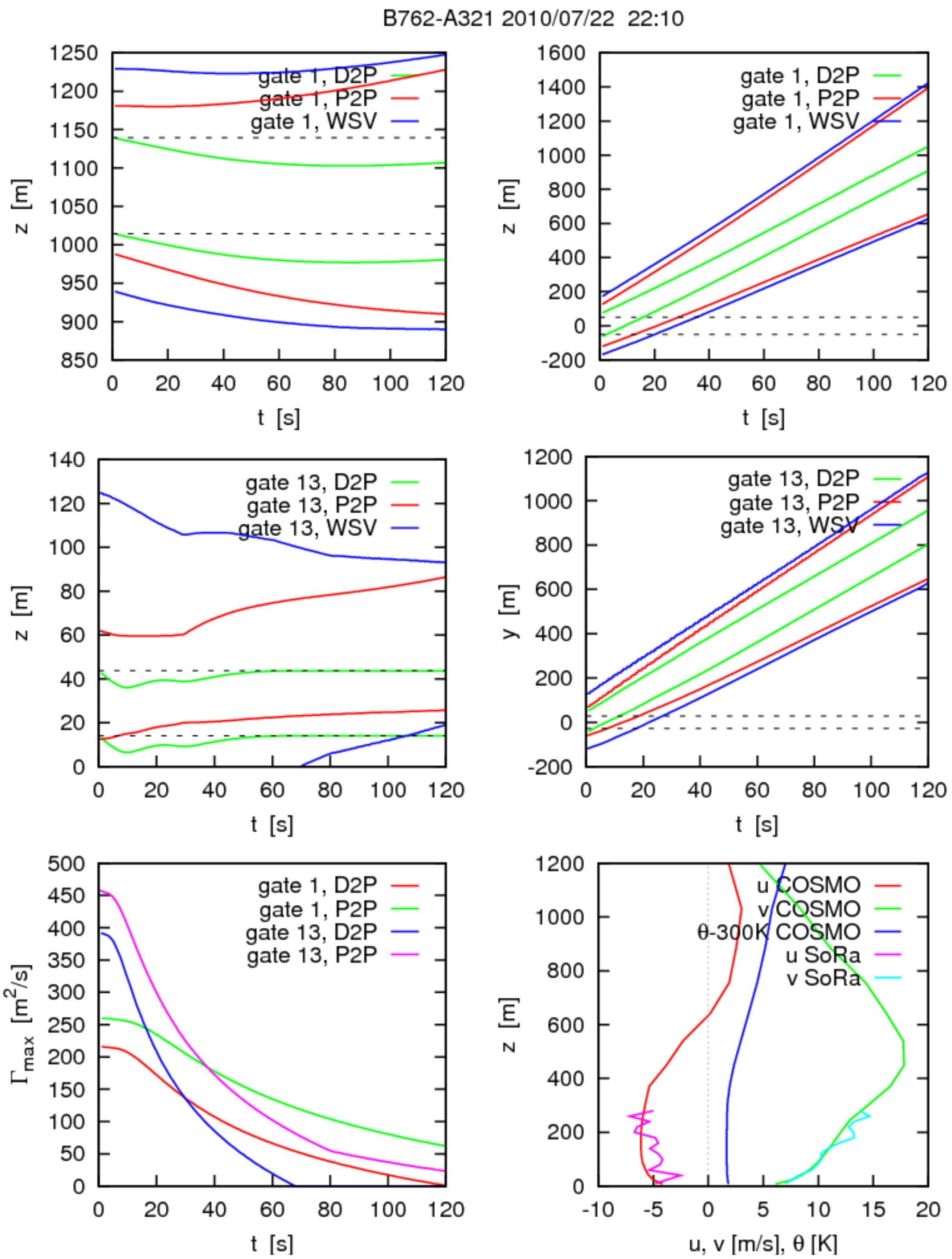

Figure 11. Predicted envelopes of wake vortex evolution and safety areas in gates 1 and 13 for strong crosswind case and setups 4 (D2P), 2 (P2P), and 1 (WSV).

Candidate explanations for the small number of critical encounters in real life are: (i) the deformation of the vortices that may alleviate vortex encounters by reducing the impact times of adverse forces and moments (Crouch & Loucel 2005, Hennemann & Holzäpfel 2011, Holzäpfel et al. 2010, Vechtel 2011), (ii) the dimensions of the flight corridor. The comparison of setups 5 and 6 indicates that the approach corridor dimensions have a strong impact on the frequency of potential reduced separations, (iii) the "self-protection mechanism" that tends to deviate an encountering aircraft from the vortex center, (iv) effects of the more or less generally prevailing headwind that may support effective vortex descent (by advecting the vortices along the inclined flight track towards higher glide path positions where the follower aircraft passes by) and vortex decay in a way which is not yet adequately considered in the WSVBS, or (v) end effects that weaken the wake vortices when they propagate along the vortex centers after touch down (Moet et al. 2005).

Conclusions

The Wake Vortex Prediction and Monitoring System WSVBS with all its components and their interactions has been described. The WSVBS consists of components that consider meteorological conditions, aircraft glide path adherence, aircraft parameter combinations representing either aircraft weight categories or individual aircraft types, the resulting wake-vortex behavior, the surrounding safety areas, wake vortex monitoring, and the integration of the predictions into the arrival manager. The elements of the WSVBS are generic and thus could well be adjusted to the runway systems at Frankfurt and Munich airports. The WSVBS predicts the concepts of operations and procedures established by DFS and it further predicts temporal separations for closely spaced parallel runways as well as for in-trail traffic.

A specific feature of the WSVBS is the usage of both measured and predicted meteorological quantities as input to wake vortex prediction. In ground proximity where the probability to encounter wake vortices is highest, the wake predictor employs measured environmental parameters that yield superior prediction results. For the less critical part aloft, which can not be monitored completely by instrumentation, the meteorological parameters are taken from dedicated numerical terminal weather predictions. For the Munich campaign the weather prediction quality was further improved by employing hourly updated time-based ensemble predictions with the assimilation of precipitation Radar, SYNOP, TEMP, and AMDAR data. The wake vortex model predicts envelopes for vortex position and strength which implicitly consider the quality of the meteorological input data. This feature is achieved by a training procedure which employs statistics of measured and predicted meteorological parameters and the resulting wake vortex behavior.

The WSVBS combines various conservative elements that presumably lead to a very high overall safety level of the WSVBS:

a) Wake vortex prediction as well as safety area prediction employs worst case combinations of aircraft parameters.
b) The wake vortex model assumes that the aircraft are situated on the envelopes of the approach corridors. Likewise, the safety area model assumes that the wake vortices are situated along the wake vortex envelopes. As a consequence the probability to actually encounter wake vortices at the edges of the safety areas is outermost small.
c) The most critical gate determines the possible aircraft separation.
d) A LIDAR that scans the most critical gates at low altitude monitors the correctness of suggested aircraft separations.

The combination of these conservative measures certainly leads to a very high but currently unknown overall safety. Once the methodology of a comprehensive risk analysis will be established, it is planned to adjust all components to appropriate and consistent confidence levels. Possibly, this will enable to somewhat relax the current stringent safety allowances of the WSVBS with the benefit of increased operation times with reduced separations. The primary purpose of the risk analysis, of course, is to convince all stakeholders of the usefulness and capabilities of the system

The WSVBS has demonstrated its functionality at Frankfurt airport in the period from 18/12/06 until 28/02/07. At Munich airport the WSVBS has demonstrated the feasibility of dynamic pairwise separations for the first time (23/6/10 – 15/9/10). These performance tests indicate that

i. the system runs stable - no forecast breakdowns occurred,
ii. in Frankfurt aircraft separations could have been reduced for the closely-spaced parallel runway system in 75% of the time compared to ICAO standards,
iii. reduced separation procedures could have been continuously applied for at least several tens of minutes and up to several hours occasionally,
iv. the Frankfurt predictions were correct as for about 1100 landings observed during 16 days no warnings occurred from the LIDAR,
v. the consideration of dynamic pairwise separations may almost double the times operating at radar separation compared to weight class combinations,
vi. an assessment of the sensitivity of the predicted dynamic pairwise separations on the aircraft type combinations indicates a higher sensitivity on the heavy leader aircraft types than on the medium follower aircraft types,
vii. the impact of the flight corridor dimensions on the achievable reductions of aircraft separations turns out to be relatively large. So the existing and in future expected improvements of navigational performance may substantially support the performance and introduction of new wake vortex advisory systems,
viii. the potential capacity gains of dynamic pairwise operations for single runways appear to be very small for the baseline setup of the WSVBS. A sensitivity analysis of eight different setups of the WSVBS indicates that the baseline setup of the WSVBS features a very conservative design. On the other hand, it is found that for perfect weather data and perfect wake vortex predictions the vortices have frequently not left the flight corridor when the follower aircraft passes the respective gates. Nevertheless, current operations are safe. A number of candidate explanations for the small number of critical encounters in real life is suggested. Deepened understanding of the high percentage of close approaches to wake vortices without severe consequences is prerequisite to an optimal setup of a wake vortex advisory system.

The WSVBS may also be further developed to provide warnings in situations where the routinely applied aircraft separations may not be sufficient in order to further increase safety during approach and landing.

Acknowledgments

The work presented here was funded by the DLR projects Wirbelschleppe and Wetter & Fliegen and benefited from the EU projects ATC-Wake (IST-2001-34729), FAR-Wake (AST4-CT-2005-012238), FLYSAFE (AIP4-CT-2005-516 167), and the European Thematic Network WakeNet2-Europe (G4RT-CT-2002-05115) and the European Coordination Action for Aircraft Wake Turbulence WakeNet3-Europe (ACS7-GA-2008-213462). We greatly appreciate the excellent support of the teams from DFS Deutsche Flugsicherung GmbH, DWD Deutscher Wetterdienst, Fraport AG, Flughafen München GmbH, and METEK GmbH.

References

Baldauf M., Seifert A., Förstner J., Majewski, D., Raschendorfer M. 2011: Operational convective-scale numerical weather prediction with the COSMO model: description and sensitivities. — Mon. Wea. Rev., Vol. 139, No. 12, 3887-3905, 2011.

J.B. Critchley, P.B. Foot, UK CAA Wake Vortex Database: Analysis of Incidents Reported Between 1982 and 1990, Civil Aviation Authority, CAA Paper 91015, 1991.

J.D. Crouch, R.E. Loucel: Flight-simulator study of airplane encounters with perturbed trailing vortices, J. Aircraft, Vol 42, No. 4, 924-931, 2005.

K. Dengler, C. Keil, M. Frech, T. Gerz, K. Kober: Comparison and validation of two high-resolution weather forecast models at Frankfurt Airport. Meteorologische Zeitschrift Vol. 18, 2009, 531-542, DOI: 10.1127/0941-2948/2009/0399.

Dengler, K., Anger, J., Keil, C. 2011: Validation of Time-Lagged Ensemble Forecasts Relevant for Predicting Aircraft Wake Vortices. Submitted to Meteorlog. Zeitschrift

G. Doms, U. Schaettler, “The nonhydrostatic Limited Area Model LM (Lokal Modell) of DWD. Part I: Scientific Documentation”, Deutscher Wetterdienst, Offenbach, 1999.

B. Elsenaar et al., Wake Vortex Research Needs for ``Improved Wake Vortex Separation Ruling" and ``Reduced Wake Signatures", Final Report of the Thematic Network 'WakeNet2-Europe', 6th Framework Programme, National Aerospace Laboratory, NLR-CR-2006-171, Amsterdam, 2006.

EUROCONTROL, Challenges of Growth 2008, STATFOR, EUROCONTROL, 2008.

FAA, NAS Enterprise Architecture / Infrastructure Roadmaps, Version 5.0, Federal Aviation Administration, 19th January 2011.

H. Frauenkron, M. Maiss, P. Nalpanis, "FLIP - Flight Performance using Frankfurt ILS", DFS German Air Navigation Services, Air Traffic Management Division, Version 2.0, 2001.

M. Frech, "A simple method to estimate the eddy dissipation rate from SODAR/RASS measurements", 16th Symposium on Boundary Layers and Turbulence, AMS, Portland, Paper 6.13, 2004, p. 4.

M. Frech, F. Holzäpfel, "Skill of an aircraft wake-vortex transport and decay model using short-term weather prediction and observation", J. Aircraft, Vol 45, 461-470, March-April 2008.

M. Frech, F. Holzäpfel, A. Tafferner, T. Gerz, "High-Resolution Weather Data Base for the Terminal Area of Frankfurt Airport", J. Appl. Meteor. Climat. Vol 46, 1913-1932, 2007.

T. Gerz, F. Holzäpfel, W. Bryant, F. Köpp, M. Frech, A. Tafferner, G. Winckelmans, "Research towards a wake-vortex advisory system for optimal aircraft spacing", Comptes Rendus Physique Vol 6 , 501-523, 2005.

T. Gerz, F. Holzäpfel, W. Gerling, A. Scharnweber, M. Frech, K. Kober, K. Dengler, S. Rahm, THE WAKE VORTEX PREDICTION AND MONITORING SYSTEM WSVBS PART II: PERFORMANCE AND ATC INTEGRATION AT FRANKFURT AIRPORT, Air Traffic Control Quarterly, Vol. 17, No. 4, 2009, pp. 323-346.

G.A. Grell, S. Emeis, W.R. Stockwell., T. Schoenemeyer, T. Forkel, J. Michalakes, R. Knoche, W. Seidl, "Application of a multiscale, coupled MM5/chemistry model to the complex terrain of the VOTALP valley campaign", Atmosph. Environ. Vol 34, 1435-1453, 2000.

Gurke T., Lafferton H., "The development of the wake vortex warning system for Frankfurt Airport: Theory and implementation", Air Traffic Control Quarterly, Vol 5, 3-29, 1997.

K.-U. Hahn, C. Schwarz, H. Friehmelt, "A Simplified Hazard Area Prediction (SHAPe) Model for Wake Vortex Encounter Avoidance", 24th International Congress of Aeronautical Sciences, Yokohama (Japan), 29 August - 3 September 2004, ICAS, 24th International Congress of Aeronautical Sciences Proceedings, 2004

T. Hall, M. Soares, "Analysis of localizer and glide slope flight technical error", 27th Digital Avionics Systems Conference, St. Paul, MN 2008.

R. Hemm, G. Shapiro, D.A. Lee, J. Gribko, B. Glaser, "Benefit Estimates of Terminal Area Productivity Program Technologies", NASA/CR-1999-208989, 1999, p. 144.

I. Hennemann, F. Holzäpfel, "Large-Eddy Simulation of Aircraft Wake Vortex Deformation and Topology", Proc. IMechE Vol. 225 Part G: J. Aerospace Engineering, 2011, pp. 1336-1350, DOI: 10.1177/0954410011402257.

F. Holzäpfel, "Probabilistic Two-Phase Wake Vortex Decay and Transport Model", J. Aircraft, Vol 40, 323-331, 2003.

F. Holzäpfel, R.E. Robins, "Probabilistic Two-Phase Aircraft Wake-Vortex Model: Application and Assessment", J. Aircraft, Vol 41, 1117-1126, 2004.

F. Holzäpfel, "Probabilistic Two-Phase Aircraft Wake-Vortex Model: Further Development and Assessment", J. Aircraft, Vol 43, 700-708, 2006.

F. Holzäpfel, M. Steen, "Aircraft Wake-Vortex Evolution in Ground Proximity: Analysis and Parameterization", AIAA J. Vol 45, 218-227, 2007.

F. Holzäpfel, T. Gerz, M. Frech, A. Tafferner, F. Köpp, I. Smalikho, S. Rahm, K.-U. Hahn, C. Schwarz, THE WAKE VORTEX PREDICTION AND MONITORING SYSTEM WSVBS - PART I: DESIGN, Air Traffic Control Quarterly, Vol. 17, No. 4, 2009, pp. 301-322.

F. Holzäpfel, M. Frech, T. Gerz, A. Tafferner, K.-U. Hahn, C. Schwarz, H.-D. Joos, B. Korn, H. Lenz, R. Luckner, G. Höhne, "Aircraft Wake Vortex Scenarios Simulation Package – WakeScene", Aerosp. Sci. Technol. Vol 13, 1-11, 2009.

F. Holzäpfel, T. Misaka, I. Hennemann, Wake-Vortex Topology, Circulation, and Turbulent Exchange Processes, AIAA Paper 2010-7992, AIAA Atmospheric and Space Environments Conference, 2-5 August 2010, Toronto, Ontario, Canada, 16 pages.

F. Holzäpfel, K. Dengler, T. Gerz, C. Schwarz, Prediction of Dynamic Pairwise Wake Vortex Separations for Approach and Landing, AIAA Paper 2011-3037, 3rd AIAA Atmospheric Space Environments Conference, 27-30 June 2011, Honolulu, Hawaii, 15 pages.

ICAO, Aircraft Type Designators; ICAO Document No. 8643 http://www.icao.int/anb/ais/8643/index.cfm

S. Lang, "NextGen – Next Generation Air Transportation System", Global Wake Vortex Conference II, San Diego, CA, USA, 1-2 December 2010.

H. Moet, F. Laporte, G. Chevalier, and T. Poinsot, "Wave propagation in vortices and vortex bursting," Phys. Fluids 17, 054109, 2005.

C.W. Schwarz, K.-U. Hahn, "Simplified Hazard Area for Wake Vortex Encounter Avoidance", AIAA Paper 2005-5903, AIAA Atmospheric Flight Mechanics Conference, San Francisco, CA, August 2005, pp. 5903.1 -5903.9.

C.W. Schwarz, K.-U. Hahn, “Full-flight simulator study for wake vortex hazard area investigation”, Aerosp. Sci. Technol. Vol 10, 136-143, 2006.

SESAR, “European Air Traffic Management Master Plan“, Edition 1, 30 March 2009, SESAR Consortium.

M. Steen, S. Schönhals, J. Polvinen, P. Drake, J.-P. Cariou, A. Dolfi-Bouteyre, F. Barbaresco, “Candidate Technologies Survey of Airport Wind & Wake-Vortex Monitoring Sensors”, 9th Innovative Research Workshop & Exhibition, Eurocontrol Experimental Centre Brétigny-sur-Orge, France, 7-9 December 2010.

Steppeler, J., G. Doms, U. Schattler, H. W. Bitzer, A. Gassmann, U. Damrath, G. Gregoric: Meso-gamma scale forecasts using the nonhydrostatic model LM. — Meteorology and Atmospheric Physics 82, 2003, 75-96.

V. Treve, discussions during WakeNet3-Europe Workshop “Research Needs for Operational Concepts and Capacity Analysis”, London, UK, 8 - 9 Feb. 2011.

Vechtel, D., Flight Simulator Study on the influence of Vortex Curvature on Wake Encounter Hazard using LES Wind Fields, The Aeronautical Journal, Volume 116, No. 1177, March 2012.

Y. Zhang, J. Shortle, L. Sherry, “Comparison of Arrival Tracks at Different Airports”, Proceedings of 4th International Conference on Research in Air Transportation. Budapest, Hungary 2010.

2.2 Concatenating Weather Monitoring and Forecast: the WxFUSION Concept

Arnold Tafferner, Caroline Forster, Thomas Gerz
Institute of Atmospheric Physics

The meteorological network of observation and prediction continuously delivers an enormous amount of various atmospheric parameters. In particular in the area of an aerodrome the observation density is typically higher than on average. In the project we spawned the idea to smartly concatenate the variety of available data which are relevant for aviation and develop new products which use the information contained in the data but describe the phenomenon of interest in a simple and unambiguous way for direct use for the aviation stakeholders. We developed this idea in a concept and related system named WxFUSION, meaning "weather forecast user-oriented system including object nowcasting".

The Concept of Combining Weather Observation and Prediction Data

Several integrated systems, which automatically combine different data sources and provide weather hazard information specially tailored to the needs of decision makers at airports, have been developed and successfully tested in the USA. Examples are the Integrated Terminal Weather System (ITWS) by the Massachusetts Institute of Technology (Evans and Ducot, 1994) and the Auto-Nowcast System developed at the NCAR (Mueller et al., 2003). In 2010 the Commission for Aeronautical Meteorology of the World Meteorological Organisation established an expert team on meteorological services for the terminal area (ET/MSTA) and a task team on the user needs (http://www.ntf.weather.gov.hk/). The German Meteorological Service, DWD, installs an ITWS together with a low-level wind shear alert system (LLWAS) at the airports of Frankfurt and Munich (http://www.dwd.de/itws). The LLWAS basically augments the standard observation means at the airports by a cloud RADAR and a Doppler LIDAR in order to detect wind shear layers and aircraft wake vortices along the glide paths of aircraft under rainy as well as dry weather conditions.

The WxFUSION concept (Figure 1) aimes at the combination of data from observation systems, nowcasting tools, and numerical models in order to detect, track, nowcast (up to about 6 hours), and forecast (beyond 6 hours) hazardous weather phenomena for aviation purposes as precisely and as consistent as possible [Forster and Tafferner, 2009a]. The combination within one integrated system can be expected to provide a greatly enhanced benefit in monitoring and nowcasting capability, i.e. an integrated system can process and contrast the assertions of the individual tools, e.g. as regards to the exact location of a particular weather system, its intensity and movement, and thus provide a more reliable assertion of the future state of a weather system as when only one data source or nowcasting tool were used (Tafferner et al., 2008).

Certainly, in order to be useful an integrated system for nowcasting and short term forecasting must be constructed in a way that it can process large data amounts within a very short time. The prime aim of such a system is to reduce the complexity of weather to a description of the event that supports users in decision making. This requirement is quite obvious in extreme weather situations where individual weather parameters change quickly and not much time is available to analyze a complex and large data set visually or by hand. Therefore, there is a need for automation in order to fulfill this requirement. The system is currently under development; several components, however, exist already and are described in the following. Examples of individual components are also presented in the following.

Figure 1 illustrates the system, various data sources and system components are represented by symbols. The elements in the top row are the cloud tracker Cb-TRAM, the radar tracker Rad-TRAM and the VERA analysis (see below). In addition polarimetric radar and lightning observations are available. Together these elements compose the observation and nowcasting part of WxFUSION. The bottom row of elements comprises numerical model forecasts and forecast validation components. Forecast data are available from the COSMO-DE (Baldauf et al., 2011) ensemble and from the high-resolution time-lagged ensemble COSMO*MUC* (Dengler et al., 2011, see Section 2.5). From these model outputs synthetic satellite ('SYNSAT') and radar images ('SYNRAD') are generated which are used as input to Cb-TRAM and Rad-TRAM. Synthetic objects are thus obtained which can be compared to the observed counterparts ('object comparison'). The best match will determine which members from the ensemble will be used for the fusion with nowcast data (Köhler, 2012).

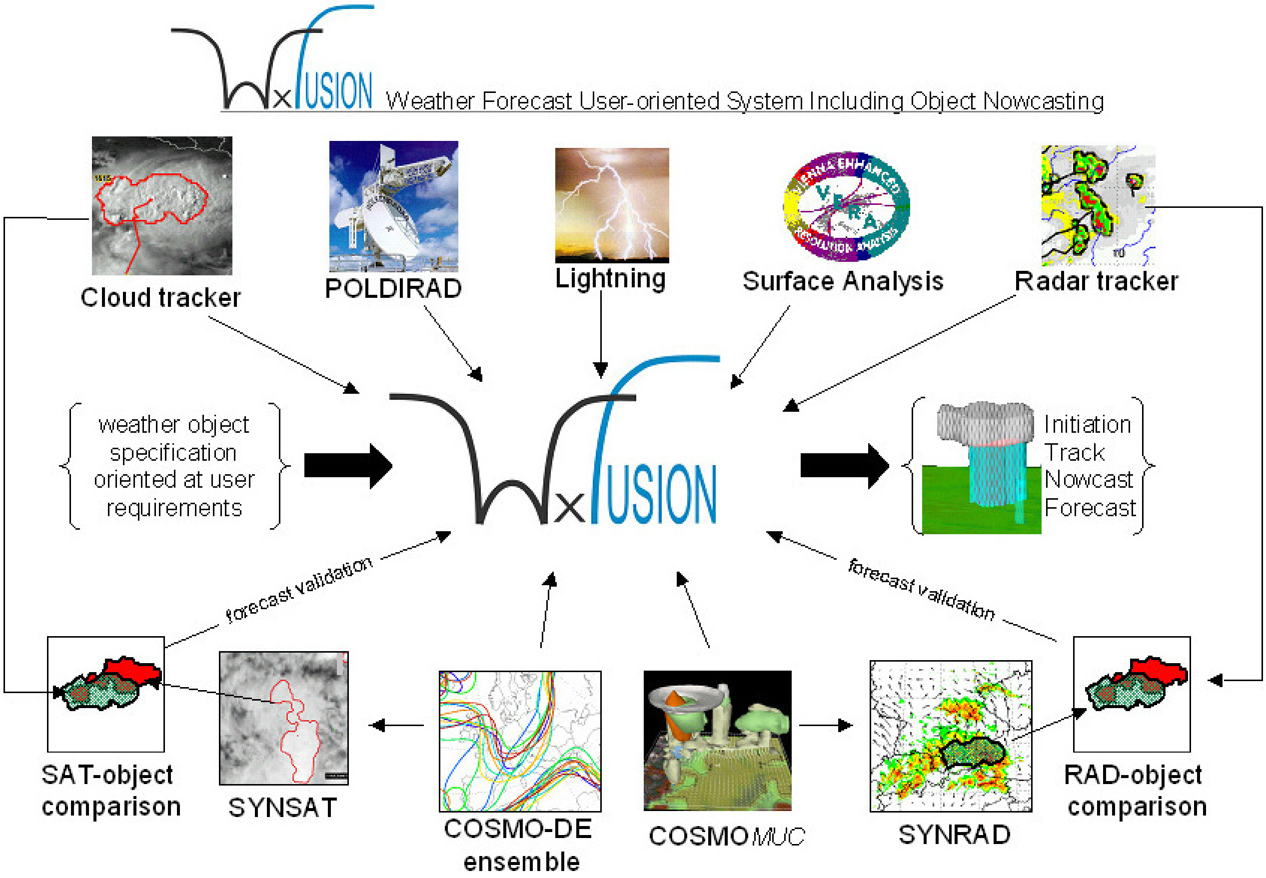

Figure 1. The concept of WxFUSION. The initiation, track, nowcast, and forecast of user specified weather objects are characterized by appropriate information through fusion of selected nowcast information (upper half) and forecast products (lower half) (adapted from Tafferner et al., 2008; Forster and Tafferner, 2009b).

Data Fusion to Get Simple Products

The central part comprises the fusion component. A weather object specification oriented at user requirements has to be provided as further input to WxFUSION. As already mentioned above, users of weather forecasts need this information in a form that can be used for decision making. Users do not want, and often do not have the background knowledge, to interpret a multitude of complex meteorological data. Instead, as noted above, users need this information in a reduced form, easy to understand, free of interpretation and tailored to their needs. Figure 2 makes this reduction of complexity visible. On the left side two photographs of two different thunderstorms are composited in order to make visible typical weather features in one image. In the upper part there is a fully developed cloud anvil typical of mature thunderstorms together with a new convective cloud developing in front of it. In the lower part the typical cloud wall in front indicates the forced ingest of moist air into the storm, in the rear heavy precipitation with corresponding downburst can be seen. Correspondingly, by use of Cb-TRAM which detects the upper part, and by use of Rad-TRAM which detects the bottom part, a composite thunderstorm object can be constructed as shown on the right hand side (see also Section 2.3). Also indicated is a surface object which shall describe the squall line generated from the thunderstorm outflow (Westermayer, 2012). Therefore, the information about the thunderstorm given to users is a top and a bottom part, each of which consisting of a polygon with bottom and top, and some descriptive parameters, as e.g. intensity, trend, rain rate, etc. which are deduced from other observation data.

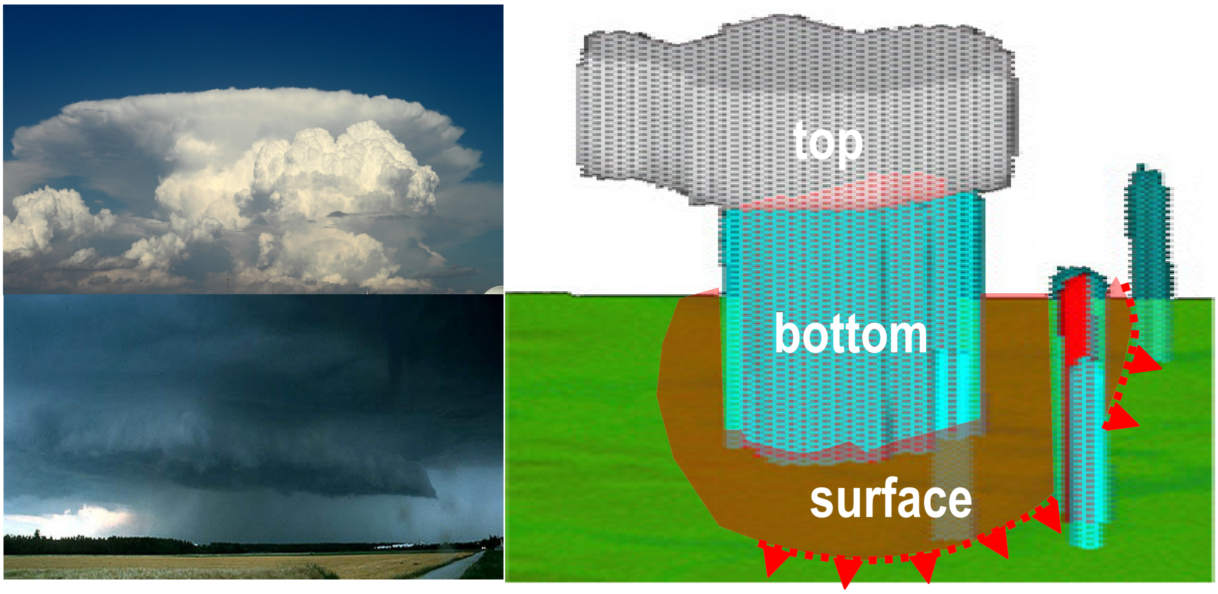

Figure 2: Real thunderstorm as seen by an observer (upper photograph by M. Köhler) and thunderstorm weather objects constructed from nowcasting tools. Explanation see text.

The heart of WxFUSION is the fusion module (centre of Figure 1). Its task is to retrieve from all available nowcast and forecast tools those data which are needed to calculate the required parameters of the weather object on output. E.g. a thunderstorm weather object on output (symbolized on the right in Figure 1) should contain information on initiation, actual state, nowcast up to one hour and forecast for later hours based on model forecasts.

The Fuzzy Logic Approach

The data fusion itself is undertaken employing fuzzy logic. The fuzzy logic procedure mimics the data analysis of an experienced forecaster. By evaluating and combining the outputs of nowcasting procedures and numerical prediction together with his knowledge about thunderstorm development (conceptual model) he composes a picture in his mind of what is going to happen. In contrast to decision trees which build on true/false branches when information contents are evaluated, fuzzy logic is a decision finding technique that allows a gradual transition between true and false, i.e. it deals with parameter ranges instead of fixed thresholds. Every contribution can be weighted with regard to its importance for the weather phenomenon by using so-called fuzzy functions. A final decision is then determined through an adequate combination of all weighted contributions. As an example let us consider the task to estimate the intensity of a thunderstorm. As contributing elements cloud top temperature, radar reflectivity and lightning density are chosen. Figures 3 and 4 show an example of the fuzzy logic evaluation. The influence (weight) of every data is taken into account by appropriately chosen fuzzy functions for low, middle or high membership grade. An observed value, e.g. a cloud top temperature of 228 K as shown by the dashed line in the top diagram (Figure 3), belongs with a membership grade of 0.8 to “cold” and with a grade of 0.2 to “middle”. The other parameters are evaluated similarly. After having collected and evaluated all possible data combinations a thunderstorm intensity value of 6.4 on a scale from 0 to 10 is found from the output fuzzy sets which are composed of 5 different thunderstorm intensity classes from very light to very strong (Figure 4).

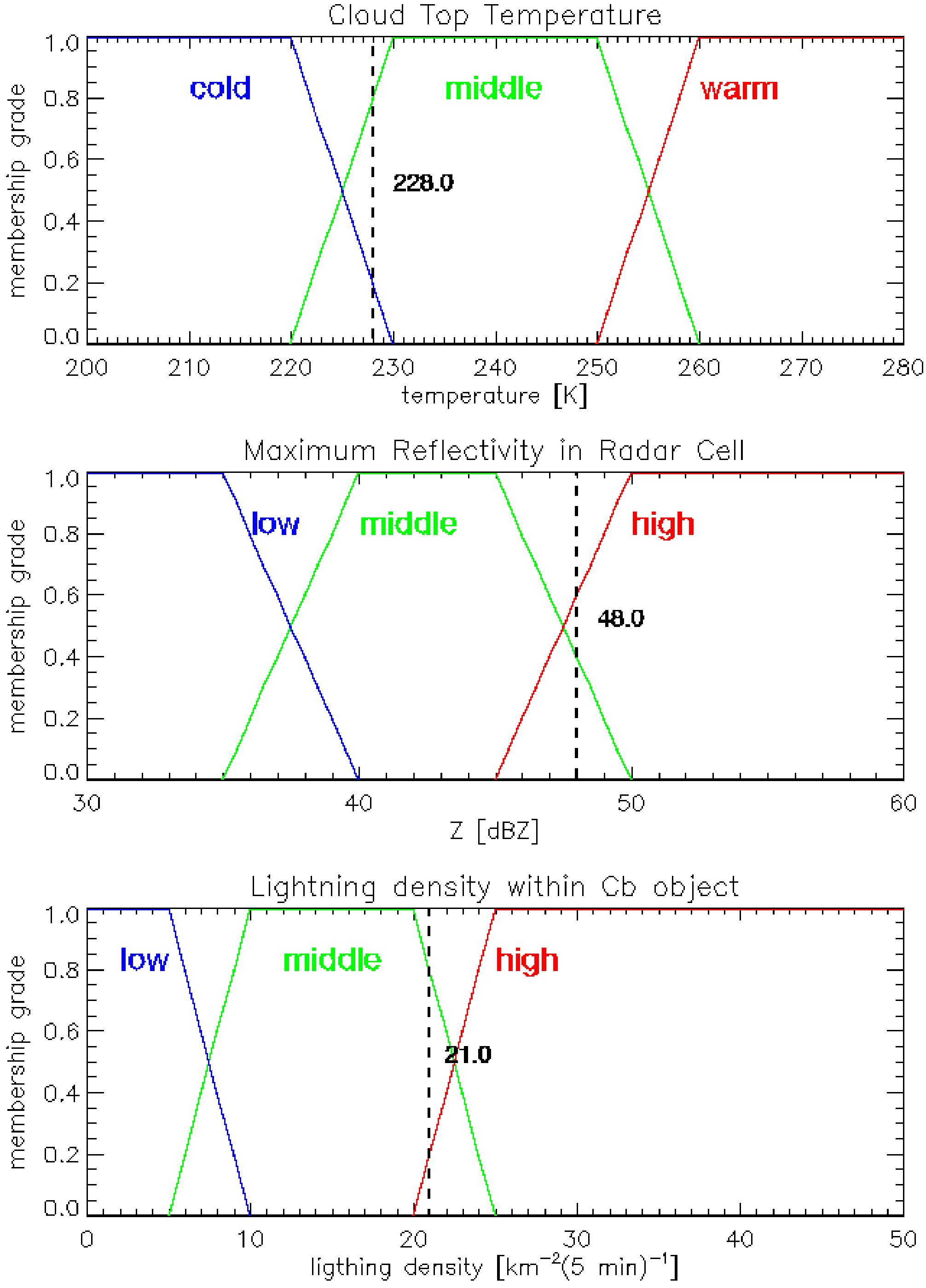

Figure 3. Fuzzy logic: input fuzzy sets with observed values of 228 K, 48 dBZ and 21 flashes km^{-2} (5 min)$^{-1}$ for cloud top temperature, radar reflectivity and lightning density; explanation see text.

The so calculated intensity is included as a descriptive parameter in the weather object together with output from the already mentioned nowcasting tools. Further detail, i.e. trend and lightning density will be included in the fuzzy logic procedure by taking into account the results of the research work of Bretl (2010) and Meyer (2010).

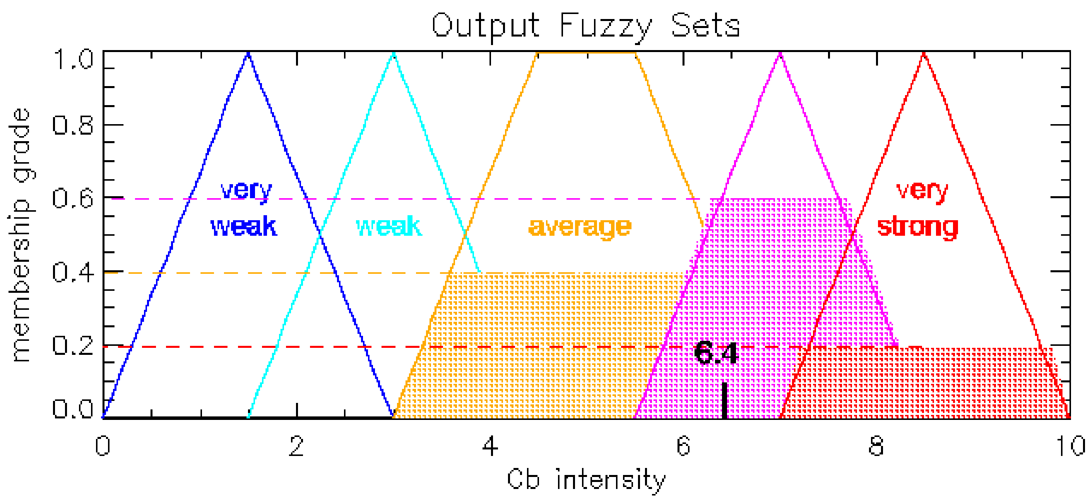

Figure 4. Fuzzy logic: Output fuzzy sets for 5 different thunderstorm intensity classes; explanation see text.

For the estimation of the future development only output from the nowcasting tools and numerical model output is available. It therefore makes sense to relax the detailed description of a weather phenomenon based on observation data to a more probabilistic estimate of how the event will evolve. This is rendered schematically in Figure 5. Whereas a 3-dimensional description of a thunderstorm is possible at analysis time together with small scale additional features, like e.g. the position of a gust front, after 30 minutes only the location of the thunderstorm is nowcast. Beyond one hour this is relaxed to a probability of occurrence.

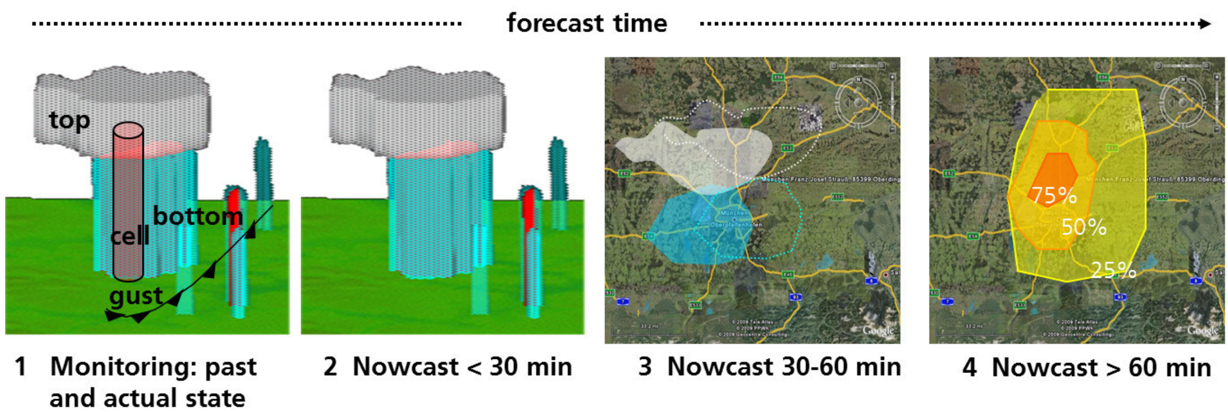

Figure 5: Nowcasting: decrease of descriptive detail over forecast time.

Considering the typical life time of thunderstorms, the uncertainties in numerical forecasting and the experience gained it would not make sense to forecast thunderstorms deterministically beyond one hour. Work is underway (Köhler, 2012) to combine output of nowcasting tools with numerical forecasts in order increase forecast accuracy. Thereby forecast evaluation plays an important role, first promising results have been achieved.

Graphical User Interface (GUI)

Figure 6 shows the graphical user interface of WxFUSION. Output data from the individual nowcasting tools, from the forecast models as well as fuzzy logic output, are ingested and processed. The GUI serves various purposes: an overlay of all data provides a synopsis of the weather event in one figure, it enables a quick evaluation of nowcasting quality, the best member out of the forecast ensemble is determined automatically, fuzzy logic procedures can be triggered by mouse over. In addition, the WxFUSION GUI can be run in real time as has been demonstrated already during the summer campaigns (see Section 2.3).

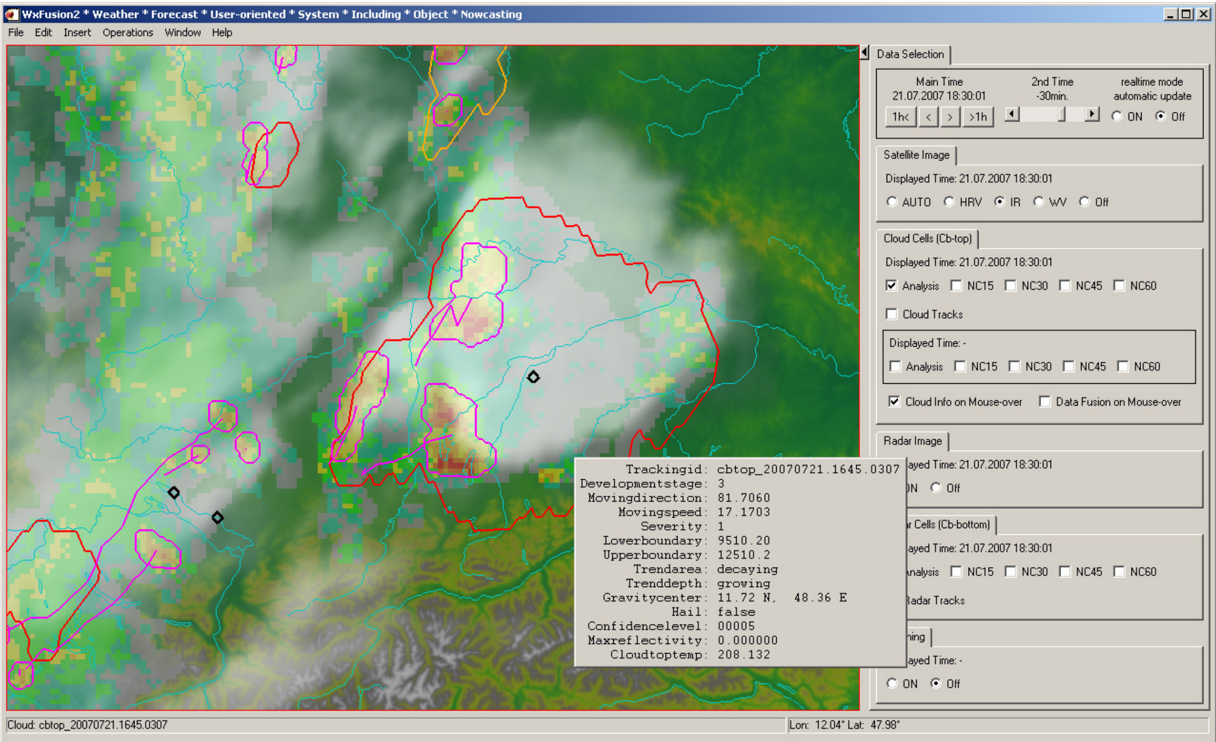

Figure 6: WxFUSION GUI: data overlay composed of satellite and radar image on geographic background together with Rad-TRAM (pink) and Cb-TRAM objects (red). Also shown tracks of cell centres and mouse over information on chosen weather object

Outlook

WxFUSION will further be developed, for both thunderstorm and wintry weather events, and finally demonstrated and validated in close cooperation with the decision makers at the ground and in the air. The aim is to bring the system to an international standard that makes it possible to apply the system European wide as a MET tool serving aviation needs in a Single European Sky. Once the LLWAS of DWD at the airports of Frankfurt and Munich is functioning, WxFUSION will also include these data into the fusion process and, eventualy, WxFUSION may become a part of DWD's Integrated Terminal Weather System (ITWS).

References

Baldauf, M., A. Seifert, J. Förstner, D. Majewski, M. Raschendorfer, T. Reinhardt, 2011: Operational Convective-Scale Numerical Weather Prediction with the COSMO Model: Description and Sensitivities. Mon. Wea. Rev., 139, 3887-3005.

Bretl, S., 2010: Untersuchung des Lebenszyklus von Gewittern in Mitteleuropa mit Hilfe von Fernerkundungs- und Modelldaten. Diplomarbeit. Ludwig-Maximilians-Universität München, März 2010

Dengler, K., J. Anger, C. Keil, 2011: Validation of Time-Lagged Ensemble Forecasts Relevant for Predicting Aircraft Wake Vortices. Meteorol. Z., 20, 625-634.

Evans J., Ducot E. 1994: The Integrated Terminal Weather System (ITWS), MIT Lincoln Laboratory Journal, Vol. 7, No. 2.

Forster, C., and A. Tafferner, 2009a: Nowcasting and forecasting thunderstorms for air traffic with an integrated forecast system based on observations and model data, WMO Symposium on Nowcasting, Whistler, B.C., Canada, 30 August - 4 September 2009.

Forster, C., and A. Tafferner, 2009b: An integrated user-oriented weather forecast system for air traffic using real-time observations and model data, Proceedings of the European Air and Space Conference (CEAS), Manchester, UK

Köhler, M., 2012: Kombination von Nowcast- und Forecastverfahren zur optimalen Kurzfrist-vorhersage von Gewittern bis zu einem Zeitraum von 6 Stunden. Doktorarbeit at IPA, in progress

Meyer, V., 2010: Thunderstorm Tracking and Monitoring on the Basis of Three Dimensional Lightning Data and Conventional and Polarimetric Radar Data. Dissertation, Ludwig-Maximilians-Universität München, Mai 2010

Mueller C., Saxen T., Roberts R., Wilson J., Betancourt T., Dettling S., Oien N., Yee J. 2003: NCAR Auto-Nowcast System, Weather and Forecasting Vol. 18, 545-561.

Tafferner, A., Hagen, M., Keil, C., Zinner, T. and Volkert, H., 2008, Development and propagation of severe thunderstorms in the upper Danube catchment area: Towards an integrated nowcasting and forecasting system using real-time data and high-resolution simulations, Meteorology and Atmospheric Physics, 101, 211-227, DOI 10.1007/s00703-008-0322-7.

Westermayer, A., 2012: Detektion und Verlagerung von Gewitter-Fallwinden und Böen aus POLDIRAD-, LLWAS- und COSMOairport –Daten. Masterarbeit at Institut für Physik der Atmosphäre, in progress

2.3 Nowcasting Thunderstorms for Munich Airport

Caroline Forster, Arnold Tafferner
Institute of Atmospheric Physics

The successful demonstration and assessment of the DLR thunderstorm nowcasting algorithms at Munich Airport during two campaigns in the summers of 2010 and 2011 are described. The algorithms Cb-TRAM and Rad-TRAM, that detect, monitor, and forecast up to one hour (nowcast) thunderstorm cells from satellite and radar data, run in real time and provided new thunderstorm products for users at the airport. The products were presented on displays the users were already familiar with as well as on webpages designed by DLR. On the webpages, also additional information like measurements with DLR's polarimetric radar and model forecasts was shown. Moreover, thunderstorm warnings were issued and sent via email to the users whenever a thunderstorm was detected in the terminal manoeuvring area of the airport of Munich. The nowcasting skills of Rad-TRAM and Cb-TRAM are encouraging, especially for lead times up to 30 minutes, and the user feedback on the DLR thunderstorm products was very positive. The Rad-TRAM and Cb-TRAM products provide a good overview on the situation and its future development, and the thunderstorm warnings were very helpful for the collaborative decision making at the airport. However, some suggestions for improvements were made like the demand for nowcasts beyond one hour. This will be considered within the integrated weather forecast system, WxFUSION, which has been further developed during the campaigns.

Introduction

Thunderstorms are related to hazardous phenomena like turbulence, icing, hail, heavy rain, lightning and reduced visibility that can lead to considerable obstructions in the air transport system. For instance, if a thunderstorm passes an airport, ground operations might have to be stopped and flights have to be re-routed in holding patterns or even diverted because of hazardous weather phenomena in the airport's terminal manoeuvring area (TMA). It is clear that delays and divertions at one airport lead to delays and divertions at other airports as well. According to Quon [2006], adverse weather is the primary reason for disruptions in the air transport system in the U.S. Over Europe, adverse weather is responsible for 40-50% of all delays [EUROCONTROL, 2007], and according to the German air navigation safety provider DFS (personal communication), more than 80% of the delays at Munich Airport (MUC), Germany, are due to weather with thunderstorms and fog as the primary reasons. These numbers indicate that there is a clear need for weather information systems that help all air space users to plan well in advance and enable the mitigation of the weather hazard's effects. If all decision makers in the air and at the ground have access to the same weather information systems, the collaborative decision making process can be accelerated considerably.

Many of the weather data and tools available to date have to be interpreted by the user before any action can be triggered. However, as air space users often have to make quick decisions especially during thunderstorm situations, they need simple and easy to read information which does not need any interpretation. Recently, the algorithms Cb-TRAM (Cumulonimbus Tracking and Monitoring) [Zinner et al., 2008; Zinner and Betz, 2009] and Rad-TRAM (Radar Tracking and Monitoring) [Kober and Tafferner, 2008] have been developed at DLR. They provide thunderstorm detections and forecasts up to one hour (nowcast) especially for aviation purposes. Hazardous areas for aircraft are represented by simple contours, see Section 5.2 for details. In addition, an integrated weather forecast system named WxFUSION (Weather Forecast User-Oriented System Including Object Nowcasting) [Forster and Tafferner, 2009b] is currently under development at DLR with the aim to combine different data from observations and numerical models in order to detect, nowcast (up to 6 hours), and forecast (beyond 6 hours) weather phenomena like thunderstorms as precisely as possible.

For the development of such algorithms and systems, feedback of the users is needed in order to optimise the output of the algorithms in terms of the user's requirements. Therefore, two summer campaigns have been initiated and performed at MUC airport during 2010 and 2011. One of the aims of these campaigns was the demonstration and test of the DLR nowcasting products at MUC in close cooperation with the German Meteorological Service (DWD) and users from DFS, the Lufthansa Hub Control Center (DLH-HCC), and the Munich Airport operations (FMG). This paper will present the results of these campaigns with regard to thunderstorm nowcasting and outline recent developments with regard to WxFUSION. Other activities during the campaigns like wake vortex forecasts and air traffic operational concepts will be described in other contributions of this report [Holzäpfel et al. 2011; Mollwitz and Korn, 2011]. In the following, we introduce the DLR nowcasting algorithms Cb-TRAM and Rad-TRAM; we describe the activities and specific goals of the two campaigns in more detail; we present an example of a typical thunderstorm situation at MUC and the products provided by DLR; then, the user feedback and the quantitative evaluation of the nowcasting products during the campaigns are discussed before we conclude our study and give an outlook.

The DLR Nowcasting Algorithms

Cb-TRAM

Cb-TRAM (Cumulonimbus Tracking and Monitoring) is a fully automated algorithm for the detection, tracking, and nowcasting of thunderstorms by using satellite data from METEOSAT SEVIRI (Spinning Enhanced Visible and Infra-Red Imager) [Zinner et al., 2008; Zinner and Betz; 2009]. The four different spectral channels high resolution visible (HRV), infra-red (IR) 10.8µm, IR 12.0µm, and water vapour (WV) 6.2µm are combined in order to identify three different stages of thunderstorm development: (1) convection initiation, (2) rapid vertical development, and (3) mature stage (Figure 1). Note that Cb-TRAM is able to detect the most active parts within huge cloud systems. Over Europe, METEOSAT data have a spatial resolution of about 5x5 km² and are available either every 15th minute (METEOSAT-9 normal scan) or every 5th minute (METEOSAT-8 rapid scan). The tracking in Cb-TRAM is based on the geographical overlap between current detections and first-guess patterns of cells detected in preceding time steps. At a time, the first-guess patterns are retrieved by using the approximate propagation direction and velocity of a detected cloud pattern during the previous 30 minutes in combination with an image-matching algorithm [cf. Zinner et al., 2008]. This algorithm extracts the general transformation vector field from several consecutive satellite images, thereby describing the cloud motion and local cloud developments. Similar to the first-guess patterns, nowcasting intervals from 5 to 60 minutes are generated by extrapolation and exploitation of the pyramidal image-matching algorithm. Additional details as well as application and validation studies of Cb-TRAM were provided by Zinner and Betz [2009], Tafferner et al. [2008], Forster et al. [2008], Dotzek and Forster [2010], and Zinner et al. [2011].

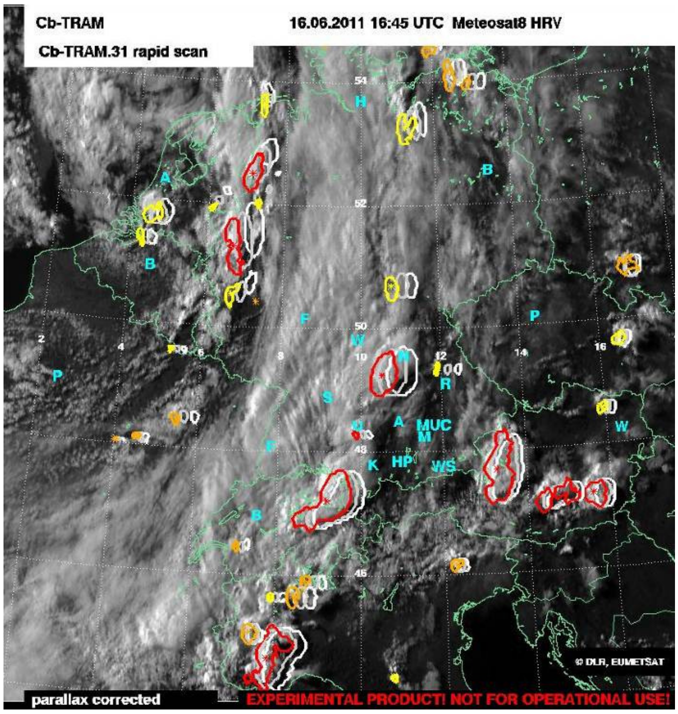

Figure 1. HRV image from METEOSAT-8 over middle Europe with Cb-TRAM objects as polygons; yellow, orange, and red indicate detected development stages 1, 2, 3. Grey and white contours indicate the 15 and 30 minutes nowcasts.

Rad-TRAM

Rad-TRAM (Radar Tracking and Monitoring) is a detection, tracking, and nowcasting algorithm for heavy precipitation cells by using weather radar data [Kober and Tafferner, 2008]. A reflectivity threshold of 37dBz is used in order to identify hazardous precipitation areas for air traffic (Figure 2). This threshold has been chosen, as precipitation with reflectivity ≥ 37dBz often corresponds to lightning activity within the most active parts of thunderstorms. In addition, experience has shown that pilots often avoid flying through precipitation with reflectivity ≥ 37dBz. During the summer campaign 2010, Rad-TRAM was based on the European radar composite (PM product) provided by the DWD. It has a spatial resolution of 2km x 2km and a temporal resolution of 15 minutes. For the summer campaign 2011, Rad-TRAM was set up on a new DWD product, the EURADCOM composite which covers Central Europe with a spatial resolution of 1km x 1km and a temporal resolution of 5 minutes. The EURADCOM product has been especially developed for aviation purposes in the Functional Air Space Block European Central (FABEC). Rad-TRAM's tracking and nowcasting is based on the same principle as in Cb-TRAM. For more details on Rad-TRAM applications see Kober and Tafferner [2008] and for details on the tracking and nowcasting technique see Zinner et al. [2008].

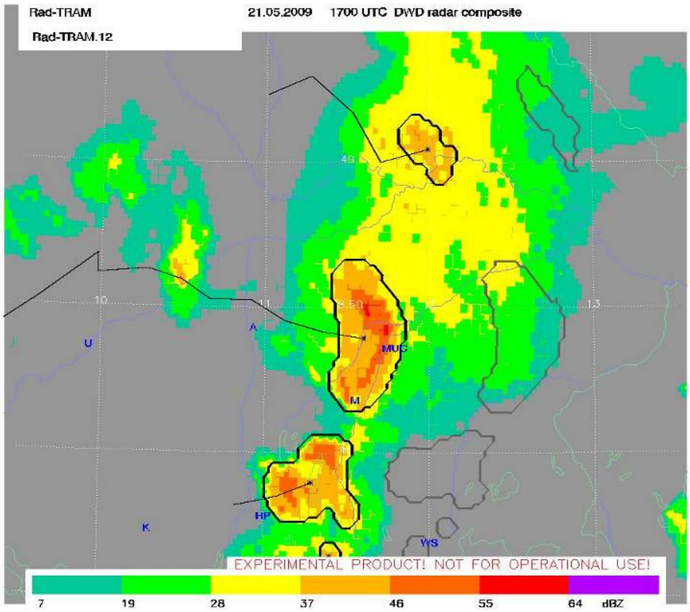

Figure 2. DWD weather radar composite (colored shading) over TMA MUC with detected Rad-TRAM Cb cells (black polygons); grey polygons indicate 60 minutes nowcast; black lines are the tracks of the objects.

The Summer Campaign 2010

During 2010, the campaign was performed within the Wetter & Fliegen project. It took place from 1 June until 15 August 2010. The focus of this first campaign was the demonstration of the products to the users who should test them and give feedback on their benefits and disadvantages. The DWD provided input data for the DLR nowcasting tools as well as other observational and forecast data and acted as an observer of the activities during the campaign. In case of a positive user feedback with regard to the DLR nowcasting tools, the DWD considers to implement Cb-TRAM and Rad-TRAM in its operational service.

Cb-TRAM and Rad-TRAM products were provided in real time directly from DLR to the DFS Center at MUC, the DFS Tower MUC, the DLH_HCC, and the FMG. They were presented on a website from DLR (http://www.pa.op.dlr.de/nowcasting/) which was updated whenever a new Cb-TRAM or Rad-TRAM product was available. During 2010, the refresh rate was 15 minutes. Both Cb-TRAM and Rad-TRAM were displayed also in real time in the Weather Image Information System (WIIS) by the company WIIS GmbH. WIIS was already well-established at LH HCC, FMG, and DFS Center MUC, i.e. the users could test the DLR products in displays they were familiar with. Feedback of the users was collected via e-mail and via a questionnaire.

In addition to the nowcasting tools, also products from the DLR polarimetric Doppler radar POLDIRAD were provided to the users. POLDIRAD is a C-Band radar with polarisation agility for transmitting, dual-channel receiving, and Doppler capability. It was operated during thunderstorm situations only, but provided the advantage that vertical scans through specific thunderstorm clouds could be performed manually if necessary and that hydrometeors could be distinguished due to the polarisation capability. These skills were very helpful to estimate the echo top of a thunderstorm and the location of hail within the cloud. If operated, POLDIRAD can provide its products in 10 minutes intervals. They were available for the users on a website (http://www.pa.op.dlr.de/poldirad/).

From the DWD COSMO-DE model, parameters important for take-off and landing procedures as well as for airport operations like wind, total precipitation, and temperature were extracted and graphically prepared for the TMA MUC (COSMO-MUC). The COSMO-MUC forecasts were updated every hour and products were displayed in 15 minutes intervals at http://www.pa.op.dlr.de/MUCSOMMER2010/.

In order to draw the attention of the users to our products during thunderstorm situations, thunderstorm warnings were issued by DLR via e-mail to all users involved in the campaign whenever thunderstorms were detected and forecast in the TMA MUC. The warnings were simple and short text messages describing the situation and giving an overview of the situation by an attached image displaying Cb-TRAM and/or Rad-TRAM output. As these warnings were issued by hand, it was necessary to permanently monitor the weather and especially the thunderstorm situation. For this, not only the nowcasting tools Cb-TRAM and Rad-TRAM, but also other weather information and tools from the DWD within in the Ninjo Workstation were used.

LH HCC offered DLR a working place in the HCC area during the whole campaign period, i.e. whenever there was a thunderstorm situation, DLR staff had the possibility to be directly in contact with the people responsible for operations at the airport and with air traffic controllers. For instance, the director of operations at the LH HCC could explain his work and its dependence on the current weather situation, while DLR staff could in turn explain the thunderstorm products and how they can be used at LH HCC. Within the course of the campaign it turned out that these conversations and discussions were very valuable for both sides. The DLR staff learned much about the chain of operations at the airport and the related needs with regard to thunderstorm information, while the users learned about modern weather information and how it can facilitate their work.

For a later evaluation of the campaign, it was necessary to collect information and establish a documentation of all thunderstorm days during the campaign period. This has been done on a campaign website, where different links to the documentation and the products offered by DLR are available (http://www.pa.op.dlr.de/MUCSOMMER2010/).

Finally, the integrated weather information system WxFUSION has been tested and further developed during the campaign period. As the system is still under development, the WxFUSION products have not yet been presented to the users at the airport, but have been tested internally.

The Summer Campaign 2011

As the summer campaign in 2010 was successful and resulted in a very positive user feedback (see below), the DFS requested a repetition of the campaign in 2011 with slightly different and additional activities described below. Since a second summer campaign could not be supported within Wetter & Fliegen, the DFS was prepared to sponsor the summer campaign 2011 within the LuFo IV project iPort. The campaign took place from 1 June until 30 September 2011. Its focus was again the demonstration of the nowcasting products and their test by the users (this time users at DFS only) as well as the collection of further and more detailed user feedback.

This time, Cb-TRAM and Rad-TRAM were test-wise installed and running at the DWD, i.e. Cb-TRAM and Rad-TRAM output was directly provided in real time to the users by the official weather data supplier for aviation in Germany. This is an important step towards an implementation of the DLR algorithms in the operational service by the DWD. It could be shown that the installation of the algorithms in the environment at DWD is not complicated, and that the algorithms were running stable over the whole campaign period. In addition, Cb-TRAM and Rad-TRAM output could easily be included in the Ninjo test version and was tested by the DWD at MUC.

The Rad-TRAM and Cb-TRAM output data were provided every 5th minute and were collected and stored by the DFS during the whole campaign period. They are used for evaluation purposes and for the test-wise integration in DFS displays like MetFROG and PHOENIX, a special weather information display for air traffic controllers and the controller display in the tower, respectively. Rad-TRAM could already be demonstrated in real time in the MetFROG test display during summer 2011. It was tested at several places within the DFS, e.g. Tower MUC, Tower Köln/Bonn, Tower Düsseldorf, and Center Operation Support. So far, detailed feedback has been received from the Tower MUC (see below).

Similar to the campaign in 2010, the DLR products were also displayed on the DLR nowcasting site (http://www.pa.op.dlr.de/nowcasting/), a documentation of all thunderstorm days has been established (http://www.pa.op.dlr.de/MUCSOMMER2011/), and DLH-HCC kindly offered the working place in the HCC again. As the thunderstorm warnings turned out to be very helpful, they have been issued again on demand of the DFS Tower MUC. In addition, new POLDIRAD products were presented to the users on a website (http://www.pa.op.dlr.de/poldirad/rainbow.html). This includes vertical cross sections through thunderstorm cells along the glide path at MUC as well as Doppler velocities and vertical wind profiles.

Finally, the Bayerische Rundfunk (BR) prepared a documentary about clouds for the series “Faszination Wissen” in which thunderstorm clouds and aviation were one of the key topics. A BR team visited DLR on 19 July 2011 in order to document the DLR activities for the nowcasting of thunderstorms for aviation. Fortunately, this day was a thunderstorm day at MUC airport, and the DLR team could demonstrate the skills of their nowcasting tools to the film team in real time. The shooting was done both at the working place in the DLH HCC at MUC and in the office of the DLR team at Oberpfaffenhofen. The documentary has been shown on the Bavarian TV on 6th of November 2011.

An Example Case: The 19th of July 2011

As an example of how the DLR nowcasting products were presented to the users, the thunderstorm case on 19th July 2011, when a BR team filmed at DLR, will be shown here. Ahead of a low pressure system, warm and humid air masses were advected to Bavaria. At 16:15 UTC, the vortex of the low pressure system over France can clearly be seen in the HRV satellite image with Cb-TRAM contours superimposed (Figure 3a). Convection initiation (yellow contours) is detected near the center of the low pressure system, and a mature thunderstorm (red contour) has already developed between Kempten and Hohenpeissenberg (marked by K and HP). It is predicted to move in a north-easterly direction (grey and white contours in Figure 3a and b) and is related to lightning activity, heavy precipitation, hail (reflectivity >55dBZ, Figure 3b). A first thunderstorm warning was sent to the users at this time with Figure3b as attachment. The thunderstorm intensified and slowly moved towards MUC. At around 16:30 UTC, POLDIRAD scans show echo tops at 10 to 12 km height within the cell (Figure 4a), and the vertical structure with the overhanging strong reflectivity indicates strong dynamical development within the cell (Figure 4b). At 18:15 UTC the thunderstorm had crossed the river Lech and reached lake Ammersee (Figure 3c). A second warning was sent to the users at this time with Figure 3c attached. Finally, the thunderstorm reached MUC at 19:45 UTC (Figure 3d).

On this day, the DLR team was present at the working place at LH HCC and could show and discuss the DLR products with the director of operations at LH HCC who asked from time to time for an update of the situation during the afternoon. It was especially important for him to know when the thunderstorm will hit MUC. At 19:30 UTC there was a peak in departing long distance flights scheduled, and LH’s interest was the departure of these flights before the thunderstorm arrived at MUC. If necessary, LH would try to accelerate the dispatch of these flights in order to avoid that they were stuck on the ground because of lightning and heavy precipitation over MUC. The DLR nowcasting products finally predicted about one hour in advance that the thunderstorm will likely hit MUC after 19:30 UTC. This information was very helpful for the dispatch at LH HCC. Unfortunately, it was not possible to talk to users from the FMG or DFS on this day, as they were under pressure because of the thunderstorm situation. However, feedback on the DLR nowcasting products from DFS and FMG was given at a later time and is presented in the following.

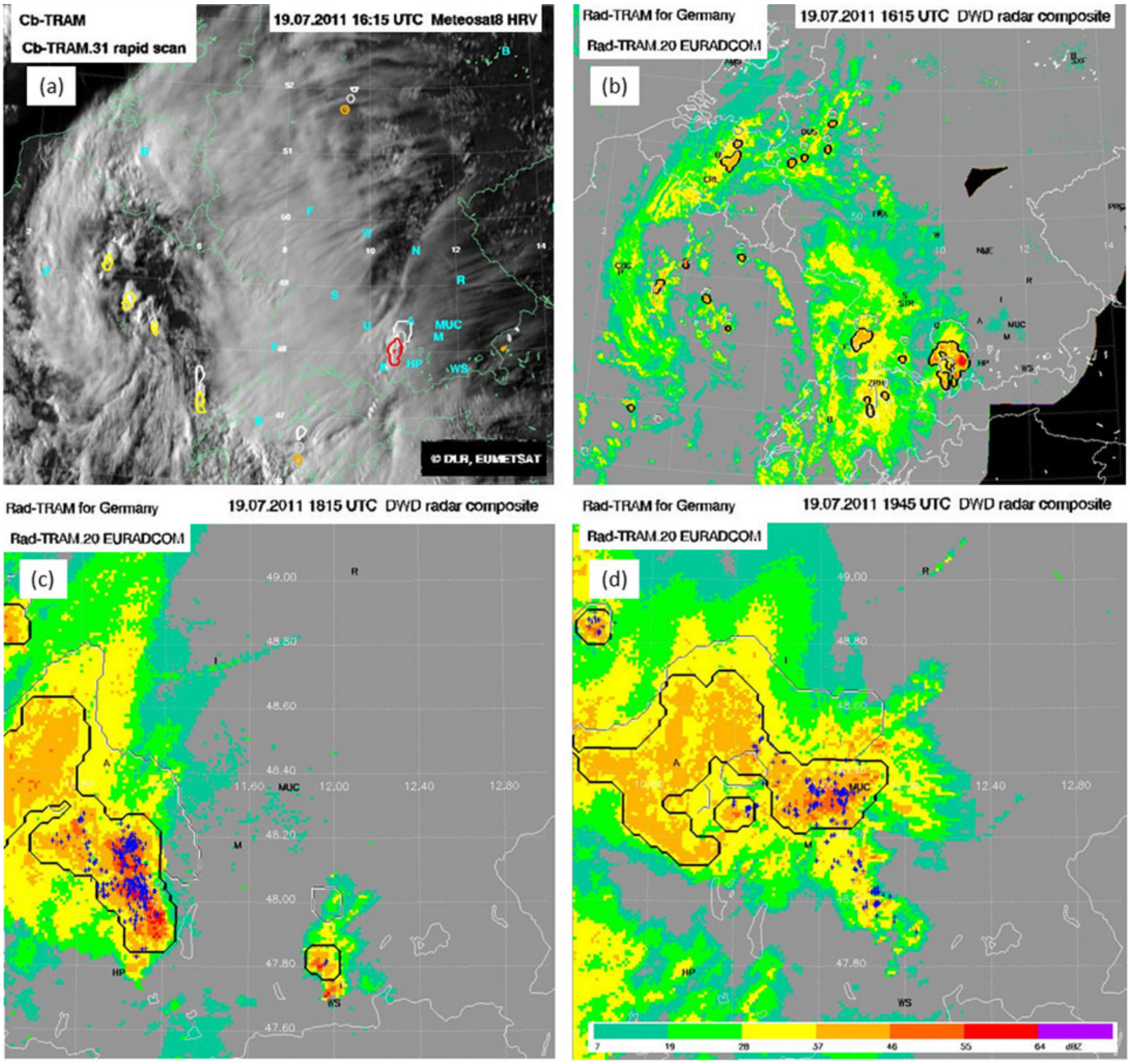

Figure 3. Thunderstorm situation on 19 July 2011. (a) METEOSAT-8 HRV image at 16:15 UTC with Cb-TRAM contours; yellow, orange, and red contours indicate the detected development stages 1, 2, 3. (b) EURADCOM radar composite with black Rad-TRAM contours at 16:15 UTC. (c, d) As (b), but for the TMA MUC at 18:15 UTC (c) and 19:45 UTC (d). The grey and white polygons in (a) and (b) are the 30 and 60 minutes nowcasts. The thin black contours in (c) and (d) are the 60 minutes nowcasts. Blue crosses in (c) and (d) represent lightning detections from the LINET system (Betz et al., 2008).

Users' Feedback

Feedback of the users on the benefits and disadvantages of new weather information products is very important for the development of these products. Based on user feedback the user's requirements can be accounted for in the output and in the presentation of the products. In addition, it can be assessed whether the application of new weather information tools help improving coordination through common situational awareness of the convective weather impacts among all affected users. For instance, in the U.S., MIT Lincoln assessed the user feedback with regard to innovative integrated terminal weather systems [Robinson et al., 2006, 2008]. They got co-ordinated feedback from traffic managers and area supervisors on convective weather impact mitigation decisions made using the new systems, on the time to monitor existing convective weather impact mitigation initiatives, and on the time associated with the mitigation plan development and execution process in relation to expected workload for similar convective events prior to the new systems [Robinson et al., 2006]. Important results of this assessment were that it took less time for the users to develop and implement operationally effective plans and that the number of such plans implemented per convective weather day significantly increased.

During the summer campaigns 2010 and 2011 at MUC, the user feedback on Cb-TRAM and Rad-TRAM was obtained via informal e-mails, personal conversations, and a questionnaire with the questions:

1. Are the thunderstorm forecasts correct (e.g. extrapolated cells, moving direction) ?
2. Is the way of displaying the products appropriate? (e.g. clear, readable, free of interpretation) ?
3. Is the thunderstorm product helpful? (e.g. for the planning and for the co-ordination of the operations) ?

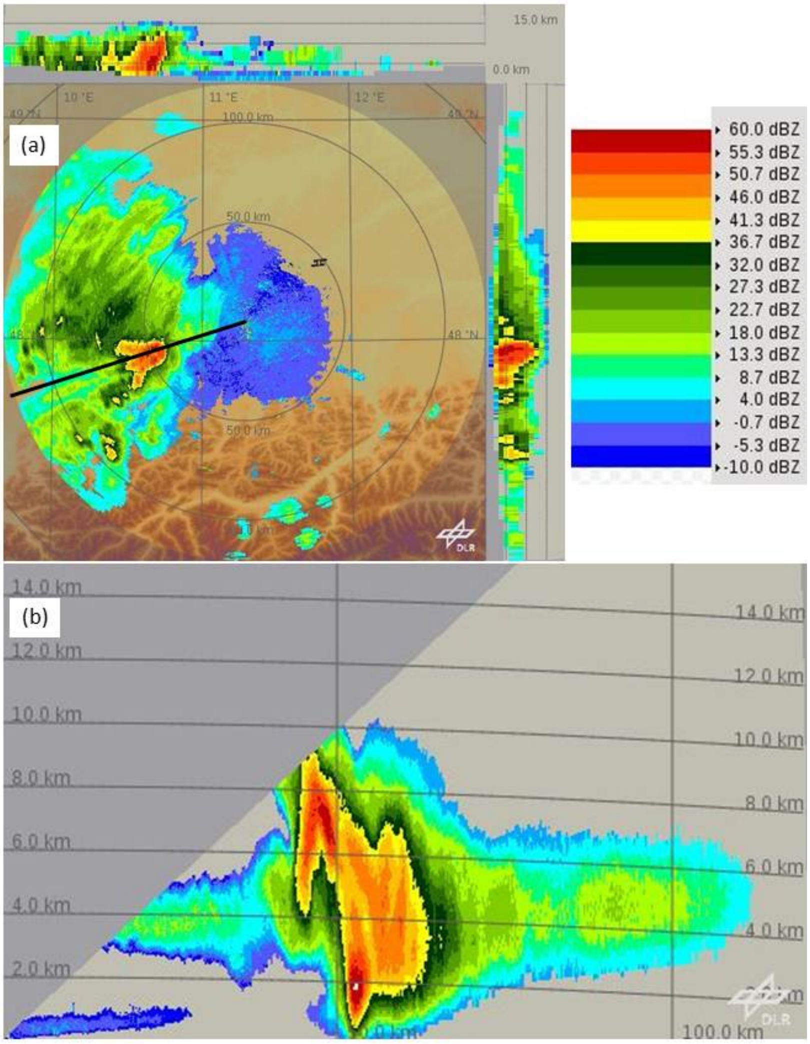

Figure 4. POLDIRAD measurements on 19 July 2011. (a) Maximum reflectivity scan at 16:31 UTC. POLDIRAD is located in the center of the image. The circles indicate the radii of 50km and 100km around POLDIRAD. MUC is indicated by a black symbol on the 50km radius north-east of POLDIRAD. (b) Reflectivity for a vertical cross section (black line in (a)) at 16:27 UTC through the thunderstorm cell at 249° azimuth.

In total 8 questionnaires were filled in and 18 e-mails were obtained from about 20 persons involved in the campaigns. Including the numerous comments and suggestions from personal conversations with supervisors at DFS Tower and Center MUC, directors of operations at LH HCC, and traffic managers from FMG, the evaluation of the questionnaires and e-mails resulted in a very positive feedback. Most of the users found the depiction of the products clear and intuitive. They appreciated the simple display of hazardous areas for air traffic as contours and the indication of the future development and moving direction. The 5 minutes updates of the products in 2011 were considered as much better than the 15 minutes updates in the year before. With the 5 minutes updates rapidly changing situations could easier and earlier be assessed. The nowcasting up to one hour was found to be accurate enough to enable a reasonable planning, e.g. the deployment of additional staff or the ordering of overtime, and it was useful to estimate how long the airport will be affected by a thunderstorm. The DFS appreciated the display and availability of data also from neighbouring countries. Thunderstorms moving towards Germany could then be recognized early and actions could be triggered with less time pressure. In general, the nowcasting products turned out to be very helpful for the planning.

However, in some cases it became clear that different users have different requirements with respect to weather information. For example on 24 August 2010 at 14:15 UTC, the 60 minutes nowcast predicted that a thunderstorm cell will directly affect MUC. One hour later, however, the cell passed just south of the airport. For the airport operations FMG, this was a wrong forecast, because the cell missed the airport and the operations on the movement area did not have to be shut down. In contrast, the DFS Tower MUC was satisfied with the forecast. Although MUC was not directly hit by the thunderstorm, there were severe obstructions in the approach, and with the help of the nowcast, the DFS could plan accordingly.

Another issue were heavy precipitation cells in Rad-TRAM close to the threshold of 37dBZ. Such cells appear and disappear from time step to time step, as their maximum reflectivity alternates between above and below the threshold. This is very confusing for the user, especially in cases when the cell clearly shows lightning activity also at time steps where it was not detected by Rad-TRAM. From these cases it is evident that a combination of different data sources (e.g. lightning and Rad-TRAM information) could guarantee a more continuous tracking of thunderstorm cells. The fusion of different data sources will be considered in WxFUSION (see below).

The DFS suggested some improvements with respect to the weather information and its presentation to the users. For instance, an indication of the height of a thunderstorm cell on the display would be very helpful in order to assess how many of the upper air sectors are affected by the cell. In addition, forecasts up to two hours would be of great advantage, as this is the timeframe for actions with regard to coordination at the central flow management unit (CFMU) in Brussels. Moreover, it would be a great advantage to have available and displayed all the innovative weather information products demonstrated during the summer campaigns in one visualization system only. At DFS, this would preferably be Met-FROG.

Finally, it turned out that the thunderstorm warnings were very useful for the collaborative decision making at the airport. During 2010, they were issued by DLR just to draw the attention of the users to the DLR products. However, as all users obtained the same warning at the same time, they all had the same situational awareness and could make decisions and trigger actions within a much shorter time period than without the warnings. Therefore, the thunderstorm warnings were also issued in 2011 on demand of the DFS. Currently, an automation of the thunderstorm warnings is discussed.

Quantitative Evaluation of the Nowcasting Products

Several evaluations of Rad-TRAM and Cb-TRAM have been performed and are still in progress based on the data collected during the summer campaigns. An economic assessment has been performed and is described by Lau [2011] within this report and by Lau et al. [2011]. These studies investigate delay data at MUC, and determine the potential for a delay reduction, if weather information from Rad-TRAM is used for the pre-tactical planning of flights. In a complementary study, the DFS plans to estimate the potential for a delay reduction, if Rad-TRAM is used by the air traffic controllers for tactical regulations. It is envisaged to perform real time simulations with controllers to assess their actions with and without the Rad-TRAM information.

In order to assess the detection and nowcasting quality of the DLR algorithms two different methods have been applied. The first method compares the nowcasting of Cb-TRAM and Rad-TRAM for different lead times with the detection in Cb-TRAM and Rad-TRAM, respectively. The second method compares the detection and nowcasting of Cb-TRAM or Rad-TRAM with the observation by an independent data source. While the first method assesses the nowcasting quality only, the second method also assesses the ability of the algorithm to detect thunderstorms at the correct location.

Comparison of Nowcast with Observation

In case of the first method, we distinguish a pixel-based from an object-based analysis, see Figure 5. The pixel-based analysis checks how many pixels of an observed Rad-TRAM (Cb-TRAM) object overlap with pixels of a Rad-TRAM (Cb-TRAM) nowcast. These are counted as hits (Figure 5a). The pixels of an observed object that do not overlap with a nowcast one are regarded as misses, and the pixels of a nowcast object that do not overlap with an observed one are regarded as false alarms. Skill scores like the probability of detection (POD) with POD=hits/(hits+misses) and the false alarm ratio (FAR) with FAR=false alarms/(hits+false alarms) are calculated and interpreted. The perfect nowcast would have a POD = 1 and a FAR = 0. Figure 6 shows the results of the POD and FAR for the pixel-based analysis of Rad-TRAM nowcasts over the whole summer period 2011 (39 thunderstorm days). As expected the POD decreases, and the FAR increases with nowcast lead time. The mean POD value over all days is 0.65 for the 15 minutes nowcast and declines to 0.27 for the 60 minutes nowcast with standard deviations between 0.06 and 0.03, respectively (Table 1). The mean FAR over all days increases from 0.36 for the 15 minutes nowcast to 0.73 for the 60 minutes nowcast with standard deviations between 0.03 and 0.06, respectively. These numbers are quite encouraging keeping in mind that the pixel-based analysis requires an exact match of observation and nowcast.

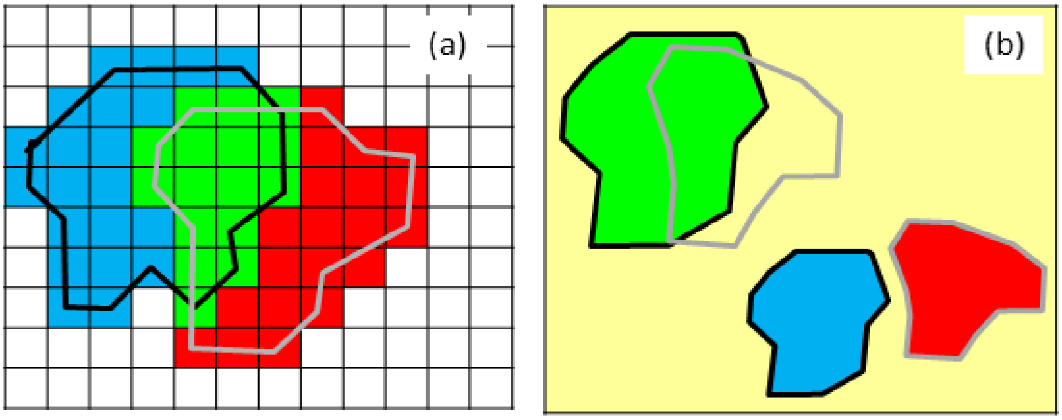

Figure 5. Observed (black) and nowcast (grey) objects. (a) Pixel-based analysis: the pixels covered by the observed and nowcast objects are counted. (b) Object-based analysis: the observed and nowcast objects are counted. Green are the hits, blue the misses and red the false alarms.

Table 1: Mean values of POD and FAR and the respective standard deviations (STD) for all thunderstorm days in 2011 for the 15, 30, 45, and 60 minutes nowcasts.

	15 min.	**30 min.**	**45 min.**	**60 min.**
POD / FAR	0.65 / 0.36	0.47 / 0.53	0.34 / 0.65	0.27 / 0.73
POD STD / FAR STD	0.06 / 0.03	0.04 / 0.05	0.03 / 0.05	0.03 / 0.06

The object-based method, however, requires just an overlap between observed and nowcast object (Figure 5b). Overlapping observed and nowcast objects are counted as hits, non-overlapping observed objects are counted as misses, and non-overlapping nowcast objects are counted as false alarms. In Figure 7 POD and FAR for the object-based analysis are shown. As only an overlap between observed and nowcast objects is required, the skill is better than for the pixel-based analysis. The mean values of the POD vary between 0.74 for the 15 minutes nowcast and 0.48 for the 60 minutes nowcast with standard deviations between 0.06 and 0.04, respectively (Table 2). FAR increases from 0.25 for the 15 minutes nowcast to 0.52 for the 60 minutes nowcast with standard deviations between 0.02 and 0.04.

Table 2: Same as Table 1, but for the object-based analysis.

	15 min.	**30 min.**	**45 min.**	**60 min.**
POD / FAR	0.74 / 0.25	0.65 / 0.35	0.56 /0.43	0.48 / 0.52
POD STD / FAR STD	0.06 / 0.02	0.05 / 0.03	0.05 / 0.04	0.04 / 0.04

An issue with the presented pixel- and object-based analyses is the fact that observed objects that appear for the first time are not nowcast and counted as misses, because Rad-TRAM cannot predict the formation of a new heavy precipitation cell. Therefore, the object-based evaluation has been repeated for only those objects that also have a nowcast. This evaluation can be considered as the best case scenario, as the weakest criterions for obtaining a hit (overlap only) and filtering misses (only objects are considered that have a nowcast) are applied for the evaluation. The main results are summarized in Table 3. From the evaluations presented here, it can be concluded that the nowcasting performance of Rad-TRAM is somewhere between the pixel-based analysis and the best case scenario. The nowcasting for lead times greater than 30 minutes has to be considered with care because of the low POD and high FAR.

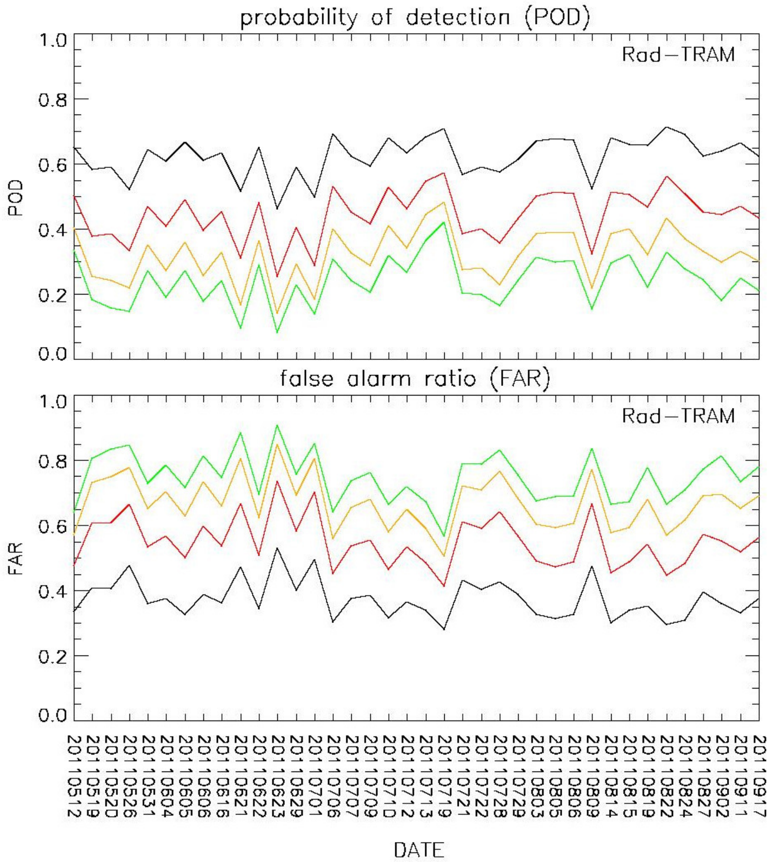

Figure 6. POD and FAR for the pixel-based analysis for all thunderstorm days in 2011. The black, red, yellow and green curves indicate the daily mean values for the 15, 30, 45, and 60 minutes nowcast

Table 3: Same as Table 2, but only for objects that also have a nowcast.

	15 min.	30 min.	45 min.	60 min.
POD / FAR	0.98 / 0.01	0.95 / 0.03	0.89 / 0.09	0.75 / 0.23
POD STD / FAR STD	0.06 / 0.004	0.06 / 0.007	0.06 / 0.01	0.05 / 0.03

One disadvantage of the presented evaluation is the fact that it is biased towards large objects. It is evident that an overlap of the nowcast and the observation of large objects is more likely than for small objects. In addition, it can happen that an observation overlaps with two different nowcast objects which have different sizes and cell centers than the observed one. The overlaps are counted as hits, although from an eyeball inspection the observed object does not match very well with the nowcast objects. In order to get a feeling on the ability of Rad-TRAM to nowcast the correct size of the objects as well as the correct location of their cell centers, further skill scores have to be evaluated like the location error of the cell centres and the area bias of the cells. Work is currently in progress to calculate such skill scores and perform additional analyses for the thunderstorm days in 2011. Similarly, work on the pixel-based and object-based analysis as well as the calculation of location errors and area bias for Cb-TRAM nowcasts is currently in progress.

Comparison with an Independent Data Source

In contrast to precipitation, lightning activity is an exclusive feature to thunderstorms. Therefore, lightning data from the LINET network [Betz et al., 2008] has been the data source of choice for the comparison with Cb-TRAM detections and nowcasts [Zinner et al., 2011]. Only Cb-TRAM cells of the mature stage have been considered here, as the other two development stages in Cb-TRAM are early warning stages and therefore not necessarily connected to lightning activity. The lightning data were clustered to lightning objects, and the overlap between Cb-TRAM detected and nowcast cells with lightning objects is determined by both a pixel-based and an object-based analysis as illustrated in Figure 5. This time, the grey contours in Figure 5 are the lightning objects, and the black contours represent either Cb-TRAM detections or nowcasts. As example, results of the object-based analysis show that for the Cb-TRAM detections the POD is around 61% and the FAR is around 29%, if an overlap of at least one pixel is required. The POD decreases to 33.4% and the FAR increases to 60.8% for the 60 minutes nowcast. These numbers are encouraging keeping in mind that some of the lightning cells are counted as misses, as they are related to another Cb-TRAM detection of stage. Sensitivity studies including all Cb-TRAM detection stages confirmed this. However, the FAR got worse because many of the Cb-TRAM stage one and two cells do not contain lightning and are counted as false alarms. Further details and results can be found in Zinner et al. [2011].

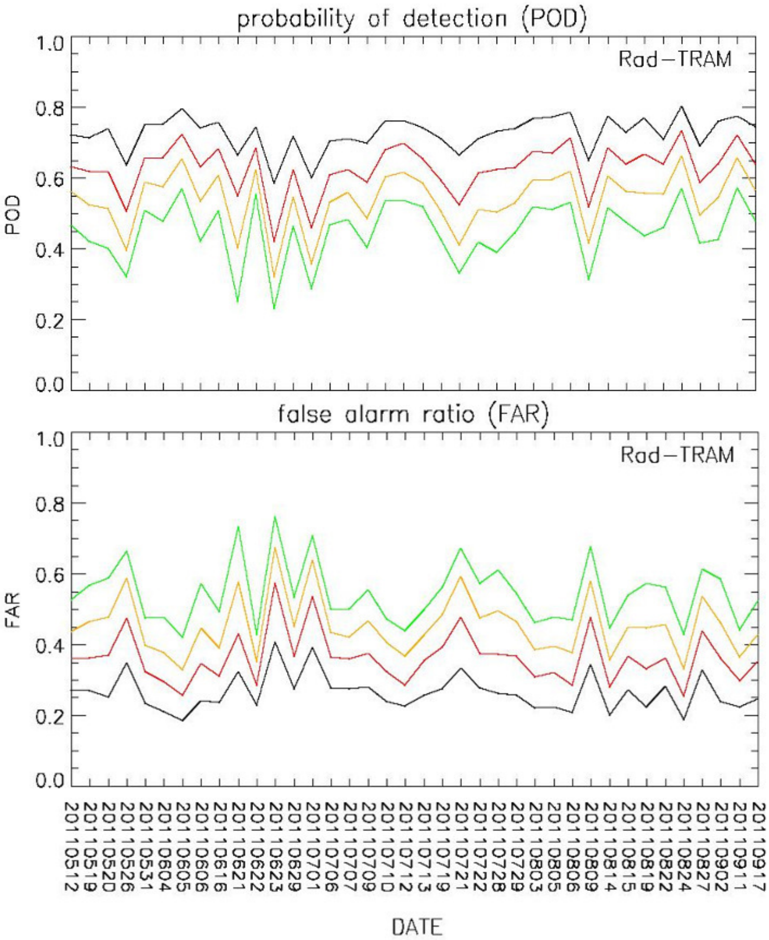

Figure 7. Same as Figure 6, but for the object-based analysis.

A study by Dotzek and Forster [2010] compared Cb-TRAM detections and nowcasts with data from the European Severe Weather Data base (ESWD). With six case studies they showed that up to 47% of all ESWD reports were located within a Cb-TRAM detection contour, and about 7% more reports were located close by these contours. The POD for an ESWD report corresponding with a Cb-TRAM detection was 24% on average in the whole summer season 2008 with maximum values up to 58% on intense thunderstorm days. These numbers are encouraging, as ESWD reports do not necessarily have to correspond exactly with a Cb-TRAM cell due to storm morphology. In addition, if a detected Cb-TRAM cell is not related to an ESWD report, this does not falsify the Cb-TRAM detection, but the convective storm might simply have not been reported to the ESWD. Likewise, the absence of a Cb-TRAM cell cannot be regarded as a proof that there was no thunderstorm. The ESWD report then might be related to storms that cannot be seen from space like small or low-topped convective storms, or those developing below cirrus layers.

Developments beyond the Nowcasting Horizon

The nowcasting quality of thunderstorms rapidly deteriorates with nowcast lead time. For lead times beyond roughly one hour they are no longer reliable and reasonable, as discussed above. On the other hand, forecasts from numerical weather prediction models are not reliable for the first hours, but have better forecast skills for longer lead times.

To fill that gap between nowcasts based on observations only and forecasts based on model data only, the concept of WxFUSION (see Section 2.2 above) is used. The graphical user interface of WxFUSION where the different data sources can be superimposed and the fuzzy logic and the numerical forecast selection algorithms can be tested has been run in real time during the summer campaigns. Work has been done and is currently going on to evaluate the results of these algorithms and to gain further knowledge on the formation and life cycle of thunderstorms that can be used in the fusion algorithm. Examples are given in the following.

One study investigated the ability of the COSMO-DE model to forecast the location of thunderstorm cells. For this, Cb-TRAM was applied to synthetic satellite images from COSMO-DE which are available up to 21 hours in 15 minute intervals. Comparing the Cb-TRAM$_{_COSMO}$ forecasts to Cb-TRAM observations revealed that 50% of all Cb-TRAM$_{_COSMO}$ forecasts overlap with an observation. The forecasts are updated every 3 hours. That means for each 15 minute interval 7 different forecasts with different initial times exist and build a so-called time lagged ensemble with ensemble member 1 as the most recent forecast and ensemble member 7 as the oldest forecast. If the different Cb-TRAM$_{_COSMO}$ forecasts from this time lagged ensemble are compared to the observation, it turned out that member 1 and member 4 are the best members in the majority of all cases, i.e. the Cb-TRAM observations overlap most often with a Cb-TRAM$_{_COSMO}$ forecast from member 1 or 4.

Another study investigated the initiation of thunderstorms by exploring the vertical velocity, the equivalent potential temperature, and CAPE (convective available potential energy) in the synoptic scale model COSMO-EU [Köhler, 2011]. It was found that in most of the areas where thunderstorms were observed COSMO-EU forecasts showed constant upward motion above 1000hPa, potential lability and elevated values for CAPE. These large scale parameters from COSMO-EU agreed better with observed thunderstorms than the thunderstorm probabilities from the high resolution COSMO-DE model.

The time series of different observational data like cloud top height, maximum radar reflectivity, lightning activity, and size of a thunderstorm as well as forecast data from the COSMO-DE model were inspected in combination in order to learn about the life cycle of thunderstorms [Bretl, 2010]. It was found that the time series of the trend of the inspected variables show a typical behaviour during the formation, mature, and decay phase of a thunderstorm. For instance, the formation phase is characterized by a growth of all inspected variables, while the decay phase is characterized by a decline of these variables.

A further study deals with the detection and nowcasting of convection initiation (CI) [Stich et al., 2011]. The aim is to improve the CI stage-1 detection and nowcasting in Cb-TRAM by a combination with different data sources from observations and numerical models. First results show that the high FAR of the Cb-TRAM's stage 1 can be considerably lowered by excluding detections and nowcasts that occur in regions with low surface equivalent potential temperatures and downward motion at 500hPa. At the same time, the POD hardly changes.

Finally, surface observations of temperature, humidity, and pressure from SYNOP observations and data from the Vienna Enhanced Resolution Analysis (VERA) System were explored to find out whether they exhibit typical characteristics along thunderstorm tracks monitored by Cb-TRAM [Klötzke, 2011]. It was found that thunderstorms related to frontal systems exhibit high pressure gradients and gradients of equivalent potential temperatures.

Conclusions and Outlook

The demonstration of the DLR products for thunderstorm detection and nowcasting at MUC during the summer campaigns in 2010 and 2011 showed the usefulness of these products for the collaborative decision making process at the airport. As all users received a thunderstorm warning at the same time and could get an overview on the current weather situation by inspecting the DLR nowcasting products, they had the same situational awareness and could make decisions and trigger actions with less time pressure than without the warnings and products. In general, the user feedback was very positive, but with suggestions for improvements of the products like an indication of the height of the thunderstorm cells in the display or the demand for nowcasts beyond one hour. The latter will be considered within

WxFUSION (see Section 2.2) which has been further developed during the campaigns, but is not yet ready to be presented to the users. Still, effort has to be made in order to integrate the knowledge gained from the studies made so far. A quantitative assessment of the nowcasting performance of the DLR tools revealed that the algorithms have good forecast skills, but for lead times greater than 30 minutes the nowcasting has to be used with care because of the increasing number of missed observations and false alarms. These results indicate that it is more suitable for longer lead times to combine observational and nowcasting data with numerical model results and express the forecasts with probabilities, e.g. the probability of the occurrence of a thunderstorm in a specific area. This will also be considered within WxFUSION.

It is envisaged to initiate another summer campaign in 2012. Not only Rad-TRAM but also Cb-TRAM products will then be available in the MetFROG display in real time. In addition, Rad-TRAM can also be tested by the controllers within the PHOENIX test display. Since the thunderstorm warnings turned out to be very important, it is planned to automate the production of such warnings on the basis of Rad-TRAM. Whenever a Rad-TRAM cell is detected and/or nowcast within the TMA MUC a text message will be issued automatically and sent to the users. As the DFS wishes to present all the information in one display, it is discussed to integrate the thunderstorm warnings in the MetFROG display. As a further activity during the summer campaign 2012, it is planned to demonstrate the link of Cb-TRAM and Rad-TRAM data into the cockpit of light aircraft. DLR is currently in contact with the companies Atmosphere (http://www.atmosphere.aero/) and TriaGnoSys (http://triagnosys.com/) in order to discuss and prepare a concept for such a demonstration.

Acknowledgements

We are grateful to the DWD who supported the campaigns 2010 and 2011 with operational weather data and enabled a test-wise installation of the DLR nowcasting algorithms Cb-TRAM and Rad-TRAM at DWD facilities. We also thank Stefan Schwanke (DFS) for supporting the summer campaign 2011 from the LuFo IV project iPort. Thank you very much to all the users from DFS, FMG and LH HCC who gave us valuable feedback on our products, especially to Peter Roth from DFS Tower MUC who promoted our products within the ProMUC consortium. LH HCC is acknowledged for offering a working place to DLR. We thank Gottfried Perschl from WIIS GmbH for giving us the opportunity to display our products in WIIS, and we thank Prof. Dr. H.-D. Betz from Nowcast GmbH for providing lightning data during the campaigns in 2010 and 2011.

References

Betz, H. D., K. Schmidt, W. P. Oettinger, and B. Montag (2008), Cell-tracking with lightning data from LINET, Adv. Geosci., 17, 55–61.

Bretl, S., 2010: Untersuchung des Lebenszyklus von Gewittern in Mitteleuropa mit Hilfe von Fernerkundungs- und Modelldaten, Diplomarbeit in Meteorologie, Ludwig-MaximiliansUniversität München, 31. März 2010.

Dotzek, N., and C. Forster, 2010: Quantitative comparison of METEOSAT thunderstorm detection and nowcasting with in situ reports in the European Severe Weather Database (ESWD), Atmos. Res., 100 (2011), 511-522, doi:10.1016/j.atmosres.2010.12.013.

Eurocontrol, 2007: Performance Review Report 2006 of the Performance Review Commission, May 2007.

Forster, C., A. Tafferner, C. Keil, T. Zinner, 2008, Validation of severe weather forecasts based on synthetic satellite data as part of an integrated thunderstorm forecast system for air traffic, Proceedings of the EUMETSAT Meteorological Satellite Conference, Darmstadt, Germany 8 - 12 September 2008, EUMETSAT P. 52, ISBN 978-92-9110-082-8, ISSN 1011-3932, 8 pages.

Forster, C., and A. Tafferner, 2009a: Nowcasting and forecasting thunderstorms for air traffic with an integrated forecast system based on observations and model data, WMO Symposium on Nowcasting, Whistler, B.C., Canada, 30 August - 4 September 2009.

Forster, C., and A. Tafferner, 2009b: An integrated user-oriented weather forecast system for air traffic using real-time observations and model data, Proceedings of the European Air and Space Conference (CEAS), Manchester, UK, 26 - 29 October 2009

Holzäpfel, F., K. Dengler, T. Gerz, C. Schwarz, Prediction of Dynamic Pairwise Wake Vortex Separations for Approach and Landing, AIAA Paper 2011-3037, 3rd AIAA Atmospheric Space Environments Conference, 27-30 June 2011, Honolulu, Hawaii, 15 pages.

Klötzke T., 2011: Signaturen von Gewitterzugbahnen in SYNOP-Beobachtungen, Bachelorarbeit in Meteorologie, Freie Universität Berlin, 28. September 2011.

Köhler, M., 2011: Untersuchung der Auslösung von Gewittern während der „Wetter & Fliegen“ Sommerkampagne 2010, Masterarbeit in Meteorologie, Ludwig-Maximilians Universität München, 6. Oktober 2011..

Kober and Tafferner, 2008: Tracking and nowcasting of convective cells using remote sensing data from radar and satellite, Meteorol. Zeitschrift, 1 (18), 75 - 84.

Lau A., C. Forster , A. Tafferner, N. Dzikus and V. Gollnick, Assessment of a Convective Weather Nowcasting and Tracking Algorithm Based on Delay Reduction Potential at Munich Airport (Part I), 11th AIAA Aviation Technology, Integration and Operations (ATIO) Conference, Virginia Beach, Virginia, USA, 20-22 September 2011.

Lau A.; Economic assessment of enhanced information on convective weather tracking and nowcasting based on the delay reduction potential, this issue.

Mollwitz V., Korn B. 2011: Concept of operations for arrival traffic in the terminal area under the influence of thunderstorms – Description of concept and first validation, this issue.

Quon, 2006: L. Modeling and Simulation Needs for Next Generation Air Transportation System Research. AIAA Modeling and Simulation Technologies Conference and Exhibit, 21-24 August 2006, Keystone, Colorado, AIAA 2006-6109, p 1-8.

Robinson, M., DeLaura, R. A., Evans, J. E., McGettigan, S., Operational Usage of the Route Availability Planning Tool During the 2007 Convective Weather Season, Project Report ATC-339, MIT Lincoln Laboratory, Lexington, MA, 2008. http://www.ll.mit.edu/mission/aviation/publications/publication-files/atc-reports/Robinson_2008_ATC-339_WW-15781.pdf.

Robinson, M., Evans, J. E., Assessment of Air Traffic Control Productivity Enhancements from the Corridor Integrated Weather System (CIWS), Executive Summary, Project Report ATC-325-1, MIT Lincoln Laboratory, Lexington, MA, 2006. http://www.ll.mit.edu/mission/aviation/publications/publication-files/atc-reports/Robinson_2006_ATC-325-1_WW-13782.pdf.

Stich, D., C. Forster , T. Zinner, A. Tafferner, 2011: Convection Initiation - Nowcasting by data fusion and its Verification, European Conferences on Severe Storms (ECSS 2011) Palma de Mallorca, Balearic Islands, Spain, 3 - 7 October 2011

Tafferner, A., Hagen, M., Keil, C., Zinner, T. and Volkert, H., 2008, Development and propagation of severe thunderstorms in the upper Danube catchment area: Towards an integrated nowcasting and forecasting system using real-time data and high-resolution simulations, Meteorology and Atmospheric Physics, 101, 211-227, DOI 10.1007/s00703-008-0322-7.

Zinner, T., Betz, H.D., 2009. Validation of Meteosat storm detection and nowcasting based on lightning network data. Proc. 2009 EUMETSAT Meteorological Satellite Conference, Bath, 21–25 September 2009. 9 pp. Available at http://www.eumetsat.int/Home/Main/AboutEUMETSAT/Publications/ConferenceandWorkshopProceedings/SP_201001515267179.

Zinner, T., C. Forster, E. de Coning, and H.-D. Betz, 2011: Validation of the METEOSAT storm detection and nowcasting system Cb-TRAM with lightning network data, in preparation for Atmos. Chem. Phys.

Zinner, T., H. Mannstein, A. Tafferner, 2008: Cb-TRAM: Tracking and monitoring severe convection from onset over rapid development to mature phase using multichannel Meteosat-8 SEVIRI data. – Meteor. Atmos. Phys. 101, 191–210, DOI 10.1007/s00703-008-0290-y.

2.4 Nowcasting Winter Weather at Munich Airport

Arnold Tafferner, Felix Keis
Institute of Atmospheric Physics

The WxFUSION concept can also be extended to handle winter weather conditions. Of particular importance here is the occurrence of in-flight and ground icing conditions at an aerodrome. Data from surface observations of precipitation type and intensity, of surface conditions (dry, liquid, frozen), of hydrometeor observations within clouds, and of aircraft observations of temperature and humidity can be fused. Work is underway to combine existing in-flight icing algorithms with the additional data sources available to build a corresponding winter weather module within WxFUSION.

Introduction

Airport operations in winter are significantly impacted by weather conditions such as snow fall, freezing rain and drizzle, and low ceiling and visibility. Delays and cancellation of flights are often resulting from these weather conditions. Runways and taxiways must be kept free of or cleared from snow and ice and aircraft have to be de-iced before take-off. Planning and conduct of aircraft traffic flow on the ground and in the air can be significantly impacted through these procedures. During the recent winters 2009 and 2010 European air traffic has been significantly disrupted by winter weather as has been the case for two major hubs shortly before Christmas in December 2010: 200 flights at Frankfurt on a single day (17.12.2010) and an almost complete still stand at London Heathrow. The photographs in Figure 1 are two examples from 30 November 2010 at Frankfurt airport and on 22 December 2010 at Berlin Tegel after heavy snow fall (left) and snow together with rain (right).

Figure 1. Winter weather impacting airport operations: Frankfurt on 30.11.2010 (left) and Berlin Tegel on 22.12.2009 (right)

In order to gain understanding of the impact of winter weather conditions on airport operations a meeting was held at Munich airport with representatives of Munich airport operations, air traffic control, local office of the German weather service and DLR institute of Atmospheric Physics on 17 December 2007. The outcome of the meeting can be compressed into the following user requirements:

Of particular interest for all stakeholders is the short-term forecasting, or nowcasting, of:

- Onset, duration and type of precipitation,
- Icing at the surface,
- Freezing fog,
- Aircraft icing at ground,
- Visibility.

The Deutsche Flugsicherung (DFS) reported in the meeting that there are 20-30 winter weather days at Munich airport and 70-90% of all delays are weather related (summer and winter). Therefore, the objective of the work package “Winterwetter” within the DLR project “Wetter & Fliegen” was to develop a winter weather nowcasting system that provides users with 0-2 hour nowcasts of the winter weather conditions described above. The following paragraphs describe the concept of the system and show first results from individual measurement platforms.

The nowcasting Concept

The task “nowcasting of winter weather at Munich airport” can be approached by a stepwise procedure:

- Check which MET data are available at the airport and within the TMA
- Analysis: combine MET data to determine winter weather conditions hazardous to aviation at every observation site within the TMA and represent these hazards by winter weather objects (WWO)
- Nowcasting: use calculated trends at observation sites within the TMA to determine changes in weather conditions at the airport
- Use forecast data from numerical model for early warning

In the following, these points are addressed.

Available data at Munich Airport

Figure 2 shows schematically the available data at and around Munich airport which can be used for the analysis of winter weather conditions. We have to distinguish in-situ data, remote sensing data and derived products.

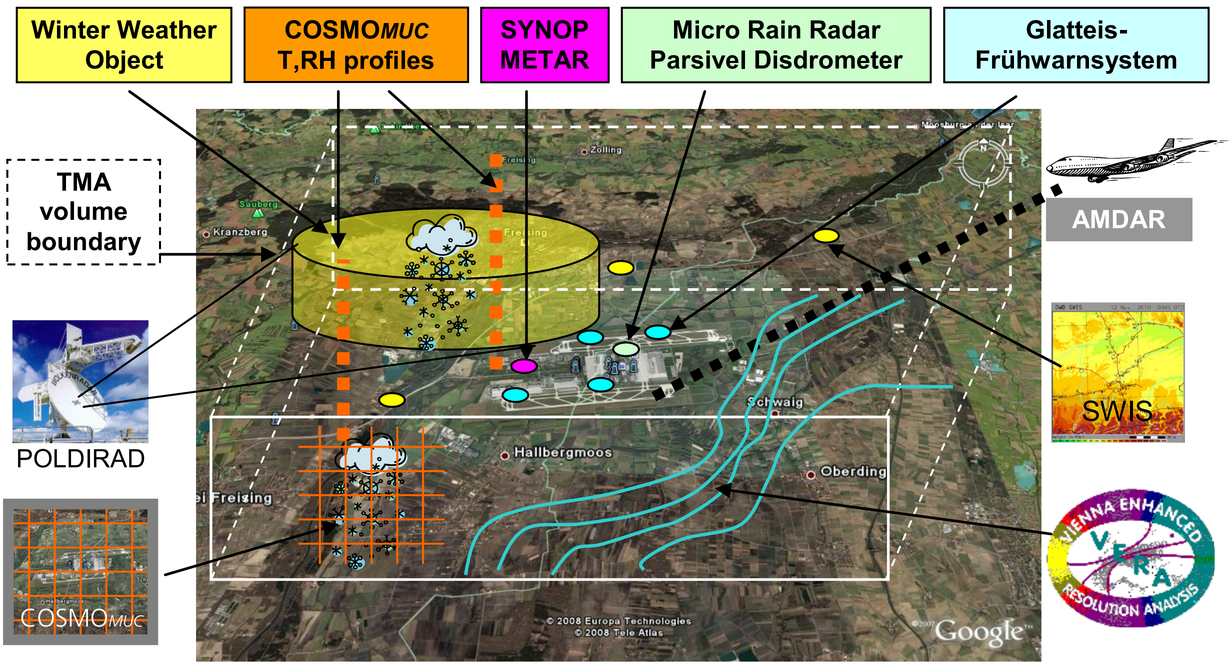

Figure 2. Available MET data at and around Munich airport

SYNOP & METAR data are reported hourly from station 10870 (München Flughafen) and cover up to 90 different parameters, including besides standard observations like pressure, wind, temperature and humidity, also cloud cover, cloud height and type, precipitation amount and type, various soil temperatures and ground state. These data therefore give valuable information also on winter weather conditions like e.g. observation of freezing rain, frozen surface, etc.

Special sensors installed in the run and taxiways record the temperatures of the near ground air, of the surface and the soil, furthermore the precipitation type, pressure, wind velocity and freezing temperature. The sensors form the hardware part of the so-called “Glatteisfrühwarnsystem – **GFS**”, an icing early warning system. It determines freezing conditions which are used to optimize the use of de-icing chemicals.

In addition to these sensors at the airport, surface conditions of roads around the airport are also evaluated by the Strassenwetterinformationssystem **SWIS** (Street Weather Information System), operated by the German weather service. Measurements include air temperature, humidity, wind velocity and direction, visibility range und precipitation amount. Similar to the sensors within the airport area SWIS sensors measure surface and soil temperature, humidity and water film on the road and in addition the salt content during the winter period.

The **Micro Rain Radar** (MRR-2) is a small low-power vertical-looking Doppler radar operating at 24 GHz. It measures the velocity spectra of falling raindrops. Raindrop size distribution and rain rate are estimated as vertical profiles. A narrow spectra with low fall speeds indicates snow, a broad spectra with higher fall speeds indicates rainfall. For further information see www.metek.de.

The **Parsivel optical disdrometer** measures size and fall speed of particles with a narrow laser beam. Fall speed and size distribution is used to estimate rain rate and precipitation type. For further information see http://www.ott-hydrometry.de. The photograph in Figure 3 (left) shows these two instruments, the observation site is indicated on the right.

Figure 3. Observation instruments at Munich airport operated by DLR, foto: Parsivel (left), micro-rain radar (right), observation site indicated by green dot in right Figure.

The Polarimetric Doppler Weather Radar **POLDIRAD** is operated for research since 1986 jointly with the DLR Institute of High Frequency Technology. The main characteristics of the C-band system comprise the polarisation agility for transmitting, the dual-channel receiving, the Doppler capability and the real time processing and display. A selection of two parameters out of the following are available for real time display: reflectivity factor for each polarisation of choice; the differential reflectivity; and the depolarisation ratio for a selected polarisation, especially the linear depolarisation ratio; or the circular depolarisation ratio; the Doppler velocities; and the Doppler spectral widths for both receiving channels. Time series products as the differential propagation phase will be available in real time soon. The radar can be used to estimate the dynamical and the connected microphysical cloud structures and their developments with their lifetimes. Snow, graupel, hail and rain can be distinguished. It is such of great value in order to reveal winter weather precipitation in real time.

AMDAR (Aircraft Meteorological Data Relay) data are reported from aircraft during flight. Data transmitted are temperature and humidity besides others. Together with pressure recordings, geographic position data and time information vertical profiles of these data can be constructed. These soundings thus provide useful information on inversion layers, cloud layers and possible icing zones.

Besides these in-situ data, forecast data from the **COSMO*MUC*** derivative of the COSMO-DE model of the DWD (COSMO, 1998) are available within the Terminal Manoeuvring area (indicated as **TMA** volume boundary) of the airport; see Section 2.5 for a description of that model.

Vienna Enhanced Resolution Analysis (**VERA**) is a objective, automatic analysis procedure for meteorological parameters over complex terrain developed by the University of Vienna (Steinacker et al., 1997). It is able to resolve mesoscale structures caused by topography by including meteorological a priori knowledge in the analysis. The scheme is used for both error detection and correction, and interpolation of irregularly distributed data onto a regular grid. The emphasis is put on the transfer of information from data sparse to data rich areas. For this purpose the so called “fingerprint technique” is used. It adjoins additional orographic information to the measurements. The error detection mode checks the single measurements concerning their spatial physical plausibility and calculates correction suggestions where necessary. The method runs independently from any first guess or model field. For the use in Wetter & Fliegen VERA has been installed at DLR/IPA over a domain with reduced size covering southern Germany. For winter weather the analysis system can provide information on surface temperature and humidity, observed precipitation and especially fronts, where the exact position, movement, strength is of great importance for timely warning and model forecast verification. Figure 4 shows an example of analysed surface temperature. The 0° C contour run close to the airport MUC, dividing colder near ground air to the northeast from warmer temperatures to the southwest. Such information could be quite valuable when there is precipitation in the area, thus allowing the estimate of possible freezing conditions at the ground.

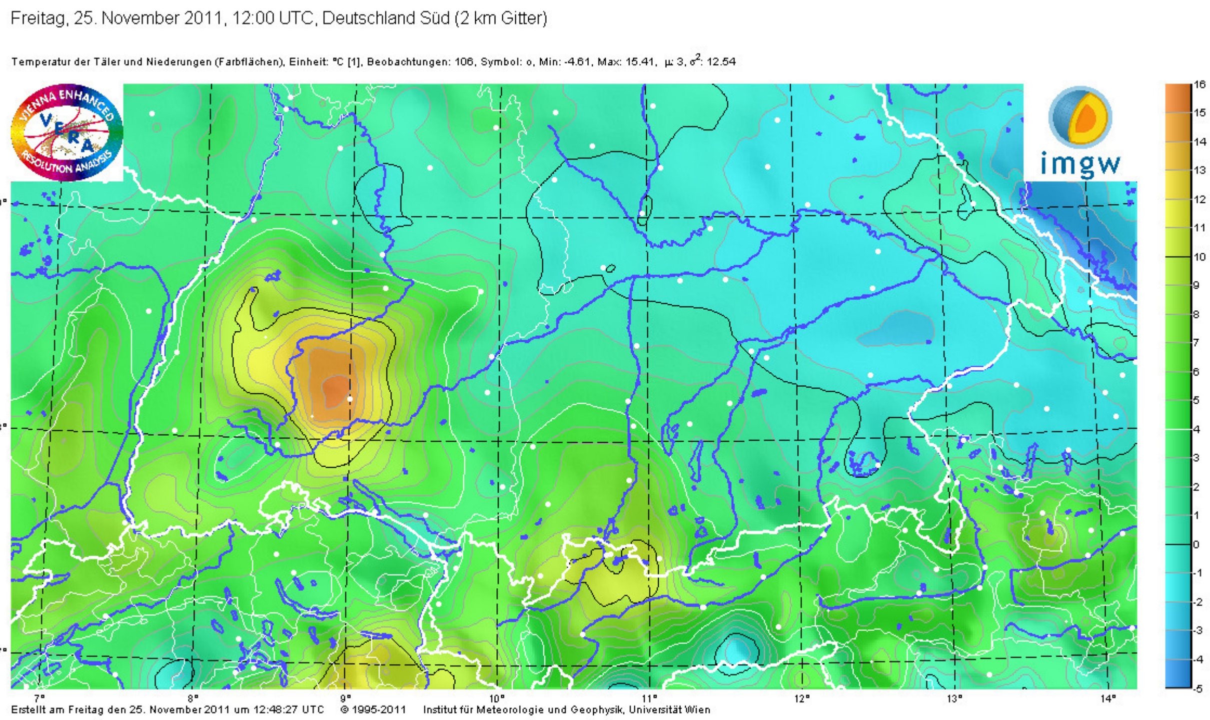

Figure 4. Vienna Enhanced Resolution Analysis: Temperature of valleys and low lands on 25/11/2011.

Fusion of Observation Data into Weather Objects Representing Hazards to Aviation

A certain winter weather phenomenon, like e.g. freezing precipitation, can be thought of a certain volume of air within which this phenomenon can be observed. Various observations, like the ones described above, are suited for describing one or the other attribute of that phenomenon, as e.g. the surface temperature, the precipitation type. With no doubt the actual weather phenomenon can be determined more precisely when data from various sensors are combined (Tafferner et al., 2008). It is therefore advisable to think of such volumes as weather objects with certain inherent attributes. Such an approach has already been successfully implemented for nowcasting thunderstorms (Forster and Tafferner, 2009; also Forster and Tafferner this volume). For our purposes, a winter weather object at a certain location, e.g. an airport, can be defined through the following parameters:

- a vertical column of air consisting of several layers
- issued time
- valid time
- next update time
- layer description, e.g.:
  - Snow: upper and lower boundary with intensity: light, moderate, severe
  - Rain: upper and lower boundary with intensity: light, moderate, severe
  - Freezing rain: upper and lower boundary
  - Freezing drizzle: upper and lower boundary
- surface conditions
- trends, e.g. intensity increasing, change to melting, etc.

This first approach addresses only the threats to aviation related to precipitation processes. In the future, further ingredients could be taken into account like wind, visibility, ceiling.

A winter weather object (WWO) is shown schematically as yellow cylinders in Figures 2 and 5. From the definition it is obvious that the object can have several different hazard layers. In Figure 5 this is exemplified within the yellow idealized object:

- there is a near surface layer with temperatures above freezing up to about 800 mb (ref. sounding to the left) which contains rain drops;
- a second layer from H1 to H2 (about 800 to 660 mb) contains supercooled droplets which result from melting of snow and ice within the “warm nose”, the the layer with positive temperatures between about 660 and 600 mb;
- on top there is a precipitating cloud layer with mixed type particles up to the radar height of precipitation (Ht).

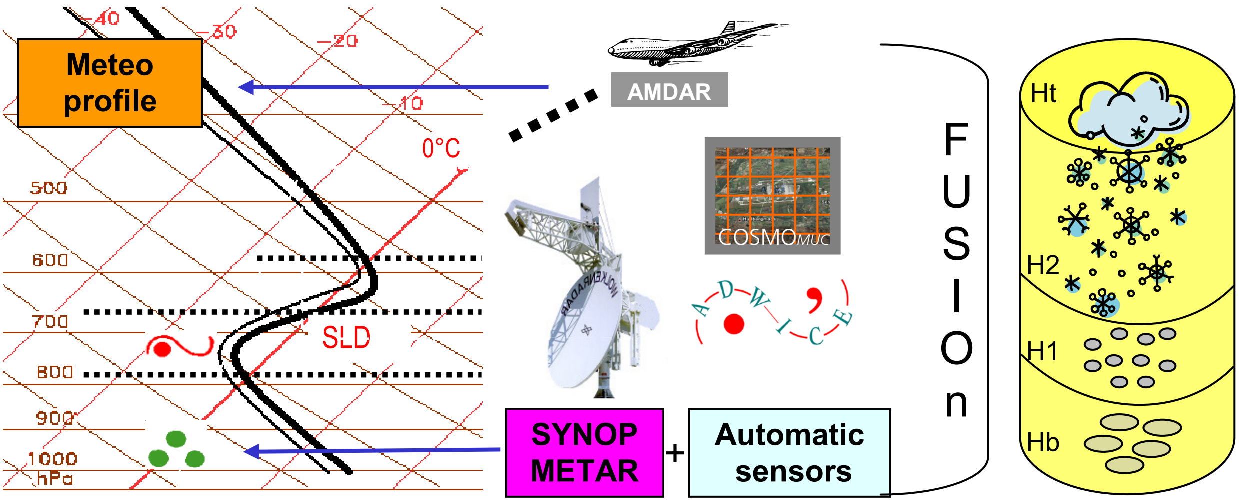

Figure 5. Fusion of data into an object

In Figure 5 various data sources are shown symbolically which would allow deriving the weather object. SYNOP and automatic sensors (e.g. from GFS) allow to determine the surface conditions, in this example rain with temperature above zero. The temperature/humidity sounding can be provided from

COSMO*MUC* model or AMDAR data, or constructed from both depending on data availability (esp. as regards to AMDAR humidity observations). POLDIRAD observes the precipitation height and is able to determine the hydrometeors within the cloud through its polarimetric capability and related algorithms. ADWICE – the Advanced Diagnosis and Warning System for Icing Environments - (Tafferner et al., 2003; Leifeld, 2004) uses the information of reported weather at the ground together with the soundings of temperature and humidity and radar measurements to determine the icing threat to aircraft in flight.

Figure 6 illustrates schematically the current algorithm for the diagnostic product which is run operationally at DWD (DWD - Luftfahrt, 2003). Starting from weather observations of SYNOP and of radar reflectivity from the European radar composite of DWD icing scenarios “freezing”, “convective” or “stratiform” are determined over the domain of the COSMO-EU model which covers roughly the area of Middle Europe. Forecast profiles of temperature and humidity from this model allow to calculate the vertical structure and extent of the icing scenarios (“3-D DIP” in the Figure). Another scenario “general” is added if temperature and humidity profiles are within certain thresholds even when not supported from ground observations. Note that within ADWICE not only precipitation is considered but also the occurrence of super-cooled droplets in general, e.g. in stratiform clouds which can pose a hazard to aircraft especially when residing for a longer time within this clouds as is the case during holding pattern. A graphical depiction of the diagnosed icing product is seen on the right. Coloured regions indicate different icing threats on flight level 65. A detailed description of both the diagnostic and prognostic icing algorithm can be found in Leifeld (2004).

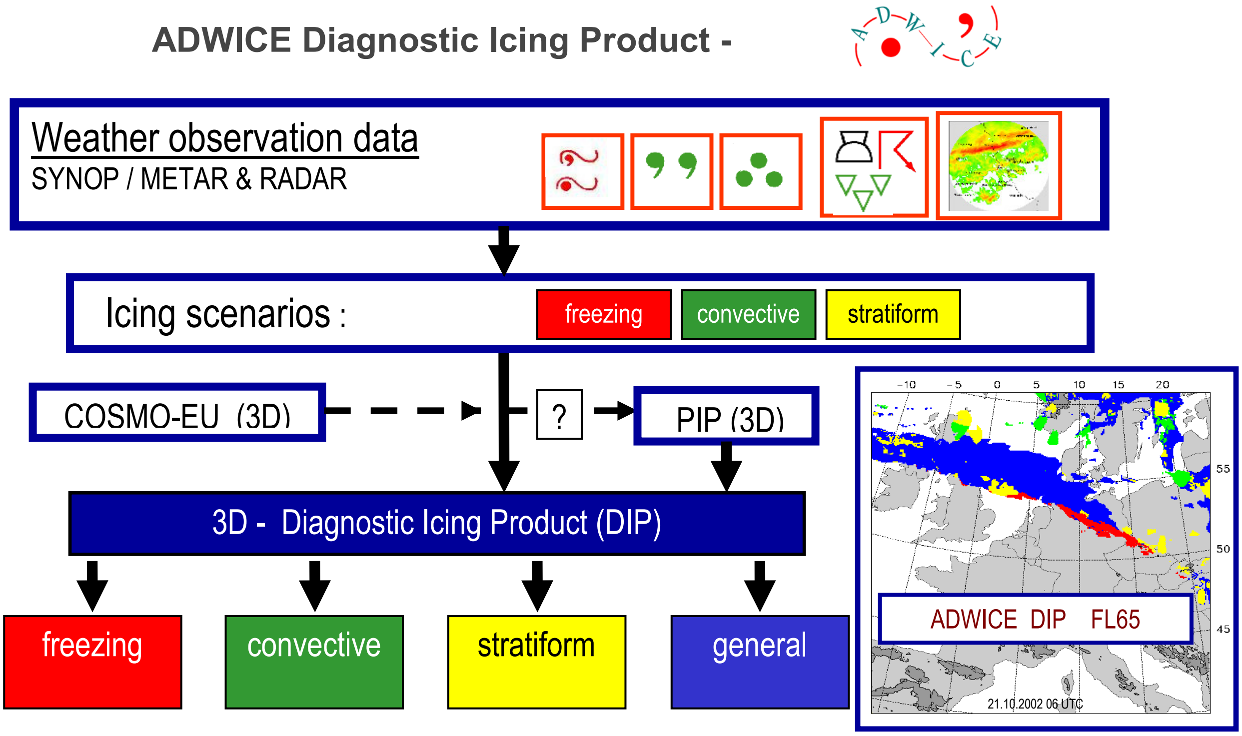

Figure 6. Data flow diagram of ADWICE algorithm for diagnostic icing product.

Up to date, ADWICE only uses radar reflectivity for the analysis. However, the quite useful polarimetric radar information and the measurements of the micro rain radar can be included in the analysis. This will be part of a data combination algorithm. It will be based on fuzzy logic which allows that the ‘ingredients’, i.e. the information contents of the various observations can be weighted and contrasted to each other using physical concepts and experience to derive the actual weather state as precisely as possible. This work is carried out within the frame of a doctoral thesis (Keis, 2010).

Nowcasting: Extrapolating Winter Weather Conditions in Time and Space

Close to actual time, air traffic control and airport operations require exact weather information as it makes a great difference whether the precipitation during the next hour will be rain, freezing rain or snow. Quite different operations have to be set into place like the planning and conduct of runway and airport road clearing, of aircraft deicing, of aircraft traffic flow on the ground and in the air. This is why users chose the nowcasting of winter weather conditions at first place when asked what they need most.

For nowcasting icing & snow conditions for the airport one has to consider weather changes due to advection of air with different characteristics and, especially demanding, possible changes resulting from precipitation and cloud physics processes which can occur within short time spans at the observation site. For capturing both of these effects an approach is followed where WWOs are determined at the various observation sites around the Munich airport where both SYNOP and polarimetric radar data are available. Changes in WWOs around the airport can then provide guidance for the expected change at the airport. Figure 7 demonstrates this approach.

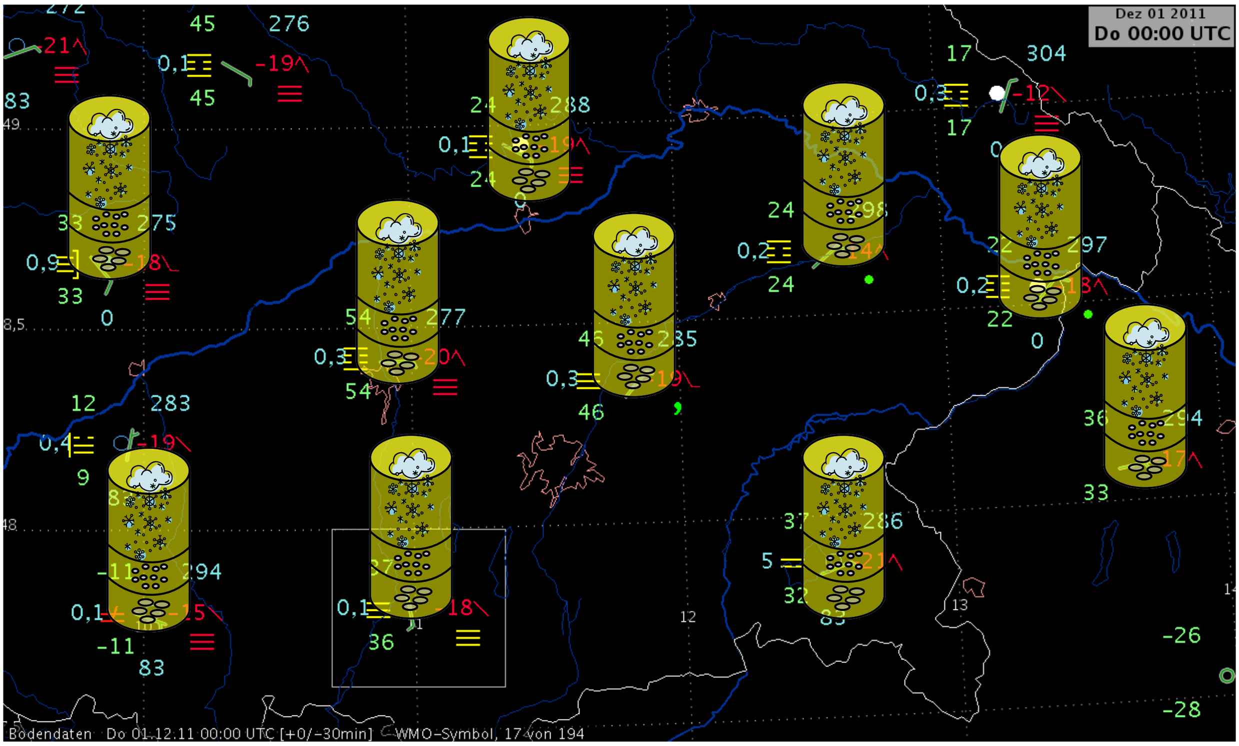

Figure 7. SYNOP stations within the TMA MUC together with winter weather objects

At every SYNOP observing station within the TMA a WWO is determined as described above using surface observations, polarimetric radar data and temperature/humidity forecast soundings from the COSMO-DE model. Note that only at MUC airport (in the centre of the Figure) AMDAR data are available for the soundings, too. For nowcasting winter weather hazards at MUC the following approach is proposed:

1) Determine WWO from observed data and forecast soundings at every observation site;
2) Calculate trends in surface parameters, e.g. temperature, humidity at the airport;
3) Use forecast temperature/humidity soundings at the airport from COSMO*MUC*;
4) Determine weather trend at the airport from observed weather at upstream stations at earlier time which can then be used to take into account advection;
5) By fuzzy logic, combine upstream weather changes with estimated trend at the airport to nowcast winter weather conditions up to 2 hours.

From data availability at Munich airport, points 1 to 5 can be updated every 30 minutes, also the calculation can be performed quite fast in order to not produce unnecessary delays.

Forecasting for Early Warning

For forecasting winter weather beyond the nowcasting range up to about 24 hours or more, one can rely on operational forecast models like COSMO-DE. Although numerical models have achieved remarkable progress during the last years in forecasting the overall weather state, e.g. the surface pressure distribution or whether it will rain or not, winter weather phenomena like freezing rain or drizzle, or light or heavy snow fall result from the subtle interplay of various factors, like the vertical distribution of temperature and humidity, cloud cover and type, snow cover, soil moisture and the composition of the atmosphere with aerosols which again influence cloud and precipitation processes. The situation gets even more complicated as these processes result from instabilities which are triggered by small changes in the atmospheric parameters, e.g. whether the temperature at the ground or through a certain depth of the atmosphere is slightly above or below 0° C. In order to better estimate the future atmospheric state ensemble models as mentioned above give better guidance than a single model run. Combined quantities like ensemble mean, spread and others allow estimating probabilities which can be used for advanced planning. Here output of the KENDA ensemble model from DWD can be used in future to provide this probability information.

First Results

Several winter weather events which occurred in 2010 have been selected as example cases for first studies. In the following some results from algorithm development and local measurements are presented, all of which are necessary steps in setting up the nowcasting procedure as described in the previous chapter.

Installation of ADWICE at DLR

The operational ADWICE algorithm run at DWD consisting of diagnostic and prognostic parts has been installed at DLR. However, in contrary to DWD the higher resolution COSMO-DE model output is used at DLR instead of COSMO-EU output as in the operational version. In a first step, it is evaluated whether this can already bring improvements. Figure 8 demonstrates these differences.

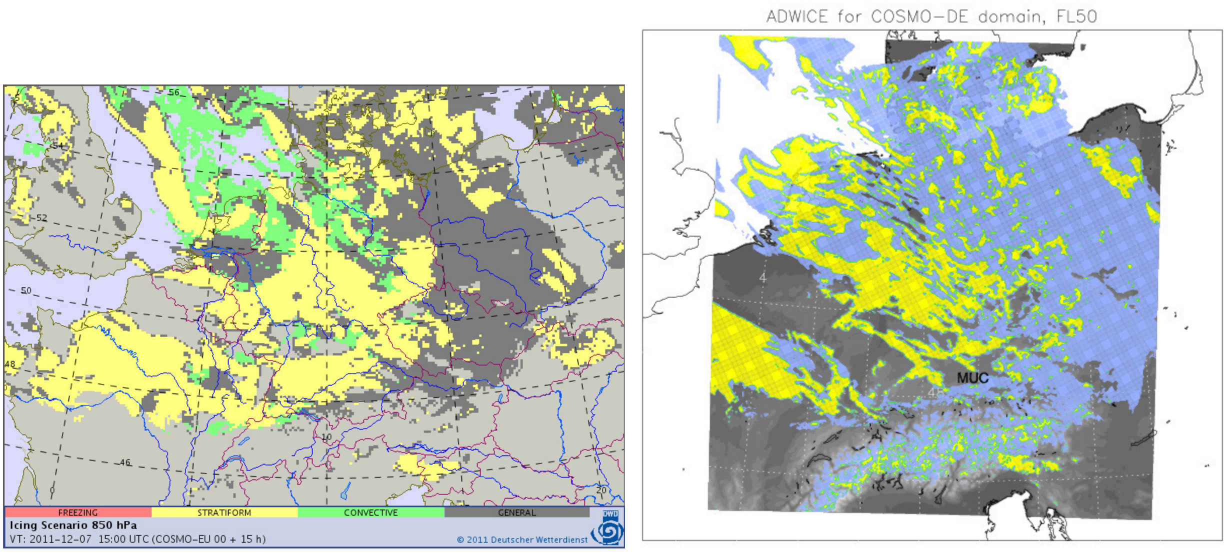

Figure 8. ADWICE forecasts for flight level 50 using COSMO-EU output left, COSMO-DE output right.

Notable differences are seen in the extent of the yellow areas which render the icing scenario “stratiform” in both Figures. Calculated from the output of the COSMO-EU model (left) these areas are much larger especially over Germany as compared to the ADWICE forecast from DLR which is calculated from COSMO-DE output (right). The too large icing fields in the operational version are well known as a problem referred to as "overforecasting". It appears that the use of COSMO-DE output is a step in the right direction, although more testing is required and results have to be verified against independent data sources.

Use of AMDAR Data

At the airport AMDAR data relayed from descending aircraft can replace the forecast soundings of temperature and humidity from the COSMO model. The benefit is demonstrated in Figure 9. Forecast temperature and dew point temperature from the COSMO-DE model are shown as black lines, crosses mark measured temperature and dew point from descending aircraft. The pink lines are lines fitted to the measurements. Whereas the temperature curves from both AMDAR and forecast show close resemblance, especially within the range 0° to -20° C degrees which is the preferred range where icing is most probable, there is a large difference in the dew point temperatures. Under the precondition that the measurements are correct, the forecast icing zone indicated as blue bar on the right is correctly dismissed by using the observation data (no respective bar). Further evaluations in this direction will be conducted together with POLDIRAD measurements and surface observations.

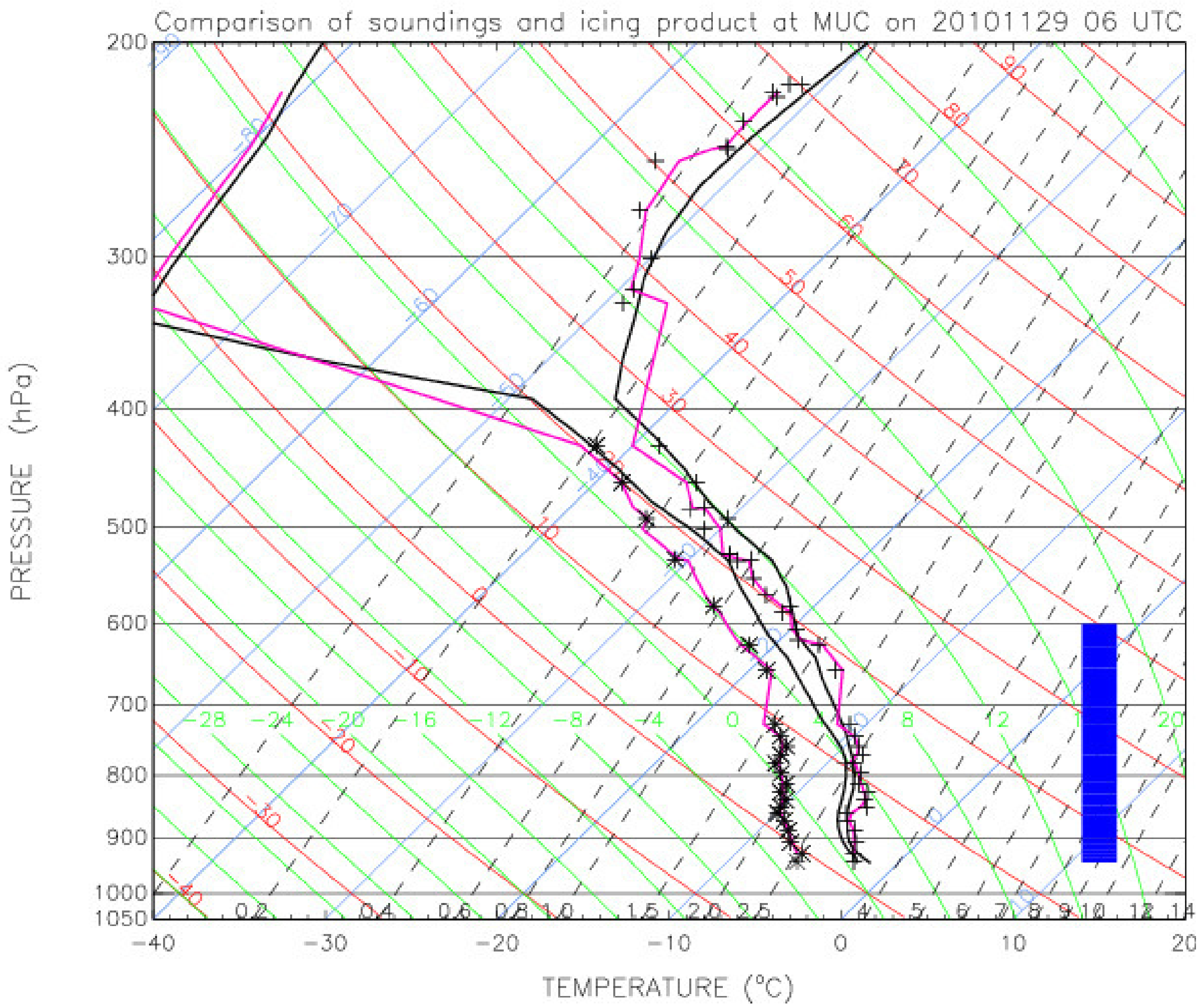

Figure 9. Comparison of forecast (black curves) and measured (pink) soundings of temperature and humidity for 29 November 2010 06 UTC. The blue vertical bar on the right indicates the ADWICE icing range as forecast by COSMO-DE.

Use of Polarimetric Radar Data

Figure 10 shows measurements from a winter time snow front which is detected as a line signal in the POLARIMETRIC reflectivity data (left). From the corresponding polarimetric information the hydrometeors can be determined as indicated in the right Figure. Clearly the possibility to distinguish between snow and rain provides a quite useful information for winter weather nowcasting as it helps in decision making at the airport, e.g. snow clearing on runways, as well as for de-icing procedures and warnings of in-flight icing threat.

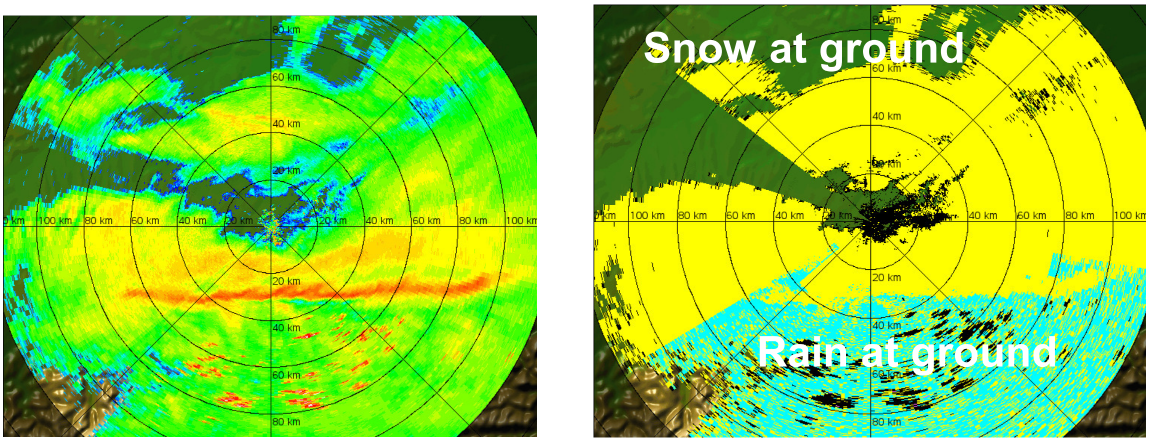

Figure 10. Snow front approaching from north towards Alps (line in left Figure) as detected by DLR POLDIRAD Alps on 21 November 2008 1330 UTC. Snow and rain areas can be distinguished through polarimetric capability.

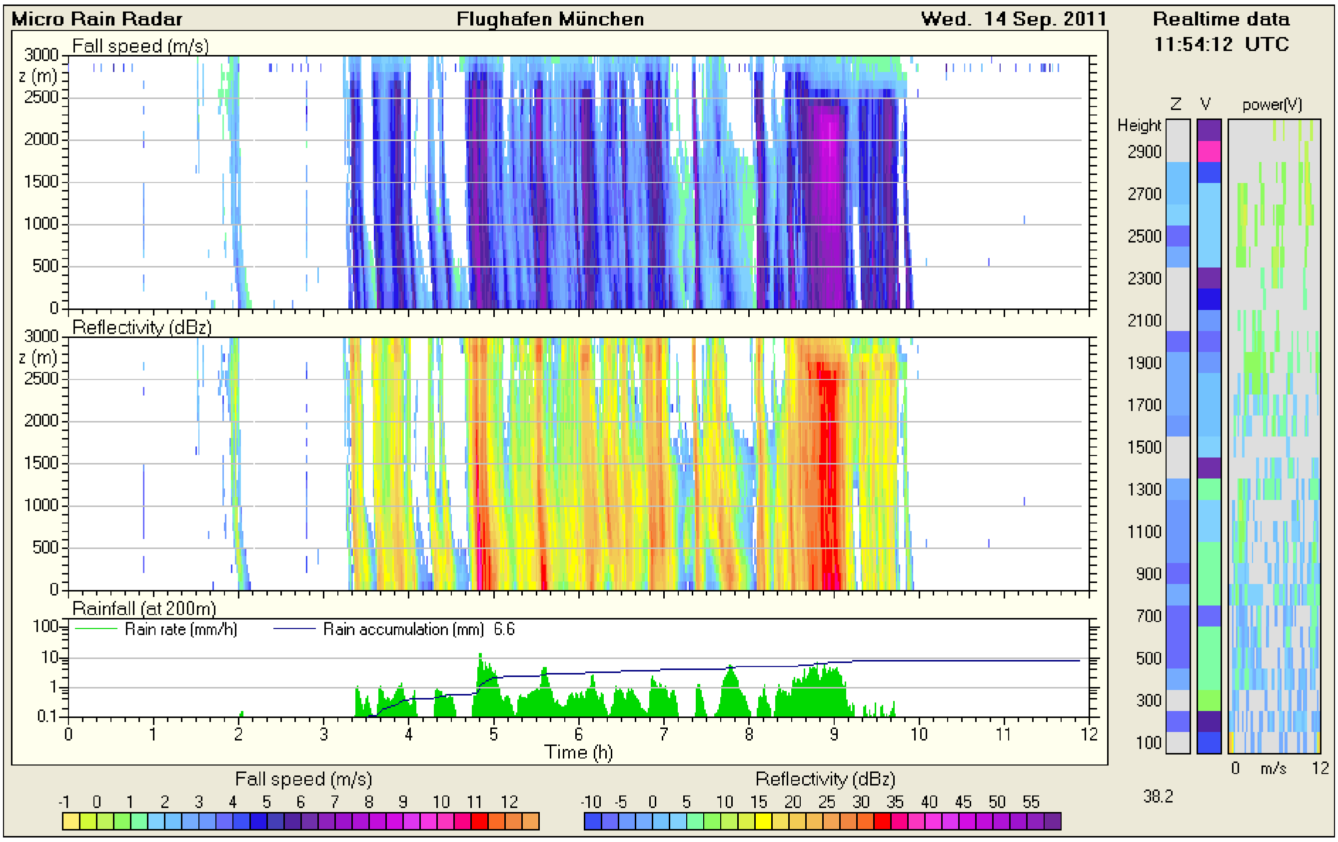

Figure 11. Measurements of the micro rain radar at Munich Airport on 14 September 2011

Use of Other Local Data

The Micro Rain Radar and the Parsivel instrument allow to observe precipitation events at the airport in real time and to provide relevant information on winter weather threats like the precipitation strength, the size and type of hydrometeors, the accumulated precipitation and the actual weather. Figure 11 shows a measurement example on 14 September 2011 with hydrometeor fall speed, reflectivity and accumulated rain fall. Figure 12 shows corresponding measurements from the Parsivel instrument. Note that also actual weather (ww) is determined from the measurements automatically. The droplet size provides useful information for estimating the icing intensity, in particular when super-cooled large droplets (SLD, range 40 – 400 µm) are detected.

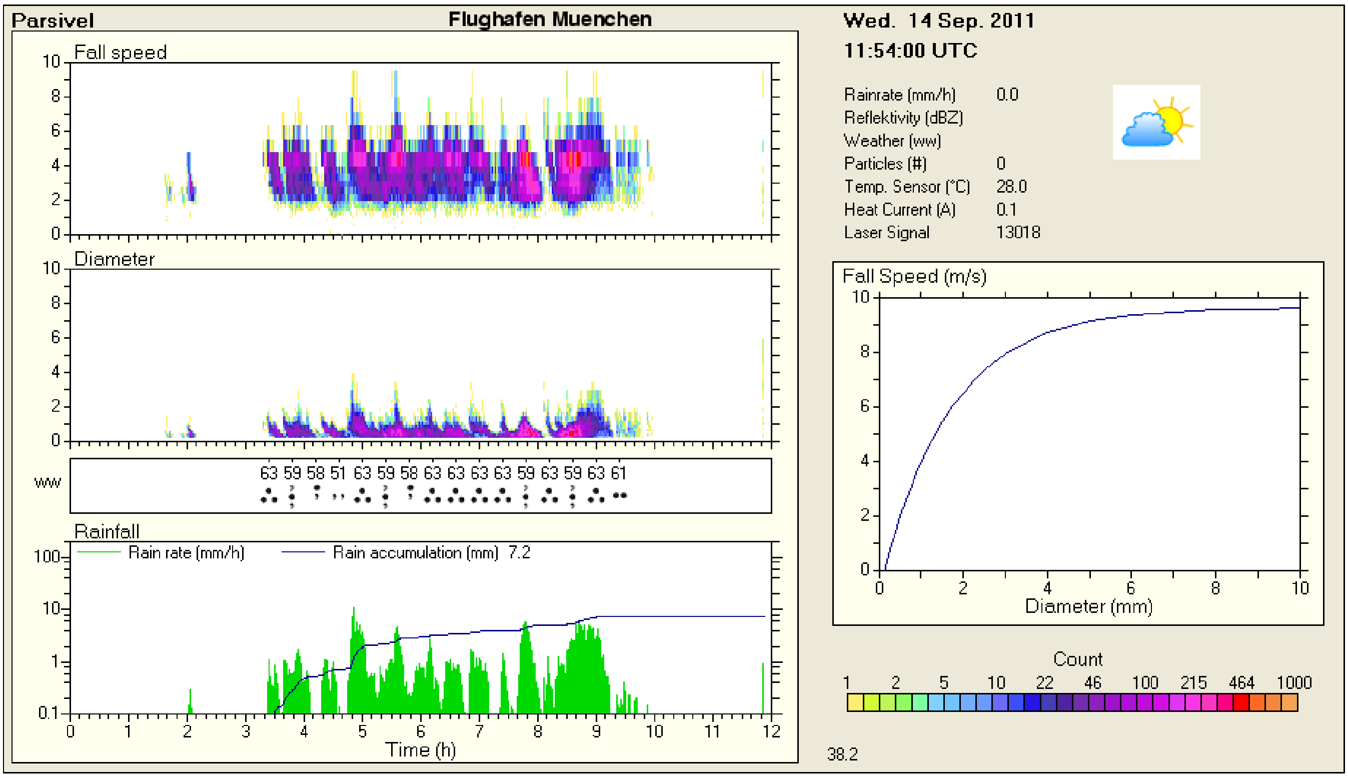

Figure 12. Measurements of the Parsivel instrument at Munich Airport on 14 September 2011

Outlook

During the winter 2011/12 cases where winter weather influences airport operations at MUC will be gathered and evaluated as regards to icing and snow fall conditions. All local observations and POLDIRAD measurements will be used to further develop the nowcasting system in the sense described above. It is expected that the experience gained from many winter weather cases will enable the build-up of a fuzzy logic procedure which can improve the nowcasting of winter weather and thus provide a reliable source of information for decision making at the Munich airport.

References

COSMO, 1998: Consortium for small scale Modeling: http://www.cosmo-model.org/content/model/documentation/core/default.htm

DWD – Luftfahrt, 2010: ADWICE Vereisungsprognosen für den europäischen Luftraum – Leitfaden zur Nutzung und Interpretation der Produkte –. DWD Abteilung Flugmeteorologie, 31.03.2010

Forster, C., and A. Tafferner, 2009: An integrated user-oriented weather forecast system for air traffic using real-time observations and model data, Proceedings of the European Air and Space Conference (CEAS), Manchester, UK, 26 - 29 October 2009

Keis, F., 2010: Nowcasting von Winterwetter am Münchner Flughafen und Umgebung durch Verbindung von Beobachtungs-, Fernerkundungs- und Modelldaten. Ph.D. work in progress at Institut für Physik der Atmosphäre, DLR

Kober K., Tafferner T. 2008: Tracking and nowcasting of convective cells using remote sensing data from radar and satellite, Meteorol. Zeitschrift, 1 (18), 75 - 84.

Leifeld, C., 2004: Weiterentwicklung des Nowcastingsystems ADWICE zur Erkennung vereisungsgefährdeter Lufträume, Berichte des Deutschen Wetterdienstes Nr. 224, Offenbach am Main, 118 S.

Steinacker, R., W. Pöttschacher, M. Dorninger, 1997: Enhanced Resolution Analysis of the Atmosphere over the Alps Using the Fingerprint Technique. Annalen der Meteorologie, 35, 235- 237

Tafferner, A., Hagen, M., Keil, C., Zinner, T. and Volkert, H., 2008, Development and propagation of severe thunderstorms in the upper Danube catchment area: Towards an integrated nowcasting and forecasting system using real-time data and high-resolution simulations, Meteorology and Atmospheric Physics, 101, 211-227, DOI 10.1007/s00703-008-0322-7

Tafferner, A. , Hauf, T. und Leifeld, C. und Hafner, T. und Leykauf, H. und Voigt, U. (2003) ADWICE - Advanced Diagnosis and Warning System for Aircraft Icing Environments. Weather and Forecasting, 18 (2) , 184-203

Zinner, T., H. Mannstein, A. Tafferner, 2008: Cb-TRAM: Tracking and monitoring severe convection from onset over rapid development to mature phase using multichannel Meteosat-8 SEVIRI data. – Meteor. Atmos. Phys. 101, 191–210, DOI 10.1007/s00703-008-0290-y.

2.5 Limited Area Numerical Weather Prediction

Thomas Gerz, Klaus Dengler, Arnold Tafferner, Frank Holzäpfel
Institute of Atmospheric Physics

Two limited area model derivatives of the numerical weather prediction model COSMO-DE operated by the German Meteorological Service are introduced. The aim is to obtain frequently updated highly resolved predictions in a limited area as an aerodrome. The predictions include dynamic parameters as wind and turbulence kinetic energy and thermodynamic quantities as temperature and humidity but also the amount of snow, rain and hail. The models are used in the airport environments of Frankfurt (COSMO-*FRA*) and Munich (COSMO-*MUC*) for aircraft wake vortex, thunderstorm activity, and wintry weather warning applications, as detailed in Sections 2.1 to 2.4.

Introduction

The demand for efficient, safe, and environmentally sustainable air traffic is steadily increasing. Major airports already today operate at their capacity limits. With increasing demand the air transport system becomes more vulnerable to distortions of all kinds. One of the major contributors to incidents, accidents, and delays in air traffic are adverse weather conditions, also en-route but especially at and around busy airports. Detailed studies of the impact of weather upon aviation show that there is a need for improved weather forecasts. Short-range wind forecasts with high resolution in space and time will become an important factor in airport operations especially for lead times of 1-2 hours.

An accurate forecast of wind, turbulence and temperature along the glide paths of an airport is also required to predict the transport and decay of aircraft wake vortices, see Section 2.1. The reason is that the atmosphere in terms of wind speed, wind direction, turbulent kinetic energy, eddy dissipation rate, and vertical stability of air surrounding the vortices affects their horizontal and vertical displacement as well as their decay (see Section 6.1).

For high quality predictions a limited area, high-resolution weather forecast model should be the appropriate choice. Such a model should take into account the orographic and land use characteristics at and around the airport in order to correctly balance the levels of energy, driven by turbulence, surface friction and sensible and latent heat of the air masses in the atmospheric boundary layer. In the past DLR has developed the 'Nowcasting Wake Vortex Impact Variables' model NOWVIV (Gerz et al. 2005) to forecast wake-vortex affecting weather parameters in airport environments. Recently, we use derivatives of the COSMO-DE model with which the German Meteorological Service, DWD, runs operational weather forecasts for Germany. The two derivatives are COSMO-*FRA* and COSMO-*MUC* for the two aerodromes of Frankfurt and Munich, respectively.

Running the model in a rapid update cycle (RUC) mode results in several forecasts with different forecast initial times for a certain forecast time. This so called Time-Lagged-Ensemble (TLE) is a single-model variant initial-condition ensemble-forecast system where the dynamics, the physical parameterisations and the numerics are the same for all members. It provides an estimate of the forecast uncertainties and reduces errors resulting from initial spin-up. An improvement especially of the short term forecasts up to 6 h is expected which is highly relevant for forecasting wake vortices (Section 2.1), thunderstorms (Section 2.3) and wintry weather conditions (Section 2.4).

The COSMO-DE Model and its Limited Area Derivative COSMO-*FRA*

The non-hydrostatic, fully compressible COSMO model has jointly been developed by the Consortium for Small Scale Modelling and is operationally used by several European Meteorological Services. The COSMO-DE version is the high resolution model of DWD using a horizontal mesh size of 2.8 km covering an area of roughly 1200 x 1300 km^2 in Central Europe (Steppeler et al. 2003).

For the application in the Frankfurt Airport area, we took the COSMO-DE model of version 4.2 as the local area model COSMO-*FRA* which is centred at the Airport encompassing an area of 280 x 280 km^2 (see Figure 1). The vertical resolution of the boundary layer is increased amounting to 16 to 90 m corresponding to 19 levels below 1600 m with a total of 50 vertical levels as in COSMO-DE. The horizontal resolution was kept as in the parent model. The numerics and physics packages follow the operational configuration (Baldauf et al. 2011), using a two time level integration scheme based on the Runge-Kutta method of 3rd order and a prognostic turbulence scheme with 2nd order closure (i.e. a prognostic equation for the turbulence kinetic energy). The roughness length used in COSMO-*FRA* is 0.47 m (forest). COSMO-*FRA* made a 24-hour forecast once a day starting at 00 UTC; initial and hourly boundary data were provided by the larger-scale COSMO-EU model and updated every three hours. COSMO-*FRA* was first applied to predict wake vortex transport and decay parameters, so the vertical profiles of wind, virtual potential temperature, and turbulence kinetic energy were output at a 10 min frequency.

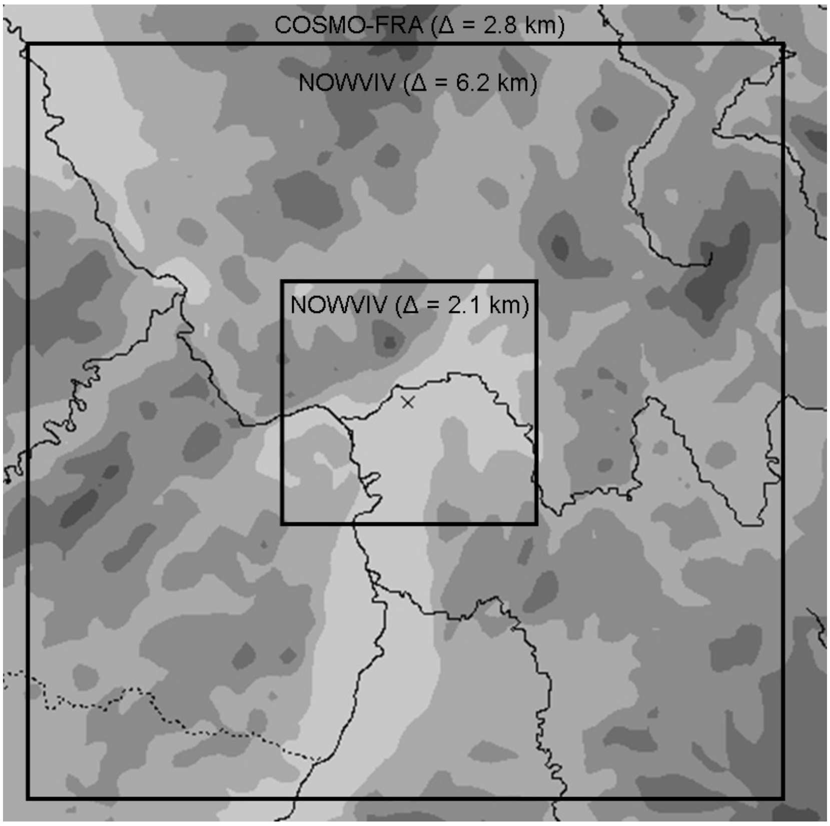

Figure 1. Domain of the high resolution models COSMO-*FRA* and nested NOWVIV centred at Frankfurt Airport. COSMO-*FRA* topography is given in grey shading, rivers in black.

The performance of COSMO-*FRA* has been assessed against NOWVIV predictions and local measurements at Frankfurt Airport by Dengler et al. (2009). One of the outcomes was that an adjusted land use data set for COSMO-*FRA*, possibly combined with higher horizontal and vertical resolutions, to account for specific topographic and land-use features at and around the airport would achieve better forecasts of wind, virtual potential temperature and turbulence kinetic energy in the boundary layer.

The next improvement was to adapt COSMO-*FRA* to version 4.8 of COSMO-DE and start the model hourly in a Rapid Update Cycle (RUC) mode providing short range time-lagged ensemble (TLE) forecasts of up to 6 hours. Figure 2 shows a schematic illustration how the TLE is created showing the available forecasts for an example time of 15:10 UTC. Forecasts starting at 10 UTC (member -5h) to 15 UTC (member -0h) are available with 10-minute output frequency. Therefore, for every 10-minute increment 6 members of the TLE are available. In addition, every full hour a forecast starting 6 hours ago is available creating a 7th member (i.e. for 15 UTC a forecast starting at 09 UTC, member -6h). Finally an equally weighted ensemble mean is calculated from the 6 available members. Further, the spread of the 6 ensemble members indicates the predictability and the related uncertainties of the respective meteorological situation. The model output comprises the three wind components, air density, virtual potential temperature, turbulent kinetic energy, eddy dissipation rate (EDR), and pressure.

The hourly forecasts of the COSMO-*FRA* model were analysed for three cases representing significantly different weather situations as experienced in winter 2006/2007: a frontal passage, stormy conditions and a high pressure system. The results were compared against the reference run starting at 00 UTC with a lead time of 24 hours as used before.

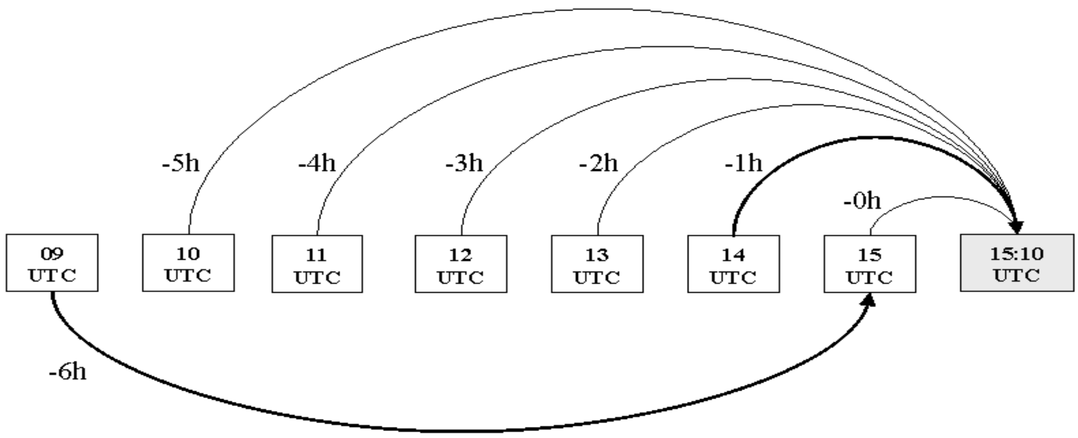

Figure 2. Schematic illustration of the creation of a time-lagged-ensemble (TLE) forecast.

The TLE forecasts were also checked and validated against measurements of vertical profiles of the three wind components, the standard deviation of vertical velocity, and virtual temperature from 60 m up to 1650 m with vertical resolution of 30 m provided by a wind and temperature radar combined with radio-acoustic sounding system run by DFS (Konopka and Fischer 2005) at the airport of Frankfurt.

A detailed discussion of the results is provided by Dengler et al. (2011). It was concluded that TLE forecasts of wind speed and the wind components parallel and perpendicular to the flight/runway direction reduce the mean bias and root-mean-square error in all three cases compared to the reference model run. The improvement of the forecast was most evident in the very short range of 1 - 2 hours as has been found in previous studies (Lu et al. 2007). The 1-hour forecast showed the lowest bias in all cases. In case of the frontal passage all forecasts overestimated the wind speed within the inversion layer up to 1000 m. In the stormy situation forecasts up to 2 hours underestimated the wind speed above 800 m while no consistent trend was observed in case of the high pressure system. The forecasts of turbulence kinetic energy improved below 900 m but not above that altitude. In contrast to the wind forecasts the 1 hour forecast of turbulence kinetic energy showed the largest error caused by initial spin-up effects. Finally, TLE forecasts of virtual potential temperature also improved except in the case of the high pressure system where the root-mean-square error increased significantly compared to the reference run.

No data assimilation had been used in the model runs. This shows that the observed improvement of the forecasts is a result of the hourly rapid update cycle which benefits from more accurate initial- and boundary conditions provided and updated every 3 hour by the COSMO-EU model. The shortest forecast range members of the time-lagged ensemble (forecasts up to 2 hours) were most accurate and the ensemble spread of the members provided useful information about the reliability of the forecasts.

To further improve the forecasts especially on the short range we aimed to assimilate local data measured in the airport environment, e.g., wind and temperature data from profilers or from aircraft (AMDAR) as well as precipitation data from radar (latent heat nudging), into the model. These technical improvements were achieved with another limited area model, this time located at the airport of Munich, COSMO-*MUC*.

The Limited Area Model COSMO-*MUC*

The COSMO-*MUC* setup used a 358 x 358 km^2 domain where the airport of Munich was located in the southeast quarter of the computational domain, i.e. downstream of the main wind direction (see Figure 4 below). The model had a horizontal resolution of 2.8 km and a vertical resolution of 16 to 144 m corresponding to 17 levels below 1100 m above ground. Again, the numerics and physics packages followed the operational configuration of COSMO-DE. The boundary conditions were treated as before with COSMO-*FRA,* COSMO-*MUC* however, calculated the initial conditions by assimilating locally available data from precipitation radar, aircraft (AMDAR), surface synoptic observations (SYNOP), and radio sounding observations (TEMPS) with an hourly update rate (Figure 3). As COSMO-*FRA* also COSMO-*MUC* started every hour instead 3-hourly like COSMO-DE. Forecast parameters included, besides standard model output, also the amount of precipitation which has been used for advanced warning of thunderstorms (Section 2.3) or in winter time (Section 2.4).

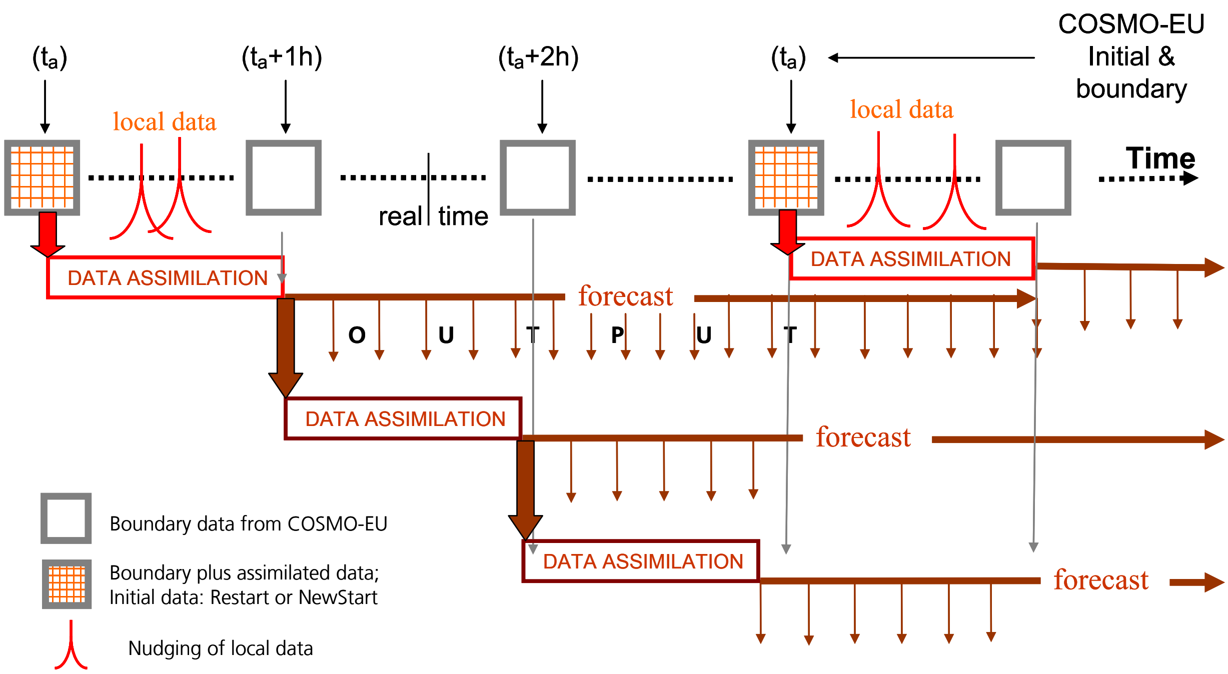

Figure 3: Schematic illustration of the hourly assimilation cycle of the operational mode of COSMO-*MUC*.

Every hour boundary conditions were provided by the operational COSMO-EU model of DWD. New initial data was available every 3 hours from COSMO-EU as indicated by the gridded squares in the upper line of Figure 3 while empty squares indicate the input of boundary data only. Every hour COSMO-*MUC* started from an initial state provided from an analysis run which assimilated local data throughout the past hour (indicated by “local data” and “data assimilation”). In case of a 6-hour forecast run 6 different model outputs were available at any analysis time (see also Figure 2). These TLE forecasts allowed the calculation of probabilities of snow or heavy convective precipitation amount for a certain time. Of course, the configuration could be changed, e.g. by running longer forecasts therefore enabling more members to be combined at any time, or perturbing initial conditions and generate more members. A quite similar approach is undertaken at DWD with the aim to spread an ensemble of 40 members (Schraff et al. 2011).

COSMO-*MUC* has also been used to analyse the improvement of precipitation forecast of convective systems (Figure 4). The predicted reflectivity fields at 850 hPa were compared to COSMO-DE forecasts and reflectivity data from radar (Figure 5) employing the displacement amplitude score (*DAS*) technique (Keil and Craig 2009). *DAS* is a field verification measure for precipitation forecasts that combines weighted distance and amplitude errors:

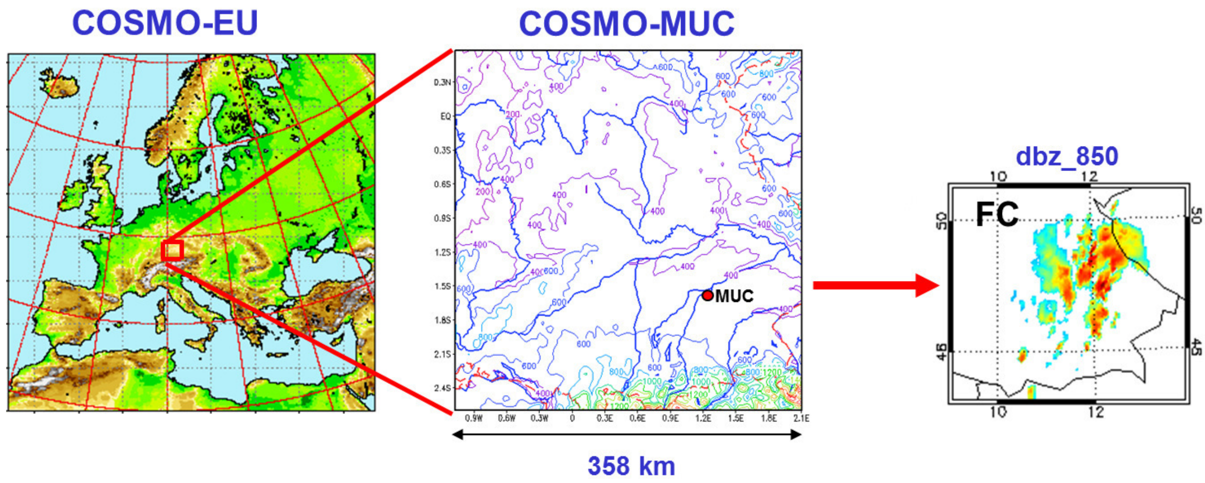

Figure 4: COSMO-*MUC* model chain for Munich Airport (MUC). Hourly boundary conditions updated every 3 hours were provided by COSMO-*EU*. COSMO-*MUC* provided forecasts of the reflectivity at 850 hPa as a guess for the amount of precipitation.

$$DAS = \frac{DIS}{D_{\max}} + \frac{AMP}{I_0}$$

It is based on an optical flow algorithm that defines a vector field that deforms, or morphs, one image to match another. When the forecast field is morphed to match the observation field, then for any point in the observation field, the magnitude of the displacement vector gives the distance to the corresponding forecast object (if any) yielding a "displacement error field" (*DIS*), while the difference between the observation and the morphed forecast is the "amplitude error" (*AMP*); I_0 is a **c**haracteristic intensity averaged out of 5 thunderstorm cases. If observed and forecast features are separated by more than a prescribed maximum search distance (D_{max}), they are not matched to each other, but they are considered to be two separate amplitude errors, i.e. a missed event and a false alarm. *DAS* constitutes a single measure of forecast quality and has the advantage to avoid double penalties. The smaller the values of *DAS*, *DIS* and *AMP*, the better is the prediction.

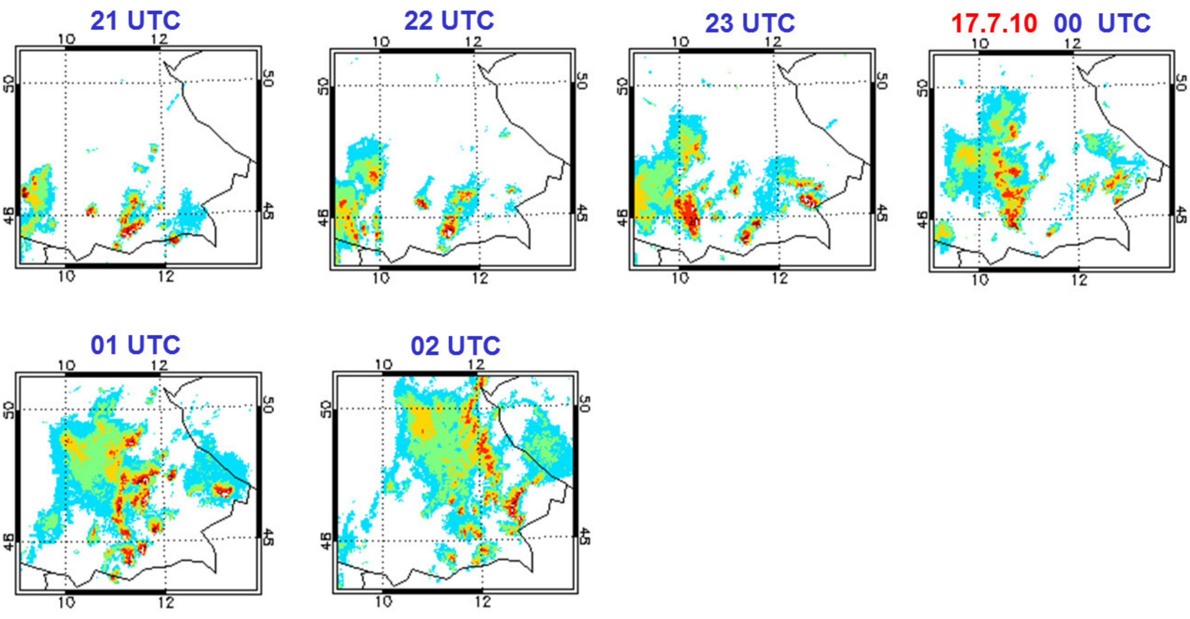

Figure 5: Observed precipitation fields of the passage of a convective system on 17th July 2010.

In our case study of a convective situation over Southern Germany from 16th of July at 21 UTC to 17th of July 2010 at 02 UTC (Figure 5), DAS compared the predicted 850-hPa reflectivity fields from COSMO-DE and COSMO-*MUC* with the observed precipitation field from radar measurements: A vector field was calculated to morph the predicted field on the observed field such that the error was minimised. Thereafter, the vector field was applied to the predicted field and by comparing with radar observations the domain-averaged errors DAS, its components DIS and AMP, as well as the false alarm ratios (FAR) and the biases (FBI) were calculated. This procedure is demonstrated in the figures below; both models started at 21 UTC on 16.7.2010 and forecasts are compared to observations at 01 UTC on 17.7.2010. Figure 6 shows the COSMO-*MUC* forecast without data assimilation, Figure 7 depicts the COSMO-*MUC* forecast including data assimilation.

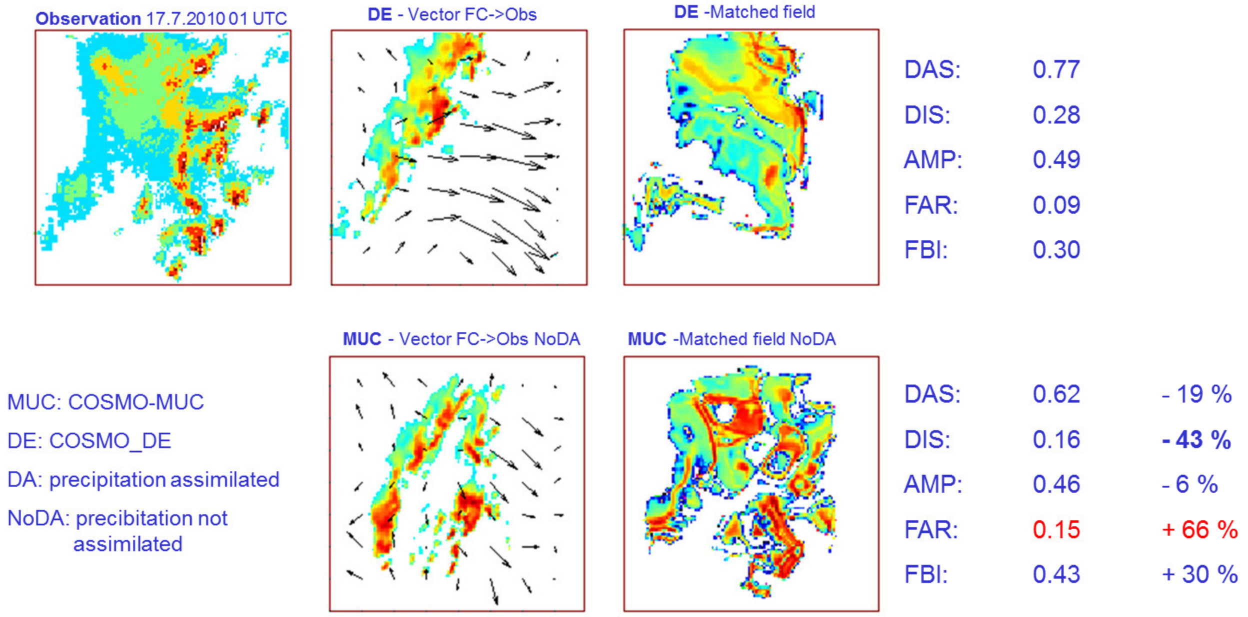

Figure 6. Four-hour COSMO-*MUC* (without data assimilation) and COSMO-*DE* runs from 16.7.2010 21 UTC: Observed precipitation from radar (upper left), operational DE-forecast with vector field (upper middle) and the matched DE field (upper right). Below the vector field and matched field for the COSMO-MUC run are shown, respectively. The values of the main error parameters are displayed as well as the change in error when using COSMO-*MUC* instead of the operational COSMO-DE.

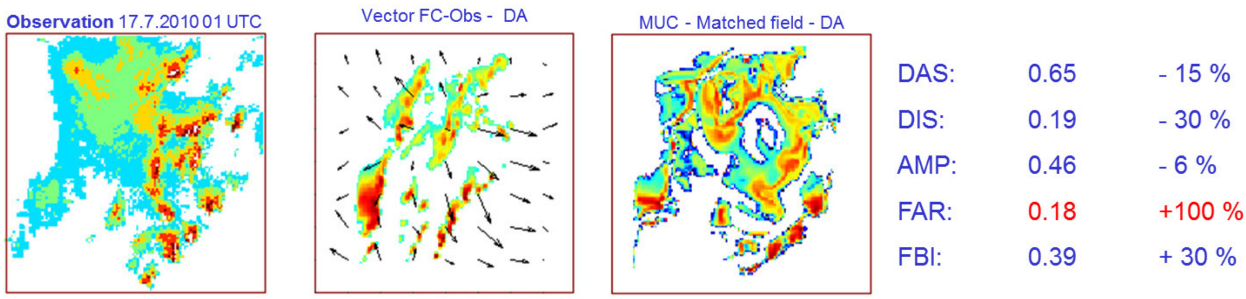

Figure 7. As Figure 6 but with data assimilation in COSMO-*MUC*.

Both figures reveal that the forecasts of COSMO-*MUC* (with and without assimilating observation data) improve compared to COSMO-DE forecasts. Although the COSMO-*MUC* runs with data assimilation are somewhat less accurate than the runs without data assimilation on average (compare the DAS values 0.65 and 0.62, respectively), it is worth to note the some details as the strong convective band in the southeast corner of the observed field are very well predicted when including data assimilation. The analysis of five more cases revealed that the displacement error was reduced in the first 3 hours but the amplitude error increased (indicating that the event was underestimated by the model).

These are preliminary results and more cases have to be analysed to get a thorough assessment. The dependency of DAS on the search radius, precipitation threshold and on the domain size and temporal value of the averaging has to be investigated in more detail. Finally, one has also to keep in mind that the comparison of the 850-hPa reflectivity filed with observation from the precipitation radar can have some notable influence on DAS, especially on AMP.

Conclusion

The two limited area models COSMO-*FRA* and COSMO-*MUC*, which were derived from their parent model COSMO-DE of the German Meteorological Service, were used to obtain frequently updated highly resolved predictions in the aerodrome areas of the airports of Frankfurt and Munich in Germany. Tests showed that the prediction accuracy of wind, turbulence kinetic energy and temperature generally improved with time-lagged ensemble forecasts when updated each hour. We then employed the recently developed displacement amplitude score technique to assess the quality of convective precipitation forecasts and confirmed the previous finding of better prediction accuracy by rapid forecast updating also for precipitation patterns. On the other hand, we found that the assimilation of local data (nudging of precipitation, AMDAR, SYNOP, and TEMP data) did not improve the forecast quality further in the statistical mean but provided some accurately forecasted rain pattern locally.

The limited area models will be evolved further in the future. We might advance to finer spatial resolutions of the horizontal and vertical scales requiring adaptations of the sub-grid closures. Also to use adequately resolved data bases of topography and land use at and around the airports is envisaged to ensure a better representation of the local boundary layer physics and energetics.

We will apply COSMO-*FRA* and COSMO-*MUC* to predict aircraft wake vortex separation minima and to combine the forecast of thunderstorms and wintry weather conditions with observations and nowcasting techniques in the WxFUSION environment, see Section 2.2.

References

Baldauf, M., A. Seifert, J. Förstner, D. Majewski, M. Raschendorfer, T. Reinhardt 2011: Operational Convective-Scale Numerical Weather Prediction with the COSMO Model: Description and Sensitivities. Mon. Wea. Rev. 139, 3887-3005.

Dengler K., Keil C., Frech M., Gerz T., Kober, K. 2009: Comparison and validation of two high-resolution weather forecast models at Frankfurt Airport. Meteorologische Zeitschrift, 18, Nr. 5, 531-542.

Dengler K., Anger J., Keil C. 2011: Validation of high-resolution time-lagged ensemble wind forecasts. Meteorol. Z. 20, 625-634.

Gerz T., Holzäpfel F., Bryant W., Köpp F., Frech M., Tafferner A., Winckelmans G. 2005: Research towards a wake-vortex advisory system for optimal aircraft spacing, Comptes Rendus Physique Vol 6 , 501-523.

Keil C., Craig G. 2009: A displacement and amplitude score employing an optical flow technique. Weather and Forecasting, 24, 1297-1308. DOI: 10.1175/2009WAF2222247.1.

Konopka J., Fischer H. 2005: The wake vortex warning system at Frankfurt Airport. — Proc. 24th Digital Avionics Systems Conf., Washington, DC, IEEE 3.A.6-31-14.

Lu C., Yuan H., Schwartz B.E., Benjamin S.G. 2007: Short-range numerical weather prediction using time-lagged ensembles. — Wea. Forecasting 22, 580-595.

Schraff C., Reich H., Rhodin A., Potthast R., Blahak U. Stephan K., Zeng Y., Epperlein D., Leuenberger D., Weusthoff T., Tsyrulnikov M., Gorin V., Iriza A., Lazanowicz M., Torrisi L. 2011: COSMO Priority Project KENDA for Km-Scale Ensemble-Based Data Assimilation, 9th SRNWP Ws. Non-hydrostatic Modelling, Bad Orb, 16 – 18 May 2011

Steppeler, J., G. Doms, U. Schattler, H. W. Bitzer, A. Gassmann, U. Damrath, G. Gregoric: Meso-gamma scale forecasts using the nonhydrostatic model LM. — Meteorology and Atmospheric Physics 82, 2003, 75-96.

3. Risk and Economic Assessments

3.1 Economic Assessment of a Wake Vortex Advisory System

Alexander Lau[1] , Sandro Lorenz[2], Alexander Scharnweber[2], Wilfried Gerling[2]
[1] *Institute of Air Transportation Systems,* [2]*Institute of Flight Guidance*

Airport capacity constraints and growing traffic demand in air transportation cause congestion and delay on the ground and in the air. Conservative wake vortex separation minima in the approach phase guarantee a minimum of in-flight wake encounters of trailing aircraft but do not always fit possible weather-based separation minima and therefore throughput performance of an airports runway system. This work estimates delay rates and economic benefits of DLR`s WSVBS regarding delay reduction potential through the application of reduced time-based approach separations for a single and dual-dependent runway system. A delay analysis provides the relevant delay data, whereas several operational scenarios enabled through the application of reduced separations are considered. Under specific implementation assumptions the results give insight about possible delay reductions and related beneficial impact. Several economic scenarios are applied to show the potential economic value of the system.

Introduction

Throughput is a major requirement for airports to generate economic value (Graham 2008). In this sense aviation and non-aviation revenues are closely related to the overall efficiency of airside and landside processes. Especially the capacity of an airports runway system represents an important technical foundation for airside performance. Many technical and operational approaches exist to safely increase throughput within the final approach and landing phase at highly congested airports.

The installation of a WSVBS is mainly driven by two points. The first is to generate additional controller information regarding the existence, the strength and the position of wake vortices within the final approach- and/or departure-corridor. The second operational and economic driven motivation is to increase runway capacity by decreasing minimum separations below conservative ICAO separations.

Increasing airport related throughput improves its quality of service to airlines, which is defined as the average delay rate per movement (Ashford 1997). This is, despite increasing the general capacity value of an airport, suspected to be the major area in which economic benefit can be generated by a Wake Vortex Advisory System within the approach phase.

Under instrument meteorological conditions (IMC) radar separation is applied between approaching aircraft. Depending on the special circumstances of the particular airport this is determined to 3 NM, 2.5 NM or even 2 NM. Due to a possible risk of wake vortices, increased separations have to be accomplished between particular categories of aircraft. At most airports the wake vortex separation rules set up by ICAO are applied which require extended separation distances of 4 NM, 5 NM, or 6 NM depending on the assigned ICAO weight classes (Heavy, Medium, Light) of the concerned aircraft (leader and follower).

To increase airport capacity for landing aircraft, DLR has developed a wake vortex advisory system named WSVBS (“Wirbelschleppen Vorhersage- und -Beobachtungssystem”). The WSVBS is intended to dynamically adjust aircraft separations dependent on weather conditions and the resulting wake vortex behaviour. It is based on a precise and sophisticated weather model (NOWVIV) which especially predicts the local wind conditions. Another model builds up the creation, propagation, migration, and decay of the vortices (P2P). Both models allow predicting the individual area of risk behind an aircraft on final approach. Possible deviations from the intended flight path are considered as well. Together with a safety area predictor model (SHAPe) the necessary separations are calculated as the required minimum time intervals between leading and following aircraft during in-trail and dependent parallel approaches.

The system originally was designed for the closely spaced parallel runways of Frankfurt Airport which cannot be operated independently, i.e. increased wake vortex separations of 4 NM, 5 NM or 6 NM have to be applied between any two aircraft established on different glide slopes (e.g. 25R and 25L) if the leading aircraft is “Heavy” or for the combination “Medium” before “Light”.

In order to enhance landing capacity at Frankfurt Airport the German Air Navigation Service Provider DFS has established three alternative modes of operation for aircraft separation for the dependent parallel runway system under instrument meteorological conditions (IMC). These can only be applied on favorable weather conditions (esp. favorable crosswind) and require the use of a wake vortex advisory system such as DLR’s WSVBS (Gerz et. al 2009) or DFS’s wake vortex warning system, WSWS (Konopka 2005). In these modes reduced separations (merely radar separation instead of wake vortex separation) may be applied between particular aircraft which are landing on different runways. However, in all modes, the aircraft in-trail (approaching the same runway) remain separated according to ICAO standards. Due to the lack of a well-accepted wake vortex advisory system these DFS modes are not operationally up to now.

As a first step in applying WSVBS for operational use the calculated separation times are transformed into the appropriate DFS modes (Staggered, Modified Staggered Left, or Modified Staggered Right). This method does not take the full advantage of the system because the applied separation times are restricted to present values which correspond to the distances laid down in the ICAO separation matrix. Sometimes the proposed minimum separations from WSVBS are below those from the ICAO standard. For that reason a second operational mode was defined which directly uses the actual WSVBS output data as minimum separations between pairs of aircraft depending on their weight categories.

However, using aircraft’s weight categories (e.g. Heavy, Medium or Light) may possibly not be the best way to assign adequate minimum separations for a pair of aircraft. New modern aircraft may be designed to produce fewer vortices and to better cope with the incursion of a vortex from another aircraft. For that reason the WSVBS was modified so that it evaluates pairs of aircraft types instead of aircraft weight categories.

The system has best performance on parallel dependent runways due to occasionally using radar separation instead of wake vortex separation. However, still a benefit can be expected for the performance of single runway operations due to the fact that calculated WSVBS-separations below ICAO separations are generated by the system.

The goal of this analysis is to determine the possible reduction of delays. This can be evaluated by fast time simulations and/or analytical computations.

Assumptions

There are several studies which discuss the subject of airport productivity enhancement through higher runway capacity in consequence of reduced approach separations (e.g. Roelen et. al 2001, Hemm et. al 1999 and Ballin 1996). Most of these studies focus on the computational background and modeling methodology laying down specific assumptions regarding the operational implementation. A performance based operational analysis of such a safety related system requires assumptions regarding system functionality and reliability.

System Failures

System failure cases of a WSVBS are defined in this study as

i) System breakdown. In this case, the controller is not obtaining any WSVBS separation information during the time of malfunction.

ii) Decrease of system reliability. In this case the WSVBS separation information the controller obtains from the system is not reliable enough for operational use.

Especially the second failure case needs to be clearly indicated to the controller, which postulates a monitoring functionality regarding the system functional states.

Both failure cases cause controller actions changing the separation mode from WSVBS-based separations back to ICAO wake vortex or individual minimum separations. The high level of complexity of high intensive approach- and runway operations will lead to adaptations of approach sequences during these transition times. Aircraft might have to be “curved out” of the final approach path or hold for a higher period of time. Those “failure” scenarios are likely to be more cost intensive than the baseline ICAO standard approach procedure compared to regular WSVBS operations. Furthermore it depends on the time of day a failure case occurs and its duration on how much cost of time and economic loss it causes. It is therefore highly speculative to integrate system failures into a performance assessment of the WSVBS. Assuming that the certification requirements for an ANSP based airport system will be defined according to EASA (2009), both failure cases will evolve with a probability of 10^{-9} each. That would mean that effects would be classified as *catastrophic*. However, irregular operations are not part of this study.

Weather Predictability

Approach controller of complex airports today are supported by the Arrival Manager AMAN. The AMAN is a tool which supports the controller who is responsible for the final approach in establishing the required approach separations, approach speeds and approach sequence for maximum throughput. It enables pre-planning for each approaching flight at the entering point into the Terminal Maneuvering Area (Metering Fix) of an airport. On the basis of traffic sample data, actual radar positioning data, A/C types, separations etc. the AMAN generates target times at which the flight needs to fly over specific fixes (e.g. threshold). By estimating possible earliest and latest threshold times, the AMAN generates an approach sequence like depicted in Figure 1. Every flight is shown as a label following a timeline shown in the center.

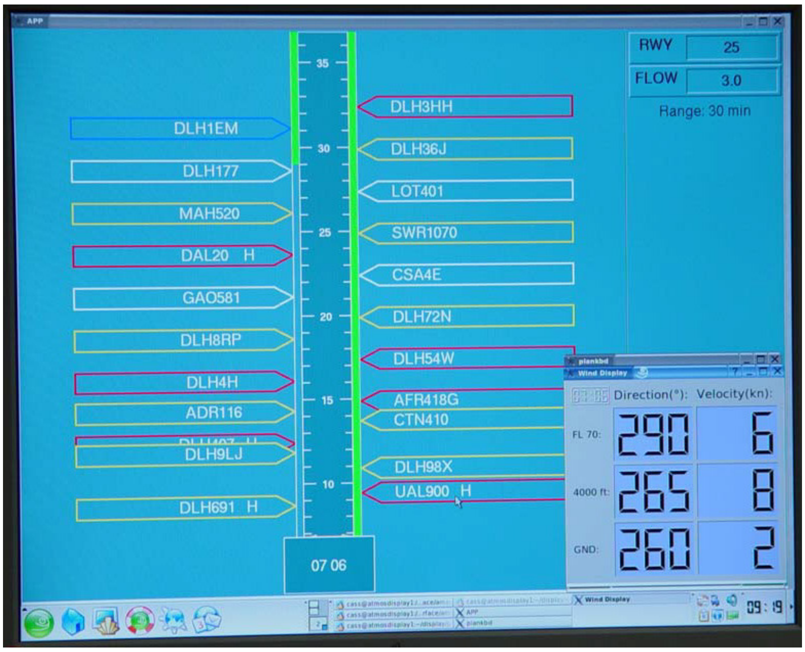

Figure 1. AMAN Display. (Gerling et al. 2008, Source: DLR)

According to Gerz et. al (2009) WSVBS separation information obtained to the controller is updated each ten minutes and predicts separations for the next 60 minutes. This information will be processed by the AMAN, which causes the possibility that the predicted time-based sequencing (which is a proposal for the controller) will change according to dynamic wind predictions. If the prediction horizon of the WSVBS is falling beneath the controller’s planning horizon, the sequence during the final approach might have to be changed, which again causes cost in time and money. In that case the transition phase for the sequencing at the final approach induces additional costs, which are not taken into account within this study. It is assumed that the vortex prediction is perfect even during highly stochastic changes of the wind direction in the approach path.

Methodological Approach

Capacity and flight planning at capacity regulated airports is subdivided into different phases. These phases have different lead times. In the strategic planning phase which starts about several months before the day of operation, the stakeholder community trades available airport slots. At that time the maximum practical capacity and therefore the maximum number of available slots at an airport has to be known, which means that a tactical capacity increase based on weather cannot be integrated into this decision process. It is therefore not appropriate to focus this study to runway capacity enhancements according to WSVBS separations.

It is rather reasonable to focus more on tactical or short-term capacity effects based on WSVBS predictions. These short-term effects are based on a delay-reduction potential. Regarding runway capacity, delay is defined as "*the difference between the time it would take an aircraft to be served without interferences from other aircraft and the actual time it takes the aircraft to be served*" (FAA 1973). Delay is a service measure impacted by runway congestion. If congestion increases, delay increases according to the arrival queuing length, which again is directly impacted by the service time per aircraft.

Figure 2 shows the variety between strategic capacity enhancements on the cost of increasing delay rates and tactical delay reduction due to improved capacity (application of WSVBS separations while keeping the number of arrivals constant). Regarding tactical delay management measures at hub airports, the service quality is mostly predefined to a specific value, usually 4 or 8 minutes.

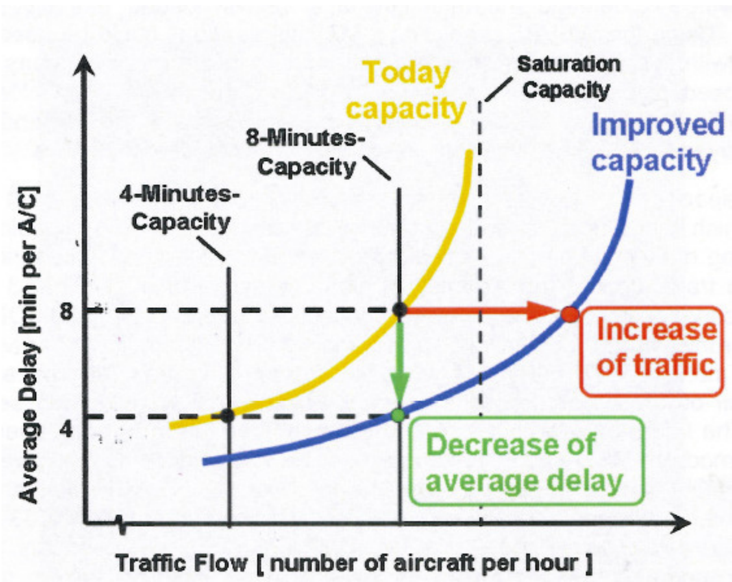

Figure 2. Relation between average delay versus traffic flow (Gerz at. Al 2008)

Delay Model

A delay model has been employed which can be categorized as process simulation model. The model integrates representative traffic data as well as WSVBS separations to generate individual delay rates according to chosen scenarios. The model uses the runway threshold as geometric reference, which allows neglecting physical flight characteristics like approach speeds along the common approach path from the final approach fix (entry gate) to the threshold. This is possible if the schedule which serves as traffic input data contains individual on-block times, from which the threshold time can be calculated by subtracting an average taxi-in time.

Figure 3 shows the time-space-dimension of the final approach and landing process. Capacity calculation models use merging or entry fixes (like stated left and middle) as reference points which allows modeling more realistic traffic scenarios and specific airport/airspace layouts. The opening case represents the scenario in which the leader has a higher approach speed than the follower (which is put down on the weight class). The closing case represents the other way in which the separation at the entry gate has to guarantee a sufficient separation at the threshold. Using the threshold as the reference point the delay model directly calculates this critical separation by applying the WSVBS minima. This does not imply that these minima are allowed to be under run at one of the outer gates along the approach path but guarantees a maximum delay performance in runway utilization.

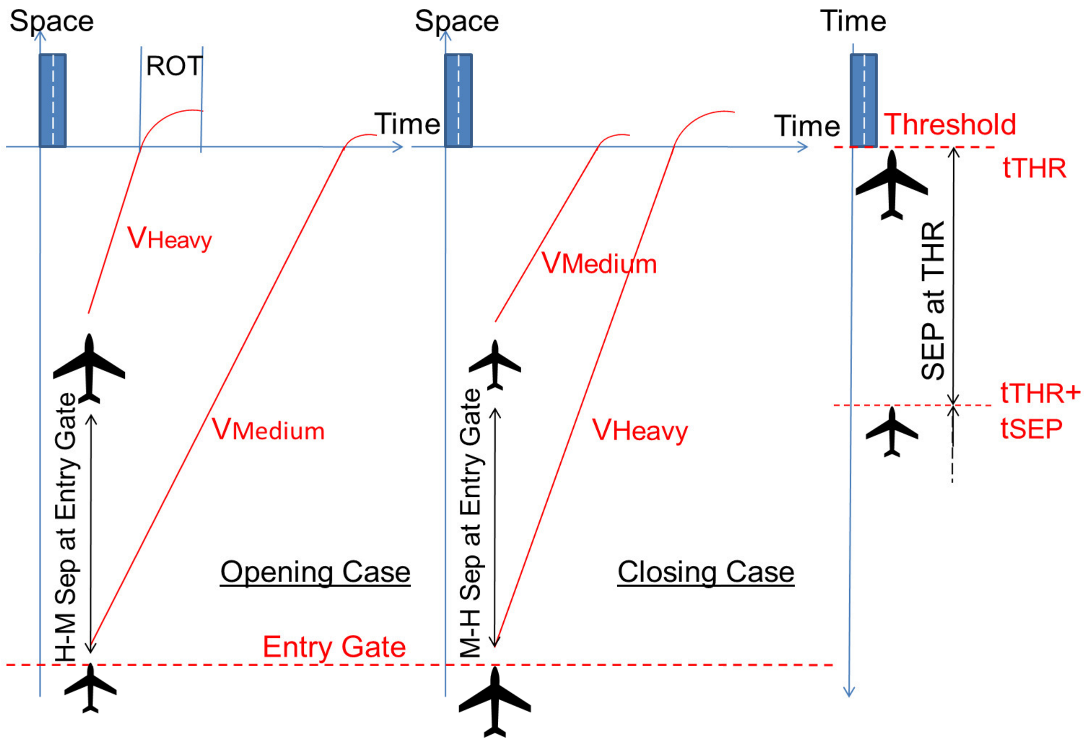

Figure 3. Time / space dimension of the final approach and landing process, left: Heavy leader, Medium follower, middle: Medium leader, Heavy follower, right: time-/separation-base delay calculation at THR.

The WSVBS generates minimum target separations which represent the lower limit under which no aircraft pairing is allowed to be separated without endanger flight safety for the trailing aircraft. In a first step these separations are processed by the delay model to account for position uncertainties so that the applied separations consist of the WSVBS minima plus an "uncertainty" share. This additional share covers controller- as well as position-inaccuracies and is usually known as separation buffer. The static part of this buffer is inserted intentionally by the controller. The dynamic part reflects the position-inaccuracies and is usually pilot-driven. The latter is normally distributed with a 2σ (95.45%) standard deviation of a predefined position-inaccuracy. Figure 4 depicts the described correlation between WSVBS separation minima and real applied separations in the delay model.

According to the fact that the applied separations depend on the standard distribution and the position violation, it is important to use realistic values. Figure 5 shows the process chain of the delay calculation model. After calculating the individual separations according to the separation mode and A/C pair the model compares the planned times of the trailing aircraft with the sum of the actual time of the leading aircraft plus separation. This is always done for the schedule of a whole day.

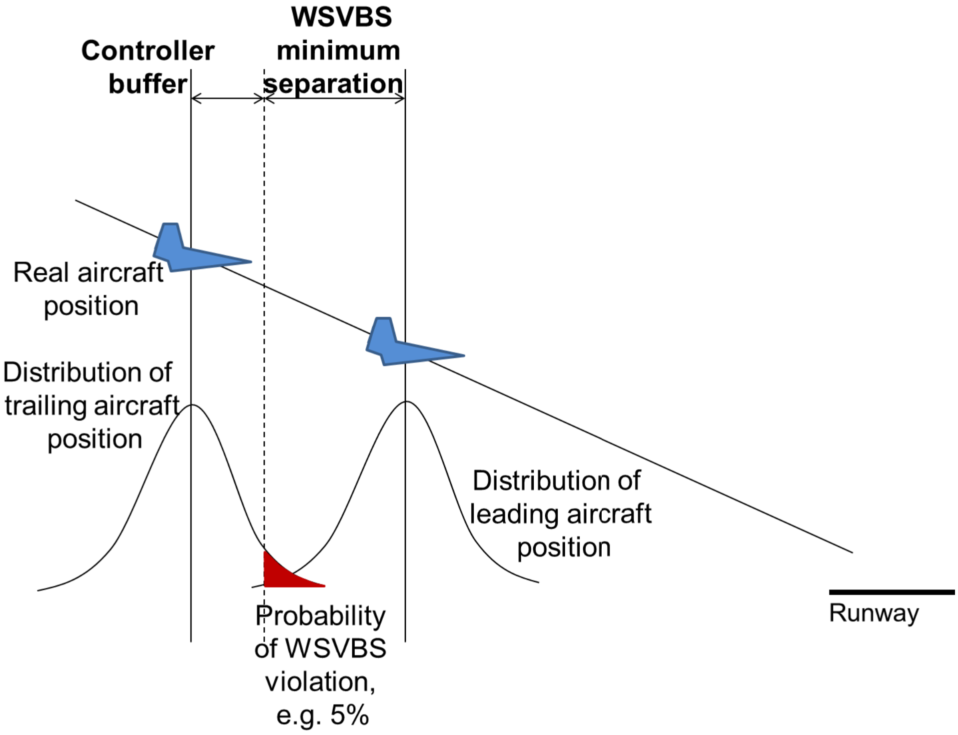

Figure 4. Separation buffer and position-inaccuracy

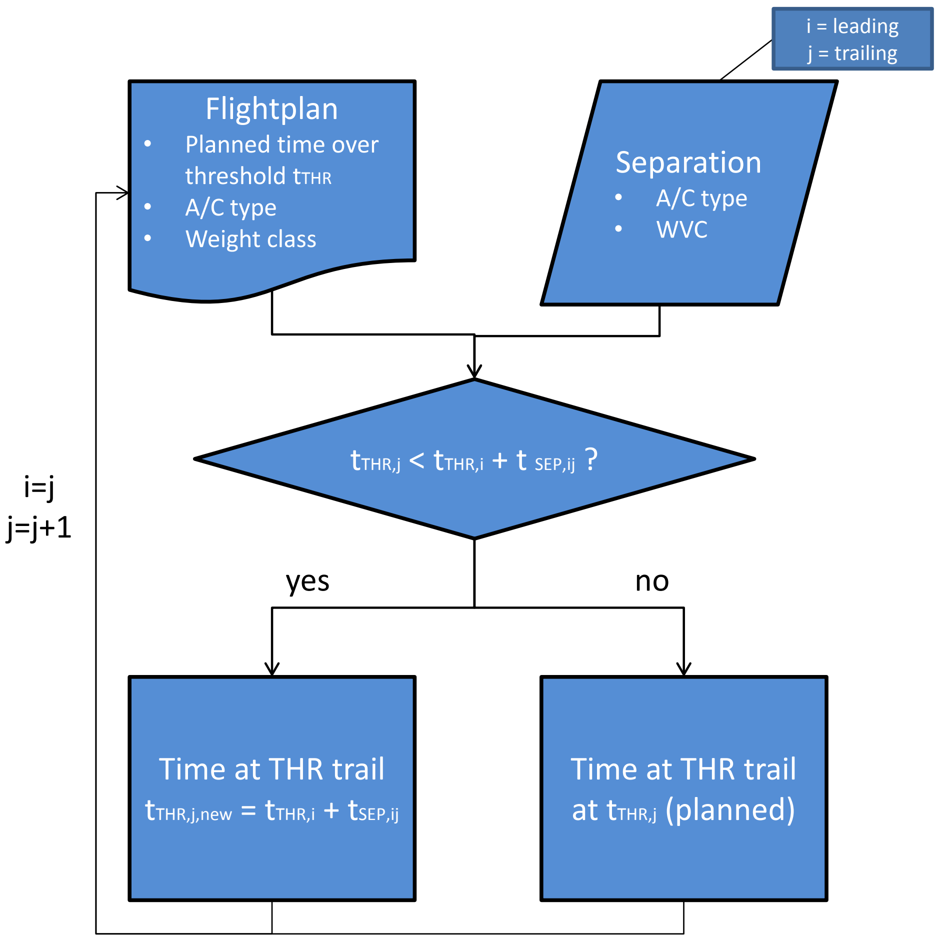

Figure 5. Process chain delay calculation

Economic Model

The economic assessment of the WSVBS is based on the analysis of arrival delay rates of ICAO and WSVBS separation modes and the subsequent economic quantification over several years. This analysis is conducted for the dual-dependent runway system.

The study gives an impression of the economic impact of a WSVBS investment decision over the life cycle of the system. This is done regarding delay reduction without partitioning costs and benefits to specific stakeholders of the aviation community. However, it is common sense that such an airport system induces costs and benefits throughout the air transportation system. Since the main interest of this work focuses on the economic potential of the WSVBS for the dual-dependent runway system the argumentation and the results in this study do not go further than this. Furthermore there is no available separation dataset for a whole year regarding the single runway system yet. At this point it is mentioned that the results are not related to a specific airport rather than giving an idea on how much a WSVBS under specific assumptions of implementation on a dual-dependent runway system can be economically worth.

The most common method to judge the economic viability of an investment is to generate its Net Present Value NPV (Wöhe 2008). The NPV is a dynamic investment calculation value which relates investments carried out at different times to one single time through compounding and discounting on a yearly basis. In other words, decision makers get an idea of better investing their capital on a bank receiving an interest *or* investing it in a business. This is the reason why the NPV is sensitive to the interest rate. It is defined by the following equation:

$$K_0 = \sum_{j=1}^{n} (E_t - A_t) * \frac{1}{(1+\mathrm{i})^2} \tag{1}$$

where E_t is the yearly investment, A_t is the yearly benefit and $\frac{1}{(1+\mathrm{i})^2}$ is the discount factor with *i* as required rate of return.

It is fundamental to generate yearly investment and benefit rates to constitute the economic viability over time. This implies traffic prognosis and weather data input for the system life cycle for a representative depreciation duration of about 10 years (for more detailed information see Bundesministerium der Finanzen 2000). The economic model therefore consists of several modules which are listed in Figure 6.

Based on realistic traffic rates of 2009 the traffic forecast has been conducted for Frankfurt Main International. Even if this study intends to focus a generic runway system, it is necessary to use traffic rates that guarantee realistic demand forecasts. Furthermore it is important that the demand forecasts represent a moderate to high level of congestion establishing a representative busy hour rate. The portioning between arrival and departure traffic rates is part of the scheduling module. The forecast is done for the years 2010 to 2020 and is based on Intraplan (2008) predicting an average growth rate in flight movements of approximately 2.4% p.a. for Frankfurt Main International.

Additionally an extrapolation of yearly traffic rates from 1991-2009 is conducted which indicates an annually growth rate of approximately 1.8%. This fits the so-called “*Prognosenullfall*”. This hypothetic case describes a static airports infrastructure without operationalization of additional runways from 2010 to 2020. However, this setup causes high delay rates. Again, the study focusses a generic dual-dependent runway system and is not related to a realistic airport case. Table 1 contains numbers of the latest Eurocontrol long-term forecast regarding IFR movements in Europe related to a base year (in brackets). These numbers imply that a yearly growth rate of 2.0% represents a conservative estimation.

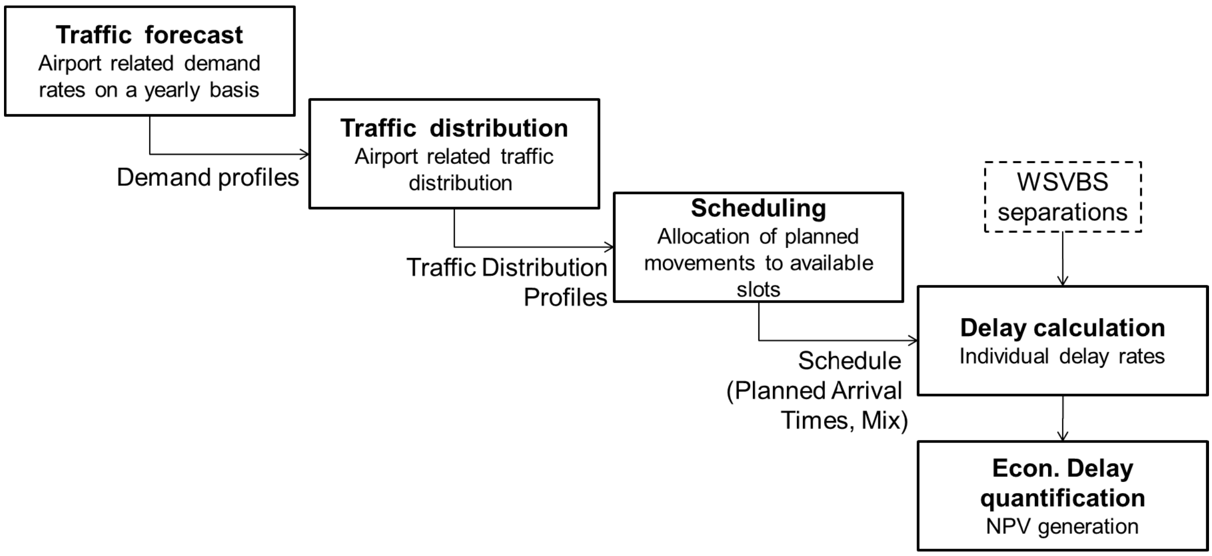

Figure 6. Economic quantification model

Table 1. Average annual growth for IFR flight movements in Europe (Eurocontrol 2010)

year (base year)	**2015** (2010)	**2020** (2015)	**2030** (2009)
growth [%]	2.9	2.5	2.8

Figure 7 shows the demand profile (dashed line) within the upper and the lower bound. The traffic distribution model generates traffic profiles for each day of a year. This is done by given monthly, weekly and daily traffic distribution profiles of the year 2009 (Fraport 2010). It is assumed that these profiles are representative for future schedules. The future traffic profiles are generated by stochastic distribution within the conditions of the given profiles and are shown exemplarily in Figure 8.

The generated demand profiles serve as input data for the generation of the schedule, which contains scheduled landing times. A representative daily schedule serves as pattern for the distribution of hourly traffic counts to available airport slots, which allows spreading the movements more realistically over one hour. An hour is thereby subdivided in 12 bins according to the 5 minute time-grid of planned arrival times each representing a single slot (5 minutes before the planned arrival time to 10 minutes after the planned arrival time). The individual *arrival* slot capacity is thereby derived from the respective capacity value multiplied by the arrival share of the representative schedule which is also cut down to pure arrival shares. Table 2 contains an extract of an exemplary schedule which contains traffic mix information and planned threshold times serving as input for the delay model.

Although delay cost affect the whole aviation industry from the passenger to the airport, airlines burden the majority of emerging delay costs. Even if not always directly accountable to an airlines cost calculation, delay cost at least concern airlines indirectly. The cost of delay can be calculated separately for strategic and tactical delay for different phases of flight. Strategic delay costs are those cost which occur by adding a buffer to the airline schedule in advance. This provides elasticity to the schedule against unpredictable events like technical malfunction or extended turnaround durations.

Tactical costs of delay are those cost which occur on the day of operation. They are mainly dominated by crew cost, passenger cost of time and fuel burn and arise if planned schedules are timely exceeded by actual operations. This is triggered by congestion and unpredictable events like weather.

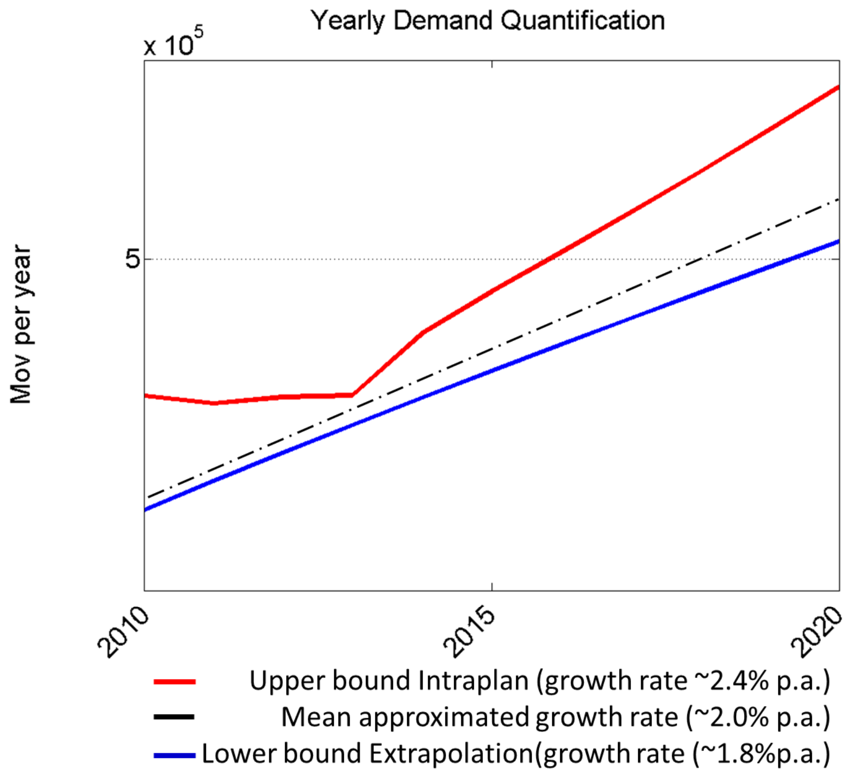

Figure 7. Demand profiles for Frankfurt Main International: yearly number of movements (*100.000) for the years 2010 to 2020. The stagnation of the upper bound prognosis left results from careful forecasts regarding the ongoing economic crisis whereas the lower bound forecast represents an ongoing demand extrapolation of the years 1991 to 2009. The upper bound profile represents the "*Planungsfall*" (additional runway capacity at an hourly capacity value of ~126Mov/h) and the lower bound profile represents the "*Prognosenullfall*" (static airport infrastructure at an hourly capacity value of ~86Mov/h). This study is based on a yearly growth rate of approximately 2,0%.

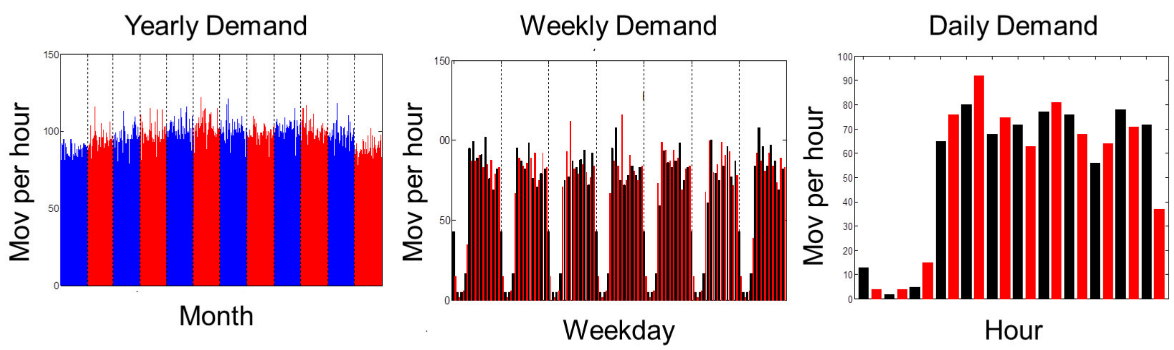

Figure 8. Modeled demand profiles for on an hourly basis for one year (left), one week (middle) and one day (right)

Crew costs are not paid uniformly throughout the airline community. Different salary types exist which complicate the way delay cost can be quantified. For example time-based salaries when the crew is paid by block hours differentiate against cycle-based salaries where the crew is paid by sectors flown. In addition cockpit crew salaries increase with the aircraft size, whereas cabin crew salaries are more or less independent against this. However, European airlines mostly pay fixed salaries with flying-time and cycle-based allowances (University of Westminster 2011).

Table 2. Exemplary schedule (excerpt)

A/C typ	Rwy	hour	minute	second
Heavy	Left	7	05	00
Heavy	Right	7	05	00
Medium	Right	7	10	00
Heavy	Left	7	15	00

Passenger delay costs are subdivided into “soft” and “hard” costs. Soft costs focus more on the passenger tolerance of delay (which can be assigned to the airline) whereas hard costs quantify the direct cost of lost time to the passenger. This of course is strictly driven by aircraft sizes and load factors.

This study focuses on delay arising in the tactical approach segment which can be scaled to the network level. At this level, another two types of delay occur: primary and reactionary delay. Primary delay arises by a single flight initially running late. This flight causes knock-on effects, e.g. by blocking gates at an airport longer than planned. These knock-on effects cause other flights to hold and therefore to be delayed. Especially when primary delays occur early in the day it is hard for an airline to reduce the amount of reactionary delay coming back to the planned schedule. At this point lays the link between strategic delay (buffering) and tactical delay. Reactionary delay costs are included as cost sensitivity into the delay cost calculation.

Potential delay reduction

Meteorological Data

The WSVBS provides a delay reduction merely under favorable weather conditions, i.e. special crosswind situations. Therefore the results of this analysis strongly depend on the selected weather scenario which is represented by system proposed separations. The selected weather scenario should either be representative for the entire cycle of a year or for a special season of the year. On the other hand only a sample of 66 days was available for evaluation provided by the DLR institute of atmospheric physics. Those were the days 2006/Dec/20 to 2006/Dec/31 and 2007/Jan/06 to 2007/Feb/28. From this winter season 6 single days were selected which meet the following requirements and conditions:

- The distribution of the 6 days selection should be quite similar to that of the total 66 days.
- The selected 6 days should be spread over the whole period from 2006/Dec/20 to 2007/Feb/28.
- The 6 days selection should comprise some changes between the DFS modes (Staggered, Modified Staggered Left, Modified Staggered Right, or ICAO separation).
- Days with the same mode in more than 90 % of time are considered as homogenous and therefore not included in the analysis.
- The WSVBS separation should sometimes be significantly below the ICAO standard.
- For selecting the representative 6 days only the day times (from 6 am to 22 pm) are evaluated.

With these constraints the following 6 days were identified for evaluation: Jan/07, Jan/18, Feb/09, Feb/11, Feb/15, and Feb/27.

Traffic Data

With regard to the analysis of a WSVBS introduction to a dual-dependent runway system as well as a single runway system, matching traffic samples have to be applied. These daily traffic samples need to represent realistic demand profiles for the respective runway systems and – to promote the optimal application of a WSVBS – need to be close to practical capacity. Representative daily traffic samples of Frankfurt Main International serve these requirements. One representative daily traffic sample for the dual-dependent runway system has been made available for the analysis (2009/Apr/04) whereas the traffic sample for the single runway system is based on prognostic data of the year 2020 (Fraport 2006). This makes it difficult to compare the results between the different runway systems. However, due to the fact, that the separation modes for the different runway systems differ from each other, a comparison of these results is not foreseen.

Aircraft Types for individual separations

For the single runway system the WSVBS also predicts conservative separations for individual aircraft. This approach requires that the approaching aircraft types are known. The selection of aircraft types is based on the used traffic sample 2020 as well as on the aircraft database of the latest WSVBS version. Not all aircraft types and especially no future aircraft types (e.g. A350) have been integrated into the WSVBS yet so that some types have been replaced according to the (estimated) MTOM to account for relevant aircraft parameters like safety-area dimension. Heavy leader aircraft types (aircraft designators according to ICAO) are A333, A332, A343, A346, B764, B772 and medium follower types are A320, A321, B733, B734, B735, B737, B738, B773, CRJ1 and RJ85.

Scenarios

Table 3 gives an overview on the scenarios undertaken for the potential delay reduction analysis. In total 29 calculation runs have been conducted. The base-case scenarios represent the ICAO separations schemes for both of the ground-laying traffic samples.

The WSVBS separation dataset for the single runway configuration contains a noticeable amount of in-trail separation values which are below 60s. Those separations are not appropriate with respect to the minimum runway occupancy time ROT for single runway operations. Due to the fact that the ROT depends on runway layouts regarding the position of runway exists, holds, etc. as well as the A/C type, ATC clearances and pilot behavior, it is not useful to define a hard value. Nevertheless it is of interest how delay reacts, when specific ROT minima are in place. For that reason additional calculations are conducted for the in-trail case using exemplary occupance time limits of 55, 60 and 65 seconds.

Results

As shown in Figures 9 and 10 a WSVBS seems to be capable of reducing the arrival delay to a certain extent. In the dual dependent arrival operation case a substantial delay reduction in relation to the ICAO base case can be observed (see Figures 9 and 12). Especially with the weight-class separation scheme (which allows separations down to zero) the system provides a considerable potential. As mentioned earlier there is presumably no airport which operates at a delay level of above 60 minutes average which is referred to as the ICAO case in this study.

For single runway operation at least one day can be identified which can handle the existing traffic demand (see Figure 11) with a significant lower delay (see Figure 10). A further analyze of the separation values provided by the WSVBS showed that most of the above mentioned inappropriate separation values below 60 s occurred on this particular day. The average delay reduction between ICAO based separations (382 s) and aircraft based separations with the 65 s ROT condition (347 s) is 35 s, which is almost no delay reduction (see Figure 13). The results of the subsequent simulation runs lead one to assume that the delay reduction could only be achieved at the expense of safe runway occupancy times.

Table 3. Scenarios of the potential delay reduction analysis

Traffic sample	ICAO Base Case	Sep schemes (single RWY)		Sep schemes (dual-dependent RWY)		ROT sensitivities (single RWY)		
		weight-class	A/C types	DFS modes	weight-class	ROT 55	ROT 60	ROT 65
2009/Apr/04 (dual de-pendent)	1 day (Apr/04)	-	-	6 days	6 days	-	-	-
PFV 2020 (single)	1 day (PFV 2020)	6 days	6 days	-	-	1 day (Feb/11)	1 day (Feb/11)	1 day (Feb/11)

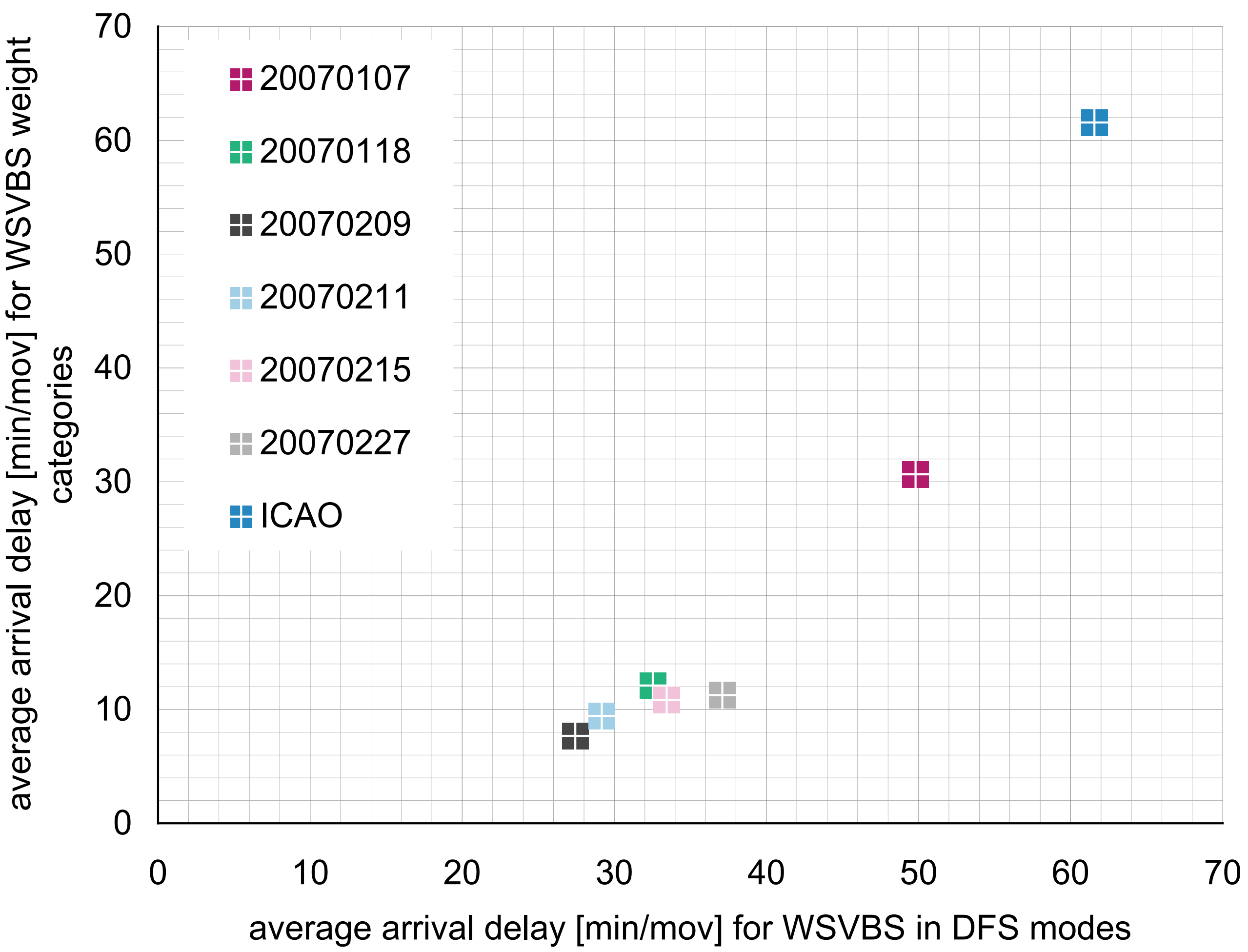

Figure 9. Average delay simulation results for the 2009/Apr/04 traffic sample

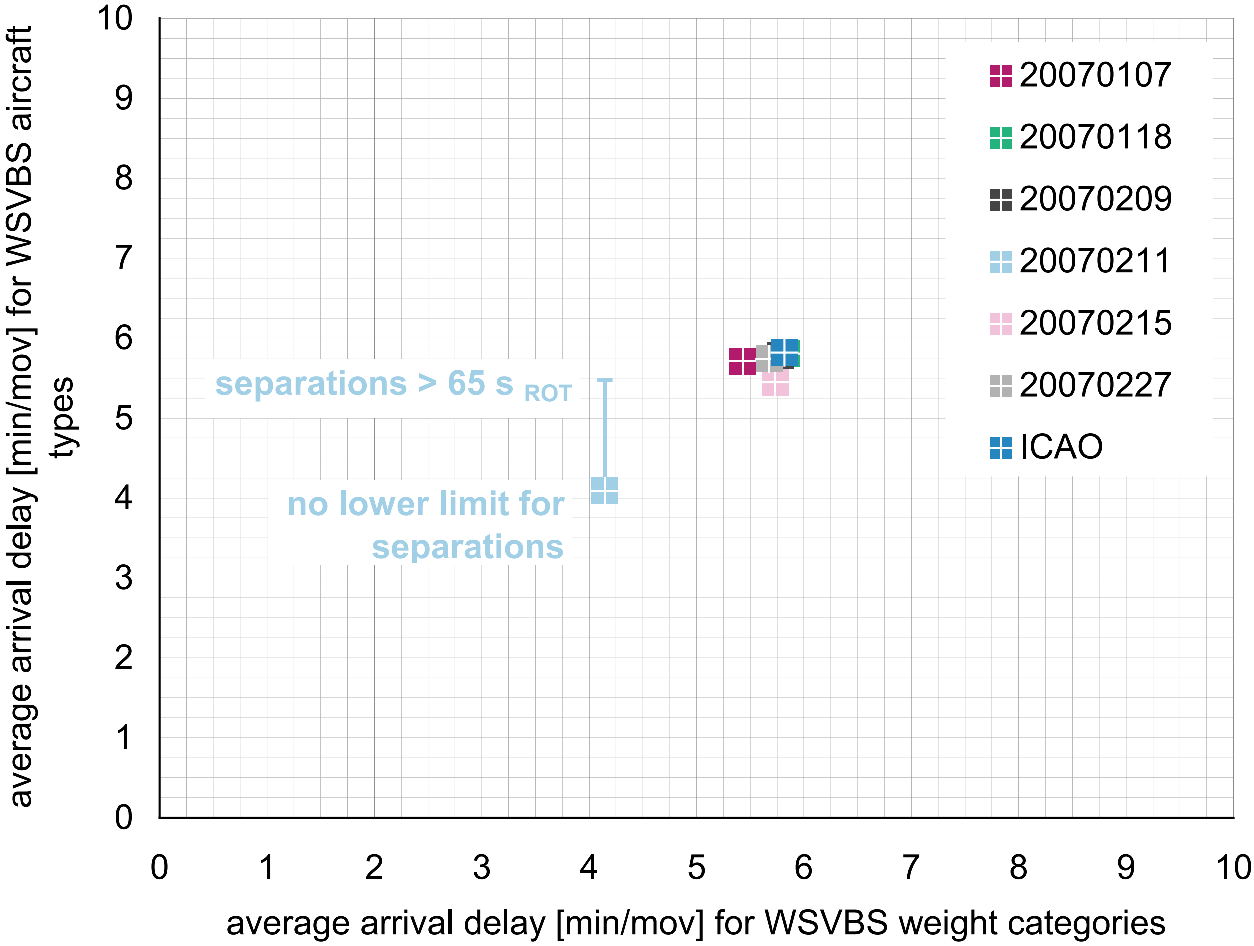

Figure 10. Average delay simulation results for the PFV 2020 traffic sample

Economic viability

Meteorological Data

An economic WSVBS assessment over several years requires a continuous separation dataset for at least one year. This dataset provided by the DLR institute of atmospheric physics contains the aircraft weight class combinations H-H and H-M based on wind data throughout the year 2004. It was used to represent the wind in every year 2010 to 2020 assuming that the average wind behavior and especially the distribution of wind directions and strength at the 13 approach gates is not significantly changing in future. The share between ICAO, MSL, MSR and STG is 40%, 34%, 23% and 3% respectively.

Traffic Data

As for the potential delay analysis the same traffic sample of 2009/Apr/04 is used in combination with forecasted demand distribution profiles as pattern to generate detailed flight plans containing the relevant times, aircraft weight class and runway assignment. The latter fulfills the requirement, that not more than 2 aircraft in a row approach the same runway which guarantees even runway utilization according to dual-dependent runway operations.

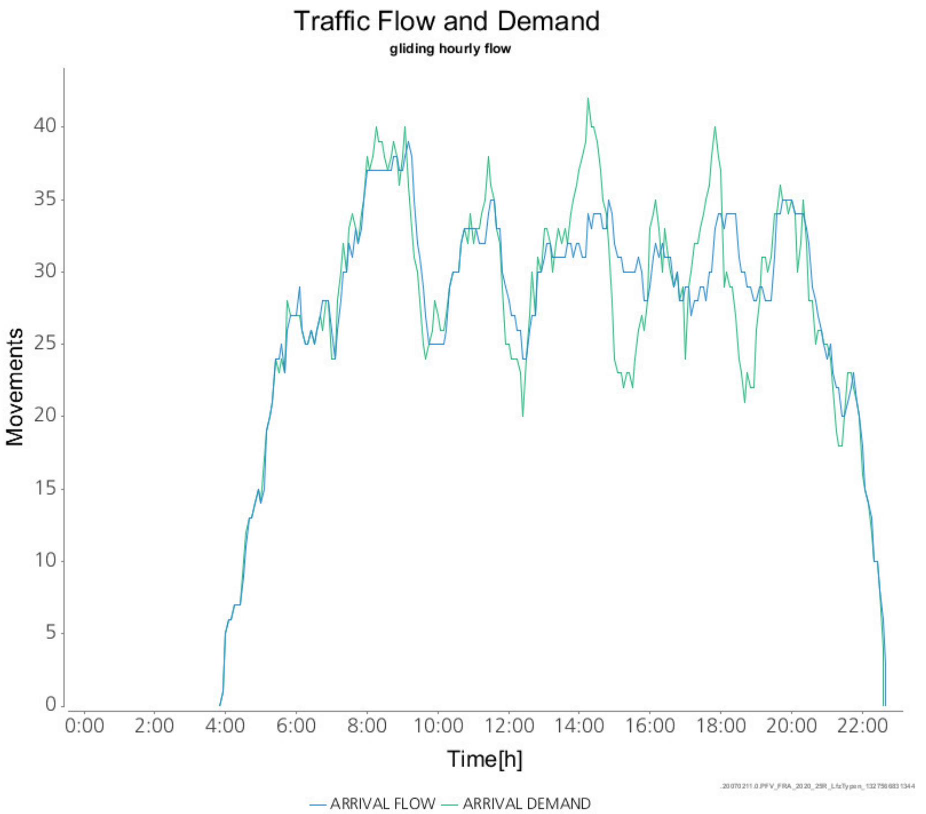

Figure 11. Traffic flow and demand for PFV 2020 traffic sample using WSVBS A/C types separation scheme data of the 2007/Feb/11

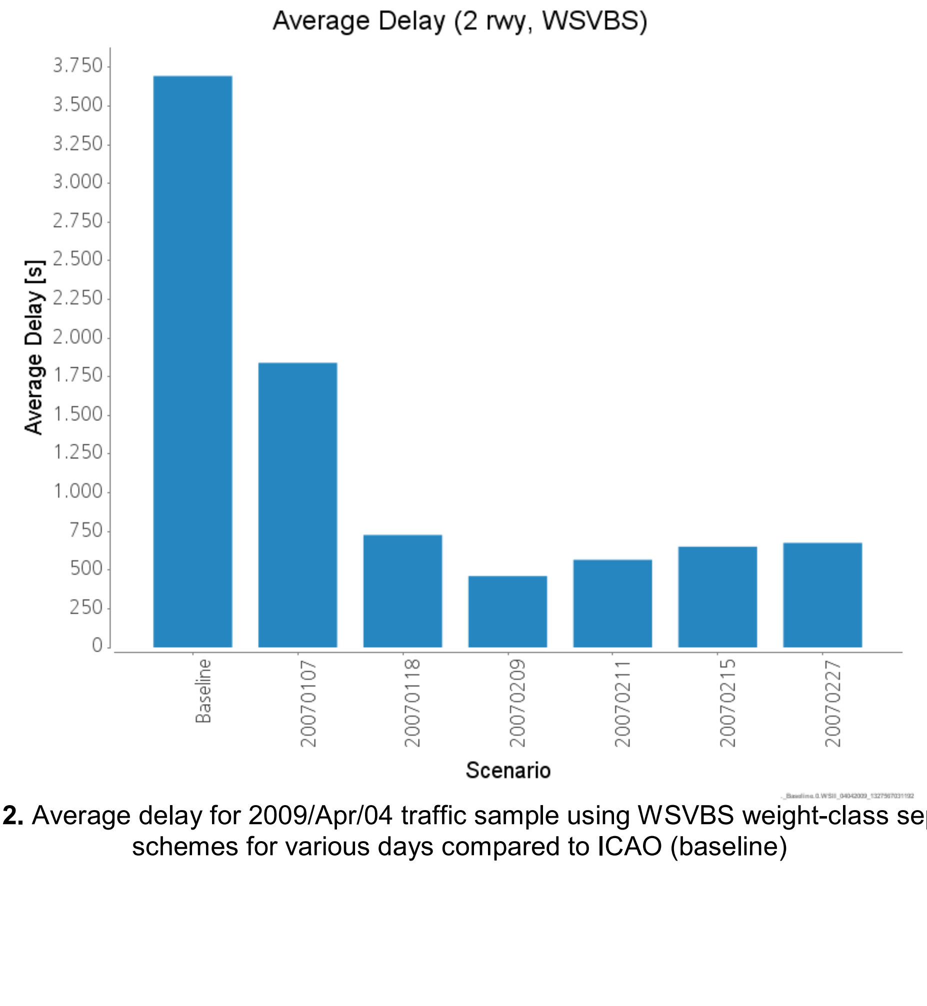

Figure 12. Average delay for 2009/Apr/04 traffic sample using WSVBS weight-class separation schemes for various days compared to ICAO (baseline)

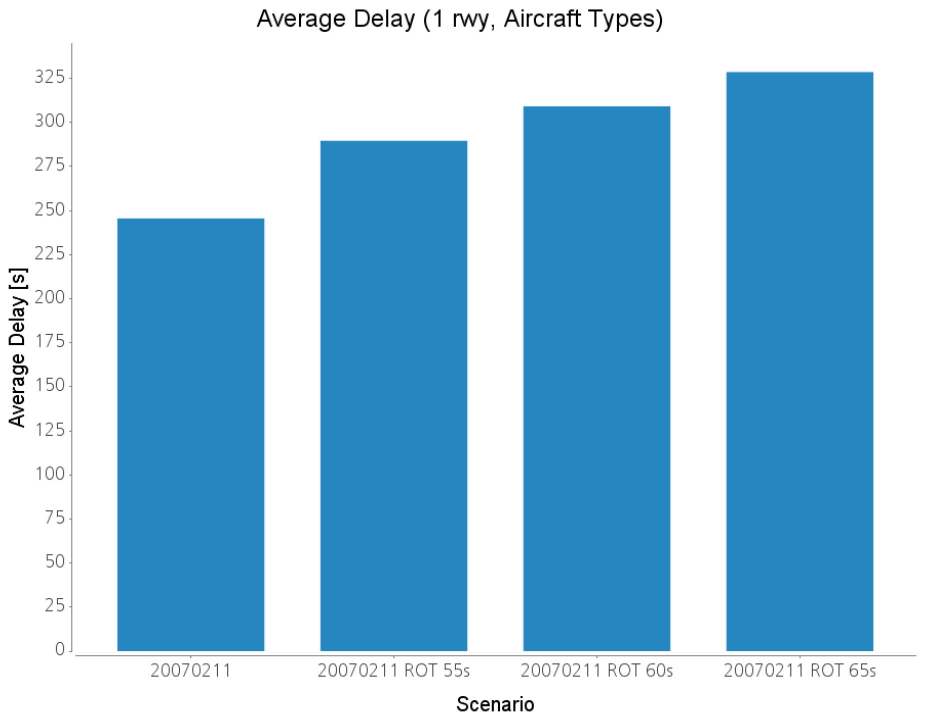

Figure 13. Average delay for 2009/Apr/04 traffic sample using WSVBS aircraft type based separation schemes for various ROT conditions on 2007/Feb/11. The left column represents no ROT condition. The average ICAO delay for this day is 382 s.

Economic Data

The cost of delay is derived from the University of Westminster (2011) report. The document contains tactical delay cost per minute induced during the arrival phase with and without network effects for the most common types of aircraft. The compilation of the cost shares has already been described. Mean values for the two weight classes heavy and medium have been adopted accounting the fact that no aircraft type based separations are applied within the economic viability assessment. Tables 4 and 5 show mean delay cost values for heavy and medium type aircraft with and without network effects. The cost estimates are corrected by a yearly escalation factor of 2%.

Table 4. Mean delay cost values for **heavy** type aircraft with and without network effect in EURO (based on University of Westminster (2011))

minutes	**5**	**15**	**30**	**60**	**90**	**120**	**180**	**240**	**300**
cost/#min w/o net	383	1.450	3.693	10.370	19.173	29.630	55.416	87.423	125.300
cost/#min with net	397	1.617	4.630	17.633	44.430	89.477	12.636	160.143	201.080

Table 5. Mean delay cost values for **medium** type aircraft with and without network effect in EURO (based on University of Westminster (2011))

minutes	5	15	30	60	90	120	180	240	300
cost/#min w/o net	170	627	1.575	4.355	7.995	12.300	22.880	35.975	51.440
cost/#min with net	160	649	1.850	6.838	17.190	31.498	42.784	57.483	76.005

Saving delay minutes by applying WSVBS separation modes instead of ICAO separations enables the economic quantification of system benefits. These benefits are compared to system costs. Cost estimates of the system can be established for the specific cost shares according to Fabrycky and Blanchard (1991): research and development, production and construction, operation and maintenance, retirement and disposal cost. Subdividing into initial and operational investments following the NPV generation:

- Initial investment cost: These costs are defined as research and development cost as well as production and construction cost. The initial investment costs are defined by the following cost items:
  - Equipment cost
  - Land use
  - Hardware connection cost
  - Initial training cost
  - Software development cost
  - Labor installation cost

  Initial licensing costs consist of the three following cost items:
  - Initial licensing cost
  - CNS operational reliably
  - Safety case

- Operational and maintenance cost are defined by the following cost items:
  - Land use
  - Equipment maintaining cost
  - Hardware connection maintaining cost
  - Software maintaining cost
  - Operational training cost
  - Operational labor cost
  - Energy consumption
  - Insurance

  Cost for maintaining the operational admission consist of the three following cost items:
  - Permanent licensing cost
  - CNS operational reliability
  - Safety case

The amount of admission costs of a wake vortex advisory system installed on a European airport depend on the question which instance operates the system. Airport systems underlying functional ICAO requirements, e.g. optical systems, are usually operated by the airport authority. Those technologies need a so-called "*Formal-*" or "*Musterzulassung*" in which technical functionalities are listed according to the respective ICAO requirements. The European level equivalent is the so called "*EG Prüferklärung*"

(European Union 2004) which demands the technological compatibility of airport technologies within a European flight management system according the EASA standards.

A wake vortex advisory system is expected to be operated by a licensed air navigation service provider. Apart from the fact that EASA is working on requirements which define the licensing process of such systems, no such process definition is in place which can be compared to CATII/III admissions. An estimation of licensing costs is difficult. However, licensing costs of a wake vortex advisory system are assumed to be one of the major cost items for the system operator.

Scenario Input

Cost of delay

Delay cost estimates are shown inTables 4 and 5. The latter reflects delay costs including network effects.

System cost

The following Table 6 contains the initial WSVBS system costs approximations subdivided in hardware (SODAR/RASS, LIDAR), software (NOWVIV, P2P, SHAPe) and licensing costs. According to the authors opinion these high, base and low cost approximations are best-choice approximations. The operational estimates are corrected by a yearly escalation factor of 2%.

Table 6. Best-choice WSVBS system cost approximations (BASE/LOW/HIGH) in Euro. Licensing cost items are composed by general admission cost, reliability proof and safety case.

	Hardware (SODAR/RASS, LIDAR)		Software (NOWVIV, P2P, SHAPe)	
	initial (year 1)	operational (year 2-10)	initial (year 1)	operational (year 2-10)
Land use	**2500/1.000/3.500**	**2500/1.000/3.500**	**240/150/350**	**240/150/350**
Equipment cost	**1.000.000/700.000/1.500.000** (SODAR/RASS) **500.000/300.000/700.000** (LIDAR)	-	**5.000/3.000/7.000**	-
Equipment maint.	-	**50.000/35.000/75.000** (SODAR/RASS) **25.000/15.000/35.000** (LIDAR)	-	**250/150/350**
Hardware connect	**1.500/1.000/2.000**	-	-	-
H connect maint.	-	**75/50/100**	-	-
Training initial	-	-	**8.000/5.000/10.000**	-
Training ops.	-	-	-	**5.000/2.000/7.000**
Software dvmt.	-	-	**720.000/600.000/ 900.000**	-
Software maint.	-	-	-	**36.000/30.000/ 45.000**
Labour inst.	**5.000/3.000/8.000**	-	**5.000/3.000/8.000**	-

Labour ops.	-	**5.000/3.000/8.000**	-	**5.000/3.000/8.000**
Energy	**380/300/500**	**380/300/500**	-	-
Insurance	**100/80/150**	**100/80/150**	**3.000/2.500/4.000**	**3.000/2.500/4.000**
Licensing initial	**6.000.000/3.000.000/9.000.000**			
Licensing ops.	**300.000/200.000/400.000**			

System acceptance and adaptation effects

The time dependence of technological benefits is dominated by operational acceptance and applicability especially in the case of a safety related system. This operational applicability is defined not only by technological functionalities but also by controller acceptance. Within the DLR project “Wirbelschleppe II”, real-time simulations have been conducted to show the feasibility of the systems integration (Gerling 2008). Nevertheless, full system performance cannot be expected during the first years of operation. To account for this behavior of conservative performance development, the calculations are adopted by learning curves, whereas positive, baseline and negative system acceptance is adopted. A difference is assumed in the duration of performance initiation or *habituation* periods regarding application by the controller and also functional system adaptions at the beginning of the life-cycle. It must be stated that full system performance will require a high level of automation on the ground and on-board, e.g. communication via data link. This causes a higher diversification of the aircraft mix reflecting different aircraft equipment levels. Those factors are represented by learning curves shown in Figure 14.

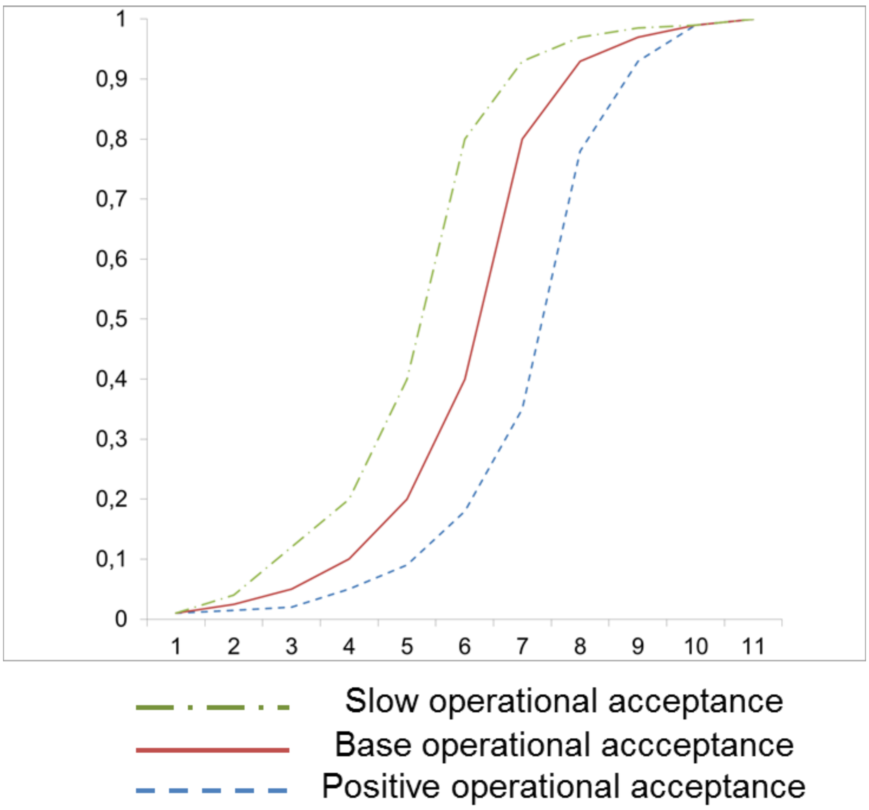

Figure 14. Exemplary learning curves representing system acceptance and adaptation

In sum 4 different scenario factors are applied: separation mode, cost of delay, system acceptance and WSVBS system cost. Not all factor combinations have been investigated. The study rather focusses on combinations which give information about system cost and application conditions.

Results

In total 4 *cutting-edge* scenarios have been considered for this report. These scenarios represent the worst-case scenarios. Nevertheless, all scenarios have highly positive 10-year-NPVs. The 4 depicted scenarios in Figures 15 and 16 contain calculation information regarding factor combinations, costs, benefits and calculated NPVs which in addition are shown in the diagrams. The total benefits represent the delta of delay minutes between ICAO separations (base case) and the respective WSVBS separations expressed in cost values. The discount is captured at a rate of 25.0%, which constitutes conservative high risks.

Expecting even higher NPVs in best-case scenarios, the interpretation of these numbers requires caution. Even if the NPVs go into the hundreds of millions, the results depend heavily on the combination of factors like demand estimation on the traffic forecasting side and cost estimations on the economic side. The more interesting information is the cost delta between the different separation modes.

DFS neg acc	pritact	HIGH COST		DISCOUNT: 25% 0,25	
Initial Cost	14003050 [€]				
Initial Benefit	0 [€]				
Years		2010 - 2020		NPV [€]	3,78E+08
Year	Total Ops Cost	Total Benefits	Net Benefit	Discount Rate	NPV
1	13300	4773230,442	4759930,442	0,25	-10195105,65
2	728600	7679280,4	6950680,4	0,25	-5746670,19
3	743172	10238705,45	9495533,447	0,25	-884957,0656
4	758035,44	27697161,56	26939126,12	0,25	10149308,99
5	773196,1488	52325750,13	51552553,98	0,25	27042049,88
6	788660,0718	109422924,7	108634264,6	0,25	55519870,54
7	804433,2732	207631426,3	206826993	0,25	98894634,75
8	820521,9387	473454313,2	472633791,2	0,25	178189426,8
9	836932,3774	576302528,1	575465595,7	0,25	255427111,6
10	853671,025	636411665,2	635557994,2	0,25	323669631,6
11	870744,4455	637998392,7	637127648,2	0,25	3,78E+08

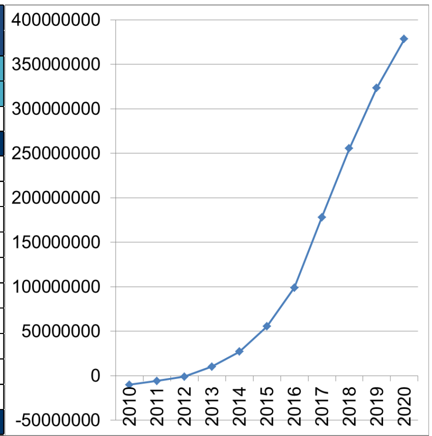

DFS neg acc	fulltact	HIGH COST		DISCOUNT: 25% 0,25	
Initial Cost	14003050 [€]				
Initial Benefit	0 [€]				
Years		2010 - 2020		NPV [€]	8,06E+08
Year	Total Ops Cost	Total Benefits	Net Benefit	Discount Rate	NPV
1	13300	9168702,471	9155402,471	0,25	-6678728,023
2	728600	15057200,37	14328600,37	0,25	2491576,213
3	743172	20267474,61	19524302,61	0,25	12488019,15
4	758035,44	55965140,1	55207104,66	0,25	35100849,22
5	773196,1488	106023312,4	105250116,3	0,25	69589207,31
6	788660,0718	225362138,7	224573478,6	0,25	128459797,3
7	804433,2732	429916626	429112192,7	0,25	218451146,6
8	820521,9387	982081175,5	981260653,5	0,25	383079366
9	836932,3774	1216077835	1215240903	0,25	546186238,9
10	853671,025	1343104436	1342250765	0,25	690309317,3
11	870744,4455	1352162655	1351291910	0,25	8,06E+08

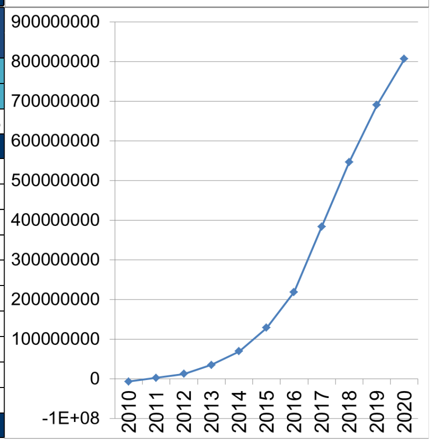

Figure 15. Worst-case pre- and full-tactical calculation: high system cost and slow system acceptance for DFS separation modes

The pre-tactical worst-case scenarios have break even durations of about three years for DFS based separations and two years for weight class based separations. The delta of the 10-year NPVs is about 190 million Euros. The present of the aircraft weight class based separations mode is approximately 30% higher. The full-tactical worst-case scenarios have break even durations of about one year, whereas the 10-year-NPS are significantly higher.

Net benefits representing the sum of delay cost for each year are within the hundreds of millions in the best-case scenarios. However, correlated with the number of movements these fairly high values represent delay reductions not more than 12 minutes per aircraft without network effect and 24 minutes including knock-on delay minutes within the final year with the highest demand rates.

GK neg acc	pritact	HIGH COST		DISCOUNT: 25% 0,25	
Initial Cost	14003050 [€]				
Initial Benefit	0 [€]				
Years		2010 - 2020		NPV [€]	5,66E+08
Year	Total Ops Cost	Total Benefits	Net Benefit	Discount Rate	NPV
1	13300	6968415,885	6955115,885	0,25	-8438957,292
2	728600	11271668,21	10543068,21	0,25	-1691393,64
3	743172	15512163,9	14768991,9	0,25	5870330,213
4	758035,44	41229435,65	40471400,21	0,25	22447415,74
5	773196,1488	75759690,6	74986494,45	0,25	47018990,24
6	788660,0718	159424276,4	158635616,3	0,25	88604365,25
7	804433,2732	311420006	310615572,7	0,25	153745172,2
8	820521,9387	698639217,1	697818695,1	0,25	270819722
9	836932,3774	867429986,6	866593054,2	0,25	387131872,8
10	853671,025	920344568	919490897	0,25	485861456,1
11	870744,4455	936824504,5	935953760,1	0,25	5,66E+08

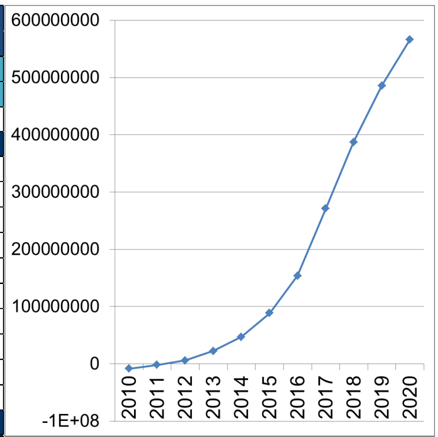

GK neg acc	fulltact	HIGH COST		DISCOUNT: 25% 0,25	
Initial Cost	14003050 [€]				
Initial Benefit	0 [€]				
Years		2010 - 2020		NPV [€]	1,10E+09
Year	Total Ops Cost	Total Benefits	Net Benefit	Discount Rate	NPV
1	13300	12429232,44	12415932,44	0,25	-4070304,045
2	728600	20423260,17	19694660,17	0,25	8534278,466
3	743172	28347142,87	27603970,87	0,25	22667511,55
4	758035,44	76559078,54	75801043,1	0,25	53715618,81
5	773196,1488	141685234,6	140912038,5	0,25	99889675,58
6	788660,0718	302819495,4	302030835,3	0,25	179065246,9
7	804433,2732	591263810,9	590459377,7	0,25	302893553,4
8	820521,9387	1331148835	1330328313	0,25	526085608
9	836932,3774	1668281897	1667444964	0,25	749886282,7
10	853671,025	1777804081	1776950410	0,25	940684880,1
11	870744,4455	1813940257	1813069512	0,25	1,10E+09

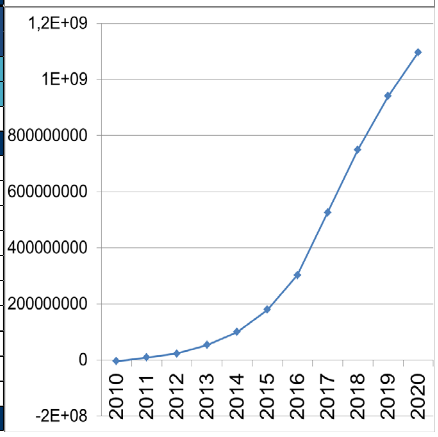

Figure 16. Worst-case pre- and full-tactical cost calculation: high system cost and slow system acceptance for aircraft weight class based separation modes

Conclusion

A WSVBS potential delay reduction analysis regarding individual aircraft-, weight class- and DFS operational separations together with a study of the economic viability applying reduced separations for the approach on a dual-dependent runway system is conducted.

Regarding the potential delay reduction analysis the WSVBS showed considerable performance with the aircraft based separation scheme. The individual aircraft separation scheme also shows delay reduction potential but is not always consistent with the ROT requirements. A ROT of about 65 seconds represents a separation limit over which no significant average delay reductions are realized.

Regarding the economic viability of the WSVBS a forecasting model has been described which creates schedule information on the basis of representative baseline demand profiles. The model output serves as input for the delay calculation model developed for the potential delay reduction analysis. Individual delay quantities for each movement in the approach phase were translated into economic cost of delay values to generate the present value of the system. Operational scenarios exist in which the system can be operated beneficially on a dual-dependent runway system under given assumptions. These assumptions are

- Constant yearly demand increase rate of 2%
- Perfect wind forecasting performance
- Identical separations distributions (representing the weather) for different years
- Initial system cost estimates between 6 and 14 million Euros
- Delay cost calculations based on delay cost incurred in the approach phase for pre-tactical and full-tactical (with network effects) approximations (see Tables 4 and 5)
- System acceptance durations after operational implementation of 2 and 5 years
- Discount rate: 25%

Total benefit values are remarkably high, while the present values at the end of the depreciation period go into the hundreds of millions. Nevertheless, it cannot be stated that these numbers fulfill reality when implemented at a real airport. Too many uncertainties exist, which have influence on the profit behavior of the system. Especially weather uncertainty, which has been treated as static on a yearly basis, will have influence on the systems benefit.

Factors from which the economic viability depend in a high degree are

- System acceptance and operability
- Initial system cost
- Forecasted demand profile
- Weather

Potential for future work:

- Capacity analysis applying fast-time simulation tools
- Application of a higher quantity of weather data for more than one year
- Economic sensitivity regarding different demand rates
- Integration of cash flows between actors of the aviation community

Safety related assessments without an integration of economic data would additionally extend the knowledge about the system in real operational environments.

Acknowledgments

The work presented here was funded by the DLR project Wetter & Fliegen. We greatly appreciate the excellent support of the teams from DFS Deutsche Flugsicherung GmbH and Fraport AG.

References

Ashford, N., ”Airport Operations”, 2nd edition, McGraw-Hill, 1997.

Ballin, M.G., Erzberger, H., „An Analysis of Landing Rates and Separations at the Dallas/Fort Worth International Airport“, NASA Ames Research Center, Technical Memorandum 110397, 1996.

Bundesministerium der Finanzen, “AfA-Tabelle für die allgemein verwendbaren Anlagegüter („AV“)“, 2000

EASA European Aviation Safety Agency, “Certification Specifications for Large Aeroplanes CS-25”, Amendment 6, 2009.

Eurocontrol, “Eurocontrol Long-Term Forecast: IFR Flight Movements 2010-2030”, Document Identifier CND/STATFOR Doc415, Brussels, 2010.

FAA Federal Aviation Administration, “Procedures for Determination of Airport Capacity”, Federal Aviation Administration Report No FAA-RD-73-11, 1973.

Fraport AG, “Luftverkehrsstatistik 2009”, Frankfurt Main, 2010.

Fraport AG, „ Ausbau Flughafen Frankfurt Main Planteil B 11 Planungsgrundlagen Kap. 5 Flugpläne“, Unterlagen zum Planfeststellungsverfahren, Frankfurt, 2006.

Gerling, W. et. al, “DLR-Projekt Wirbelschleppe II Echtzeitsimulationen mit Wirbelschleppenvorhersage“, DLR Institut für Flugführung, IB 112-2007/18, 2008.

Gerz et. al, „The Wake Vortex Prediction and Monitoring System WSVBS Part II: Performance and ATC Integration at Frankfurt Airport”, DLR Project Wake Vortex, Forschungsbericht 2008-15, 2008.

Gerz et. al, „The Wake Vortex Prediction and Monitoring System WSVBS Part II: Performance and ATC Integration at Frankfurt Airport“, ATC Quarterly, Vol. 17(4)323-346, 2009.

Graham, A., “Managing Airports”, 3rd edition, Elsevier Ldt., 2008.

Hemm, R. et. al, “Benefit Estimates of Terminal Area Productivity Program Technologies”, NASA Langley Research Center, NASA/CR-1999-208989, 1999.

Holzäpfel, F., Dengler, K., Gerz, T.,“Prediction of Dynamic Pairwise Wake Vortex Separations for Approach and Landing“, 3rd AIAA Atmospheric Space Environments Conference, Hawaii, 2011.

Intraplan Consult GmbH, “G8 Luftverkehrsprognosen 2020 für den Flughafen Frankfurt Main und Prognose zum landseitigen Aufkommen am Flughafen Frankfurt Main”, Unterlagen zum Planfeststellungsverfahren, München, 2008.

Konopka, J., Fischer, H., “The wake vortex warning system at Frankfurt airport”, 24th Digital Avionics Systems Conference, 2005.

Roelen, A.L.C. et. al, “A cost benefit analysis of wake vortex measures”, National Aerospace Laboratory NLR, NLR-CR-2001-610, 2001.

University of Westminster, “European airline delay cost reference values”, Final Report (Version 3.2), London, 2011.

Wöhe, G., Döring, U., “Einführung in die Allgemeine Betriebswirtschaftslehre”, 23. Auflage, Verlag Franz Vahlen, München, 2008.

3.2 Wake Vortex Scenarios Simulation Package for Take-Off and Departure

Frank Holzäpfel[1], Jan Kladetzke[2]
[1]Institute of Atmospheric Physics, [2]Institute of Robotics and Mechatronics

The WakeScene-D software package (Wake Vortex Scenarios Simulation Package for Departure) has been developed for comprehensive airspace simulations of take-off and departure. WakeScene-D consists of modules that model traffic mix, aircraft trajectories, meteorological conditions, wake vortex evolution, and potential hazard area. The software package estimates the probability to encounter wake vortices in different traffic and crosswind sce-narios using Monte Carlo simulation in a domain ranging from the runway to an altitude of 3000 ft above ground. A comparison to measured vortex tracks of about 10,000 departures from runway 25R of Frankfurt airport indicates good agreement of global wake vortex transport characteristics in ground proximity. The standard departure situation employing a two-minute aircraft separation is compared to scenarios with reduced departure separations and various crosswind conditions. Comprehensive sensitivity analyses have been conducted which are briefly recapitulated. Effects related to departure route combinations and wind direction sectors are reported in more detail. Finally, an advanced scenario with an asymmetric crosswind criterion is introduced.

Introduction

Aircraft generated wake vortices pose a potential risk to following aircraft in various flight phases, whereas most wake vortex encounters are reported for approach and landing and for take-off and climb (Elsenaar et al. 2006). The ICAO wake-vortex aircraft separation standards (ICAO 2001) established in the 70's increasingly degrade aviation efficiency when traffic congestion limits airport capacity during landing and take-off. Research has shown that the transport and persistence of wake vortices are highly dependent on meteorological conditions (Gerz et al. 2005, Hallock et al. 1998), so that in many cases the separation standards are over-conservative. For single-runway operations, analyses (de Bruin et al. 2003, Frech & Zinner 2004, Frech & Holzäpfel 2008) suggest that, above a certain crosswind threshold, vortices are blown out of the flight corridor and pose no further threat to following aircraft.

The EU-project CREDOS (Crosswind-Reduced Separations for Departure Operations, see www.eurocontrol.int/eec/credos/) intends to demonstrate the operational feasibility of a concept of operations that uses measures of the prevailing crosswind component to allow temporary suspension of the need to apply wake vortex separations between successive departing aircraft. The focus on the combination of crosswind and departures has significant advantages: The follower aircraft is still on the ground when the controller schedules the separation. So the controller always has the possibility to extend the separation without requiring the pilot to make a maneuver. This beneficial situation also reduces the time horizon for which crosswind conditions must be anticipated. Secondly, in contrast to arrival situations the leader aircraft is generally faster so that the actual separations tend to increase.

WakeScene-D (Wake Vortex Scenarios Simulation Package for Departure) (Holzäpfel et al. 2009-2, Hozäpfel & Kladetzke 2011) is an extension of WakeScene which has been developed for approach and landing and is described in detail in (Holzäpfel et al. 2009-1). WakeScene-D estimates the probability to encounter wake vortices in different traffic and crosswind scenarios using Monte Carlo simulation in a domain ranging from the runway to an altitude of 3000 ft above ground. In cases with potential wake encounters all relevant parameters can be provided to VESA (Vortex Encounter Severity Assessment, Höhne et al. 2004, Luckner et al. 2004, Kauertz et al. 2012), a tool developed by Airbus, which may subsequently perform detailed investigations of the severity of the encounter. WakeScene-D consists of elements that model traffic mix, aircraft trajectories, meteorological conditions, wake vortex evolution, and potential hazard area. The process and data flows are controlled and evaluated by the MATLAB-based environment MOPS (Multi Objective Parameter Synthesis, Joos et al. 2002). Within CREDOS

WakeScene-D is used to support the definition of suitable crosswind criteria that allow reducing aircraft separations, to identify the sensitivity and interplay of the employed sub-models and parameter combinations, and to support risk analyses taking into account a broad range of variables which determine the probability and risk of a wake vortex encounter.

Related models have been developed for approach and landing: (1) WAVIR (Wake Vortex Induced Risk, Speijker et al. 2000) which is capable to estimate frequencies of certain risk events in a given scenario. (2) ASAT (Airspace Simulation and Analysis for TERPS where TERPS stands for Terminal Instrument Procedures) is a multifaceted computer tool for aviation related simulations and safety evaluations which has not been specifically designed as a wake vortex risk assessment model. Similar to WakeScene, ASAT has an interface to VESA that permits subsequent wake vortex encounter severity assessment. (3) The Vortex Risk Analysis Tool has been employed for the risk assessment of the High Approach Landing System / Dual Threshold Operation (HALS/DTOP) implemented at Frankfurt airport. HALS/DTOP aims at increasing the capacity of the closely spaced parallel runway system by employing a second threshold displaced by 1500 meters for the southern runway. (4) A comprehensive air traffic control wake vortex safety and capacity integrated platform has also been generated in the EU project ATC-Wake (Speijker et al. 2007). Elsenaar et al. (2006) provides a comprehensive survey on operational concepts designated to increase airport capacity and the regulatory framework which is relevant for the associated risk assessments as well as many other wake vortex related issues.

First, this paper describes the operating sequence of WakeScene-D and the employed sub-models. Next, a reference scenario is introduced which shall represent the real current departure situation. Then the statistics achieved with reduced aircraft departure separations and different crosswind thresholds are discussed. The paper highlights a selection of the most interesting results found in the conducted comprehensive sensitivity analyses. The investigated parameters of these sensitivity analyses comprise effects related to different departure route combinations, variations of flight path adherence, different wake vortex models, the development of aircraft separations during the departures, the sample size of the Monte Carlo simulations, aircraft type combinations, aircraft take-off weights, meteorological conditions, and airport operation times. Vortex tracks of about 10,000 departures collected during a six-month measurement campaign at Frankfurt airport are compared to WakeScene-D simulations and a comparison of the arrival and departure situation is conducted. On one hand, the sensitivity analyses help to increase the confidence in the software package and, on the other hand, they allow identifying the parameters that control encounter probabilities during takeoff and departure. In a next step the knowledge of these key parameters enables the optimization of criteria for reduced aircraft separations under favorable crosswind conditions. The current report is based on Holzäpfel et al. (2009) and Holzäpfel & Kladetzke (2011); a more detailed description of the sensitivity analysis is available in Holzäpfel & Kladetzke (2009).

Survey on Operating Sequence

The flowchart depicted in Figure 1 sketches the operating sequence of WakeScene-D. Via simulation control (MOPS) the types of the generator aircraft and follower aircraft, the departure routes (see Figure 2), and a number of aircraft and pilot parameters are selected. The Trajectory Model provides time, speed, position, attitude, lift and mass of generator and follower aircraft along the flight paths.

Wake vortex evolution is predicted within control gates which are released along the flight path of the wake vortex generator aircraft in predefined time increments of e.g. 5 s. The gates' orientations are perpendicular to the aircraft true heading and perpendicular to the flight path angle (see Figure 3). Based on vertical profiles of wind speed and direction, air density, virtual potential temperature, turbulent kinetic energy, and eddy dissipation rate (Meteorological Data Base) and aircraft position, speed, attitude, lift, and span (Trajectory Model) at one gate, the Wake Vortex Model simulates the development of wake vortex trajectories, circulation, vortex core radius, and attitude of wake vortex axes. The Simplified Hazard Area Prediction model (SHAPe) computes the distance between wake vortex and follower aircraft within each gate and discriminates between potentially critical cases and cases where safe and undisturbed flight is guaranteed. From all these data MOPS computes defined criteria, like minimal distance between wake vortex and follower aircraft and the respective vortex circulation and height, which are interpolated between the gates and statistically analysed. Finally, data needed for further investigations with VESA are deduced and stored. The results are optionally visualised in graphs of the statistics, 2D and 3D views (see Figure 3) or animations of the approaches of subsequent aircraft.

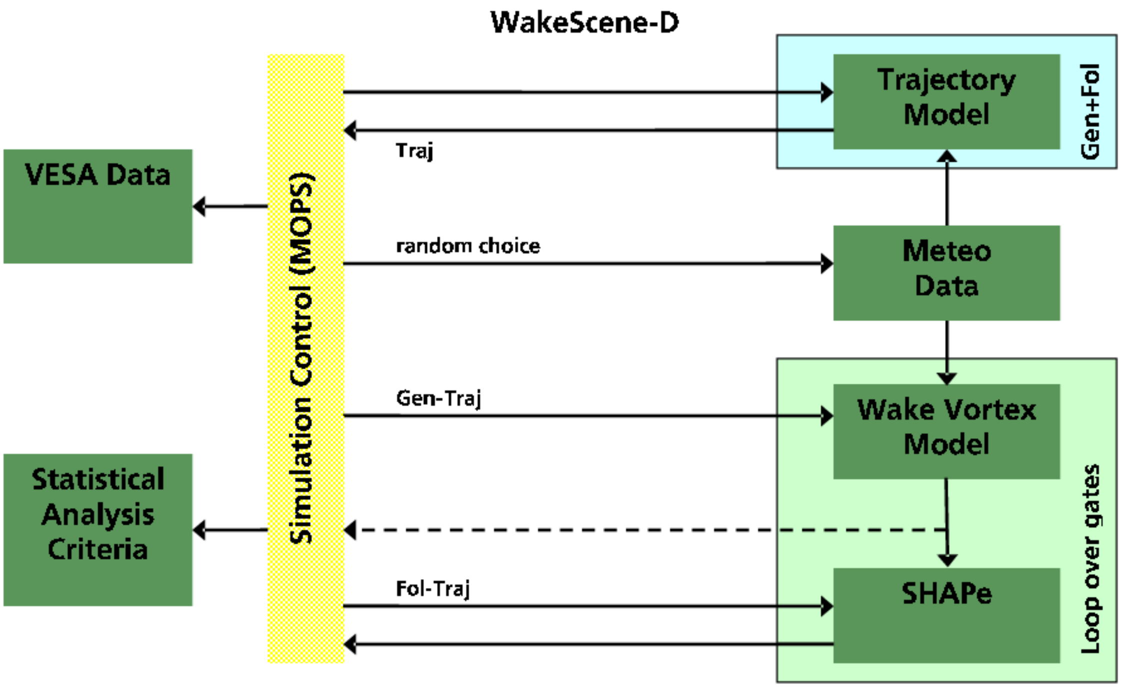

Figure 1. WakeScene-D flowchart. Arrows denote the data flow.

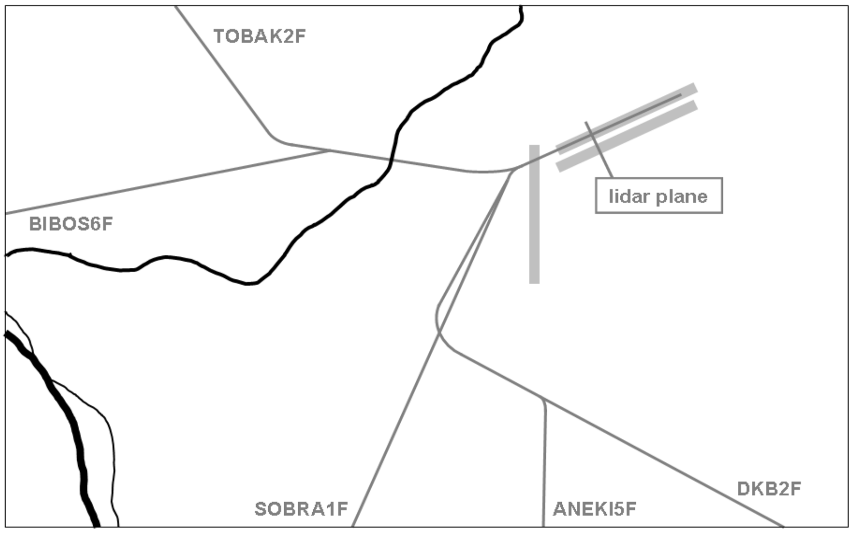

Figure 2. Runways, standard instrument departure routes (SIDS), and lidar measurement plane.

Employed Models and Data Bases

The sub-models and data bases which are employed by WakeScene-D are briefly introduced in the subsequent paragraphs followed by a brief estimation of the related uncertainties.

Meteorological Data Base

The variety of parameter combinations observed in the planetary boundary layer and their transformation on wake vortex behavior lead to a significant manifold of situations. To capture this diversity an extensive one-year simulation of realistic meteorological conditions has been produced for the Frankfurt terminal area with the non-hydrostatic mesoscale weather forecast model system NOWVIV (NOwcasting Wake Vortex Impact Variables, Gerz et al. 2005). NOWVIV comprises a full physics package including boundary layer turbulence, surface energy and momentum balance, soil physics, radiation processes including cloud effects, cumulus convection, and cloud physics (Grell et al. 2000).

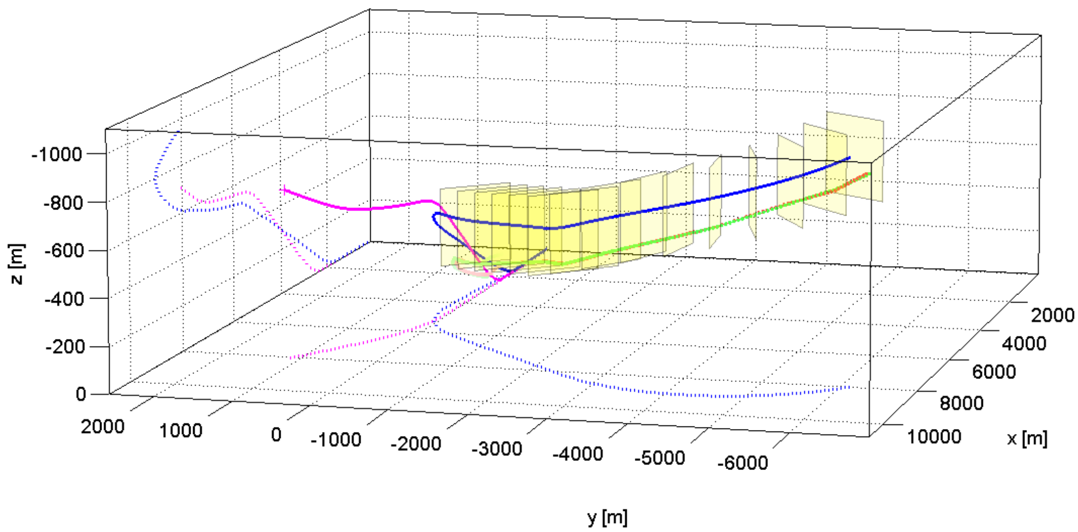

Figure 3. Perspective view of trajectories of wake-generating aircraft (blue) and follower aircraft (magenta) together with wake vortex positions (starboard vortex green, port vortex red). Projections of aircraft trajectories on vertical and horizontal planes and a number of gates used for wake vortex prediction are displayed for convenience.

NOWVIV has previously been successfully employed for predictions of wake vortex environmental parameters in five field campaigns (Holzäpfel et al. 2009). The one-year meteorological data base has been validated against a 30-year wind climatology and a 40-days subset has been compared to ultrasonic anemometer, SODAR/RASS, and lidar measurement data (Frech et al. 2007). Assessments of wake prediction skill based on predictions of meteorological conditions with NOWVIV can be found in Frech & Holzäpfel (2008) and Holzäpfel & Robins (2004).

The data base consists of about $1.3 \cdot 10^6$ vertical profiles of meteorological data at locations separated by one nautical mile and an output frequency of 10 minutes. The meteorological quantities comprise the three wind components, air density, virtual potential temperature, turbulent kinetic energy, eddy dissipation rate (EDR), and pressure.

Trajectory Model

The risk to encounter a wake vortex is strongly correlated with the actual flight paths of the vortex generating aircraft and the encountering aircraft in space and time. Aircraft trajectories are modeled beginning on runway 25R along five different standard departure routes until 3000 ft above ground (see Figure 2). A large number of environmental and aircraft specific parameters influence an aircraft trajectory. The trajectory model (see Amelsberg & Luckner, 2007 for details) simulates the impact of the most relevant parameters that are: the selected runway and the standard departure route; meteorological conditions including air temperature, density, pressure, wind direction and strength; aircraft type; aircraft takeoff weight; takeoff thrust that can be either takeoff go around (TOGA) thrust, or flex takeoff thrust (reduced thrust); start position on the runway; and pilot behavior that is described as a control model considering delayed pilot reaction time and a cross track error.

These factors are varied within defined boundaries and given probability distributions employing Monte Carlo Simulation to generate a set of trajectories for different aircraft types and departure conditions. The aircraft trajectory is adequately described with the equations of motion for three translational degrees of freedom. A deterministic verification has been accomplished by comparing results of the trajectory model with high-fidelity simulation data of departures that were simulated on the certified A330-300 full-flight simulator (A330-FFS) at TU Berlin. Furthermore, a statistical validation was performed by comparing Monte Carlo Simulation results of the trajectory model with 20,000 measured departures at Frankfurt airport provided by DFS Deutsche Flugsicherung GmbH.

Figure 4 shows exemplarily results of 1000 simulated A320 departures. The simulations are based on variations of pilot behavior, aircraft weight, thrust mode and wind conditions. In Figure 4 the resulting mean trajectory and its standard deviations (blue) are compared to the respective measurement data (red). The agreement of the lateral flight path, the climb profile, and the speed profile is sound.

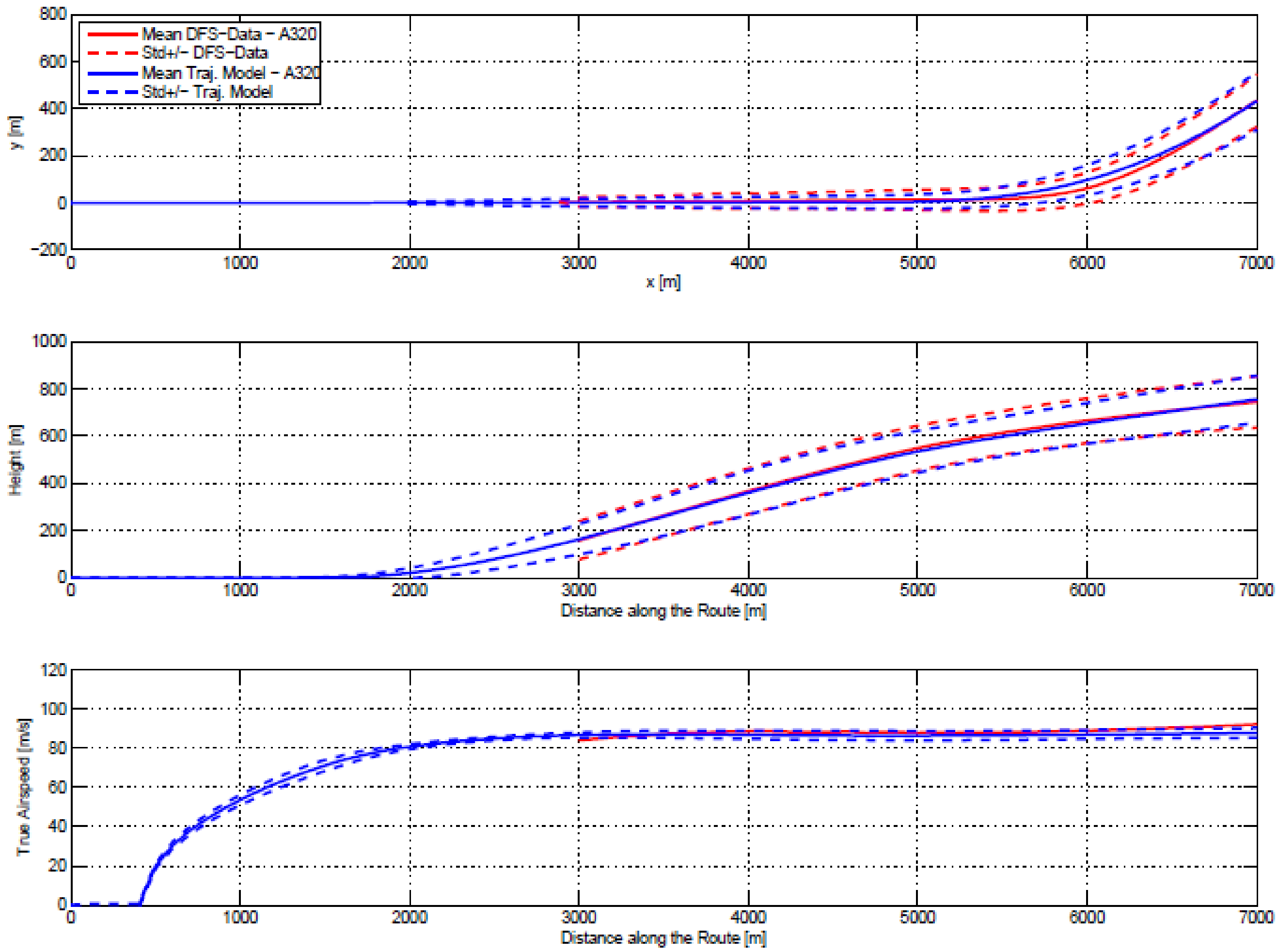

Figure 4. Statistics of 1000 departures of A320 aircraft. Lateral and vertical positions and speed profile.

Wake-Vortex Prediction Models

In the CREDOS project WakeScene provided a choice between two different parametric wake-vortex prediction models. These are the Deterministic Two-Phase wake-vortex decay model (D2P) and the Deterministic wake Vortex Model (DVM). Both vortex models have been validated for departing aircraft by evaluating statistics of the deviations between measured and predicted wake vortex behavior employing data acquired during the two CREDOS field measurement campaigns at Frankfurt airport. The alternative application of two wake vortex models allows assessing the sensitivity of WakeScene-D results on wake vortex parameterizations.

A few adaptations were necessary to comply with the architecture devised for WakeScene-D. The control gates in which the vortices evolve (see Figure 3) are inclined by the flight path angle γ with respect to the vertical direction. For curved flight the vortices are initialized in positions rotated by the bank angle Φ such that the vortices descend in a direction tilted by Φ. The wake vortex transport by headwind or tailwind is modeled by the respective transport of the gates. Because the gates have arbitrary orientations and move through the space, the determination of the closest distance between wake vortex and follower aircraft requires somewhat complex calculations.

The probabilistic vortex model P2P, which constitutes the basis of its deterministic version D2P, is described in detail in Holzäpfel (2003). Applications, assessments and further developments are reported in Frech & Holzäpfel 2008, Holzäpfel & Robins 2004, Holzäpfel 2006, and Holzäpfel & Steen 2007. In total, P2P has been validated against data of over 10,000 cases gathered in two US and six European measurement campaigns. D2P accounts for the effects of wind, axial- and crosswind shear, turbulence, stable thermal stratification, and ground proximity. Figure 5 delineates a comparison between measured wake vortex positions and circulation and the predictions of the two wake vortex models. Note the effective lateral transport of the vortices in a case with a crosswind of about 4 m/s. Further output provided to VESA includes vortex core radii and the interception angles between aircraft flight path and vortex axis, the so-called encounter angles.

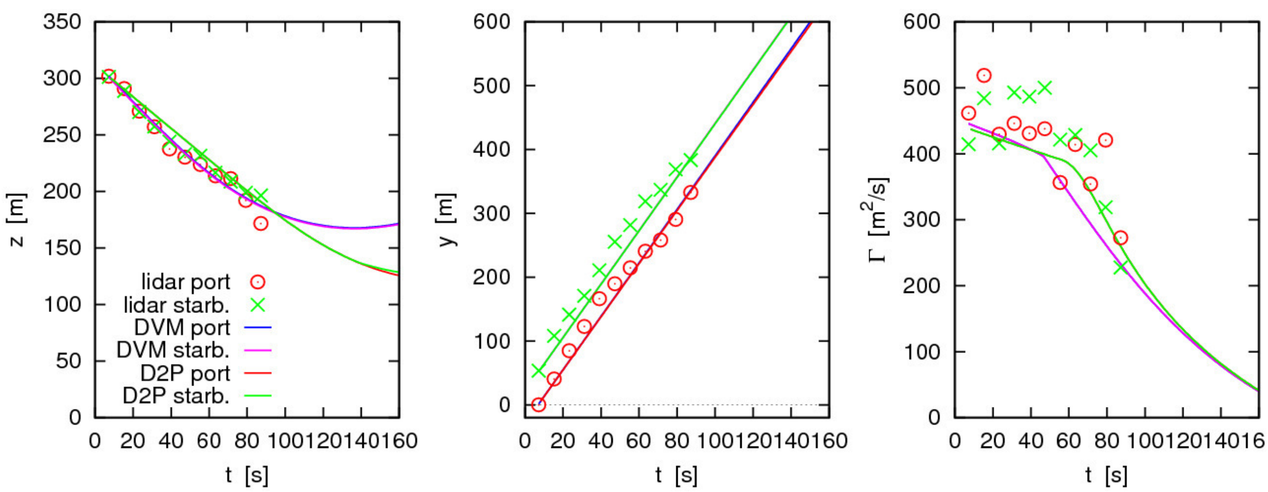

Figure 5. Example for evolution of vertical and lateral positions and circulation in a case with a crosswind of about 4 m/s from CREDOS EDDF-1 campaign. Measurements by lidar (symbols) and predictions with D2P and DVM wake vortex models (lines).

The Deterministic wake Vortex Model (DVM) is the new wake vortex predictor software developed by UCL, establishing a step forward in terms of robustness, modularity and performance. It is based on the numerical methodology and the physical models of the Vortex Forecast System (VFS), originally developed by an international (Jackson et al. 2001) and further improved and calibrated (against two US and two EU campaigns, and against LES) since 2002 in the framework of various EU-funded projects. The

DVM accounts for the effects of wind transport (cross and axial), wind shear, decay due to turbulence, stratification, and ground proximity (Winckelmans et al. 2005). It also includes improvements regarding the evaluation of the vertical profiles of environmental conditions and of the In-Ground-Effect model. The Probabilistic wake Vortex Model (PVM) is using the DVM in a Monte Carlo approach, taking into account the uncertainties and variations of the impact parameters from the aircraft and meteorological side and of some physical model coefficients of the DVM.

Hazard-Area Module

The Hazard-Area Module computes the distance of the follower aircraft (center of gravity) to the vortex centers within each gate along the flight path. Then the closest distance between the follower aircraft and the vortex pair over all gates along the flight path is determined by interpolating aircraft trajectories and wake trajectories between the gates. This closest approach is used for further statistical analysis with WakeScene-D (e.g. vortex age and circulation for this point in time).

In order to estimate the severity of the potential wake vortex encounter an Area of Interest can optionally be defined around the vortices. If the trailing aircraft penetrates this Area of Interest the wake vortex encounter is classified as potentially hazardous. This is considered as a preliminary severity assessment. A corresponding concept called Simplified Hazard Areas has been developed in Schwarz & Hahn (2006) and adapted for take-off and departure. Cases violating the Area of Interest can be subject to more detailed severity assessment with VESA.

Estimation of Uncertainty

Any software which may be employed to assess the safety of a wake-vortex advisory system must constitute a sufficiently accurate representation of the projected operation. However, for complex risk assessment tools straightforward validation appears not feasible, because the significant manifold of modeled parameters can not be measured simultaneously and reconstructed consistently in a simulation. For WakeScene-D the identification of the relevant processes and the definition of the appropriate degree of details with which they have to be modeled rely on thorough discussion and expert opinion. For the validation of the employed sub-models we refer to the studies cited above.

Here we perform exemplarily a simple estimation of uncertainty for the most important parameter, which is lateral vortex transport, at a vortex generator height of about 50 m, which is within the most critical height range of 100 m above ground (Elsenaar et at. 2006). For B744 and A343 aircraft the difference of predicted and measured standard deviations of lateral aircraft position amounts to σ_{ac} = 6.8 m. For these aircraft types the median RMS deviation of measured and predicted wake vortex positions employing the D2P model has been estimated to σ_{vort} = 19.2 m (Holzäpfel & Steen 2007). For our purposes here the statistics only need to be accurate on average; i.e. the predictions do not need to be correct in space *and* time. Because the vortex position uncertainty is dominated by spatial and temporal variations between the measured crosswind and the crosswind sensed by the vortices the latter estimation is outmost conservative. Therefore, it can be understood that the vortex prediction uncertainty also implies uncertainties from numerical weather prediction. Assuming that these uncertainties are independent and statistically stationary, the overall uncertainty amounts to $\sigma_{tot} = (\sigma_{ac}^2 + \sigma_{vort}^2)^{1/2}$ = 20.3 m. For this scenario and 120 s old vortices WakeScene-D determines a vortex spreading with σ_{obs} = 337.3 m. Hence, a very conservative estimation of the relative uncertainty of lateral vortex positions in ground proximity can be estimated to 6.0.

Reference Scenario

The described scenario serves as a reference which shall represent the real current departure situation. The working hypothesis assumes that the encounter frequencies estimated for reduced separations under appropriate crosswind conditions shall not be higher than in the reference scenario. Note that the encounter frequencies denote the fraction of encounters within a given scenario. In order to obtain the absolute probability of encounters in a scenario, the encounter frequency must be multiplied by the frequency of the considered crosswind situation.

The reference scenario employs a sample size of 1,000,000 aircraft pairings. A306, A310, A333, A343, B744 and B772 aircraft are used as vortex generators and A320, AT45, B733 and CRJ as followers. The traffic mix is modeled according to the statistics of Frankfurt airport in 2006 (Anon. 2006). All follower aircraft obey the 120 s ICAO separation. The following parameters of the generator and the follower aircraft are randomly distributed: start point, take-off weight, thrust mode (TOGA take off go around or FLEX take off (reduced) thrust), departure route combination, trajectory deviation, and pilot delay parameter. We employ randomly chosen meteorological data of the NOWVIV one-year data base within the operational hours of Frankfurt airport (6:00 – 23:00). Furthermore, cases with tailwinds above 5 knots are excluded. The constraints regarding operational hours and tailwind are also applied for all other investigated cases.

Figure 6 singles out the fraction of departures (70,167 cases or 7.0%) in which the follower aircraft approach the vortices closer than 50 m and the vortices still have at least a circulation of 100 m2/s. These cases potentially correspond to an encounter and should be understood as cases of interest or potential encounters. Detailed investigations with VESA are necessary to identify the risks related to such potential encounters. For convenience we call these cases simply encounters without regard to the real connected risks.

Remarkably, 66% of these “encounters” are restricted to heights below 300 ft above ground (see Figure 6a). Within this altitude range clearance of the flight corridor by descent and advection of the vortices is restricted: stalling or rebounding vortices may not clear the flight path vertically and weak crosswinds may be compensated by vortex-induced lateral transport (Holzäpfel & Steen 2007). This culmination of vortex encounters at low altitudes indicates that the sought crosswind criterion could be limited to this height range, which would substantially facilitate the implementation of an operational system.

Further, minor peaks at 1300 ft and at 1800 ft occur in Figure 6a. These minor peaks can be attributed to flight path changes which increase the encounter risk compared to approximately parallel flight of the leader and follower aircraft. Figure 7 exemplifies a typical situation: At about 1500 ft the leading aircraft reduces thrust and thus the climb rate; at the same time it initiates a turn towards a southerly direction. The combination of this flight path diversion with a strong headwind component which counteracts the vortex descent and a southerly wind direction leads to the displayed encounter at 1250 ft. The second cluster of encounters at 1800 ft is related to the resumption of climb when the aircraft reach the final climb speed. A number of other combinations of flight path diversions and adverse wind directions have been identified, both for identical and different departure routes of the leader and follower aircraft.

Figure 6b reveals that within the 50 m distance the encounter frequency depends only weakly on the separation between aircraft and wake vortices. Figure 6c and d indicate a considerable range of vortex ages between 80 s and 150 s corresponding to vortex strengths between 100 and 430 m2/s. The irregular circulation distribution in Figure 6d is mostly related to differing vortex decay characteristics of the different generator aircraft types in combination with different decay rates in ground proximity and aloft. Figure 6e illustrates that in 19% of the encounters the vortices still approximately retain their initial vortex spacings ranging from 34.5 m to 50.6 m for the selected vortex generator aircraft types. The cluster of vortex separations beyond 100 m represents the range typically occurring after vortex rebound in ground proximity.

Figure 6f displays encounter frequencies dependent on the minimum distance between the follower aircraft and the vortex during the whole departure and the respective circulation, Γ. The frequency of encounters with $\Gamma > 100\ m^2/s$ reduces from 7.0% for vortex distances below 50 m to 0.20% for distances below 2 m. For circulations stronger than 350 m^2/s the encounter frequencies are 0.10% for vortex distances below 50 m and reduce to 0.0037% (37 cases of 1,000,000 departures) for distances below 2 m.

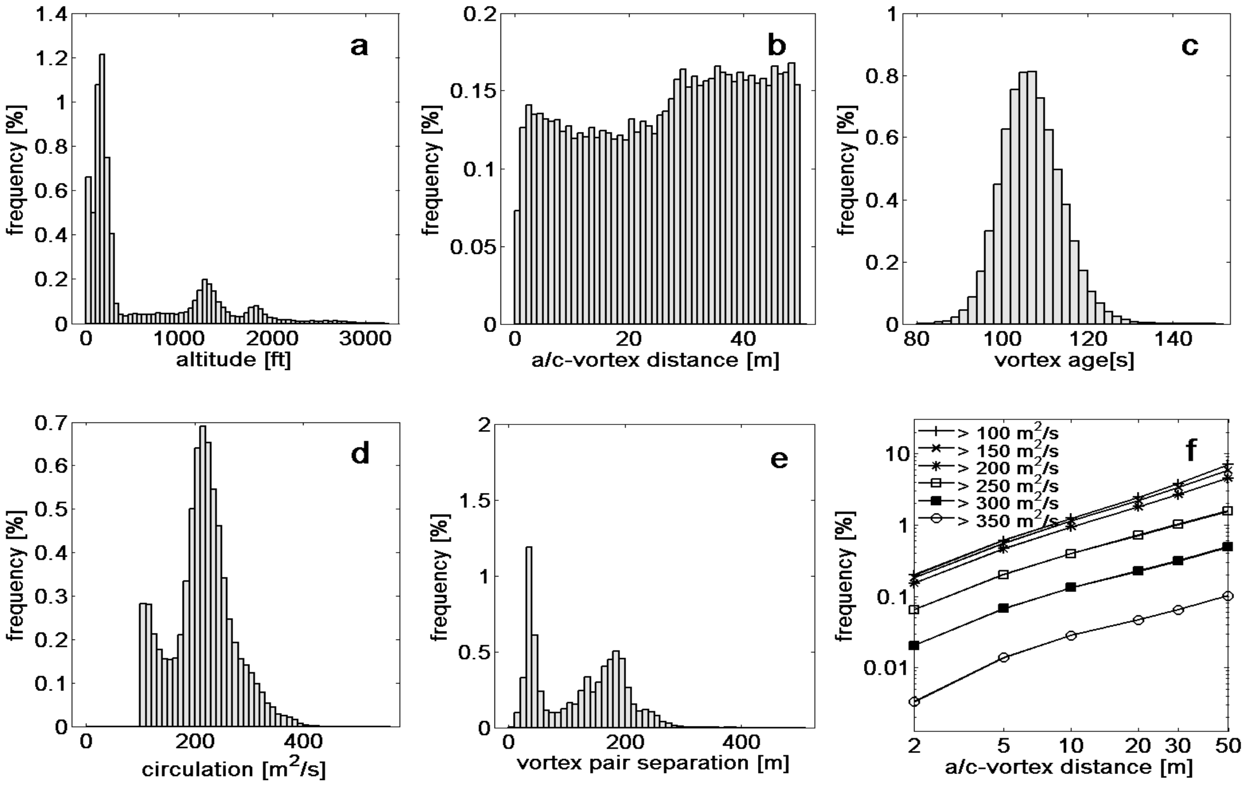

Figure 6. Statistics of cases of interest in the reference scenario. a) Aircraft altitude, b) distance between follower aircraft and wake vortex, c) vortex age, d) vortex circulation, e) vortex pair separation, and f) encounter frequencies dependent on distance to the vortex and circulation.

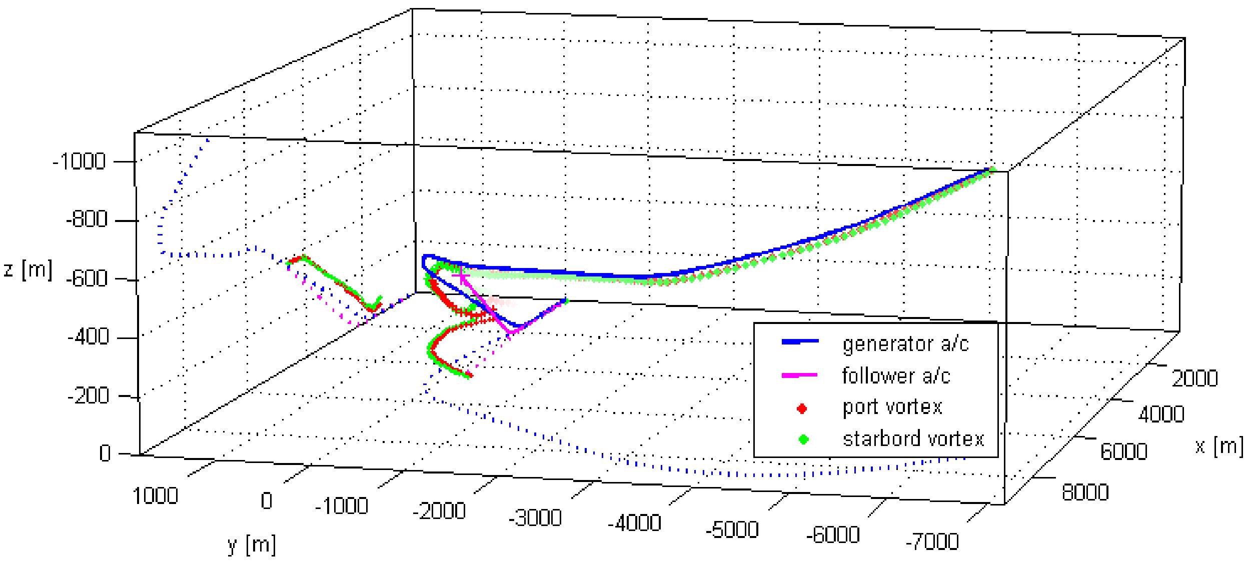

Figure 7. Perspective view of trajectories of wake-generating aircraft (blue) and follower aircraft (magenta) together with wake vortex positions (starboard vortex green, port vortex red). Projections of aircraft and vortex positions on vertical and horizontal planes are added for convenience.

The considered range of distances to the vortex and circulation strengths was chosen such that, on one hand, no cases of interest are missed and, on the other hand, the rarest strong encounters are captured. Note that the weakest potential encounters (Γ > 100 m^2/s, aircraft-vortex distance < 50 m) in many cases may not lead to any perceptible interference. On the other hand, close encounters on the order of 2 m to 5 m are almost not feasible because they are impeded by wake vortex induced aircraft reactions. In this approach factors like encounter angles, flight attitude and altitude of the follower aircraft are neglected. Therefore, only VESA which fully considers the encounter situation including the interaction of aircraft and wake vortex may really evaluate the related risks. Because VESA investigations are out of the scope of this paper, the metrics of Figure 6f are used to relatively compare the risks of the different scenarios. A target scenario is considered safe when all these joint frequencies are below the reference scenario.

Crosswind Dependency

Statistics of encounter frequencies and encounter conditions have been produced for 60 s and 90 s departure separations and crosswind thresholds from 0 to 10 knots in 2 knot increments, respectively. All other parameters correspond to the reference scenario. The crosswind criterion is met when the crosswind at 10 m height above ground exceeds a predefined threshold. This crosswind criterion has been selected because (i) 10 m is the standard height for surface wind measurements and thus constitutes the operationally simplest approach for crosswind dependent reduced separations. (ii) Most encounters are restricted to heights below 300 ft above ground. (iii) An investigation of wind conditions at Frankfurt airport (Dengler & Wiegele 2008) reports a 95%-correlation of the crosswind at 100 m height with the 10 m wind measurement.

Three independent analyses of field measurement data of wake vortices generated by departing aircraft in an altitude range from 0 to 400 m at Frankfurt airport have been performed within the CREDOS project to determine crosswind thresholds which ensure that the wake vortices have left a safety corridor at certain aircraft separation times (Dengler et al. 2011). Although the three analyses employ different assumptions on the safety corridor definition and size, the employed confidence levels, and the crosswind measurement sources and definitions, they consistently yield crosswind thresholds on the order of 4 m/s to make sure that the wake vortices have escaped a safety corridor at a vortex age of 60 s with a high probability based on good quality wind measurements. Note that such studies do not allow quantifying the related risks and setting the risks into relation to the current ICAO operations.

The corresponding WakeScene-D results for aircraft separations of 60 s and crosswinds above 8 knots (4.1 m/s) are displayed in Figure 8. The overall frequency of encounters of 3.1% (31,239 cases) is clearly below the corresponding frequency of 7.0% of the reference scenario. Figure 8 shows in agreement with the experimental results that the strong crosswind in ground proximity is outmost effective. The remaining 56 encounters below 300 ft can be almost neglected compared to the corresponding 45,962 encounters in the reference scenario. Now the peak at 1800 ft related to flight path diversions clearly dominates the scenario.

The encounter synopsis in Figure 8f indicates that despite of the reduction of the overall encounter frequencies the encounters with circulations stronger than 350 m^2/s are still 2 to 4 times more frequent than in the reference scenario in Figure 6f. This can be explained by the halved time for vortex decay. Two facts may potentially reduce the hazard of the current encounters compared to the reference scenario. The encounters occur at sufficiently high altitudes to provide ample time for pilots to recover. The encounter angles are increased which could potentially reduce adverse effects for the follower aircraft.

Figure 9. Figures 9 and 10 depict the so-called encounter angles γ and ψ which denote the inclination angle and the azimuth angle between vortex axis and flight path of the follower aircraft, respectively. Negative inclination angles γ denote situations where the aircraft approach the vortex from below. Negative azimuth angles ψ refer to encounters from the left, i.e. the aircraft hit in general the port vortex.

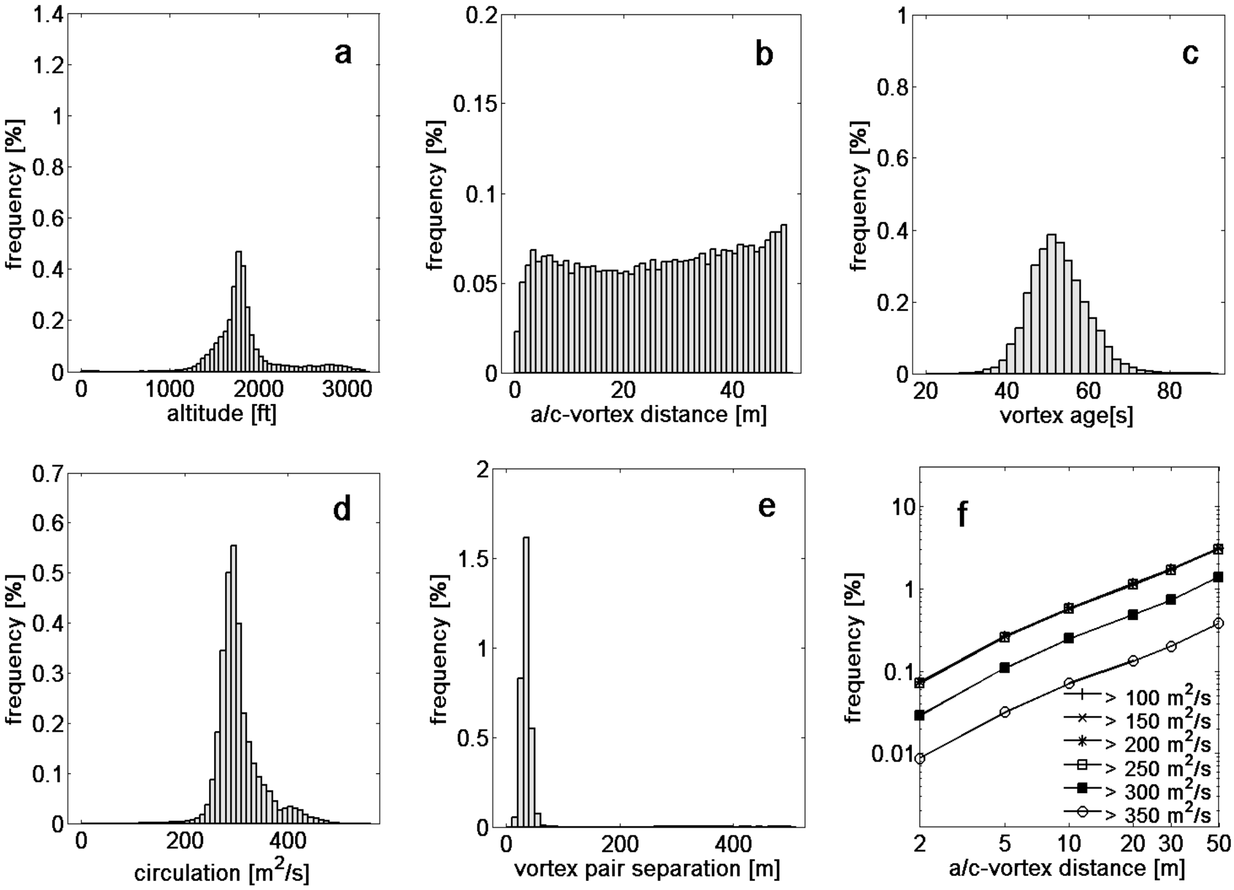

Figure 8. Statistics of cases of interest for aircraft separated by 60 s and a crosswind threshold of 8 kn.

Figure 9 shows the encounter angles with color-coded circulation values for the reference scenario. The predominantly negative inclination angles γ below 300 ft correspond to cases where the aircraft approach the wake vortices from below after the vortex rebound. Due to the ground induced decay the corresponding circulation values are relatively low. Aloft the inclination angles on average are slightly negative. This can be explained to some extent by the steeper climb rates of the follower aircraft and to some extent by reduced descent rates of aged wake vortices. At about 1500 ft the aircraft reduce the climb rate in order to accelerate. Below that altitude range the aircraft with higher climb rates encounter less inclined vortices ($\gamma < 0$, see Figure). Inversely, positive inclination angles (encounter from above) occur in the altitude range where the follower aircraft with lower climb rates encounter wake vortices which were generated by aircraft which have already resumed climb when they have reached the final climb speed.

The azimuth angles ψ are on average negative. This can probably be attributed to the more frequent south-westerly winds. Crosswinds directed from port to starboard are tilting the vortices in azimuthal direction because the longer residence times of older vortex segments lead to larger transport distances. The turns around 1500 ft and 2000 ft (see Figure 2) lead to increased encounter azimuth angles with either sign depending on the departure route combinations and the wind direction (see Figure 7).

Figure 10 shows the encounter angles for 60 s aircraft separations with crosswinds above 8 knots. Now encounters at low altitudes have almost completely disappeared. Most of the remaining encounters are occurring above 1000 ft and can be explained by the flight path changes discussed above. A remarkable concentration of encounters with strong vortices between 1000 ft and 1700 ft occurs with inclination angles centered on zero and azimuthal angles around 30 deg. These strong encounters mainly occur if the leading aircraft follows a southerly departure route. In these cases the leading aircraft have already initiated a turn without reducing the climb rate and south-westerly winds compensate vortex induced descent.

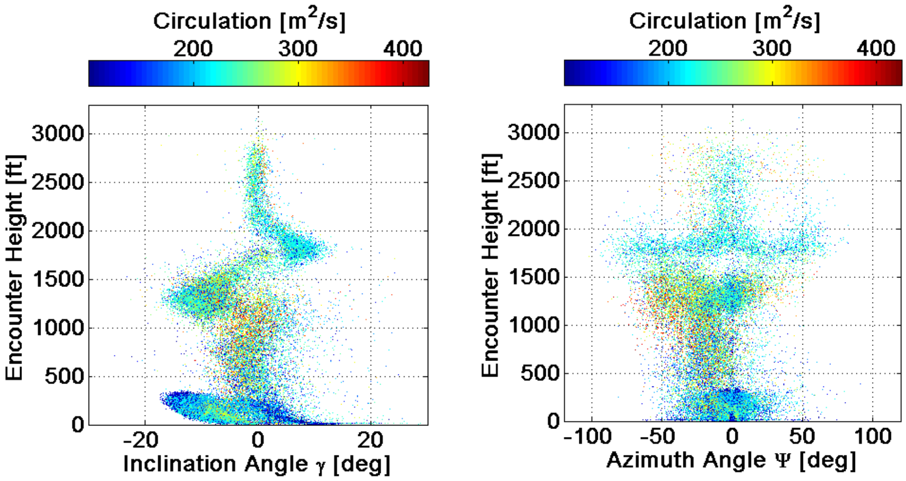

Figure 9. Encounter angles γ (inclination angle) and ψ (azimuth angle) dependent on altitude with color-coded circulation for the reference scenario.

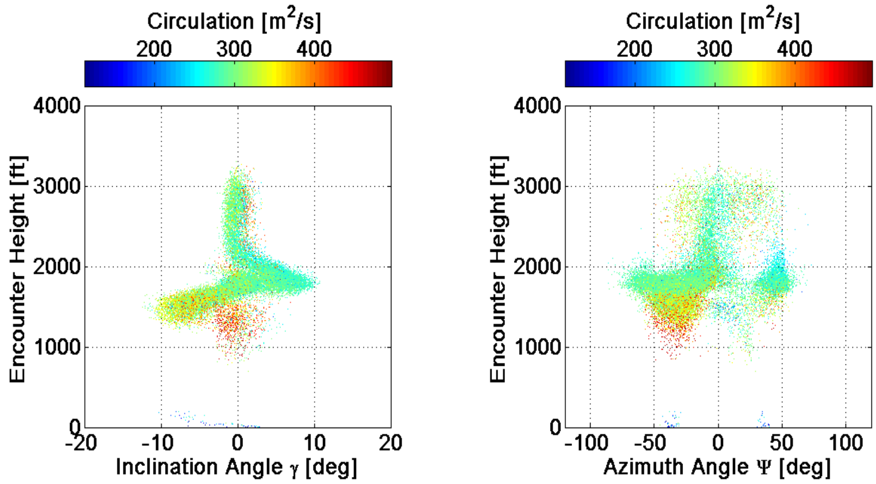

Figure 10. Encounter angles dependent on altitude with color-coded circulation for 60 s aircraft separations with crosswinds above 8 knots.

Table 1 provides a synopsis of the encounter frequencies for the investigated crosswind and departure separation scenarios. The crosswind threshold and aircraft separation combinations where the encounter frequencies fall below the reference scenario (highlighted in dark grey) are highlighted in light grey. A In summary crosswinds are very effective to reduce encounter frequencies close to the ground already for crosswinds stronger than 4 knots (6 knots) at 90 s (60 s) aircraft separations. As a consequence, the encounters at higher altitudes become more prominent. Due to the reduced time for vortex decay worst case encounter frequencies aloft are not reduced very effectively by increasing crosswinds.

Figure 11 shows the frequencies of the crosswinds in the meteorological data base in 0.5 knot increments (All CWs) and the respective encounter frequencies versus crosswind speed for aircraft separations of 60 s, 90 s, and 120 s. The left plot displays absolute frequencies whereas the relative frequencies shown on the right are normalized to 100%. Figure 11 indicates that the highest encounter frequencies are not observed for zero crosswinds. For the reference scenario 120 s and the 90 s departure separations they occur instead around crosswinds of ± 1 to ± 1.5 knots. If the aircraft separation is reduced to 60 s, the most critical crosswinds amount to ± 2.5 knots. This is due to the fact that weak crosswinds may compensate the vortex-induced lateral propagation speed of wake vortices generated in ground proximity such that the luff vortex is hovering above the runway (Holzäpfel & Steen 2007). For the 60 s separation the critical crosswind magnitude is higher because the crosswind has less time to transport the vortices out of the flight corridor.

Table 1. Synopsis of encounter frequencies for different aircraft separations and crosswind scenarios.

Scenario	120 s all CWs	90 s 60 s all CWs	90 s 60 s CW > 2kts	90 s 60 s CW > 4kts	90 s 60 s CW > 6kts	90 s 60 s CW > 8kts	90 s 60 s CW > 10kts
total encounter frequency	7.0%	12.8% 19.9%	7.5% 17.7%	3.7% 8.3%	2.6% 3.8%	2.2% 3.1%	1.9% 2.7%
encounter frequency below 300 ft	4.6%	9.4% 15.8%	2.9% 13.1%	0.057% 3.5%	0.0003% 0.10%	0.0002% 0.0056%	0.0% 0.0044%
worst case encounter frequency	0.0037%	0.023% 0.11%	0.011% 0.056%	0.0073% 0.020%	0.0041% 0.010%	0.0026% 0.0086%	0.0017% 0.0025%

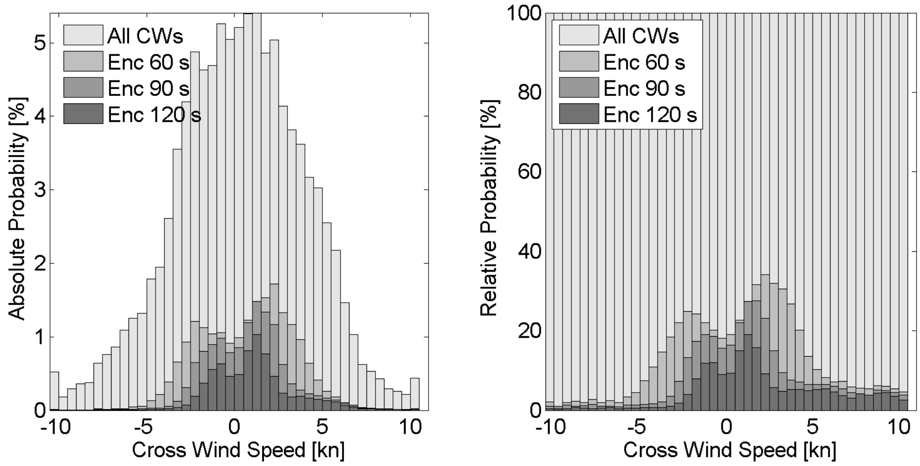

Figure 11. Left: Crosswind distribution in 0.5 knot increments and respective absolute encounter frequencies for different aircraft separations. Relative encounter frequencies right. Winds blowing from the port side are positive.

Figure 11 right indicates that for the 120 s separation crosswinds above 2.5 knots do not significantly reduce the relative encounter frequencies. For the 90 s separation this is the case above about 4 knots and for the 60 s separation the corresponding threshold is at about 6 knots. Beyond these thresholds the encounters at high altitudes related to flight path diversions constitute the dominant risks.

Somewhat surprisingly the histograms are not symmetric. Note that already at -5 to -5.5 knots the relative encounter frequency for 60 s separations is lower than the encounter frequency for 5 to 5.5 knots for the 120 s reference scenario. Several reasons for the asymmetry can be identified: (i) the realistic meteorological data base contains distributions of wind speed and direction which are not only the result of predominant synoptic patterns but are also influenced by the orography in the vicinity of the airport, in particular the Taunus mountain ridge. (ii) The winds aloft generally deviate from the winds at 10 m altitude and (iii) the departure routes are not symmetric with respect to the runway. (iv) The most important and fundamental effect, however, is related to the turning of the wind direction to the right with increasing height (Ekman Spiral). This effect is described in more detail below.

Comparison to Field Measurement Data

The validation activities for the individual sub-models and data bases of WakeScene-D and an estimation of the related uncertainties are described above. Here we perform a *global* comparison of wake vortex transport characteristics achieved with long-term measurements and WakeScene-D simulations. Note that this comparison assumes that the employed data sample is sufficiently large to provide converged wake vortex transport statistics in a climatological sense. During the six months CREDOS measurement campaign EDDF-2, vortex tracks of about 10,000 departures from runway 25R of Frankfurt airport were collected with the WindTracer lidar (Dengler & Wiegele 2011). The lidar measurement plane was situated 2961 m from the threshold of runway 25R (see Figure 2) where 99% of the vortices were measured at heights below 135 m. Wake vortices that might have been advected from runway 25L to 25R are not part of the data set.

To mimic the lidar measurements with WakeScene-D we have simulated 10,000 departures with randomly chosen aircraft types and meteorological data. Wake vortex predictions are interpolated within the lidar measurement plane. The lidar scan pattern leads to vortex observations roughly each 8 s. To provide similar visual impressions of the scatter plots the WakeScene-D wake vortex data are also plotted each 8 s where the instant for the first data point is varied randomly.

Figure 12 shows scatterplots of lateral positions of the port vortex against time based on the lidar measurements and WakeScene-D simulations. Additionally, the medians and distributions for one to three standard deviations are plotted. The comparison of the measurements (left) to the simulated lidar data (center) indicates that the domain covered by the lidar constitutes a sub-domain of the real wake vortex transport distances. Zooming the WakeScene-D simulation data on the area covered by the lidar (right) reveals an excellent agreement between measured and simulated lateral vortex transport characteristics. The main differences are related to shorter lidar observation times caused by a loss of the coherent vortex structure during the decay. This good agreement indicates that WakeScene-D supports investigating realistic wake vortex behaviour in domains and height ranges that are far out of reach of measurements. Because the modelling of wake vortex transport in ground proximity is quite complex it could be assumed that the agreement with observations would be even better at higher altitudes.

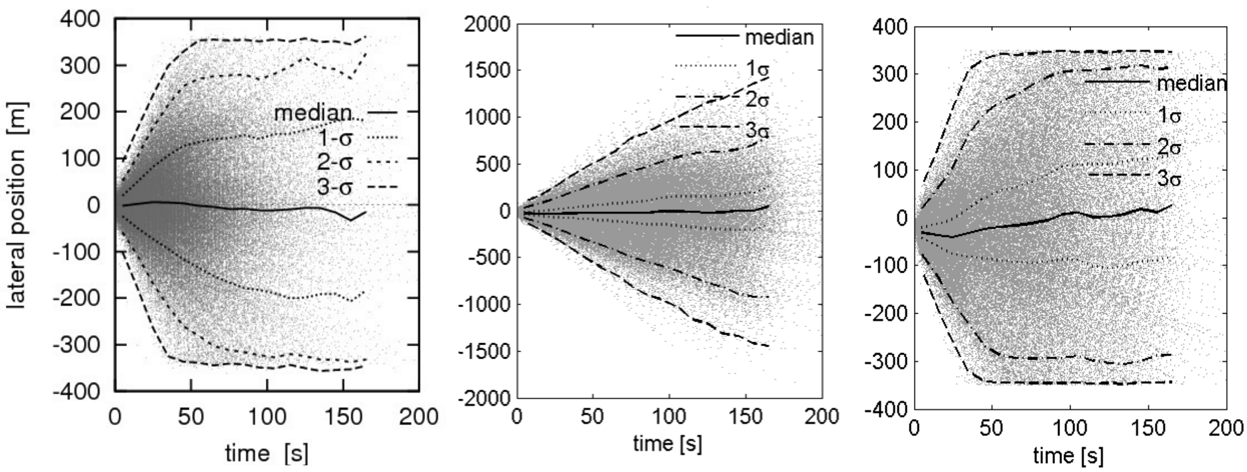

Figure 12. Scatterplots and statistical distributions of lateral positions of the port vortices against time for 10,000 departures. Field measurement data (left) and WakeScene-D predictions within different domains (center and right).

Sensitivity Studies

Comprehensive sensitivity analyses regarding the impact of various sub-models and parameter selections have been performed. A detailed description of all the studies is available in Holzäpfel & Kladetzke (2009).

Wind Directions

Now effects of wind directions on the encounter frequencies are considered. Four different wind direction sectors are distinguished: headwind, tailwind, crosswind from port side, and crosswind from starboard side. Here the wind directions are defined with respect to the runway direction. So headwinds are blowing from 315° < RWA < 45° where RWA denotes the relative wind angle with respect to the runway direction. Winds from the starboard side correspond to the wind direction range 45° < RWA < 135°.

Table 2 lists the encounter frequencies dependent on the four different wind direction sectors for the reference scenario. Headwind situations lead to the highest encounter probabilities because headwind transport of the wake vortices may compensate wake vortex descent or even lead to rising wake vortices with respect to the generator aircraft trajectory. This effect increases encounter frequencies because the medium weight class followers usually take off earlier than the leader and climb steeper than the leading aircraft and therefore usually fly above the wake vortices. In contrast, the encounter frequencies for tailwind situations are much lower (more than a factor of five), because tailwinds support wake vortex descent.

Table 2. Encounter frequencies dependent on four different 90° wind direction sectors for the reference scenario. The wind sector icons assume a flight direction from right to left.

SID-comb. wind dir.	all	N-N (16.0 %)	N-S (24.0 %)	S-N (24.0 %)	S-S (36.0 %)
CW port (20.9 %)	5.2%	4.6%	4.3%	5.3%	6.1%
CW starb. (18.9 %)	1.7%	1.6%	1.6%	1.5%	1.9%
tailwind (22.4 %)	2.5%	2.3%	2.1%	2.4%	2.9%
headwind (37.8 %)	13.3%	13.4%	13.3%	13.0%	13.4%

However, the smallest encounter frequencies are observed for crosswinds from the starboard side. Here the crosswinds close to the ground reduce encounter frequencies. With increasing height the wind direction turns on average to the right. Consequentially, a tailwind component is added to the crosswind which supports vortex descent and thus reduces encounter frequencies aloft.

The turning of the wind direction with altitude is related to the concept of the Ekman spiral depicted in Figure 13: Above the atmospheric boundary layer with a thickness on the order of 1 km the wind direction is mainly controlled by the equilibrium of the driving pressure gradient force and the Coriolis force. The resulting wind is called geostrophic wind. In the atmospheric boundary layer the friction force causes a deviation of the wind direction to the left (on the northern hemisphere).

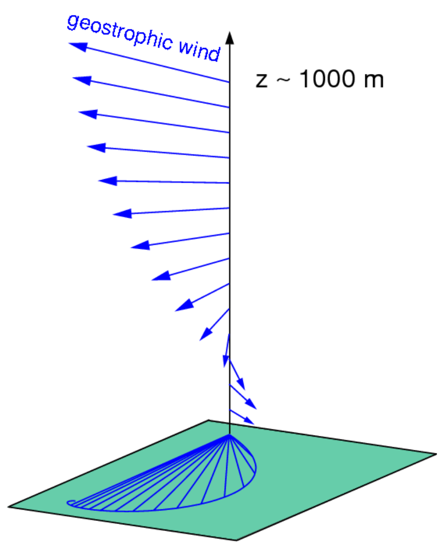

Fig. 13. Schematic sketch of Ekman spiral.

Due to the same mechanism crosswinds from port side receive a headwind component with increasing height. As a consequence, the port crosswind situation leads to three times more encounters than the starboard side crosswinds. Additionally, crosswinds from the port side also support encounters for departures of the leading aircraft on the southerly departure routes. There is also some weak trend that the strongest circulation values occur for the headwind encounters (not shown).

Table 3 lists the wind direction effects for 60 s aircraft separations and crosswinds above 6 knots. Because cases with tailwinds above 5 knots are excluded from operations, the wind sector for tailwinds has no contributions. The encounter frequencies for headwinds and for crosswinds from the port side are now almost identical. Considerable differences occur between the different departure route combinations. Small encounter frequencies are observed for headwinds and crosswinds from the port side (southerly winds) for leading aircraft on the northern departure routes and, conversely, for crosswinds from the starboard (northerly winds) side for leading aircraft on the southern departure routes. Hence, encounters can be avoided if the crosswind after the turn transports the vortices away from the former flight track, i.e. southerly crosswinds are favorable for turns to the north.

The smallest encounter frequencies occur for crosswinds from the starboard side combined with the S-N SID combination. Here two favorable effects are combined: the turning of the crosswind to a tailwind at increasing altitudes and the fact that the vortex generating aircraft uses the downwind departure route. Crosswinds above 8 knots show similar characteristics with further reduced encounter frequencies.

Table 3. Encounter frequencies and corresponding circulation strengths dependent on four different 90° wind direction sectors for 60 s aircraft separations and crosswinds above 6 knots.

SID-comb. wind dir.	all	N-N (16.0 %)	N-S (24.0 %)	S-N (24.0 %)	S-S (36.0 %)
CW port (38.0 %)	5.5%	1.8%	1.4%	7.7%	8.5%
CW starb. (44.7 %)	1.5%	0.9%	3.5%	0.2%	1.3%
tailwind (0 %)	–	–	–	–	–
headwind (17.2 %)	5.8%	1.6%	2.7%	7.9%	8.3%

Key Results of Remaining Studies

Sample size: It must be guaranteed that the sample size of the Monte Carlo simulations is sufficiently large to provide converged simulation results also for rare events. For this purpose statistics of encounter frequencies derived from sample sizes of 10^4, $5{\cdot}10^4$, 10^5, $2{\cdot}10^5$, $5{\cdot}10^5$, and 10^6 departures of aircraft pairings have been analysed for different scenarios. It was found that a reasonable representation of the frequencies of the most critical and rare encounters requires sample sizes of 500,000 departures of aircraft pairings. Therefore, the one million sample size used for the current investigations guarantees well converged statistics.

Operation times: By default the meteorological data of the NOWVIV one-year data base is employed only within the operational hours of Frankfurt airport (06:00 – 23:00). A comparison to 24 h operations indicates a minor increase of encounter frequencies for nocturnal meteorological conditions. This can potentially be explained by the reduced turbulence in the residual layer which increases vortex lifetimes and the increased temperature stratification which reduces vortex descent.

Flight path adherence: Deviations from nominal flight tracks in vertical and horizontal direction have been determined being on the order of 100 m. Therefore, the sensitivity of encounter frequencies of the standard flight path deviation model has been compared to a version in which these deviations were deactivated. The study indicates that the deactivation of aircraft trajectory deviations only slightly reduces the encounter frequencies.

Pull-away effect: In contrast to arrivals where a close-up effect on average reduces aircraft separations, an increase of average aircraft separations is expected for departures. The reason is that at a given time the leading aircraft has arrived in general already at a higher flight speed than the follower aircraft. The simulations indicate that the separation increases are spread between 0 to 3 NM that is the minimum initial separation is never reduced. The pull-away effect is the more pronounced the more the initial aircraft separations are reduced.

Departure Routes: For the encounter statistics with crosswinds above 8 knots the differences between the departure route combinations are quite prominent because the encounters in ground proximity (which are independent from SID combinations) are already quite rare (see Figure 8) and many encounters aloft are related to flight path diversions. As a result for a generic airport the SID combination study indicates that reduced departure separations could be supported by crosswinds above 8 knots for a straight departure route. For diverging departure route combinations the procedure could be refined by using only SID combinations where the leading aircraft is flying on the downwind SID.

Wake vortex model: Wake vortex modeling constitutes a very important element of WakeScene-D. Therefore, the statistics achieved with the D2P wake vortex model have been compared to results of the Deterministic Vortex Model (DVM). The two wake vortex models deliver very similar characteristics of encounter altitude, the distance between follower aircraft and wake vortex, and vortex age. The circulation distributions exhibit different characteristics but almost identical ranges. In ground proximity the D2P model predicts more pronounced vortex spreading. For the statistics of encounter strength and distance between aircraft and vortex similar characteristics are found. The corresponding deviations are naturally more pronounced for the rare encounters and reside typically within a range of 5% to 30%. Because the encounter frequencies of equal strength vary between the different scenarios by up to almost two orders of magnitude, the agreement between the encounter statistics of the two wake vortex models is considered as good. In particular, the conclusions derived from the synopsis of the encounter frequencies in Table 1 would be identical with the DVM wake vortex predictions.

Aircraft-type combinations / Take-off weight: The encounter frequencies of the considered scenarios have been filtered to attribute the encounters to the 24 possible leader/follower combinations. As expected encounters are avoided if the leading aircraft take off late and climb slowly whereas the follower aircraft take off early with a steep climb rate. Thereby, the respective flight tracks are well separated. In contrast, if the leading aircraft take off early and climb steeply whereas the follower aircraft take off relatively late, the resulting flight tracks may be close to each other leading to high encounter probabilities. The same interrelations also apply to the take-off-weight distributions (which correlate with take-off positions and climb rates) within specific aircraft type combinations.

Comparison to arrival situation: The comparison of the current reference scenario (see Figure 6f) to WakeScene results for arrivals obeying the ICAO minimum separation of 5 NM between heavy and medium aircraft in (Holzäpfel et al. 2009-1) indicates that encounters (Γ > 100 m^2/s and distances to the vortices below 30 m) are 5.6 times more frequent for arrivals (21.5%) than for departures (3.8%). For approaches the accumulation of encounters within a height range below 300 ft is with about 95% even more pronounced. The reason for these differences can mainly be attributed to the much more pronounced spreading of aircraft trajectories for the departure situation which is caused by e.g. large variations of rotation point and climb rate. Note that the considered departure and arrival scenarios can not be directly compared due to differences regarding sample size and traffic mix. Further, in the arrival simulations the aircraft are already installed on the glide slope whereas for departures waypoints with diverging flight routes are considered.

Implementation of Lessons Learned

Here we investigate an advanced crosswind scenario which is based on the lessons learned from the sensitivity analysis. First, we restrict the analysis on the northern departure routes used by default at Frankfurt airport where encounters are relatively rare. Second, we differentiate crosswinds blowing from the port side and the starboard side of the departing aircraft. Encounter frequencies for 60 s departure separations and a crosswind threshold of 6 knots indicate that for positive crosswinds (wind from port side) the worst case encounter frequency of 0.0082% is higher than in the reference scenario (see Table 1). However, for crosswinds below -6 knots (wind from starboard side) the encounter frequencies of all circulation and distance thresholds are smaller than in the reference scenario (worst case encounter frequency is 0.0031%). In conclusion, the consideration of the northern departure routes as used routinely at Frankfurt airport yields encounter frequencies below the reference scenario for all considered vortex distances and circulation strengths for crosswinds below -6 knots (wind from starboard side) and for crosswind magnitudes above 8 knots. The assessment of the related encounter risks with VESA leads to the same conclusions (Kauertz 2009, Kauertz et al. 2012).

Conclusions

WakeScene-D is a software package to determine wake vortex encounter probabilities for departures. The severity of potential encounters identified by WakeScene-D can subsequently be evaluated with VESA (Kauertz et al. 2012). In this paper first the components of WakeScene-D which model traffic mix, aircraft trajectories, meteorological conditions, wake vortex evolution, and potential hazard area are briefly introduced. Then various investigated scenarios are discussed which shall support the identification of suitable crosswind criteria that allow reducing aircraft separations for departures.

Measured vortex tracks of about 10,000 departures from runway 25R of Frankfurt airport are compared with WakeScene-D simulations. For lateral vortex transport, which for crosswind departures constitutes the most important quantity, good agreement between the characteristics of measurement and simulation is achieved. This good agreement indicates that WakeScene-D is an instrument which allows investigating realistic wake vortex behaviour in domains and height ranges that are far out of reach of measurements.

Monte Carlo simulations of the Frankfurt traffic mix with a sample size of 1,000,000 cases indicate that for current operations 66% of the potential encounters are restricted to heights below 300 ft above ground. Within this altitude range clearance of the flight corridor by descent and advection of the vortices is restricted: stalling or rebounding vortices may not clear the flight path vertically and weak crosswinds may be compensated by vortex-induced lateral transport (Holzäpfel & Steen 2007). Further, minor peaks at altitudes of 1300 ft and at 1800 ft occur which can be attributed to flight path diversions (change of climb rate and heading) in combination with adverse wind conditions (headwind and crosswind) which increase the encounter risk compared to approximately parallel flight of the leader and follower aircraft. For example, increased encounter frequencies are observed when the leading aircraft conducts a turn towards the main wind direction. The resulting headwind component may compensate wake vortex descent and may advect the vortex trail into the flight path of the follower aircraft.

Statistics of encounter frequencies and encounter conditions have been established for 60 s and 90 s departure separations and minimum crosswinds from 0 to 10 knots in 2 knot increments, respectively. The reduction of aircraft separations from 120 s to 60 s approximately triples the number of encounters, whereas the fraction of strong encounters increases due to the reduced time for vortex decay. If aircraft separations are reduced to 60 s and crosswinds at 10 m height above ground exceed a threshold of 8 knots, the overall frequency of potential encounters of 3.1% clearly is falling below the corresponding frequency of 7.0% of the reference scenario. The strong crosswind in ground proximity very efficiently reduces the encounters below 300 ft from 4.6% in the reference scenario to 0.0056%. Unfortunately, the 10 m crosswind criterion alone is not sufficient to reduce encounters which are related to flight path diversions along the departure routes. Due to the by 50% reduced time for vortex transport and decay, encounters with circulations stronger than 350 m^2/s are still 2 to 4 times more frequent than in the reference scenario.

An investigation of wind direction effects on the encounter frequencies reveals an intriguing phenomenon: Headwind situations lead to the highest encounter probabilities because headwind transport of the wake vortices may compensate wake vortex descent or even lead to rising wake vortices with respect to the generator aircraft trajectory. This effect increases encounter frequencies because the medium weight class followers usually take off earlier and climb steeper than the leading aircraft and therefore usually fly above the wake vortices. In contrast, the encounter frequencies for tailwind situations are much lower because tailwinds support wake vortex descent.

However, the beneficial effects of crosswinds are not symmetric. The smallest encounter frequencies are observed for crosswinds from the starboard side. Here the crosswinds close to the ground reduce encounter frequencies. With increasing height the wind direction turns on average to the right. Consequentially, a tailwind component is added to the crosswind which supports relative vortex descent and thus reduces encounter frequencies aloft. This turning of the wind direction with height is related to the concept of the Ekman spiral which describes the resulting wind direction in the atmospheric boundary layer by equilibrium of the driving pressure gradient force, the Coriolis force, and the friction force. Due to the same mechanism crosswinds from port side receive a headwind component with increasing height. As a consequence, the port crosswind situation leads to significantly more encounters than the starboard side crosswinds.

From a WakeScene-D perspective it can be concluded that for 60 s departure separations along the northern departure routes as used routinely at Frankfurt airport acceptable encounter frequencies are found for crosswinds below -6 knots (wind from starboard side) and for crosswind magnitudes above 8 knots. The respective assessment of the related encounter risks with VESA leads to the same conclusions also for straight departure routes (Kauertz 2009, Kauertz et al. 2012). Crosswind departure procedures could be refined by using only departure route combinations where the leading aircraft is flying on the downwind route.

Crosswind transport certainly is the most effective mechanism to clear a flight corridor from wake vortices. However, the applicability of purely crosswind based wake vortex advisory systems covering vertically extended domains is impeded by the veering wind with altitude. As a consequence, either the flight tracks of subsequent aircraft must be separated already at quite low altitudes such that the crosswind does not change significantly within the considered height ranges or the advisory system must also consider vortex descent and/or vortex decay either explicitly or implicitly as in the presented concept.

Acknowledgement

The financial support from the EU project CREDOS (AST5-CT-2006-030837) is greatly acknowledged. Thanks are addressed to many CREDOS colleagues for numerous discussions and valuable comments. In particular, the contributions from Swantje Amelsberg, Helge Lenz (trajectory model), Carsten Schwarz (hazard area module), and Ivan De Visscher (DVM wake vortex model) are highly acknowledged.

References

Amelsberg, S., and Luckner, R., "Parametric Aircraft Trajectory Model for Takeoff and Departure," 1st CEAS European Air and Space Conference, CEAS-2007-273, Berlin, Germany, Sept. 2007, pp. 785-795.

Anon., „Frankfurt Airport Luftverkehrsstatistik 2006," Fraport AG, Frankfurt am Main, Germany, 2007.

de Bruin, A.C., Speijker, L.J.P., Moet, H., Krag, B., Luckner, R., and Mason, S., "S-Wake – Assessment of Wake Vortex Safety," Publishable Summary Report, National Aerospace Laboratory, NLR-TP-2003-243, Amsterdam, 2003.

Dengler K., Wiegele A., "EDDF-1 Data Collection Campaign Report," CREDOS, D2-1, 25 Nov. 2008.

Dengler K., F. Holzäpfel, T. Gerz, A. Wiegele, I. De Visscher, G. Winckelmans, L. Bricteux, H. Fischer, and J. Konopka, Crosswind Thresholds Supporting Wake-Vortex-Free Corridors for Departing Aircraft, Meteorological Applications, 2011, DOI: 10.1002/met.261.

Elsenaar B. et al., "Wake Vortex Research Needs for Improved Wake Vortex Separation Ruling and Reduced Wake Signatures", Final Report of the Thematik Network 'WakeNet2-Europe', 6th Framework Programme, National Aerospace Laboratory, NLR-CR-2006-171, Amsterdam, Mar. 2006.

Frech, M., and Holzäpfel, F., "Skill of an Aircraft Wake-Vortex Model Using Weather Prediction and Observation," *Journal of Aircraft*, Vol. 45, No. 2, 2008, pp. 461-470.

Frech, M., and Zinner, T., "Concept of Wake Vortex Behavior Classes," *Journal of Aircraft*, Vol. 41, No. 3, 2004, pp. 564–570.

Frech, M., Holzäpfel, F., Tafferner, A., and Gerz, T., "High-Resolution Weather Data Base for the Terminal Area of Frankfurt Airport," *Journal of Applied Meteorology and Climatology*, Vol. 46, No. 11, 2007, pp. 1913-1932.

Gerz, T., Holzäpfel, F., Bryant, W., Köpp, F., Frech, M., Tafferner, A. and Winckelmans, G., "Research towards a wake-vortex advisory system for optimal aircraft spacing," Comptes Rendus Physique, Vol. 6, No. 4-5, 2005, pp. 501–523.

Grell, G.A., Emeis, S., Stockwell., W.R., Schoenemeyer, T., Forkel, T., Michalakes, J., Knoche, R., and Seidl, W., "Application of a multiscale, coupled MM5/chemistry model to the complex terrain of the VOTALP valley campaign, Atmospheric Environment, Vol. 34, No. 9, 2000, pp. 1435-1453.

Hallock, J.N., Greene, G.C., and Burnham, D.C., "Wake Vortex Research - A Retrospective Look," Air Traffic Control Quarterly, Vol. 6, No. 3, 1998, pp. 161–178.

Höhne, G., Luckner, R., and Fuhrmann, M., "Critical Wake Vortex Encounter Scenarios," *Aerospace Science and Technology*, Vol. 8, No. 8, 2004, pp. 689-701.

Holzäpfel, F., "Probabilistic Two-Phase Wake Vortex Decay and Transport Model," *Journal of Aircraft*, Vol. 40, No. 2, 2003, pp. 323-331.

Holzäpfel, F., "Probabilistic Two-Phase Aircraft Wake-Vortex Model: Further Development and Assessment", J. Aircraft, Vol. 43, 700-708, 2006.

Holzäpfel, F., Frech, M., Gerz, T., Tafferner, A., Hahn, K.-U., Schwarz, C., Joos, H.-D., Korn, B., Lenz, H., Luckner, R., and Höhne, G., "Aircraft Wake Vortex Scenarios Simulation Package - WakeScene," *Aerospace Science and Technology*, Vol. 13, No. 1, 2009, pp. 1-11, doi:10.1016/j.ast.2007.09.008.

Holzäpfel, F., Kladetzke, J., "Wake vortex encounters during take-off & departure: Sensitivity analysis and worst case search," CREDOS D3-9, 5 Nov. 2009.

Holzäpfel, F., Kladetzke, J., Assessment of Wake Vortex Encounter Probabilities for Crosswind Departure Scenarios, Journal of Aircraft, Volume 48, Number 3, May-June 2011, pp. 812-822. DOI 10.2514/1.C000236

Holzäpfel F., Kladetzke J., Amelsberg S., Lenz H., Schwarz C., De Visscher I., "Aircraft Wake Vortex Scenarios Simulation Package for Takeoff and Departure," *Journal of Aircraft*, Vol. 46, No. 2, 2009, pp. 713–717, also AIAA Paper 2008-8921.

Holzäpfel, F., and Steen, M., "Aircraft Wake-Vortex Evolution in Ground Proximity: Analysis and Parameterization," *AIAA Journal*, Vol. 45, No. 1, 2007, pp. 218- 227.

Holzäpfel F., R.E. Robins, "Probabilistic Two-Phase Aircraft Wake-Vortex Model: Application and Assessment", J. Aircraft, Vol. 41, 1117-1126, 2004.

ICAO, Procedures for Air Navigation Services - Air Traffic Management, Doc 4444, ATM/501, 2001.

Jackson, W., Yaras, M., Harvey, J., Winckelmans, G., Fournier, G., Belotserkovsky, A., "Wake Vortex Prediction - An Overview," Project Final Report, Transport Canada and its Transportation Development Center, Montréal, Canada, March 2001, http://www.tc.gc.ca/tdc/summary/13600/13629e.htm.

Joos, H.-D., Bals, J., Looye, G., Schnepper, K., and Varga, A., "A multi-objective optimisation based software environment for control systems design," Proceedings of 2002 IEEE International Conference on Control Applications and International Symposium on Computer Aided Control Systems Design, CCA/CACSD, Glasgow, Scotland, U.K., 2002.

Kauertz S., "Workpackage 3 Final Report" CREDOS, D3-11, 25 Nov. 2009.

Kauertz S., F. Holzäpfel, J. Kladetzke, "Wake Vortex Encounter Risk Assessment for Crosswind Departures," Journal of Aircraft, accepted, 2012, 11 pages.

Luckner, R., Höhne, G., Fuhrmann, M., "Hazard criteria for wake vortex encounters during approach," *Aerospace Science and Technology*, Vol. 8, No. 8, 2004, pp. 673-687.

Schwarz, C.W., and Hahn, K.-U., "Full-flight simulator study for wake vortex hazard area investigation," *Aerospace Science and Technology*, Vol. 10, No. 2, 2006, pp. 136-143.

Speijker, L.J.P., Kos, J., Blom, H.A.P., and van Baren, G.B., "Probabilistic wake vortex safety assessment to evaluate separation distances for ATM operations," 22nd Congress of the International Council of the Aeronautical Sciences, NLR TP 2000 326, Harrogate, United Kingdom, Sept. 2000.

Speijker, L.J.P., Vidal, A., Barbaresco, F., Frech, M., Barny, H., and Winckelmans, G., "ATCWake: Integrated Wake Vortex Saftey & Capacity System," Journal of Air Traffic Control, Vol. 49, No. 1, 2007, pp. 17–32.

Winckelmans G., Duquesne T., Treve V., Desenfans O., and Bricteux L., "Summary description of the models used in the Vortex Forecast System (VFS)," Univ. Catholique de Louvain, Louvain-la Neuve, Belgium, Apr. 2005.

3.3 Economic Assessment of Enhanced Information on Convective Weather

Alexander Lau
Institute of Air Transportation Systems

An assessment of delay reduction potential of Rad-TRAM is presented, which detects, tracks and predicts up to one hour heavy precipitation cells by using weather radar data. Rad-TRAM has been developed at DLR and will be assessed by analyzing delay data at Munich Airport during convective weather events. Delay reduction potential underlying operational adaptation through advanced weather information serves as assessment metric to quantify the economic benefit of the algorithm. Advanced weather information refers to the tracking, nowcasting and visualization of severe areas within thunderstorms. Delay data is evaluated during convective impact within the boundaries of terminal airspace of Munich airport and coverage areas within this airspace are considered regarding delay behavior. Arrival traffic is affected by mean individual delay rates of up to 21 minutes whereas departure traffic is more evenly impacted during convective impact. The analysis which represents the first part of an extensive assessment concludes with an approximation of potentially avoidable yearly delay costs at Munich airport.

Introduction

It is widely understood today that adverse weather is one of the major reasons causing delay in the air transportation system. Many studies in particular at North American airports have been conducted to show the potential benefit of ITWSs. (Allan and Evans, 2001, Evans et al., 2005, Robinson et al., 2004) The majority of these analyses compare airport delay rates before and after system implementation. Due to the fact that the algorithm is not operationally implemented yet, the presented work focuses on the assessment of delay reduction potential without evaluating delay data of post implementation phases. To do so it is expedient from an economic point of view to introduce delay related impact sensitivities of the technology to be assessed. This is especially recommendable to account for the uncertainty of weather impact on air traffic.

Safety and reliability as well as delay reduction (potential) are the most important performance indicators regarding the operational assessment of convective weather tracking and nowcasting (forecasting up to 1 hour) algorithms. It is postulated that the product confidence level regarding the consistency of the convective cells in time and space is sufficient for operational utilization within the defined nowcast horizon.

Convection itself represents the most severe weather phenomena for air traffic. Wind-shear, icing and hale are main properties which have to be avoided by pilots. Due to regulatory traffic flow activities, e.g. slot re-allocation and holdings, conducted by the CFMU and Radar Control (-FMPs) in Europe, flight schedules are affected and delay arises. Referring this to traffic flow disruptions at an airport like Munich one can speak of delay rates because of the high number and diversity of movements being affected by severe weather in the vicinity of the airport.

The conduction of economic assessments of specific technologies like e.g. Rad-TRAM requires the capability of modeling the technological impact within an integration framework, e.g. an airport or an ATC system. (FAA, 1999) Airport throughput as another important KPI of airport efficiency mainly depends on surface infrastructure and operational conception. (Eurocontrol, 2009) The latter is impacted by nearby airspace performance, especially during periods of convective weather impact. Airport arrival capacity today is therefore dependent on flexible radar-based routing procedures in the arrival sequencing and metering area (ASMA).

Advanced weather decision support tools take an important role in optimizing airport efficiency during convective weather impact especially at highly congested airports and airspaces. The assessment of weather information systems needs to be appropriately adapted to individual parameters like infrastructure and weather occurrences.

Economic Impact of Integrated Weather Information Systems

Due to the unique infrastructural and operational setup of airports or airport systems (here defined as a number of nearby located airports affecting each other's airside arrival and/or departure operations), efficiency programs and/or technologies are likely to induce economic impact, which is dependent on individual airport characteristics. Following the goal of economic feasibility in the context of system implementation, not only site dependent infrastructural and weather factors but also adapted controller procedures and regulations as a result of additional weather information may influence its share on efficiency improvements. These improvements mainly stabilize VMC airport capacity during IMC conditions. In this manner weather information systems serve as enabler for local capacity improvements, which are

- Reduced Spacing during Approach,
- Advanced Low Visibility Operations during Flight and on the Ground,
- Decreased Runway Occupancy Times,
- Predictive Airport Configuration Planning, and
- Delay Reduction during Convective Impact through Arrival and Departure Area Closure and Reopening.

For each of these improvements a number of integrated ATC applications exist to provide respective weather information to decision makers. In addition to important baseline weather information like wind-direction and -strength, ceiling and visibility, these Integrated Weather Systems combine weather- and ATM information to facilitate the execution of operational decisions. (Evans, 2006) The integration of both domains enables decision support, which is based on a real-time ATC representation in which weather now- and forecasts are represented with sufficient parametric and time accuracy.

An assessment of a variety of Integrated Weather- and Decision Support Systems at 10 major U.S. airports is conducted in Hemm et al. (1999). The assessed technology portfolio as part of the NASA TAP Program contains A/C Vortex Spacing, High-Speed Roll-out and Turn-off during low visibility conditions, Dynamic Runway Occupancy Measurement and Real-Time Data Link Interaction between Center ATC and on-board FMS. Arrival delay serves as benefit metric which is analytically generated by airport capacity and delay models. Each technology is represented in the capacity calculation whereas demand profiles and weather data serve as input for an analytic queuing model. Examples for capacity impacting parameters which represent the technological impact are arrival sequences, individual runway declarations and adapted buffer times in aircraft spacing. Concluding the economic quantification a delay- and a system-life-cycle-cost breakdown completes the economic quantification.

Allan and Evans (2001) present an assessment of an ITWS at the New York Terminal Area. Two types of weather events are examined with respect to delay reduction through application of ITWS and a TCWF algorithm: convective weather and strong vertical wind shear. To determine to which extend delay reduction benefits with ITWS/TCWF in use can be realized, two delay models have been used. Beside a linear delay model, in which delay is represented as a linear function of pertinent variables like weather occurrence, the queuing model represents weather related delay as a function of actual airport capacity, demand and event duration. The latter is interpreted by weather event duration and the time period in which airport capacity is decreased by regulatory action. The comprehensive studies of Robinson et al. (2004 & 2006) focus on operational benefits obtained through the introduction of the CIWS. The ground laying concept is based on an identification and quantification of benefit categories during en-route real-time utilization at several ARTCCs. This approach allows the alignment of detailed statistics on how controllers use the system during severe weather events. Beside improving situational awareness major benefit categories could be identified in keeping routes open longer and proactive requests of optimized routes. Table 1 contains selected information about yearly economic benefits of the three introduced systems assigned to the related benefit categories.

Nowcasting Thunderstorms Using Weather Radar Data: Rad-TRAM

Due to the average lifetime of convective cell systems of only 20-30 minutes and the lack of knowledge about the detailed state of the atmosphere it is challenging to now- and forecast their evolution. The Institute of Atmospheric Physics at DLR developed weather information systems to identify, track and nowcast convection with high precision within the time window of one hour ahead.

One of these information systems is Rad-TRAM[0] (Radar Tracking and Monitoring) which uses weather radar data from the DWD European radar composite (2km x 2km horizontal resolution available every 15th minute) to detect, track, and nowcast up to 60 minutes areas with reflectivities higher than 37 dBZ. (Kober and Tafferner, 2009) These detected and nowcast areas represent aviation hazards like heavy precipitation, turbulence and hail in the lower part of a thunderstorm and are highly relevant for take-off and landing procedures at airports. The threshold value of 37 dBZ is based on the experience that pilots tend to request diversion clearances when reflectivity of a convective cell crossing their trajectory exceeds this magnitude of reflectivity. Rad-TRAM outputs contours of the detected and nowcast precipitation cells together with their characteristic attributes (e.g. moving speed, moving direction, hail occurrence, maximum reflectivity and gravity center) into files in XML format which is an easy to read international standard.

Table 1. Economic benefit of weather information systems [Mio$/Year] at selected U.S. Airports. (Allan and Evans, 2001, Hemm at al., 1999, Robinson et al., 2004) The exemplary information gives anticipation about the economic quality of advanced weather information related to delay reduction. As depicted weather information systems are not intended to serve information for all benefit categories which is case-related to individual weather conditions and ATC needs.

Airport / Year		Benefit Categories					
		Decreasing ROTs	A/C Routing	A/C Sequencing	A/C Spacing	High Wind Ops	Increased Flow Rates
NASA TAP Technologies	Atlanta Hartsfield/ 1997	*12.3*	*42.0*	*42.0*	*37.9*		
ITWS / TCWF (during adverse weather)	New York (EWR,JFK,LGA)/ 1999		*24.0*			*61.9*	*75.0*
CIWS (during adverse weather)	Chicago O`Hare/ 2002-2003		*32.1*				

To date, the operational weather information representation philosophy differentiates throughout the user community. As mentioned air traffic controllers have different information from partly different data sources in comparison to airline hub operations staff and pilots which leads to different levels of situational awareness. As can be seen in Figure 1, a ground-based information system like Rad-TRAM is capable to provide an overview of the thunderstorm situation and its evolution by just showing contours encompassing the hazardous areas. Resulting benefits from an operational perspective are stated in the following points:

- Identification of active storm cells
- Intuitive representation of “No-Go-Areas” in a specific airspace
- High accurate information of geometry location and future development of hazardous areas.

Especially the third point enables decisions with considerably higher time precision during the tactical capacity planning process. If this information is made available to all stakeholders, the community’s situational awareness would be substantially improved, and there would be a great potential for throughput optimization and delay reduction.

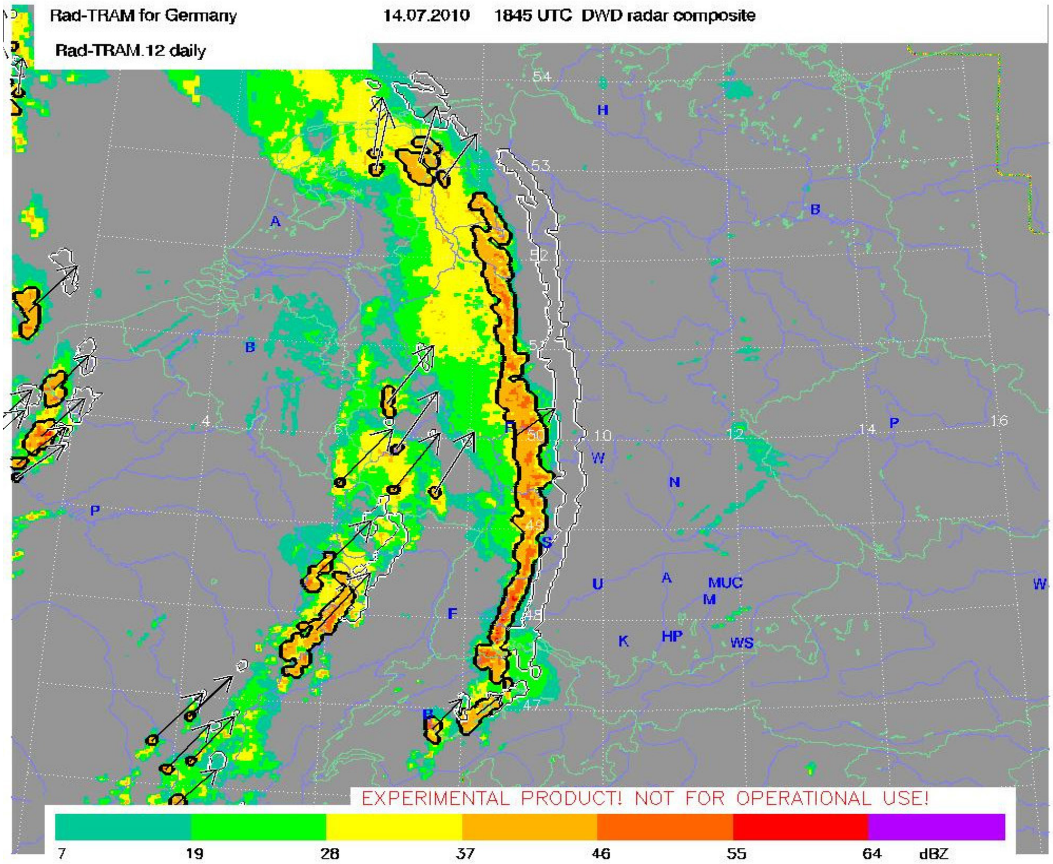

Figure 1. Rad-TRAM information. DWD European radar composite (color shading) on 14th July 2010 at 6:45pm UTC with Rad-TRAM contours encompassing areas with heavy precipitation. The thin white contour is the 60 minutes prediction; arrows indicate the movement of the cells.

Methodology

Munich Franz Josef Strauß International (MUC) has been chosen for an analysis of delay reduction potential. The airport has a high average of days with convective activity in its vicinity. Due to its location in southern Germany, where atmospheric conditions foster the development of convective weather during the summer season (for detailed information, refer to Hagen et al. (1999)), convection along with high precipitation and wind represents a major weather impact on the airports flow rates. In 2010, 41 days with convective activity near the airport have been observed. In the majority of the cases convective cells approach the airport from westerly or from northern directions whereas single cells with low moving speeds, moving cell systems and convective fronts are observed (Source: DLR).

MUC is Germany`s second major Hub Airport after Frankfurt/Main International. Yearly passenger and freight numbers continuously grew since its opening in 1992. Until 2005 the yearly movement rate grew up by a total of 108% whereas the passenger rate grew by 138%. (Intraplan, 2007) Beside general growth rates in air transportation this is due to the utilization through Lufthansa as the airlines second major hub. In 2010 the airport handled 34.7 Million Passengers.

MUC operates two independent runways with operational orientations 08 and 26. All thresholds are ILS equipped and can be operated during ILS CATIII conditions. The airports capacity benchmark is actually defined with 90 movements per hour for each of the two configurations, which represents high flow rates during hours of peak demand today.

MUC is a capacity-coordinated airport. It is integrated into the European ATFCM conducted by the CFMU in Brussels. This process is structured in three phases (Eurocontrol, 2009): The Strategic Flow Management takes place until seven days prior to the day of operation and approximates a capacity plan for the next year. The Pre-Tactical Flow Management is conducted during the six days prior to the day of operation and finds best ways to match available capacity resources with upcoming demand rates. Flow measures like airspace reorganization are considered if needed. A daily plan is constructed which will be updated during the Tactical Phase, which is applied during the day of operation. This phase is dominated by actual traffic and weather conditions, for which the CFMU achieves information from the flight management positions. Due to the fact that the majority of flights within the CFMU`s area of responsibility last approximately two hours, CFMU sets a regulation deadline of two hours in advance. In the case of forecasted convection in the next two hours, ATC has to decide whether to rearrange operations or to down-regulate capacity. It is straightforward, that the precision of weather information affects this process. With this background especially the edge times of existence of hazardous areas within terminal airspace are focused in this work.

Hypothesis

The assessment methodology for Rad-TRAM is based on an analysis of delay rates at MUC. Terminal and therefore airport capacity can be optimized by minimizing severe weather impact times to the minimum amount possible. This shall be shown by means of the following two basic assumptions:

1) The time-dependent delay rate of an airport (which from an airside-capacity-point-of-view is defined by its terminal airspace structure, its runway system and the corresponding concept of operations) is potentially adaptable to existence times of hazardous areas within the vicinity of the airport.

2) The time-dependent delay rate of an airport is directly related to individual disruption times of traffic flows over terminal fixes and to the corresponding now- and forecasting quality of these block times.

There are not many previous studies addressing the interplay of convective weather characteristics to ATC operations in Europe. For this reason and due to the fact that a detailed operational analysis of Rad-TRAM benefits in a controller environment is not available yet, it is assumed, that controllers and supervisors will rely on the algorithm and will follow it in terms of using the information as a basis for tactical planning as well as optional routing actions.

Database

Next to the (Rad-TRAM) XML-format-based weather data, METAR-format-based weather data and Eurocontrol CFMU traffic data with relevant timestamps is applied. Two types of CFMU data sources are being incorporated: Airport related flight lists contain estimated and actual take-off and arrival times, aircraft IDs, flight based regulations and associated delays. Movement related point profiles contain routing data and the associated scheduled and actual time-over declaration. METAR data is applied to constitute convection related delay rates during VMC and IMC conditions.

Approach

The assessment leads to an economic quantification of delay rates. The identification of convective weather events by analyzing the corresponding weather and traffic data is conducted in a first step. Giving this information as input, an analysis of delay rates during periods of convective coverage is conducted. Three steps have to be undertaken to quantify the amount the relevant amount of delay:

1) Identification of evaluable convective weather events.

This is done by evaluating Rad-TRAM data. In the summer season of 2009, a total of 32 days with adequate convective activity at MUC have been observed. On 25 of these days Rad-TRAM output is available. The mean existence duration of these areas covered by detected Rad-TRAM cells within the TMA is three hours, whereby Rad-TRAM cells with a life-time greater than 30 minutes have been tracked 42 times. The majority of these events took place between 2.00pm and 8.00pm UTC.

2) Analysis of Flow and Delay data during these convective weather events.

Flow and delay data can be extracted from the CFMU point profiles by comparing scheduled and actual arrival times for each arrival movement during the day. Figure 2 shows aggregated flows and the respective hourly delay rates for a convective weather impacted day and a day without convection.

3) Identification of potentially avoidable delay rates.

Average delay rates during convective coverage within the TMA are analyzed and compared to delay rates without convective impact. Only from these numbers it is possible to derive a maximum amount of delay minutes to be reduced by enhanced convective information.

For more detailed information please refer to Lau et al. (2011) in which delay rates according to the fraction of coverage within the TMA as well as delay behavior before and after convective impact are considered.

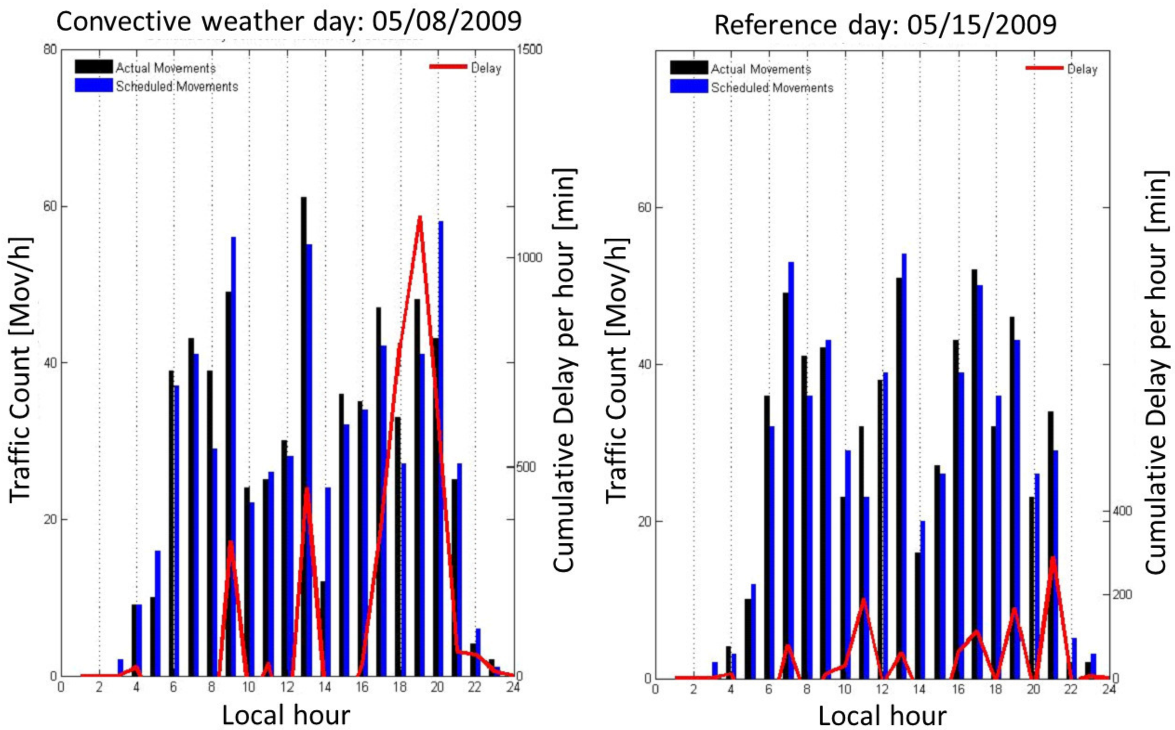

Figure 2. Scheduled/actual arrival counts with hourly delay rates. Left: Convective weather impacted day (05/08/2009) with a maximum delay rate at 7:00pm. Right: Reference day without convective weather impact (05/15/2009). Blue bars represent scheduled/estimated movement counts, blue bars represent actual movement counts.

Results and Discussion

Relevant landing and take-off times are represented by time-over point profiles of the CFMU database. Relevant time stamps are used to generate accumulated arrival and departure delays:

$$D_A = \sum (A/TA - E/C/TA) \quad (1)$$

$$D_D = \sum (A/TOT - E/C/TOT) \quad (2)$$

Accumulated arrival and departure delays D_A and D_D are given by the difference of actual and estimated/calculated times of arrival (A/TA and E/C/TA) and respectively take-of times (A/TOT and E/C/TOT). Weather impact times are generated by the existence of hazardous areas within terminal airspace. Two specific airspace boundaries have been applied as shown in the example in Figure 3. The inner airspace C (inner TMA) contains the final approach (ARR) and initial turning (DEP) fixes. The outer airspace C (outer TMA) covers an area of around 40x35 square-miles around the airport and contains the initial fixes.

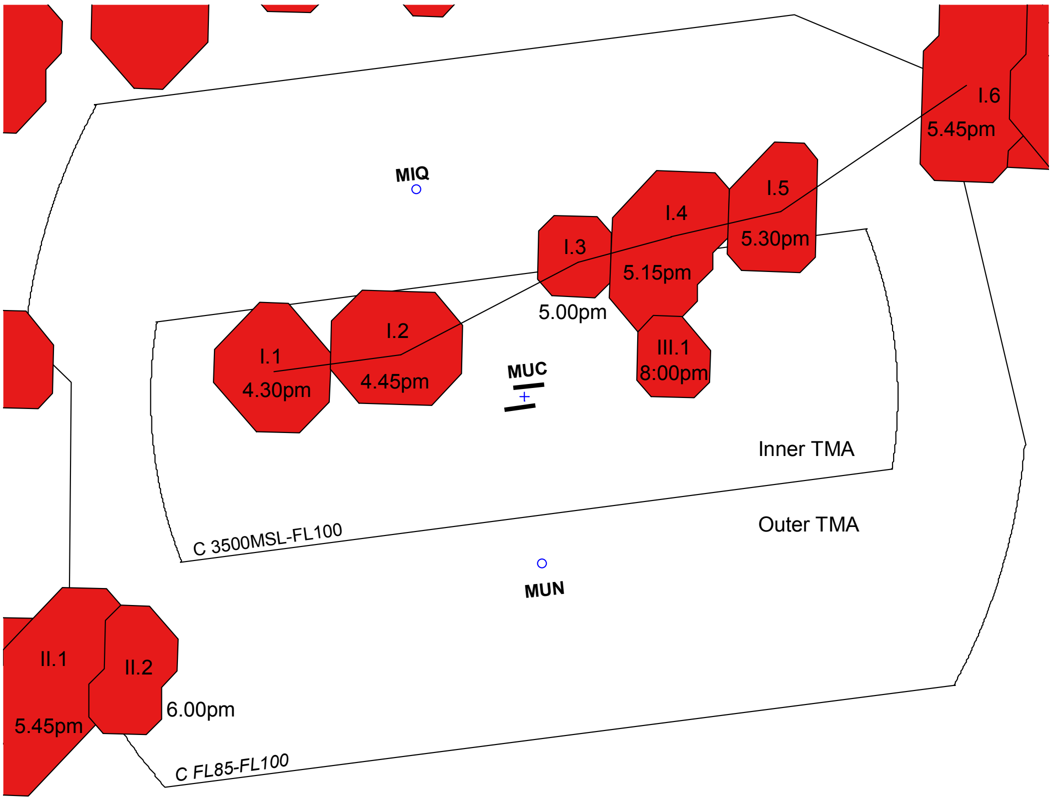

Figure 3. Hazardous areas within terminal airspace. The weather scenario is taken from 05/08/2009, where in total 3Rad-TRAM cells where observed (red areas with roman numbers). The timestamps are quarterly analysis times of Rad-TRAM. The first cell appeared at 4.30pm within the TMA and moved eastward leaving the outer TMA at around 5.45pm. This is a typical example where northbound departure routes are restricted.

Table 2 shows results of the statistical analysis of delay rates during all observed days for times when hazardous areas where observed and during times when no hazardous areas where observed by Rad-TRAM. This is done for the inner and the outer TMA during IMC and VMC conditions. The data reveals that high delay sensitivity is present when parts of the inner TMA are blocked by convective weather. Because of the dynamic behavior of moving convection the most times when convective weather appears within TMA boundaries, mostly both the inner and the outer TMA is covered. The difference lies in the range of opportunities for air traffic control to adapt operations. For both arrival and departure movements, the median and the 75th percentile of delay values are high during IMC and VMC conditions when Rad-TRAM cells are detected, whereas it is low during times when no Rad-TRAM cell is observed. The median departure delay values are generally higher than the median arrival delay values whereas median delay rates of arrival movements typically reach higher individual values of up 21.8 minutes.

This can be referred to effects of network operations, which will be focused within the second part of this study.

The cost of delay is derived from University of Westminster (2011). Tactical delay cost per minute with and without network effects for the most common types of aircraft are provided in Table 3. Tactical costs of delay are those cost which occur on the day of operation. They are mainly dominated by crew cost, passenger cost of time and fuel burn and arise if planned schedules are timely exceeded by actual operations. This is triggered by congestion and unpredictable events like weather.

Mean cost values for total delay minutes during all days with convective activity in the outer TMA and only for periods of convective coverage during those days are derived. The accumulated costs for all relevant arrival movements on days with convective activity are given in Table 4. The cost shares of arrival delay minutes during coverage periods in the outer TMA are also depicted.

Nearly the half of the total arrival delay costs emerge during convective activity in the TMA. The yearly cost reduction potential of enhanced convective weather information can be quantified as a proportion of these costs. Periods directly before and after convective activity are not yet included in these cost values.

Table 2. Delay sensitivities to the existence of hazardous areas [Delay/Mov]. Delay data was divided in 10-minute-steps to reflect delay behavior within the gliding hour. The abbreviation 'Cov' stands for coverage of hazardous areas output by Rad-TRAM. Individual delay rates during convection are approximately higher. NOTE: The data only reflects delay behavior within the 30 days of observation during all hours of the day and does not reflect the general delay situation at MUC.

Outer TMA	Arr Delay [min]		Dep Delay [min]	
	Median	75th	Median	75th
VMC / No Cov	*0.9*	*6.5*	*2.0*	*5.8*
VMC / Cov	*5.8*	*14.3*	*7.4*	*13*
IMC / No Cov	*1.2*	*5.6*	*2.3*	*5.7*
IMC / Cov	*6.5*	*16.3*	*7.8*	*13.9*

Inner TMA	Arr Delay [min]		Dep Delay [min]	
	Median	75th	Median	75th
VMC / No Cov	*1.0*	*6.8*	*2.2*	*6.0*
VMC / Cov	*7.9*	*17.0*	*8.0*	*16.0*
IMC / No Cov	*1.3*	*6.2*	*2.5*	*6.0*
IMC / Cov	*8.5*	*21.8*	*8.3*	*16.0*

Table 3. Mean delay cost values with and without network effect in EURO

minutes	**5**	**15**	**30**	**60**	**90**	**120**	**180**	**240**	**300**
cost/#min w/o net	276	1.038	2.634	7.362	13.584	20.965	39.148	61.699	88.370
cost/#min with net	278	1.132	3.240	12.236	30.810	60.488	84.661	108.813	138.542

Table 4. Delay cost values with and without network effect [Mio. EURO]. In 2009 nearly all arrival movements during days with convective activity have been evaluated so that these cost estimates represent the yearly cost approximations.

Cost of Delay	Arr Delay Cost [Mio. Euro]	
	all effected days	all effected days (during coverage periods)
Total Delay Cost pre-tactical	*20.5*	*8.5*
Total Delay Cost full-tactical	*35.5*	*14.6*

Delay rates at MUC in 2009 before, during and after the existence of hazardous areas within the TMA have been investigated as a first step of the assessment of Rad-TRAM. Arrival flows are highly sensitive to convection regarding individual delays, especially during (convection related) IMC operations at MUC. Departure flows show a higher median value of delay rates during convective impact. Delay shares during convective activity are dominant according to the costs they constitute. The analysis shows that from a delay reduction perspective, the benefit of enhanced convective weather information will be in the millions. Especially better information in the context of pre-tactical and tactical flow management is expected to be highly beneficial, whereas the concept of system-wide information management of integrated weather information will enable these potentials.

Outlook

The need to identify the stake of different delay types and the assignment to the respective mission segments (ground origin, en-route, approach) is important to be analyzed as a next action. This allows a detailed assignment of delay rates to convective activity in the vicinity of MUC related to significant approach fixes. This analysis needs to be corrected by METAR based weather factors like wind and visibility at the airport level.

With this information ATFM and ATC actions need to be investigated to find out, if the needed time accuracy to decrease delay rates could be achieved and if more sophisticated convective weather information can be applied in that way. Fore- and nowcast quality metrics need to be introduced.

To specify detailed economic values, use case surveys on individual flight missions and daily rotations impacted by representative convective events have to be conducted. The aim of this work will lie on the formation of delay, especially with respect to network operations.

References

Allan, S.S.,Gaddy, S.G., and Evans, J.E., “Delay Causality and Reduction at the New York City Airports Using Terminal Weather Information Systems.” Project Report ATC-291, MIT Lincoln Laboratory, Lexington, MA, 2001.

Eurocontrol, “ATM Airport Performance (ATMAP) Framework”, Report by the Performance Review Commision, Brussels, 2009.

Eurocontrol, “Air Traffic Flow&Capacity Management Operations ATFCM Users Manual”, 14th edition, 2010.

Evans, J. E., Robinson, M., Shawn, A., “Quantifying convective delay reduction benefits for weather/ATM systems”, 6th Eurocontrol/FAA ATM R&D Seminar, Baltimore, 2005

Evans, J. E.,”Implications of a Successful Benefits Demonstrations for Integrated Weather/Air Traffic Management (WX/ATM) System Development and Testing.”, 12th Conference on Aviation, Range, and Aerospace Meteorology (ARAM), Atlanta, GA, Amer. Meteor. Soc., 2006.

FAA, Office of Aviation Policy and Plans, “FAA Airport Benefit-Cost Analysis Guidance”, Washington, DC, 1999.

Hagen, M., Bartenschlager, B., Finke, U.: „Motion characteristics of thunderstorms in southern Germany“, Meteorol. Appl. 6, 227-239, 1999.

Hemm, R., Shapiro, G., Lee,D.A., Gribko, J., Glaser, B., “Benefit Estimates of Terminal Area Productivity Program Technologies”, NASA/CR-1999-208989, 1999.

Intraplan Consult GmbH, “Luftverkehrsprognosen 2020 für den Flughafen München”, Planfeststellungsverfahren 3. Start- und Landebahn, Munich, 2007.

Kober, K., Tafferner, A., “Tracking and nowcasting of convective cells using remote sensing data from radar and satellite”, Meteor. Zeitsch., Vol. **1**, No. 18, 075-084, 2009.

Lau A., C. Forster , A. Tafferner, N. Dzikus and V. Gollnick, Assessment of a Convective Weather Nowcasting and Tracking Algorithm Based on Delay Reduction Potential at Munich Airport (Part I), 11th AIAA Aviation Technology, Integration and Operations (ATIO) Conference, Virginia Beach, Virginia, USA, 20-22 September 2011.

Pyrgiotis, N., Kerry, M., Odoni, A., “Modelling Delay Propagation Within An Airport Network.”, 12th WCTR, Lisbon, 2010.

Robinson, M., Evans, J. E., Crowe, B., Klingle-Wilson, D., Allan, S., “Corridor Integrated Weather System Operational Benefits 2002-2003: Initial Estimates of Convective Weather Delay Reduction.” MIT Lincoln Laboratory Project Report ATC-313, 2004.

Robinson, M., Evans, J. E., Hancock, T. R., “Assessment of Air Traffic Control Productivity Enhancements from the Corridor Integrated Weather System (CIWS)”, MIT Lincoln Laboratory Project Report ATC-325, 2006.

University of Westminster, “European airline delay cost reference values”, Final Report (Version 3.2), London, 2011.

4. Advanced Flight Control Systems for Atmospheric Disturbance Mitigation

4.1 Wake Impact Alleviation Control Functions and Sensor Requirements

Christian Horn, Dominik Niedermeier, Jana Ehlers
Institute of Flight Systems

Active control technology can be applied to alleviate wake vortex effects on aircraft and support the pilot to carry out his control task. Aircraft equipped with such a controller will be less affected by unforeseen wake vortex encounters or will even be able to follow another aircraft closer than authorized by the current separation distances without any compromise concerning safety. The application of such an approach requires the accurate determination of the flow disturbance to calculate the necessary countermeasures. Modern LIDAR technology has the potential to measure the flow field in front of the aircraft and to provide the required disturbance information in advance before it affects the aircraft. This paper summarizes the status of the work performed during the last years and the current activities. This includes the assessment of a wake vortex impact alleviation strategy with forward-looking sensors in offline simulations and flight tests as well as the derivation of required characteristics of the LIDAR sensor. For the analysis of the sensor requirements different sensor models are developed and a detailed sensor parameter sensitivity study is performed.

Nomenclature

C_{l,δ_a}	Rolling moment coefficient due to aileron deflection
C_{l,δ_r}	Rolling moment coefficient due to rudder deflection
$C_{m,\delta_{DLC}}$	Pitching moment coefficient due to DLC flap deflection
C_{m,δ_e}	Pitching moment coefficient due to elevator deflection
C_{n,δ_a}	Yawing moment coefficient due to aileron deflection
C_{n,δ_r}	Yawing moment coefficient due to rudder deflection
$C_{Z,\delta_{DLC}}$	Vertical force coefficient due to DLC flap deflection
f_s	Sinusoidal shaping function
l_μ	Mean aerodynamic chord
L_{WV}	Wake vortex induced rolling moment
M_{WV}	Wake vortex induced pitching moment
N_{WV}	Wake vortex induced yawing moment
$\bar{q}$	Dynamic pressure
s	Half of the wing span
S	Wing reference area
x_g	Geodetic x-coordinate
$\boldsymbol{y}$	Output vector
y_g	Geodetic y-coordinate
z_g	Geodetic z-coordinate
Z_{WV}	Wake vortex induced vertical force
$\Delta\delta_a$	Deflection angle of ailerons commanded by IRLIS
$\Delta\delta_{DLC}$	Deflection angle of direct lift control flaps commanded by
$\Delta\delta_e$	Deflection angle of elevator commanded by IRLIS
$\Delta\delta_r$	Deflection angle of rudder commanded by IRLIS
Φ	Bank angle

Control Concept

Experiences with the application of forward-looking sensors applied to atmospheric flow disturbance alleviation have been collected at the Institute of Flight Systems for several decades. Based on the former work, a similar approach was used for the active control concept of wake vortex encounters with the aim to improve the aircraft behavior.

The principle of the control concept is illustrated in Figure 1. Knowing the wake vortex flow field in front of the aircraft from forward-looking sensor information the flow disturbance distribution along the aircraft in space and time can be computed. Using a suitable Aerodynamic Interaction Model (AIM) the resulting additional forces and moments induced by the flow disturbances can be determined [1]. For the wake vortex control concept an AIM taking into account the wing, the horizontal tail, the vertical tail and the fuselage is used. Knowing the aircraft aerodynamics and the control surface efficiencies the required control surface deflections to compensate the wake vortex induced disturbances can be determined. Due to the fact that the control deflections can be calculated in advance from the look-ahead sensor information the application of the control deflections can be perfectly synchronized with the arrival of the respective flow disturbance at the aircraft's wing, the horizontal and the vertical tail.

This approach of controlling moments and forces is understood to be the initial version of the Integrated Ride and Loads Improvement System (IRLIS) which is supposed to cope with wake vortices and natural atmospheric turbulence. These basic functions of the system will be further extended and completed in the future.

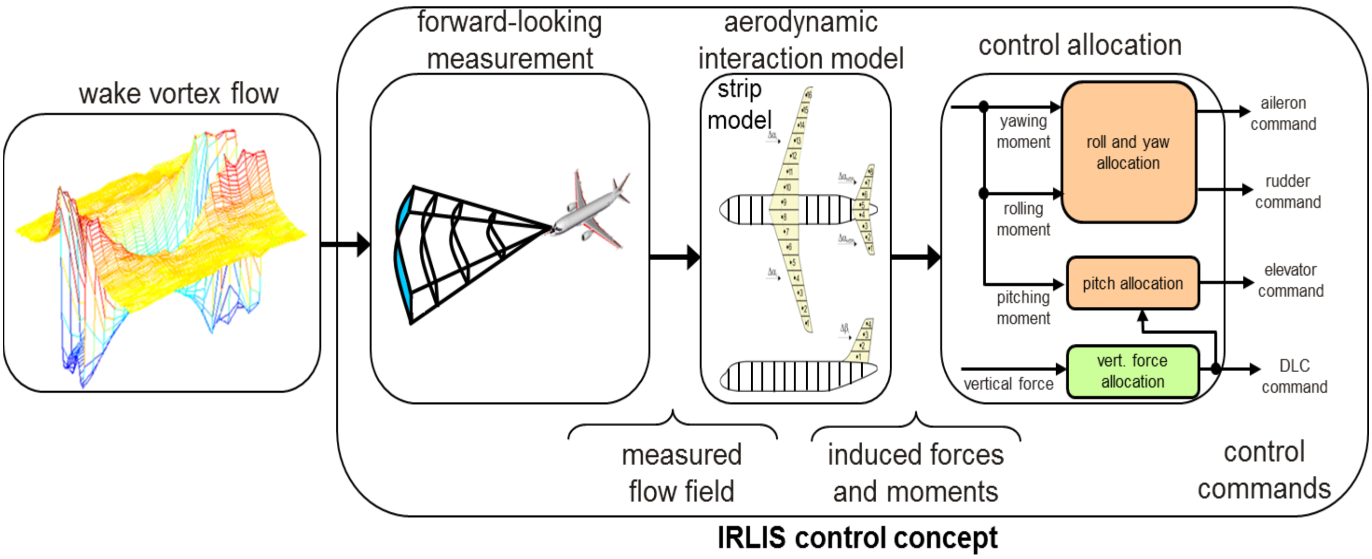

Figure 1. Principle of the IRLIS flight control system

Measurement Concepts and Measurement Point Handling

For the assessment of the feasibility of a wake vortex impact alleviation control strategy and the derivation of sensor requirements models of three different forward-looking measurement concepts have been implemented. All concepts assume that a so-called LIDAR (Light Detection and Ranging) system is applied as forward-looking sensor. Its measurement principle is based on the Doppler effect like Radar. However, the laser is in the infrared or ultraviolet range.

In all cases the sensor models do neither include the physics of light of a real sensor nor the physical rules of measurement but only the principle of forward-looking measurement. The LIDAR models calculate the positions of a specified number of measurement points first. These positions are then used to determine the wake vortex induced velocity vector either by using an analytical wake vortex model or by applying look-up table flow field data derived from large eddy simulations [2]. Today's LIDAR sensors are only capable of measuring the line-of-sight component of the wake vortex induced velocities. However, the research in the field of forward-looking sensors indicates that the determination of the full velocity vector might be possible in the future. For that reason both possibilities have been considered for the implementation of the different sensor models. We now describe the differences of the three measurement concepts that form the basis for the applied sensor models.

In case of the 1-D measurement concept the airflow is scanned and measured along a line (1-D) in wing span direction at a certain distance in front of the aircraft (cf. Figure 2). It is assumed that the angle of view of the sensor is rotated by -4.5° about the aircraft pitch axis to let the LIDAR look roughly in flight path direction. For this measurement concept it is assumed that the LIDAR is able to determine all three components of the wake vortex induced velocity vector. This concept is used for the pilot assessment during flight tests described below.

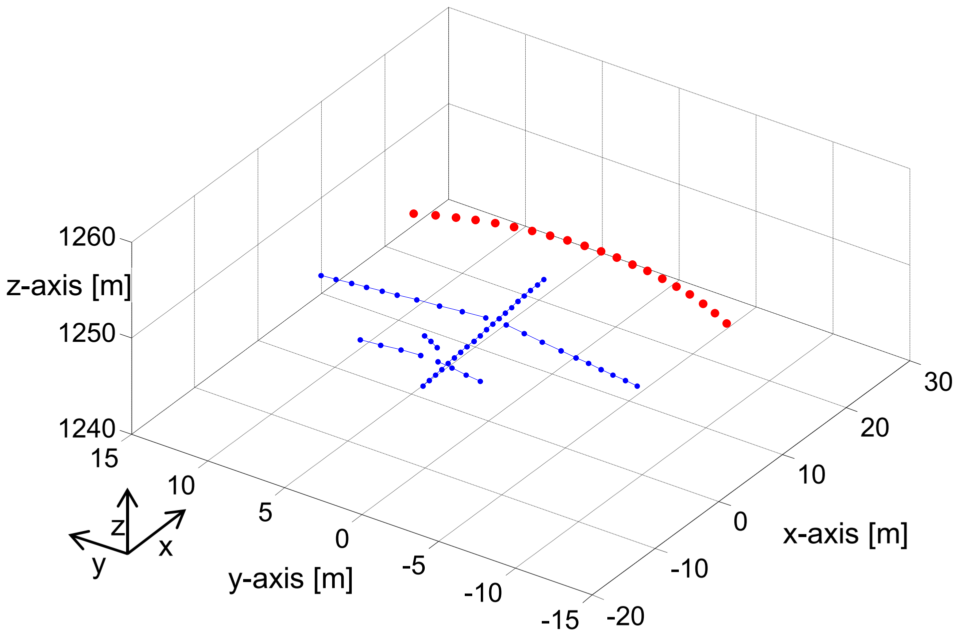

Figure 2. Measurement line (red) and AIM strip locations (blue). The Aerodynamic Interaction Model (AIM) divides the aircraft geometry into strips and computes the induced forces and moments for each strip. [1] The illustrated strip locations represent the center of area of each strip.

The 2-D LIDAR sensor model calculates a specified number of measurement points which are evenly distributed along horizontal and vertical lines in the virtual scanning plane in front of the aircraft. Figure 3 exemplarily shows the 2-D measurement plane. The size of the measurement plane is expressed in multiples of the aircraft wing span and height. Depending on the applied wake vortex flow field, the wind velocities at the measurement points are determined either by an analytical wake vortex model or a look-up table.

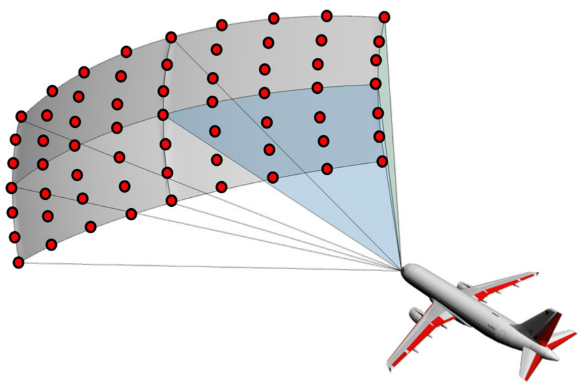

Figure 3. 2-D measurement plane

Physically, the LIDAR is only able to detect the average flow velocity in a specific blur range in beam direction, the so called line-of-sight (LoS). To account for this effect in the LIDAR model a blur range with additional sampling points is located around the nominal point of measurement (cf. red points in Figure 4). It turned out that the effect plays only a minor role and is not investigated further.

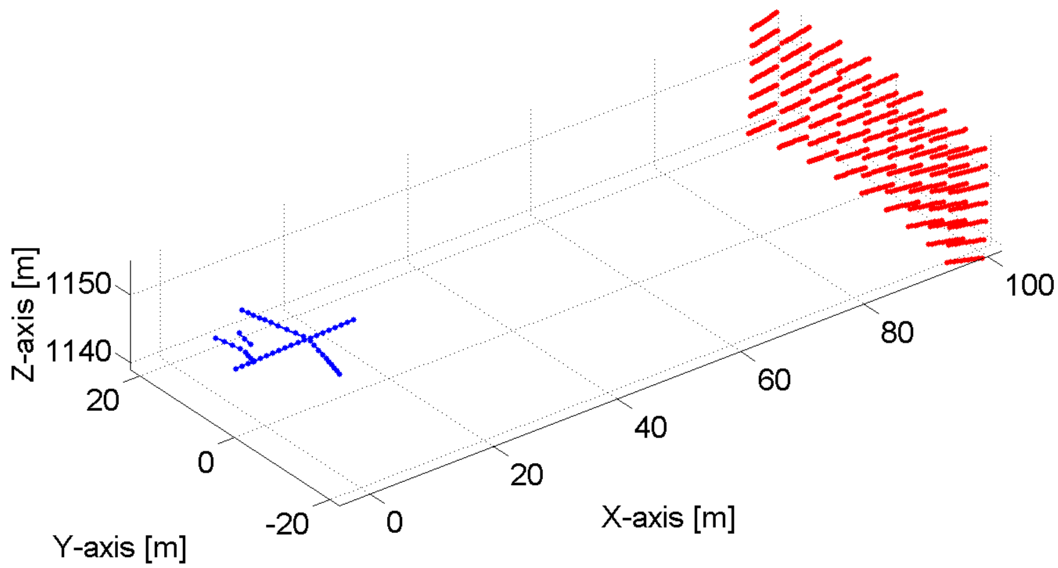

Figure 4. Measurement plane (red) and aircraft AIM strip locations (blue)

In addition measurement errors due to noise are modeled as zero mean, normally distributed values with a given standard deviation and are superimposed on the nominal velocity. For a first approach a simple measurement error model is used. All three velocity components (in x-, y- and z-direction) of the flow disturbance vector are perturbed by the normally distributed errors.

For sensor parameter sensitivity studies the following parameters are freely adaptable:

- Measurement range
- Measurement frequency
- Measurement error
- Number of measurement points in horizontal and vertical scanning direction
- Plane size defined as multiples of the aircraft wing span and height
- Output of line-of-sight velocities or all three components of the velocity vector

In case of this basic 2-D model it has to be noted that all measurement points in the measurement plane are measured simultaneously at each time step. The measurement frequency thus corresponds to the frequency with which the entire 2-D measurement plane is updated.

In addition to the basic 2-D measurement concept, another more detailed approach of modeling the LIDAR sensor and processing the sensor data has also been realized. This more complex LIDAR model represents an enhancement of the basic 2-D measurement concept. It has so far not been included in the sensor parameter sensitivity studies described in the subsequent chapter. Detailed analyses of the enhanced measurement concept will however be part of future work performed at the Institute of Flight Systems.

The main differences between the two 2-D sensor models are the measurement concept and the processing of the measured data. The enhanced sensor model also assumes a curved 2-D measurement plane as illustrated in Figure 3, but each measurement direction is now measured sequentially as it is likely for a real LIDAR sensor that can only measure at one measurement point at a time. The result is a slightly distorted measurement plane as shown in Figure 5 for a straight level flight at constant speed. The number of measurement points as well as the point-to-point sampling rate can be varied. For the first approach 35 measurement points with a point-to-point update rate of 350 Hz (resulting in a sampling rate of 10 Hz for each direction) has been chosen. The scanning of each measurement plane starts at the measurement point at the left bottom corner of the measurement plane and proceeds row wise from the left to the right for each row subsequently.

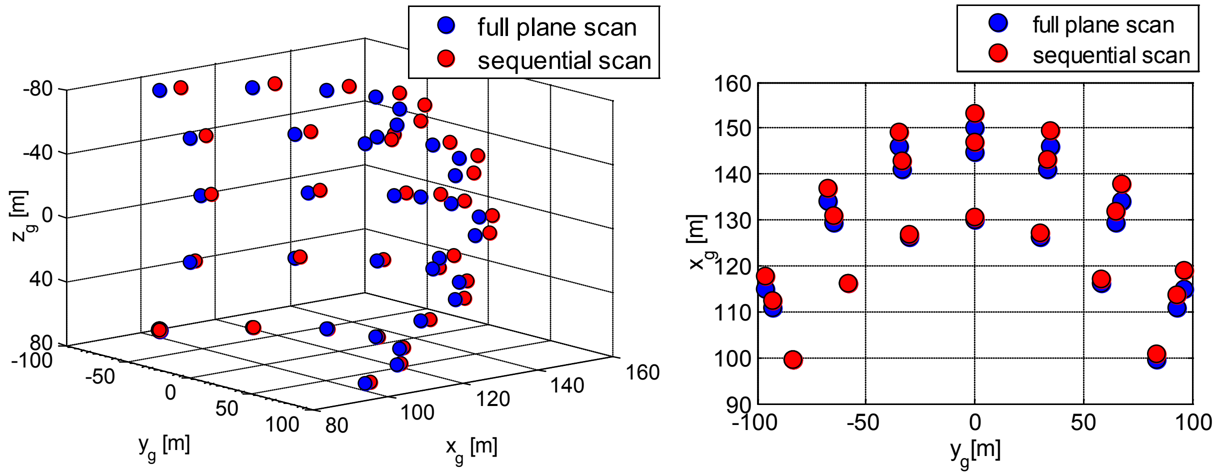

Figure 5. Measurement planes for full plane and sequential scans (left 3-D view, right top view). For clarity only the measurement points of the bottom half of the measurement plane (with $z_g \geq 0$ m) are shown in the top view.

The AIM determines the overall induced forces and moments at each time step by summing up the in-duced forced and moments of each strip at the current time step. The required input for the AIM conse-quently consists of an array of the wind velocities at all strips at each time step. But the LIDAR sensor only provides the wind velocities of a single measurement point at each time step. This LIDAR model thus requires a more complex processing of the measured wind velocities. The data for each measure-ment point are stored first. The allocation of the measured wind velocities to the different strips of the AIM is accomplished in a separate step. A benefit of this approach is that changes in flight path and attitude of the aircraft between the moment of the measurement of the wind velocities and the moment when they actually affect the aircraft can be taken into account (cf. Figure 6).

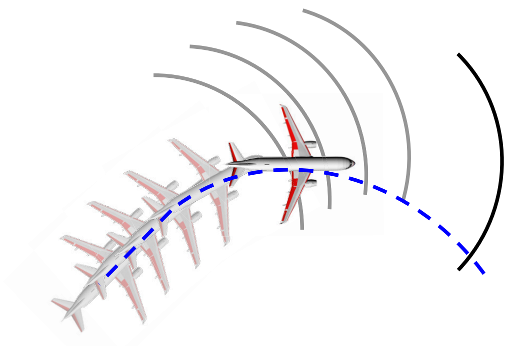

Figure 6. Position of aircraft relative to planes of stored points

In detail the enhanced modeling of the LIDAR measurement and data processing is implemented in the following way: The wind velocities are detected point by point for each measurement direction. After each measurement the measured wind velocities and the position of the measurement point are stored in spatially fixed coordinates. For the detection of the relevant wind velocities at the different strips of the AIM the stored data of measurements of a certain timeframe can now be used. Out of the stored measurement points an algorithm selects the five closest measurement points of each strip. The relevant wind velocity for each strip is then determined by calculating a weighted mean of the velocities at these measurement points. The weights are the inverses of the distances to the actual strip. To account for the time delay due to processing time and actuator delays the algorithm does not evaluate the current position of each strip but considers estimated aircraft position and attitude after this known time delay as a basis for the position of the strips.

Control Allocation

Using the measured wind velocity vectors the aerodynamic interaction model computes the forces and moments induced by the wake vortex, which are then fed to the control allocation block of the wake vortex controller (cf. Figure 1). Considering the elevator, the ailerons and the rudder as primary control surfaces for the basic wake vortex controller, the respective control commands are computed from the induced wake vortex moment vector as follows:

$$\begin{bmatrix}\Delta\boldsymbol{\delta_a}\\ \Delta\boldsymbol{\delta_e}\\ \Delta\boldsymbol{\delta_r}\end{bmatrix} = -\frac{\mathbf{1}}{\bar{q}\cdot \boldsymbol{S}}\cdot\begin{bmatrix}\boldsymbol{C_{l,\delta_a}(y)\cdot s} & \mathbf{0} & \boldsymbol{C_{l,\delta_r}(y)\cdot s}\\ \mathbf{0} & \boldsymbol{C_{m,\delta_e}(y)\cdot l_\mu} & \mathbf{0}\\ \boldsymbol{C_{n,\delta_a}(y)\cdot s} & \mathbf{0} & \boldsymbol{C_{n,\delta_r}(y)\cdot s}\end{bmatrix}^{-1}\begin{bmatrix}\boldsymbol{L_{WV}}\\ \boldsymbol{M_{WV}}\\ \boldsymbol{N_{WV}}\end{bmatrix}. \tag{1}$$

This wake vortex impact alleviation control strategy is implemented in a simulation model of the DLR research aircraft ATTAS (Advanced Technologies Testing Aircraft System) and is used for the offline simulations and for the flight tests.

It is assumed that the longitudinal and lateral controls are decoupled and that the control allocation equations are linear in the control surface deflections. Generally the control surface efficiencies, such as C_{l,δ_a} and C_{l,δ_r}, are nonlinear functions of the output vector y. In case of the ATTAS model the aileron control efficiencies are functions of aircraft angle of attack.

In the region between two wing tip vortices an encountering aircraft is exposed to strong downdrafts causing very high sink rates. In such a situation the short-term vertical motion of the aircraft can be improved, if the aircraft is equipped with special flaps for independent direct lift control (DLC flaps) in addition to the primary controls. DLC flaps are considered to be fast moving flaps at the trailing edge of the aircraft's wing with a size similar to that of the landing flaps. The DLR research aircraft ATTAS is equipped with DLC flaps that can be used optionally.

If the DLC flaps of ATTAS are used in addition to the primary controls their influence has to be considered for the control allocation of the wake vortex impact alleviation. The effect of the elevator deflection on the vertical force is neglected in this regard. This allows solving the Z-force equation independently from the elevator deflection. In the case of the ATTAS aircraft model the relation between the Z-force change generated by the DLC deflections and the DLC deflection angles is modeled as third-order polynomial. This third-order polynomial is solved for the DLC deflections in order to compensate the wake vortex induced vertical force. The pitching moment resulting from the DLC flap deflections is then considered for the determination of the required elevator deflection. Corresponding to the Z-force due to DLC flap deflections, the relation between DLC flap deflection and its pitching moment coefficient contribution is modeled as third-order polynomial, denominated as $f(\Delta\delta_{DLC})$ in Equation 2, which shows the modified equation for the calculation of the required elevator deflection.

$$\Delta\delta_e = -\frac{\mathbf{1}}{\boldsymbol{C_{m,\delta_e}}}\left[\frac{\boldsymbol{M_{WV}}}{\bar{q}\cdot S\cdot \boldsymbol{l_\mu}} + \boldsymbol{f}(\Delta\boldsymbol{\delta_{DLC}})\right] \tag{2}$$

The computation of the lateral control commands is not affected by the application of the DLC flaps and corresponds to Equation 1.

Sensor Parameter Sensitivity Study

As outlined above, several simulations have been conducted using the basic 2-D measurement concept. in order to perform a sensor parameter sensitivity study. As aircraft model a nonlinear 6-degrees-of-freedom model of the DLR research aircraft ATTAS was used. The wake vortex flow field is modeled by an analytical model. It consists of two superimposed counter rotating wing tip vortices. It is assumed that each vortex can be described by the velocity model of *Burnham-Hallock* [4]. The wake vortex generating aircraft is chosen to be a category 'heavy' aircraft with a MTOW of 190 t and a wing span of about 60 m. The age of the wake is set to 130 s which is equivalent to a separation distance of 5 nm (9265 m).

The induced velocities are fed to the aerodynamic interaction model in order to calculate the induced forces and moments that disturb the aircraft's motion. The wake impact alleviation controller (see above) is included to counteract the wake vortex disturbances. The DLC flaps described above are not used for the sensor parameter sensitivity study. The wake impact alleviation controller is composed of a second aerodynamic interaction model that uses the output of the sensor model to compute the induced forces and moment which are finally fed to the control allocation part. Moreover the simulation model contains a basic autopilot that controls the flight path of the aircraft.

The following paragraphs describe the nominal simulation case and shows the corresponding results in Figure 7. The autopilot holds the aircraft on the ILS beam. The nominal reference flight path (green dashed-dotted line) in the vertical plane (glide slope) is inclined by 3° which represents a typical landing approach situation on a standard ILS beam. The lateral position of the nominal flight path in the horizontal plane (localizer) is in the geodetic coordinate system y_g = 0 m. The wake of the generating aircraft is assumed to be y_g = -30 m off the center line, the respective wake vortex lines are aligned horizontally and located parallel to the vertical plane of the localizer signal at an altitude of 1 km. Thus, the right wing tip vortex line (black dashed line) is at a lateral distance of about y_g = -6.3 m of the nominal flight path, the left wing tip vortex line is at a lateral distance of about y_g = -53.7 m (out of the diagram). This represents a situation where the aircraft is passing the wake on its right-hand side.

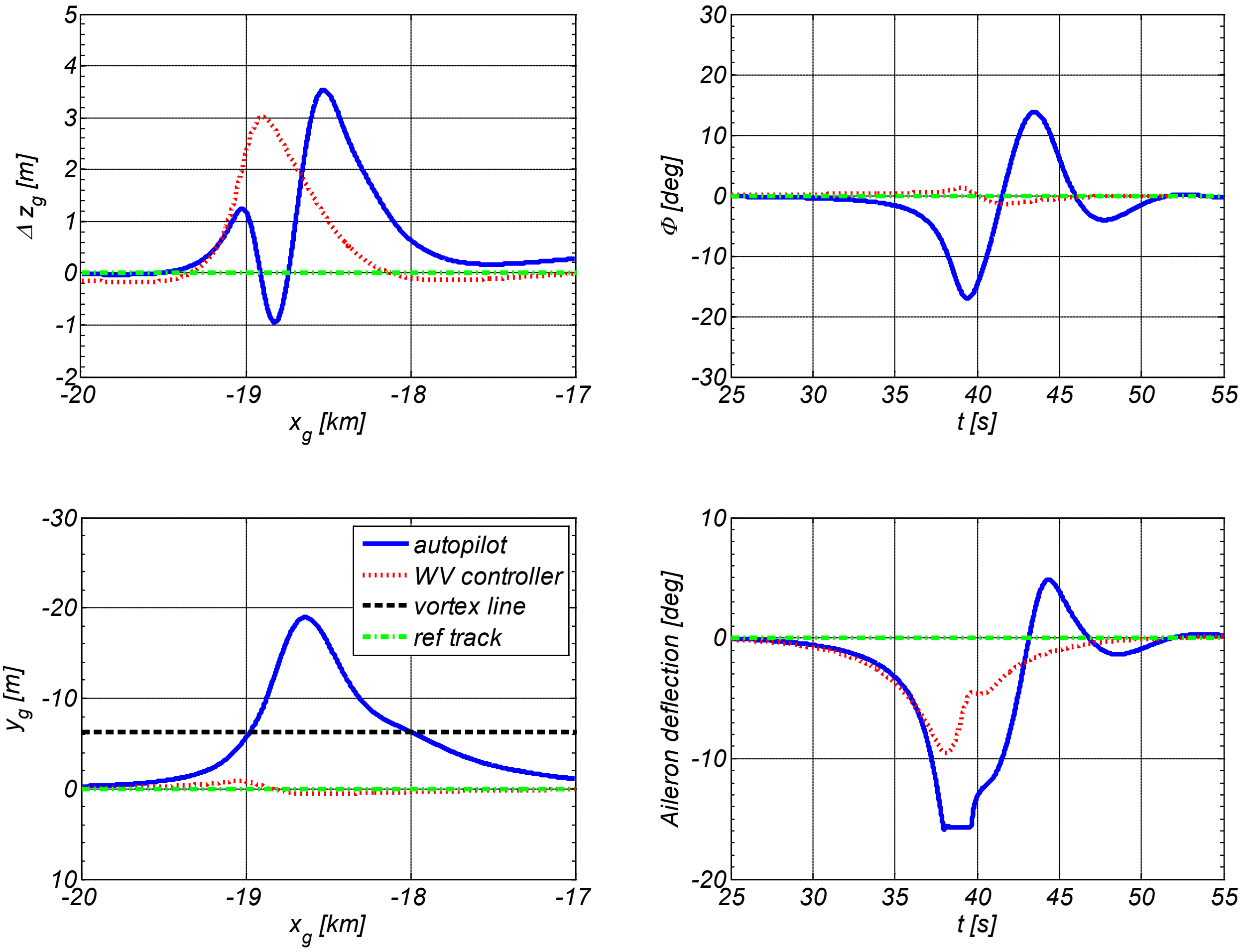

Figure 7. Flight track and time histories of a flight through a wake vortex flow field (offline simu lation with autopilot exclusively and autopilot supported by wake vortex controller)

The nominal set of sensor parameters is chosen based on advices of LIDAR manufacturers. The plane size in horizontal direction is twice the wing span and equal to the aircraft height. The measurement point matrix is of size 9x7. The measurement range is 100 m. The complete matrix is scanned with a frequency of 10 Hz. The blur range is set to ±2.5 % of the nominal measurement range with 10 sampling points. For the nominal case no measurement error is considered and the LIDAR delivers all three components of the velocity vector.

The blue curves in Figure 7 illustrate the flight with an autopilot trying to keep the aircraft on the ILS beam. The autopilot is designed to be representative for the aircraft type and cannot prevent high bank angles Φ and large lateral deviations Δy_g from the reference flight path. The approach situation when the autopilot is supported by the wake vortex impact alleviation controller is given by the red curves. It can be seen that the flight path deviations and bank angle excursions are reduced considerably. With respect to the results it can be stated that the wake vortex controller works properly, if the flow disturbance is known exactly.

Having demonstrated that the control concept works in principle the LIDAR model parameters were examined in more detail. For this purpose several simulations with parameter variations of the main LIDAR model parameters were performed. The following LIDAR model parameters have been changed for the sensitivity study:

- Number of measurement points (2x2 up to 9x9 points)
- Size of the measurement plane (varying between one time to four times of the wing span in horizontal dimension and one time to four times of the aircraft height in vertical dimension)
- Measurement noise (normally distributed, mean 0 m/s, standard deviation 0 m/s – 3 m/s)
- Measurement range (50 m up to 400 m)
- Measurement frequency (between 1 Hz and 100 Hz)
- Output of line-of-sight velocity or all three components of the velocity vector

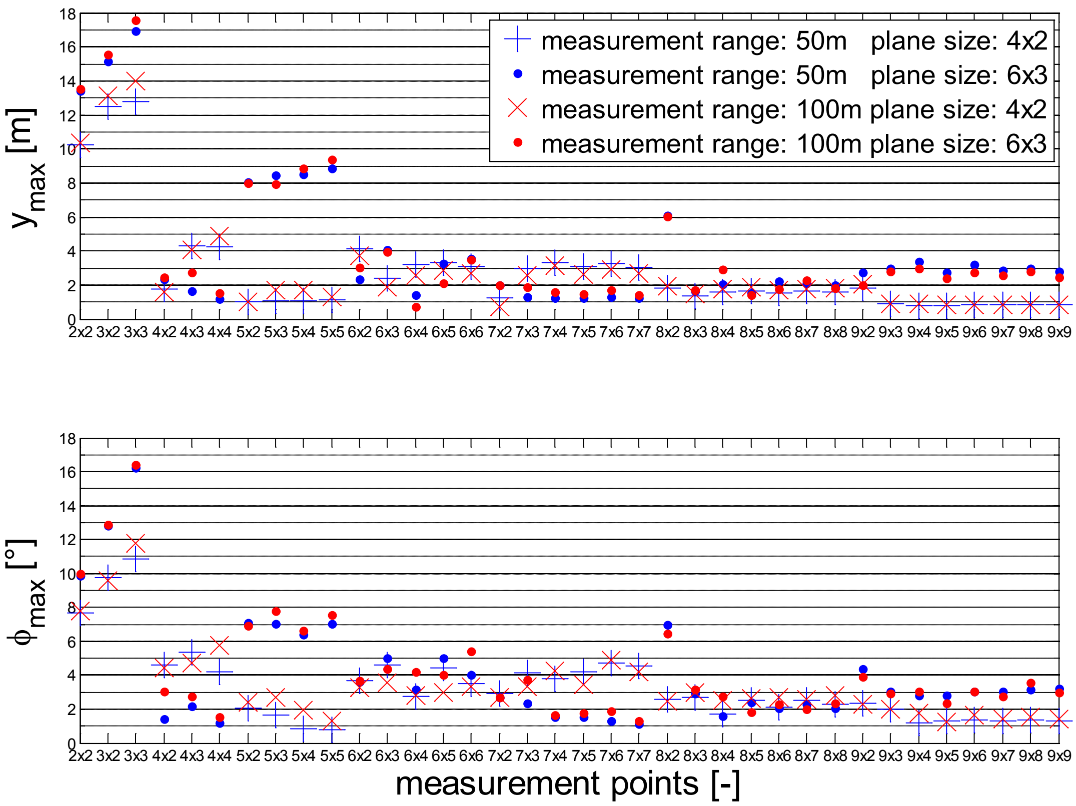

Figure 8. Lateral (y) deviation and bank angle for varying measurement points at 50 m and 100 m measurement range and plane sizes of 4x2 and 6x3

The results of the variation of measurement points are shown in Figure 8. It can be seen that an increased number of horizontal measurement points reduces the maximum devia-tion from the flight path in y-direction and the bank angle, while the number of vertical measurement points has only a small influence on the deviations.

Considering the complete number of simulation runs several unexpected results were produced. They are visible in the plots as peaks (c.f. Figure 8). The wake vortex flow field is highly nonlinear. The attempt to linearly interpolate with a limited number of measurement points leads to significant interpolation errors. The change of the number of measurement points implies a change of measurement point locations. Consequently the reduction of measurement points may coincidentally lead to more advantageous locations of the available measurement points for the linear interpolation. However a very large increase of the number of measurement points tends to result in smaller bank angles and cross-track errors.

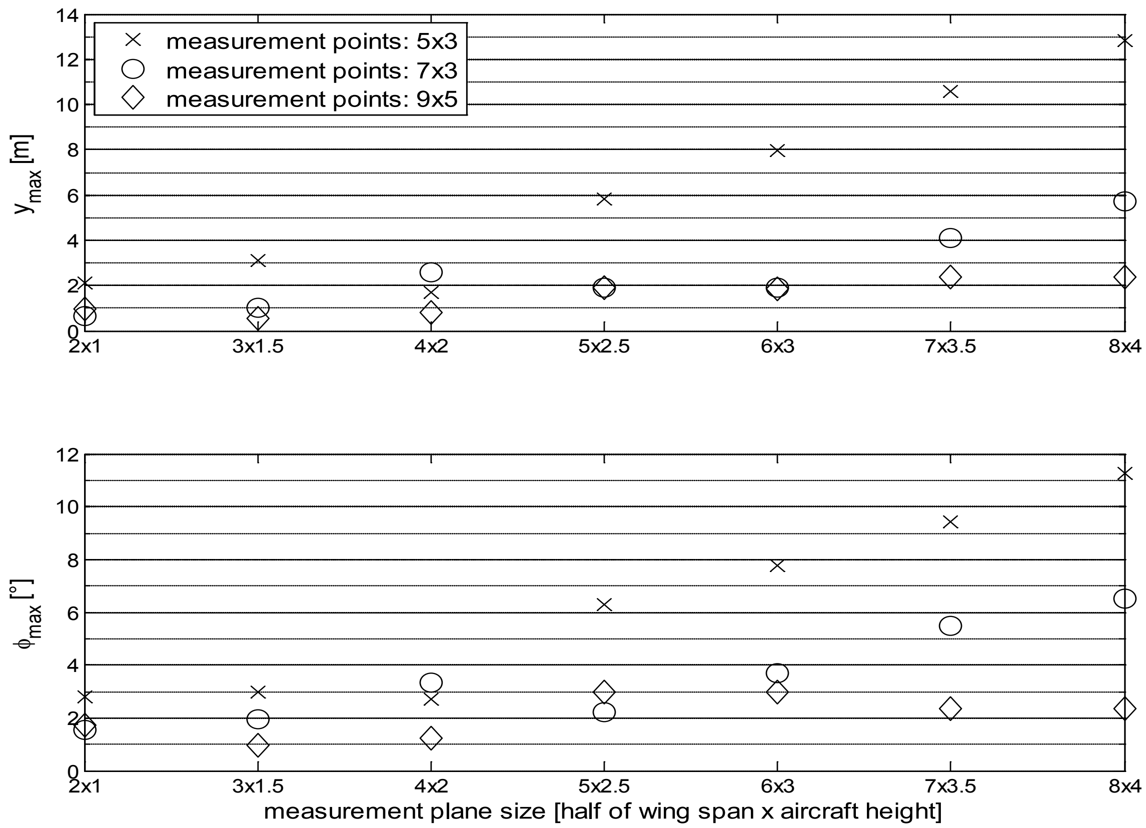

Figure 9. Lateral (y) deviation and bank angle for varying measurement plane with 5x3, 7x3 and 9x5 measurement points at 100 m measurement range

Based on the results of Figure 8, 5x3, 7x3 and 9x5 measurement points were chosen for the next simulations regarding the other parameters. The results for varying the size of the measurement plane are shown in Figure 9. Again an increasing number of horizontal measurement points has a positive effect on the maximum deviations. Therefore a horizontal measurement point number of at least nine is desirable. For the analysis of the measurement range the same set of measurement points (i.e. 5x3, 7x3, 9x5) was used. The results are given in Figure 10. As expected, it is better to use a shorter measurement distance. The suggested measurement range is up to 250 m with a maximum measurement error of 2 m/s in each velocity direction. Based on the simulations performed so far a LIDAR measurement should have at least 9x3 measurement points and should not exceed a distance of 250 m as well as a measurement error of 2 m/s. The measurement plane size should be at least twice the wing span and the aircraft height.

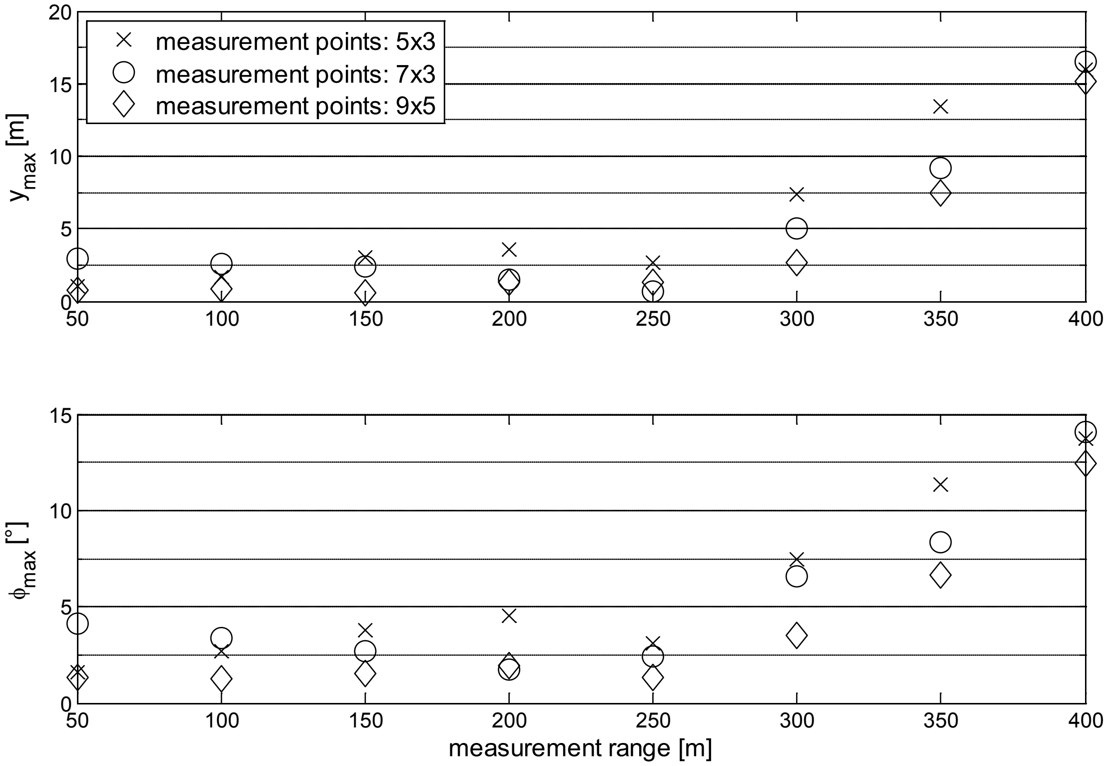

Figure 10: Lateral (y) deviation and bank angle for varying measurement range with 5x3, 7x3 and 9x5 measurement points

Pilot Assessment

The feasibility of a forward-looking control concept has been shown in several offline simulations. However, the acceptance of such an assistance system by the pilots is crucial, because the system uses a significant part of the control authority in order to compensate the wake vortex effects. Several flight test sessions have been conducted to rate different wake vortex encounters without and with the wake impact alleviation controller and without and with DLC flaps in order to evaluate the benefit of a wake vortex impact alleviation system from a subjective point of view. In former flight test sessions it could be shown that the application of the automatic assistance system (in both cases with and without DLC flaps) was rated good by the pilots [3]. However, in those flight tests ideal disturbance measurements were assumed and no airframe fixed measurement direction of the LIDAR sensor was considered. These effects have been accounted for in the updated flight tests described in this report.

The flight tests were conducted by using the in-flight simulation capabilities of the DLR research aircraft ATTAS, which is a modified VFW 614. By using nonlinear model-following control the aircraft acts like the simulated aircraft model encountering a wake vortex. As the pilots are experienced with the VFW 614 ATTAS, the simulated model is a VFW 614.

Flight Test Scenario

The flight test scenario is chosen similar to the simulation scenario. The flight tests consist of two flights with several approaches. The first of these flight tests was performed in 2009 at Holzdorf military air base. During this experiment the differences between wake vortex encounters with and without the wake vortex impact alleviation controller are investigated. The DLC flaps were not used for the wake vortex impact alleviation during this flight experiment. The second flight test was conducted in 2010 at Parchim International Airport and at Airport Braunschweig-Wolfsburg. This flight test allows a comparison of wake vortex encounters without any wake vortex impact alleviation controller, with the alleviation system without DLC flaps and with the alleviation system including DLC flaps.

The flight test scenario for both flights was identical. The encountering aircraft type is a VFW 614 with a MTOW of 21 t (ICAO class “medium”). The vortex generating aircraft is a category “heavy” aircraft (MTOW = 190 t) with a separation distance of 4 nm. The experiment scenario consists of an ILS ap-proach at a constant approach speed of 140 kt, with an inclination angle of γ_{GLS} = 3°, beginning 6 nm before the runway threshold and a go-around after flare initialization (cf. Figure 11). The initial altitude was at 2000 ft MSL corresponding to 1850 ft AGL at Parchim and 1700 ft AGL at Braunschweig and Holzdorf.

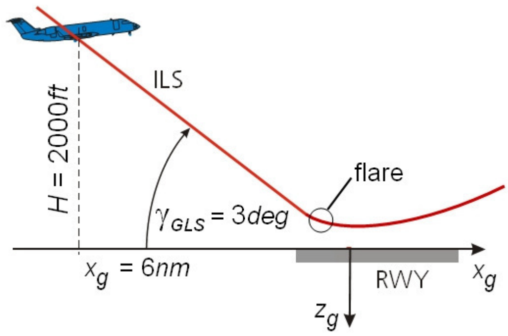

Figure 11. Approach scenario (side view)

The pilots who participated in the experiments are two professional pilots experienced in performing wake vortex encounters simulated in flight. The experimental pilot had to intercept the glide slope and maintain the nominal glide path. The flaps were already set to landing configuration, whereas the landing gear extension was commanded by the pilot at an unspecified altitude. The wake vortex encounters were initiated between 600 ft and 1100 ft AGL during the descent. The pilots were not informed about the encounter altitude in order to consider the element of surprise. The real turbulence during these flight experiments was considered to be light to moderate.

The additional forces and moments resulting from the wake vortex encounter were recorded in offline simulations. In these offline simulations it was assumed that the aircraft moves on a fixed flight path, leading the aircraft either along the upper, the lower or the lateral parts of the wake vortex wind field. The horizontal encounter angles were varied between 0° and 30°. The recorded forces and moments were then replayed during the flight after the crossing of the initiation altitude above ground which was varied for each encounter. This type of encounter model is often referred to as time-fixed encounter.

The wind field of the wake vortices was calculated either by using the Burnham-Hallock [4] model or by data sets of wake vortex flow fields coming from large eddy simulations [2]. During the flight test in 2009 both wake vortex models were used whereas during the flight test in 2010 only Burnhan-Hallock wake vortices were applied. The maximum required roll control ratio resulting from the wake vortex disturbances was 0.814. The roll control ratio is defined as the absolute value of the ratio between the wake vortex induced rolling moment and the maximum available rolling moment from an aileron (and roll spoiler) deflection.

Additionally to the wake vortex forces and moments acting on the aircraft, the forces and moments resulting from the wind field as “measured” by the LIDAR model (i.e. considering the airframe fixed measurement direction and the lead time of the sensor information) are recorded in the offline simulation. During the simulated encounters these recorded forces and moments are then fed to the automatic assistance system in order to compute the required control deflections.

The sensor model used for the flight tests is the 1-D sensor concept described above. This sensor model was used because the flight tests have been performed at an early stage of the sensor analysis when the 2-D sensor model had not been completed yet. It is as-sumed that the measurement range of the 1-D sensor is fixed to approximately 20 m and the number of measurement points is equal to the number of wing strip elements used to calculate the forces and moments acting on the aircraft. The y-components of the measurement points are equal to the y-components of the corresponding aircraft AIM wing strips.

The chosen measurement range corresponds to the minimum range and time required for the calculation of the control deflection commands at a calibrated airspeed of 140 kt considering the computational time delay and the actuator dynamics of ATTAS. Consequently the measured data points do not have to be buffered but can be directly fed into the wake impact alleviation system. The fact that the outer measurement points are located closer to the wing than the inner ones is neglected in this approach.

Pilot Rating Scale

The pilot rating of each vortex encounter was performed by means of the wake vortex encounter rating scale [9]. The ratings for each approach comprise four categories: aircraft control, demands on the pilot, aircraft deviations from flight state and flight path, and hazard. Each category is graduated into four levels, with a rating of 1 denoting an uncritical case and a 4 denoting an unacceptable one. Ratings of 1-3 are considered acceptable. A rating of 4 in any category leads to an unacceptable overall rating for the respective wake vortex encounter. In case of a go-around decision, the "aircraft deviations" category has to be rated with 4, whereas the rating in "hazard" category does not necessarily need to be unacceptable, i.e. a go-around is not necessarily hazardous. The ratings were performed immediately after each encounter.

Evaluation Results

Figure 12 shows the effect of the pilot assistance system on the average pilot ratings. The results of former experiments based on 20 piloted approaches are given in Figure 12 a presenting the clear tendency of improved ratings when the wake impact alleviation controller is engaged [7,8]. For those experi-ments the same forces and moments as those directly acting on the simulated aircraft were fed into the control allocation part. According to the former results the same trend is clearly confirmed for the wake impact alleviation controller using the 1-D sensor-concept as described in this report (cf. Figure 12 b). Again the wake impact alleviation system gets better ratings than the unassisted encounters. The ratings are even slightly better than in Figure 12 a. The reason for the improvement was identified to be the consideration of the required computation and actuator response time when determining the forces and moments that have to be compensated. However, it has to be kept in mind that in both flight experiments only a limited number of approaches (20 approaches in the former experiment with ideal disturbance measurement and 16 approaches in the latest flight test with realistic disturbance measurement) have been performed.

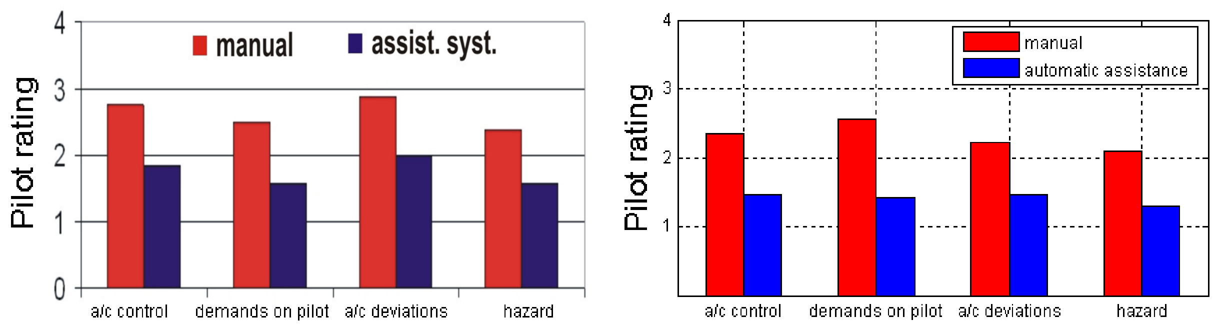

Figure 12. Average pilot ratings for IFS wake vortex encounters. Left: ideal disturbance measurement [6,7], right: realistic disturbance measurement

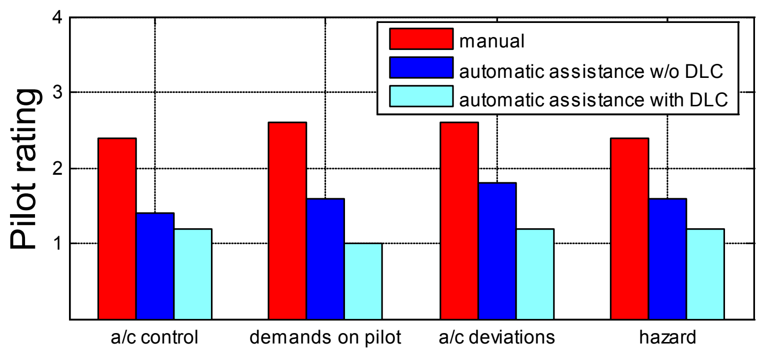

Figure 13. Comparison of average pilot ratings for IFS wake vortex encounters

Figure 13 shows the pilot ratings coming from the IFS experiments in 2010 with additional use of DLC surfaces. Due to flight time restrictions, the number of wake vortex encounter trials is also very small in this case. For each of the three control concepts five approaches have been performed. But the pilot's perception of the response improvement of the aircraft is evident. Applying IRLIS results in an aircraft response during wake vortex encounters which is nearly not affected by the induced disturbances (ratings close to 1).

Conclusions and outlook

In all phases of flight the flow field of wake vortices can strongly affect the passenger comfort and the safety when encountered by aircraft, hence, such encounters are to be avoided in any case. In case of an unintended wake vortex encounter an active control concept can be applied to alleviate the wake vortex effects on aircraft motion. It can be shown that the aircraft response encountering wake vortex turbulence can be improved significantly by using an active control concept as presented in this paper.

Future work on this topic will focus on the measurement concept including the sensor model and the data processing. The presented enhanced 2-D measurement concept will be developed further and used in subsequent projects. It will be applied to a new aircraft simulation model, which is representative for a single aisle aircraft of a MTOW of about 80 t.

References

[1] Fischenberg, D., 2012: Wake Vortex Encounter Modelling and Validation by Flight Tests“ in Section 4.4.

[2] Hennemann, I., 2010: “Deformation und Zerfall von Flugzeugwirbelschleppen in turbulenter und stabil geschichteter Atmosphäre”, PhD Thesis, Technische Universität München, DLR-FB 2010-21, 145 pp.

[3] Schwarz, C.W., Hahn, K.-U. and Fischenberg, D., “Wake encounter severity assessment based on validated aerodynamic interaction models,“ *AFM/ASE/GNC/MST Conference*, Toronto, Ontario, Aug. 2010.

[4] Burnham, D.C. and Hallock, J.N., “Chicago Monoacoustic Vortex Sensing System,” Vol. 4, Wake Vortex Decay, Springfield, VA, National Information Service, 1982.

[5] Hahn, K.-U., Schwarz, C. and Friehmelt, H., “A Simplified Hazard Area Prediction (SHAPe) Model for Wake Vortex Encounter Avoidance”, *24th International Congress of Aeronautical Sciences (ICAS)*, Yokohama, Japan, Aug./Sept. 2004.

[6] Vechtel, D. and Amelsberg, S., “Full Flight Simulator Study for Evaluation of Aircraft Dynamics While Encountering Curved Wake Vortices,” Institute Report IB 111-2009/17, DLR Institute of Flight Systems, Braunschweig, Germany, July 2009.

[7] Schwarz, C. and Hahn, K.-U., “Automated Pilot Assistance for Wake Vortex Encounter,” *Deutscher Luft- und Raumfahrtkongress 2007, First CEAS European Air and Space Conference*, Berlin, June 2007.

[8] Hahn, K.-U. and Schwarz, C., “Safe Limits for Wake Vortex Penetration,” AIAA Guidance, Navigation and Control Conference and Exhibit, Hilton Head, South Carolina, Aug. 2007.

[9] Schwarz, C. and Hahn, K.-U., „Subjective wake vortex encounter evaluation“, Institute Report IB 111-2011/46, DLR Institute of Flight Systems, Braunschweig, Germany, December 2011.

4.2 Simulated Lidar Signals for Wake Vortex Detection ahead of the Aircraft

Markus C. Hirschberger[1], Takashi Misaka[1], Frank Holzäpfel[1], Christian Horn[2]
[1]*Institute of Atmospheric Physics,* [2]*Institute of Flight Systems*

Within the DLR-project "Wetter & Fliegen" a feasibility study of airborne lidar sensors for active control at flying through wind shear and turbulent air masses (specifically wake vortices) was carried out. The main goal of such sensors is delivering sufficiently precise real-time measurements of the wind field in a short range in front of an aircraft under clear air conditions up to cruising speed at every altitude, so that a dangerous disturbance in terms of turbulent air motion at an encounter can be alleviated by an active control system with an automatic feed-forward controller. So far, no realized lidar sensor meets the requirements with regard to accuracy, rapidity and spatial resolution of wind measurements necessary for active control. For this reason, we investigate the potential of two suited systems by means of simulations including the physical properties of lidars and atmosphere: a Fringe-Imaging(FI) Doppler Wind Lidar (DWL) similar to the one developed within the project AWIATOR and a Backscatter Lidar (BL) for wind measurements. Though a totally new optical design might be necessary for the latter device to operate at a sufficiently high spatial resolution, the signal processing offers wind components in the *y*- and *z*-directions (transversal to the aircraft's propagation axis *x*) in very short time. From the results of DWL and BL simulations it turns out to be advisable to combine a Fringe-Imaging DWL for the *x*-component measurements with a BL for the *y*- and *z*-component measurements.

Introduction

The superior goal of airline passengers is to arrive on schedule in preferably short time and especially to fly in a safe way at the same time. Although nowadays bigger aircraft are able to transport more passengers per flight, the proliferation of passenger numbers expected in the near future will inescapably raise the number of air activities [3]. In this context, an essential tool for enhancing aircraft throughput while at least preserving the flight safety standards presently in force will be a reliable aircraft-based forward-looking remote sensor or an ensemble of sensors capable of wind measurements at least in a short distance (50-150 m) in front of the airplane, so that a dangerous disturbance in terms of turbulent air motion at an encounter can be compensated by an active control system by means of an automatic feed-forward controller [5,21]. The goal is a lowering of the gust load and an increase in flight comfort by alleviation of incidents with passenger injuries.

Such an active controller application requires precise knowledge of the (turbulent) flow to determine the required counteractions. The forward-looking time should not exceed 0.5 seconds. However, measuring in a shorter time than this is also difficult, due to the lead time necessary for the actuator dynamics and the time needed for the processing of the data measured by the sensor and the subsequent controller positioning computations.

Horizontal or vertical wind shear may cause severe danger for an encountering aircraft, especially near the ground. Turbulence may appear in clouds or in clear air, mainly in the friction layer between about 2000 ft and 3000 ft [23]. The most challenging turbulence phenomenon to cope with are the wake vortices (WV), self-generated by aircraft, that are the major hazard at departure or landing [4]. More flights in the future results in smaller spacings between the separated air corridors, thus the risk of WV encounters increases. Due to their small scale flow structure, wake vortex characteristics are extremely hard to identify by sensors in general. Simple detection of wake vortices is unsatisfactory since their strength varies with age and under the prevailing environmental conditions. Spatial resolution of detection preferably on the order of magnitude of one meter is desirable.

Lidars are remote sensing devices that are capable of wind measurements at high spatial resolution and also in clear air. Here we present two different approaches of useful monostatic pulsed lidars for wind measurements based on simulations. On the one hand a DWL based on the already engineered and flight-tested gust sensor of AWIATOR, that is suitable for measurements even at cruising altitude, will be analyzed numerically, including a critical analysis of the signal processing of the 2D fringes of such a FI-DWL with a FPI, which has not been conducted or published so far for cruise altitude before. On the other hand a more experimental and visionary approach is investigated in detail by simulating a backscatter lidar (BL). The design of this device in combination with its measurement geometry and signal processing is novel.

The objective of this contribution is to show the feasibility of such airborne wind lidar sensors under minimum sensor requirements (for active control).

Measurement Requirements

The general measurement situation is described below in Figure 1 for the DWL case and in Figure 2 for the BL case. Via the radiation backscattered from particles (aerosols or molecules) of the atmosphere, their motion can be captured and this way the wind, which transports them.

While one or multiple lidar(s) situated in the wings of the aircraft should be excluded from analysis (because wings may oscillate strongly and the position of the sensor therefore may vary between the point of radiation emission and detection of the backscattered signal that is analyzed), the aircraft's nose is the only really adequate place for a laser remote sensing device. Thus we restrict our analysis on a monostatic lidar in or near the nose, which also increases the time between measurement in front of the aircraft and actual contact of the wings.

Specifications for a forward-looking sensor for feed-forward control were determined and evaluated based on non-physical sensor models that calculate the measurement points in front of the aircraft. Concerning the necessary data precision of DWL measurements there is a difference between the demands for determination of the disturbance phenomenon from pure LOS-velocities $v_{\mathrm{LOS}} = (v_x^2+v_y^2+v_z^2)^{0.5}$ with the respective components [24], and the use of the full 3D wind vector $(u,v,w)^T$ for flight control in the case of a landing approach [10]. Both are compared in Table 1. The requirements for determining the disturbance phenomenon are higher since it does not take three LOS-directions which are necessary to determine one 3D wind vector, but only one LOS-velocity component v_{LOS} each time. Because of the small viewing angles of the LOS-directions in forward-looking lidar configuration, the errors for v_y and v_z (transversal to the propagation direction of the aircraft) are much higher than for v_x.

Table 1: Measurement requirements for (Doppler wind) lidar systems.

Measurement property	disturbance phenomenon (only LOS-velocities)	flight control (full 3D wind vectors)
range	150 m (- 500 m)	30-150 m (120-600 m)
points per slab	min. 63 LOS-directions	min. 20 full 3D wind vectors
frequency (slabs per second)	min. 10 Hz	min. 10 Hz
volume (depth of each slab)	max. 3% of range, i.e. 4.5 m (-15 m)	max. 10% of range, i.e. 3-15 m (12-60 m)
error (standard deviation)	max. 0.5 m/s for v_{LOS}	max. 2.5 m/s for each of u, v, w

For the flight control case knowledge of full 3D wind velocity vectors in front of an aircraft in suitable distances allows the derivation of forces and moments on the aircraft caused by the wind, so that the necessary control commands for compensation can be derived. The measurement error is modelled using normally distributed values with a given standard deviation.

All requirements in Table 1 are valid for landing approach, except the ones in brackets, which are valid at cruising speed (4-5 times higher). In general, the smallest possible value is preferred for the measurement range at flight control depending on the actual air speed. The scan angle depends on the measurement range and should be adapted in order to cover the full wingspan.

Similar parameter values were defined in the project Greenwake [22]. A minimum number of measurement points of 100 for WVs and less than 10 for wind shear is assumed there, with a LOS velocity accuracy of 1 m/s. Operation at all flight levels up to FL400 must be guaranteed.

For the feed-forward controller to work, two kinds of input by measured lidar data are possible:

1. Measured full 3D wind velocity vector (i.e. 3rd column in Table 1). Then the feed-forward controller can directly derive the required control commands.
2. Knowledge of wake vortex circulation, core radius and wake vortex position. Then idealized models like Burnham-Hallock or Lamb-Oseen help derive the necessary wind velocity vectors.

With the first point met with sufficient resolution, the second can also be fulfilled. We aim at measuring the v_x,v_y,v_z components of a single v_{LOS} as good as possible and then take a look at the feasibility of real time processing. Mainly two kinds of lidars have proven their potential to measure wind in the past.

Doppler Wind Lidars (DWL)

While pulsed onboard Doppler radar are capable of long-distance, range-gated wind field measurements under the presence of hydrometeors (e.g. in clouds, fog or rainfall), they are mainly suited for detection of cumulonimbi with high water drop density or for large-scale wind shears only, but not for CAT. Via pulse compression, spatial resolution in the meter-range is possible. Nevertheless, radar will perform poorly under clear air conditions outside clouds, without raindrops or thick optical depths [23]. Compared to Doppler radars, DWL operate well in clear atmosphere. Pulsed DWL measure the wavelength (frequency) shift Δλ, that is caused by the optical Doppler effect, between the emitted laser pulse at the wavelength λ_0 and the received, backscattered photons (including solar photons) at $\lambda_0 \pm \Delta\lambda$ by the LOS-velocity v_{LOS} mentioned above, according to the Doppler shift formula

(1) $$v_{LOS} = -\frac{\Delta\lambda\, c}{2\,\lambda_0},$$

where $c \approx 3.0 \cdot 10^8$ m/s is the speed of light under the assumption of a refraction index of 1 in clear air. The measurement geometry is displayed in Figure 1.

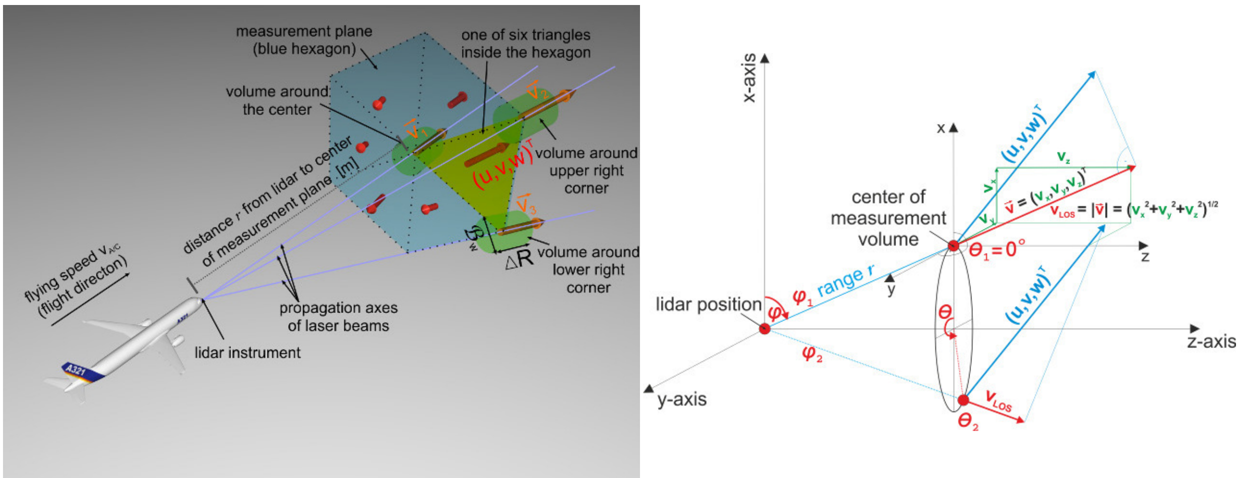

Figure 1. (Left) Measurement geometry with three LOS-vectors $\vec{v}_1, \vec{v}_2, \vec{v}_3$ (orange), i.e. three directions, and full 3D wind vectors $(u,v,w)^T$(red) generated from three LOS-measurements each (B_W: beam diameter, ΔR: range bin). (Right, taken from [8]) Azimuth and elevation angles with the LOS-velocity components v_x, v_y, v_z of a single LOS-vector $\vec{v}$ (in optical x-,y-,z-coordinates), whose magnitude is v_{LOS}.

Successful aircraft-based measurements of wake vortices with DWL in the past were either near the ground with high aerosol density or in the higher atmosphere only with the help of smoke-seeders or in hazy environment [17]. The angle for the velocity components was very advantageous (huge v_y- and v_z-contributions by measuring the WV from above, and perpendicular to the WV axis, thus the v_y- and v_z-errors are reduced here).

While coherent DWL sensors engineered and tested in projects like MFLAME, I-Wake or FIDELIO were designed for far range measurements (500-2375 m) via heterodyne detection and aerosol backscattering at lower spatial resolution (measurement intervals of ca. 75 m), the incoherent (direct detection via fringe imaging (FI)) FI-DWL sensor of the project AWIATOR was developed for the near field (50-150 m) in front of the aircraft at a slightly higher spatial resolution (ca. 30 m) including the capability of wind detection at cruising altitude by analyzing photons backscattered from molecules [12,19].

The FI-technique of the AWIATOR-sensor allows a combined analysis of the aerosol together with the molecular part of photons in one step, making use of the broadened fringe patterns created by a Fabry-Pérot-interferometer (FPI) on a 2D intensified charge-coupled device (ICCD) localized at the focal plane behind it.

For our needs none of those will be truly satisfactory. Even though big progress has been made concerning the range resolution (ca. 15 m) of heterodyne systems [11] only recently, and with autodyne detection systems being considered [1], all of them are at least today limited in flight altitude because of their need for backscattering aerosols (which are nearly missing completely in cruise altitude) by their measurement principle. The AWIATOR-sensor yields only four LOS-components at a rate of 15 Hz (state 2010), thus nearly no information is gained about a complex structure like a WV. However, this FI-DWL-principle can be extended to more LOS-directions in the future [22].

Backscatter Lidars (BL) for wind measurements

The big advantage of a BL for wind measurements compared to a DWL is its independence of frequency (or wavelength) shifts. This means the Doppler shift needs not be measured and an analyzing interferometer like the FPI is not necessary. The BL works solely with detecting the backscattered intensities (photons) from slabs, i.e. range bins, with a certain thickness in different LOS-directions. The drawback is that two slab measurements at slightly different points of time have to be taken in order to determine the movement of the particles, i.e. the wind velocity. The big advantage is that even under for DWL bad angles (v_y and v_z tiny) and at larger ranges, transversal wind components v and w perpendicular to the flight axis can be measured more quickly and perhaps precise. These transversal wind vector components are crucial to the flight stability of an aircraft. Slab thicknesses for the BL may be smaller than 5 meters and the true air speed needs not be extracted from the results, which is the case for the Doppler shift of DWLs.

The wind evaluation procedure for the v- and w-components of the BL has its origin in Particle Image Velocimetry (PIV) [16]. What is done is a cross-correlation (CC) of two images, taken either from two spatially different slabs d and $d+\Delta d$ at the same point of time t or, more favorable, from the same slab d at two slightly different points of time t and $t+\Delta t$. This laboratory laser principle is applied in the scanning, ground-based Volume-Imaging Lidars (VIL) in the free atmosphere [2,18,20]. The retrieved data are temporarily averaged over volume backscattering measurements, which will not be possible in our airborne case. The flight speed also requires a different scanning device for pulse emission to the directions. Speckle Imaging Velocimetry (SIV) is another lidar method similar to PIV. In SIV the density distribution of the air molecules is measured [6], so far only up to a range of 100 m. Backscattering signals from the slabs include statistically distributed laser-speckle, that serve as indicators for the air motion determined from two CCD image recordings in a small time interval of a small air region. A directional scanner is missing in this device. No tracer particles are added in VIL and SIV measurements.

Figure 2 shows the simulated general principle of an airborne BL for wind measurements proposed in this study. Only a few of the directions of the laser beams are visualized as green lines; in reality or the simulations the whole measurement plane has to be scanned in a resolution as high as the backscatter images shown. To our best knowledge, so far no fully working airborne BL system for wind measurements has been built or flight-tested. This means, the difficulties arising from a moving platform for the BL system and the signal processing have not been solved yet.

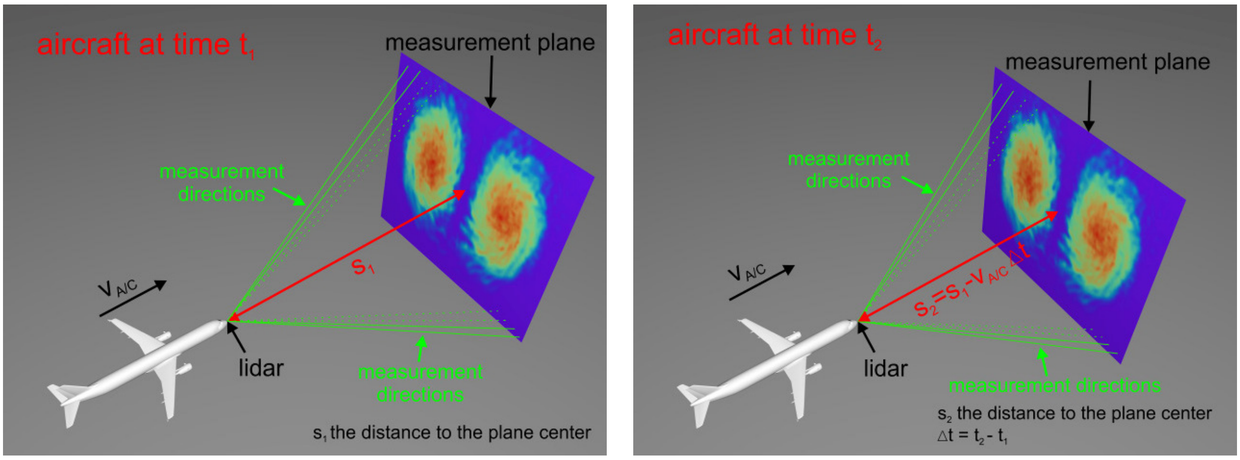

Figure 2. General measurement principle of the simulated airborne BL for wind measurements at times t_1 (left) and $t_2=t_1+\Delta t$ (right). Shown are the backscattered intensity distributions of the simulations. Note that the angles of the measurement directions have to be adapted, i.e. enlarged for the plane at t_2, to scan exactly the same points.

Simulations of a Fringe-Imaging Doppler Wind Lidar

We summarize the results of a paper on simulations of a FI-DWL with a FPI [8]. The interferometric fringe patterns generated by the FPI are simulated including atmospheric conditions as well as laser and detector properties. We focus especially on the noise disturbing the 2D CCD-images in the forward simulation. The backward simulation, i.e. the signal processing, delivers the accuracy achievable via calculation of the ring radii difference of the 2D CCD fringe images between emitted and received photons, and by the Doppler shift formula (1) the LOS-velocity accuracy.

Figure 1 again illustrates the measurement situation for a 3D wind vector geometrically. From three LOS-velocities v_{LOS} in different directions (orange) one full 3D wind vector $(u,v,w)^T$ (red) can be determined (see Figure 1 left, in the centre of the triangle (yellow) formed by the centres of the three LOS-volumes as corners). The question now is: “How exact can a single v_{LOS} be measured?

Because of the quickly changing wind field the measurement plane should be quite close to the aircraft in order to fly through nearly the same wind field as predicted by the DWL (or BL). Thus time for measurement and signal processing is highly limited. The number of backscattered photons would be too low for far-range measurements, since they have to be distributed on a high-resolution CCD (here: 960x780 pixels) for analysis in the FI-DWL-case. The measurement volume is ≈0.05 m^3 for the distances r = 56 (76) m of Table 2 and a range bin of ΔR = 10 m, with assumed values of 0.025 m for the radius of the outgoing laser beam and a divergence angle of 500 µrad at full angle, resulting in a beam width of B_w≈ 0.08 m in the LOS-volume’s center.

Table 2 summarizes the parameters used for the simulations. The backscatter and extinction coefficient values are the ones determined for an altitude of 8500 m. Other properties are the laser wavelength, the instrument constant and the telescope area. The number of backscattered photons received at the CCD is calculated by the single scattering lidar equation. It is n=1.3×10^7 for a LOS-volume range of 76 m and n=2.4×10^7 for a range of 56 m.

Then realistic fringe patterns of a FPI on a 2D CCD localized at the focal plane behind it are simulated, taking atmospheric and instrument properties like scattering and noise into account. The received 13

(24) million photons per pulse are transformed to photoelectrons and distributed on a CCD with 960×780 pixels without intensification. The noisy pixel signals are modeled by Poisson-distributed random numbers for shot (or photon) noise, Gamma-distributed random numbers for speckle noise, and Gauß-distributed random numbers for the read-out noise. Solar background noise plays a minor part due to the short range gates (i.e. low exposure time of Δt = 6.7×10^{-8} s) and can be neglected. Figure 3 (left) shows such a simulated 2D FPI ring pattern on a CCD, that includes strong broadening by Rayleigh scattering. Similar patterns (without atmospheric influences) can also be simulated by 3D ray-tracing of plane waves with random properties, that are emitted towards a FPI (with lenses around it) and finally intersect the 2D CCD-plane. A result is shown in Figure 3 (right).

Table 2. Single scattering lidar equation parameters for a transmitted pulse energy of E_L = 70 mJ and pulse length τ_p = 10 ns at a flight height of h=8500 m used for the FI-DWL simulations.

n	photons received at the CCD	1.3×10^7 / 2.4×10^7
λ_L	center pulse wavelength	354.7 nm
r	range	76 m / 56 m
$\beta(\lambda_L,h)$	backscatter coefficient	3.104×10^{-6} m^{-1} sr^{-1}
A_r	area of the telescope	0.13 m^2
k	instrument constant	0.15
$\alpha(\lambda_L,h)$	extinction coefficient	2.70×10^{-5} m^{-1}
ΔR	range bin of atmospheric volume	10 m

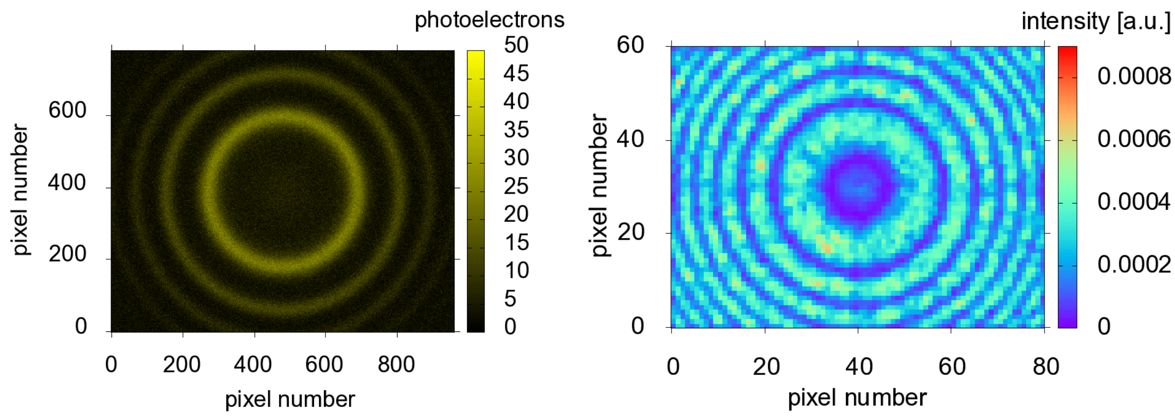

Figure 3. (Left) 2D broadened fringe pattern including atmospheric properties. (Right) 2D fringe pattern on a CCD created via 3D ray-tracing of a multitude of plane waves with random properties.

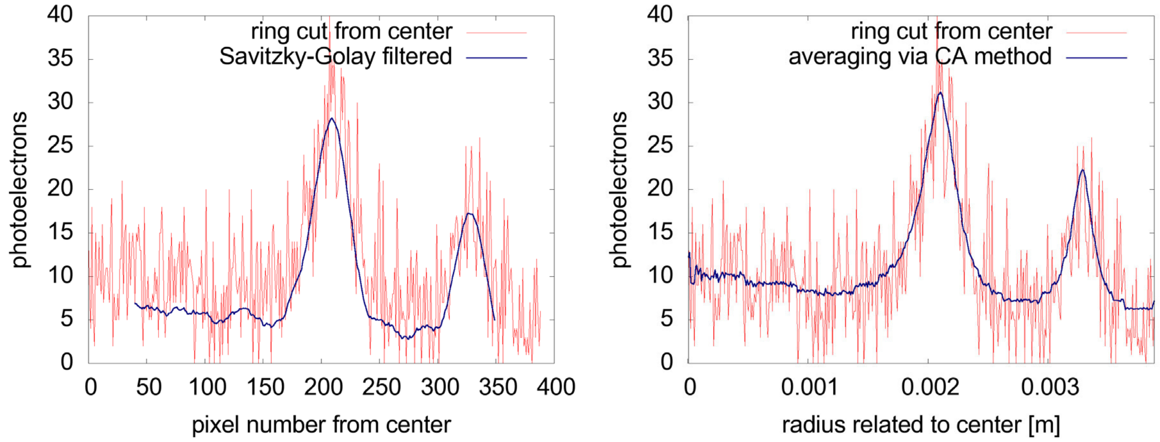

Figure 4. (Left) Cut through a ring from the center to the edge of a 2D-CCD fringe pattern (red) and improvement by Savitzky-Golay-filtering 360 of such noisy cuts in steps of 1° (blue); (Right) Same cut through a ring as in the left image (red), but noise reduction by Circular-Averaging (CA)-method (blue).

The main focus of the signal processing is on two novel radii evaluation strategies including a center determination that make use of the complete 2D information given on the CCD. Thus the noise of single 1D cuts (see red curves in Figure 4) through the 2D rings can be significantly reduced. After calculation of the ring center as exact as possible via the so-called Circular-Averaging(CA)-method, again CA or the so-called Midpoint-Line(ML)-method can be applied to compute ring radii from the CCD-images. CA, when applied to the noisy data, performs better than e.g. a Savitzky-Golay-filter, as visible in the blue curves of Figure 4. In [8], results computed by the ML- and CA-method for a v_{LOS} of 0 m/s and a v_{LOS} of 50 m/s are compared and visualized. The gaps between these curves are tiny; fitting them by the Levenberg-Marquardt method a more precise peak position, which corresponds to the ring radius (i.e. wavelength), is determined.

In the analysis of the results, we have to distinguish the measurement or calculation bias from the standard deviation. The CA-type of signal processing proves to nearly reach the accuracy necessary for LOS-velocity measurements. A standard deviation of 2.5 m/s including centre determination can be achieved with only 20 CCD images to average. The bias is 7 m/s. For exactly known ring centres, bias and standard deviation can be better than 2 m/s for the innermost ring. Especially because of the low number of images (i.e. pulses) necessary to average, the methods are suited for DWL measurements and for use in a velocity sensor on board of aircraft.

However, the precision for the LOS-velocity of more than 0.5 m/s from Table 1 can (if possible) only be reached with even more time-consuming signal processing. Many ways of parallel processing can reduce the computation time. Intensification of a CCD, i.e. an ICCD, may reduce the noise in relation to the received signal, which would result in a higher accuracy. Resolution reduction concerning the pixels to accelerate calculations would yield degraded results.

A FI-DWL may be suitable for short-range wind-shear detection, but not for small-scale phenomena like wake vortices. The Doppler-principle in forward-looking configuration of the lidar favourably measures the v_x-component of v_{LOS} with low error, while results will be more defective for the v_y- and v_z-components due to the small elevation and azimuth angles. Especially these *y*- and *z*-contributions of v_{LOS} are often dangerous for aircraft encountering i.e. a WV. Therefore an alternative approach for the v_y and v_z or the *v*- and *w*-components of a 3D wind vector should be investigated.

Simulations of a Backscatter Lidar for Wind Measurements

A BL has certain advantages in measuring cross-flow velocities compared to a DWL. To simulate such a device we need realistic slabs from complex turbulent structures like wake vortices and a program that takes these profiles as extinctions for backscatter simulations in 3D. The photons backscattered from a slab of wake vortices for the different directions are distributed on a screen as seen by the following aircraft. Finally a cross-correlation procedure and an alternative novel procedure calculate the *v*- and *w*-components of two full backscatter images at slightly different points of time. The software elements necessary to do BL simulations of wake vortices for wind measurements are described now.

Wake Vortex Extinction Profiles from Large Eddy Simulations

For simulation of an airborne BL that measures WVs first of all realistic 3D wind velocity fields generated by WVs are needed. The incompressible Navier-Stokes codes LESTUF and MGLET simulate the circulation decay and vortex topology of WVs as well as the turbulent exchange processes of passive tracers under varying environmental conditions [7,9,13].

For our purpose 3D data from MGLET-simulations of WVs with passive tracers in combination with their velocity field are most suited. (Combined velocity-profiles $(v^2+w^2)^{1/2}$ of LESTUF-simulations also deliver velocity fields similar to Figure 6 left top, that could also be converted to extinction profiles, though these may be physically incorrect structures.)

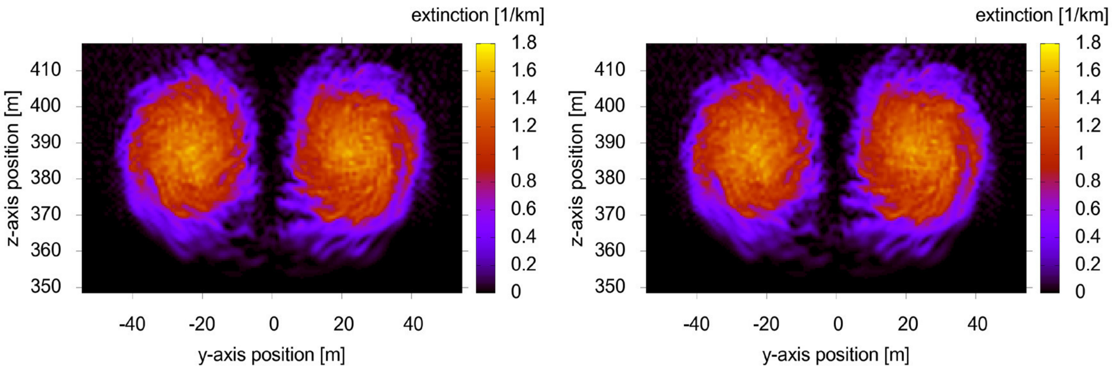

Figure 5. Extinction profiles generated from MGLET simulations at times (left) t_1 and (right) $t_2=t_1+\Delta t$ with Δt=0.1 s for a single slab at high spatial resolution (219×139 pixels). Differences may at least be visible with the naked eye at the dark-yellow centers of the distributions.

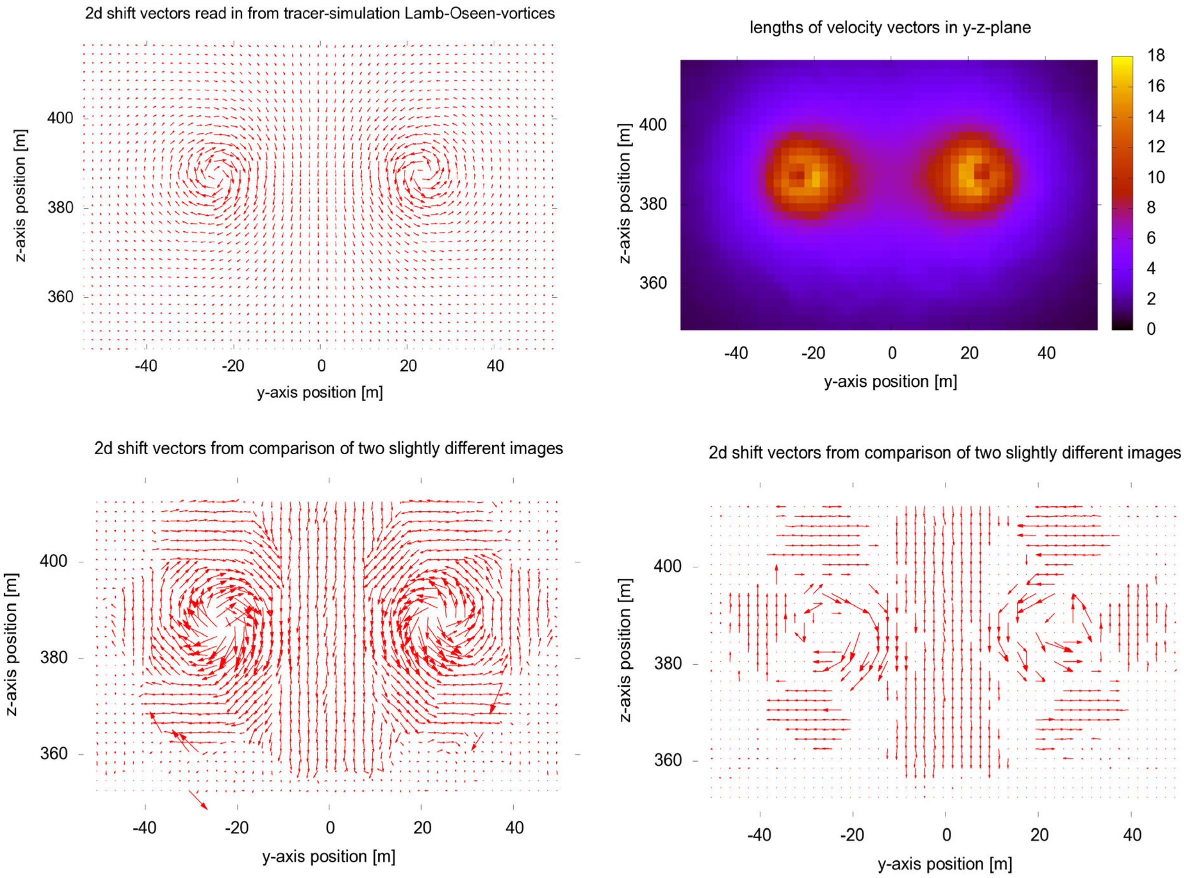

Figure 6. *v*- and *w*-wind velocity components from MGLET-simulations used as an optimal structure (left top), the retrieved wind field from cross-correlation calculations (left bottom) and from weight-shift calculations (right bottom). The lengths (in m/s) of the *v*-and *w*-velocity vector components of the left top image are visualized in the image on the right top.

The resolution of the tracer distributions and the corresponding wind field is usually one meter in all three spatial directions. A case at a vortex age of 40 seconds was chosen, with a normalized eddy dissipation rate (describes the intensity of atmospheric turbulence) of ε *=0.01 and a normalized Brunt-Väisälä-frequency (describes the degree of stable thermal stratification) of N*=0.35, i.e. a still very structured WV without much decay. The WVs generated by a A340 aircraft were modelled in the MGLET simulations as two counter-rotating Lamb-Oseen vortices with a vortex separation of 47.1 meters and a vortex core radius of 3 meters, see Section 6.1.

Since measurements of slabs (planes) should take place at least 10 times per second (see the requirements in Table 1), the movement of the tracers may take only Δt=0.1 s between two images. This is also optimal for the CC-based wind evaluation procedures. However, data from LES-simulations are saved at least every few seconds. Therefore we use 2D velocity fields (*v*- and *w*-component) of slabs perpendicular to the *x*-axis and move the first particle image at time t_1 according to the velocities (e.g. a velocity of 10 m/s means a movement of 1 m in 0.1 s), so that a second particle image at time $t_2=t_1+\Delta t$ is generated. For this short time interval the particle motion should be described physically adequate by this method, and it will serve for a proof-of-principle for the wind-measuring BL later on. Only very close to the vortex centres this method yields artificial radial velocity components (divergence).

As a result from tests with the evaluation algorithms, a higher spatial resolution than 1 m is needed. Therefore the tracer distributions as well as the velocity field from MGLET-simulations taken for the calculation of the second image were spatially interpolated to obtain a resolution of 0.5 meters. This way the images have 219×139 = 30441 pixels and are sufficient to visualize and reconstruct the rotational wind velocity features of the wake vortices in axial view.

Finally, the values of the continuous distributions from MGLET-simulations are raised or lowered to realistic extinction values, while the relative structure of the profile is maintained. Here a stretching factor of 2.0 seems to be suitable. Figure 5 shows the extinction profiles at t_1 and t_2 that are read in for the backscatter simulations. Figure 6 at the left top shows the *v*- and *w*-velocities of a slab at *t*=40 s as given from the MGLET-simulations (optimal) and the same velocity field obtained by the CC-evaluation method (bottom left) and the new Weight-Shift-method (WS) (bottom right) for the extinction profiles to be read in. For better visibility the 2D wind vectors were scaled by a factor of 0.2. Figure 7 shows the differences of the lengths and the directions of the via CC and WS reconstructed velocity vectors from the optimal profile in Figure 6, left top.

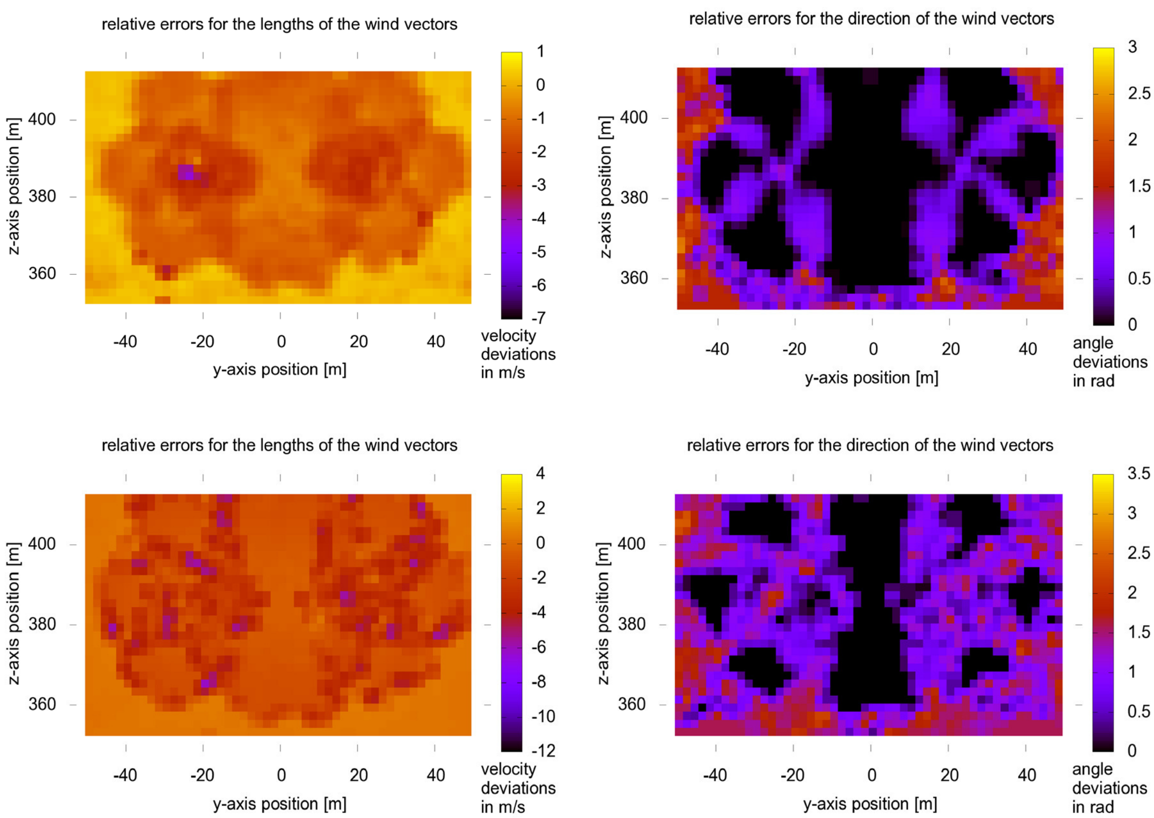

Figure 7. Relative deviations of the velocity magnitudes (in m/s) between the wind field of the large eddy simulation and the wind field calculated from the extinction profiles via CC (top left) and corresponding relative deviations of the wind speed directions (in rad) (top right). The bottom images show the same as the top images for the WS method.

Monte-Carlo Simulations

To perform backscatter simulations we use a Monte Carlo program for polarized backscatter signals (pbs, [14,15]). The contribution of photons hitting a receiver in backward direction is calculated taking polarization into account. The formerly latest version of pbs was adapted concerning its measurement geometry to the necessities of airborne wind-measuring backscatter lidar simulations. The structure of the backscattering volume can be reconstructed more or less exactly if single (weak) pulses are emitted to a multitude of directions with small emitter field of view (equivalent to one beam that is split in multiple directions) rather than emitting a strong single pulse with a large emitter field of view. One reason for this is the lower number of photons in the edge regions of a spatially widened laser pulse.

These problems are eliminated here by a high number of simulated directions (219×139) from a fixed position for the times t_1 and t_2 at 1 million emitted photons per direction. The divergence of each beam, i.e. the emitter field of view is 2 mrad, while the semi-aperture of the receiver is 5 mrad, i.e. the receiver field of view 10 mrad. A Gaussian laser beam is simulated with an input radius of the emitter of maximum 0.1 m, and the radius of the receiver is 0.5 m. Multiple scattering is considered here, although the first scattering order clearly dominates because of the thin slabs and the assumed environmental extinction of 0.1 km^{-1}. The slabs have extinctions up to 1.8 km^{-1}, see Figure 5, and are only 2.5 meters thick.

At the first point of time, t_1, the measurement distance from the lidar to the beginning of the slab we want to measure is 500 m, thus azimuth angles of $-6.2° \leq \theta \leq 6.2°$ with 219 equidistant subdivisions and elevation angles of $-3.9° \leq \varphi \leq 3.9°$ with 139 equidistant subdivisions are simulated. At the second point of time, t_2, the distance is only 485 m, i.e. we assume an aircraft flight speed $v_{A/C}$ of 150 m/s in x-direction and an aircraft movement directly to slab, so the aircraft has moved 15 m for the assumed Δt=0.1 s. The maximum angles must be increased: azimuth angles are now $-6.4° \leq \theta \leq 6.4°$ and elevation angles are $-4.1° \leq \varphi \leq 4.1°$ at the same resolutions from above. The measurement time intervals are chosen in a way that at θ=0° and φ=0° (beams hitting the center of the slab) just the Δx=2.5 m thick slab is completely measured. This stays the same for the angles outside the center, where the beam will pass a distance slightly longer than 2.5 m. Every part of the slab is (fully) hit by the laser beams.

The scattering Mueller matrices are randomly oriented prolate spheroids at a wavelength of 532 nm (i.e. laser wavelength 532 nm), which have the scattering properties of aerosols. Mueller matrices for molecular scattering could also be used.

The received backscattered photons are then ordered on a screen according to the emission direction of the laser beam, i.e. again 219×139 points. This way the images of Figure 8 are created. Not the absolute photon numbers retrieved are used for analysis, but the backscattering intensities that are normalized according to view angle and measurement distance, so that a comparison by the CC- and WS-algorithms is possible.

A difficulty in reality may be the short time for distinguishing the arriving backscatter contributions from the single directions and slabs (if this is necessary), as well as the adaption of the angle from the first measurement of the plane to the second measurement in a shorter distance in front of a plane. The same plane has to be measured at t_1 and t_2, and this plane has to have exactly the same x-,y- and z-positions and sizes. The particles in it move from t_1 to t_2 according to the extinction profiles.

Calculation of Wind Velocities

The data processing algorithms will be described in detail in the doctoral thesis of M. Hirschberger. The algorithms used here are mainly based on searches for best matches between a chosen reference template of the image 1 at t_1 and a number of equally sized templates in a certain region of the image 2 at t_2.

The cross-correlation (CC)-method first calculates the cross-correlation coefficient functions and searches for a peak value between a reference template of image 1 and all the templates of a certain region of image 2 around this reference template position for these CC-functions. Then the movement of the particles from image 1 to image 2 can be calculated at pixel-accuracy. Finally a Gaussian peak fit filter is applied to determine the vector shifts at subpixel accuracy [16]. The weight-shift(WS)-method does not use the CC-coefficient functions for best match calculations, but takes the center-of-masses of the templates and computes the best match concerning position of the center-of-mass of a reference template of the image at t_1 and the templates of a region of the image at t_2 around it. Subpixel-accuracy can be reached by filtering with center-of-mass positions. For both methods 8x8 reference templates were used with a search region of 16x16.

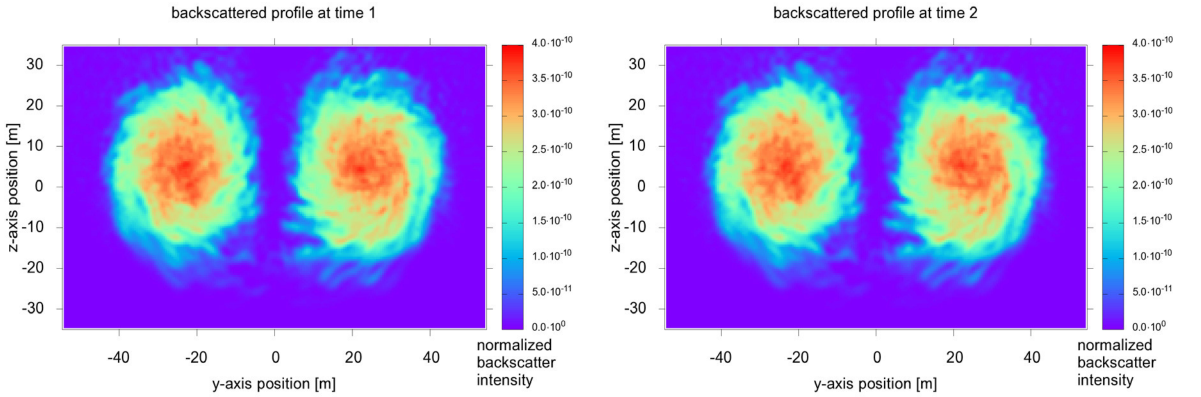

Figure 8. Backscatter images at time t_1 (left) and t_2 (right) from normalized backscatter simulations. The backscattering intensities are normalized according to view angle and measurement distance, so that a comparison by CC- and weight-shift-algorithms is possible.

Results and Discussion

Backscatter Lidar Simulations

Results from the backscatter simulations are presented in Figure 8. Intensities are already normalized, so that the images at t_1 and t_2 can be used for the wind-vector evaluation algorithms. Results of these are shown in Figure 10. Figure 9 visualizes the relative differences of the extinction profiles taken for the simulations (see Figure 5) and the resulting backscatter profiles (see Figure 8). Values are normalized to the averaged values of each image, i.e. each pixel value of both images is divided by this mean value; the difference of these two fractions then yields the differences. Figure 11 finally compares the calculated velocity fields from the extinction profiles (see Figure 6, bottom) with the computed velocity fields from the backscatter profiles (see Figure 10), again for the CC and WS algorithms. See captions of Figures 8 to 11 for more details.

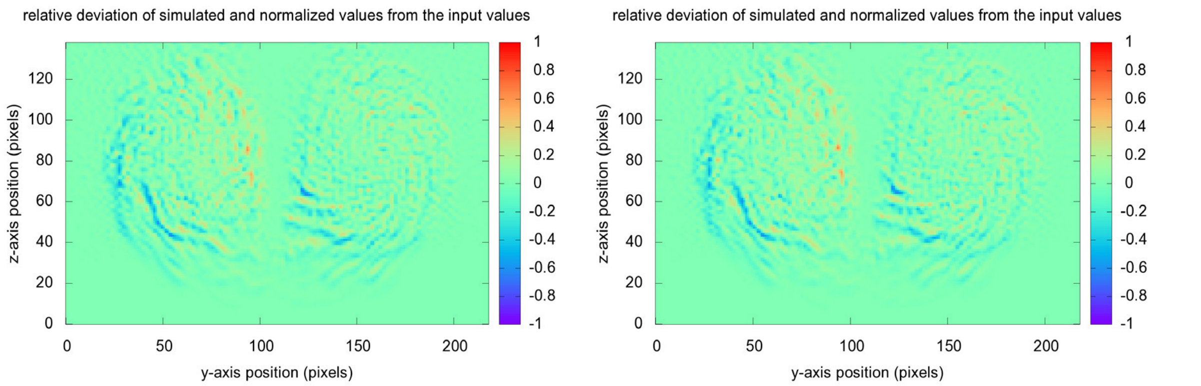

Figure 9. Relative deviations of the average values of read in extinction profile at t_1 and the corresponding backscattered profile at t_1 (left) and the same for the t_2-images (right).

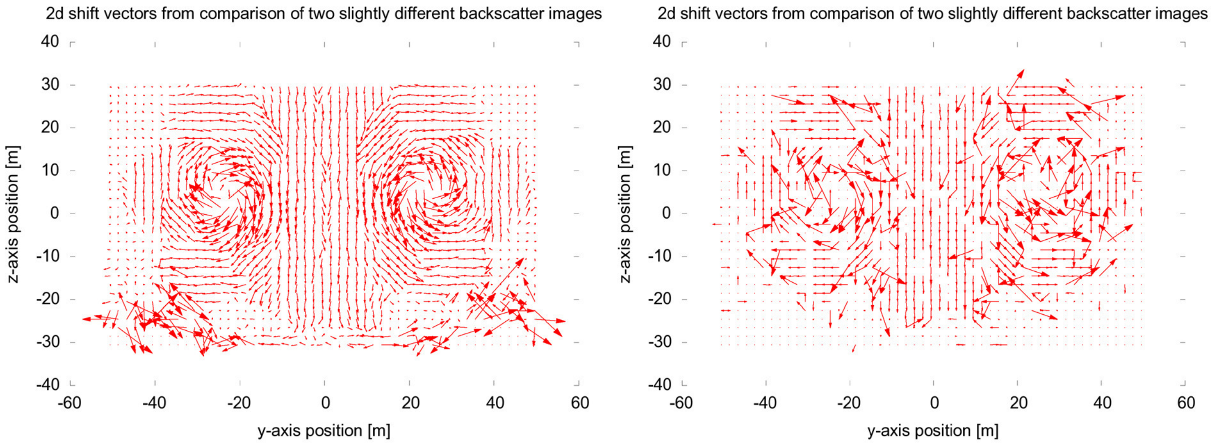

Figure 10. Unfiltered CC-calculated wind vectors (left) and WS-calculated wind vectors (right) in *v*- and *w*-direction from the backscatter images of Figure 8.

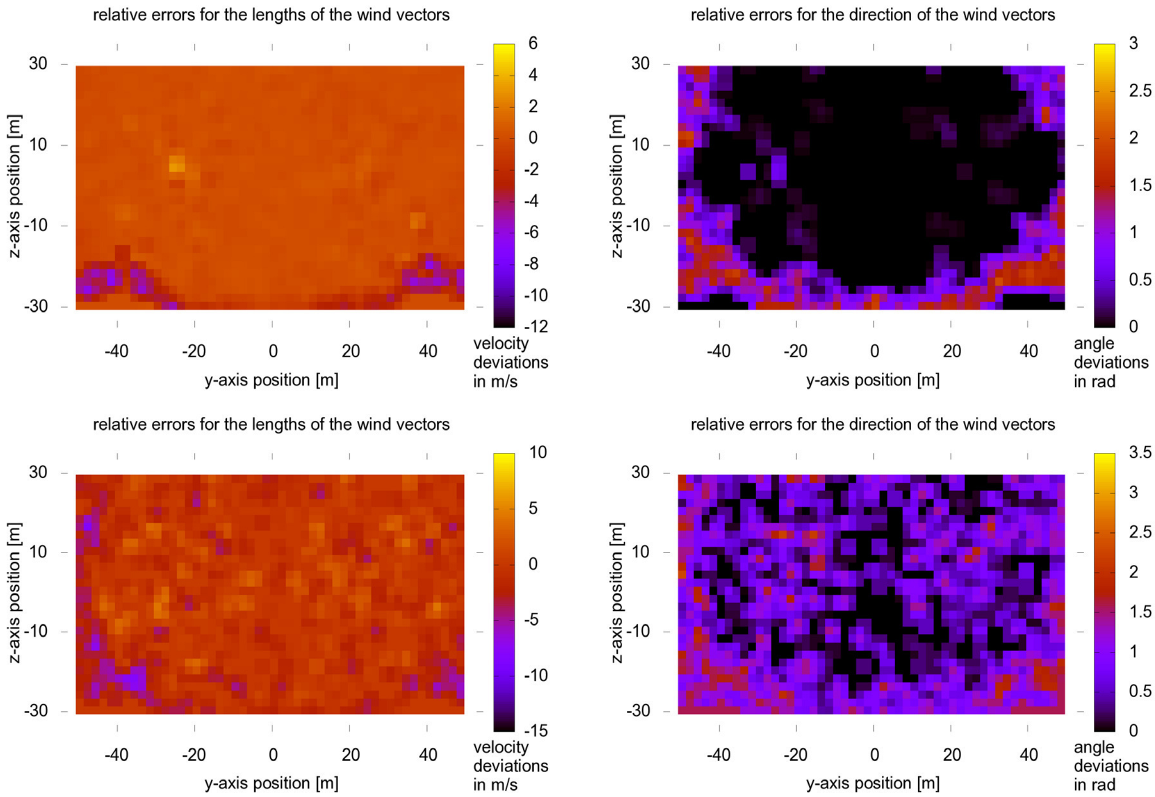

Figure 11. Relative deviations of the velocity magnitudes (in m/s) between the extinction fields and the backscattered fields both calculated via CC (top left) and corresponding relative deviations of the wind speed directions (in rad) (top right). The bottom images show the same as the top images for the WS method.

The results of the simulations of a BL for wind measurements via a proof-of-principle method show the feasibility of detecting the rotational features of vortices, especially with the CC-based algorithm. Errors in the lengths and directions of the retrieved wind vectors are quite low in the center region (see Figures 7 and 11). The number of wind vectors per plane is more than sufficient. However, the *u*-component of wind cannot be simulated so far with backscatter simulations. The main difficulty of this kind of BL in reality is the necessity of many high-resolution slab measurements in very short time gaps, since the CC-algorithms for evaluation are only suited for extremely short time intervals (Δt=0.05-0.2 seconds in our case; see also PIV) between the two images. The movement of the particles is hardly visible for such small Δ*t*. However, the algorithms can detect them.

The spatial resolution of 219×139 pixels is necessary for detection of the rotational vortex structures and should not be lower to our experience. In PIV laboratory measurements and under useful measurement geometries usually much higher resolutions on ICCD-cameras are measurable. Since time is severely limited for the BL at flight speeds of 70-200 m/s and more, the lidar has not much time to do measurements. A lidar device for measuring in ten-thousands of directions in a few milliseconds seems not to have been built yet. Fibers and beamsplitters could provide a solution for emission of pulses, but in the receiver the backscatter signals may have to be detected according to a time gate for each direction, i.e. the signals from the directions may have to be clearly separated in the detector.

Solar background noise is not relevant at such short time gates (2.5 m slabs) and can be excluded from analysis.

Comparison of Doppler Wind Lidar and Backscatter Lidar

For exactly known FPI ring center at a measurement distance of 56 m and a range bin of 10 m only 20 ring diagrams are sufficient for a bias and a standard deviation better/lower than 2 m/s. (FI-)DWL has big measurement errors for the *v*- and *w*-components of wind. Signal processing is very slow and time-expensive so far. Therefore a BL with new and quick signal processing was analyzed as an alternative. The advantages are visible from the results. The principle of BL would be useful also for wind power stations, where no moving platform must be considered, to measure the wakes behind them or to optimize their orientation to the wind direction. Such a lidar might be much easier to build than for aircraft. Especially the analysis could be extended to 3D, since the lidar could measure more than just a few slabs (see also [20]).

Conclusion and Outlook

So far, no suitable lidar sensor for active flight control is available. From the results of DWL and BL simulations it turns out to be advisable to combine a FI-DWL for the *x*-velocity component measurements with a BL for the *y*- and *z*-velocity component measurements. Possibly, the vortex velocities in flight direction are less important for active flight control such that crossflow measurements with a BL would be sufficient.

Concerning the BL as a wind-measuring device, the simulations should also be possible for a measurement distance lower than 500 meters, although this may be difficult in the simulations (not in reality) because of the wider angles of view; slabs thinner than 2.5 m could alleviate this problem. Photon noise should be included in the analysis, and laser wavelengths different from 532 nm should be simulated, since lasers at 532 nm might not be eye-safe. There is still a lot of potential in the analysis algorithms for the BL. The analysis for BL could for example be extended to the 3D case, so a full 3D wind vector would become available. At *y*- and *z*-resolutions of 0.5 m this means slabs of only Δx=0.5 m thickness and a high number of such thin slabs to be measured. Simulations could become too time-consuming for realization in that case.

Acknowledgements

We would like to thank G. Ehret, N. Hannemann, I. Hennemann, M. Moser, O. Reitebuch, F. Steinebach and C. Wolkensinger. A special thanks to U.G. Oppel and to M. Wengenmayer for the former latest version of pbs, as well as to T. Gerz and C. Schwarz for managing the project.

References

[1] M.C. Cates, J.N. Paranto, T.A. Larsen (2011), Multifunction Aircraft Light Detection And Ranging (LIDAR), Patent-No. WO/2011/022164 A1.

[2] E.W. Eloranta, J. King, J.M. Weinman (1975), The determination of wind speeds in the boundary layer by monostatic lidar, J. Appl. Meteorol. 14, 1485-1489.

[3] EUROCONTROL (2004), Challenges to Growth 2004 Report (CTG04), European Organization for the Safety of Air Navigation, Edition Number 1.0, EATMP Infocentre Reference 041109-01, Brussels, Dec. 2010.

[4] T. Gerz, F. Holzäpfel, D. Darracq (2002), Commercial aircraft wake vortices, Progress in Aerospace Sciences 38, 181-208.

[5] K.-U. Hahn, D. Fischenberg, D. Niedermeier, C. Horn (2010), Wake Encounter Flight Assistance Based on Forward-Looking Measurement Processing, In: AIAA Guidance, Navigation, and Control Conference, 2-5 August 2010, Toronto, Ontario Canada, AIAA 2010-7680.

[6] T. Halldórsson, A. Langmeier, A. Prücklmeier, V.A. Banakh, A. Falits (2006), Particle and speckle imaging velocimetry applied to a monostatic lidar, Proc. SPIE 6522, 65220A.

[7] I. Hennemann, F. Holzäpfel (2011), Large-eddy simulation of aircraft wake vortex deformation and topology, Proc. IMechE Vol. 225 Part G: J. Aerospace Engineering, published online 23. September 2011, DOI: 10.1177/0954410011402257.

[8] M.C. Hirschberger, G. Ehret (2011), Simulation and high-precision wavelength determination of noisy 2D Fabry-Pérot interferometric rings for direct-detection Doppler lidar and laser spectroscopy, Appl. Phys. B 103, 207-222, link: http://www.springerlink.com/content/u3311lvg67060665/ .

[9] F. Holzäpfel, T. Misaka, I. Hennemann (2010), Wake-Vortex Topology, Circulation, and Turbulent Exchange Processes. In: AIAA Atmospheric and Space Environments Conference, 2-5 August 2010, Toronto, Ontario, Canada, AIAA 2010-7992.

[10] C. Horn, C. Schwarz (2009), Sensor Requirements for a feed forward controller, internal report of the DLR project “Wetter und Fliegen”, June 2009.

[11] H. Inokuchi, H. Tanaka, T. Ando (2009), Development of an Onboard Doppler Lidar for Flight Safety, J. Aircraft 46, 1411-1415.

[12] G. Jenaro Rabadan, N.P. Schmitt, T. Pistner, W. Rehm (2010), Airborne Lidar for Automatic Feedforward Control of Turbulent In-Flight Phenomena, J. Aircraft 47, 392-403.

[13] T. Misaka, F. Holzäpfel, T. Gerz, M. Manhart, F. Schwertfirm (2011), Large-Eddy Simulation of Wake Vortex Evolution from Roll-Up to Vortex Decay, In: 49th AIAA Aerospace Sciences Meeting including the New Horizons Forum and Aerospace Exposition, 4-7 January 2011, Orlando, Florida, USA, AIAA 2011-1003.

[14] U.G. Oppel, M. Wengenmayer (2003), Diffusion of the lidar beam seen from the receiver. In: C. Werner, U.G. Oppel, T. Rother: 12th International Workshop on Lidar Multiple Scattering Experiments (MUSCLE XII), 10-12 Sept. 2002, Oberpfaffenhofen, Germany, Proc. SPIE 5059, pp. 21-30.

[15] U.G. Oppel, M. Hirschberger, M. Wengenmayer (2006), Simulation of the azimuthal dependence of cross-polarized lidar returns and its relation to optical depth and a comparison with measurements by N. Roy, G. Roy, L.R. Bissonnette, and J.-R. Simard. 14th International Workshop On Multiple Scattering Lidar Experiments (MUSCLE XIV), Université Laval, Québec, Canada, 4-7 Oct. 2005, pp. 27-40. Defence R&D Canada, Valcartier.

[16] M. Raffel, C. Willert, S. Wereley, J. Kompenhans (2007), Particle Image Velocimetry - A Practical Guide (2nd ed.), Springer-Verlag Berlin Heidelberg.

[17] S. Rahm, I. Smalikho, F. Köpp (2007), Characterization of Aircraft Wake Vortices by Airborne Coherent Doppler Lidar, J. Aircraft 44, 799-805.

[18] Y. Sasano, H. Hirohara, T. Yamasaki, H. Shimizu, N. Takeuchi, T. Kawamura (1982), Horizontal wind vector determination from the displacement of aerosol distribution patterns observed by a scanning lidar, J. Appl. Meteorol. 21, 1516-1523.

[19] N.P. Schmitt, W. Rehm, T. Pistner, P. Zeller, H. Diehl, P. Navé (2007), The AWIATOR airborne LIDAR turbulence sensor, Aerosp. Sci. Technol. 11, 546-552.

[20] J.L. Schols, E.W. Eloranta (1992), Calculation of Area-Averaged Vertical Profiles of the Horizontal Wind Velocity From Volume-Imaging Lidar Data, J. Geophys. Res. 97, 18395-18407.

[21] C. Schwarz, K.-U. Hahn (2011), Automated pilot assistance for wake vortex encounters, Aerosp. Sci. Technol. 15, 416-421.

[22] C. Schwarz, S. Bowater (2011), UV Imaging Lidar for Wake Vortex Detection - The GreenWake Project, Project Progress Review, May 2011, link: http://www.wakenet.eu/fileadmin/user_upload/3rd%20Major%20Workshop/presentations/WN3E_3rdMW_day2_Greenwake.pdf (Nov. 2011).

[23] C. Wolkensinger (2010), Vergleich messtechnischer Konzepte zur bordgestützten Ermittlung atmosphärischer Störphänomene, DLR Institut für Flugsystemtechnik, Braunschweig, IB 111-2010/35, 59 pages.

[24] C. Wolkensinger (2011), Autonomous Wake-Vortex Approximator (AWA): Autonomes Verfahren zur Erkennung von Wirbelschleppen aus Line-of-Sight (LoS) Messdaten eines vorausschauenden Sensors, DLR Institut für Flugsystemtechnik, Braunschweig, IB 111-2011/14, 35 pages.

4.3 Wake Characterisation Using LIDAR Measurements

Dietrich Fischenberg
Institute of Flight Systems

Due to the physical principle of a LIDAR (Light Detection and Ranging) sensor it is only possible to get velocity measurements in the line of sight (LoS) direction of the laser beam. Velocities perpendicular to the laser beam cannot be detected. Since a vortex flow field in general presents a concentric tangential flow around its vortex line the angle between laser beam and wake vortex lines is very important for the measurement. The smaller this measurement angle is the less information about the flow field can be obtained from the LIDAR signal. Hence, a processing of the LIDAR measurements is necessary. We describe two processing concepts: the Online Identification (O-ID) method and the Autonomous Wake-Vortex Approximator (AWA) method.

Wake Online Identification

A processing concept is now described and verified which is capable to reconstruct the vortex strength, its position and orientation from LIDAR line-of-sight measurements. Key element is the application of an online identification (O-ID). The outcome of the presented approach is an approximation of the wake flow field velocities by an analytical wake model. This approximated flow field can provide the wake velocities in any spatial resolution (as opposed to the LIDAR measurements).

The LoS measurement information is very dependent on the wake vortex encounter and measurement scenario. At small encounter angles the LoS measurements would detect only small parts or even nothing of the wake vortex velocities. To obtain the relevant velocities in the wake, a post-processing of the LoS measurements is indispensable before using it, e.g. in a feed-forward disturbance compensation controller. An important element of the concept is that not only single-time line-of-sight (LoS) measurements (see Figure 1 with 27 LoS measurement directions) are interpreted but also the LoS velocity time histories for all measurement directions.

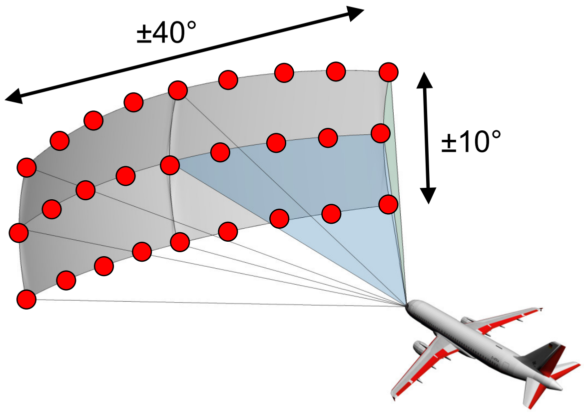

Figure 1: Forward looking LIDAR sensor with 27 measurement directions

The overall O-ID concept is shown in Figure 2. The idea is to fuse the information of the LoS measurements with that of a wake predictor. The wake predictor gives a first rough guess of the wake's position, strength and orientation and is based on available information from other aircraft in the area of interest and from horizontal wind speed information. A minimum requirement for data transfer from other aircraft is actual aircraft mass, position and flight path. Both parts of information, the LoS-measurements and the wake predictor's first guess, are then used as inputs into an online identification algorithm, which determines the wake strength and its orientation as well as the positions of both single vortices.

The O-ID is based on algorithms developed for offline wake determination with flow measurements from 5-hole-probes [2], where the respective data were recorded during the passage of the flow field of interest. In the present case, the algorithms are modified in order to apply them for online computations with forward looking LoS measurements. The outcome can be a precise representation of the flow field in front of the aircraft before getting into contact with a wake.

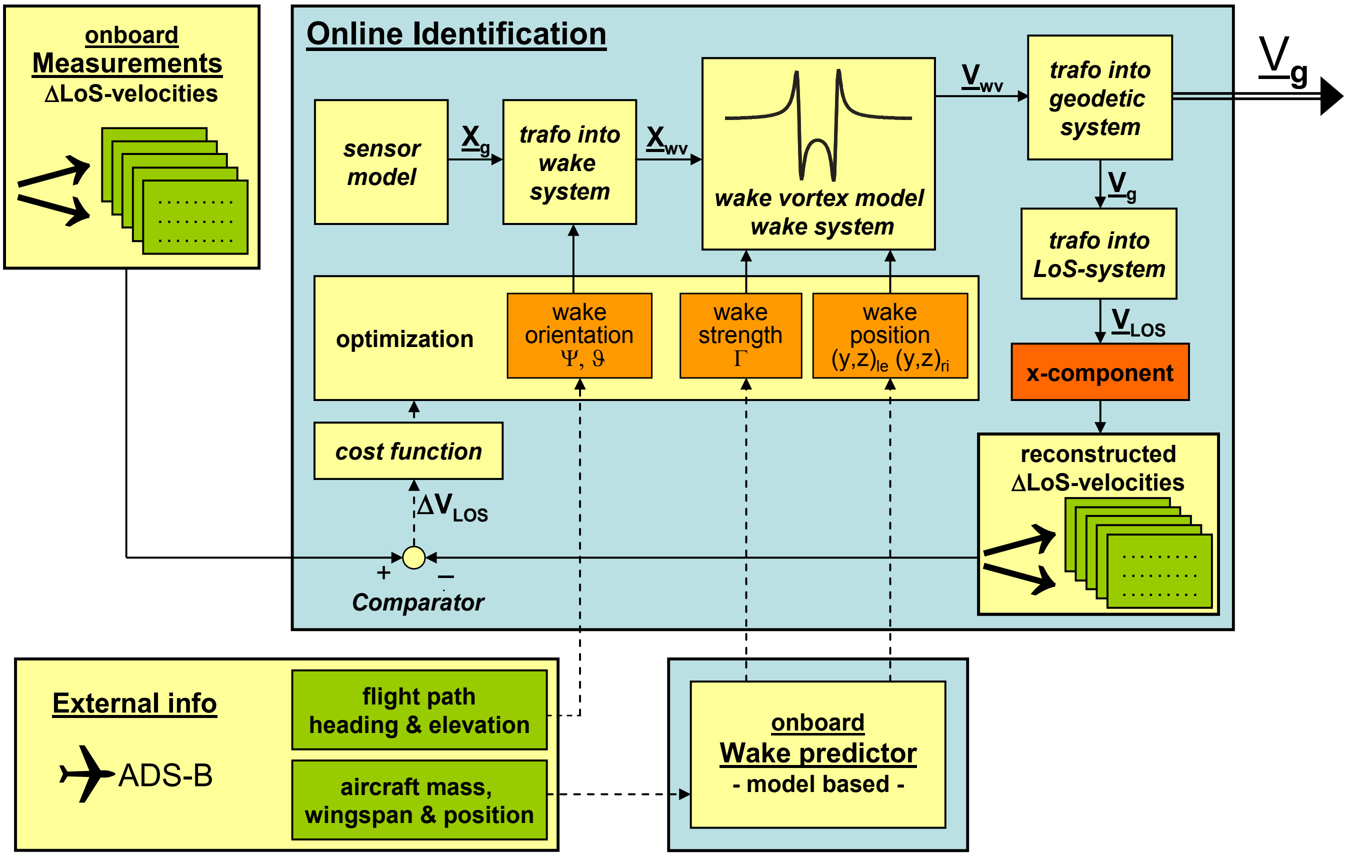

Figure 2: O-ID concept for determination of wake vortex strength, position and orientation from line-of-sight measurements

The O-ID determines the parameters of an analytical wake model iteratively by minimizing the differences between measured and reconstructed LoS measurements. This is done by using the time histories of all available measurement directions within a suitable, distinct time window. Ideally, the time window is permanently scrolled and updated every time after a new measurement snapshot vector is available. The O-ID algorithm works iteratively and should converge ideally within the measurement update rate, e.g. within 0.1 s. The update rate as well as the time window depend on the encounter scenario and the airspeed. A typical time window for many scenarios is less than 10 s.

The analytical vortex model by *Burnham-Hallock* [3] was found to be very adequate for online application. The model describes the radial velocity distribution V_t within a vortex with only two parameters: *circulation* Γ and *core radius* r_c:

$$V_t(r) = \frac{\Gamma}{2\pi}\frac{r}{r_c^2 + r^2}$$

A wake is described with two superposed vortices counter rotating with the same strength. As the vortex core radius is relatively constant during wake aging, it was found adequate to apply a constant value of 4% wing span [2]. This fixed value depending on wing span is also used here for online application. Assuming an elliptical load distribution in most flight phases, the core radius can be formulated as a function of only lateral vortex spacing *b'* which is calculated from the identified y-coordinates of the two vortices:

$$r_c = 0.04\frac{4}{\pi}b'$$

Thus, seven parameters are necessary to describe the wake flow field in front of an aircraft analytically. All parameters can be identified applying the O-ID:

(1) vortex strength (circulation Γ)
(2-3) lateral position of left and right vortex (or lateral vortex spacing *b'*)
(4-5) vertical position of left and right vortex
(6-7) wake orientation w.r.t. the geodetic ref. frame (elevation ϑ_{wv}, azimuth Ψ_{wv}).

The algorithm based on an analytical wake model can be applied with LoS measurement data for wake ages a few wing spans after generation (wake rollup complete) and prior to a moderate level of wake deformation [2].

The O-ID algorithm (Figure 2) uses a simple parametric LIDAR sensor model, which covers main sensor features like pulse frequency, update rate, measurement geometry, resolution and accuracy. The sensor model computes the position vectors $\underline{X}_g$ for all measurement points in the geodetic reference frame. These positions, transformed into the wake system, result in $\underline{X}_{WV}$. Applying the analytical wake model, the wake velocities $\underline{V}_{WV}$ at each measurement position are computed. These velocities, transferred back into the geodetic reference frame, result in $\underline{V}_g$. Finally, they are transformed into the LoS system, resulting in $\underline{V}_{LOS}$. Only the components in LoS measurement direction are then compared to the measured ones ("comparator" in Figure 2). A cost function is evaluated and an optimizer tries to minimize any differences between the measured and reconstructed LoS velocities by tuning the seven model parameters.

Note: not a snapshot is fed into the optimisation but a distinct evaluation time window. After convergence the fully reconstructed wake vector in the geodetic frame ($\underline{V}_g$) is available for use e.g. in a feed-forward disturbance compensation. As the algorithm is iterative, a robust and fast convergence is essential. This is supported by a minimum number of model parameters (7) and by suitable a-priori values from the wake predictor. The convergence should be achieved ideally before a new measurement vector is available (e.g. in 0.1 s).

The O-ID determination of the model parameters is done using the Maximum Likelihood parameter estimation method. The Maximum Likelihood output error method is widely used for system identification. It is described in ref. [4].

Verification of the O-ID Method

For verification, the algorithm is tested by simulation. As no real measured LIDAR data are available, the LoS measurements are generated using a simple LIDAR sensor model (Figure 3). The assumed LIDAR is specified by:

- measurement distance 150 m ahead of the aircraft
- measurement angles: 80° horizontal (±40°), 20° vertical (±10°)
- measurement directions: 27 (9 horizontal, 3 vertical)
- 10Hz update rate; each measurement direction is updated 10 times a second
- accuracy 3% of measurement distance (= 4.5 m)
- measurement noise with a standard deviation σ = 0.5 m/s

The wake velocity field is generated with computational fluid dynamic methods (Large Eddy Simulation – LES). The wake velocities are generated for different wake ages of an Airbus A340 aircraft in a temperature stable (Brunt-Väisälä frequency N* = 0) but turbulent weather condition (dissipation rate of ε^* = 0.23).

13 measurement scenarios are evaluated with the O-ID algorithm. In all cases, the encounter aircraft is approaching the wake of a preceding aircraft with a constant speed of VTAS = 70 m/s without any rotational motion. The assumed LIDAR measurement distance is 150 m ahead of the encounter aircraft. Simulation variation parameters are:

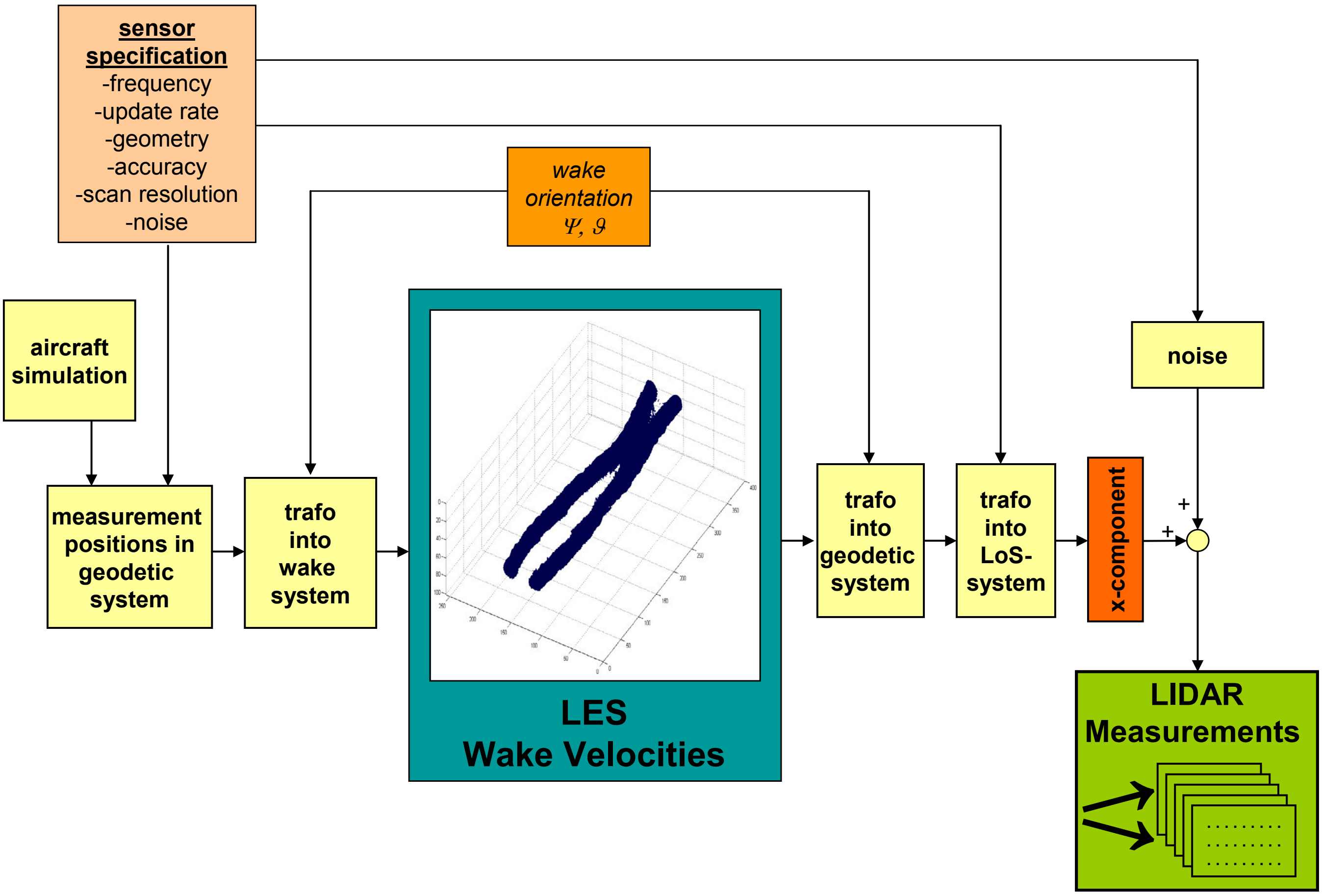

Figure 3: Simulation of LIDAR measurements using LES wake velocity fields

a) LES vortex age (16 s, 32 s, 48 s, 64 s, 80 s, 120 s, 136 s)
b) wake orientation relative to the flight path of the aircraft (lateral 10°, 30°, 50°)
c) vertical wake position offset
d) evaluation time window

Table 1 summarizes the identified parameters, their initial settings (init), the results achieved by the O-ID (id), and the reference values (ref). The LES reference values are determined by identification of the y/z-velocity distribution of the LES-fields with the analytical *Burnham-Hallock* model for each x-position separately and then averaging the determined values for all x-positions. This is done for wake strength Γ and lateral wake spacing *b'*.

Table 1: LES simulation scenarios and O-ID results, initial and reference values (nomenclature: b' lateral vortex spacing (equivalent to y_{le} and y_{ri}), Γ circulation, ψ wake orientation, Z_{le} altitude left vortex, Z_{ri} altitude right vortex; green cases: acceptable match, orange cases: unacceptable match)

case	wake age [s]	# LoS	evaluation time [s]	b' id/ ref / init [m]	Γ id / ref / init [m^2/s]	ψ id / ref / init [°]	z_{le} [m]	z_{ri} [m]
1	16	27	7	48/ 47/ 30	440/ 487/ 250	29.9/ 30/ 25	945	946
2	16	6	7	48/ 47/ 30	457/ 487/ 250	30.6/ 30/ 25	945	945
3	16	6	8	51/ 47/ 30	464/ 487/ 250	10.6/ 10/ 15	945	946

4	32	6	7	52/ 47/ 30	443/ 482/ 250	32.1/ 30/ 25	948	956
5	32	6	4	56/ 47/ 30	449/ 482/ 250	53.6/ 50/ 45	954	952
6	32	6	7	47/ 47/ 30	441/ 482/ 250	29.3/ 30/ 25	973	978
7	48	6	7	46/ 48/ 30	403/ 470/ 250	26.6/ 30/ 25	950	955
8	64	6	7	58/ 48/ 30	373/ 460/ 250	30.0/ 30/ 25	969	955
9	64	6	8	45/ 48/ 30	416/ 460/ 250	9.5/ 10/ 15	949	950
10	80	6	7	61/ 49/ 30	403/ 448/ 250	32.9/ 30/ 25	956	957
11	120	6	7	21 / --- / 30	35/ --- / 250	20.6/ 30/ 25	932	934
12	120	6	8	61/ --- / 30	107/ --- / 250	16.3/ 10/ 15	965	931
13	136	6	7	-80/ --- / 30	-398/ --- / 250	-331/ 30/ 25	970	----

In all test cases, the O-ID initialisation is done manually. Initial value for wake strength is always $\Gamma = 250$ m^2/s, lateral spacing initialisation is always $b' = 30$ m. The initial lateral wake orientation relative to the aircraft flight path is always set with an error $\Delta = 5°$. The position error is set to 5….20 m.

A LES wake plot example (iso-surface plot 6 m/s) is presented in Figure 4 (wake age 80 s). Wake deformation can be seen clearly. As a quite turbulent case is simulated, only at the early wake age of 16 s there is almost no deformation. A first wake linking between left and right vortices is seen at an age of t = 80 s. For 120 s and 136 s wake age heavy linking occurs.

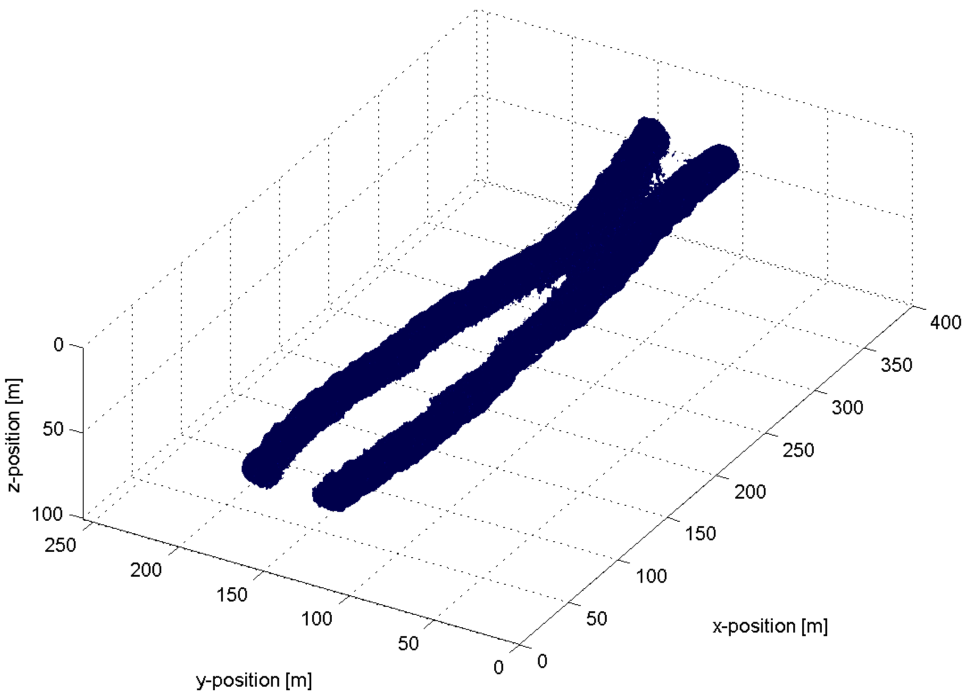

Figure 4: LES A340 wake simulation, wake age 80 s, dissipation rate e* = 0.23 (turb.), N* = 0

Wake age 16 s (cases 1, 2, 3)

A good fit is achieved for all measurements. The identification results are very near to the reference values, only the vortex strength is about 10% smaller than the reference. In case 1 the O-ID algorithm uses the information of all 27 LoS measurement directions. Using only six LoS-directions (the left ones as the wake is approaching from the left), i.e. cases 2 and 3, there is a quite similar result: slightly different orientation (0.7°) and a wake strength error of 6%. A reduction of the evaluation time to a small 4 s window gives the (not shown) identical result. However, using an evaluation time window reduced to 3 s the O-ID does not converge, as no measurement information from the second vortex is available.

For small encounter angle scenarios (case 3) the information needed for the O-ID is mostly in the outer measurement directions (horizontal -40° and -30° directions). Furthermore, the necessary evaluation time window is increasing for small encounter angle scenarios.

Wake age 32 s (cases 4, 5, 6)

The O-ID result of case 4 achieves a good fit for the left 6 weighted LoS-directions. However, the other (only simulated) LoS velocities in vertical 0° direction have discrepancies. This is an outcome of the approximation of a deformed wake with a straight wake model. Case 5 is a scenario with a high lateral encounter angle of $\Delta\Psi = 50°$. Now there is only a very short time period between left and right vortex measurements and, applying a 10 Hz measurement rate, there is only little information about the wake in the measurement. Only the LoS measurement directions 30° and 40° (left) capture both single vortices, which is necessary for O-ID application. In all other LoS measurements at least one vortex is missing. So, for scenarios with great encounter angles, a higher measurement rate is necessary.

Case 6 is a vertical offset scenario. The achieved result is very similar to the no vertical offset scenario of case 4.

Wake age 48 s (case 7)

There is a similar ID result as for the 32 s wake age case, and the wake can be approximated.

Wake age 64 s (cases 8, 9)

Wake deformation is ongoing, but the O-ID wake approximation is still acceptable for both a 30° and a 10° encounter scenario. Some discrepancies are now even in the weighted LoS measurements (case 9), and the identified values show some differences to the reference values, e.g. the wake strength error is 19% in case 8.

Wake age 80 s (case 10)

Figure 5 shows – as an example – the O-ID result using the LES wake field of 80 s wake age (Figure 4). Wake deformation is considerable, and the O-ID wake approximation is getting more inaccurate. The position inaccuracies grow to several meters, however, the wake strength determination is still acceptable for a 30° encounter.

Wake age 120 s (cases 11, 12)

Wake deformation is now too strong to get a reasonable result from the O-ID. Position and orientation results are inaccurate, and the LoS fits show clear discrepancies.

Wake age 136 s (case 13) Heavy wake linking is on-going, and no approximation via O-ID is possible.

Limitations of the O-ID Method

Some general tendencies and constraints that were observed during the O-ID tests are listed in the following:

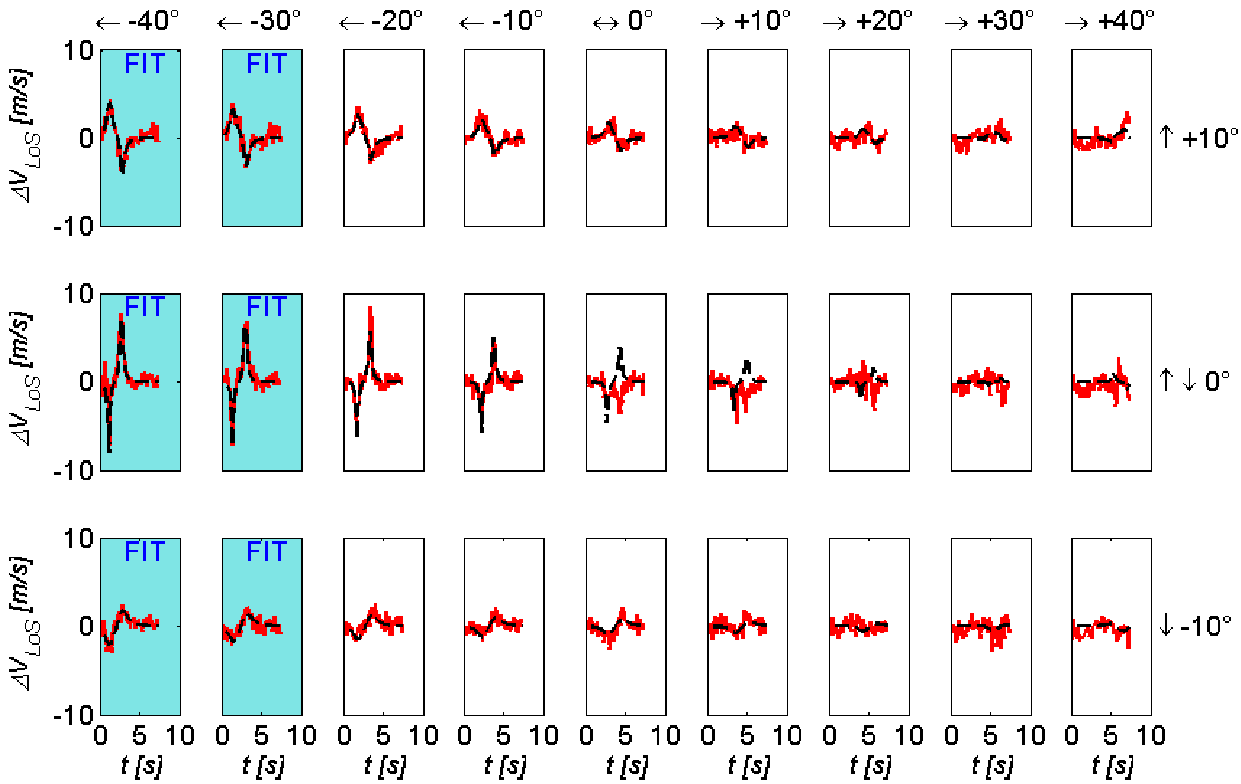

Figure 5: O-ID approximation of LoS measurements (case 10): 6 weighted directions, LES age 80 s, lateral encounter angle 30°; —— 'measured'; —— O-ID reconstruction

- the approximation of a deformed wake using a straight, simple analytical wake model is only appropriate for a limited degree of wake deformation
- the applied measurement rate of 10 Hz is sufficient for encounter scenarios with encounter angles up to approx. 40°…50° (for aircraft flying at typical approach speed), to cover higher encounter angles or wake encounter scenarios in cruise flight a higher measurement rate would be necessary
- there seems to be a tendency that the wake strength is determined a little smaller than it really is
- the accuracy of the wake predictor for delivering the O-ID parameter starting values is assessed as a critical parameter, especially the prediction of the wake position (example: a position estimate within 20 m at 100 s wake age would require a wind speed information accuracy better than 0.2 m/s)
- if the wake generator would fly a turn, a straight analytical model would provide inaccurate results
- for O-ID convergence, it is necessary that the measurement information of both vortices is contained in the data

Autonomous Wake-Vortex Approximator

A second processing concept of line-of-sight (LoS) measurements is the Autonomous Wake-Vortex Approximator (AWA). Similar to the O-ID concept, the AWA is capable to reconstruct the vortex strength, its position and orientation from LIDAR LoS-measurements. However, the AWA is a *stand-alone method* which uses as input only LIDAR LoS measurements.

The method is described in detail and applied to simulated vortex flow fields in reference [6]. In this context, the overall AWA structure is presented, showing the four main modules (Figure 6):

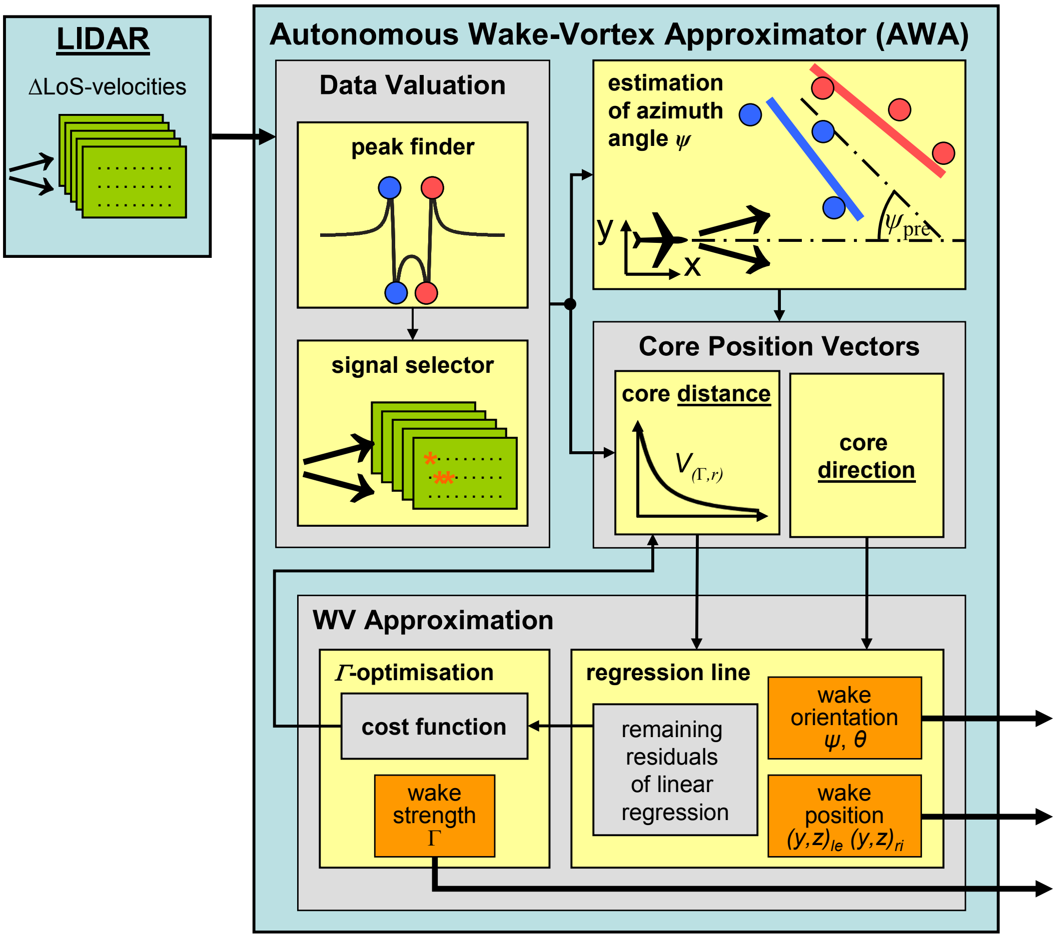

Figure 6: Structure of the Autonomous Wake-Vortex Approximator (AWA)

1. data valuation with peak finding and signal selection
2. wake azimuth angle estimation
3. core position vectors computation
4. wake vortex (WV) approximation – reconstruction of wake orientation and position (ψ, θ, $(y,z)_{le}$, $(y,z)_{ri}$) und estimation of wake strength (Γ)

Applied to LES wakes [6], the method gives appropriate results up to slightly curved vortices. Similar to the O-ID method, the AWA implies two straight vortices and tries to approximate the wake trajectory with a linear regression curve. Heavily curved wakes or a wake curvature originated by a turning aircraft may cause approximation problems. However, different altitudes of left and right vortices can be covered by the method.

The method is limited to wakes in the horizontal plane or to very limited elevation angles. A wake elevation, evident during take-off and approach/landing, reduces the accuracy of the method.

The method also implies that there are two measurement peaks in the selected directions from the left and the right vortex, respectively. The selected measurement directions (step 1) should cover both vortices in the measurement window and the scenarios are limited to much higher lateral encounter angles than vertical ones.

The core position vector computation (step 3) uses the pre-estimated azimuth from step 2. A more exact reconstruction of the azimuth as well as the elevation is then done iteratively. An orientation correction of the core direction vectors is not done so far, only the length of these vectors is recalculated. So, an improvement could be to recalculate also the wake elevation and the azimuth in every iteration step. However, the additional parameters would affect adversely the speed of convergence.

The computation of the core position vectors (step 3) is done with the simple potential wake model. This model is incorrect within the vortex core. A better model would cover also the region within the core, e.g. the *Burnham-Hallock* velocity distribution model. However, those models have more parameters (e.g. the core radius), and, more disadvantageously, two solutions for the length r of the core position vectors: outside of the core radius and within the core. For this, a solution would be necessary to improve the method's accuracy.

Resumee and Outlook

Generally, the O-ID method is capable to reconstruct the vortex strength, wake position and orientation from LIDAR line-of-sight measurements. The outcome of the presented approach is an approximation of the wake flow field velocities by an analytical wake model. Applying the identified wake model, the flow field can be reconstructed in any spatial resolution.

The O-ID concept was verified by performing multiple scenario tests with simulated LIDAR measurements and LES wake velocity fields of an A340 aircraft. The principle functioning could be shown, and good results were achieved for wakes with a limited degree of wake deformation. For stronger wake deformation and wake linking, the results are more inaccurate or the method does not converge at all.

As the method works iteratively, appropriate starting values for the model parameters are essential. The starting values can be provided by a model based wake predictor using information from other aircraft in the area of interest. Since both the wake predictor as well as the information from other aircraft may contain inaccuracies, only rough first estimates of the starting values are available. A preliminary study showed different parameter sensibilities for O-ID convergence: the starting values for wake strength and lateral spacing are quite robust, in all cases they were initialized to $\Gamma = 250$ m^2/s and b' = 25 m, and convergence was achieved. The initial values for wake orientation and position of both single vortices are more critical: 5° in orientation and 20 m in position are considered to be the maximum tolerable errors. However, applying starting values within these limits, convergence is often, but not always achieved.

To cover also curved vortices, the analytical model using two straight vortices could be extended by a superimposed oscillation, requiring a minimum of three additional parameters (amplitude, frequency, phase). Then, 10 parameters would have to be identified.

Rotational aircraft motion was not yet included in the test scenarios and in the O-ID algorithms.

A constraint of the O-ID is the need for appropriate starting values for the model parameters. They may be available from an onboard wake predictor, whose inputs are from other aircraft via ADS-B and own measurements (wind). A better solution would be an autonomous method based on measurements of the own aircraft only. One solution for this could be the autonomous wake-vortex approximator, AWA.

References

[1] Hahn, K.-U.; Fischenberg, D.; Niedermeier, D.; Horn, C. *Wake Encounter Flight Control Assistance Based on Forward-Looking Measurement Processing* AIAA Guidance, Navigation and Control Conference, Toronto, Canada (2010)

[2] Fischenberg, D. *Determination of Wake Vortex Characteristics from Flight Test Data (in German: Bestimmung der Wirbelschleppencharakteristik aus Flugmessdaten)* German Aerospace Congress, Stuttgart, 23.-26. Sept. 2002

[3] Burnham, D. C.; Hallock, J. N. *Chicago Monoacoustic Vortex Sensing System* Vol. 4, Wake Vortex Decay, Springfield, VA, National Information Service (1982)

[4] Jategaonkar, R. V. *Flight Vehicle System Identification: A Time Domain Methodology* Progress in Astronautics and Aeronautics Series, Vol. 216, Published by AIAA, ISBN-10: 1-56347-836-6 (2006)

[5] Fischenberg, D. *Verfahren zur Bestimmung der Stärke und Position von Wirbelschleppen aus line-of-sight (LOS)-Messungen* DLR IB 111-2010/04 (2010), patent pending

[6] Wolkensinger, C. *Autonomous Wake–Vortex Approximator (AWA), Autonomes Verfahren zur Erkennung von Wirbelschleppen aus line-of-sight (LOS)-Messdaten eines vorausschauenden Sensors* DLR IB 111-2011/14 (2011), patent pending

[7] Wolkensinger, C. *Vergleich messtechnischer Konzepte zur bordgestützten Ermittlung atmosphärischer Störphänomene* DLR IB 111-2010/35 (2010)

4.4 Wake Vortex Encounter Modelling and Validation by Flight Tests

Dietrich Fischenberg
Institute of Flight Systems

A method is presented for assessing the accuracy of aerodynamic wake encounter models (also named “aerodynamic interaction models”). The method uses real world data from in-situ measurements to produce the best possible fit of a given model structure. This process requires: (a) suitable encounter flight test data, (b) a high precision flight path reconstruction, (c) suitable parameters of an analytical vortex model, and (d) a high quality basic aerodynamic model. The vortex model parameters are identified in an a-priori step from the same wake encounter flight test data used for the subsequent validation of the aerodynamic interaction model. The accuracy assessment is done by analysing the errors between model outputs and the corresponding flight test data. The paper reflects the used incremental Strip Model structure and recommends appropriate a-priori data. Simulation results are analysed, and strip model extensions are implemented which imply a notable model quality improvement.

Wake Vortex Encounter Flight Tests

Precise flight test data are essential for wake vortex encounter model validation. As explained in detail in the next chapter, the validation procedure is done in two parts: (a) wake determination including a flight path reconstruction (FPR) and (b) the validation step, where the determined wake model parameters from (a) are used as an input.

The wake characteristics are identified from the measured test data. For this it is essential that the wake encountering aircraft gathers as much wake information as possible. This is ensured best for lateral wake crossing, where the pilot adjusts the flight path such that both vortices are hit near their cores. As there are strong up- and downwinds in a wake, the encounter aircraft should not stay too long in the wake field, but on the other hand the period of data collection during the passage of the vortex flow should not be too short because of limited measurement information. A good compromise is a 2-4 sec duration which gives 200-400 samples of flow measurements at a 100 Hz rate. That is sufficient to cover the high velocity gradients near the vortex core and to identify the vortex core radius. The lateral encounter angle should be within 5°-20°.

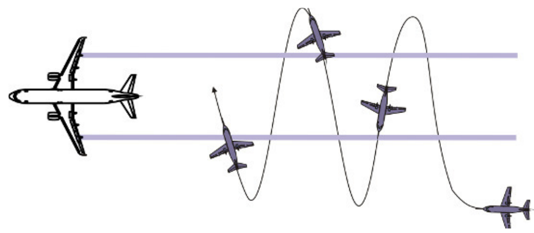

Figure 1. Flight test scenario for wake determination and encounter model validation; in practice the lateral encounter angles are considerably smaller (25° maximum)

Figure 1 shows a typical test scenario. Wake visualization is important for appropriate vortex hits and can be done (a) with a smoke generator mounted on the wing, (b) by oil injection into the engine exhaust, or, for flight tests in cruising altitude, (c) simply by the generator contrails.

Flow Sensor Measurements

For wake identification, a high measurement quality of the available flow probe signals on the wake encountering aircraft is fundamental for the overall evaluation procedure. As a minimum requirement, one AoA-sensor and one AoS-sensor must be installed on the encounter aircraft for wake identification. The more flow sensors are available at different positions on the encounter aircraft, the better the information about the encountered wake will be [14, 16]. The measurement signals should be calibrated carefully and ideally be available at a sampling rate > 50 Hz. The calibration can be done with the FPR method and suitable flight test data, as documented in [15].

Measurements with Several 5-Hole-Probes on Booms

The ideal case: the test aircraft for in-situ wake vortex measurements is equipped with several 5-hole-probes mounted on booms. The booms ensure minimum influence of the fuselage and wing of the encountering aircraft on the measurements. The 5-hole-probes also allow high frequency measurements that are less influenced by dynamic effects as from vane measurements. An aircraft with these features is the Do 128 (MTOW = 4.3 t; ICAO weight class LIGHT) of the Technical University Braunschweig: wind velocities are measured in all 3 axes (corresponds to equivalent wind angles of attack and sideslip) with 100 Hz at four distinct positions: a/c nose, left and right outer wing, and vertical tail [18].

Typical Do 128 measurements from an encounter with the wake of a MEDIUM class aircraft (MTOW = 21 t) are shown in Figure 2. From those data, vortex strength, core radius, left and right vortex positions and the wake orientation can be determined (see below).

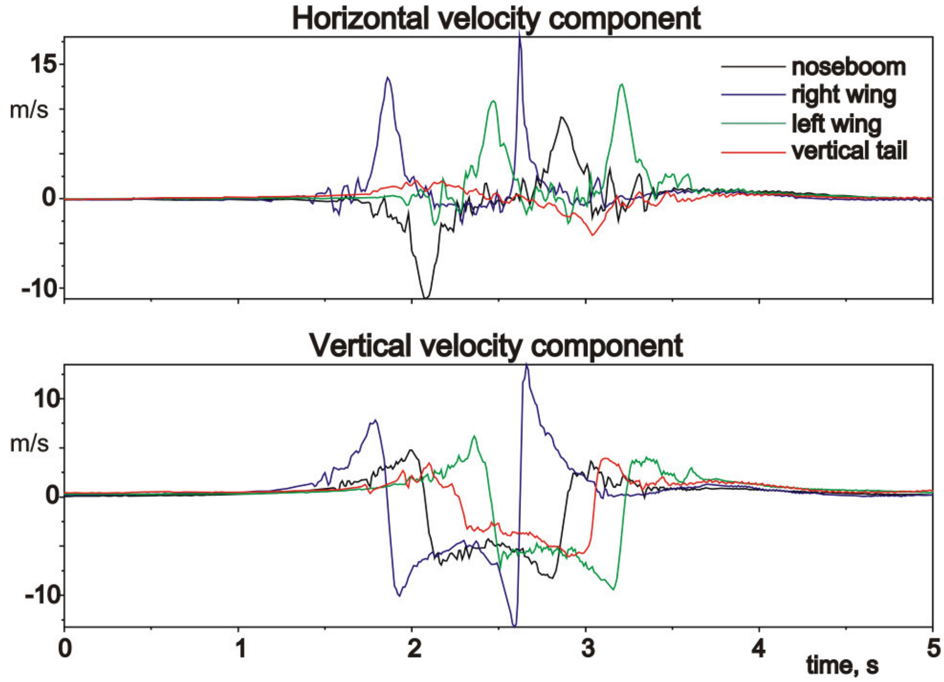

Figure 2. High quality 100 Hz flow probe measurements of the Do 128 aircraft during a lateral wake encounter. Horizontal and vertical wake velocities at the four measurement positions.

Measurements with Fuselage Vanes

Alternatively, aircraft equipped with one or two fuselage-mounted angle of attack vanes and angle of sideslip sensor (besides inertial measurements) can also provide valuable wake encounter flight test data. Despite fuselage and wing influences on the measurements, it is possible to determine the overall wake characteristics like wake strength and vortex positions from those data. An example will be shown below.

Calibration

Flow sensors have to be calibrated carefully. This can be done using suitable flight test data in undisturbed air which are evaluated applying the FPR method [15]. Boom-mounted flow sensor calibration can be done using linear approximations. Fuselage-mounted vanes require more calibration effort, as they are influenced by the fuselage itself. In the linear region, a factor, a bias, and a luff/lee influence in the AoA measurement can be found and calibrated.

$$\alpha_1 = F_1\,\alpha_{1,i} + \Delta\alpha_1 + F_{\alpha\beta}\beta_i \;\; \text{(AoA left)}; \quad \alpha_2 = F_2\,\alpha_{2,i} + \Delta\alpha_2 - F_{\alpha\beta}\beta_i \;\; \text{(AoA right)}; \quad \beta = F_\beta\,\beta_i + \Delta\beta \;\; \text{(AoS)}$$

It has to be pointed out that for wake vortex measurements the flow at the fuselage vane positions suffers from unsteady und other effects like fuselage/wing interferences. Those effects are beyond the scope to be calibrated in a classical manner and have to be accepted when evaluating fuselage vane measured AoA/AoS.

Wake Identification

Wake strength and position have to be known for wake encounter simulation and validation. For validation with flight test data, the wake model parameters are derived in an a-priori step from measurements. This step consists of a flight path reconstruction in the wake axis system and the identification of the parameters of an analytical wake vortex model, see Figure 3 and [14, 16].

The inertial measurements (accelerations, rotational rates, Euler angles) of the encounter aircraft are used to reconstruct precisely the encounter aircraft flight path in the wake axis system. From this step, also the inertial flow angles α_i, β_i are obtained. They consider the aircraft's flow angles without any local flow. These inertial flow angles are reconstructed for all AoA/AoS measurement locations. The differences between these inertial local flow angles and the measured AoA/AoS during a lateral wake fly-through are clearly seen in Figure 4 (left). It is assumed that they are produced by the flow field of the encountered wake.

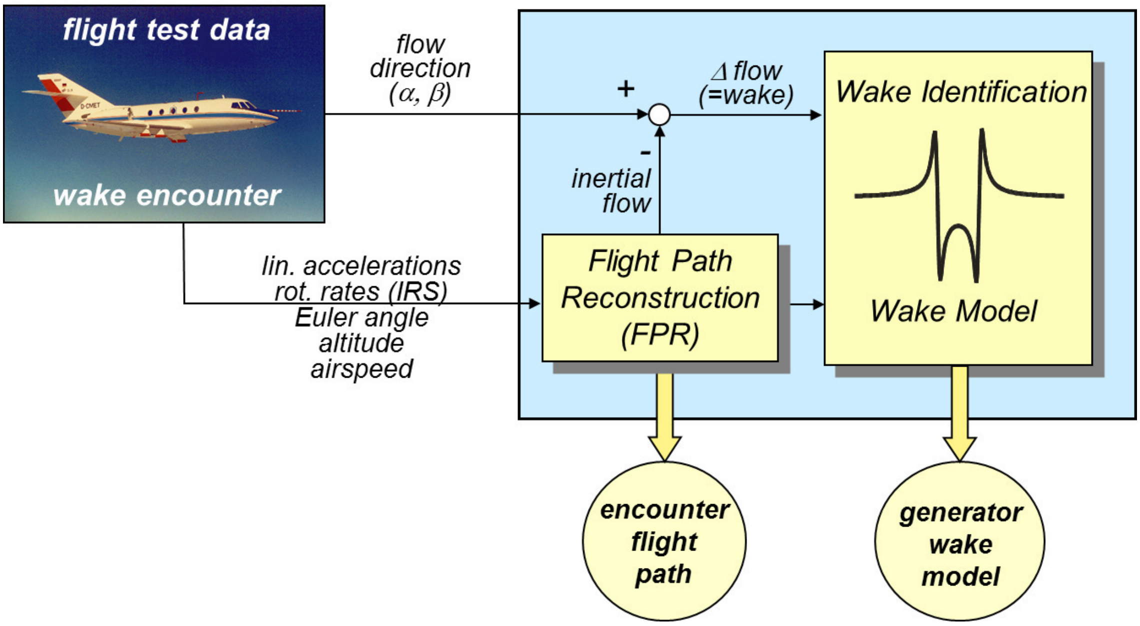

Figure 3. Principle of wake identification and flight path reconstruction

Using parameter identification methods [15], these differences are minimized by tuning the parameters of an analytical vortex model. The model outputs α_{wv}, β_{wv} are added to the reconstructed inertial flow angles α_i, β_i. In the present evaluation, the analytical Burnham-Hallock vortex model [4] is used for flow field description. Model parameters are vortex strength (circulation), position in the wake axis system, and wake orientation. The procedure as well as the parameter quality is discussed in detail in [14, 16]. The identification result is shown in Figure 4 (right).

Aircraft Basic Aerodynamic Model

For wake encounter simulation, forces and moments are computed in two independent submodels: (a) the classical basic aerodynamic model, and (b) the wake encounter model (also named aerodynamic interaction model, AIM), which describes increments of forces and moments in a spatial wind field.

For the validation of the forces and moments generated by the wake, it must be ensured that model deficiencies are not originating from the basic aero model. A high quality basic model is needed. This quality can only be achieved by tuning the model with parameter identification techniques using suitable flight test data that are recorded far away from any wake influence. In the flight tests the aircraft's eigenmodes should be excited [15]: e.g. 3211 elevator inputs for short period excitation, elevator impulse for phugoid excitation, bank to bank manoeuvres (aileron inputs), rudder doublets (Dutch roll excitation). All manoeuvres should be repeated with different amplitudes. An operating point model is sufficient, which is derived for the same velocity/altitude/thrust setting envelope point as chosen for the wake encounter tests.

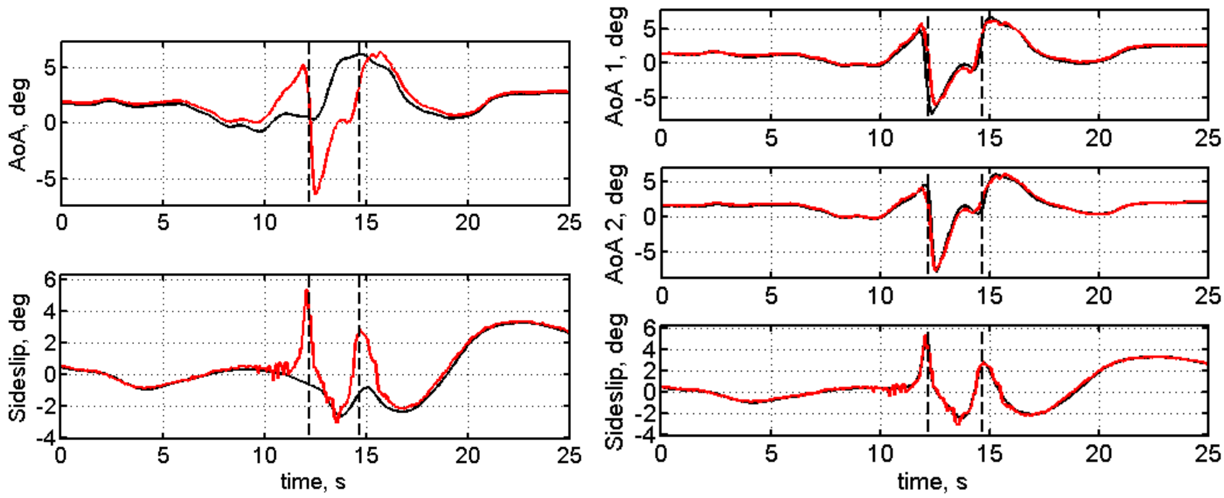

Figure 4. Lateral wake fly-through, fuselage vane equipped aircraft; left: reconstructed inertial AoA/sideslip (——), right: reconstructed inertial AoA/sideslip and local wake induced flow angles (——), flight test measured (——)

Wake Encounter Model (Strip Method)

A popular and easy to use encounter model is the strip model. It is based on lifting line theory and describes the additional aerodynamic forces and moments acting on an aircraft in a spatial wind field, e.g. a wake vortex. The lift generating surfaces of an aircraft (wing, horizontal and vertical tail) are divided into strips, Figure 5. Well proven numbers of strips in simulation are 16 (wing), 8 (horizontal tail), and 4 (vertical tail). At the 25% chord location of each strip the additional angles of attack (wing, horizontal tail) and angles of sideslip (vertical tail) due to the local wind/wake field are computed. Using a suitable lift gradient, additional lift is obtained for each strip. These local lift increments are weighted in span direction elliptically and then summed up. Additionally, the corresponding moments of all strips are computed and summed up. No drag effects are considered so far, so the present strip model describes wake effects in 5 degrees of freedom. More details are given in [9, 17].

The model is based on several a-priori data, which are depending on the aircraft's geometry and aerodynamics. The geometry of wing, horizontal and vertical tail, and the lever arms for moment computation are generally well known from 3-D drawings. The aerodynamic derivatives (lift gradients for wing, horizontal and vertical tail, downwash gradient) may be known, if not, they can be estimated. The Helmbold equation, which considers the aspect ratio (AR) influence on lift gradients, leads to good a-priori values for the lift curve slope [17].

$$C_{L\alpha} = C_{L\alpha\infty} \frac{AR}{2 + \sqrt{4 + AR^2}}$$

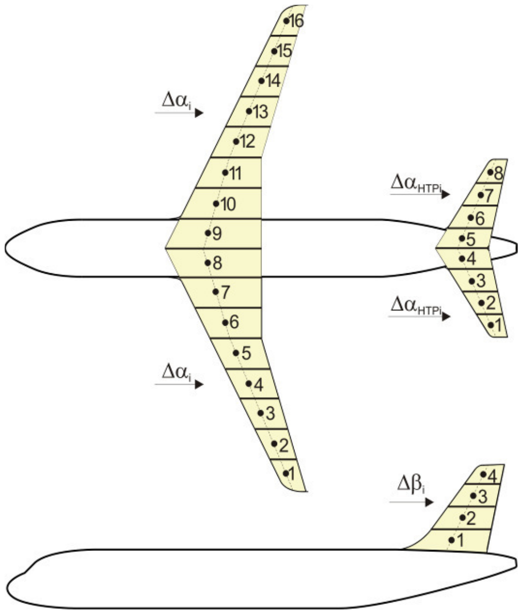

Figure 5. Strip model

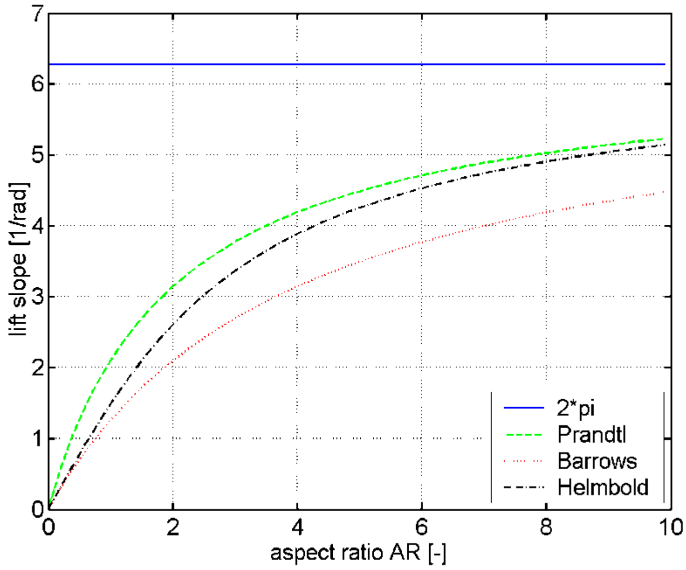

Figure 6. Different approximations for lift curve slope depending on aspect ratio AR

The Helmbold equation is an approximation for high aspect ratio wings as well as low aspect ratio tails and a compromise between the Prandtl and Barrows formulations, see Figure 6. The lift curve slope is also depending on wing sweep Λ. A simple approximation to account for this is given in [17].

Mach number dependency of the lift curve slope can be modeled acc. to Prandtl-Glauert:

$$C_{L\alpha} = C_{L\alpha,M=0} \frac{1}{\sqrt{1-M^2}}$$

Validation

The overall validation method is illustrated in Figure 7. The model computes the sums of forces and moments of (a) the basic aerodynamic model and (b) the aerodynamic interaction model, which provides Δ-forces and -moments due to wake influence. The simulation is driven by the flight test measured control inputs (elevator, aileron, rudder etc.). The model outputs are compared to the corresponding measured flight test data, typically linear and rotational accelerations, rotational rates, altitude, and velocity.

Besides a high quality basic aerodynamic model, the exact knowledge of the wake model parameters (strength and vortex positions) for each encounter should be known. As already described above, these model parameters are determined in an a-priori step, using flight test measurements of the encounter aircraft to reconstruct precisely its flight path and inertial flow angles α_i, β_i. Secondly, the aerodynamic interaction model should be driven with the reconstructed flight path and Euler angles, which are also the outcome of the above mentioned a-priori step. This “driven mode” stabilizes the wake encounter simulation and proved to be essential, as wake induced forces and moments are very sensitive to small flight path inaccuracies. The accuracy is assessed by computing the standard deviations of the errors between model outputs and the corresponding flight test data and the maximum errors. Each degree of freedom is considered separately.

A typical validation example from a lateral fly-through flight test with a Do 128 aircraft (about 4 t) into the wake of the VFW-614 aircraft (about 20 t) is shown in Figure 8, applying the method in Figure 7. Typical model outputs (red lines) in all 6 DoF are compared to the corresponding flight test data (black lines).

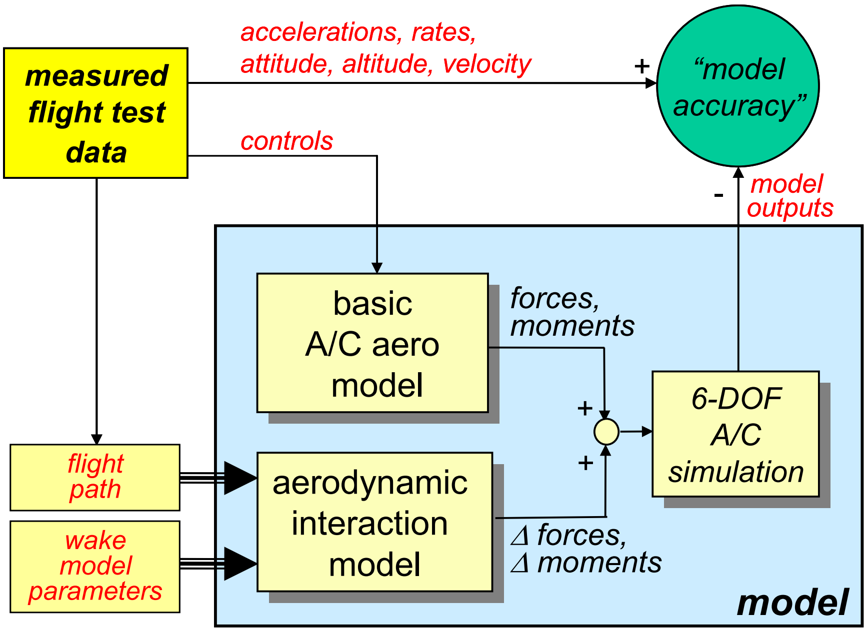

Figure 7. Method to validate wake encounter models from flight test data

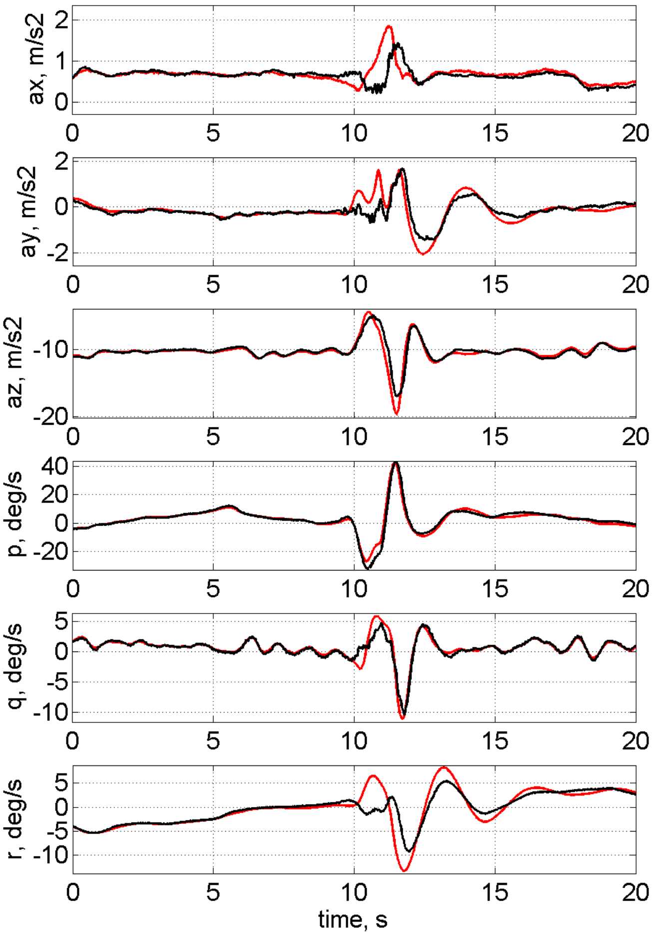

Figure 8. Do128 lateral wake fly-through: simulation model output (——) compared to flight test data (——)

Looking at each DoF separately and keeping in mind that this is a typical encounter out of more than 50 Do 128 encounters, the model quality can be assessed as follows: the rolling motion (roll rate p) and the vertical motion (vertical acceleration *az*) during a wake fly-through can be simulated in high quality. This can be considered to be an outstanding result for the strip model with its widely linear structure, applying the elaborate validation procedure including sensor calibration and wake identification. Both degrees of freedom (*p, az*) are the most important inputs into todays wake hazard assessment tools. The pitching motion (pitch rate *q*) is also simulated in good quality, despite some minor deficiencies at the beginning of the wake encounter. The lateral motion (acceleration *ay*) has some minor, but tolerable discrepancies. The longitudinal motion (acceleration *ax*) has discrepancies as no drag effects are modelled. However, this degree of freedom is considered to be not very important for a wake encounter.

However, the simulation quality in the yawing motion (yaw rate *r*) is rated more critical: the initial model response is opposite to what the flight test shows. This is a typical result found in many Do 128 encounter validations. If such a model lacking a correct yaw response is used for pilot training in simulators, it could have a fatal training effect.

Strip Model Extensions

Some efforts were undertaken to further improve the model quality, with special emphasis on the yawing motion. In many validation cases, a correlation was found between the model faults in the longitudinal axis and the yawing motion. Obviously, drag effects have considerable impact on the yawing degree of freedom.

So, the model was extended with drag effects. Drag depends on angle of attack in a nonlinear manner. Nonlinearities cannot be implemented in the strip model independent of the basic aero model. However, the fundamental idea of the strip model is this independency. To keep this, a linear formulation with one drag derivative, applied to each single strip, was used to consider wing and tail drag. Applying corresponding lever arms, the drag increments were also added to the yawing moment.

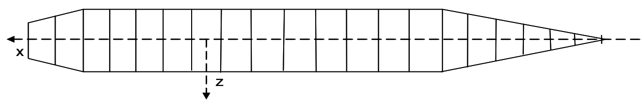

Figure 9. Strip model fuselage effect modeling

Moreover, the strip model does not consider any fuselage effects. An empirical model was implemented to account for this. The fuselage is divided typically into 20 strips (Figure 9), computing a wake induced local sideslip angle at each strip. Using a suitable fuselage strip derivative, the summation of the strip increments gives a lateral fuselage force, and, considering the corresponding lever arms, a fuselage yawing moment.

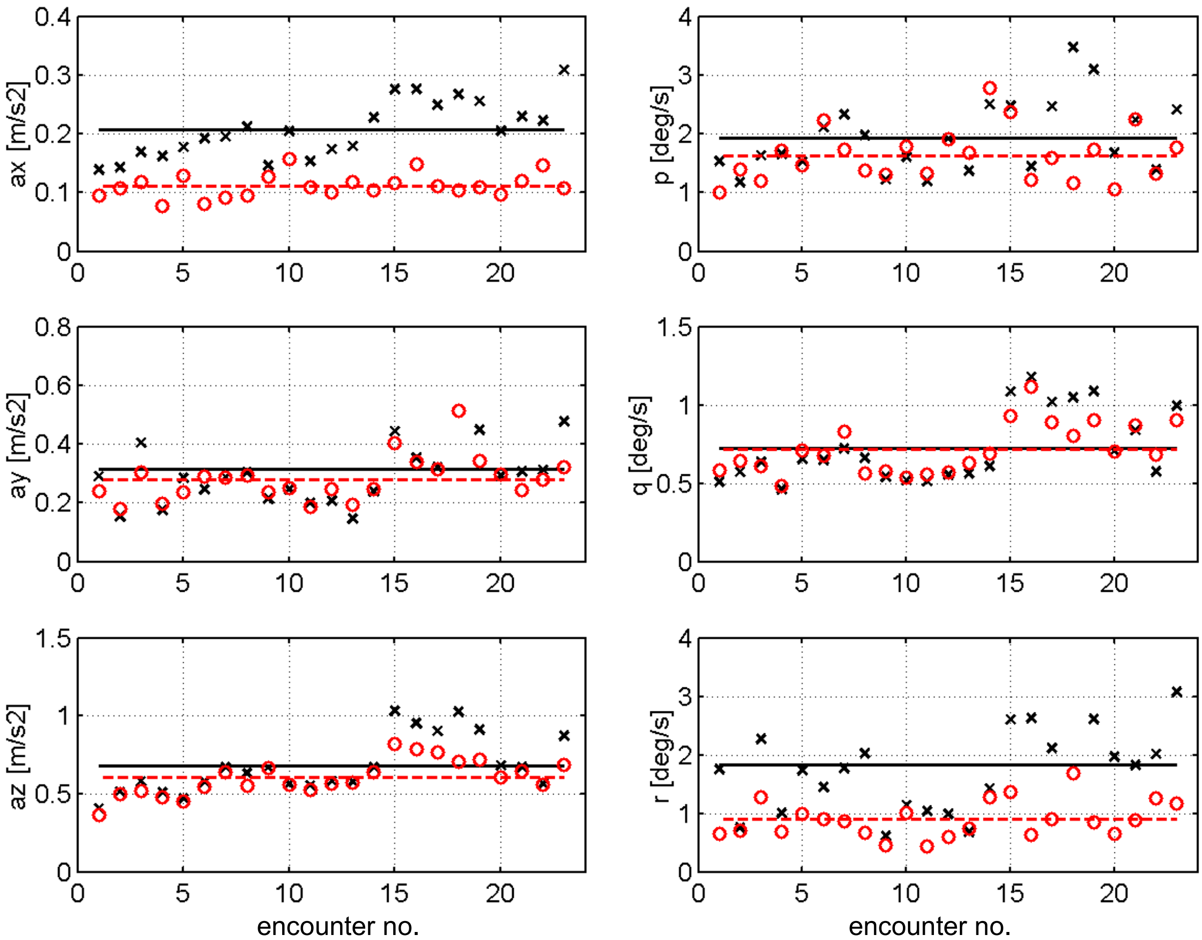

Figure 10. Model improvements for 23 wake encounter simulations: standard deviations of the errors between model outputs and the corresponding flight test data; without (x) and with (o) wing and fuselage drag effects; the lines give the mean error standard deviation of all 23 encounters

The determination of the two additional parameters, a wing drag derivative and a fuselage derivative, was done using the total validation procedure (Figure 7) in an optimization mode to minimize the discrepancies between model output and flight test data. This identification process was performed using 23 high quality encounters of the Do 128 aircraft into the VFW-614 ATTAS wake. The result: both derivatives were identified to a value of about 0.8, and a considerable model improvement concerning the mean error standard deviations can be stated: about 51% in the yaw and 48% in the longitudinal axis for all 23 encounters. Through coupling effects, improvements also in the roll axis (16%), in the lateral axis (10%), and the vertical axis (11%) are achieved. Figure 10 summarizes the results for all evaluated wake encounters.

Figure 11 shows the Figure 8 example, now applying the described model extensions. Despite some discrepancies in the lateral motion, a considerable improvement in the longitudinal axis (ax) and the yawing motion (r) is seen. The initial opposite model reaction in the yawing motion is now largely eliminated. However, one constraint is evident: no general formulation was found for the semi-empirical drag derivatives. Suitable values can be determined from flight test data applying the method described in this paper. If those flight test data are not available, the value of 0.8 may be taken in an empirical manner, but the validity of this has still to be proven for other aircraft.

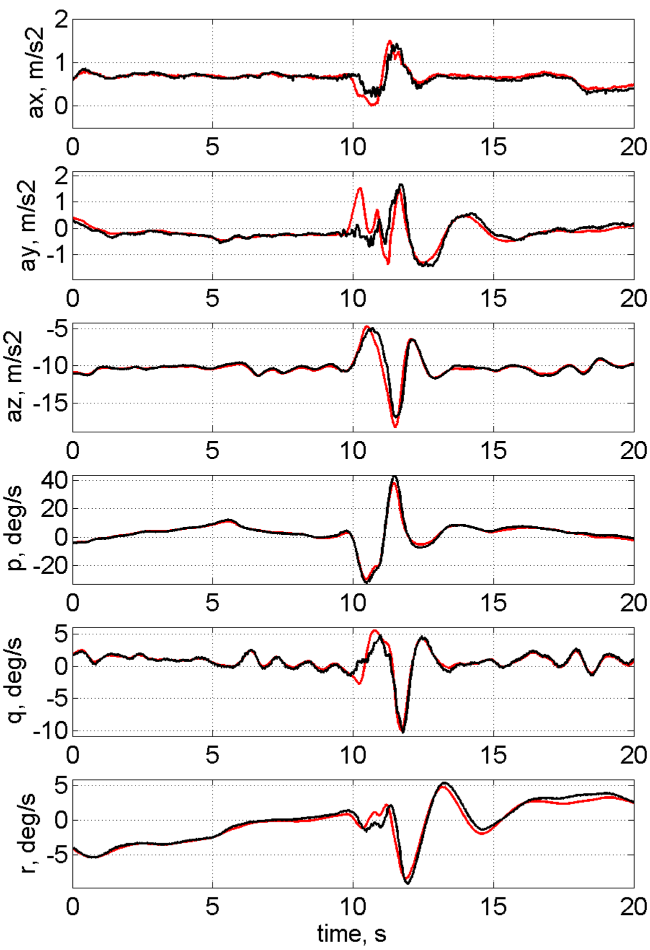

Figure 11. Do128 lateral wake fly-through: simulation output with wing and fuselage (——) compared to flight test data (——)

Resumee and Outlook

A method was presented to analyse the quality of an aerodynamic interaction model for wake encounter simulation by comparing the model outputs to corresponding wake encounter flight test data. The method consists of an elaborate procedure which requires several inputs: (a) suitable encounter flight test data, (b) a high precision flight path reconstruction, (c) suitable parameters of an analytical vortex model (e.g. Burnham-Hallock), and (d) a high quality basic aerodynamic model. Having all these data available, the encounter model quality can be assessed and analysed. The model used in the present case study is the strip model, which is based on lifting line theory. It describes the forces and moments acting on an aircraft in a wake as increments in addition to the basic aerodynamics in five degrees of freedom (drag effects are neglected).

Analysing 23 wake encounters, it could be shown that the strip model is capable of reproducing the most important inputs into wake hazard assessment tools, the vertical and roll degrees of freedom, in high quality. This is an excellent result for the widely linear model structure, which is achieved by applying the elaborate validation procedure including sensor calibration and wake identification. The pitching motion is represented also with sufficient quality. However, the quality of the yawing motion is rated more unfavourable: in many encounters the model response is found opposite to what the flight test shows.

Analysing the yaw degree of freedom, a clear correlation between longitudinal model deficiencies (drag neglected) and the yawing motion was found. A simple model extension for drag effects was derived, keeping the idea untouched, that the strip model should have an incremental structure, independent from the basic aero model. Moreover, the strip model was extended for fuselage effects. Doing the validation step again, a considerable model improvement regarding the mean error standard deviations was achieved for all 23 encounters: about 50% in the yaw and in the longitudinal axis, and also further improvements in roll (16%), the lateral axis (10%), and in the vertical axis (11%) were achieved.

The currently reached simulation quality is considered to be close to the maximum of what is achievable using a linear strip model structure which can be treated independently from the aircraft's basic aero model. However, the validity of the presented model and its extensions to account for drag and fuselage effects should be validated for other aircraft configurations.

References

[1] International Civil Aviation Organization (ICAO) *Procedures for Air Navigation Services - Air Traffic Management*, Doc 4444-RAC/501, 14th Edition (2001)

[2] Hahn, K.-U. *Coping with Wake Vortex* International Congress of Aeronautical Sciences, Toronto (Canada), 8-13 September 2002, ICAS, 23rd International Congress Proceedings (2002)

[3] Hahn, K.-U., Schwarz, C. *Safe Limits for Wake Vortex Penetration* AIAA Guidance, Navigation and Control Conference and Exhibit, 20-23 August 2007, Hilton Head, South Carolina, (2007)

[4] Burnham, D. C., Hallock, J. N. Chicago *Monoacoustic Vortex Sensing System* Vol. 4, Wake Vortex Decay, Springfield, VA, National Information Service (1982)

[5] Holzäpfel, F., Robins, R. E. *Probabilistic Two-Phase Aircraft Wake Vortex Model: Application and Assessment* Journal of Aircraft, Vol. 41, No. 5, 2004

[6] Harris, M., Young, I., Köpp, F., Dolfi, A., Cariou, J. *Wake Vortex Detection and Monitoring* Aerospace Science and Technology 6 2002 325-331 (2002)

[7] Rahm, S., Smalikho, I. *Aircraft Wake Vortex Measurement with Airborne Coherent Doppler Lidar* Journal of Aircraft Vol. 45. No 4, July-August 2008

[8] de Bruin, A. S-WAKE *Assessment of Wake Vortex Safety – Publishable Summary Report* NLR-TP-2003-243 (2003)

[9] Fischenberg, D. *S-WAKE Results of Flight Test Data Analysis* DLR internal report IB 111-2002/11 & SWAKE-TN-222-1 (2002)

[10] Reinke, A., Fischenberg, D. *Validation of Aerodynamic Models for Wake Encounter Response with Flight Test Data Analysis* DLR internal report IB 111-2003/14 & SWAKE-TN-222-2 (2002)

[11] Nagel, P., Düßmann, R. *Simulation and Flight Test of Wake Encounters with Eurofighter Typhoon (in German: Simulation und Flugtest von Wirbelschleppeneinflügen bei Eurofighter Typhoon)* German Aerospace Congress, Aachen, September 2009

[12] Lelaie, C., Reinke, A. *Airbus Wake Vortex Flight Test Campaigns and General Conclusions* WakeNet3-Europe Workshop on Wake Turbulence Safety in Future Aircraft Operations, Paris Januar 2009

[13] Lelaie, C. *A new Way to Define Wake Separations* Global Wake Conference, Bruxelles Nov. 2009

[14] Fischenberg, D. *Determination of Wake Vortex Characteristics from Flight Test Data (in German: Bestimmung der Wirbelschleppencharakteristik aus Flugmessdaten)* German Aerospace Congress, Stuttgart, 23.-26. Sept. 2002

[15] Jategaonkar, R. V. *Flight Vehicle System Identification: A Time Domain Methodology* Progress in Astronautics and Aeronautics Series, Vol. 216, Pub. by AIAA, ISBN-10: 1-56347-836-6 (2006)

[16] Jategaonkar, R., Fischenberg, D., von Gruenhagen, W. *Aerodynamic Modeling and System Identification from Flight Data – Recent Applications at DLR* Journal of Aircraft Vol. 41, No. 4, July-August 2004

[17] McCormick, B. *Aerodynamics, Aeronautics and Flight Mechanics* John Wiley & Sons, Inc. (1995)

[18] Cremer, M. *All Integrated Nose Boom for Wind and Turbulence Measurement* 30th Annual Symposium, Society of Flight Test Engineers, St. Louis, USA (1999)

[19] Fischenberg, D. *A Method to Validate Wake Vortex Encounter Models from Flight Test Data* 27th International Congress of the Aeronautical Sciences (ICAS), Nizza, France (2010)

4.5 Design and Flight Testing of Feedback Control Laws

Gertjan Looye, Thomas Lombaerts, Thiemo Kier
Institute of Robotics and Mechatronics

This Section gives an overview of RMC-SR activities in feedback flight control design and flight testing within the project Wetter & Fliegen. All results have been, or are about to be, published at AIAA and IFASD conferences. Main focus has been handling of severe atmospheric disturbances in the design of flight control systems, both for manual as well as automatic flight. The work has concentrated on handling disturbances like wind shears, turbulence, and wake vortices, just by means of feedback control, without prior knowledge of upcoming events. The core problem hereby is to fulfil primary functionalities, like aircraft stabilization and tracking (e.g. speed and flight path, or manually commanded attitude) as far as aircraft performance allows, while keeping engine and actuator control activity at an acceptable level, especially avoiding control saturation. In the design of flight control laws, these challenges have been addressed in control law structure design, synthesis of signals used for feedback, and in tuning of control law parameters by means of multi-objective optimization. An integrated set of manual and automatic flight control law functions has been designed and successfully flight tested on DLR's ATTAS aircraft. For analysing flight loads aspects, a new modelling approach, especially applicable to considerably flexible airframes has been developed in parallel to the project. Its full integration in the flight control law design process will be pursued in planned follow-on activities.

Introduction

The aircraft flight control system has a major influence on how the aircraft responds to atmospheric disturbances. In fulfilling basic functions, like stability and command augmentation, automatic tracking of speed commands and flight path tracking, rejection of such disturbances is a major design goal. However, different types of disturbance need to be distinguished in and by design. For example, it does not make sense to try to compensate for higher frequency turbulence, since due to the high inertia of the aircraft and the limited power of its control system and engines, this will just result in unnecessary actuator activity, causing even more nuisance and –worse– wear. Lower frequency turbulence and wind shear must be addressed, since these may result in severe airspeed and altitude deviations. Rejection of disturbances like severe wind shears and wake vortices may go beyond the aircraft performance limits, easily driving controls to their limits. The latter in addition poses a risk of pilot-induced oscillations.

A complicating factor is that, unless sophisticated detection algorithms are available, the feedback control system initially is not able to distinguish between classes and severities of disturbances. For example, although a wind gradient is easily detected using the air data and inertial reference systems, in advance it is not possible to tell if this gradient is caused by a wind shear, or just a longitudinal gust encounter. The flight control system must thus be able to cope well with all types of disturbances, trade-offs have to be made between tracking accuracy and control and engine throttle activity, and means for handling control saturation must be incorporated.

In the frame of the project Wetter & Fliegen, an integrated manual and automatic flight control system has been developed and flight tested with special emphasis on these aspects. This article gives a brief overview of these activities, including references to published results at conferences and in journals. The overview is structured as follows. In the following paragraph, the over-all control law architecture and aspects of the design will be presented. Next, the flight tests will be briefly described. Finally, a brief overview of relevant flight loads aircraft modelling activities will be given.

Flight Control Law Architecture and Design

The over-all flight control law architecture is depicted in Figure 1.

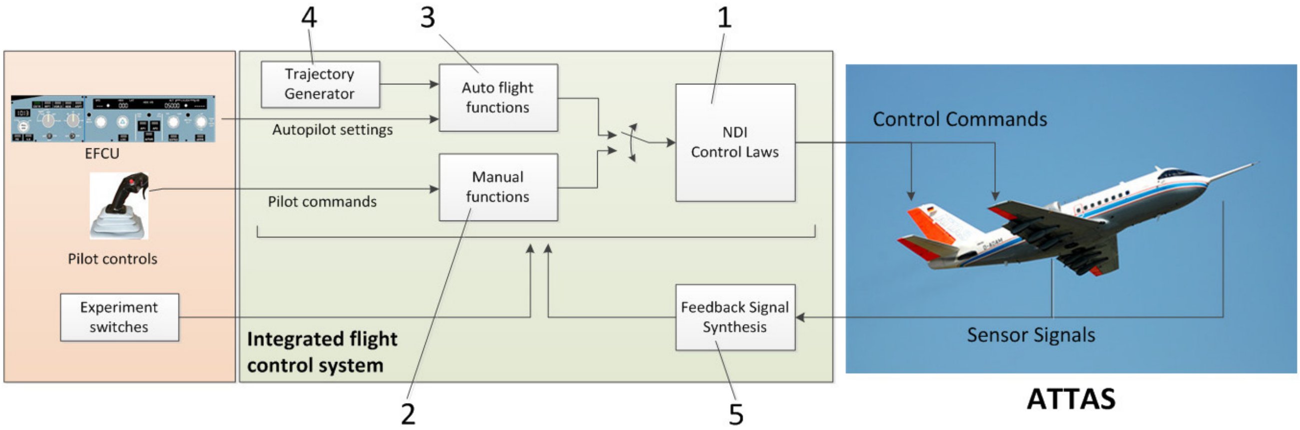

Figure 1. Over-all flight control law architecture

The principal elements are:

1. An inner loop core, based on inverse model equations (“Nonlinear Dynamic Inversion” method), tracking angular acceleration commands as provided by all control law functions in a decoupled way. Besides decoupling of angular acceleration responses, the beauty of this method is that commanded control deflections are automatically adapted as a function of the flight condition and other (approximately) known parameters, like centre of gravity location and aircraft mass. RMC-SR’s Modelica-based modelling environment allows these control algorithms to be generated fully automatically, see [7].

2. Rate-Command-Attitude-Hold (RCAH) manual control algorithms for manual control of the aircraft. This component follows pitch and roll attitude rate commands from the pilot, holding attitude as soon as the stick or column is released. Beyond certain limits, pilot commands are interpreted as attitude references. For example, as soon as the roll angle exceeds 27.5 degrees (left or right), the roll attitude becomes proportional to the stick input up to a maximum of 35 degrees (ATTAS fly-by-wire limit). Pedal inputs are interpreted as proportional side slip commands. Although pitch, roll and side slip responses are very well decoupled by design, artificial coupling is re-introduced for automatic turn compensation (increasing pitch in order to increase lift as required for a level turn) and a roll response proportional to pedal input, causing the course to be maintained when side slip is commanded. All these features can be switched on and off in flight on request. It is also possible to switch-off the attitude hold feature on pitch and roll commands. In case of wake vortex encounters with attitude hold, the flight control system would restore the original attitude of the aircraft as soon as the disturbance is gone. Without attitude hold, the aircraft’s attitude just stabilizes after driving the angular rate to zero. A comparison has been one of the piloted evaluation objectives in flight tests.

   The design of the manual control functions is discussed in detail in [1].

3. Auto flight algorithms for automatic tracking of speed, course, flight path angle and 3D trajectory references. These references are provided by a basic trajectory generator, to be discussed subsequently, or from the glare shield experimental flight control unit (EFCU) in the cockpit. During the project, two completely different design methodologies have been used: the Total Energy Control System (TECS) with Nonlinear Dynamic Inversion (NDI) inner loops, which has been applied by RMC-SR in various projects since the nineties, and multi-loop Nonlinear Dynamic Inversion using time scale separation between respectively attitude rate; angle of attack, roll and side slip; and flight path angle, course angle and speed command functions. The TECS approach al-

lows for easy arbitrary combination of tracking references and control resources in case engine limits are encountered or in case of partial manual control. The system includes practically all modes and protections as available in contemporary auto pilot systems, including automatic landing. The latter feature has been further improved in the frame of the DLR TOPGAL project. The NDI approach allows for easier envelope protection, handling of actuator limits, and can be automatically generated for each individual aircraft type. Part of the NDI system was developed in the frame of add-on defence resources (WTF).

The design of the auto flight control functions is discussed in detail in [2].

4. This function contains a basic trajectory generator, executing 3D flight test manoeuvres by appropriately tasking the autopilot functions. Examples are helical flight paths, symmetrical altitude profiles, and energy exchange test manoeuvres. In the frame of the project VAMP, this generator has been redesigned, allowing aircraft flight missions as described using DLR's XML-based Common Parametric Aircraft Configuration Schema (CPACS) to be interpreted and flown. The combination of auto flight functions, the redesigned trajectory generator, and a point mass simplification of the aircraft flight dynamics is used for mission simulations in aircraft (pre-) design [8].

   Trajectory generation for helical flight paths is discussed in detail in [3, 5].

5. This function, called "feedback signal synthesis" includes all sensor signal processing functionalities, like (complementary) filtering, state estimation, cross track and altitude deviations from the ILS path, etc. Tuning of complementary filters on air speed plays a decisive role in the trade-off between accurate tracking of speed commands and engine control activity under turbulent and wind shear conditions.

The over-all system allows smooth switching between manual and auto flight modes in any combination and at any time. The auto flight functions may be commanded from the glare shield control unit ("selected" operation) or from the trajectory generator ("managed" operation).

All flight control functions have been implemented in the Matlab/Simulink environment, allowing for easy transfer to ATTAS by means of automatic code generation. The tuning parameters have been optimized by means of multi-objective optimization using the RMC-SR MOPS (Multi-Objective Parameter Synthesis) environment. This has been done considering criteria like tracking performance, stability and stability margins, control activity, etc. The major strength of MOPS is that best trade-offs between scaled criteria can be achieved automatically. The design approach is detailed in [7]. In the frame of this project, criteria have been incorporated that are based on turbulence response simulation analyses; see the references [1], [2] for details.

Handling of Control Saturation Limits

As already stated in the introduction, handling of control saturation is one of the most important design aspects, especially in case of severe atmospheric disturbances. It has been addressed in three ways:

- By parameter tuning, trading off control activity and tracking accuracy of commanded references (manual or automatic). This mainly aims at avoiding rate saturation of actuated control surfaces and on achieving smooth engine responses. The latter has been emphasized in the design of ATTAS, after its temporary grounding due to engine problems.
- By integrator wind-up prevention. Stopping an integrator as soon as the control effector downstream saturates is not so much a measure, but rather a necessity, since delayed responses, instability and plain runaways may occur otherwise.
- By on-line choking all command paths upstream, such that actuator limits are never exceeded. This method naturally applies to methods like NDI and is called "Pseudo Control Hedging" (PCH). The great advantage of PCH is that it avoids full saturation, which would basically open the feedback loop, causing major problems in case of (nearly) unstable airframes. The design and im-

plementation of this feature in the flight control system was funded from additionally provided defence funds in 2010.

- Within the autopilot, speed or altitude control priority can be selected. Either of which is controlled via aircraft pitch when the engines reach their command limits.

Further details and references to its origins of PCH can be found in references [1] and [2].

Flight Testing of Control Laws

The Wetter und Fliegen project offered various opportunities to test the feedback control laws in flight. Add-on defence funding allowed for three additional test flights. Although ATTAS offers the option of in-flight simulation (simulation of an aircraft model and control laws, while making ATTAS replicate acceleration and attitude responses), it was strongly preferred to have the control laws directly control the aircraft. Focusing on atmospheric disturbances, a main challenge has therefore been to actually demonstrate control law performance in wind shear, turbulence, and wake vortices in flight. Obviously, such circumstances are not available on request. Therefore, the following approach was followed:

- Turbulence is relatively commonly encountered during spring and summer, especially when crossing cloud layers or due to thermals. Although experiments were mostly performed at higher altitudes, the flight control laws were left active during descent when returning to the airport. When crossing turbulent atmospheric layers, the descent was interrupted (after ATC approval) and control law behaviour was evaluated in level flight. The control laws were alternately switched on and off for 30 seconds, allowing ride comfort and control activity to be assessed qualitatively in flight and quantitatively afterwards.

- Wind shear (lateral and longitudinal) is easily generated by turning flight in constant wind. Hereby it is most important to fly circles relative to the ground while maintaining airspeed. As a consequence, ground speed varies and bank and crab angles have to be continuously adapted by the controller. At nonzero flight path angle, a flight path in form of a helix arises. Flight mechanical details are described in reference [3].

- Wake vortices were generated by means of partial in flight simulation. Control surface deflections used for in-flight simulation of aircraft responses during wake encounters were recorded and provided for use by the Flight Systems Institute. The flight test engineer could activate artificial wake encounters via experiment buttons. The recorded control deflections were then added to the control commands by the control laws. This approach provided a best compromise solution and turned out to work very well.

  A notable inaccuracy is that the air data signals provided to the controller are only modified due to the induced aircraft motion. As a result, inertial and air mass referenced aircraft responses are practically identical. In reality obviously, this is not the case, since the airdata system picks up local wind variations immediately, whereas the airframe has a delayed response due to its inertia and the wind disturbances are not uniform over the airframe. This aspect actually is addressed in models used for off-line simulation.

The flight control laws as used in this project have been evaluated in seven flights:

1. Flight 1: Objective: evaluation of auto flight control laws in wind shear and turbulent conditions. Three helical manoeuvres were performed in the form of final approaches to Braunschweig airport. Considerable (steady) winds were encountered and turbulence was present at the top of the manoeuvres. The flight control laws performed exceptionally well and engine responses were moderate, pleasing the flight crew. By incorporating the helix manoeuvers in final approaches, the flight test allowed the evaluation of a noise abatement procedure proposed in the project TIVA-II. This so-called Helical Noise Abatement Procedure (HeNAP) allows the aircraft to approach the runway at a considerably higher altitude. By performing the final descent in the imme-

diate vicinity of the runway threshold, noise on the ground is concentrated in this area (Figure 2). In order to validate the effect on noise levels on the ground, a noise measurement campaign was organized by means of twelve microphone stations below the helix and standard approach paths. For comparison reasons, two standard ILS approaches and two steep approaches (~-7 degrees glide path) were performed as well, see Figure 3.

After flight test, the helix manoeuvre turned out to be highly valuable for auto flight control law testing. For this reason, the helix was proposed as a standard flight test manoeuvre for auto flight control laws and the technicalities for making a given auto pilot perform such a manoeuvre was published at the DGLR and the first ICAS Aerospace Guidance and Control conference, see references [3] and [5]. The HeNAP and noise measurement results have been published in reference [4].

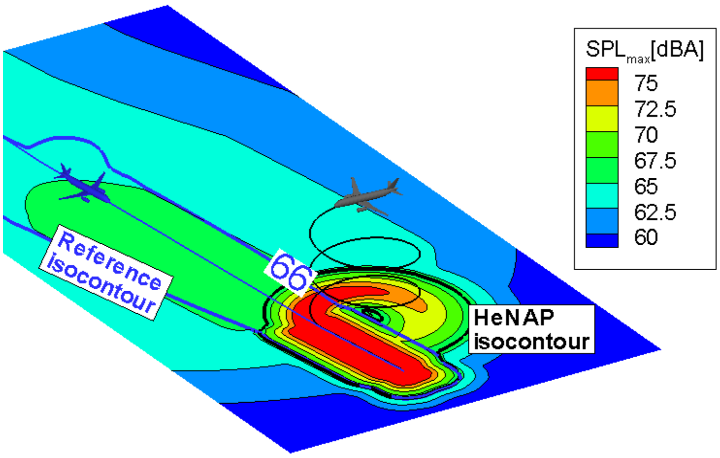

Figure 2. Concentration of ground noise near the runway by the HeNAP. The 66dB contour for a standard ILS approach has been added for comparison

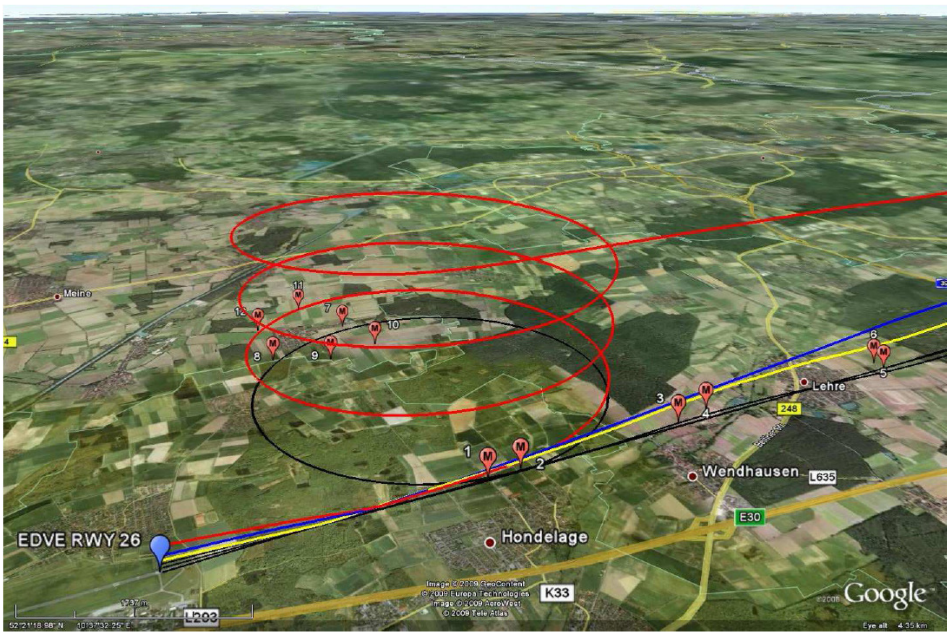

Figure 3. Flight test trajectories of 3 helical flight paths (in red: not distinguishable due to high controller tracking accuracy), 2 steep approaches (blue), one manual ILS approach. Note that the black ground tracks of the helix (9 full circles) are not distinguishable, in spite of up to 30kts wind. The red markers indicate microphone stations

2. Flight 2. Objective: evaluation of the manual control laws. During this flight, all functionalities were tested at two flight conditions. First of all, basic functionalities were tested, such as rate command responses with and without attitude hold, decoupling of command responses, steady-heading and wings-level side slip responses, turn co-ordination, simulated engine failures, etc. The experiment pilot performed tasks such as side slip, roll and pitch attitude captures, course changes, ILS tracking, etc. The control laws worked very well and valuable suggestions for improvements in command responses were obtained. No turbulence was encountered whatsoever on the clear winter day the flight took place.

3. Flight 3 (WTF funded). Objective: evaluate manual control laws, extended with Pseudo Control Hedging functionality for handling of actuator limits. During this flight, more or less the same test programme was followed as for flight 2. However, tight artificial limits were applied to control surface deflections, in order to evaluate control law behaviour close to saturation. The control laws performed very well. In addition, a dedicated auto throttle was successfully tested. During descent, turbulence was encountered and the control laws were switched on and off alternately for 30 seconds. Behaviour turned out to be highly satisfactory. Unfortunately, with control laws off, the basic ATTAS rate command system was active. This prevented a comparison of ride quality between attitude hold tracking and open loop (in fact, alpha controlled) command responses.

   The control law evaluation results have been published in reference [1].

4. Flight 4 (WTF funded). Objective: evaluate new NDI auto flight control laws and inner loops with PCH-based control limit handling. This flight included to full system, both with manual and automatic functions. Arbitrary switching in between turned out to be very smooth. Inner loop tracking worked out well, both with and without artificial control surface limitations. Auto flight testing was postponed because of a sensor signal processing problem. No significant atmospheric disturbances were encountered.

5. Flight 5 (WTF funded). Objective: test the complete autopilot system, including speed, pitch, roll and thrust limiting protections, as well as all manual control functions. The core feedback control laws for auto flight were largely the same as during flight 1. The emphasis was on mode functionalities and protections. To this end, the auto pilot could be fully operated from the ATTAS Experimental Flight Control Unit (EFCU). Since this system has been designed for the A320 and since for experiment reasons far more functionality was accessible as compared with in-service designs, the human interface is not intended for day-to-day operations. Helical manoeuvres were performed up-and-away, but no significant wind was encountered on the day of flight. In order to test engine control activity, so-called energy exchange manoeuvres were performed. During such a manoeuvre, a combined altitude and speed change is commanded, such that the total energy level (potential plus kinetic) remains constant. As a main means of control for the aircraft energy state, the engines should hardly respond. The results have been recorded and were intended for comparison with future flight tests of new systems.

   The control law evaluation results will be published in reference [2].

6. Flight 6. Objective: repetition of flight 4, at all flap settings. This time, the autopilot functions could be fully and successfully tested. For comparison reasons, helical and energy exchange manoeuvres as in flight 5 were performed up and away. The NDI control laws showed considerably more engine responses as compared with the TECS-based design in flight 5. Unfortunately, no turbulence was encountered.

7. Flight 7. Objective: flight testing of the complete auto flight and manual control system under artificial wake vortices. During this flight artificial wake encounters from the left and the right could be introduced on command by the flight test engineer. The following tests were performed at two flight conditions, with and without artificial control limitations:

a. Auto flight on. Observe how the auto flight functions restore speed, course, and level flight after encounters from the left and the right;

b. Manual control with attitude hold, without pilot action. Observe how the attitude control laws restore roll and pitch attitude and minimize side slip. The experiment pilot then restores course, level flight, and speed (Figure 5, lower plot);

Figure 4. ATTAS take off for flight 7 (Photo by M. Felux, KN)

c. Manual control with attitude hold, with immediate pilot intervention in order to restore course, level flight, and speed;

d. Manual control without attitude hold, without pilot action. Observe how the attitude is stabilized after encounter (Figure 5, upper plot);

e. Manual control *without* attitude hold, with immediate pilot intervention in order to restore course, level flight, and speed.

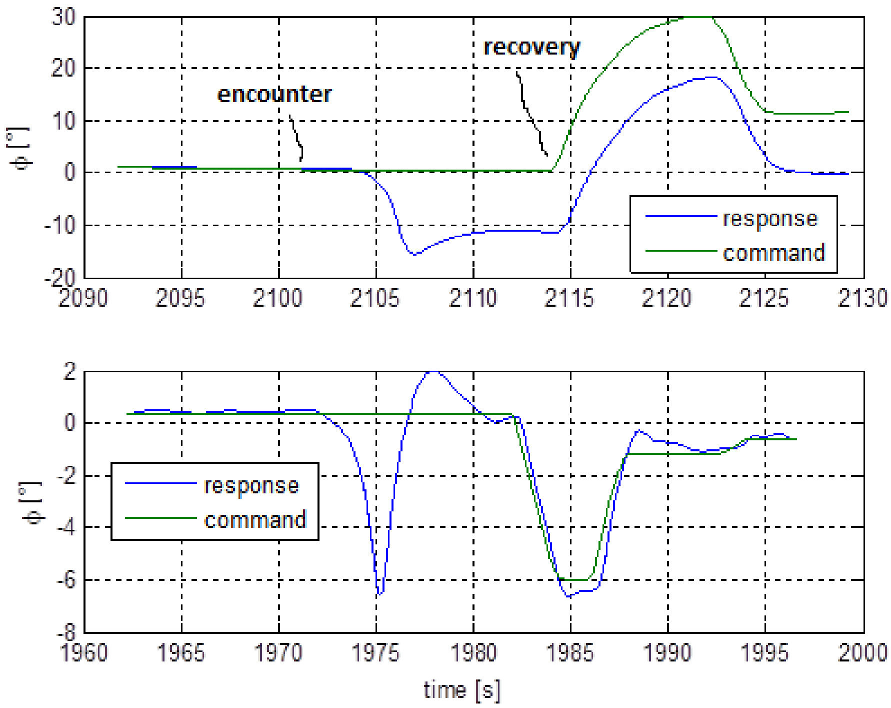

Figure 5. Wake encounter (from left), without and with attitude hold (roll). Pilot monitors aircraft response until encounter is over. Then approximately recovers course. With attitude hold, the controller recovers wings level flight automatically.

The control laws behaved very well. The expected major difference between attitude hold on and off did not occur. It was expected that the combined effort of the control laws and the pilot to restore the initial roll attitude would cause problems. The indication of the commanded roll angle within the controller (driven by pilot stick input) showed the pilot where the control law action was going, allowing him to anticipate this.

Unsteady Aeroelastic Modelling

Atmospheric disturbances are a major focus in determining and validating design loads on an aircraft. To this end, responses to continuous turbulence and discrete gusts are to be simulated. The distribution of the wind field over the airframe together with unsteady aerodynamic effects plays a very important role in the level and distribution of the aerodynamic loads on the airframe (Figure 6). Of course, it is interesting to see what levels of flight loads are achieved during wake vortex encounters. For this reason, a modelling process and simulation environment were developed and integrated in RMC-SR's Dynamic Aircraft Model Integration Process (DAMIP) [9]. The resulting models allow for simulation of flexible aircraft flight dynamics and flight loads responses to arbitrary wind fields, including wake vortex encounters. Unsteady and wind field penetration effects are accurately accounted for. One major problem is that unsteady aerodynamic effects are computed in the frequency domain. For simulation in the time domain, so-called rational function approximations are necessary. For this work, a new physical approach was developed, requiring only one term to be actually approximated, improving over-all accuracy. This work, although not in the frame of, but closely related to the project, has been published in reference [6] and was well received by the aeroelasticity community.

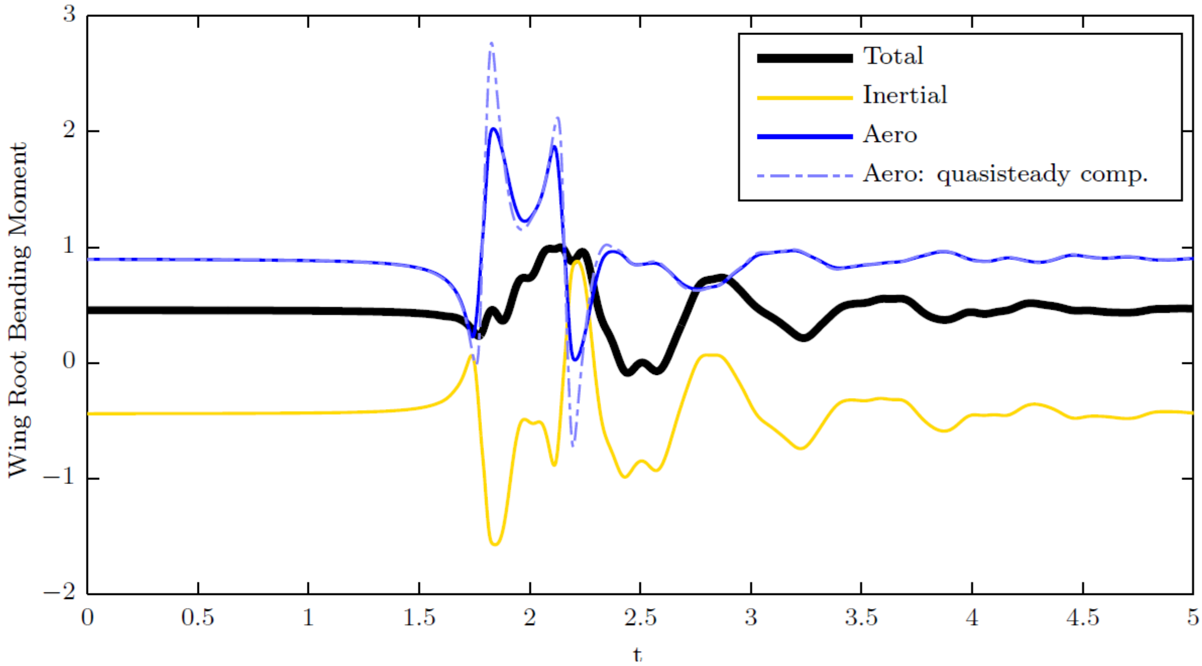

Figure 6. Wing root bending moment components (normalized w.r.t. maximum total loads) of a flexible large transport aircraft perpendicularly crossing a pair of wake vortices. Note the alleviating effect of unsteady aerodynamics

For future work, this modelling approach will be integrated in control law design models, allowing for more accurate simulation of wake vortex encounters, including local air data sensor readings, and for including flight loads criteria in the tuning process of control laws.

Conclusions and Future Work

The results achieved during the Wetter & Fliegen project can be summarized as follows:

- An integrated manual and automatic feedback flight control system was designed and very successfully evaluated in flight tests. The auto flight functions based on two methods have been developed (multi-loop NDI) or extended (TECS / NDI).

- A new flight test procedure for testing auto flight control laws under lateral and longitudinal wind shear conditions was proposed, based on so-called helical flight path trajectories.
- The auto flight functions allowed the so-called Helical Noise Abatement Procedure to be tested in a combined flight experiment and noise measurement campaign. Since tracking of helical trajectories is not a standard feature, DLR has been the first to actually test this type of approach fully automatically.
- The manual flight control system has a lot of functionalities that may be switched on or off in flight and simulator experiments. This will be very useful for future research in wake vortex encounters. An initial flight test (flight 7) showed very promising results.

Future work has been planned for the WOLV project:

- Integration of the flight control system within the IRLIS flight control system, developed in co-operation with the institute of Flight Systems.
- Incorporation of the new flight loads model in the parameter tuning process.
- Detailed evaluation of control law behaviour with more detailed air data sensor models.

Acknowledgment

The authors would like to thank the following persons for their contributions to the work summarized in this chapter: Dirk Leißling (FT), for helping in preparations of the flight tests, for implementation of the control laws in the simulator and on ATTAS, and for implementing the in-flight simulated wake-vortices; Christian Horn (FT) for providing the inversely simulated wake vortex encounter, Michael Preß, Hans-Jürgen Berns, Stefan Seydel, Axel Widmann, Andreas Hahn, Regina Gebhard (all FX) for preparing and conducting the ATTAS flight tests. We also highly appreciate the additional support from the DLR Programme Office, for providing additional WTF funds.

References

[1] Lombaerts, Thomas and Looye, Gertjan (2011) Design and Flight Testing of Manual Nonlinear Flight Control Laws. In: Proceedings of the AIAA 2011 GNC Conference and Exhibit. AIAA 2011 Guidance, Navigation and Control Conference and Exhibit, 7.-11. Aug. 2011, Portland, Oregon, USA.

[2] Lombaerts, Thomas and Looye, Gertjan (2012) Design and Flight Testing of Automatic Nonlinear Flight Control Laws. Submitted to the AIAA 2012 GNC Conference and Exhibit. AIAA 2012 Guidance, Navigation and Control Conference and Exhibit, 13.-16. Aug. 2012, Minneapolis, Minnesota, USA.

[3] Looye, Gertjan (2011) Helical Flight Path Trajectories for Autopilot Evaluation. In: Selected Papers of the First CEAS Specialist Conference on Guidance, Navigation and Control Advances in Aerospace, Guidance, Navigation and Control. Springer. Pp. 79-90. ISBN 978-3-642-19816-8.

[4] Bertsch, Lothar and Looye, Gertjan und Anton, Eckhard und Schwanke, Stefan (2011) Flyover Noise Measurements of a Spiralling Noise Abatement Approach Procedure. Journal of Aircraft, 48 (2), Pp. 436-448. DOI: 10.2514/1.C001005.

[5] Looye, Gertjan (2009) Flight Testing of Autopilot Control Laws: Fly the HELIX! Deutscher Luft- und Raumfahrtkongress 2009, Deutschland.

[6] Kier, Thiemo M. (2011) An Integrated Loads Analysis Model Including Unsteady Aerodynamic Effects for Position and Attitude Dependent Gust Fields. IFASD 2011 - 15th International Forum on Aeroelasticity and Structural Dynamics, Paris, France.

[7] Looye, Gertjan (2008) An integrated approach to aircraft modelling and flight control law design. Ph.D. thesis, Delft University of Technology, The Netherlands.

[8] Looye, Gertjan (2010) Aircraft mission simulation for environmental analysis with flight test validation. Presentation at the DGLR workshop on "Umweltfreundliches Fliegen", June 2010, Braunschweig, Germany.

[9] Kier, Thiemo; Looye, Gertjan; Scharpenberg, Moriz, and Reijerkerk, Marion (2007) Process, Methods and Tools for Flexible Aircraft Flight Dynamics Model Integration. IFASD 2007 - 13th International Forum on Aeroelasticity and Structural Dynamics, Stockholm, Sweden, IF-060.

5. Flight Systems to Increase Situational Awareness and Avoid Hazards

5.1 System and HMI Design of a Wake Encounter Avoidance and Advisory System

Tobias Bauer, Dennis Vechtel, Christian Raab
Institute of Flight Systems

The encounter of wake vortices of preceding aircraft can present a substantial hazard to the follower. Separations as procedural means are applied to avoid such encounters; however, the multitude of parameters governing vortex evolution makes them overly conservative (and thus capacity limiting) in the majority of cases without preventing incidents altogether. The German Aerospace Center DLR is working on a Wake Encounter Avoidance and Advisory (WEAA) system to allow pilots to avoid potentially dangerous wake vortex encounters by a small scale tactical evasion manoeuvre. Such manoeuvre tries to adhere to the planned flight track as closely as possible and is not intended to require ATC permission. Work on the system is on-going with a larger time horizon but initial solutions will be presented: the system conceptual design and selected components such as wake vortex prediction and hazard evaluation, avoidance trajectory generation, and a human-machine interface for increased situational awareness.

Introduction

The encounter of a sufficiently strong wake vortex of a preceding or crossing aircraft can pose a threat to the follower as a consequence of

- significant induced (linear and angular) accelerations leading to injuries of passengers / crew or structural damages,
- induced forces and moments (often predominantly rolling moments) leading to a poorly controllable flight condition or even (temporary) loss of control,
- hazardous flight path deviations resulting from the above effects, including altitude loss in the downdraft of the wake.

Wake vortices are often encountered in departure and approach operations – even close to the threshold, which makes them particularly dangerous due to ground proximity – but encounters also occur during cruise. Separations are defined under IFR to prevent hazardous encounters [17]; these have generally proven acceptably safe but the level of safety still could be increased

- under VFR, or
- in extreme meteorological situations when vortices behave abnormally, or
- in situations where separations are inadvertently violated, cf. Learjet 45 accident in Mexico City in 2008 [24].

In these cases an encounter avoidance system could improve flight safety by providing a safety net function. As current wake vortex separations limit (especially approach and departure) capacities unnecessarily in most cases, such a system could alternatively assist in increasing airspace capacity because of its mitigating effect on the encounter probability.

The aim of WEAA (Wake Encounter Avoidance and Advisory) system development as undertaken by DLR is to support pilots in avoiding hazardous small scale atmospheric phenomena such as wake vortices without necessity to change the flight plan or violate the active clearance. To that effect, potentially hazardous conflicts are detected and where possible evasive manoeuvres are defined, guided and monitored. Increasing the pilots' situational awareness in case of a predicted encounter is one of the main design objectives.

Where circumstances do not allow encounter avoidance, timely alerts can help the pilots to prepare themselves. Here the potential benefit of dedicated wake encounter alleviation functions of the flight controller has already been successfully demonstrated in flight experiments [1-3]. Such functions can be seamlessly integrated with WEAA even if they are not part of the avoidance system.

WEAA is initially intended as a safety net, i.e. to improve the existing level of safety. It is conceivable to use it alternatively as a means to increase capacity in as much as separations may be reduced for future aircraft so equipped; however, the system itself is not designed to suggest appropriate separations. The approach is in principle extendable to other phenomena such as small fields of clear air turbulence (CAT) but, due to the lack of suitable instruments for their detection, investigations currently focus on wake vortices. DLR work in this respect is complementary to earlier (I-WAKE [4], FLYSAFE [31]) and on-going (SESAR [5]) efforts.

Initial Considerations for System Concept

Due to the stochastic nature of wake evolution and transport, zones of potential danger become very large over time especially if meteorological parameters and those of the generating aircraft (weight, air-speed and configuration) are unknown. The complete avoidance of these zones of uncertainty is not compatible with current operations and traffic densities. Thus a viable avoidance system requires a more exact knowledge of the actual wake position, which is only attainable with improved prediction based on more accurate generator and meteorological parameters and/or remote detection of the wake position.

Remote detection of wake vortices could be performed using forward-looking LIDAR sensors. Unfortunately most of these sensors are only able to measure the line-of-sight (LoS) component of the flow field velocity. As wake encounters often occur when the involved aircraft have the same nominal flight path (as during approach and landing) the main vorticity components of the wake are not measurable with LIDAR. Additionally the measurement resolution and update rate of current instruments at distances relevant for avoidance manoeuvres are below requirements by several orders of magnitude [21]. Conceptually, however, it appears desirable to combine the measurement with a prediction based on data of the leading aircraft, which might be received via Automatic Dependent Surveillance ADS-B. A combination of ADS-B-based prediction and LIDAR measurement appears promising for this purpose [21].

Once position and spatial orientation of the wake are known an evasion trajectory can be calculated. Aim of system development is to initiate the manoeuvre early enough so that it requires only small accelerations and ideally is not perceived by the passengers. With the expected small deviations from the original flight path 30 to 40 s appear a sufficient tentative time horizon; this value will be further analysed in simulation and ultimately in flight experiments.

Avoidance Manoeuvre Design Restraints

The WEAA system enables avoidance of small scale phenomena with immediate return to the original flight path so by definition a change in the flight plan is not envisaged, nor does the small time horizon allow requesting changes of the current clearance from ATC. This requires manoeuvres to be designed such that informing ATC about their execution suffices.

As a consequence, the airspace available for wake evasion is limited. In the absence of dedicated ATC procedures the idea is to restrain manoeuvring to the tolerable navigation deviations. In principle evasive manoeuvres can be performed either vertically or laterally, or by adapting airspeed only. All three options may be combined if compatible with the capabilities of the flight guidance and control functions.

Airspace and Navigational Restraints

Under normal conditions each aircraft has to acquire the desired flight path as accurately as possible given its capabilities. ICAO’s Required Navigation Performance (RNP) concept [17-19] specifies a minimum navigational accuracy (Navigation System Error, NSE) to be met by the on-board equipment for 95% of the time, cf. Figure 1.

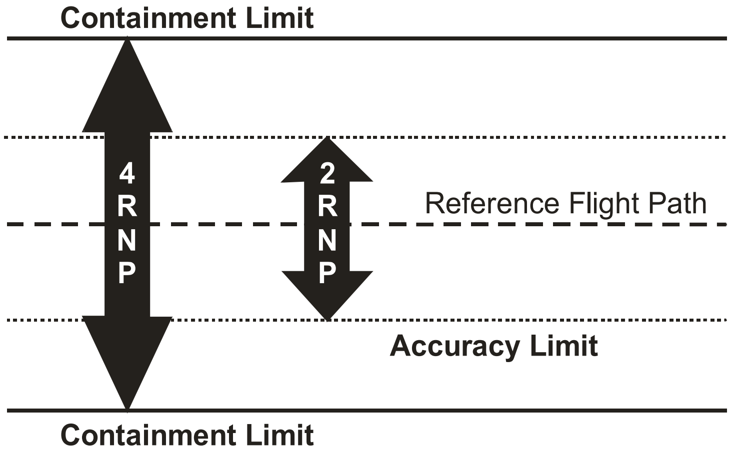

Figure 1. RNP containment and accuracy limits (redrawn from [25])

The concept includes on-board monitoring thus an estimation of the current NSE is available. Numerical RNP requirements are set by ICAO member states dependent on type of airspace and flight phase. Typical values are ±2 NM for cruise, ± 1 NM for arrival and departure and ± 0.3 NM for approach [19].

Twice the width of the accuracy limit defines the containment limit where, assuming Gaussian distribution of NSE, the indicated position is located with a probability of 99.999%. Taking into account horizontal navigation performance achieved by modern aircraft for most flight phases [25] and confidence intervals of wake vortex habitation volume predictions, see below, it appears that often sufficient lateral margin exists for manoeuvring, cf. Figure 2.

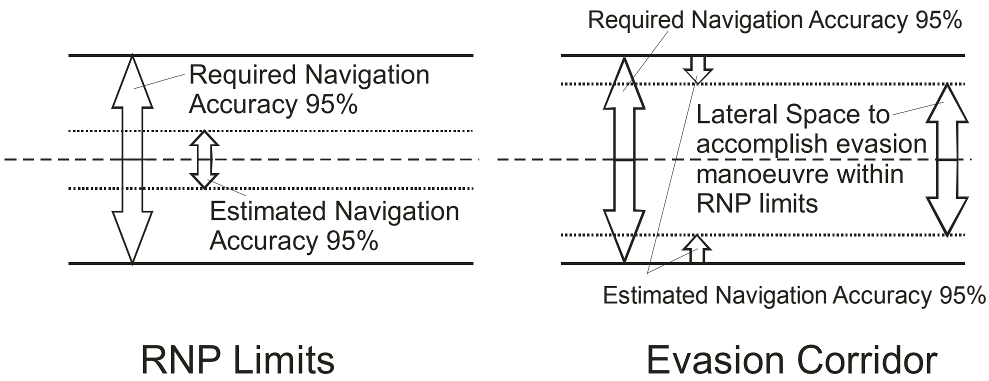

Figure 2. Definition of lateral evasion corridor limits

The tolerances on vertical position deviation, listed in Table 1, are significantly smaller than those in lateral direction. This is due to the high accuracy of barometric height measurement and the much lower vertical separations. However, as the vertical motion of the vortices is limited, this option is not precluded per se. Considering that ATC should be informed when the altitude deviates ±100 ft from the cleared flight level (FL), it is conceivable though that for this type of manoeuvre a quick, possibly automated go/no-go decision from ATC would be required.

As to speed adaptations, true airspeed has to be maintained within a tolerance margin of ±5% [20]. On its own this option does not appear effective during the envisaged time horizon. Moreover, configuration and airspace dependent speed restrictions (such as the limit of 250 kt below FL100) need to be taken into account.

Table 1: Tolerable vertical flight path deviations due to pilotage errors ([19] II-A-6).

	Level flight segments and climb/descent intercept altitude region of specified altitudes	*Climb/descent along specified vertical profile (angle)*
At or below 1 500 m (5 000 ft)	45 m (150 ft)	60 m (200 ft)
1 500 m to 3 000 m (5 000 ft to 10 000 ft)	73 m (240 ft)	91 m (300 ft)
Above 3 000 m (10 000 ft)	73 m (240 ft)	91 m (300 ft)

Interoperability Restraints

In addition to navigational and ATC requirements interoperability restraints must be observed during an evasive manoeuvre such that it is not impaired by triggering alerts from other systems. It is the intention of the WEAA system design that the independent safety net functions of terrain and traffic collision avoidance are not affected by the avoidance manoeuvre. These functions obviously need to have higher priority than wake avoidance.

Navigating in areas close to ground, mountains or other obstacles it must be assured that the performance of an evasive manoeuvre does not result in an (Enhanced) Ground Proximity Warning System ((E)GPWS) alert. Therefore at low altitudes or in mountainous areas information about the proximity of ground must be considered for the generation of the evasion trajectory, with regard to the fact that (E)GPWS not only takes into account height above ground but also terrain closure rates.

As to surrounding traffic, the WEAA system is not intended to handle existing TCAS conflicts, which take priority over wake avoidance. However, it must be assured that the wake evasive manoeuvre does not trigger new TCAS alerts during its execution. This does not necessarily mean that the wake evasion system must comprise a built-in TCAS functionality but the TCAS principle of operation needs to be taken into account for trajectory generation. In analogy to (E)GPWS, not only actual proximity of the aircraft is evaluated but also closure rates are observed.

Performance Restraints

When determining an evasion trajectory, the aircraft performance, manoeuvrability and passenger comfort (small accelerations and load factors) need to be taken into account. These restraints depend on the flight phase (e.g. in final approach passengers can be assumed to be seated with seatbelts fastened such that higher accelerations can be tolerable). The general aim is to achieve sufficient lead time for the manoeuvre such that, unlike TCAS, hard manoeuvring is not required. Beneficial for reaching this aim is that usually only small flight path deviations will be required.

WEAA System Architecture

With the above restraints in mind, system architecture for WEAA has been developed, a high-level overview of which is presented in Figure 3.

According to requirements, the following tasks have to be performed by the system:

- predict wake vortex transport and decay for surrounding traffic using meteorological data and information on the traffic (aircraft type, track, velocity; performance data and planned trajectories where available), possibly enhanced by remote wake vortex detection employing a suitable forward-looking (LIDAR) sensor. Such prediction can include own vortices as they might be encountered under special circumstances;
- detect wake conflicts, using prediction of own trajectory and that of other traffic (assuming in absence of better information that its flight track is properly described by extrapolating the current

flight path vector), followed by hazard assessment where required. These two functions are closely interconnected, see below;

- in case a conflict is detected, alert the flight crew and generate an evasion trajectory, taking into account terrain and traffic collision avoidance requirements as well as own ship flight performance, flyability restraints and passenger comfort;
- provide guidance for the necessary evasive manoeuvres to the pilots, e.g. on Primary Flight Display (PFD) and Vertical Speed Indicator (VSI);
- monitor manoeuvre execution (by pilot via flight director in manual flight or by the automatic flight system when autopilot is in use); and
- display an overview of the situation to increase the pilots' situational awareness, e.g. on the Navigation Display (ND).
- The WEAA system constantly updates the trajectory upon reception of new input data. The stability of the prediction remains a major point for further investigations.
- Two design options have been defined for the determination of necessary wake parameters:
- The basic design is based on prediction of the wake vortex location using information and sensors that are in principle available and on-board a transport aircraft today.
- The enhanced system design employs wake characterisation from prediction and vortex measurement by means of a suitable sensor such as LIDAR [12]. These have not yet achieved sufficient technological maturity [21] and their installation on transport aircraft is not foreseeable in the near future. Hence, this option is seen as a long term one but one of the aims of further WEAA system assessment is to evaluate benefits and necessity of a LIDAR sensor.

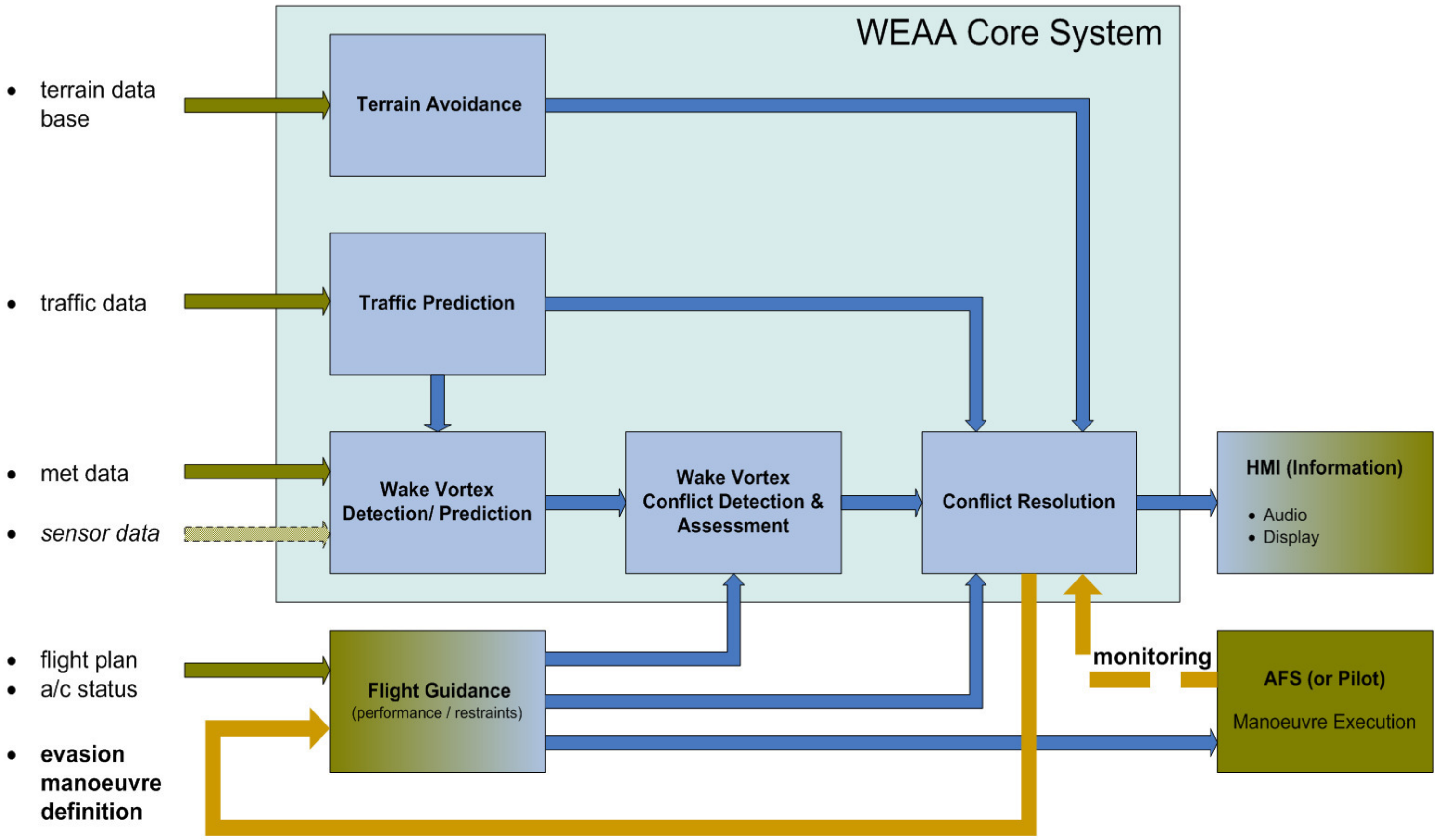

Figure 3. Simplified top-level functional architecture of WEAA system

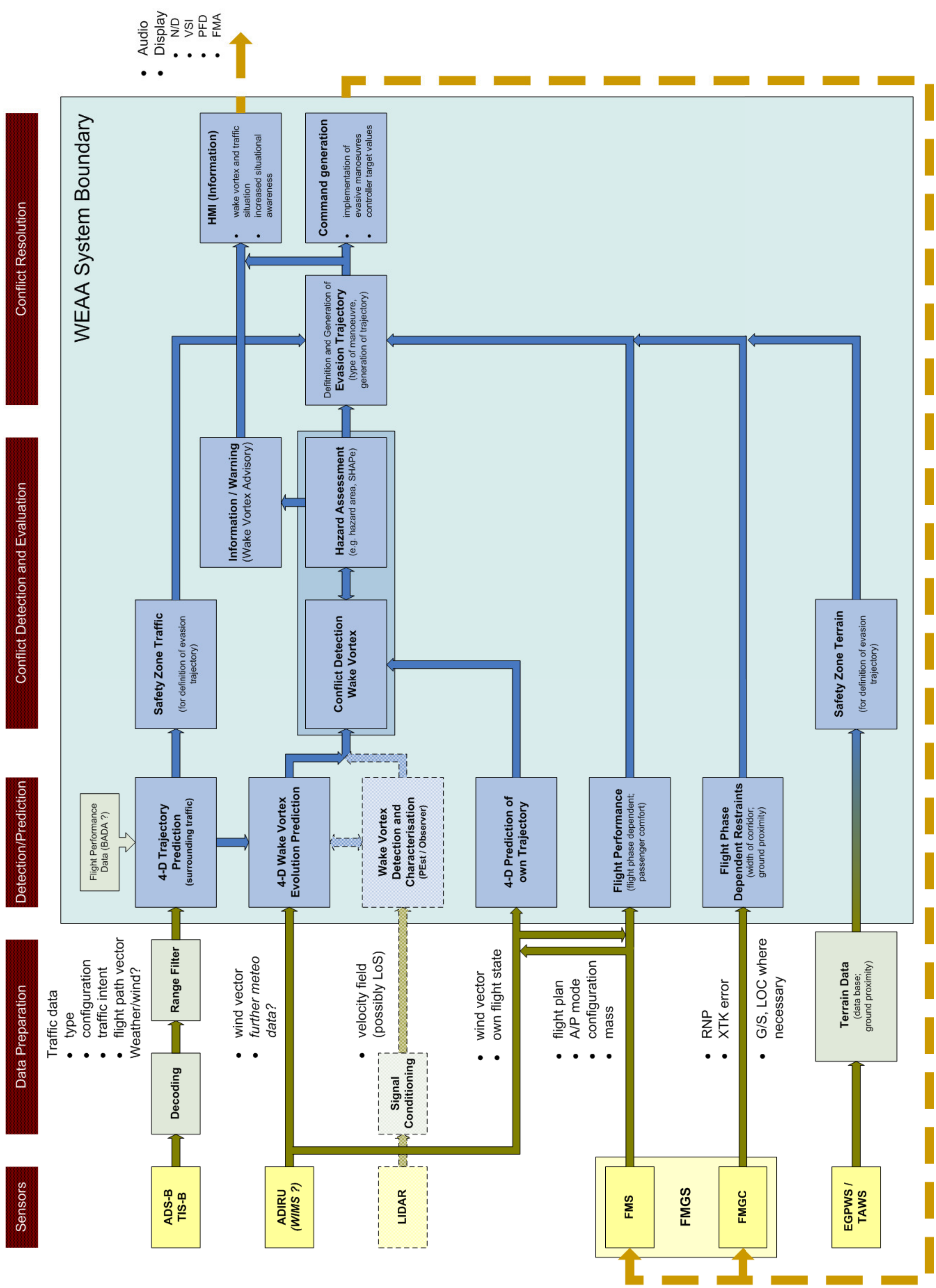

Figure 4: Functional architecture of WEAA system (with optional LIDAR detection) (see Glossary)

Figure 4 shows a more detailed functional system break-down of the WEAA system with the two design options. The system architecture is as generic as possible but where necessary adapted to DLR's ATRA research aircraft (Figure 5) which is the envisioned test-bed for future in-flight system integration and evaluation.

Figure 5. DLR's ATRA Research Aircraft

System Components and Initial Results

The WEAA system realisation, which is a work-in-progress, uses a modular architecture to allow a step-by-step implementation of components and to allow trade-off studies for different configurations. For instance, the benefit of using a LIDAR sensor in addition to a pure wake prediction will be evaluated. Various existing and on-going component implementations are discussed hereafter.

Wake Vortex Prediction

Wake vortex prediction is effected with Holzäpfel's P2P tool [6,7], a real-time capable probabilistic two-phase wake vortex prediction model. P2P takes into account effects of aircraft configuration, wind, wind shear, turbulence, stratification and ground proximity. It has been extensively validated on LIDAR measurements and numerical (LES) simulations [7,8], cf. Figure 6. Alternatives to the P2P model could be NASA's APA [10] or PVM [11].

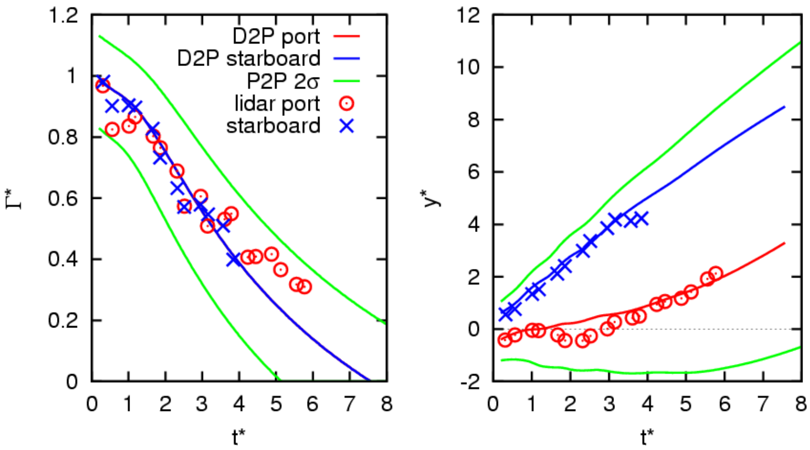

Figure 6. Sample wake vortex prediction from P2P showing calculated nominal (D2P, red and blue lines) and measured (symbols) values for vortex decay Γ^* and lateral positions y^*. Green lines are associated 2σ confidence intervals for prediction (P2P) [9]

Hazard Assessment

WEAA's hazard assessment function uses the Simplified Hazard Area Prediction (SHAPe) method by HAHN and SCHWARZ [13-15] to quantify the severity of a potential wake encounter. In relation to the nominal wake vortex positions, areas are determined outside of which no hazard due to the wake exists (Figure 7), i.e. where flight operations can be considered as safe and undisturbed.

The hazard assessment criterion used by SHAPe is the roll control ratio *RCR* defined as

$$RCR = \left| \frac{C_{l,WV}}{C_{l\,max,\delta_l}} \right|, \tag{1}$$

where $C_{l,WV}$ is the coefficient of the rolling moment induced by the vortex wake and $C_{l\,max,\square}$ is the coefficient for the maximum rolling moment obtainable by roll motivator deflection (roll control power). Numerical values for acceptable RCR have been derived experimentally from piloted trials [15].

The extent *a*, *b* of the hazard areas given by SHAPe (Figure 7) is added to the wake vortex habitation volumes predicted by P2P. Hazard assessment thus is closely connected to conflict detection, as the permissible distances *a*, *b* to the assumed position of the vortex cores determine the size of the volumes for which conflict detection is necessary (with *a* = *b* = 0 meaning the wake does not represent a relevant hazard any longer). In addition, the level of hazard and hence *a*, *b* may depend on the encounter geometry.

Evasive Trajectory Generation Using a Potential-Field-Based Method

The conflict resolution function, cf. Figs. 3 and 5, has the task to modify the flight path in order to evade the wakes while avoiding other hazardous zones (terrain and the safety zones around other traffic) and diverting as little as possible from the originally planned trajectory. The method chosen uses a potential field approach which is well known in robotics [29] and also often applied for trajectory planning of unmanned aerial vehicles [30]. In order to take into account the limited manoeuvrability of transport aircraft a super-elliptical shape for the potential field surrounding the wake vortex hazard zone was chosen (Figure 9). The parameters of such ellipses can be easily adapted as a function of airspeed to always ensure a smooth evasive manoeuvre taking passenger comfort into account. The intended flight path is characterised by an attracting potential so that after the wake evasion the trajectory automatically leads back to the original flight path. Navigational restraints are represented with a repulsive potential so that manoeuvring within the cleared airspace is assured. In addition danger zones for surrounding traffic and terrain are modelled by penalty barrier functions. Thus it is assured that an evasive manoeuvre does not lead to a conflict with TCAS or (E)GPWS without the necessity of a built-in TCAS and (E)GPWS functionality.

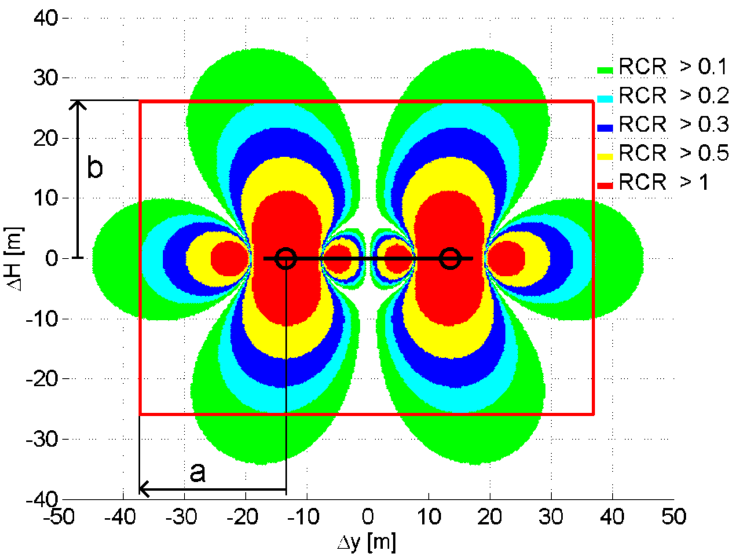

Figure 7. Sample result from SHAPe hazard assessment showing a simplified hazard area (red rectangle) based on roll control ratio *RCR* (cf. Eq. 1) around nominal wake vortex positions (black circles) (modified from [16])

The current aircraft performance is taken into account for the trajectory generation. Depending on airspeed, altitude and passenger comfort criteria the maximum bank angle as well as the maximum roll acceleration during lateral evasive manoeuvres are restricted. Also boundaries are set on the maximum vertical load factor during vertical evasion. These constraints limit turn radii and changes in flight path angles.

If a conflict free avoidance trajectory (in terms of traffic and/or terrain) can be found, this approach guarantees maximum possible proximity to the originally planned flight path and, in contrast to TCAS, automatic reacquisition of the nominal flight path after clearance of the danger zone. If there is no possible conflict free trajectory the wake encounter is accepted and the crew alerted accordingly.

For first studies the evasion options have been restrained to pure lateral or vertical motion. A decision algorithm, based on encounter geometry, cf. Figure 8, calculates the most effective direction of evasion (vertical or lateral) so that the wake evasion leads to the smallest deviations from the original flight path. Motion in all three spatial dimensions plus adjustment of flight speed, i.e. 4-D evasion, is conceivable although it has to be analysed whether evasion by speed adjustment is viable in view of ATC and configuration dependent speed restrictions.

Figure 8. Sequence of avoidance trajectory generation (modified from [22])

The trajectory generated by the algorithm is smoothed to ensure flyability. The smoothing algorithm consists mainly of a moving average filter in conjunction with some additional trajectory optimisation functions. Trap situations are avoided by means of the special shape of the potential field.

The algorithm has been successfully tested in flight simulation in cruise conditions with autopilot engaged [22]. The simulator trials showed that with this experimental setup the evasive manoeuvres in vertical as well as in lateral direction effectively avoided the wake habitation areas with deviations to the original flight path lower than 150 m (vertically and laterally). An example is depicted in Figure 9 where the initial and the smoothed flight paths are shown.

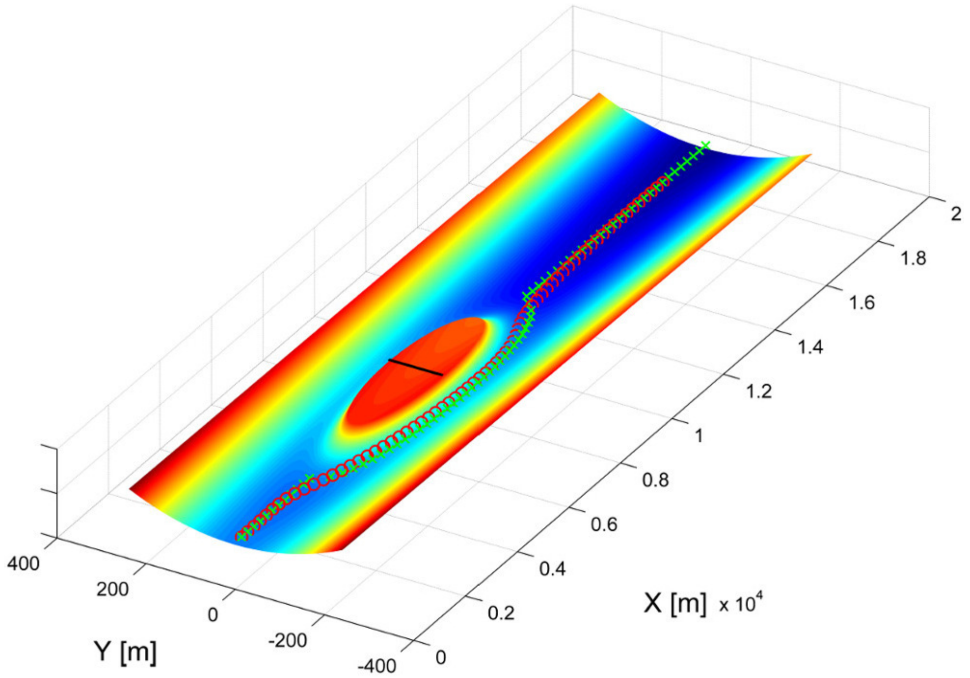

Figure 9. Example of generated avoidance trajectory on a potential field represented by the coloured surface [22]. Black line indicates wake segment to be avoided. Initial (green ×) and smoothed (red O) trajectories are shown.

Future work comprises refinement of the conflict resolution algorithm for other flight phases and adaptation to manual flight control: here the evasion trajectory must be designed such that a pilot is able to fly it, and the degraded precision of manoeuvre execution has to be taken into account for the trajectory generation. Similar to the Airbus autopilot-TCAS system APTCAS the WEAA system concept provides that the manoeuvre is performed manually if in manual flight and automatically if the autopilot is activated.

Human-Machine Interface

Design Requirements

Information about the wake hazard zone and the intended avoidance trajectory is essential for pilot situational awareness. For the WEAA system a human-machine interface (HMI) was developed with the intention to test the overall system with the DLR A320-ATRA research aircraft (Figure 5) [26]. Therefore, considerations were made on how to integrate the system into the ATRA cockpit environment providing additional functions to a conventional Airbus A320 flight control and guidance system. Design of the human-machine interface is influenced by existing systems like TCAS, wind shear protection function and flight envelope protections. Main sources of information for the concept were the A320 Flight Crew Operating Manual [27] and designs developed in the European project FLYSAFE [31].

Primary Flight Display (PFD) and Navigation Display (ND) are the central sources of information for the pilot during flight. A textual warning message is displayed on the PFD if the WEAA system has detected a hazardous wake encounter conflict. In case of a vertical avoidance manoeuvre the proposed trajectory is indicated by coloured markings in the vertical speed indicator (similar to TCAS). Hazard zones, the lateral evasive trajectory and headings currently to be avoided are depicted in the ND.

In addition to the indications on PFD and ND a Vertical Situation Display (VSD) is proposed in the introduced concept as shown in Figure 10. It was originally developed for pilot assistance during approach manoeuvres [28] but can be modified to display wake hazard zones in order to improve pilot spatial situation awareness. During the evasive manoeuvre the pilot is guided by aural messages to assure that the aircraft flies the intended trajectory. The proposed HMI concept was tested and evaluated by pilots in an engineering simulator with an A320-like cockpit environment.

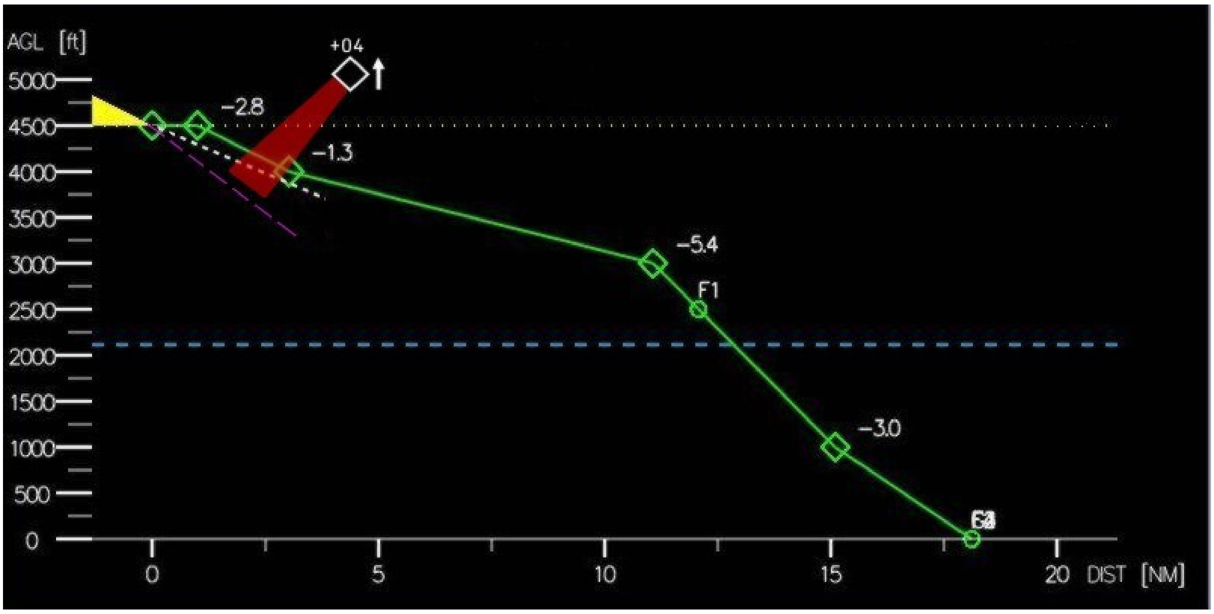

Figure 10. VSD during a vertical wake vortex evasion manoeuvre showing the recommended flight path (violet dashed line), active flight plan (green lines and symbols), the hazard zone (red polygon) and the intruder aircraft causing the wake (white diamond).

Operational Aspects

As already stated earlier the WEAA system calculates a trajectory with a minimum deviation from the current flight plan. Evasive manoeuvres are flown manually by the pilot or automatically with the Autopilot (AP) engaged. Depending on flight phase, traffic situation and flight performance three basic single evasion manoeuvres are possible: vertical, lateral and speed adjustment. Trajectory optimization may lead also to a combination of these three basic manoeuvres, subject to further investigations.

The proposed system adds three new AP modes to the existing A320 auto flight system listed in Table 2. Each AP mode guides the aircraft away from a wake vortex hazard zone with a single flight path change manoeuvre. Although speed change restrictions are very tight the Speed Adjustment Mode was considered for research purposes. Clear of conflict status is reached when the aircraft has passed the wake hazard zone in a safe distance. After the aircraft has been led back to the original flight path navigation is continued in accordance with the last ATC clearance.

The designed HMI considers three phases of conflict resolution:

- Wake Vortex Conflict Detected
  Having detected a wake hazard zone endangering the aircraft the WEAA system calculates an avoidance trajectory and chooses an appropriate evasive manoeuvre. The pilot is informed by an

aural warning and a text message in the PFD. The location of the wake hazard zone is displayed in the ND. Depending on the time to conflict two levels of warnings with different colouring, yellow and red, are applied.

- Wake Vortex Evasion
  According to the optimal avoidance trajectory the Flight Director (FD) is engaged at this state with a corresponding autopilot mode indicated in the Flight Mode Annunciator (FMA). If activated at this point of flight the evasion manoeuvre is flown by the autopilot, if not the manoeuvre is flown manually by the pilot. In both cases the FD is shown in the PFD either to guide the pilot with desired steering inputs in order to avoid the hazard zone or otherwise (with autopilot activated) to inform about the intended manoeuvre. Additional indications about the avoidance trajectory are shown on PFD and ND. Synthetic voice messages guide or inform, respectively, the pilot during the evasive manoeuvre.
- Wake Vortex Encounter Avoided
  This state is entered after the wake vortex encounter conflict has been resolved. Navigation is resumed in accordance with the last ATC clearance and the AP modes are switched accordingly. The pilot is informed about the successful avoidance manoeuvre by a text message in the PFD and an aural confirmation.

Table 2. Additional AP modes provided by the WEAA system.

Mode	Description
WV VERT	Wake Vortex Vertical Evasion – The system calculates a vertical speed resulting in a climb or descent manoeuvre preventing the aircraft from encountering a wake vortex.
WV LAT	Wake Vortex Lateral Evasion – An aircraft track is calculated resulting in a flight path that is not conflicting with the vortex. The aircraft is flying a horizontal turn towards a safe track with no change in altitude.
WV SPD	Wake Vortex Speed Adjustment Manoeuvre – The Flight Management and Guidance Computer adjusts the aircraft ground speed by changing the target indicated airspeed for the auto-thrust system in order to avoid a wake vortex encounter. Speed changes may result in acceleration so that the aircraft does not encounter e.g. a descending wake from above. On the other side a deceleration manoeuvre may increase the range to a wake right in front of the aircraft's flight path.

Simulator Trials

Benefit and applicability of the introduced HMI concept was examined with simulator trials in the DLR Institute of Flight Systems engineering simulator [23]. Manoeuvre indications on PFD and ND as well as the logic for aural messages were triggered by a simple geometry-based conflict detection and resolution algorithm. The pilots had to fly manual cruise and approach scenarios both with lateral and vertical evasive manoeuvres. After each test manoeuvre pilot workload was evaluated by a questionnaire. During debriefing of the simulator trial the pilots were asked specific questions on the acceptance of the operational function, graphical design and aural messages. In general the graphical design was accepted by the pilots and they responded to the directed evasive manoeuvres quickly and clearly. Considering the workload vertical manoeuvres were less demanding than lateral ones. In summary the following main points were observed from the simulator study:

- Automatic guidance back to the last active flight plan was preferred.
- Synthetic voice messages supporting the evasive manoeuvre were found useful.
- An additional caution with enough lead time is preferred as the pilot may need some time to draw his attention to the system and to fully comprehend the traffic situation.

As these early simulator trials were focused on HMI evaluation a simple conflict resolution algorithm was used with an intruder object remaining steady in space. When dealing with wake vortices, their transport and decay will have to be taken into account, and different flight phases impose different restrictions on the allowable avoidance trajectory. In future simulator trials the progressive integration of the WEAA system and the interaction of all its components will be investigated further.

Conclusions

DLR is developing a Wake Encounter Avoidance and Advisory System (WEAA) that allows tactical small-scale evasion to avoid possibly hazardous wake encounters. WEAA initially has a pure safety net function, assuring interoperability with existing safety functions TCAS and (E)GPWS / TAWS (Terrain Awareness and Warning System). The pilots' situational awareness is a key driver in system design and development.

DLR's objectives in WEAA development are a system proof-of-concept and in-depth investigation of selected components. This includes trade-off studies to assess the necessary level of detail in modelling and hence complexity of the system functions.Pre-existing DLR knowledge has been exploited in the form of the P2P wake vortex prediction model, wake parameter identification from forward-looking sensor measurements (as a long term option) and severity assessment for a predicted encounter (SHAPe method). This means that several key system components are already available and well tested.

Initial development work has focused on the approach and cruise phases, encompassing a method for evasion trajectory generation using a potential-field-based approach, an investigation into forward looking sensor requirements for wake detection, and the enhancement of a pilot display concept for manoeuvre guidance and increased situational awareness. Current stand-alone implementations of these functions have been successfully tested in flight simulation. Further testing of the HMI and the wake prediction in a flight experiment with DLR's research aircraft ATTAS is planned.

On-going work includes further development of component functions such as conflict detection concept and algorithms as well as a refinement of the conflict resolution algorithms taking into account (E)GPWS & TCAS interoperability, passenger comfort and aircraft performance. Next steps comprise enhancing severity assessment (graded hazard assessment, non-roll dominated encounters) and further studies on enhanced wake characterisation using (LIDAR) measurements. The WEAA concept of operation will be assessed for all flight phases (current implementations focus on cruise flight and the approach phase). Different concepts for pilot assistance will be analysed with respect to workload and situational awareness.

System integration is a major task for the future; the proof-of-concept implementation in an engineering flight simulator is already on-going. As a perspective increasingly complete functions are planned to be evaluated in motion-based simulation and during flight-testing with ATRA. These experiments will support an eventual benefit analysis under realistic conditions.

Acknowledgements

The authors gratefully acknowledge contributions from the following colleagues: Jobst H. Diekmann (trajectory generation via force field method), Christian Gall (HMI), Frank Holzäpfel (P2P wake vortex prediction model) and Carsten Schwarz (SHAPe severity assessment).

References

[1] Hahn, K.-U. and Schwarz, C., "Alleviation of atmospheric flow disturbance effects on aircraft response", ICAS 2008, Anchorage, 14th – 19th Sep. 2008. proceedings: Edinburgh, 2008.

[2] Hahn, K.-U., Fischenberg, D., Niedermeier, D. and Horn, C., "Wake Encounter Flight Control Assistance Based on Forward-Looking Measurement Processing", AIAA ASE 2010, 2nd – 5th Aug. 2010, Toronto, Canada.

[3] Schwarz, C. and Hahn, K.-U., "Automated pilot assistance for wake vortex encounters", Aerospace Science and Technology, Vol. 15, 2011, pp. 416-421.

[4] Rouwhorst, W., Groeneweg, J., Winckelmans, G. and Luckner, R., “Piloted Simulation Results of an Onboard Wake Vortex Detection, Warning and Avoidance System and Cockpit Display Aspects”, ICAS 2008, Anchorage, 14th – 19th Sep. 2008.

[5] Kauertz, S., Reinke, A., “SESAR projects 9.11 & 9.30 ‘Aircraft Systems for Wake Encounter Alleviation’ ”, 3rd Major WakeNet3-Europe Workshop, Southampton, 10th – 11th May 2011.

[6] Holzäpfel, F., “Probabilistic Two-Phase Wake Vortex Decay and Transport Model”, Journal of Aircraft, Vol. 40, No. 2, 2003, pp. 323-331.

[7] Holzäpfel, F., “Probabilistic Two-Phase Aircraft Wake-Vortex Model: Further Development and Assessment”, Journal of Aircraft, Vol. 43, No. 3, 2006, pp. 700-708.

[8] Holzäpfel, F. and Steen, M., “Aircraft Wake-Vortex Evolution in Ground Proximity: Analysis and Parameterization”, AIAA Journal, Vol. 45, No. 1, 2007, pp. 218- 227.

[9] Holzäpfel, F. et al., “The Wake Vortex Prediction and Monitoring System WSVBS – Part I: Design”, in: Holzäpfel, F., Gerz, T., The DLR Project Wirbelschleppe – Detecting, Characterizing, Controlling, Attenuating, Understanding, and Predicting Aircraft Wake Vortices, DLR research report FB 2008-15, Köln, 2008, pp. 73-88.

[10] Sarpkaya, T., Robins, R. E. and Delisi, D. P., “Wake-Vortex Eddy-Dissipation Model Predictions Compared with Observations”, Journal of Aircraft, Vol. 38, No. 4, 2001, pp. 687–692.

[11] Winckelmans G., The Vortex Forecast System (VFS): prediction of trajectories and decay for aircraft wake vortices in an operational environment, Proc. Conference on Capacity and Wake Vortices, Imperial College, London, UK, 11th – 14th Sep. 2001.

[12] Schönhals, S., Steen, M. and Hecker, P., “Wake vortex prediction and detection utilising advanced fusion filter technologies”, The Aeronautical Journal, Vol. 115, No. 1166, 2011, pp. 221-228.

[13] Hahn, K.-U., Schwarz, C. and Friehmelt, H., “A simplified hazard area prediction (SHAPe) model for wake vortex encounter avoidance”, ICAS 2004, Yokohama, 29th Aug. – 3rd Sep. 2004. proceedings: Edinburgh, 2004.

[14] Schwarz, C. and Hahn, K.-U., “Full-Flight simulator study for wake vortex hazard area investigation”, Aerospace Science and Technology, Vol. 10 No. 2, 2006, pp. 136-143.

[15] Hahn, K.-U. and Schwarz, C., “Safe limits for wake vortex penetration”, AIAA GNCC 2007, Hilton Head, 20th – 23rd Aug. 2007. Paper AIAA-2007-6871.

[16] Schwarz, C., Hahn, K.-U., Holzäpfel, F. and Gerz, Th., “DLR Wake Solutions in Development”, WakeNet USA Meeting October 2010, Cambridge, MA, 20th -21st Oct. 2010.

[17] ICAO Doc 4444 ATM/501, “Procedures for Air Navigation Services – Air Traffic Management”, 15th Edition, Montreal, 2007.

[18] ICAO Doc 8168 OPS/611, “Procedures for Air Navigation Services – Aircraft Operations, Volume II, Construction of Visual and Instrument Flight Procedures”, 5th Edition, Montreal, 2006. here: Part III, Sec. I, Chap. 7.4.

[19] ICAO Doc 9613 AN/937, “Performance-based Navigation (PBN) Manual”, Volume II, 3rd Edition, Montreal, 2008.

[20] ICAO Annex 2, “Rules of the Air”, 10th Edition, Montreal, 2005.

[21] Wolkensinger, C., “Vergleich messtechnischer Konzepte zur bordgestützten Ermittlung atmosphärischer Störphänomene”, DLR internal report IB 111-2010/35, Braunschweig, 2010.

[22] Diekmann, J. H., “Entwicklung eines Softwaremoduls zur Generierung von Trajektorien zum kleinräumigen Ausweichen vor Wirbelschleppen”, DLR internal report IB 111-2010/59, Braunschweig, 2010.

[23] Gall, C., “Entwicklung und Systembetrachtung eines Assistenzsystems zur Durchführung von Ausweichmanövern”, DLR internal report IB 111-2011/10, Braunschweig, 2010.

[24] Malkin, E., “Mexico Crash Inquiry Points to Pilot Error in Turbulence”, The New York Times, New York, 15th Nov. 2008.

[25] AIRBUS Flight Operations Support & Services, “Getting to Grips with RNP-AR”, Blagnac, 2009

[26] Raab, C., “Wake Impact Attenuation and Avoidance Systems – Conceptual Design for Operation and Human Machine Interface”, DLR internal report IB 111-2010/21, Braunschweig, 2010.

[27] Airbus Industrie, “A320 Flight Crew Operating Manual – Vol. 1 Systems Description”, Blagnac, December 2009.

[28] Immisch, T., “Entwicklung und Validierung eines Pilotenassistenzsystems für das Konfigurationsmanagement eines modernen Verkehrsflugzeugs”, DLR internal report IB 111-2010/34, 2010.

[29] Koren, Y., Borenstein, K., “Potential field methods and their inherent limitations for mobile robot navigation”, IEEE International Conference on Robotics and Automation, Proceedings Vol. 2, pp. 1398-1404, 1991.

[30] Klüßendorf, F., “UAV navigation in GNSS-denied urban environments”, Technical University Braunschweig, 2006.

[31] Barny, H. (ed.), “Flight simulator test results on wake predictor”, FLYSAFE project deliverable D2.3.1-2, 2008.

5.2 Situational Awareness about Thunderstorms On-board an Aircraft

Thomas Gerz, Caroline Forster, Arnold Tafferner
Institute of Atmospheric Physics

Thunderstorms are top-ranked by pilots as weather situations compromising the flight safety. The information for pilots about adverse weather like thunderstorms today is, if at all, based on significant weather charts. Such services, however, do not give the required information for a particular flight in a particular circumstance because thunderstorms are relatively short-living phenomena. Information is required in the time-scale of up to about one hour with frequent updates clearly outlining the dangerous areas which should be avoided. Tools and products are descried which deliver that information tailored along the aircraft's trajectory. The information is produced on ground by weather expert systems and delivered to and stored in a ground-based weather processor which serves as a data base and interface between the expert system and the aircraft. Concepts and first tests are described where the information on thunderstorms is up-linked from the data base to the aircraft.

The FLYSAFE Project

The worldwide growing air traffic raises an unprecedented challenge for its safety. New tools have to be invented and implemented, in particular on-board aircraft, to maintain the current low level of accidents in aviation. In that perspective, 36 partners from industry, research centres, weather services, universities, and small and medium enterprises together with the European Commission in its 6th Research and Development Framework Programme launched and run the integrated project FLYSAFE from 2005 to 2009 (http://www.eu-flysafe.org/Project.html). The project focused on the areas identified as the main causes of accidents around the world: loss of control, controlled flight into terrain, approach and landing, and addressed three types of threats: traffic collision, ground collision, and adverse weather conditions. FLYSAFE developed new systems and functions, both on board and on ground, allowing the most comprehensive and accurate awareness of the aircraft safety situation during all phases of flight. These functions included situational awareness, advance warning, and new human-machine interface [Fabreguettes, 2010].

To raise the situational awareness of flight crews for atmospheric disturbances, weather expert systems for wake vortices, thunderstorms, in-flight icing and clear-air turbulence have been designed and developed, see Figure 1. In the project, DLR was responsible for the weather expert systems for aircraft wake vortices and thunderstorms. The expert system for thunderstorms provided forecasts on a local (TMA) scale, a regional (continental) scale (both derived from systems developed at Météo France and DLR), and a global scale (provided by output from the Unified Model of the UK Met Office). These scale products differ in terms of area covered, spatial resolution and time between updates. Moving from global via continental to local scale, they provide increasingly more high-resolution forecasts and at a faster rate, while reducing the area covered. According to their designation, the global product covers (nearly) the whole earth surface, the continental product covers an area such as that of Europe in this case, while the local (TMA) product is limited to roughly 100 km around an airport.

The products are delivered to a ground weather processor (developed by the UK Met Office) as thunderstorm bottom and top volumes (see below), representing a hazard in the airport vicinity or en-route, respectively. In case of a request by an aircraft the ground weather processor selects the product with the finest resolution and up-links relevant data for the flight corridor of the aircraft into the cockpit. The workflow is depicted in Figure 2. The functionality of delivering the products from the thunderstorm expert system to the weather data base and further on to the cockpit has been demonstrated during a FLYSAFE demonstration and validation effort, which included a full flight simulator and flight tests with an operational data link from ground to the test aircraft.

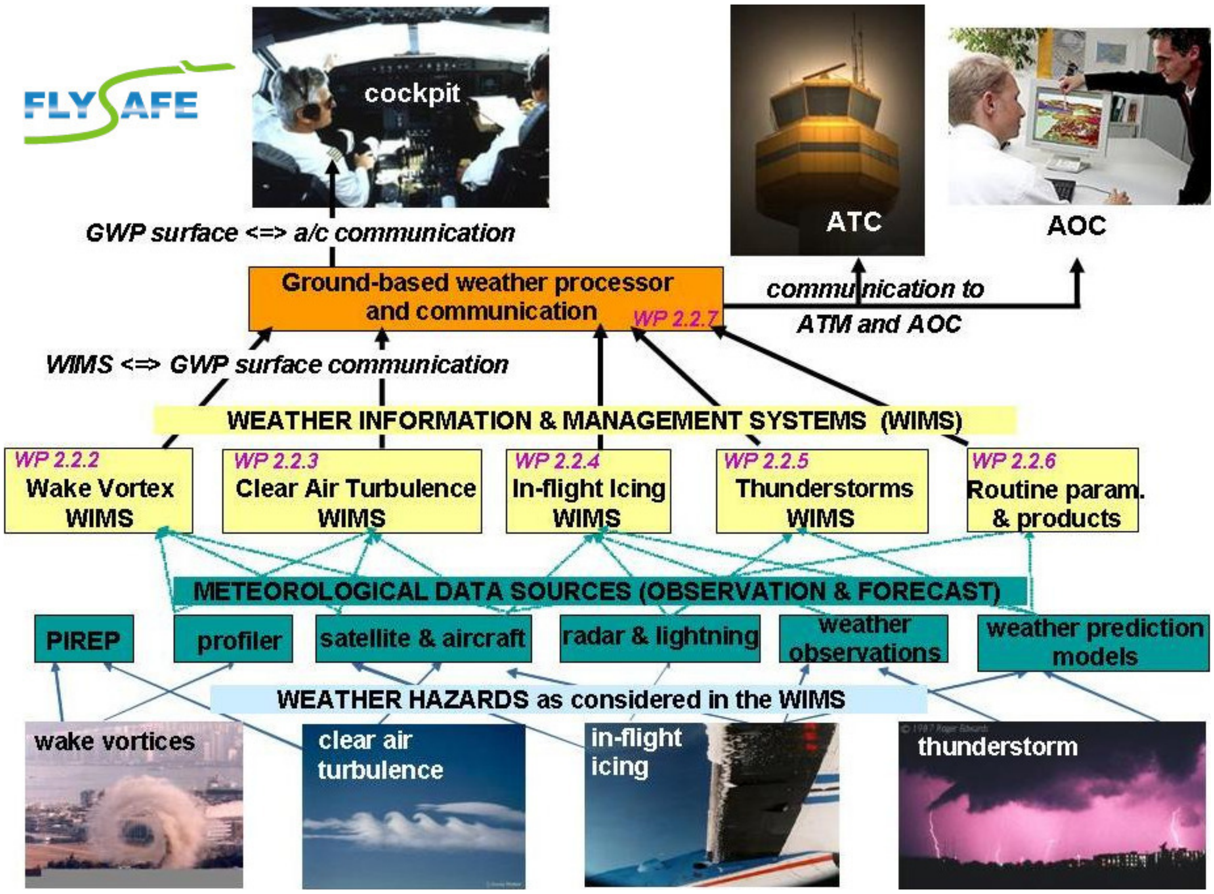

Figure 1. Provision of consistent, timely and tailored information on hazards like wake vortex, clear-air turbulence, in-flight icing and thunderstorm through ground-based weather expert systems, named WIMS, to the ground-based weather processor and communication platform from where the data are sent to cockpits as well as air traffic controllers (ATC), airline operating centres (AOC) and airports.

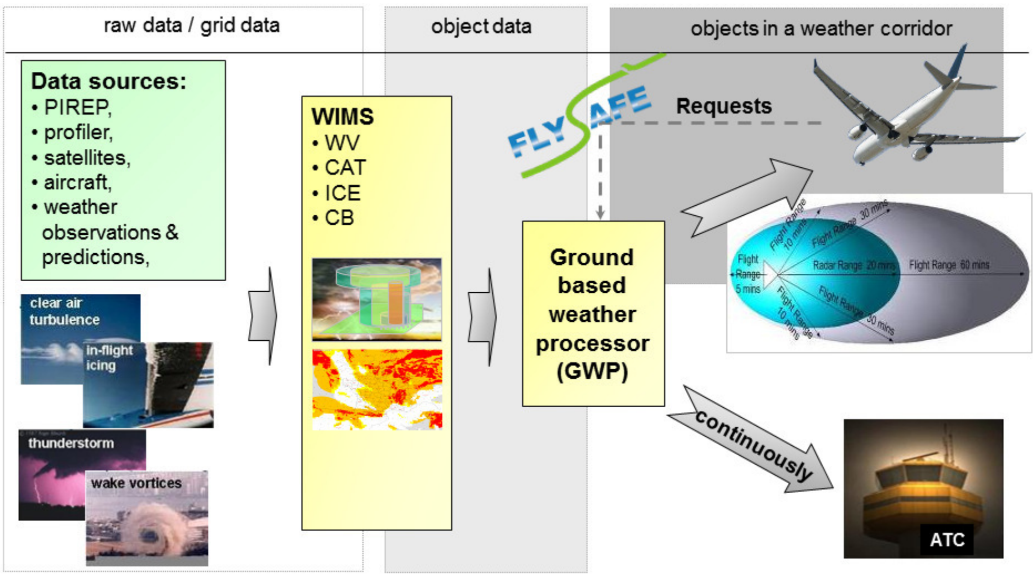

Figure 2. The workflow: Concatenating the weather data from various sources, producing simple products in the weather expert systems WIMS, transferring these products into a data base of the ground-based weather processor, and sending the relevant and tailored information to the aviation partners.

Reducing physical complexity to simple hazard areas

Thunderstorms can appear in various sizes from small convective cells to meso-scale convective systems and convective lines with corresponding life times from a few minutes to several hours. Remote sensing with satellite, radar, and lightning measurements gives detailed information on initiation, life cycle and dissipation of thunderstorms, but this detailed information is not very useful for air traffic controllers, airline dispatchers or pilots for decision making. Therefore, the strategy is not to describe thunderstorms to any observable detail, but reduce them to simplified weather objects representing the hazard levels “moderate” (avoid, if possible) and “severe” (no go area) for aircraft. This is the job of the weather expert system WIMS. Figure 3a shows a photo of a real thunderstorm with its idealized simplification as cylinder contours. The top volume represents the upper anvil part of the thunderstorm with the hazards turbulence and lightning; the bottom volume covers the hazards wind shear, heavy rain, hail, and lightning at mid-tropospheric and near ground levels. Outer and inner volumes indicate the hazard levels “moderate” and “severe”, respectively. The top volume can be identified by using the Cumulonimbus tracking and monitoring (Cb-TRAM) algorithm which is based on satellite data (see Section 2.3 and Forster et al. [2008]) in combination with lightning data [Betz et al. 2004]. Cb-TRAM detects and nowcasts the outer top volume, i.e. turbulent areas within the anvil, while the lightning density exceeding a certain threshold marks the inner severe part of the top volume. Bottom volumes describing two severity levels can be detected with the aid of radar data exceeding certain thresholds, e.g. 33 and 41 dBZ as has been used in the CONO software [Hering et al., 2005] by Météo-France during the FLYSAFE campaign [Tafferner et al., 2008, 2009, Pradier et al., 2009]. If polarimetric radar information and/or lightning data are available in addition, the detection of the severe part can be refined as regards to occurrence of hail and/or lightning. The horizontal shapes of the top and bottom volumes do not have to be circular or elliptical, but can be polygon shaped as indicated in Figure 3b which displays the top and bottom volumes as detected for a real situation. Note that the three smaller pillars are convective cells which have not yet produced the characteristic thunderstorm cloud anvil, therefore they appear without top volume.

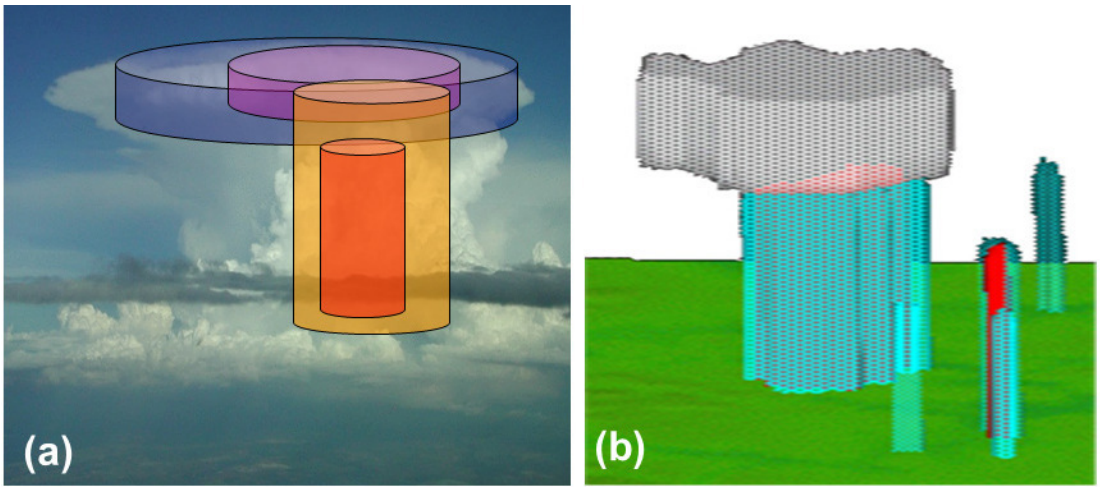

Figure 3. A thunderstorm rendered as a weather object with top and bottom volumes. (a) Photography of a thunderstorm with its idealized objects; (b) 3-dimensional view of objects as produced from a real thunderstorm by using detection algorithms based on satellite and radar data. Grey indicates top volumes, bluish colours indicate bottom volumes with level “severe” in red. Green is the ground surface.

Up-link of Data and Fusion with On-board Information

When the weather objects indicate and predict the hazardous volumes around thunderstorms simply and unambiguously, they are stored as ASCII files in standard XML format in a data base of the weather processor on ground. Upon request and depending on the flight trajectory of an aircraft, the weather processor takes the relevant XML coded objects for the flight corridor from the data base and transfers just those to the cockpit. This keeps data uplink costs to a minimum. In the cockpit the ground data can be displayed on electronic flights bags or fused with data from the on-board weather radar to get a comprehensive view of the situation. Figure 4 sketches that process of tailoring, up-linking, fusing and displaying.

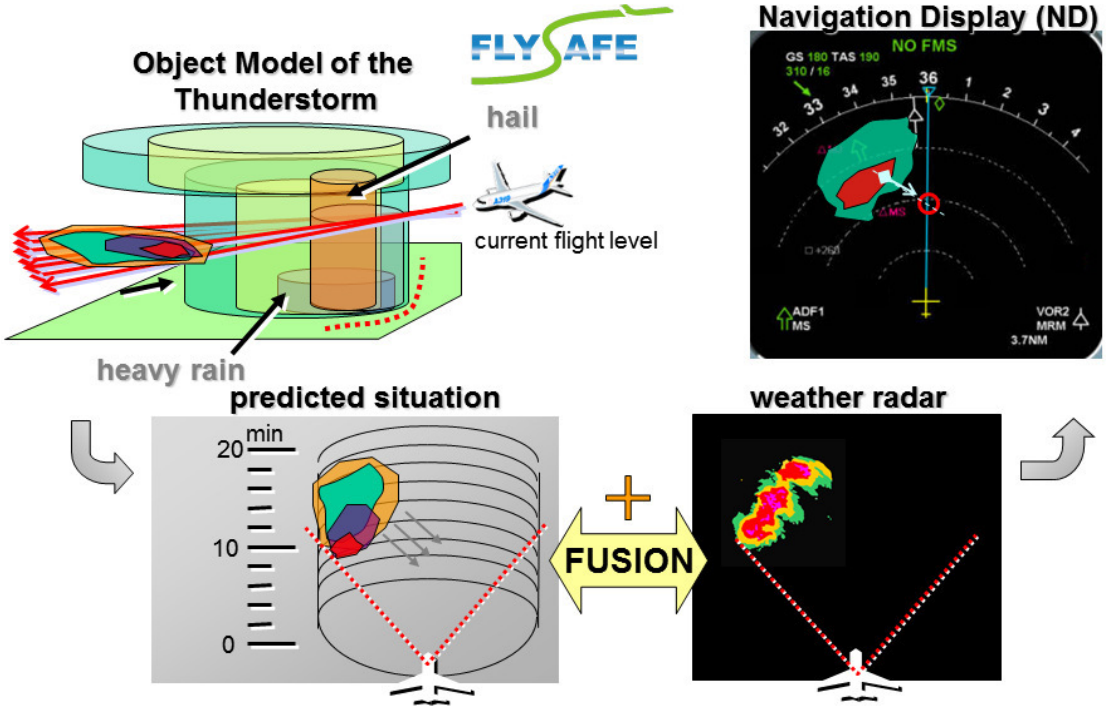

Figure 4. Sketch of the process of tailoring, up-linking, fusing and displaying the thunderstorm objects from the weather expert system on ground to the navigational display in the cockpit.

Analysis from the Flight Tests

During the flight trials we could demonstrate the functionality of the data up-link in real time. Data fusion or a common display with the on-board weather radar data could only be achieved *a-posteriori* when analysing the flights. Nevertheless, it could be shown that the delivered and up-linked objects compare well to the weather radar depiction on board the test aircraft. Most importantly, the ground data complete the picture of the weather hazard on board the aircraft as they survey a much larger area than the on-board radar and combine data from several observational sources.

How the situational awareness of the pilots could be significantly enhanced is outlined in Figure 5. It shows snapshots of the radar display recorded during a test flight over south-easterly France on 19th of August 2008 in a 10 min sequence [Sénési et al., 2009]. Objects from Cb-TRAM and the heavy precipitation cells for two different precipitation intensities are indicated as coloured contours. The spatial distribution of the thunderstorm objects agrees well with what the on-board radar sees on the right side of the intended flight track near the 50 nautical miles range circle (Figure 5 a). However, beyond that range, the on-board radar sees much less reflectivity although the expert system indicates additional thunderstorm activity (blue circle in Figure 5 a); and even a third cell is indicated by the objects beyond the 100 nautical miles range circle (red rectangle). Both cells cannot be seen by the radar at 14:05 UTC because the radar beam is attenuated by the first and closest cell and 100 nautical miles is about the detectable distance of that radar. After 10 and 20 minutes, though, these cells indicated by the objects already at 14:05 get confirmed by the on-board radar as the flight continues (Figure 5 b/c at 14:15 / 14:25 UTC, respectively). Note that the radar returns on the left side of the intended flight track (red circle in Figure 5 a) are not corroborated by the expert system. Figure 5 d reveals that these returns are not from thunderstorm activity but stem from the reflecting ground of the mountain region (so-called ground clutter).

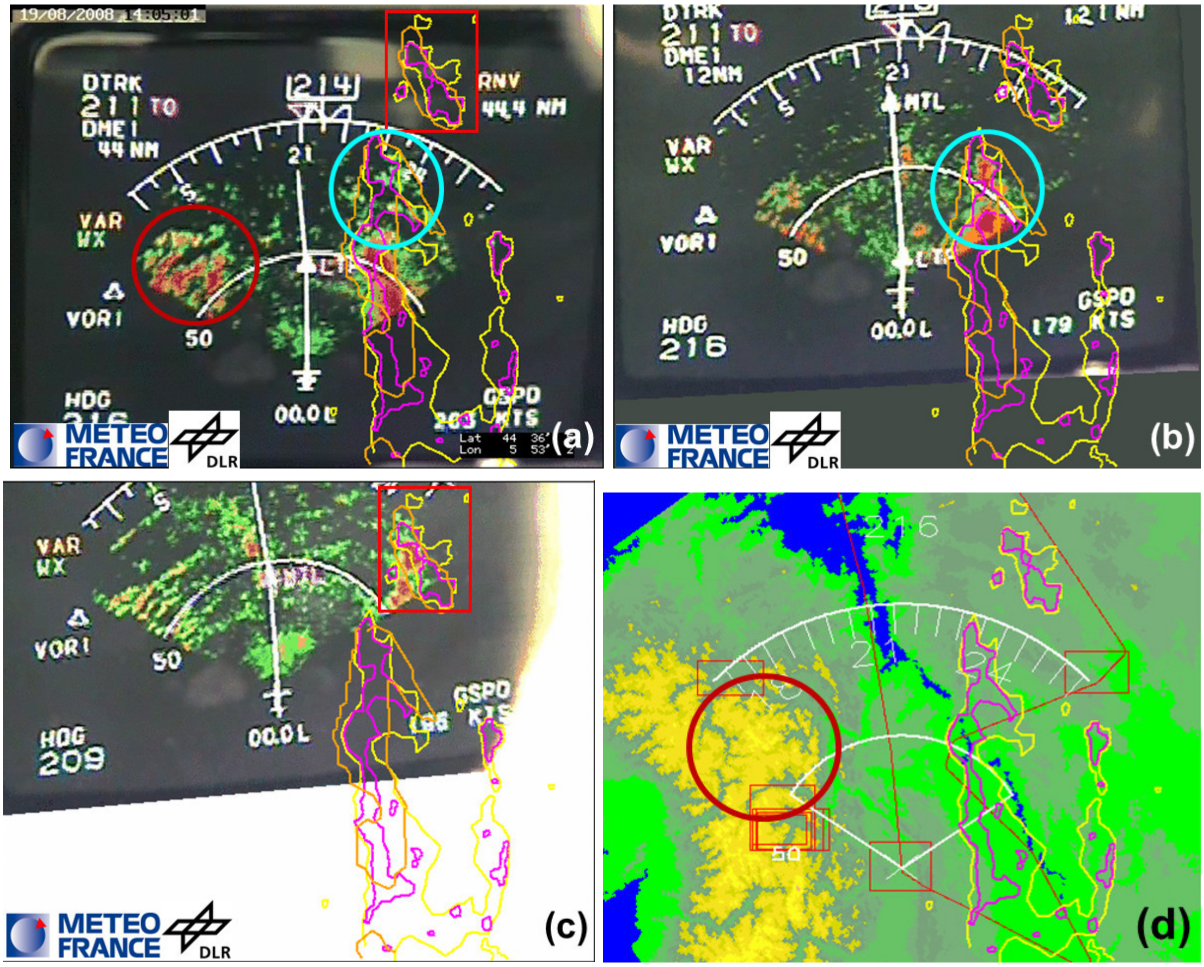

Figure 5. On-board weather radar images on 19th of August 2008 at (a) 14:05, (b) 14:15 and (c) 14:25 UTC with superimposed weather object contours from the ground system. Orange contours indicate Cb-TRAM objects, yellow and pink contours indicate heavy precipitation cells for two different intensities representing moderate and severe precipitation. (d) ground map of the flight area showing a mountain region in yellow.

Lacking Proper Weather Information in a Safety Critical Case

On Sunday 31 May 2009 at 22:29 UTC (19:29 Rio time), the Airbus A330-200 registered F-GZCP, operated by Air France under flight number AF447, took off from Rio de Janeiro Galeão airport bound for Paris Charles de Gaulle. The airplane was carrying 216 passengers of 32 nationalities as well as 12 crew members. Around 3 hours 45 minutes after take-off, the airplane crashed into the Atlantic Ocean about 435 nautical miles north-north-east of Fernando de Noronha Island, in the middle of the night and without any emergency message being sent. The last contact between the airplane and Brazilian Air Traffic Control (ATC) had been made around 35 minutes previously [BEA, Dec. 2009].

Soon after the accident a detailed meteorological analysis was presented by Vasquez [2009] on the internet. Whatever the reason for the crash finally was, the flight definitely crossed through a thunderstorm complex. Figure 6 shows the convective situation over the Atlantic at four different times from the satellite cloud analysis [Tafferner et al. 2010]. Red contours mark the convective updrafts as detected by Cb-TRAM. The flight track is indicated by a white line combining the way points INTOL and TASIL. The convective cloud feature which is traversed by the flight route is seen to grow remarkably from 0 to

01:30 UTC. At that time when the aircraft reported waypoint INTOL to air traffic control an approximate radar range of 80 nautical miles is drawn as a yellow circle around the aircraft. This is to demonstrate that at this time the pilots could not foresee the strong convective activity on their future track from the on-board radar signal returns (also a longer-range radar would not change the situation).

Also, just from looking out of the window it was probably impossible for them to recognise the thunderstorm complexes in the far distance due to the darkness at night. Furthermore, there are no lightning discharges observed from the networks for this region at this time (noted by Vasquez' report) which could have warned the pilots. Half an hour later, at 02:00 UTC, when the aircraft was close to the major convective complex (Figure 6 c), the on-board radar should have detected the cells, but now indicating convective activity almost everywhere in front of the aircraft which makes it difficult for the pilot to decide whether to penetrate the system or to go around and in which direction. This is complicated by the fact that the on-board radar signal is strongly attenuated by precipitation, due to its short wave length of 3 cm (as compared to ground based radars) with the effect not being able to render the real extension of the storm. In this case the pilots obviously chose to go through the convective complex. Figure 6 d shows the aircraft in its last known position when it had almost crossed the major storm cell at 02:10 UTC.

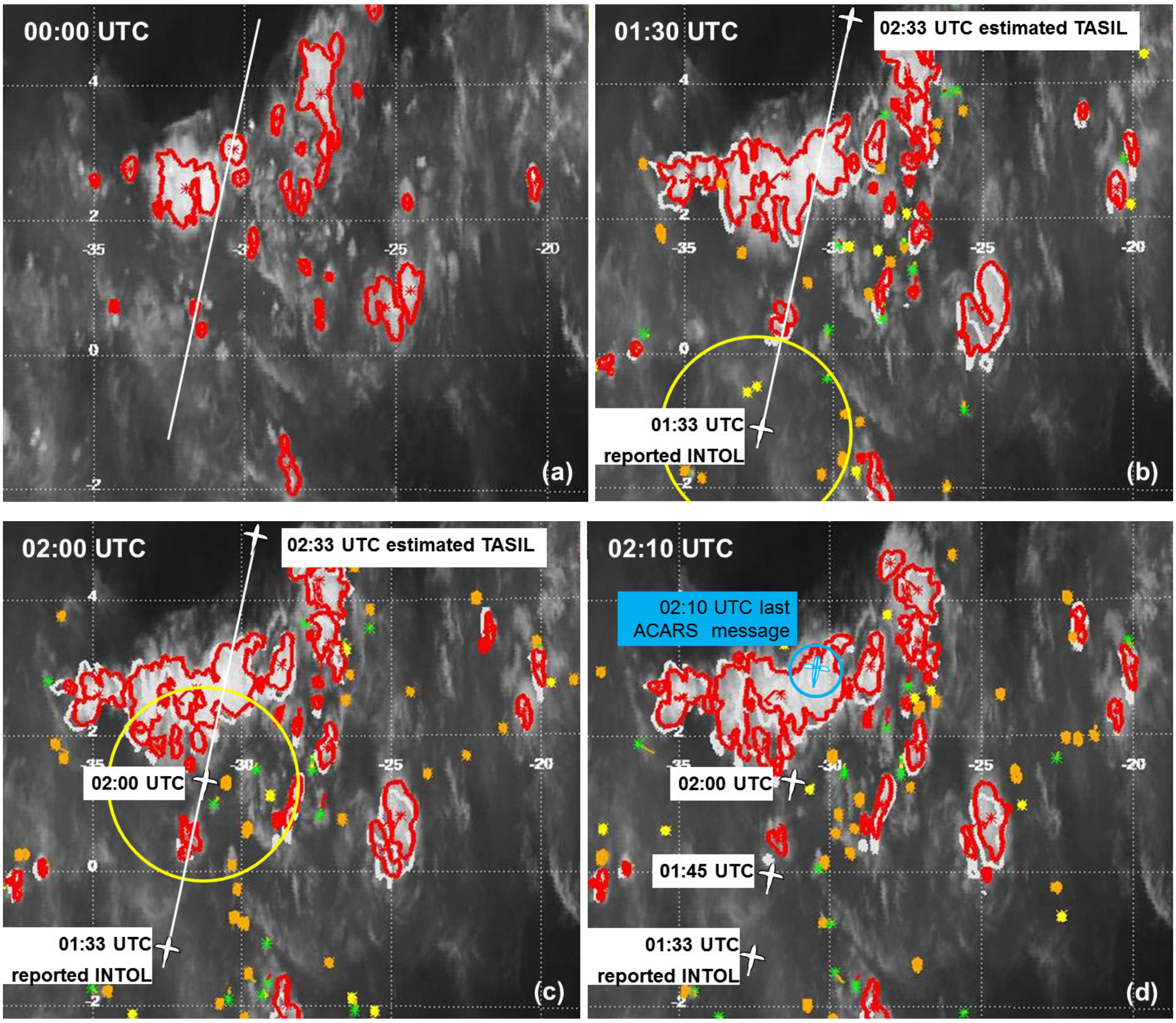

Figure 6. Meteosat infrared images over the Atlantic east of Brasil together with convective clusters (red contours) as identified from the Cb-TRAM cloud analysis on 1 June 2009 at four different time instants. Also marked is the flight route between the way points INTOL and TASIL. The yellow circle indicates a radar range of about 80nm. Yellow, orange and green little patches mark initial developments not relevant for this analysis and not discussed.

What can and what cannot be seen on the on-board radar deserves more attention, especially for aircraft flying through tropical convective complexes at high altitudes. From an investigation undertaken by Air France [Flightglobal, 2009] it looks like that the setting of the sensitivity, i.e. the gain switch, has a great influence on what is seen on the navigational display. In that report it is stated: "Several other flights - ahead of, and trailing, AF447 at about the same altitude - altered course to avoid cloud masses. Those included another Air France A330 operating the AF459 service from Sao Paulo to Paris. That crew crossed a turbulent area that had not been detected on weather radar and, as a result, increased the sensitivity - subsequently avoiding a "much worse" area of turbulence." And further in the report it is noted that: "France's Bureau d'Enquetes et d'Analyses says the crew of AF459, which had been 37 min behind AF447, detected echoes on the weather radar which 'differed significantly' depending on the radar setting."

It is also known that often aircraft fly through these storms without any problems. Obviously, it is not only the mere presence and location of these storms that is relevant but also their evolution; whether they are growing in size or depth, their movement and possibly more elaborate attitudes like height, precipitation rate and type, lightning activity and turbulence level.

However, regardless whether strong or weak returns can be seen on the navigational display, the sequence of satellite images and object contours in Figure 6 elucidates that the information from ground-based weather expert systems is able to represent the real situation about the convective activity and that this information, when brought to the cockpit, would help pilots in making decisions. Ideally, an alternative route in a given situation would be proposed by the integrated surveillance system on board the aircraft, as was demonstrated in the FLYSAFE project. Such a surveillance system would propose a detour to the flight crew after considering all aspects of the flight and the airspace as fuel capacity and consumption, other traffic or further hazards.

Next steps

Currently incorporation of weather information into avionics systems is still within the domain of research and development, and many hurdles will need to be overcome before such systems are considered to be a part of the primary systems. Some of the hurdles are not related to the technology but more related to institutional issues, such as certification, quality management and legal, etc. However, today it is noted that there is an increasing trend in the use of electronic flight bags which are preloaded with weather information. For aircraft used for passenger transport, cabin internet services become more and more available. Thus, it is not beyond the realms of possibility to foresee weather information being uplinked via the cabin internet services then subsequently routed to an electronic flight bag. However, until primary systems are in place, services for weather information would have to be regarded as advisory.

On a European level research and development are underway in the ESA-co-funded project planet2 for a certified airborne collaborative network to exchange real-time atmospheric data and meteorological conditions from/to business and regional aircraft. The goal is to get in-flight information updates on weather conditions and hazards, and at the same time, to contribute to the global weather observations by providing complementary atmospheric measurements to the existing Aircraft Meteorological Data Relay system. The European Commission is co-funding the project ALICIA to develop new cockpit information systems applicable to multiple types of aircraft and helicopters and enabling robust worldwide operations in all weather conditions.

Acknowledgements

The work presented here was funded by the DLR project Wetter & Fliegen (2008 - 2011) and the EU project FLYSAFE (2005 - 2009).

References

BEA, Dec. 2009: Update on the Investigation into the Accident to flight AF 447 on 1st June 2009. Bureau d'Enquêtes et d'Analyses (BEA) pour la Sécurité de l'Aviation.

Betz, H.-D., Schmidt, K., Oettinger, W. P., and Wirz, M. 2004: Lightning detection with 3D-discrimination of intracloud and cloud-to-ground discharges, Geophys. Res. Lett., 31, L11108, doi:10.1029/2004GL019821.

Fabreguettes M. 2010: FLYSAFE final publishable report, D6.7-3 Public, FLY_673THA_PUB_A, 97 pp. See also http://www.eu-flysafe.org/EU-Flysafe_Public/Download/Forums/Final-Forum.html.

Flightglobal, Kaminski-Morrow, 2009: Air France reviewing weather-radar use after AF447 crash: http://www.flightglobal.com/articles/2009/07/09/329492/air-france-reviewing-

Forster, C., A. Tafferner, C. Keil, T. Zinner, 2008, Validation of severe weather forecasts based on synthetic satellite data as part of an integrated thunderstorm forecast system for air traffic, Proceedings of the EUMETSAT Meteorological Satellite Conference, Darmstadt, Germany 8 - 12 September 2008, EUMETSAT P. 52, ISBN 978-92-9110-082-8, ISSN 1011-3932, 8 pages.

Hering, A, S. Sénési, P. Ambrosetti, and I. Bernard-Bouissières 2005. Nowcasting thunderstorms in complex cases using radar data. WMO Symposium on Nowcasting and Very Short Range Forecasting, Toulouse, France.

Pradier, S., C. Forster, W. W. M. Heesbeen, C. Pagé, S. Sénési, A.Tafferner, I. Bernard-Bouissières, O. Caumont, A. Drouin, V. Ducroq, Y. Guillou, P. Josse, 2009: Description of convective-scale numerical weather simulation use in a flight simulator within the Flysafe project, Meteorology and Atmospheric Physics, doi:10.1007/s00703-008-0317-4

Sénési, S., Y. Guillou, A. Tafferner, and C. Forster, 2009: Cb nowcasting in FLYSAFE: Improving flight safety regarding thunder-storm hazards. WMO Symposium on Nowcasting, 30 August - 4 September 2009 , Whistler, B.C., Canada

Tafferner A., Forster C., Senesi S, Guillou Y., Laroche P., Delannoy A., Lunnon B., Turb D., Hauf T., Markovic D., 2008: Nowcast-ing thunderstorm hazards for flight operations: the Cb WIMS approach in FLYSAFE, Proceedings of the 26th International Con-gress of the Aeronautical Sciences (ICAS), Anchorage, Alaska, 14 -19 September 2008.

Tafferner, A., C. Forster , Y. Guillou, S. Sénési, Nowcasting thunderstorm hazards for flight operations: the CB WIMS approach in FLYSAFE, Prodeedings of the European Air and Space Conference (CEAS), Manchester, UK, 26 - 29 October 2009.

Tafferner, A., C. Forster , M. Hagen, T. Hauf, B. Lunnon, A. Mirza, Y. Guillou, T. Zinner, 2010: Improved thunderstorm weather information for pilots through ground and satellite based observing systems, 14th conference on Aviation, Range, and Aerospace Meteorology (ARAM), 90th AMS Annual Meeting, Atlanta, 17-21 January 2010.

Vasquez, T., 2009: Air France Flight 447: A detailed meteorological analysis.http://www.weathergraphics.com/tim/af447/<

5.3 Air Traffic Operational Concept for Mitigating the Impact of Thunderstorms

Vilmar Mollwitz
Institute of Flight Guidance

An operational concept has been developed that uses digital thunderstorm nowcast to mitigate the impact of thunderstorms on arrival traffic at an airport. By uplinking thunderstorm nowcast to the Flight Management Computer of an aircraft, the on-board computer is enabled to find the shortest possible route around the nowcasted thunderstorms to the arrival runway. This route is negotiated via datalink with Air Traffic Control leading to reduced workload for the involved controllers and pilots as well as shorter, more fuel-efficient routes.

Introduction

From a flight guidance perspective it was the aim to develop an air traffic operational concept for mitigating thunderstorms, taking into account the new available information on these events (see Section 2.3). Currently thunderstorms are avoided on a tactical basis only, reacting when the disruption occurs already. Air traffic controllers see a picture of the current thunderstorms on their radar screen and try to lead aircraft around those areas. Most aircraft certified for instrument flight and thus being controlled by an air traffic controller have an on-board radar. This radar scans the environment in front of the aircraft and shows thunderstorms on a dedicated display in the cockpit to the pilots. From what the pilots see out of their window (at least in daytime) and from what is depicted on their radar display, the pilots decide which way around thunderstorms they want to take. If a pilot's idea of how to avoid a particular thunderstorm and the controller's idea of how to lead that particular aircraft around this particular thunderstorm do not agree, the pilot and controller decide together on the way of the aircraft around the thunderstorm via radio communication. Because one controller usually handles several aircraft at once all wishing to avoid thunderstorms, a day with thunderstorms at a certain airport usually leads to much more workload both for the pilots as well as the controller compared to a clear and sunny day.

Part of the work in Wetter & Fliegen was the development of a tool for thunderstorm nowcasting that provides thunderstorm information up to one hour as a digital file (see below). This digital information can be made available to the controller as well as via a datalink to the pilots in the cockpit. It was assumed in this work, that a datalink capable of continually uplinking new thunderstorm nowcasts with the necessary bandwith and reliability exists. Uplinking the thunderstorm nowcast to the cockpit has two main advantages: By bringing the whole relevant picture to the cockpit, the pilots could for the first time see on their cockpit displays also thunderstorms that lie on their route but are currently blocked by another thunderstorm in front of the particular thunderstorm. Those thunderstorms behind yet another can today not be observed from the cockpit by looking out of the front window or on the on-board radar display. With this new information a more strategical avoidance of thunderstorms is enabled. The second advantage of uplinked digital thunderstorm nowcast information in the cockpit is that it can be feeded into the Flight Management System (FMS). The FMS purpose is to guide the aircraft by coupling to the autopilot along the most efficient trajectory. For this the FMS constantly receives information from different sources, e.g. GPS, altimeter etc. and compares them to a planned flight trajectory. With the information about thunderstorms around the aircraft within the next hour, the FMS is enabled to find the most efficient route and thus trajectory around the thunderstorms standing in the way to the destination.

A concept for an efficient way to organise the arrival traffic at an airport impacted by thunderstorms in the vicinity has been developed. Not only efficient trajectories have to be found for just one aircraft, but for all aircraft approaching the airport as well as trajectories that do not lead to conflicts between different aircraft. For this purpose it is also helpful that the information contained in the thunderstorm nowcast is identical to both all pilots approaching the airport as well as to the controller.

Operational Concept

An aircraft receives the current thunderstorm nowcast from the ground-based weather processor and data base (Figure 1, see also the previous Section 5.2). Assumed one or several thunderstorms are forecasted to block the intended route of the aircraft, the on-board tool as a new part of the FMS calculates a trajectory that avoids the thunderstorm(s). This route is the shortest route around all thunderstorms and thus the calculated arrival time at the airport is the earliest possible for this aircraft as it is assumed that each aircraft calculates its trajectory with the highest possible airspeed. The new calculated arrival time is then sent to a ground tool keeping track of all planned arrival times of all aircraft intending to land at the airport. If that new calculated arrival time creates a conflict with the intended arrival time of another aircraft, the ground tool will send via datalink to the aircraft a requested arrival time. This time has been calculated by the ground tool to be free of any conflicts with other aircraft on the runway as well as be after the arrival time proposed by the aircraft as it is assumed that this was calculated with maximum speed and thus the aircraft is only able to arrive later by reducing its airspeed.

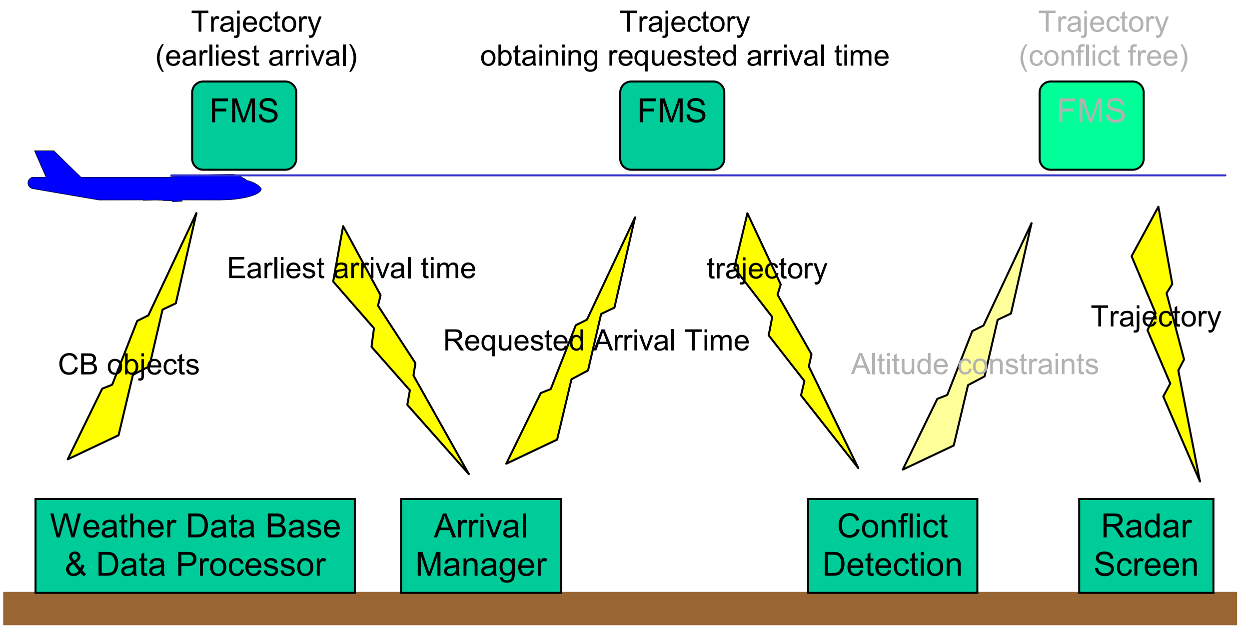

Figure 1. Trajectory negotiation between air traffic control and aircraft.

With this new requested and a bit delayed arrival time received, the FMS calculates yet another trajectory that avoids all thunderstorms but is also flown with a reduced airspeed in order to meet the requested time of arrival. This new trajectory is sent to another ground tool which checks the trajectory for conflict-freeness with any other aircraft on its way to the airport. This is necessary because the requested arrival time only assures conflict-freeness on the runway, but not on the way toward it. If a potential conflict is detected with another aircraft by the ground tool, it issues to the aircraft an altitude constraint, that is the aircraft has to fly the same route at the same speed as intended but has to fly at another (usually lower) altitude at the point of the potential conflict in order to avoid the other aircraft vertically. The FMS calculates yet another trajectory that also fulfils the altitude constraints and this trajectory is again sent to the ground so that the controller can see the trajectory the aircraft will fly on his radar screen for his information. In this way the trajectory avoids all thunderstorms laterally, avoids conflicts on the runway by time and speed control and avoids other traffic on its way to the runway vertically. Of course the route also takes care of restricted areas, terrain, etc.

So far this concept has only been described to work with aircraft equipped with a datalink and an FMS capable of thunderstorm avoidance trajectory calculations. The concept can work with aircraft without this equipment as well. Today only a part of the airline fleets are equipped with a datalink, the tool to avoid thunderstorms does not exist in any commercial airliner yet. If the thunderstorm nowcast can not be uplinked to an aircraft because it lacks a datalink, the thunderstorm information is still available to the controller for information on the ground. The same tool that calculates trajectories avoiding thunderstorms on board could run on a PC at air traffic control. Thus the calculation of a thunderstorms avoiding trajectory could also be conducted on the ground according to the same rules as for on-board calculations. This information is then presented to the controller who uses it as a suggestion to lead the aircraft efficiently around the thunderstorms to the runway. This will even work in a mixed environment, where some aircraft are equipped with datalink and the appropriate FMS functionalities and some are not. All equipped aircraft create their own trajectory and negotiate it with the ground as described above. The agreed trajectory is made visible on the controllers radar screen. For all unequipped aircraft a trajectory is created on the ground and made visible to the controller on its radar screen as well. The controller then uses the trajectories of the equipped aircraft as information of the aircraft's intent and future flight path, while the trajectories of the unequipped aircraft calculated by a ground tool are used as a suggestion to lead the aircraft around thunderstorms but also to avoid conflicts with other aircraft since all trajectories are delivered as conflict-free from the tools.

Validation

The operational concept explained above was validated and compared against todays operations. In summer 2010 a campaign was conducted at Munich Airport by the Institute of Physics of the Atmosphere validating their tools for thunderstorm nowcasting. During that campaign, traffic data was collected by the German ANSP (DFS) on two days for three consecutive hours in identified times in which thunderstorms played a role in the terminal area, i.e. for the traffic landing at Munich. During these identified hours, the position and altitude along with the aircraft type of all aircraft bound for Munich was collected from when the aircraft entered the terminal area until touchdown on the runway. The thunderstorm data of the same time frame as the traffic data was collected by the thunderstorm nowcasting tool. At DLR Institute of Flight Guidance, a traffic scenario was created for its tool TrafficSim based on the traffic data provided by DFS. In this simulation, all aircraft where set to appear in the scenario at exactly the same time, position and altitude as in the traffic sample. From there, a trajectory was calculated by the tools developed by DLR Institute of Flight Guidance according to the operational concept described above.

The trajectory avoided all thunderstorms that were provided as a replay from the thunderstorm nowcasting tool, it avoided conflicts on the runway by speed control and conflicts on the way to the runway vertically. Thus for each aircraft that landed at Munich airport during thunderstorm activity in the vicinity of Munich, both a real trajectory actually flown in the real world existed as a data file as well as a simulated trajectory calculated by TrafficSim. Both trajectories started at the same point and time and ended at the same point while avoiding the same thunderstorms. These trajectories for all and each aircraft were then compared to obtain the benefit of the concept. Figure 2 shows the time and fuel gained on the average over all simulated flights compared to its real-world counterpart for the traffic sample of 2nd and 12th of August 2010.

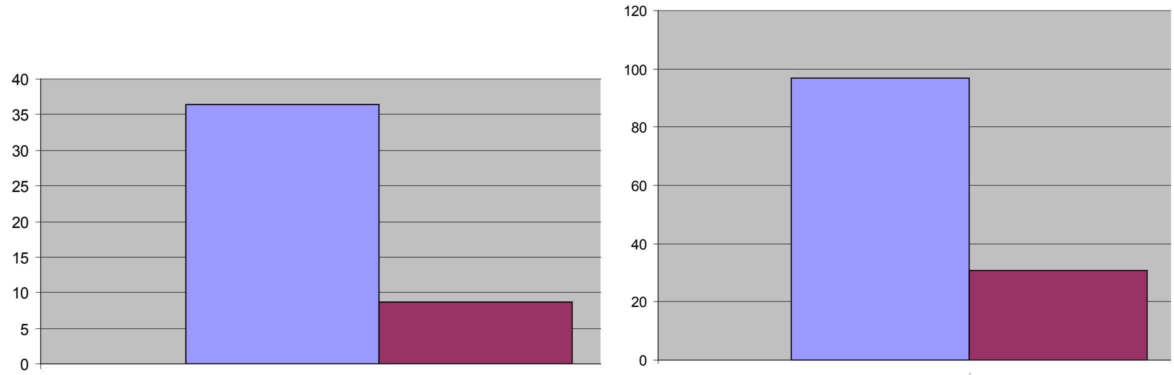

Figure 2. Time (blue in s) and fuel (red in kg) savings traffic samples for 2nd (left) and 12th of August 2010 (right).

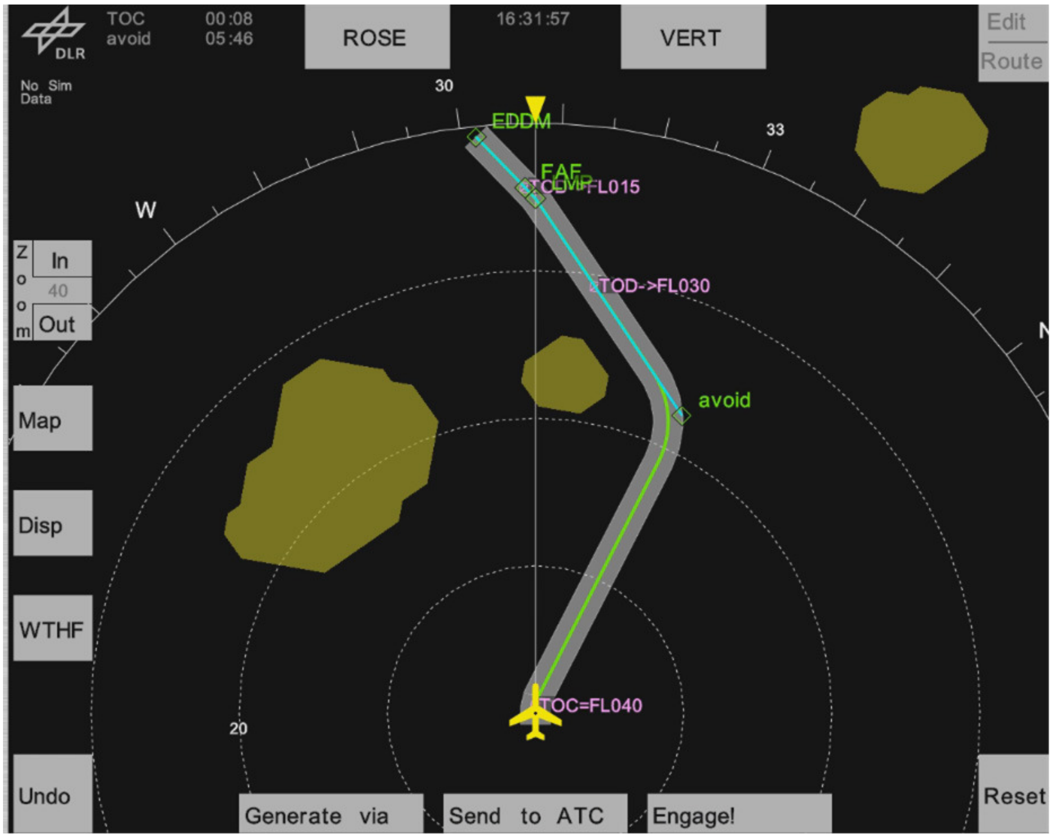

Figure 3. View of the Navigation Display with thunderstorms and indicated evasive route

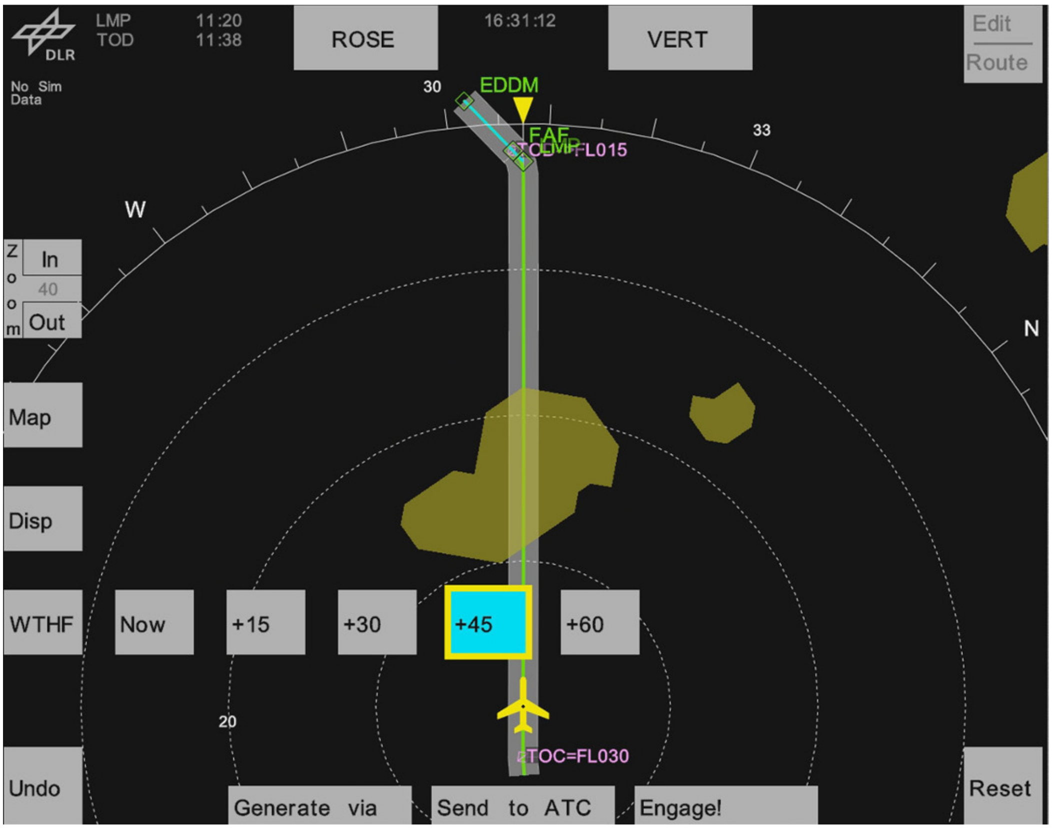

Figure 4. View of the Navigation Display with thunderstorms forecasted 45 minutes ahead of time

This shows that the concept has a clear advantage compared to nowadays operations without tool assistance by an up-linked thunderstorm nowcast object and new FMS functionalities. It has to be stated though that the traffic simulation made some simplifying assumptions that are not met in real life. Departing traffic, which crosses the routes of the arriving traffic was not simulated. In real life, arriving and departing traffic is separated laterally to avoid conflicts which of course create detours for both the arriving and departing traffic. Without departure traffic simulated, those detours did not take place which gave the simulation a little unfair advantage. Also areas of flight restrictions were not considered in the simulations. Therefore the numbers obtained for the benefit of the concept are not perfectly accurate. Nevertheless, these numbers show that the concept is quite promising and shall be further developed to include departures, restricted areas and even more real-world constraints.

The Navigation Display

The thunderstorm nowcast objects (see Sections 2.2, 2.3, and 5.2) were used to enhance the depiction of thunderstorms on board an aircraft as well as to facilitate the routing around thunderstorms by the flight crew in the Navigation Display of DLR Institute of Flight Guidance. The thunderstorm nowcast object is uploaded via datalink to the aircraft every time a new nowcast is provided, usually every 5 to 15 minutes. The natural place to depict these data is on the Navigation Display or the Electronic Flight Bag (Section 5.2). The Navigation Display (Figure 3) shows the route of an aircraft from above (2D) along with waypoints and any additional information the pilot selects to be displayed on this moving map like airports, other aircraft in the vicinity etc.

The Navigation Display also depicts the information from the on-board weather radar. The big disadvantage of the on-board radar is that its range is limited and it can not detect thunderstorms that lie behind another thunderstorm as seen from the radar antenna. With uplinked thunderstorm nowcast objects this information can also be made available on the pilots' displays. Thunderstorms are displayed as yellow areas on the Navigation Display (Figure 3). Here, the on-board tool has already found a route around the thunderstorms to the runway. The aircraft will soon turn to the right to follow the evasive route. On Figure 4 the pilot has selected to display the thunderstorm situation forecasted for 45 minutes ahead of the time the current nowcast has been issued. The different situations at different times can be selected by simply pushing the WTHF button on the touchscreen Navigation Display and then selecting the time ahead to be displayed by clicking the appropriate button.

Conclusions and Outlook

The developed operational concept and the new on-board tools to find routes around thunderstorms are very helpful for pilots and controllers and show a clear advantage in fuel and time savings compared to current operations. The concept has only been validated in a simplified environment compared to current operations. Further development and validation of the concept and innovative tools, especially regarding more real-world constraints like areas of flight restrictions, additional traffic (departing and crossing) etc. are currently conducted in the follow-up DLR project flexiGuide.

Acknowledgements

We thank the German Air Service Provider DFS for providing us with the anonymised traffic data of two sample days with thunderstorms at the Munich Airport that allowed us to validate our concept against real-world data. DFS provided us these data free of charge to support aviation research and DFS' staff was very helpful to us in interpreting the provided data.

6. Wake Vortex Physics and Encounter Consequences

6.1 Wake-Vortex Topology, Circulation, and Turbulent Exchange Processes

Frank Holzäpfel, Takashi Misaka, Ingo Hennemann
Institute of Atmospheric Physics

Large eddy simulations (LES) of aircraft wake vortex evolution in various turbulent and stably stratified atmospheric environments have been conducted with two different LES codes. Passive tracers are used to investigate exchange processes between the vortex cores, the vortex oval and its environment as well as redistribution processes along the vortex tubes. A post processing method is employed to identify the vortex center lines even in progressed states of vortex decay where the coherent vortex structure is getting lost. This method allows, for example, analyzing the circulation evolution of vortex rings, establishing statistics of vortex deformation, and revealing the mechanisms of the vortex bursting phenomenon. Vortex bursting is related to the collision of secondary vorticity structures propagating along the vortex lines. In neutrally and weakly stratified environments long-living vortex rings are observed where circulation decay proceeds in three phases. During the initial diffusion phase vortex decay may depend on integral turbulence length scales. On average, the detrainment of a passive tracer from the primary vortices is correlated with circulation decay.

Introduction

The comprehensive and detailed understanding of wake vortex behavior is crucial for the development of wake vortex systems that aim at increasing the awareness of wake vortex risks or tend to increase airport capacity. The first part of this paper focuses on aspects of the development of vortex topology and circulation decay that may both be relevant for the severity of potential vortex encounters. Another topic is the turbulent mixing and detrainment of the ice crystals generated from the exhaust jets. Their dispersion during the vortex descent is an important parameter in order to quantify the vertical extent, optical thickness, and lifetime of the contrails produced during cruise. Currently, it is not yet clear how strong the contribution of contrails to global warming might be (Schumann 2011).

It turns out that both topics are complementary allowing an improved understanding of wake vortex physics. In particular, two issues raised by Spalart (1998) in his Annual Review of Fluid Mechanics are picked up: (i) the controversial concepts of “predictable decay” and “stochastic collapse.” Here it is found that depending on the environmental conditions circulation decay characteristics may either feature two-phase or three-phase behavior or continuous decay. (ii) The mechanisms leading to the vortex bursting phenomenon. Here the analysis indicates that collisions of secondary vorticity structures propagating along the vortex lines lead to local spreading of tracers which is not connected to local vortex decay.

From lidar observations it is known that wake vortices may frequently live much longer than anticipated by the aircraft separations that have to be obeyed during approach and landing or during departures. One reason why the procedures are safe nevertheless certainly is related to the transport of the vortices away from the flight corridor by crosswind and vortex descent. Another potential reason is the fact that the vortices do not remain straight but are rapidly deformed by the relatively strong turbulence prevailing in the atmospheric boundary layer. The deformation of vortex segments may reduce the impact time of adverse forces and moments experienced by an encountering aircraft and thus may alleviate the severity of the encounter.

In order to establish statistics of vortex deformation in terms of curvature radii a post processing method is employed to identify the vortex center lines even in progressed states of vortex decay where the coherent vortex structure is getting lost. Moreover, this method allows investigating circulation decay characteristics depending on eddy dissipation rate, integral turbulence length scales, and temperature stratification in greater detail.

Further, the turbulent exchange processes between the descending vortex oval and its environment are investigated. For this purpose we track the mixing and detrainment of a passive tracer for various initial tracer distributions within the vortex pair and for different environmental conditions.

This report is based on AIAA Paper 2010-7992 by Holzäpfel et al. (2010). More detailed descriptions and results concerning the LES code LESTUF, the vortex core tracking method, vortex decay and descent characteristics, the impact of turbulence length scales, vortex topology, and validation of the LES can be found in Hennemann and Holzäpfel (2011). Additional detailed descriptions of the LES code MGLET, vortex decay, descent, and topology, the phenomenon vortex bursting, the generation of vortex funnels, as well as turbulent exchange and detrainment processes can be found in Misaka et al. (2011).

Numerical Methods and Initial Conditions

We have conducted Large Eddy Simulations (LES) of wake vortex evolution in environments with various degrees of atmospheric turbulence and stable temperature stratification employing two different LES codes. The numerical features of the first LES code LESTUF are described in detail in Kaltenbach et al. (1994). LESTUF solves the Boussinesq-approximated Navier-Stokes equations in staggered and Cartesian coordinates with a finite differences method of second order accuracy (central finite differences in space and Adams-Bashforth scheme in time). A modification of the Smagorinsky subgrid scale closure (Holzäpfel 2004) reduces wake vortex core growth rates.

The second LES code MGLET (Manhart 2001) also solves the Boussinesq-approximated Navier-Stokes equations discretized by a finite-volume zonal-grid method with non-equidistant staggered variable arrangement. A fourth-order compact scheme is used for the implicit spatial interpolation and differentiation of variables by solving a tri-diagonal system which can achieve spectral-like resolution (Hokpunna & Manhart 2010). The third-order Runge-Kutta method is used for time integration. The pressure field is calculated iteratively employing the HSMAC (Highly Simplified Marker-And-Cell) method in order to reduce the divergence of the velocity field below a prescribed threshold value. Equations for passive scalars have been implemented for investigations of turbulent mixing. Parallel computation is realized by a domain decomposition approach. The Lagrangian dynamic subgrid scale model (Meneveau et al. 1996) accounts for reduced turbulent mixing in the centrifugally stable vortex core regions.

Domain sizes of $L_x \times L_y \times L_z = 400 \times 256 \times 256\ m^3$ have been applied for LESTUF and of $400 \times 384 \times 512\ m^3$ for MGLET with a uniform grid of 1 m, where x denotes flight direction, y spanwise direction, and z vertical direction. Periodic boundaries are employed in all directions. The trailing vortices of an A340-300 aircraft are represented by two counter-rotating Lamb-Oseen vortices with a vortex separation of $b_0 = 47.1$ m and a vortex core radius of $r_c = 3$ m. LESTUF simulates an aircraft during approach with an initial root circulation of $\Gamma_0 = 458$ m²/s whereas MGLET employs a slightly higher value of $\Gamma_0 = 530$ m²/s to represent cruise conditions. In order to account for jet and boundary layer turbulence entrained into the vortices during vortex roll-up an additional rms velocity with a maximum of 2 m/s is added in the vortex core radius vicinity.

The employed combinations of environmental parameters are listed in Table 1. The intensity of atmospheric turbulence is expressed in terms of normalized eddy dissipation rates $\varepsilon^* = (\varepsilon\ b0)^{1/3}/w_0$ and the stable temperature stratification in terms of normalized Brunt-Väisälä frequencies $N^* = t_0\ (g/\theta_0\ d\theta/dz)^{1/2}$. In these equations $w_0 = \Gamma_0 /(2\pi\ b_0)$ corresponds to the initial wake vortex descent speed, $t_0 = 2\pi\ b_0^2 /\Gamma_0$ to the time scale of the vortex pair, and θ to the potential temperature of the atmosphere. Prior to the inset of the counter-rotating vortex pair, the atmospheric turbulence in the differently stratified environments was allowed to develop from prescribed spectral distributions to a state with a distinct inertial subrange and a constant eddy dissipation rate. Series of LESTUF simulations with varying integral turbulence scales, L_t, at $\varepsilon^* = 0.23$ and 0.4 in neutral stratification complement the cases listed in Table 1.

The analysis of in-situ measurements of the Falcon research aircraft (Schumann et al. 1995) at altitudes between 9 and 11 km indicates Brunt-Väisälä frequencies typically ranging from 0.011 s^{-1} to 0.023 s^{-1}

and dissipation rates between 10^{-8} m^2/s^3 and $2{\cdot}10^{-7}$ m^2/s^3. For the MGLET simulations we employ N* = 0.35 (0.013 s^{-1}) and ε^* = 0.01 ($1.2{\cdot}10^{-7}$ m^2/s^3) as a typical reference case for cruise conditions. This reference case is complemented by adjacent atmospheric conditions of enhanced or reduced turbulence and stratification, respectively.

Table 1: Environmental conditions simulated with LESTUF (L) and MGLET (M).

N^* / ε^*	0	0.35	1.0
0		M	
0.01	L/M	L/**M**	L/M
0.05	L	L/M	L
0.23	L	L	L

In order to investigate turbulent mixing processes, MGLET solves equations for two different passive tracers in the left and right vortex. We employed three different initializations: two rather academic cases where the tracers are either trapped in the vortex cores or in the vortex oval and a more realistic case derived from photographs of contrails. Here the tracers are confined within streamlines such that half of the vortex oval is covered by the tracers (for details see Misaka et al. 2011).

Circulation Decay Characteristics

Figures 1 and 2 show the temporal evolutions of normalized radii-averaged circulations for the different investigated environmental conditions achieved with LESTUF and MGLET simulations. Solid lines indicate $\Gamma^*_{5\text{-}15}$-values that are determined in planes oriented perpendicular to the flight direction. This approach corresponds to the standard method for the evaluation of numerical simulations and to scanning strategies of field measurements of wake vortices with lidar.

We have developed a post processing method that is capable to identify the vortices even in progressed states of vortex decay where the coherent vortex structure is getting lost (Hennemann & Holzäpfel 2011). For this purpose the method first determines the orientation of a local vortex segment based on the vorticity vector. The next vortex line position found along the direction of the vorticity vector is corrected by a center-of-gravity method based on the pressure minimum. The pressure minimum turned out to be a very robust criterion for the determination of the vortex center position because it results from an integration of the centrifugal forces of the surrounding, also incoherently rotating fluid elements. In Figures 1 and 2 circulation values determined perpendicular to the identified local vortex segments $\widetilde{\Gamma}^*_{5-15}$ are denoted by symbols.

In contrast to the well established two-phase circulation decay characteristics (solid lines), the vortex circulation estimated perpendicular to the deformed vortex core lines (lines with symbols) reveals a three-phase decay sequence in weakly or neutrally stratified conditions (see Figs. 1 and 2). The initial phase of gradual decay termed “diffusion phase” is followed by a “rapid decay phase” which typically commences shortly before the vortices link. The circulation decrease during the short rapid decay phase is caused by the mutual annihilation of vorticity in the linking area. Subsequently, in neutrally stratified environments long-living vortex rings are observed with gradual vortex decay. This third phase may be termed “ring diffusion phase”. The small axial extension of the vortex ring (cf. Figure 5 at the normalized vortex age of t* = 8.1) may explain why conventional data evaluation procedures, that evaluate circulation only in planes oriented perpendicular to the flight direction, may estimate erroneously that the vortex has rapidly decayed to small circulation values.

The differences between the circulation evolutions achieved by the two different codes are relatively small in the stably stratified cases. However, in the neutrally stratified case the differences are considerable. Substantial uncertainties in neutrally stratified cases are also reported in other numerical studies and experiments. In stably stratified environments the baroclinic vorticity generated around the vortex oval appears to be a robust phenomenon controlling the wake vortex behavior (Holzäpfel et al. 2001). On the other hand, in neutrally stratified environments peculiarities of the turbulence fields appear to have a strong impact on maximum vortex lifetimes and descent distances. Numerical simulations (Gerz & Baumann 2006) demonstrate that even simple displacements of the initial wake vortex positions in a statistically identical background turbulence field may substantially shift the time of vortex linking and subsequent decay. The authors state that the sensitivity to local turbulence topology may be explained by the excitation of different modes of vortex distortion due to locally different spectral power of the atmospheric turbulence.

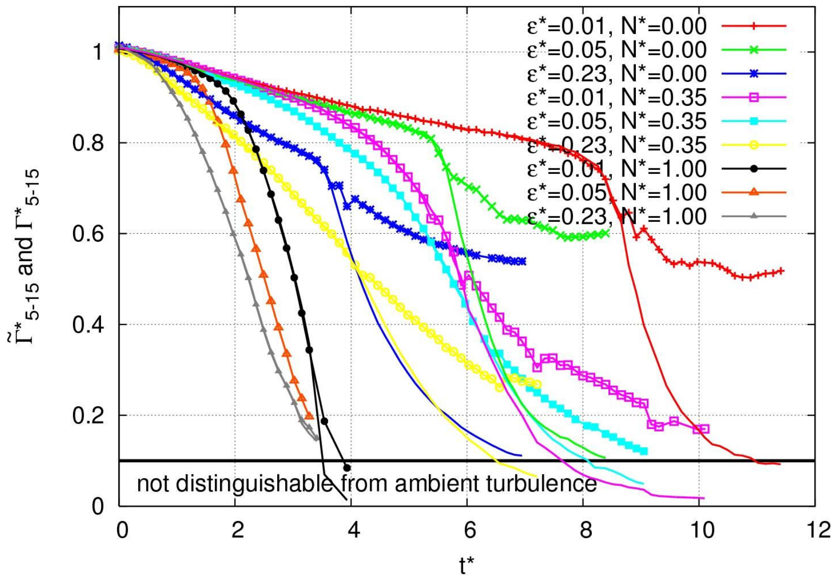

Figure 1: Circulation evolutions of LESTUF simulations for different degrees of ambient turbulence and temperature stratification.

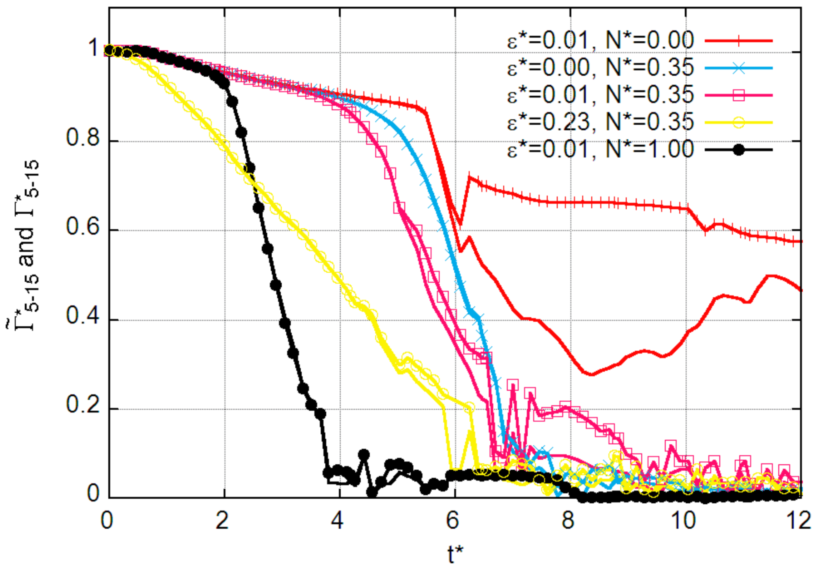

Figure 2: Circulation evolutions of MGLET simulations for different degrees of ambient turbulence and temperature stratification.

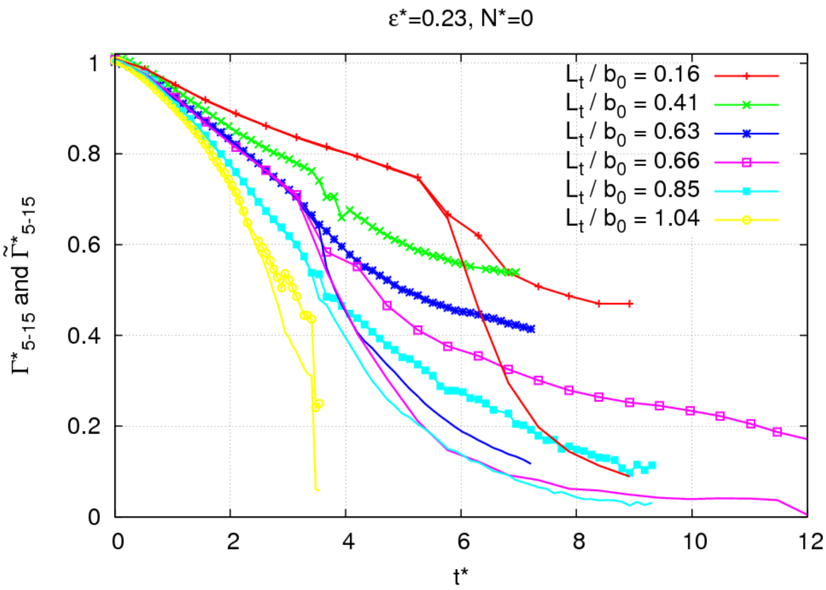

Figure 3: Circulation evolutions of LESTUF simulations for different integral turbulence length scales, L_t ($\varepsilon^* = 0.23$, $N^* = 0$).

Results of a simulation series with $\varepsilon^* = 0.23$ and $N^* = 0$ and varying integral turbulent length, L_t, scales are shown in Figure 3. Except for $L_t/b_0 = 0.16$ the onset of rapid decay occurs at similar instants of time, but the corresponding circulation evolution differs strongly already in the diffusion phase. With increasing L_t/b_0 the circulation decay in the diffusion phase speeds up and, as a consequence, the three-phase decay is more and more concealed.

Figure 4 indicates that with increasing L_t/b_0 the amount of the generated secondary vorticity structures is significantly increased during the diffusion phase. In neutrally stratified cases secondary vorticity is exclusively generated by tilting and stretching of the surrounding turbulent eddies. During the stretching process the primary vortices perform work on the secondary vortices whereby the primary vortices, in turn, lose rotational energy as delineated in Holzäpfel et al. (2003). Note that for constant eddy dissipation rates increased integral turbulence length scales correspond to more energetic turbulence fields. This suggests that the intensity of environmental turbulent kinetic energy impacts circulation decay in the diffusion phase and may conceal the two-phase and three-phase decay characteristics.

For integral length scales exceeding one initial vortex spacing the influence of L_t should be negligible as a parameter for vortex decay characterization (Crow & Bate 1976). However, if $L_t/b_0 < 1$ it should be considered together with ε^* to characterize vortex decay driven by atmospheric turbulence. For example, in the atmospheric surface layer L_t depends on the distance to the ground and can reach small values in ground proximity. In field experiments it has been observed that wake vortex decay in ground proximity is only very weakly dependent on the eddy dissipation rate (Burnham & Hallock 1998, Holzäpfel & Steen 2007). The described sensitivity on L_t/b_0 suggests that this may be related to the reduced turbulence length scales in the surface layer. Consequently, vortex decay mechanisms at the ground are mainly controlled by the interaction of the wake vortices with the secondary vortices detaching from the boundary layer.

We suppose that the good agreement between simulated decay rates and decay rates measured by lidar in the diffusion phase achieved with older numerical simulations are related to diffusive subgrid scale models or numerical schemes leading to overestimated vortex core growth rates. Only with increasing computational performance and advanced numerical schemes and subgrid scale closures it has become feasible to allow for the simulation of compact vortex cores in sufficiently large simulation domains allowing for large integral turbulence length scales.

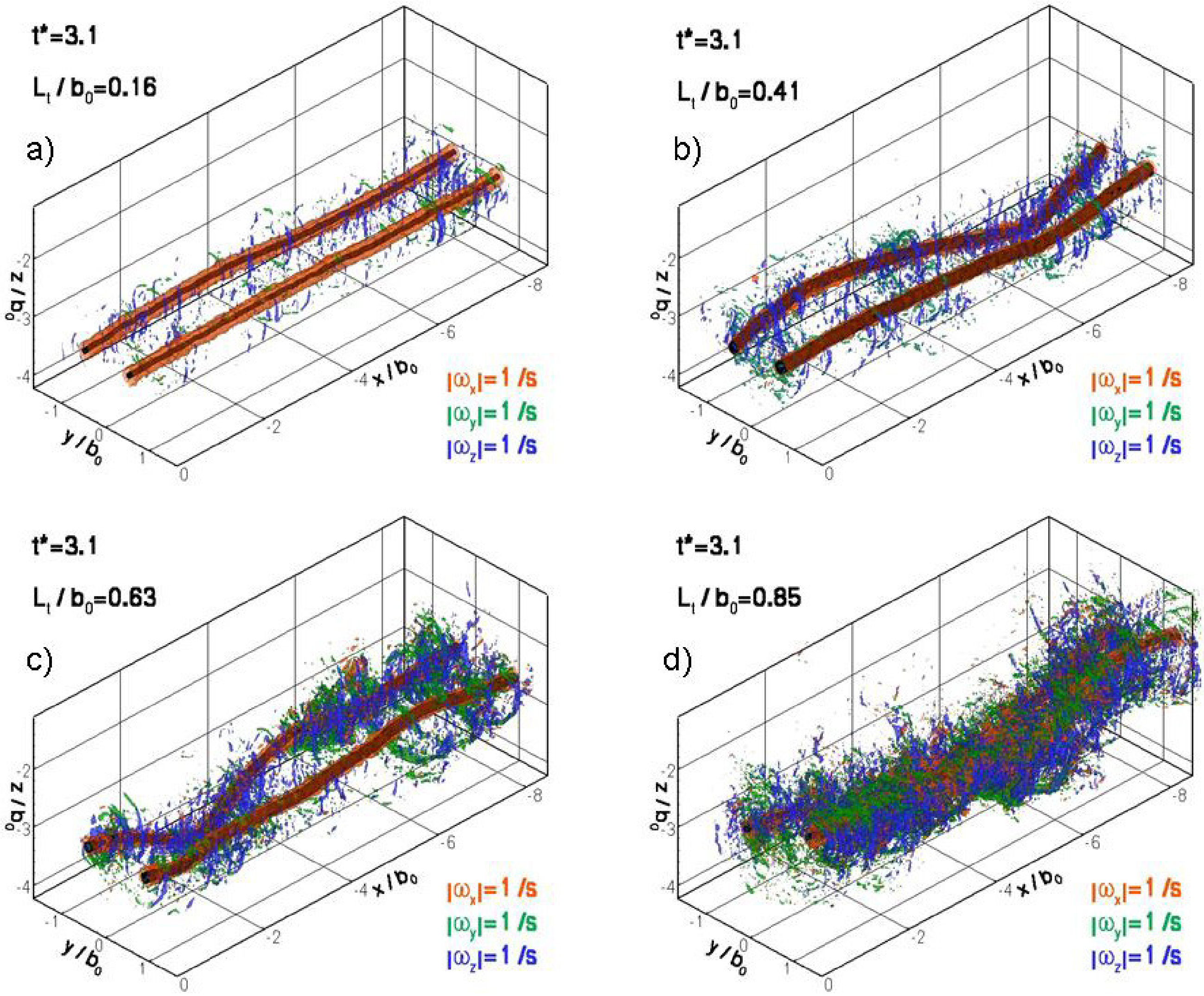

Figure 4: Vortex topology and secondary vorticity for different integral turbulence length scales at t*=3.1 (ε* = 0.23, N* = 0, LESTUF).

Vortex topology

The evolution of the vortex topology from the initial sinusoidal oscillations, the subsequent vortex linking and vortex ring formation up to the axial contraction and the lateral spreading of the vortex ring (see Figure 5) can be explained phenomenologically by mutual velocity induction. For example, at t* = 5.9 the lower ends of the vortex rings do not only mutually induce a vertical descent speed but due to their partially vertical orientation also induce a propagation velocity in flight direction leading to an axial compression of the vortex rings. Similarly, the upwards bended vortex pairs at t* = 8.1 cause a sustained widening of the vortex rings.

A comparison of Figures 5 and 6 indicates that with increasing turbulence intensity and increasing turbulence integral length scales the vortex topology is becoming more complex and the classical shape of the Crow instability and the ring formation is getting lost in favor of superimposed random deformations caused by large scale turbulent eddies. Another interesting aspect illustrated in Figure 5 is the shifting of the local minimum of radii-averaged circulation, $\widetilde{\Gamma}^{*}_{5-15}$, from the linking area at t* = 5.9 to the transverse side at t* = 6.7 and back to the former linking area at t* = 8.1. This shifting process goes along with a variation of the vortex core radii where large radii correspond to small $\tilde{\Gamma}^*_{5-15}$ values. It can be explained by stretching and compression of the respective vortex segments again caused by mutual velocity induction and, complementarily, by the propagation of pressure waves along the vortex tubes that increase core radii when the waves collide (Moet et al. 2005).

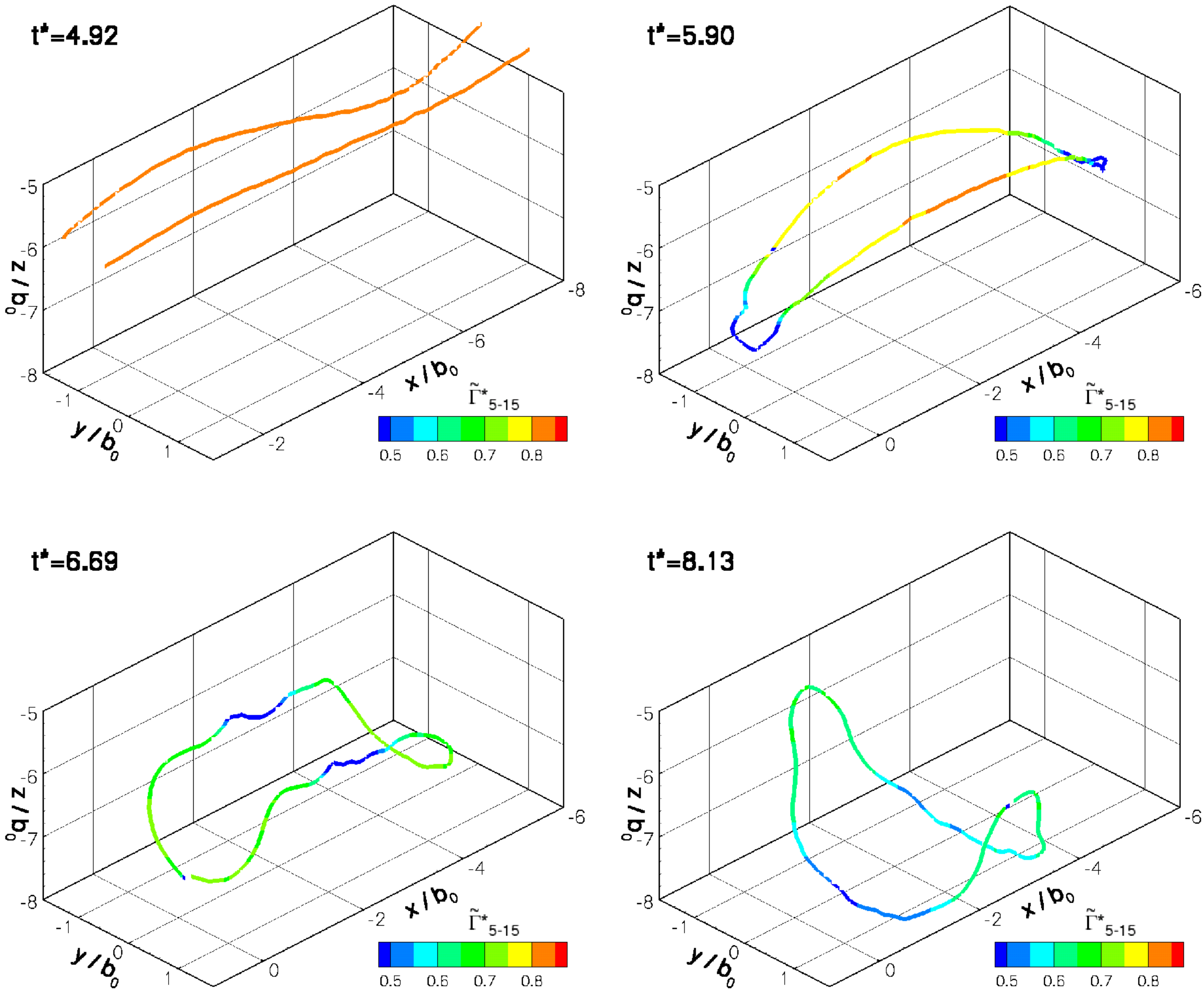

Figure 5: Temporal evolution of wake vortex topology with color-coded circulation in a neutrally stratified environment with weak to moderate turbulence (ε^* = 0.05, L_t/b_0 = 0.41, LESTUF).

Figure 7 below indicates that during vortex reconnection pressure disturbances are generated that subsequently are traveling as pressure waves along the vortices and are visualized in terms of helical instabilities (Moet et al. 2005). At t* = 6.2 the waves collide leading to a temporal local increase of core radii and a corresponding decrease of $\tilde{\Gamma}^*_{5-15}$ followed by a reorganization of the vortex structure and of $\tilde{\Gamma}^*_{5-15}$ values (cf. Fig. 5). The pressure waves continue to propagate along the vortices and collide another time in the former reconnection area. Moet et al. (2005) argue whether the vortex collision might lead to the vortex bursting phenomenon described by Spalart (1998). However, the tracer distributions in Fig. 7 do not indicate lateral spreading of the passive tracer associated with vortex bursting. In the following we suggest an alternative explanation for the vortex bursting phenomenon observed during smoke visualizations or at contrails. The formation of helical instabilities is still observed in weakly stably stratified conditions (ε^* = 0.01, N* = 0.35) but the interaction of the helical instabilities with the baroclinic vorticity prevents the reorganization of the vortex ring.

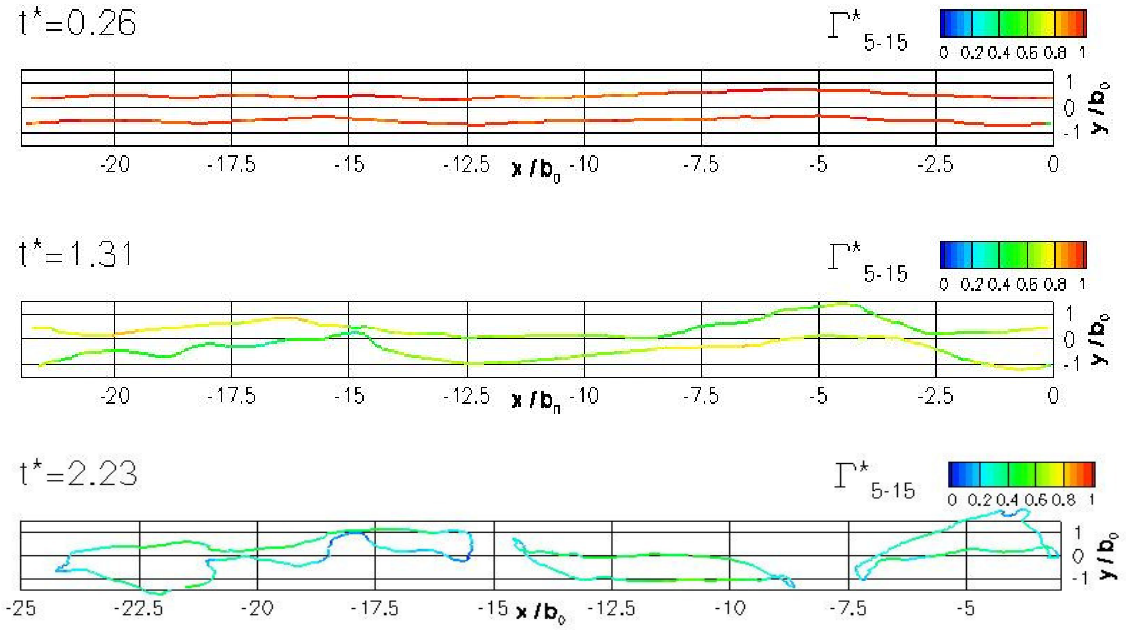

Figure 6: Formation of complex vortex ring topologies with color-coded normalized circulation in a neutrally stratified environment with moderate to strong turbulence ($\varepsilon^* = 0.4$, $N^* = 0$, $L_t^* = 2.2$, domain size $1024 \times 1024 \times 1024$ m³, $1.1 \cdot 10^9$ grid points).

Further, Figure 7 delineates that after $t^* = 10$ the vortex ring transforms into a double ring. The unusual recovery of $\Gamma^*_{5\text{-}15}$ after $t^* = 8$ of case ($\varepsilon^* = 0.01$, $N^* = 0$) in Fig. 2 is related to an increase of the ring segment length oriented in flight direction and a redistribution of circulation along the vortex rings. Note that the typical structures of the bridging process also appear during the formation of the double ring. The photo in Fig. 7 above indicates that the various stages of ring formation can also be observed visualized by contrails.

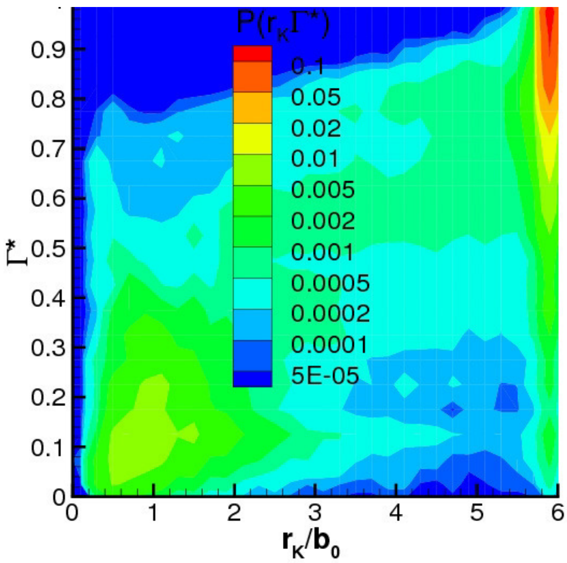

Figure 8: Joint probability density distribution of curvature radii and circulation averaged for the nine parameter combinations of ε^* and N^* of the LESTUF simulations.

For segments of the deformed vortex core lines with lengths of 1.5 initial vortex spacings, b_0, we characterize the vortex deformation in terms of curvature radii (Hennemann & Holzäpfel 2011). Despite the wide range of meteorological conditions and the resulting vortex lifetimes and varying decay characteristics, the statistics of vortex curvature radii look quite similar for all the conducted LES with LESTUF (see table 1). An inspection of the investigated cases reveals that the development of the curvature radii distributions is well correlated with circulation decay. Figure 8 displays joint probability density distributions (JPDDs) of curvature radii dependent on normalized circulation which have been established from the post-processing of the nine LES.

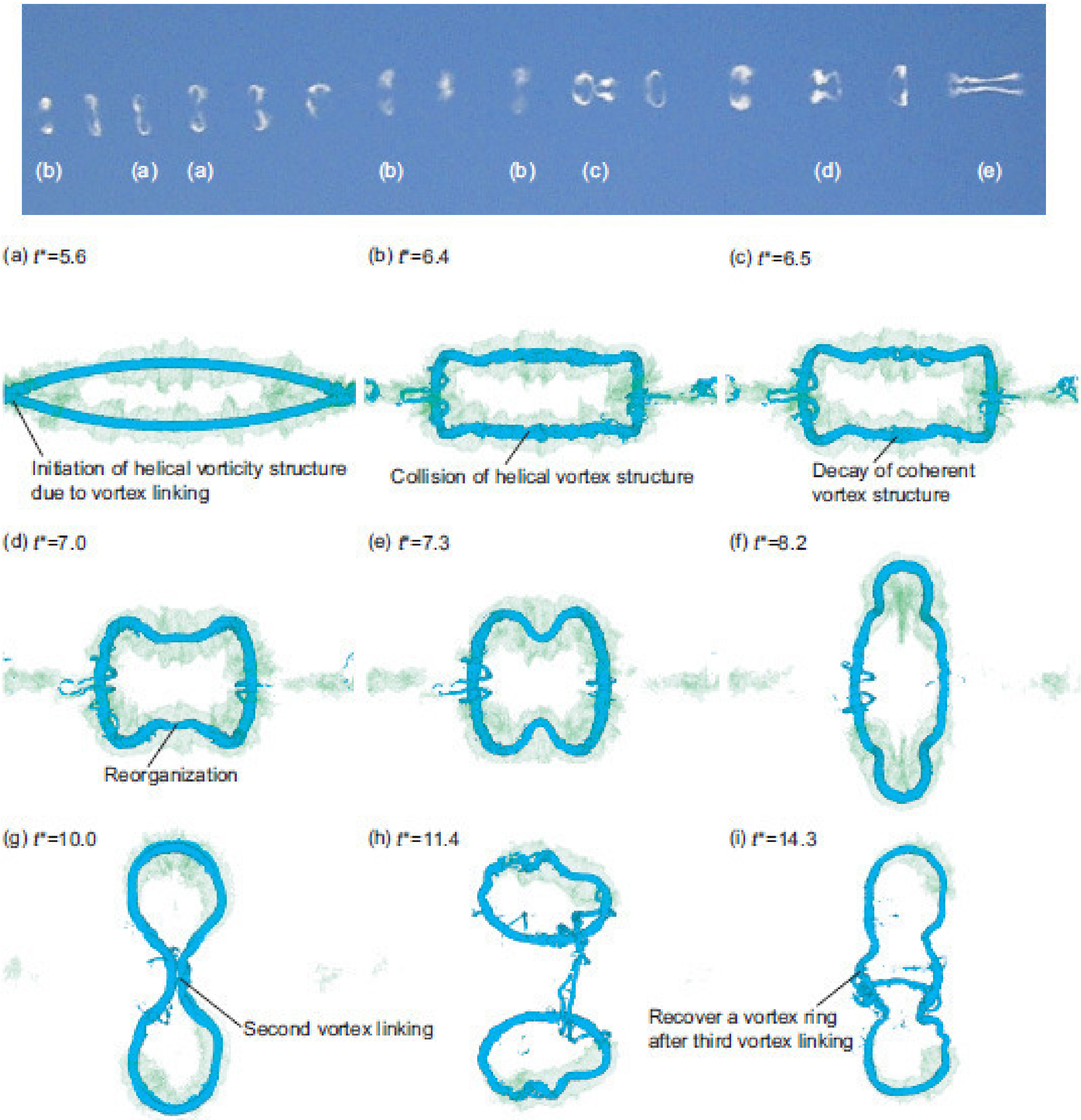

Figure 7: Above: Various stages of vortex rings; flight direction from left to right (photo Sven Lüke, 16 Nov. 2006). Below: LES of vortex ring formation in neutrally stratified and weakly turbulent environment. (ε^* = 0.01, N* = 0, L_t/b_0 = 0.85, MGLET).

Because the method to derive curvature radii, r_κ, employs a maximum of r_κ/b_0 = 6, vortex segments with $r_\kappa/b_0 > 5$ are considered to be straight in principle. Curvature radii r_κ are completely larger than $5b_0$ only for $\Gamma^*_{5\text{-}15} > 0.95$. Already at $\Gamma^*_{5\text{-}15} = 0.8$ curvature radii below $r_\kappa/b_0 = 1$ show up. At $\Gamma^*_{5\text{-}15} \approx 0.6$ about 50% are still straight. At a late stage of vortex evolution the established statistics indicate a predominance of curvature radii on the order of one initial vortex separation, b_0. In order to investigate whether such strongly deformed vortex segments may still pose a risk to follower aircraft, idealized vortex flow fields and LES data have been applied within flight simulator tests (Vechtel 2012). Encounter flights of the DLR research aircraft Falcon behind an A380 indicate that already pronounced sinusoidal oscillations prior to vortex linking might significantly reduce the severity of encounters.

Turbulent Exchange Processes of Passive Tracer

The investigation of turbulent exchange processes of passive tracers within the descending vortex oval and between the oval and its environment is of interest with respect to several aspects: (i) The dispersion of the ice crystals during the vortex descent is an important parameter in order to quantify the vertical extent, optical thickness, and lifetime of the contrails produced during cruise. These parameters are important to estimate the contribution of contrails to global warming. (ii) For inviscid point vortices the circulation can only decay as a result of diffusion of vorticity across the centerline between the vortices (Donaldson & Bilanin 1975). So the exchange processes between the passive tracers may be indicative of the annihilation of the counter-signed vorticity. (iii) The simultaneous investigation of the topology of the tracer distribution and the vortex dynamics may indicate to which extent visual observations of contrails or vortices visualized by smoke actually represent the dynamical vortex evolution.

Figure 9 displays a photograph of a contrail generated by a two-engine commercial jet airplane. The vortex cores appear hollow indicating reduced ice crystal concentrations within the cores. This may be explained either by reduced turbulent mixing of the jet exhaust into the vortex cores caused by their centrifugal stability (Holzäpfel 2004). Alternatively, the ice particles may be centrifuged out of the core by the centrifugal forces of the strongly rotating cores. Third, it could be attributed to warm jet exhaust gases accumulating inside the centrifugally stable vortex core driven by buoyancy effects and causing local subsaturation with respect to ice crystals. Possibly, a combination of more than one of these effects is responsible for the generation of the hollow vortex tubes.

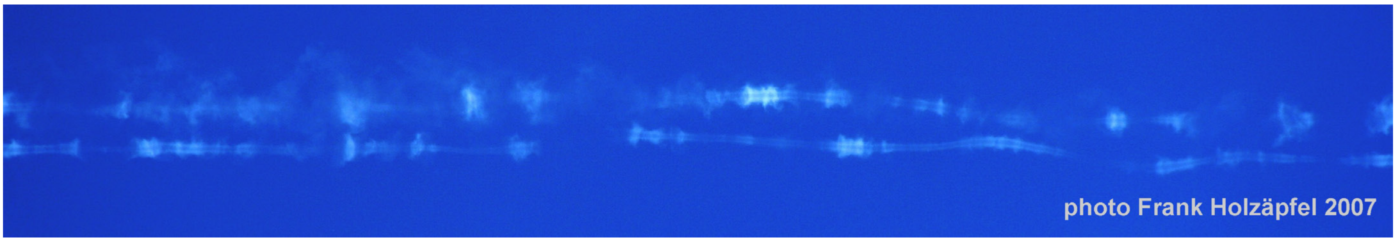

Figure 9: Photograph of a contrail generated by a two-engine commercial jet airplane indicating ice crystal redistribution along vortex lines.

Another prominent feature of Fig. 9 is the pronounced axial redistribution of ice crystals along the vortex tubes, a phenomenon termed vortex bursting, puffs or pancake vortices (Spalart 1998): The region marked by ice crystals contracts in portions of the vortices and expands in others.

The MGLET simulations of the reference case for cruise conditions ($\varepsilon^* = 0.01$, $N^* = 0.35$) exhibit a comparable tracer topology (see the red and green isosurfaces in Figure 10,). For this qualitative comparison a similar phase of vortex evolution prior to vortex linking ($t^* = 4.6$) has been chosen as depicted in the photograph of Figure 9. Clearly, the tracer is being pushed along the vortex tubes and accumulates in distinct areas where it spreads out indicating the vortex bursting phenomenon. At some locations the tracer has started to pass over to its neighboring vortex. In between the tracer accumulations, the tracer is restricted to the vortex core regions. For increased turbulence intensity the redistribution process is even more pronounced: More significant accumulations of the passive tracers at less axial positions occur at earlier times (see Misaka et al. 2011).

A more detailed analysis (see Misaka et al. 2011) indicates that the secondary vortex structures (SVS) formed by simultaneous stretching and tilting of baroclinic vorticity and of turbulent eddies (Holzäpfel et al. 2003) drive the axial redistribution process. Figure 10 features rip-shaped and helical SVS (blue) that induce themselves a propagation velocity and thus push the tracer along the vortex tubes. Behind the SVS the tracer remains in the core region whereas the puffs are produced by approaching and colliding SVS. Figure 11 illustrates this process schematically in a perspective view (left) and a cross-sectional view (right). The mechanism may also lead to the generation of vortex funnels that have been observed by research aircraft (Brown 2010, Misaka et al. 2011).

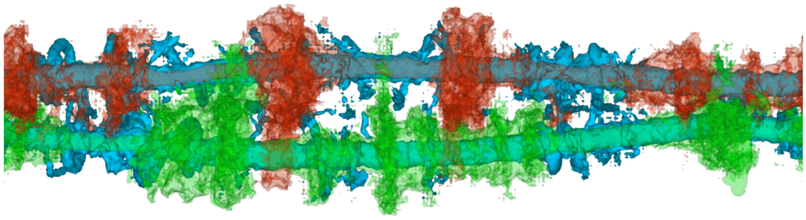

Figure 10: Topview of isosurfaces of vorticity magnitude (|ω| = 1.2 s^{-1}, blue) and of passive tracer distributions (red and green) at t* = 4.6 (ε* = 0.01, N* = 0.35, L_t/b_0 = 0.95, MGLET).

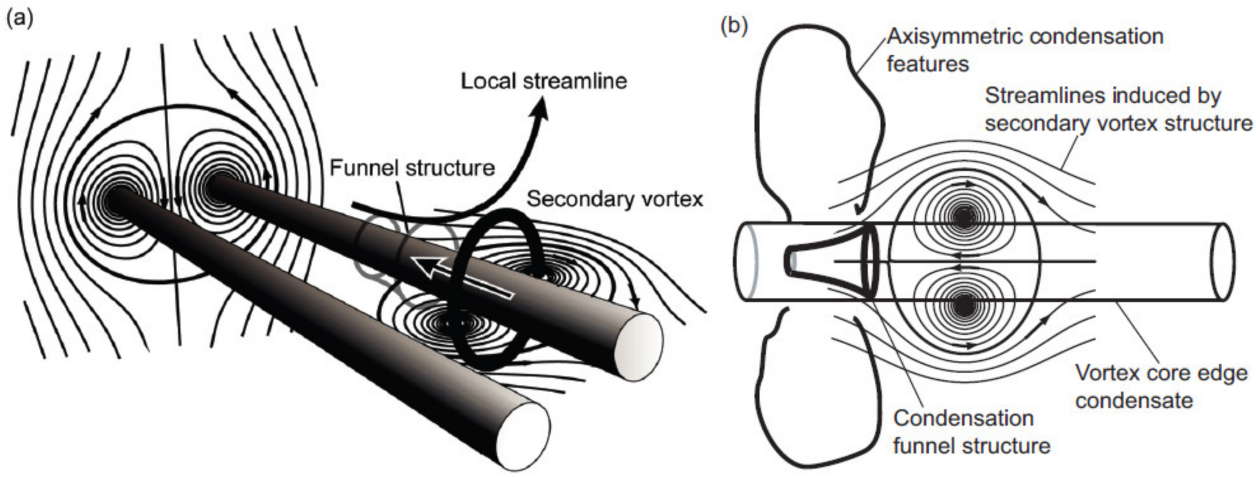

Figure 11: Schematic of (a) local passive tracer transport by secondary vortices, (b) cross-sectional sketch inspired by Brown (2010).

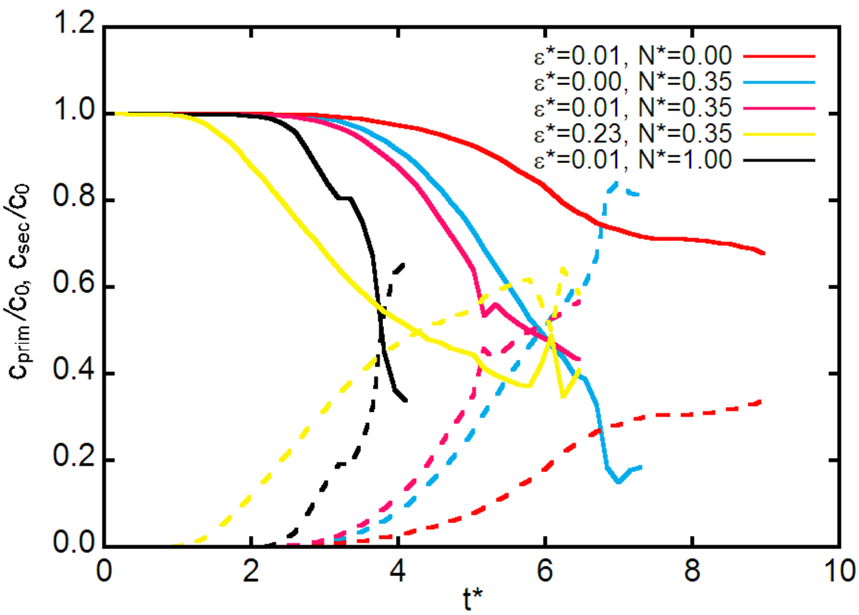

Figure 12: Temporal evolutions of tracer concentrations in primary (solid lines) and secondary wakes (dashed lines). Tracer initialized in half oval (MGLET).

Figure 12 illustrates the detrainment of the passive tracer from the primary wake (solid lines) and the corresponding tracer concentration increase in the secondary wake (dashed lines). The tracer is attributed to the primary wake when it resides within a cylindrical volume with a radius of b_0 centered on the identified vortex tracks. This method allows distinguishing between primary and secondary wake also for extensively deformed vortices and during the vortex-ring regime. Figure 12 shows results of the simulations where the tracer initially covered 50% of the oval cross-section.

The vortex detrainment characteristics feature striking similarities with the circulation decay characteristics (see Fig. 2). The sequence of the different cases with respect to the onset of rapid circulation decay and the onset of detrainment is the same. The times when the circulation has reached 50% of its initial value approximately coincide with the times when 50% of the tracer has been detrained. However, in several cases the primary wake may still contain approximately 40% of its initial tracer concentration when the wake has already fully decayed.

Conclusion

Large eddy simulations of wake vortex evolution in various turbulent and stably stratified atmospheric environments have been conducted with two different LES codes. Passive tracers are used to investigate exchange processes between the vortex cores, the vortex oval and its environment as well as redistribution processes along the vortex tubes. A post processing method is used to identify the vortex center lines even in progressed states of vortex decay where the coherent vortex structure is getting lost. This method allows, for example, analyzing the circulation evolution of vortex rings and revealing the mechanisms of the vortex bursting phenomenon.

In contrast to the well established two-phase circulation decay characteristics, the vortex circulation estimated perpendicular to the deformed vortex core lines reveals a three-phase circulation decay sequence in weakly or neutrally stratified conditions. The initial phase of gradual decay termed “diffusion phase” is followed by a “rapid decay phase” which typically commences shortly before the vortices link. In the subsequent “ring diffusion phase” long-living vortex rings are observed with gradual vortex decay in neutrally stratified environments. It may be argued that the typical weak stable temperature stratification prevailing at cruise altitudes may prevent wake vortices from excessive descent distances reaching beyond adjacent flight levels.

We find that variations of integral turbulence length scales, L_t, of the atmospheric turbulence may strongly impact vortex decay characteristics for given eddy dissipation rates, ε. With increasing turbulence length scales the circulation decay in the diffusion phase speeds up and, as a consequence, the three-phase decay is more and more concealed. The responsible mechanism corresponds to the classical concept of turbulence theory stating that the energy transfer from large eddies (wake vortices) to smaller eddies (environmental turbulent flow or baroclinic vorticity) is related to the work conducted by the large eddies by stretching of the smaller eddies. It appears that the amount of environmental vorticity (turbulent eddies) controls the circulation decay in the diffusion phase. It can be anticipated that for sufficiently large turbulence length scales ($L_t/b_0 > 1$) the effect of turbulence can be fully parameterized solely based on eddy dissipation rates. Conversely, this means that for $L_t/b_0 < 1$ (for example in ground proximity) the effect of eddy dissipation is reduced and both parameters L_t and ε are necessary to parameterize vortex decay.

The evolution of the vortex topology from the initial sinusoidal deflection, the subsequent vortex linking and vortex ring formation up to the axial contraction and the lateral spreading of the vortex ring can be explained phenomenologically by mutual velocity induction. Stretching and compression of vortex segments by mutual velocity induction and, complementarily, by the propagation of pressure waves along the vortex tubes modify vortex core radii and thus radii-averaged circulation. Pressure waves generated during vortex linking become manifest in helical instabilities. Colliding pressure waves cause a temporary and local decrease of radii-averaged circulation followed by a recovery. During this collision spreading of the tracer attributed to the vortex bursting phenomenon is not observed.

Pronounced axial redistribution of the tracer and the so-called vortex bursting phenomenon (formation of puffs or pancake vortices) is observed prior to vortex linking. It is revealed that the mechanism of vortex bursting is related to secondary vorticity structures generated from environmental turbulence or baroclinic vorticity. These ring-shaped or helical vortex structures propagate along the vortex lines thus accumulating the passive tracer ahead. Colliding secondary vortex structures lead to abrupt spreading of the tracer and thus provoke vortex bursting as it can be observed visualized by smoke or contrails. This course of events may also lead to the formation of vortex funnels.

The detrainment of passive tracer from the primary wake progresses similar as the circulation evolution. For example, the half-life periods of the tracer concentration in the primary wake and the circulation are quite close. Subsequently, the detrainment rates are reduced such that the primary wake may still contain approximately 40% of its initial tracer concentration when the wake has fully decayed. The sensitivity of detrainment rates on particular initial tracer distributions within the wake appears low.

Acknowledgements

The provision of the LES code MGLET and the kind support during its modifications by Florian Schwertfirm of Kreuzinger + Manhart Turbulenz GmbH and by Michael Manhart of Technische Universität München is greatly acknowledged. The supply of computation time on the supercomputers IBM p575 system at Deutsches Klimarechenzentrum (DKRZ) and of SGI Altix 4700 system at Leibniz-Rechenzentrum (LRZ) is greatly appreciated.

References

Brown A.P., “On the specification of wake vortex encounter gust-fields from flight data,” AIAA Pap. 2010–7678 (2010).

Burnham, D. C., and Hallock, J. N., “Measurements of Wake Vortices Interacting with the Ground, AIAA Paper 98-0593, 1998.

Crow, S. C., and Bate, E. R., “Lifespan of Trailing Vortices in a Turbulent Atmosphere,” Journal of Aircraft, Vol. 13, No. 7, 1976, pp. 476-482.

Donaldson, C. d., and Bilanin, A. J., “Vortex Wakes of Conventional Aircraft”, NATO, AGARD-AG-204., 1975.

Gerz, T., Baumann, R., “Decay characteristics of single and double wake-vortex pairs in different atmospheric flow realisations”, ICAS 2006, 25th International Congress of the Aeronautical Sciences, Hamburg, ICAS 2006-3.8.1., Sept. 2006, pp. 13.

Hennemann I., Holzäpfel F., “Large-eddy simulation of aircraft wake vortex deformation and topology,” Proceedings of the Institution of Mechanical Engineers, Part G: Journal of Aerospace Engineering, Volume 225, Issue 12, December 2011, pp. 1336-1350, DOI: 10.1177/0954410011402257.

Hokpunna, A., and Manhart, M., “Compact Fourth-order finite volume method for numerical solutions of Navier-Stokes Equations on Staggered grids,” Journal of Computational Physics, accepted for publ. 2010, doi: 10.1016/j.jcp.2010.05.042.

Holzäpfel F., Gerz, T., and Baumann R., “The turbulent decay of trailing vortex pairs in stably stratified environments,” Aerospace Science and Technology, Vol. 5, No. 2, 2001, pp. 95-108.

Holzäpfel, F., Hofbauer, T., Darracq, D., Moet, H., Garnier, F., Ferreira Gago, C., “Analysis of wake vortex decay mechanisms in the atmosphere,” Aerospace Science and Technology, Vol. 7, 2003, pp. 263-275.

Holzäpfel, F., “Adjustment of Subgrid-Scale Parametrizations to Strong Streamline Curvature,” AIAA Journal, Vol. 42, 2004, pp. 1369-1377.

Holzäpfel, F., and Steen, M., “Aircraft Wake-Vortex Evolution in Ground Proximity: Analysis and Parameterization, AIAA Journal, Vol. 45, No. 1, 2007, pp. 218-227.

Holzäpfel F., Misaka T., Hennemann I., “Wake-Vortex Topology, Circulation, and Turbulent Exchange Processes, “AIAA Paper 2010-7992, AIAA Atmospheric and Space Environments Conference, 2-5 August 2010, Toronto, Ontario, Canada, 16 pages.

Kaltenbach, H.-J., Gerz, T., and Schumann, U., “Large-eddy simulation of homogeneous turbulence and diffusion in stably stratified shear flow,” Journal of Fluid Mechanics, Vol. 280, 1994, pp. 1-40.

Manhart, M., “A Zonal Grid Algorithm for DNS of Turbulent Boundary Layers,” Computer & Fluids, Vol.33, 2001, pp. 435-461.

Meneveau, C., Lund, T. S. and Cabot, W. H., “A Lagrangian Dynamic Subgrid-scale Model of Turbulence,” Journal of Fluid Mechanics, Vol. 319, 1996, pp. 353–385.

Misaka T., Holzäpfel F., Gerz T., Manhart M., Schwertfirm F., “Vortex bursting and tracer transport of a counter-rotating vortex pair,” Physics of Fluids, accepted Dec. 2011.

Moet, H., Laporte, F, Chevalier, G., and Poinsot, T., “Wave propagation in vortices and vortex bursting,” Physics of Fluids, Vol. 17, 2005, pp. 054109-1 - 054109-15.

Schumann U., Konopka P., Baumann R., Busen R., Gerz T., Schlager H., Schulte P., and Volkert H., “Estimates of diffusion parameters of aircraft exhaust plumes near the tropopause from nitric oxide and turbulence measurements,” Journal of Geophysical Research, Vol. 100, No. D20, 1995, pp. 14147-14162.

Schumann, U., “A contrail cirrus prediction tool,” Geosci. Model Dev. Discuss., 4, 3185–3293, 2011, doi:10.5194/gmdd-4-3185-2011.

Spalart, P. R., “Airplane Trailing Vortices,” Annual Review of Fluid Mechanics, Vol. 30, 1998, pp. 107-138.

Vechtel D., “On the influence of vortex curvature on wake encounter hazard”, this report.

6.2 Large-Eddy Simulation of Wake Vortex Evolution from Roll-Up to Decay

Takashi Misaka, Frank Holzäpfel, Thomas Gerz
Institute of Atmospheric Physics

The development of an aircraft wake vortex from the roll-up until vortex decay is studied. An aircraft model and the surrounding flow field obtained from high-fidelity Reynolds-averaged Navier-Stokes simulation are swept through a ground-fixed computational domain to initialize the wake. After the wake initialization, the large-eddy simulation of the vortical wake is performed until vortex decay. The methodology is tested with the NACA0012 wing and applied to the DLR-F6 wing-body model. The roll-up process of the vorticity sheet from a main wing and the merge of an inboard wing vortex into the wingtip vortex are simulated. Vortex parameters such as the averaged circulation, vortex core radius and vortex separation are also evaluated. The growth rate of the vortex core radius is relatively small during the roll-up where the fine mesh resolution in the LES is required to capture the tiny vortex core in the RANS simulation. A high-lift configuration of a landing large transport aircraft was also studied where the wingtip vortices merge with the co-rotating and stronger outboard flap vortices.

Introduction

Wake vortices generated by a flying aircraft pose a potential risk for following aircraft due to the strong and coherent vortical flow structure [1]. In addition, condensation trails (contrails) originated from the interaction of jet exhaust, wake vortices and the environmental atmosphere may trigger the formation of cirrus clouds (contrail cirrus) which have influence on the climate [2,3]. Wake vortex is related to a broad scale of flows. Flows around aircraft's main wing, fuselage, slat, flap, jet engine and tail plane, and their interactions may affect the generation of wake vortex in particular in a high-lift condition [4]. On the other hand, contrails generated by cruising aircraft spread several tens kilometers.

The evolution of an aircraft wake can be divided into several phases, for example, (1) roll-up phase, (2) vortex phase, and (3) dissipation phase [1]. Although numerical simulation is one of the effective approaches to tackle this problem, the applicable flow scale of a numerical simulation code is usually limited to each of those regimes. High-fidelity Reynolds-averaged Navier-Stokes (RANS) simulations can handle flows around aircraft and subsequent roll-up process of wake vortex in the jet regime [5]. In addition, experimental measurements of near field wake evolutions have been conducted [4,6]. On the other hand, the dynamics of rolled-up wake vortex in the vortex and dissipation regimes has been studied mainly by large-eddy simulation (LES) or direct numerical simulation (DNS). In these researches, detailed temporal evolution of a vortex pair with a longitudinally constant velocity profile is investigated, where short-wave (elliptic) instability and Crow instability may develop. In addition, various atmospheric conditions of turbulence, stability and wind shear are considered to assess the effect of these factors on wake vortex evolution and decay [7-9]. The LES of wake vortex in the late dissipation and diffusion regimes is performed along with microphysical processes of contrails in Ref. [10].

The present study aims to develop a methodology which enables to simulate the wake vortex evolution from the generation until vortex decay, i.e., from the roll-up phase to the end of the vortex phase. We investigate the evolution of vortex parameters such as the averaged circulation, vortex core radius and vortex separation from the wake roll-up until vortex decay. By sweeping a local and stationary flow field obtained around the wing and fuselage of an aircraft with high-fidelity RANS through the LES domain to initialize the wake, it is possible to simulate the entire life cycle of a wake vortex system from realistic wake roll-up processes. The temporal integration of wake vortex until vortex decay is straightforward except for the treatment of longitudinal boundary conditions. Here we consider a simple NACA0012 wing for the numerical tests of the approach. Then the DLR-F6 model in a cruise condition is investigated with and without employing an ambient turbulence field. The roll-up process and subsequent wake evolution of a large transport aircraft case in high-lift configuration from the AWIATOR project are also simulated. The study, bridging the gap between the roll-up and the vortex phases, shall provide more realistic insights into the aircraft wake vortex evolution expressed in terms of vortex circulation and vortex core radius. It also allows investigating the entrainment of jet exhaust by considering tracers, which might be useful for detailed contrail modeling studies.

Methods

Flow Solver

In this study, the incompressible Navier-Stokes code MGLET is employed for LES [11]. An equation for potential temperature is also solved to take into account buoyancy effects employing Boussinesq approximation. The equations are discretized by a finite-volume approach with the fourth-order finite-volume compact scheme [12]. Lagrangian dynamic model is employed for a turbulence closure [13]. The third-order Runge-Kutta method is used for time integration [14].

Wake Initialization Using RANS Flow Field

The present approach which is schematically shown in Figure 1 could be a numerical realization of the catapult wind tunnel [15]. The numerical approach has several advantages for investigating an aircraft wake. The decay of a vortex pair strongly depends on environmental conditions such as ambient turbulence, temperature stratification and wind shear. Therefore the control of these conditions is crucially important to assess the influence of the ambient conditions on vortex decay. Unlike the consideration of realistic inflow conditions in an aircraft fixed LES domain, the generation of controlled turbulence fields in the ground fixed LES domain is straightforward. The other reason is that the present approach does not need a long computational domain in the flight direction for obtaining longer vortex age compared to an aircraft fixed LES domain.

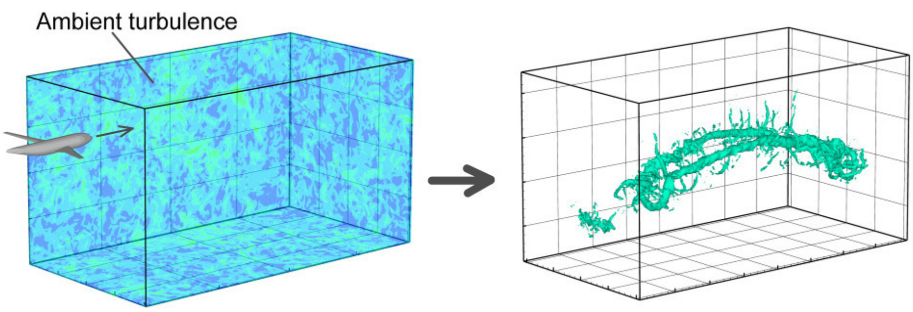

Figure 1. Schematic of the approach, (a) wake initialization, (b) wake evolution until vortex decay.

An aircraft model and the surrounding stationary flow field obtained from a high-fidelity RANS simulation are swept through a ground fixed LES domain to initialize the aircraft's wake [16]. The RANS flow field is added as a forcing term to the Navier-Stokes equations in the LES. Similar approach might be referred to as the fortified solution algorithm (FSA) [17] or a nudging technique used in data assimilation [18]. The resulting velocity field is represented by the weighting sum of RANS velocity field $\mathbf{V}_{\mathrm{RANS}}$ and LES velocity field $\mathbf{V}_{\mathrm{LES}}$,

$$\mathbf{V} = f(y,\alpha,\beta)\,\mathbf{V}_{\mathrm{LES}} + \left[1 - f(y,\alpha,\beta)\right]\mathbf{V}_{\mathrm{RANS}}\,. \tag{1}$$

The weighting function $f(y,\alpha,\beta)$ could be a smooth function of the wall-distance y or of other physical quantities such as velocity magnitude. Figure 2 schematically shows the combination of RANS and LES flow fields. Here, we employ the following function of wall-distance to realize smooth transition between the flow fields,

$$f(y,\alpha,\beta)=\frac{1}{2}\left[\tanh\left[\alpha\left(\frac{y}{\beta}-\frac{\beta}{y}\right)\right]+1.0\right], \qquad (2)$$

where the constants α and β represent the slope of the transition and the wall-distance where solutions of RANS and LES are equality weighted, respectively. These constants can be determined by trial and error, as well as by optimization techniques.

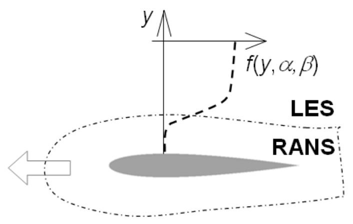

Figure 2. Schematic of the present approach for combining RANS and LES.

The mapping of the RANS flow field onto the Cartesian LES mesh is performed by a linear interpolation only once before the wake initialization. An additional computer memory is prepared to store the mapped RANS flow field, however, the additional computational cost for the forcing term is minimal. The forward movement of an aircraft is represented by simply shifting the mapped flow field for a certain mesh spacing, which is also possible for a decomposed LES domain if the increments of the advancement is smaller than the halo region of the domain decomposition for parallel computation.

Reproduction of eddy viscosity

Since we only use a RANS velocity field to initialize the wake, the eddy viscosity in the LES domain appears to be low compared to that in the original RANS flow field. Therefore it is required to reproduce velocity fluctuations modelled in the RANS flow field. It is pointed out that the correct representation of eddy viscosity in the wake is important to simulate the wake evolution [19]. Most crude but still useful representation of such velocity fluctuations may be white noise. Here we add white noise to the RANS flow field in the region of RANS-LES transition so that the time-averaged LES eddy viscosity matches to the RANS eddy viscosity in the wake. The magnitude of the fluctuations is modified by the proportional-integral (PI) controller during the advancement of the model through the LES domain.

$$\mathbf{V'}_{\mathrm{RANS}}=\mathbf{V}_{\mathrm{RANS}}+K\mathbf{V}_{\mathrm{WN}}, \qquad (3)$$

$$K=a_1(\mu_{t,\mathrm{RANS}}-\overline{\mu}_{t,\mathrm{LES}})+a_2\int(\mu_{t,\mathrm{RANS}}-\overline{\mu}_{t,\mathrm{LES}})dt, \qquad (4)$$

where $\mathbf{V}_{\mathrm{WN}}$ is a white noise field and K is a gain to control the magnitude of the velocity fluctuations. The gain is defined by the difference between the RANS eddy viscosity $\mu_{t,\mathrm{RANS}}$ and the time-averaged LES eddy viscosity $\overline{\mu}_{t,\mathrm{LES}}$. These eddy viscosities for calculating the gain are integrated in the wake region with the weighting of the RANS eddy viscosity. The magnitude of the added white noise fluctuation is also weighted locally using the RANS eddy viscosity. The constants a_1 and a_2 are set according to the convergence of the gain and numerical stability but the results are not too sensitive to these values.

Optimization of the RANS-LES Interface

In the above formulation, RANS and LES solutions are switched using a certain threshold, i.e., a constant distance from the body surface (wall-distance). On the other hand, it is possible to define the distance locally by using optimization techniques with respect to an appropriate cost function. We tested a cost function defined by the difference of axial vorticity magnitudes between two longitudinal positions,

$$J(\alpha,\beta)=\frac{1}{2}\left(\omega_{x2}-\omega_{x1}\right)^2, \qquad (5)$$

$$\omega_{x1}=\omega_x\big|_{x=x1},\ \omega_{x2}=\omega_x\big|_{x=x2},\ \omega_x=\left(\nabla\times\mathbf{V}\right)_x. \qquad (6)$$

This cost function is evaluated locally, i.e., the upstream axial vorticity magnitude ω_{x2} at x_2 and the downstream axial vorticity ω_{x1} at x_1 are evaluated at each (x,y,z) position in the transition region. The cost function is minimized by gradient-based optimization methods. The gradients of the cost function are obtained as follows,

$$\nabla_\alpha J(\alpha,\beta) = \left(\frac{\partial f}{\partial \alpha}\right)^T (\delta\omega_{x2} - \delta\omega_{x1})(\omega_{x2} - \omega_{x1}), \tag{7}$$

$$\nabla_\beta J(\alpha,\beta) = \left(\frac{\partial f}{\partial \beta}\right)^T (\delta\omega_{x2} - \delta\omega_{x1})(\omega_{x2} - \omega_{x1}), \tag{8}$$

$$\delta\omega_{x1} = \delta\omega_x\big|_{x=x1},\ \ \delta\omega_{x2} = \delta\omega_x\big|_{x=x2},\ \ \delta\omega_x = \left[\nabla \times \left(\mathbf{V}_{\mathrm{LES}} - \mathbf{V}_{\mathrm{RANS}}\right)\right]_x. \tag{9}$$

Here the derivations of the switching function f can be obtained analytically from Eq. (2). Using this gradient, the search direction is defined based on the conjugate gradient method. Smoothing of the parameters α and β is required to achieve a sufficiently smooth transition between the flow fields.

Results and Discussion

The NACA0012 Wing

Numerical tests of the present approach are performed by using a simple rectangular wing. The wing has NACA0012 cross-section and a rounded wingtip. Inflow velocity of 52 m/s and angle of attack of 10 degrees are considered. Wind tunnel test of this configuration was conducted by Chow *et al.* [20] and numerical studies followed that configuration to investigate higher-order schemes, turbulence models and so on [21]. Figure 3 shows a computational domain for RANS to obtain the near flow field and a longer domain for sweeping the RANS flow field based on the present approach. In Figure 3, the velocity magnitude and the computational mesh are shown in the RANS domain. In addition, the pressure on the root-side wall and the iso-surface of the vorticity magnitude are shown in the LES domain. For the RANS simulation, an incompressible flow solver from a free CFD software package, OpenFOAM, is used [22].

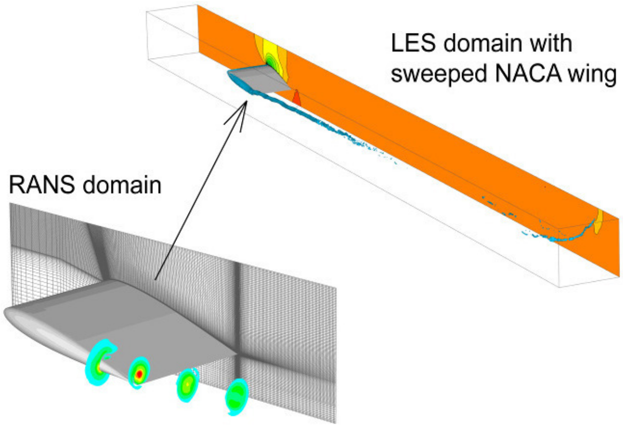

Figure 3. Computational domains for RANS simulation and for sweeping the RANS flow field.

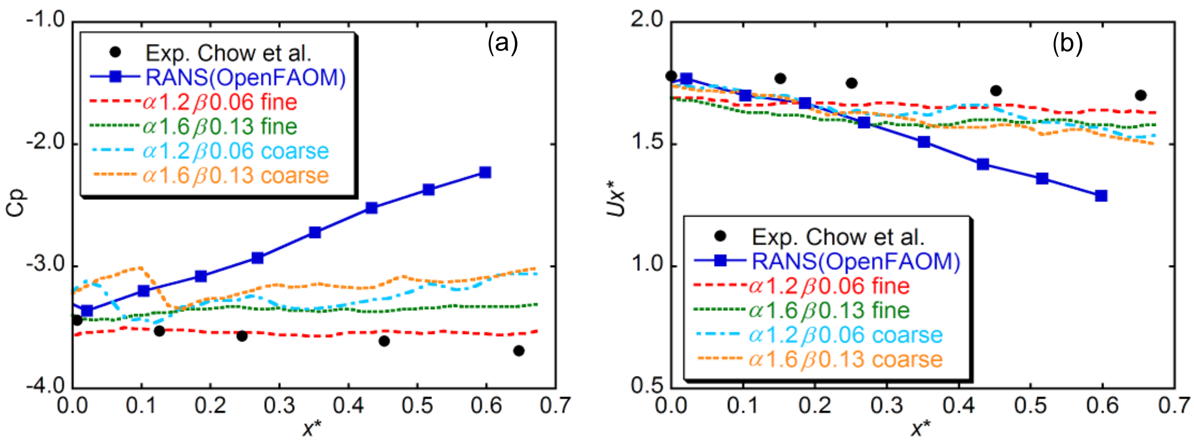

Figure 4. Vortex parameters along vortex centerline (a) pressure coefficient, (b) axial velocity.

The experimental and RANS results as well as the results from the present approach with two sets of parameters (α = 1.2, β = 0.06), (α = 1.6, β = 0.13) for two different mesh resolutions (dx^* = 0.005, 0.01) are compared in Figure 4. Figure 4(a) shows the pressure coefficient along the vortex centerline where the origin of x^* is set to the trailing edge of the wing and it is normalized by a wing chord length. The pressure in the vortex centre increases quickly in the RANS case which indicates an early diffusion of the vortex in the present RANS simulation. This is mainly due to the coarser grid resolution and the low order numerical scheme compared to other RANS simulations [21]. On the other hand, the present approach uses only the RANS near field data around the body, therefore, it shows better results compared to the RANS case. The case with the parameter set (α = 1.2, β = 0.06) and fine mesh appears closest to the experiment. In the coarse mesh cases, there are kinks of the pressure coefficient near the switching wall-distances of β = 0.06 and 0.13. Figure 4(b) shows the axial velocity along the vortex centreline. All the cases from the present approach appear to be low compared to the experiment. Unlike the pressure coefficient, there is no kink near the switching wall-distance in the coarse mesh cases.

Figure 5(a) and (b) show the switching wall-distance of the RANS and LES flow fields by green transparent surfaces before and after the optimization, respectively. The vorticity iso-surface in red shows the wingtip vortex. The switching distance is decreased near the wingtip vortex in Figure 5(b). Figure 5(c) shows the result with optimization of the switching wall-distance based on the cost function in Eq. (5). The kink of the pressure coefficient in coarse mesh cases is alleviated by modifying the switching wall-distance locally.

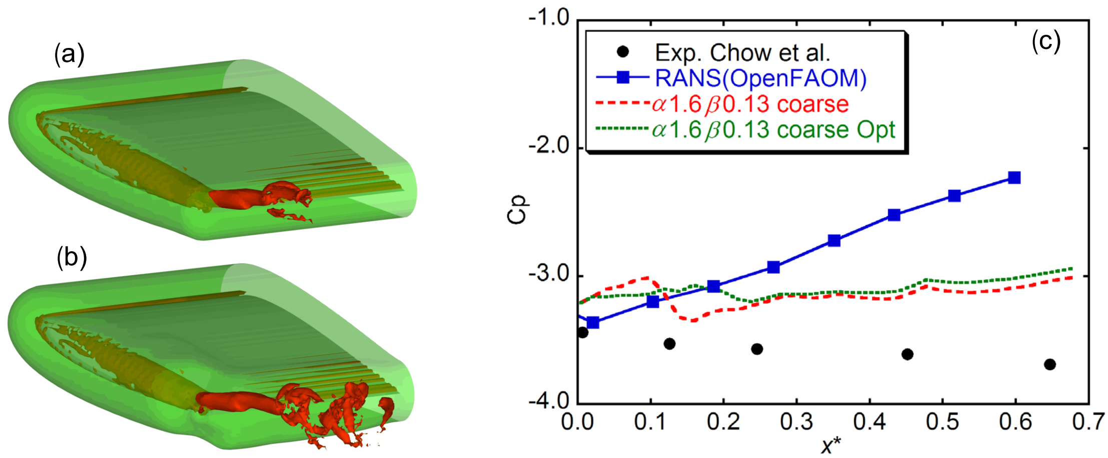

Figure 5. Iso-surfaces of the threshold β (green transparent) and vorticity magnitude (red) for (a) constant β = 0.13, (b) locally optimized β using the cost function Eq. (5), and (c) pressure coefficient with and without optimization based on the cost function.

The DLR-F6 Model

As for a more realistic case, we employed the DLR-F6 wing-body model in clean (low-lift) configuration to initialize the wake. The RANS solution is obtained by the DLR TAU-code with hybrid unstructured mesh, where the number of mesh points is approximately 8.5 million [23]. The flow conditions of Mach number M=0.75 and Reynolds number Re=5.0x10^6 are considered. Note that the RANS flow field used here is not prepared for wake investigations but for the accurate prediction of aerodynamic forces such as lift and drag coefficients. Therefore, the mesh resolution behind the trailing edge is not enough to sharply capture wingtip vortices, which is a similar situation as in the previous NACA0012 wing case. To normalize the quantities, we use the reference values, assuming an elliptic load distribution of the wing,

$$\Gamma_0 = \frac{2C_L U b}{\pi\Lambda}, \quad b_0 = \frac{\pi}{4}b, \quad w_0 = \frac{\Gamma_0}{2\pi b_0}, \quad t_0 = \frac{b_0}{w_0}, \tag{8}$$

where C_L, U, b, and Λ represent a lift coefficient C_L = 0.5, uniform flow speed U = 270 m/s, wingspan b = 1.172 m, and wing aspect ratio Λ = 9.5, respectively. These values are from the experimental conditions. Using these numbers the reference values for the normalization become Γ_0 = 10.5 m^2/s, b_0 = 0.92 m, w_0 = 1.8 m/s, and t_0 = 0.5 s, respectively.

Figure 6 shows the axial vorticity distribution on a plane at the distance of x^* = 5.3 from the trailing edge of the wingtip, which corresponds to t^* = 0.03 after the passage of the wingtip through the plane. The peak vorticity is labeled at the vortices. Here the mesh resolution and the switching wall-distance are varied. Comparing the three different mesh resolutions shown in Figures 6(a), (b), and (e), it is evident that the finest mesh clearly preserves the vorticity distribution during roll-up the best. Especially, the roll-up of a vorticity sheet from the main wing with many details is clearly seen in Figure 6(e). The vorticity peaks are also maxima in this finest mesh case. The influence of the switching wall-distance is observed from Figures 6 (b), (c), and (d), where the result with β = 0.07 in Figure 6(d) is close to the result of the finest mesh with the same switching wall-distance β = 0.07.

The dependence of the results on the switching wall-distance is reduced by using a RANS flow field with mesh refinement in the wake region [5]. The other possibility to alleviate the dependency is to use the optimization of the switching wall-distance locally as shown in the previous NACA0012 case. The optimization of the switching wall-distance is effective to obtain a sharp wake while realizing smooth transition of RANS-LES flow fields in other regions.

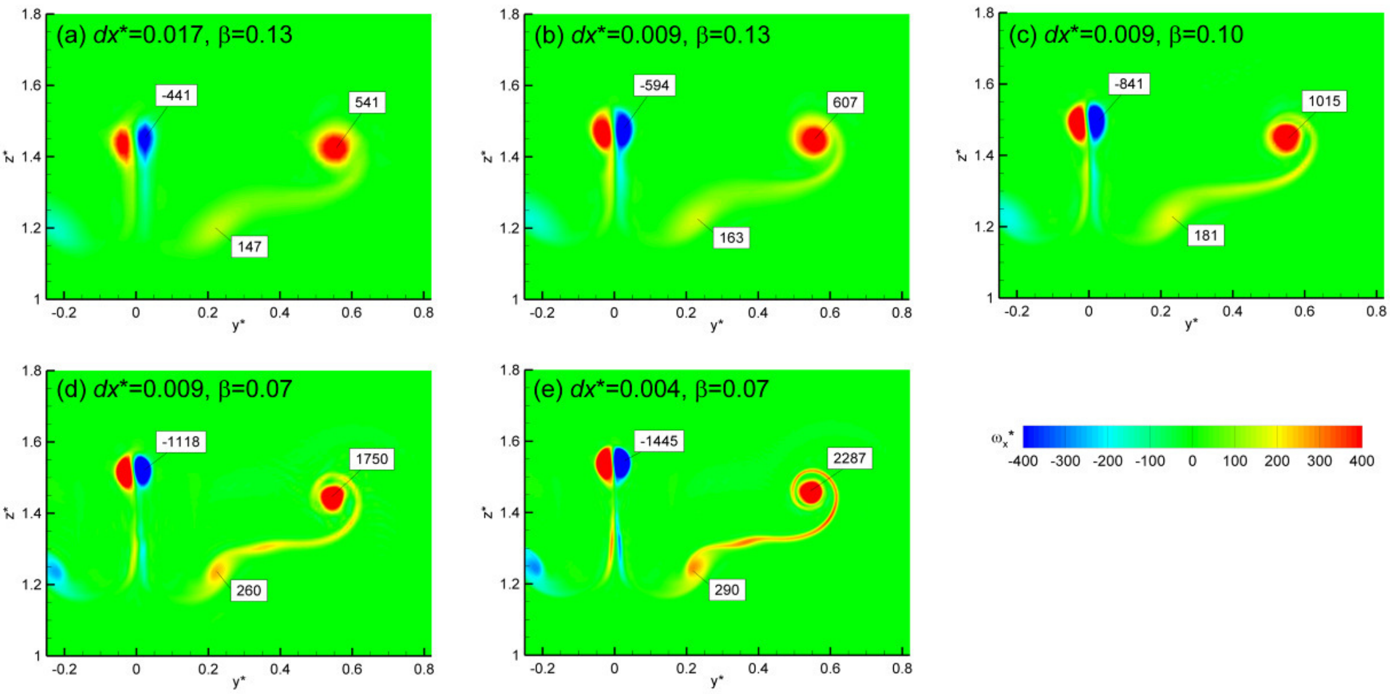

Figure 6. Vorticity distributions at x^* = 5.3 during the roll-up of DLR-F6 model's wake.

For the following analysis of the F6 model wake, the parameters used are dx*= 0.009 and β = 0.1; the optimization technique is not applied. Figure 7 shows the wake roll-up and the subsequent evolution of a vortex pair. Here the ambient turbulence is characterized by eddy dissipation rate of ε^* = 0.01. Temperature stratification is not considered. The flow field is visualized by two levels of iso-vorticity surfaces (red: $|\omega^*|$ = 250, blue transparent: $|\omega^*|$ = 65). The midpoint of the visualized wake in flight direction corresponds to the labelled position and time. The wingtip vortices and the fuselage wake have large vorticity magnitudes in the beginning. The jet-like fuselage wake decays relatively quickly while the wingtip vortices preserve large vorticity. The decayed fuselage wake and the vorticity from inboard wing (see also Figure 6) wrap around the wingtip vortices adding disturbances around them. A stable vortex pair appears between t* = 1 and 2 (cf. Figure 7 f and g). At t^* = 8.8, the vortex pair is highly disturbed and almost decayed.

Note that there is a difference of the vortex age between the both sides of the domain in flight direction after the wake initialization. Here the flow field is inverted slicewise to close the domain periodically. The resulting LES domain is two times larger than the original one, i.e., two times larger computational cost, but it is possible to apply periodic boundary conditions also for the longitudinal boundaries. The inverted part of the domain is not shown in Figure 7, where it is confirmed that the influence of the boundary treatment is not noticeable.

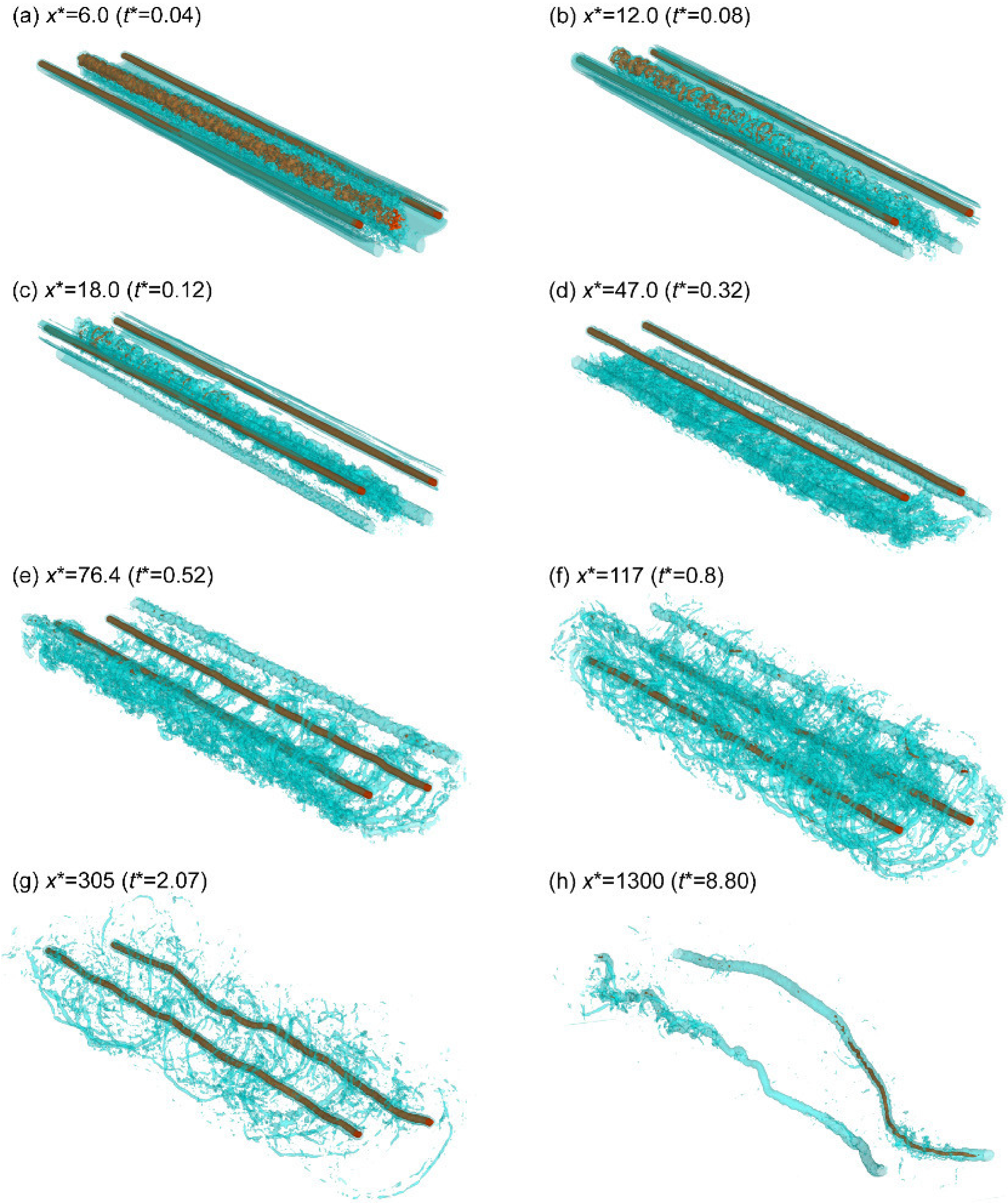

Figure 7. Temporal evolution of the vorticity distribution (red: $|\omega^*| = 250$, blue transparent: $|\omega^*| = 65$) of the wake behind the DLR-F6 model.

Figure 8(a) shows the circulation averaged between the non-dimensional vortex core radii of 0.106 to 0.318, which corresponds to the circulation averaged between core radii of 5 to 15 m, denoted as $\Gamma^*_{5\text{-}15}$, used in real-scale field measurements. Here the $\Gamma^*_{5\text{-}15}$ is averaged along vortex centerlines in the domain. The plot shows ε^* = 0.01, N^* = 0.0 and ε^* = 0.01, N^* = 0.35 cases as well as the case using Lamb-Oseen vortex model as in the conventioal LES of a vortex pair. The horizontal axes denote the distance from the wingtip (bottom) and the time (top). The start time of Lamb-Oseen model case is shifted because the Lamb-Oseen model represents a fully rolled-up vortex pair. There is a peak of the averaged circulation during the roll-up, and the initial decay rate is larger than in the Lamb-Oseen case. The circulation peak corresponds to the completion of the roll-up process (see also Figure 7), whereas the stronger decay rate might reflect the effect of the entrainment of the turbulence from the fuselage wake. It is also confirmed that the stable stratification effectively enhances circulation decay.

Figure 8 (b) shows the evolution of the vortex separation. It exhibits a local minimum followed by a local maximum value during the roll-up process. After about t^* = 2, the neutrally and stratified cases differ, the vortex spacing increases monotonously in the former case, whereas it stays first constant and then decreases slightly in the latter case. A similar evolution is noticed for the stratified Lamb-Oseen case. Figure 8 (c) shows the evolution of vortex core radii. The initial value of the core radius in the Lamb-Oseen case is set to 0.045. In all cases the vortex core radii evolve identically for six time units or about 900 vortex spacings behind the aircraft. Then the stratified cases show an abrupt increase; the neutral case follows about 2 t_0 later. The peak tangential velocities shown in Figure 8 (d) rapidly drop after the roll-up at t^* = 1, while the root-mean-square (RMS) velocity fluctuations along the vortex increase sharply. These observations corroborate the effect of the entrainment of fuselage turbulence into the main vortex pair and the larger decay rate of the averaged circulation in the early vortex phase (Figure 8a).

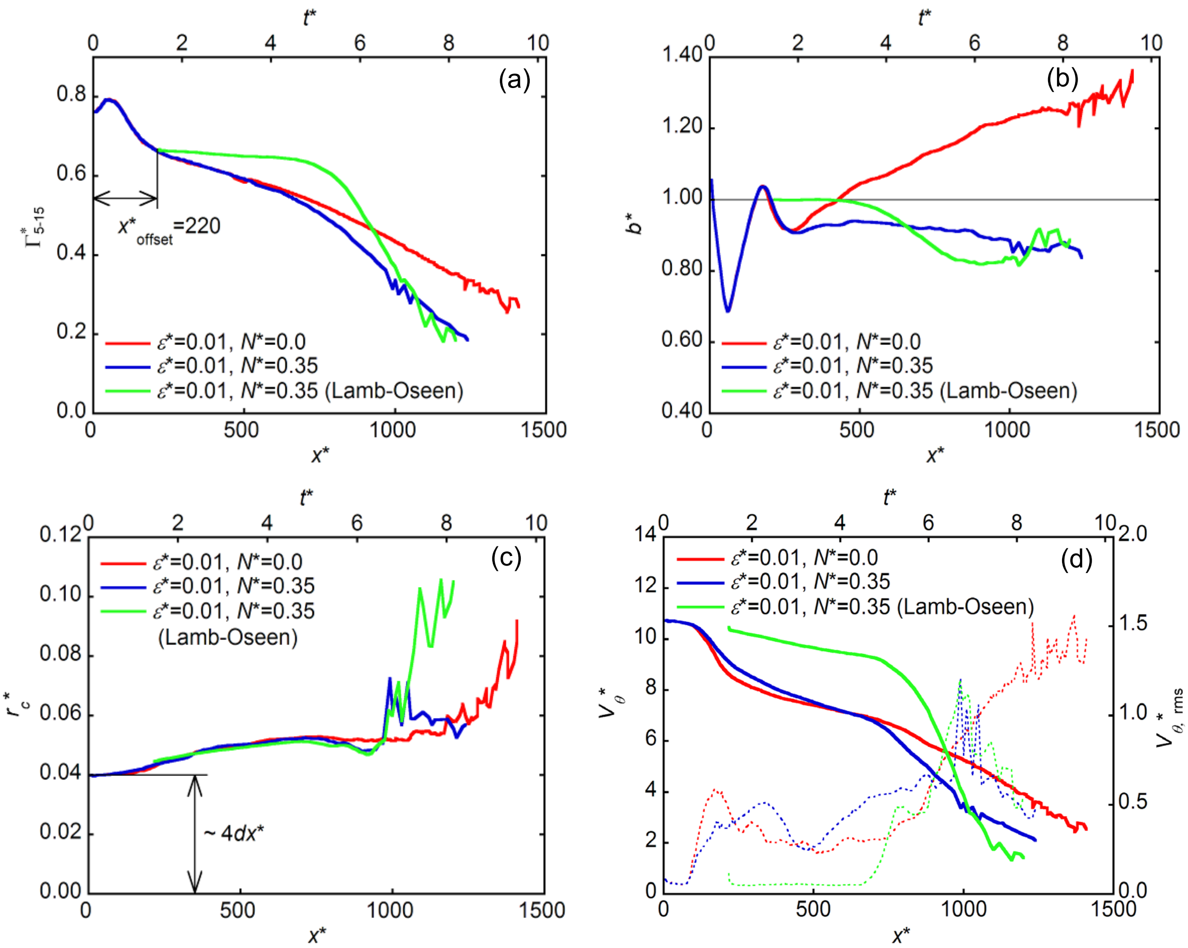

Figure 8. Temporal evolutions of (a) averaged circulation, (b) vortex separation, (c) vortex core radius, and (d) peak tangential velocity generated by the DLR-F6 model.

The AWIATOR case of a large transport aircraft

Another realistic configuration is a large transport aircraft model used in ONERA's catapult tunnel during the European AWIATOR project. The 1/27 scaled model has span width of 2.236 m. The experiment conditions are Re = 5.2×10^5, U_∞=25 m/s, and C_L = 1.4. Applying similar normalization as the previous DLR-F6 case, we have Γ_0 = 5.36 m^2/s, b_0 = 1.756 m, w_0 = 0.49 m/s, and t_0 = 2.0 s. The RANS solution is obtained by the DLR TAU-code with the adaptive mesh refinement for wingtip and flap vortices as well as for fuselage wake. The RANS/LES coupling was achieved with the setting dx*= 0.009 and β = 0.07; the optimization technique is not applied.

Figure 9 shows the evolution of vorticity distribution on a ground fixed vertical plane from t^* = 0.32 until 1.631. In this high-lift configuration, the vortices from the deployed outboard flap are stronger than wing-tip vortices. As a result, the wingtip vortex rotates around the outboard flap vortex and merges to the outboard flap vortex at t^* = 0.742. The vorticity shed by the fuselage is relatively large in the beginning, however, the magnitude decreases quickly due to mutal cancellation across the symmetry line. The vorticity shed by the through-flow nacelles also decays quickly. Similar to the DLR-F6 case it takes about one time unit to complete the roll-up process.

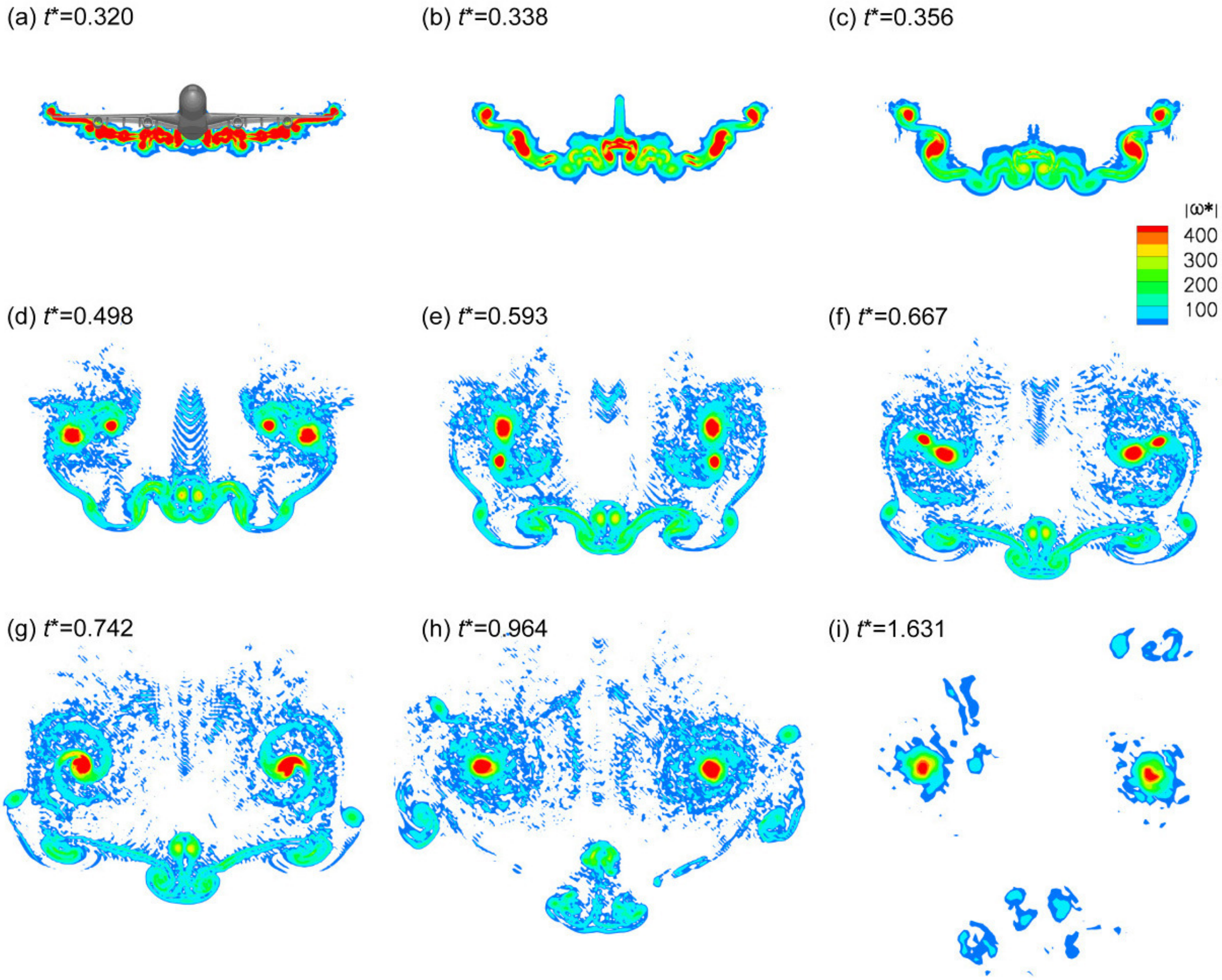

Figure 9. Evolution of vorticity distribution during roll-up of the wake of the large transport aircraft model

Conclusions

LES of wake vortex evolution from its generation until vortex decay is performed by combining RANS and LES flow fields. The RANS flow field is employed in the LES as a forcing term sweeping through the ground-fixed LES domain. An eddy viscosity initialization to match the time-averaged LES and RANS eddy viscosities, as well as an optimization technique to obtain the best switching wall-distance in the RANS/LES coupling are proposed.

The methodology is tested using the NACA0012 wing. The present approach achieves comparable results with the experiment by using the RANS flow field very near around wings and fuselage and LES elsewhere. This way the wingtip vortex properties observed in the experiment are well reproduced. The RANS alone is too diffusive to reproduce the experimental results downstream the trailing edge.

Further, the roll-up process of the wake initialized by the DLR-F6 model in low-lift configuration is simulated. The roll-up processes of the vorticity sheet emanating from the wing and tight vortices from the wingtip are simulated. A stable vortex pair appears after this. The growth of the vortex core radius is small especially after the roll-up, where the vortex core radius still depends on the mesh resolution considered here. Finally, the methodology is applied to a model of a large transport aircraft. In this high-lift case, the vortices generated from the outboard flaps are stronger than the wingtip vortices. Therefore, the wingtip vortices wrap around the outboard flap vortices, merging occurs at $t^* = 0.74$. The roll-up process is completed about one time unit after “fly-by” as in the clean low-lift case of the F6 model.

Acknowledgements

We would like to thank Olaf Brodersen, Niko Schade and Bernhard Eisfeld (Institut für Aerodynamik und Strömungstechnik) for providing the RANS data of the DLR-F6 model and Stefan Melber (Institut für Aerodynamik und Strömungstechnik) for the RANS data of the large transport aircraft model. We also thank Prof. Michael Manhart and Dr. Florian Schwertfirm for the provision of the original version of LES code MGLET. Computer time provided by Leibniz-Rechenzentrum (LRZ) is greatly acknowledged. We thank Airbus for the allowance to use the near field wake data of the large transport aircraft model for our computations.

References

[1] Gerz, T., Holzäpfel, F., and Darracq, D., “Commercial Aircraft Wake Vortices,” Progress in Aerospace Science, Vol. 38 (2002), pp. 181-208.

[2] Minnis, P., Young, D. F., Ngyuen, L., Garber, D. P., Smith Jr., W. L., and Palikonda, R. “Transformation of Contrails into Cirrus during SUCCESS,” Geophysical Research Letters, Vol. 25 (1998), pp. 1157-1160.

[3] Schumann, U., Graf, K., and Mannstein, H., “Potential to Reduce the Climate Impact of Aviation by Flight Level Change,” AIAA Paper 2011-3376, 2011.

[4] Breitsamter, C., “Wake vortex Characteristics of Transport Aircraft,” Progress in Aerospace Science, Vol. 47 (2011), pp. 89-134.

[5] Stumpf, E., “Study of Four-Vortex Aircraft Wakes and Layout Corresponding Aircraft configurations,” Journal of Aircraft, Vol. 42 (2005), pp. 722-730.

[6] Rossow, V. J., “Lift-Generated Vortex Wakes of Subsonic Transport Aircraft,” Progress in Aerospace Science, Vol. 35 (1999), pp. 507-660.

[7] Holzäpfel, F., Hofbauer, T., Darracq, D., Moet, H., Garnier, F., and Gago, C. F., “Analysis of Wake Vortex Decay Mechanisms in the Atmosphere,” Aerospace Science and Technology, Vol. 7 (2003), pp. 263-275.

[8] Holzäpfel, F., Gerz, T., Frech, M., and Dörnbrack, A., “Wake Vortex in Convective Boundary Layer and Their Influence on Following Aircraft,” Journal of Aircraft, Vol. 37 (2000), pp. 1001-1007.

[9] Proctor, F. H., Hamilton, D. W., and Han, J., “Wake Vortex Transport and Decay in Gound Effect: Vortex Linking with the Ground,” AIAA Paper 2000-757 (2000).

[10] Unterstrasser, S., Sölch, I., “Study of Contrail Microphysics in the Vortex Phase with a Lagrangian Particle Tracking Model,” Atmospheric Chemistry and Physics, Vol. 10 (2010), pp. 3922-.

[11] Manhart, M., “A Zonal Grid Algorithm for DNS of Turbulent Boundary Layer,” Computer and Fluids, 33 (2004), pp. 435-461.

[12] Hokpunna, A., and Manhart, M., “Compact Fourth-order Finite Volume Method for Numerical Solutions of Navier-Stokes Equations on Staggered Grids,” Journal of Computational Physics, Vol. 229 (2010), pp. 7545-7570.

[13] Meneveau, C., Lund, T. S., and Cabot, W. H., “A Lagrangian Dynamic Subgrid-scale Model of Turbulence,” Journal of Fluid Mechanics, Vol. 319 (1996), pp. 353-385.

[14] Williamson, J. H., “Low-storage Runge-Kutta Schemes,” Journal of Computational Physics, Vol. 35, No. 48, 1980, pp. 48-56.

[15] Coton, P., “Study of Environment Effects by Means of Scale Model Flight Test in a Laboratory,” 21st ICAS Congress, ICAS-98-391, Melbourne, September 1998.

[16] Misaka, T., Holzäpfel, F., Gerz, T., Manhart, M., and Schwertfirm, F., “Large-Eddy Simulation of Wake Vortex Evolution from Roll-Up to Vortex Decay,” AIAA Paper 2011-1003, 2011.

[17] Fujii, K., “Unified Zonal Method Based on the Fortified Solution Algorithm,” Journal of Computational Physics, Vol. 118 (1995), pp. 92-108.

[18] Kalnay, E., Atmospheric Modeling, Data Assimilation and Predictability, Cambridge University Press, 2003.

[19] Czech, M. J., Miller, G. D., Crouch, J. D., and Strelets, M., “Near-field Evolution of Trailing Vortices Behind Aircraft with Flaps Deployed,” AIAA Paper 2004-2149, 2004.

[20] Chow, J., Zilliac, G., and Bradshaw, P., “Turbulence Measurements in the Near Field of a Wingtip Vortex,“ NASA TM-110418, 1997.

[21] Dacles-Mariani, J., Zilliac G., Chow, J., and Bradshaw, P., “Numerical/Experimental Study of a Wingtip Vortex in the Near Field,“ AIAA Journal, 33 (1995), pp. 1561-1568.

[22] http://www.openfoam.com/

[23] Brodersen, O., Eisfeld, B., Raddatz, J., and Frohnapfel, P., “DLR Results from the Third AIAA Computational Fluid Dynamics Drag Prediction Workshop,“ Journal of Aircraft, 45 (2008), pp. 823-836.

6.3 Experimental Study on Wake Vortices Impacted by Turbulence and Surfaces

Reinhard Geisler, Robert Konrath
Institute of Aerodynamics and Flow Technology

Wake vortices from a generic aircraft wing model have been investigated experimentally in a water towing tank. The impact of environmental turbulence has been studied as well as the interaction of the vortices with surfaces of different contours. The experimental methods include time-resolved stereo Particle Image Velocimetry (PIV) and vortex core visualization.

Introduction

As a consequence of lift generation by aircraft wings of limited span width, vortex sheets shed off the wings, roll up and form a pair of counter-rotating vortices. The evolving two-vortex systems persist in the aircraft wake for a long period of time, possessing a high amount of kinetic energy and thereby posing a potential hazard to following aircraft. To avoid wake vortex encounters, regulatory separation distances between aircraft, dependent on their size, have to be met, which leads to a limit in the possible handling capacity of the airport. Therefore, the investigation on the decay of wake vortices is an important issue in commercial aviation (Gerz et al., 2002, 2005; Spalart, 1998).

It is well known that a stable pair of equal-strength counter-rotating vortices is subject to cooperative instabilities which can lead to their decay in the far field (Bristol et al., 2004; Crouch, 2005; Jacquin et al., 2003, 2005; Rennich and Lele, 1999; Winckelmans et al., 2005; Konrath, 2009). In the case of the long-wavelength ($\lambda \approx$ 5-10 spans) Crow instability (Crow, 1970), both tip vortices re-connect in the far wake across the mid plane in a series of ring-like vortex structures, after having experienced strong sinusoidal undulations. The development of the Crow instability is promoted by ambient turbulence, which can reduce their lifetime significantly (Sarpkaya and Daly, 1987; Han et al., 2000, Holzäpfel et al., 2003; Delisi, 2006). In the first part of the present study the development of the Crow instability as dependent on the ambient turbulence level is investigated up to the very far field, including the vortex re-connection and the formation of vortex rings by the volumetric measurement of the three-dimensional space curves of the evolving vortex core lines. The tests are performed in a towing tank using a small generic wing model to produce a two-vortex system. A well-defined turbulence field is produced in the tank by a grid towed through the tank prior to the model, similar to the setup used by Delisi, 2006. The turbulence is characterised quantitatively with respect to the turbulence intensity and length scales by performing high-speed PIV measurements.

During the last decade, the evolution of wake vortices close to the ground has received much attention. As shown by Robins and Delisi, 1993 or Türk et al., 1999, wake vortices in ground proximity can also persist for a long period and still pose a hazard for following aircraft. The evolution of a wake vortex system in ground proximity results in a complex three-dimensional flow. When counter-rotating vortices approach the ground or are generated at low altitudes, the proximity of a flat surface causes a lateral movement of the vortices resulting in an increase in their separation distances. Induced by the vortices an outboard directed flow on the surface establishes and vorticity of opposite sign is produced in a boundary layer, which causes a rebound motion of the vortices (Harvey and Perry, 1971). The induced flow near the surface experiences an adverse pressure gradient when passing the vortex cores, which is strong enough to cause a flow separation, leading to the formation of a separation bubble on the ground. Flow simulations performed by Dufresne et al., 2005; Spalart et al., 2001 and Proctor and Hamilton, 2000 show how pairs of secondary vortices are produced from the separation region; these then detach and interact with the primary vortices. The simulations of Türk et al., 1999 show also that the generated number of secondary vortices depends on the Reynolds number. Experimental results of Konrath et al., 2008 obtained in a towing tank reveal the formation of a separation bubble which is followed by the generation of a series of multiple smaller vortices enrolled by the primary vortex. In order to predict the behaviour of a two vortex system in ground proximity and its decay in the far field, additional tests were performed in a second part of the current study; here experiments were performed in the same towing tank using the same model but introducing a flat ground and varying the altitudes of the model above the plate. In addition, the investigations comprise cases with ground irregularities to clarify whether such disturbances are able to destabilize the vortices and to promote their decay.

Experimental Set-up

Water towing tank "WSG"

The present study has been performed at the DLR water towing tank in Göttingen ("Wasserschleppkanal Göttingen", WSG). This facility consists of an 18 m tank of cross-section 1.1 m by 1.1 m equipped with a carriage capable of crossing the tank at a maximum speed of 5 m/s. Models under investigation can be attached to this carriage and are propelled along the tank at defined velocities while the water inside the tank is at rest. Compared to a recirculating water tunnel, this approach permits measurements far behind the model. In addition, experiments can be performed at very low turbulence levels. This requires, however, enough time for the turbulence to settle down. Thus, the water in the tank was left to rest for at least 20 minutes prior to each run.

Since one part of this work deals with the influence of turbulence, a means of generating turbulence in a controlled way was needed. A pilot carriage with a drive system independent of the model carriage was constructed. Attached to this carriage, a square grating (20 mm profiles, pitch 200 mm) can be towed through the water upstream of the model at a maximum velocity of 1 m/s. This generates a turbulence field with temporal decay. By changing the delay between pilot and model carriage the turbulence level thus can be selected. Magnetic switches along the track are used to monitor the carriages and synchronize the measurement system.

F13 Model

To rule out the influence of the towing tank side walls, a minimum distance of one model span between walls and vortices is required. To ensure this limit, a small version of the DLR F13 model was build. This model has a main wing span of 175 mm and a chord length of 35 mm. An optional tail wing with the same chord length but different spans can be attached for 4-vortex system investigations. The profile in both cases is a Wortman FX63-137B-PT. Embedded in the wing tips are outlets for contrast agents to trace the vortex cores. The model is supported by a profiled strut attached to the carriage via a translation stage. By this means the vertical position of the model can be adjusted. For the present experiments, the angle-of-attack is set to 10° and the tail wing is replaced by a cone tail. The initial vortex distance is b_0 = 153 mm.

Stereo PIV

The velocity vector fields of the wake vortices are measured by means of a time-resolved stereo PIV system. Polyamide particles of 20 µm average diameter are suspended into the water as tracer particles. They are illuminated by a Lee LDP 200-MQG laser at 1 kHz repetition rate and with a pulse energy of 25 mJ. The laser beam is expanded and refocused by a telescope and finally spread out to a light sheet by a cylindrical lens. Depending on the application, this light sheet is brought into the towing tank either from the side or from the bottom with a final orientation perpendicular to the towing direction.

Two Photron APX-RS high-speed cameras record the light scattered by the polyamide particles from both sides of the light sheet. To reduce aberrations, glass prisms filled with water are attached to the sides of the tank with their air-glass interfaces perpendicular to the respective camera line of vision. Scheimpflug correction is applied to ensure image sharpness for the complete field of view. The total camera setups are attached to motorized translation stages which can follow the descent of the vortices. The imaging system is calibrated by taking photos of a calibration grid printed on a glass plate in the water at the light sheet position. Laser, cameras and translation stages are controlled by a programmable sequencer triggered by a magnetic switch from the model carriage.

Wake vortices show a decreasing dynamic range of velocities. Thus, the delay used for PIV recordings has to be adapted accordingly. In the current application, PIV images are recorded at the relative times of 0, 2, 5, 10 and 20 ms. This sequence is repeated every 50 ms (compare Figure 1). Using this scheme, the PIV delay can be selected and adapted to the actually occurring velocity range after the recording while maintaining a sufficient time resolution of 20 vector fields per second as well as a long total observation time (limited by camera RAM).

The acquired images are evaluated using a well-established multigrid cross-correlation analysis with image deformation. Disparity correction with the final light sheet is applied to compensate for the refraction caused by the glass calibration grid carrier.

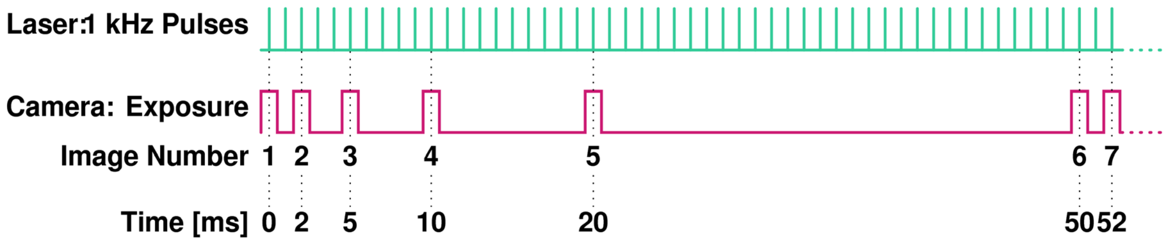

Figure 1. Timing for PIV measurement

Vortex core visualization

Since PIV provides only local planar information on the wake vortices, vortex core visualization has been applied. Driven by gravity, a contrast agent from a vessel 0.5 m above the water surface is fed into the tube system of the model and finally released into the vortex core through outlets at the wing tips. Two configurations are used:

a) Polyamide particles are used as contrast agent in the turbulence measurements. Two Rapp OptoElectronic NGW10 Xenon flash lamps illuminate the measurement volume from both sides of the towing tank. The light scattered by the particles is recorded at two frames per second with three PCO.4000 Cameras from below the towing tank. The cameras are arranged in a plane perpendicular to the towing direction with a central camera imaging along a vertical line of vision, and the other two cameras recording the volume along tilted lines of vision from opposite sides. The camera system is calibrated with a calibration grid in three parallel planes throughout a volume of at least 700 * 360 * 600 mm³. Quantitative results can be obtained.

b) Black ink is used as contrast agent in the investigation of vortices close to surfaces. Since here the view from below the tank is spoiled by constructions supporting the transparent ground plate and the humps as well as by bubbles below the ground plate, the ink traces are recorded with background illumination from above the tank by a consumer grade HD video camcorder. Since calibration and quantitative evaluation here are hindered by the surface waves of the water, only qualitative results can be obtained in this configuration.

Results

Wake vortices in a turbulent environment

The first part of the present study covers the impact of turbulence on the wake vortices. First, the time-dependency of the turbulence generated by the pilot grating is characterized by PIV (Figure 2, left). The vortex velocity of descent is estimated once at the negligible turbulence level of the towing tank after a settling time of 20 minutes. In all following PIV measurements, the translation stages move the cameras at a constant velocity to follow the descent of the vortices.

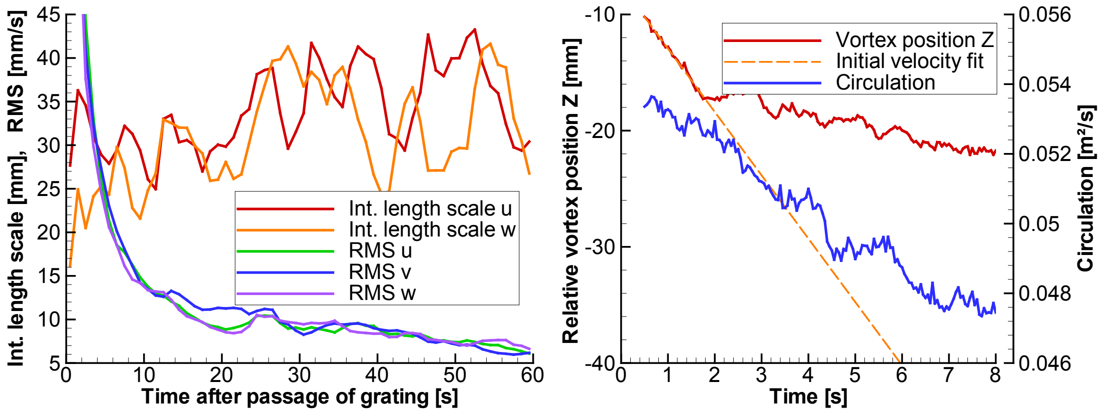

Figure 2. Characterisation of turbulence (left) and dynamic parameters of wake vortices in a low turbulence environment (right). Vortex position is relative to the coordinate system moving downwards with 44 mm/s.

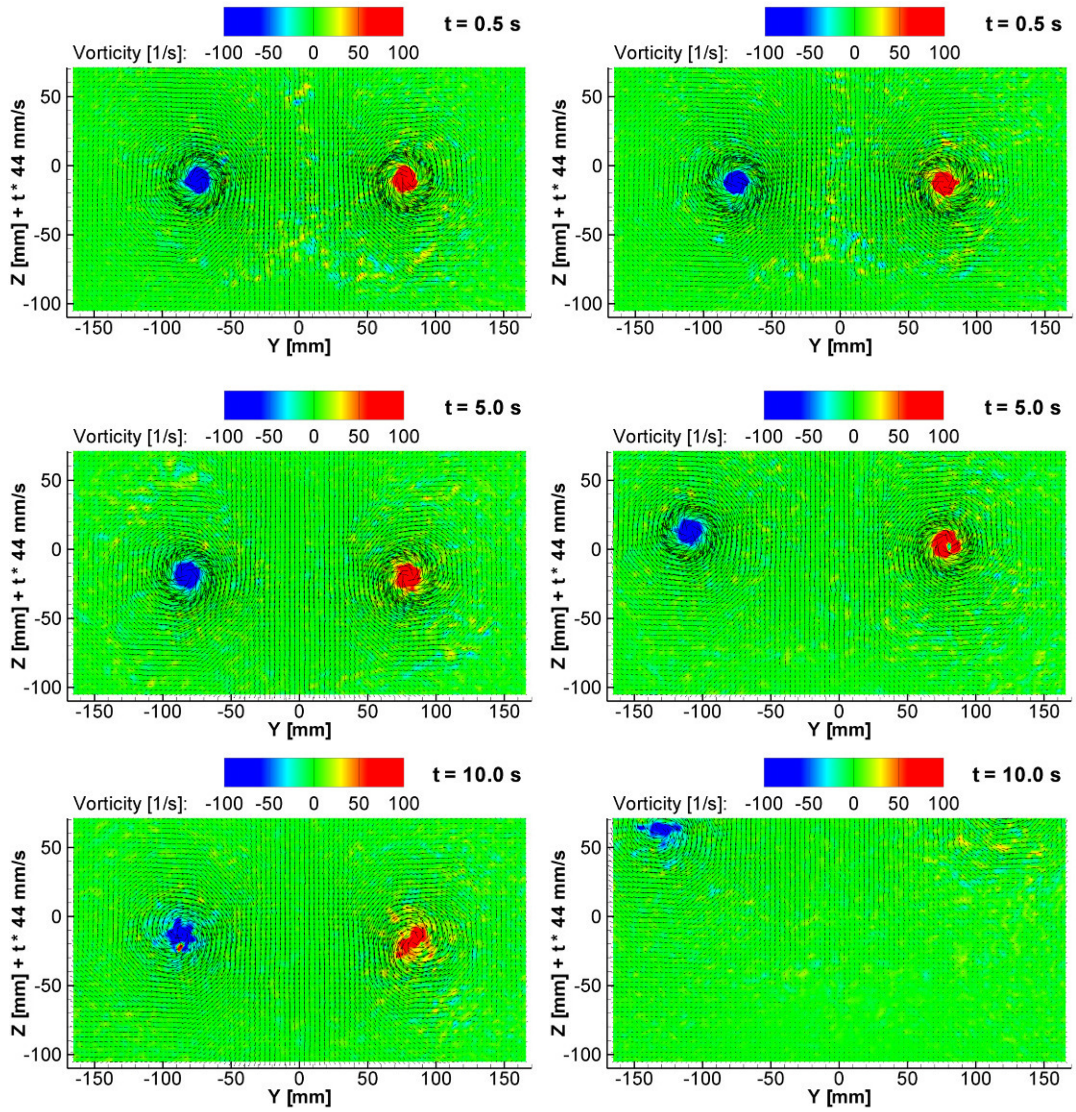

Figure 3. Wake vortices without (left, reproducible) and with (right, example) environmental turbulence. Snapshots within the first 10 seconds (i.e. t/t_0 = 3.2 or a distance of 159 b_0 behind the model). Model velocity 2.44 m/s, turbulence rms 5 mm/s (2‰), coordinate system moving downwards with 44 mm/s.

Table 1: Parameter matrix for PIV measurements

Configuration	**1**	**2**	**3**	**4**	**5**	**6**
Time after passage of grating [s]	**Without grating**	**Without grating**	**80**	**80**	**40**	**40**
Turb. rms [mm/s]	0	0	5	5	8	8
Model velocity [m/s]	**1**	**2.44**	**1**	**2.44**	**1**	**2.44**
Reynolds number: Chord based	35000	85000	35000	85000	35000	85000
Circulation based	17000	52000	17000	52000	17000	52000
Initial circulation [m²/s]	0.019	0.052	0.019	0.052	0.019	0.052
Initial velocity of descent w_0 [mm/s]	21	49	21	49	21	49
Reference time $t_0 = b_0 / w_0$ [s]	7.2	3.1	7.2	3.1	7.2	3.1

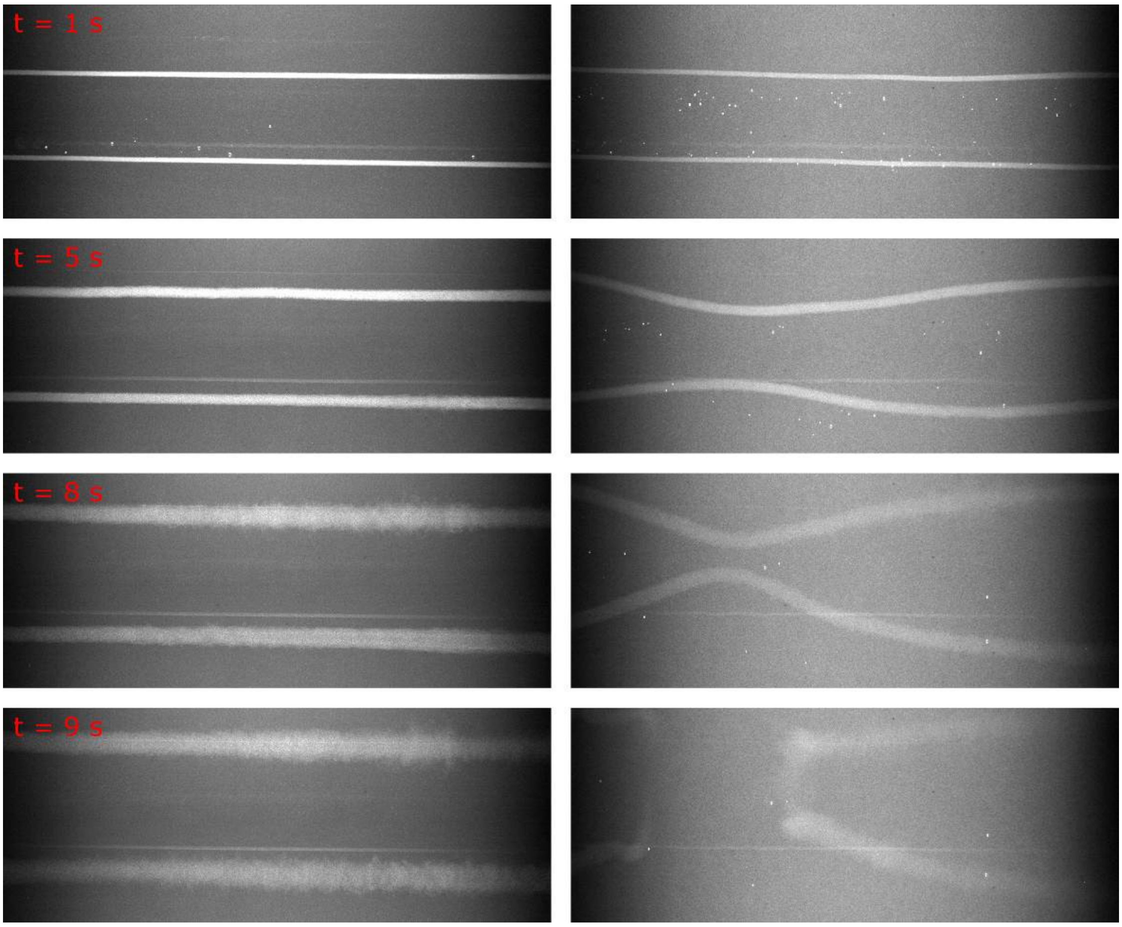

Figure 4. Vortex core visualization without (left, reproducible) and with (right, example) turbulence. Selected snapshots within the first 9 seconds (i.e. t/t_0 = 2.9 or a distance of 144 b_0 behind the model). Model velocity 2.44 m/s from right to left, turbulence rms 5 mm/s (2‰).

To rule out an influence of the towing tank floor, the measurements were interrupted when the vortices reached a distance of around 200 mm (>b_0) from the floor. Thus, the vortices have a free vertical path of around 450 mm. Since the laser light sheet has to cover an area defined by this path and the vortex distance, it was fed into the towing tank from underneath. As a result, the complete water height inside the tank was illuminated to a width of at least 350 mm. To image this field, the high-speed cameras have been equipped with Nikkor 1.8/50 lenses operated at an aperture setting of F/# 5.6. Vortex parameters like initial velocity of descent and circulation are measured at the negligible turbulence level (Figure 2, right). In Table 1, a summary of the parameter matrix measured by PIV is given.

Due to the mandatory settling time between two measurements, it takes a long time to gain a statistically significant number of runs. Thus, the maximum number of runs per configuration had to be restricted to ten. A typical result is depicted in Figure 3. The wake vortices without environmental turbulence (left side; configuration 2) show a stable behaviour. The positions of the vortex cores are almost fixed within the coordinate system moving at a constant speed of 44 mm/s (see also Figure 2, right). In contrast, the low turbulence level of 5 mm/s (2‰) is already sufficient to destabilize the vortices and divert the movement of the cores (example in Figure 3, right side; configuration 4). The exact behaviour here is not predictable. Figure 4 shows corresponding vortex core visualizations recorded from below the towing tank. In the turbulence-free configuration on the left side, the vortex cores just sink with constant velocity and separation. The apparent growth in the core distance is caused by perspective. In the turbulent configuration (right side), a Crow instability is visible. Since this instability is not artificially triggered but dependent on the turbulent nature of the environment, it is not possible to predict either the position of the vortex-linking, or, in fact, whether vortex linking will happen at all.

Wake vortices in proximity to surfaces

In the second part of this study the development of the wake vortices in proximity to the ground has been investigated for flat ground as well as for selected generic 2d-topologies (Figure 5). At about half the water depth of the towing tank, a flat PMMA (acrylic glass) ground plate has been installed along the complete path of the model carriage. The model support is attached to a translation stage on the carriage to allow the model distance *h* from the ground plate to be adjusted. Since this distance is a maximum of 160 mm only, the cameras in this configuration are not required to follow the movement of the vortex core and thus are left at rest. Equipped with Contax 2.8/21 lenses (aperture setting F/# 8), they capture a field of 400 mm x 240 mm, which covers the complete relevant development of one vortex generated by the model. The second vortex generated by the model is not recorded since the setup is symmetric and hence no additional information is to be expected. Again, to rule out undesirable influences, the field of view has to be limited to a minimum distance of b_0 from the side walls. The laser light sheet in this case is coupled into the tank through a side wall.

In an initial parameter study the influence of the model distance *h* from the ground is investigated (Figure 6). As is known, the vortex is deflected sideways and finally rises again. It is worth noticing that the angle at which the vortex rises again after deflection is around 23° and almost independent of the distance *h* as well as from the model velocity. Vorticity and vortex stability, however, do depend on *h*.

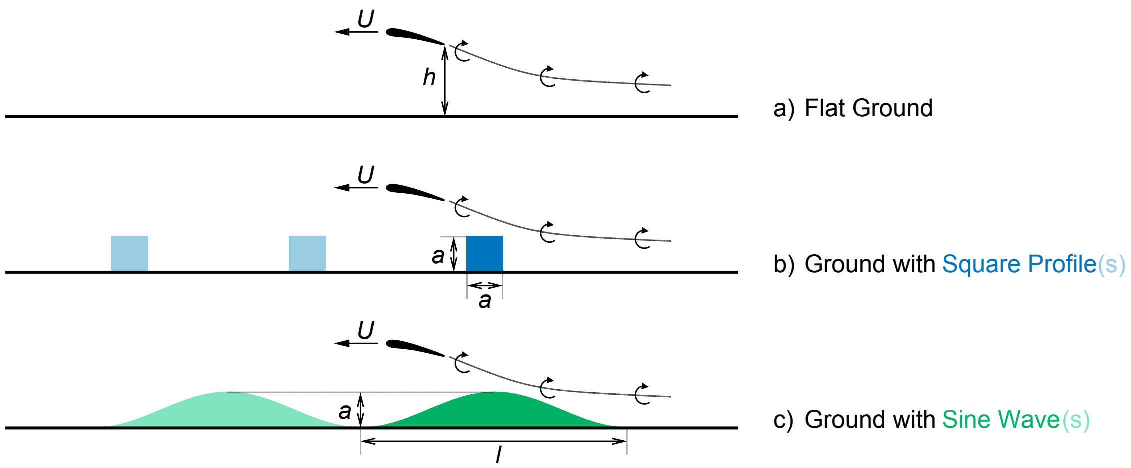

Figure 5. Ground topologies investigated.

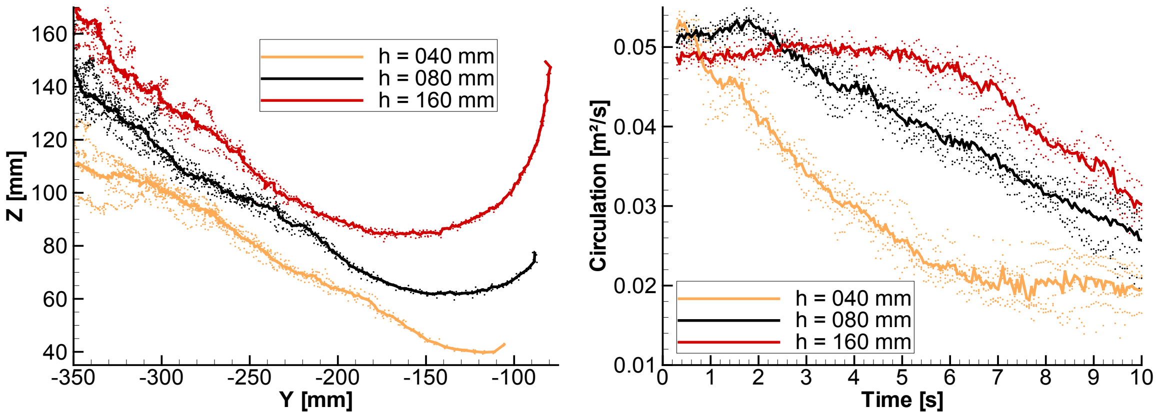

Figure 6. Vortex core trajectories (left, vortices moving from right to left) and time-dependent circulation (right) derived from PIV for different heights *h* over a flat ground. Depicted are individual runs (dotted) and their averages (lines). Model velocity *U* = 2.44 m/s, ground at *Z* = 0 mm.

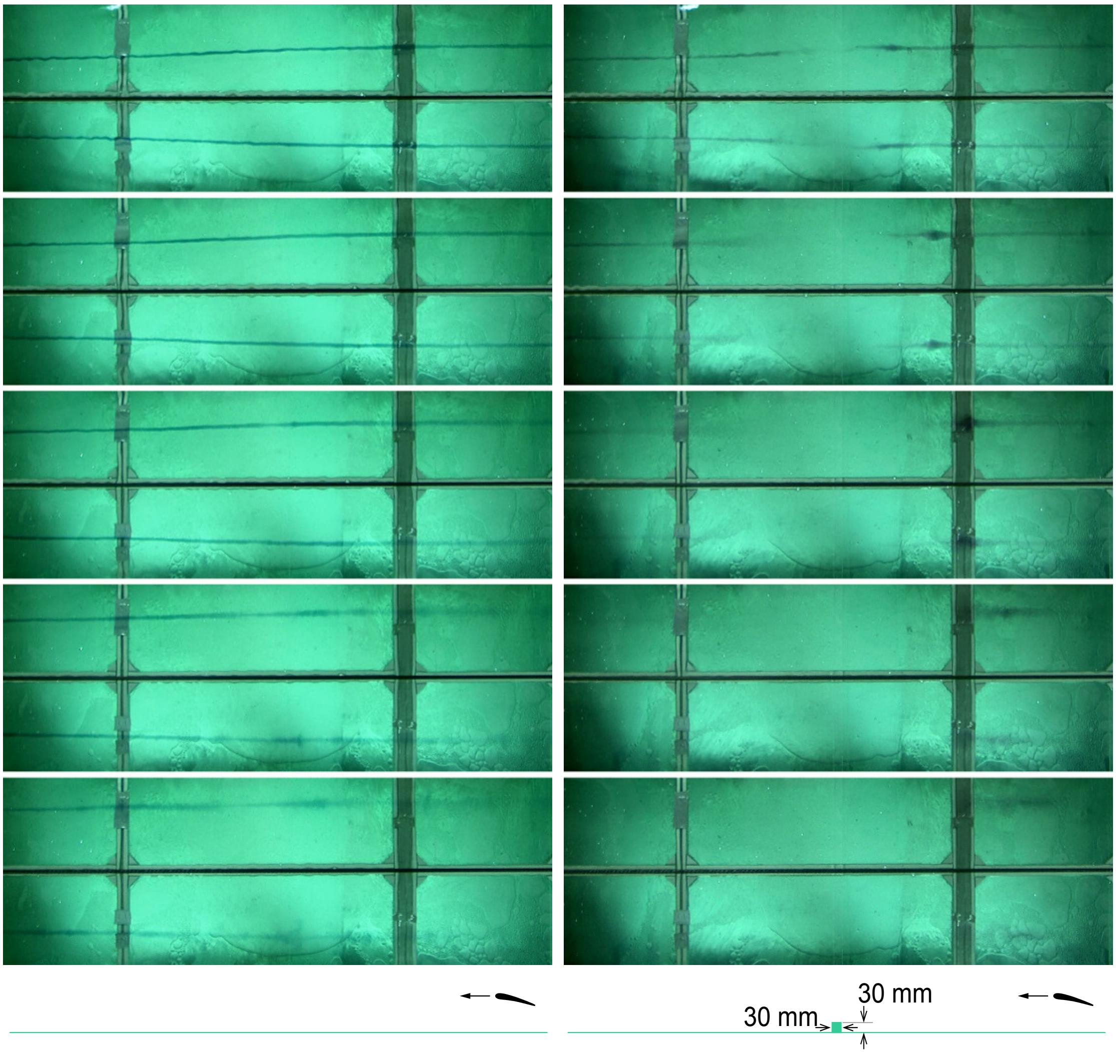

Figure 7. Vortex core visualization of the interaction with a flat ground (left) and a 30 mm square profile perpendicular to the towing direction (right, transparent profile in the centre of the image). Upper images 1.6 s after model passage, consecutive images with 0.4 s interframe time. Model velocity *U* = 2.44 m/s from right to left, ground distance *h* = 80 mm, image width approx. 2 m.

The main part of the investigation is performed at a constant ground distance *h* = 80 mm with different configurations of 2d humps along the path of the model (Figure 5 b, c). Square profiles with a side length of 10 mm, 20 mm and 30 mm in single, double or triple sequence and a sine wave of total (double) amplitude 40 mm with a length of 1300 mm (2π) and 2600 mm (4π) have been used. All ground topologies are constructed from transparent PMMA (acrylic glass) so as to giving minimal obstruction for the visualization analysis.

To get a first qualitative impression, video visualizations have been recorded from the top of the towing tank. Black ink was released from the wing tips to trace the vortex cores (see above). Without additional humps, the ground only directs the vortices sideways (Figure 7, left). With a 30 mm square profile perpendicular to the towing direction (Figure 5 b), disturbances emerge travelling upstream and downstream from the point where the vortex first hits the profile (Figure 7, right).

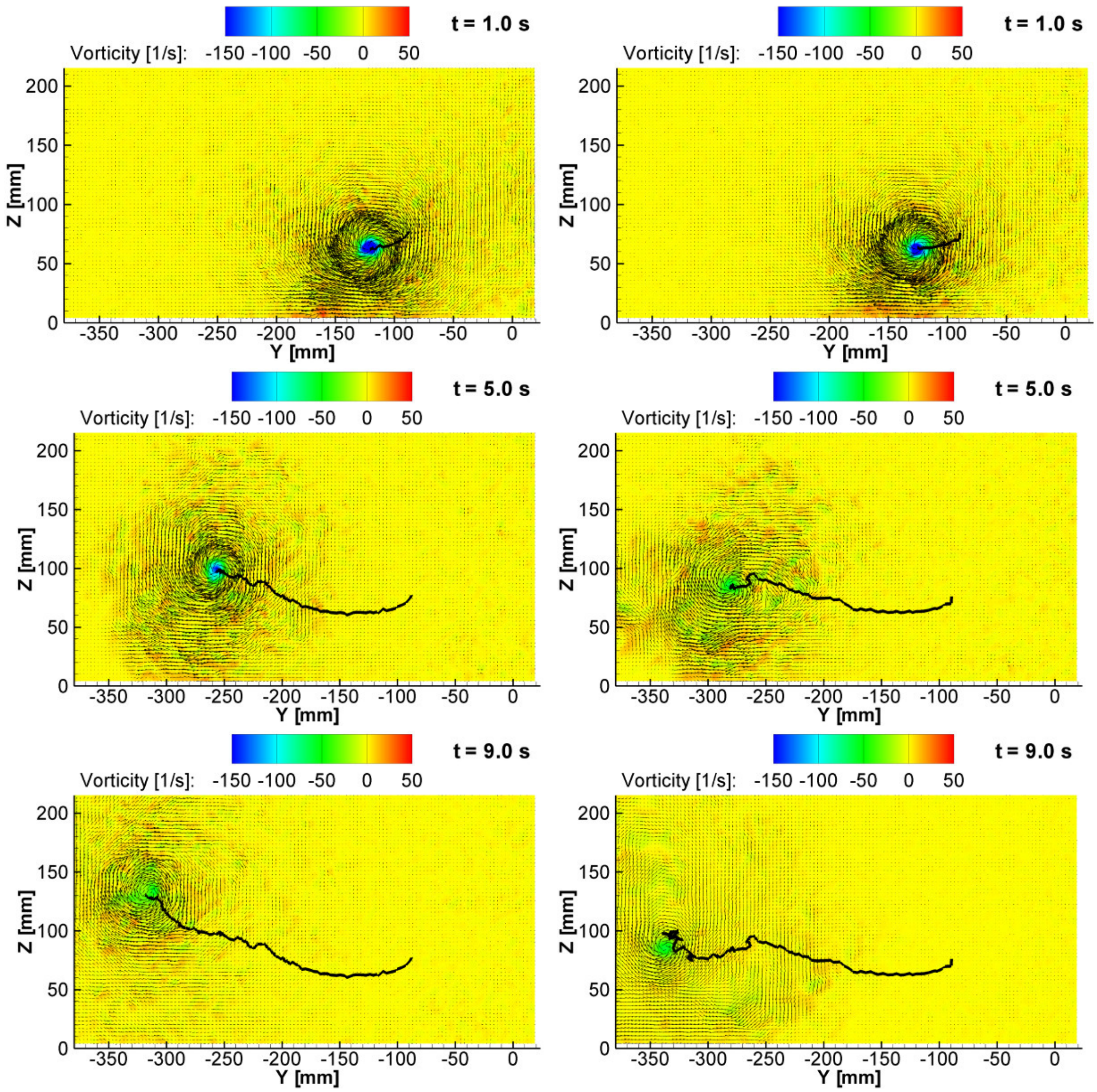

Figure 8. PIV results (vorticity, colour coded) of the vortex interaction with a plain flat ground (left) and a 30 mm square profile perpendicular to the towing direction 160 mm ahead of the PIV plane (right). Model velocity *U* = 2.44 m/s, ground distance *h* = 80 mm, ground at *Z* = 0 mm. Black arrows mark the velocity vectors in the (Y,Z) plane; the thick black curve traces the vortex path.

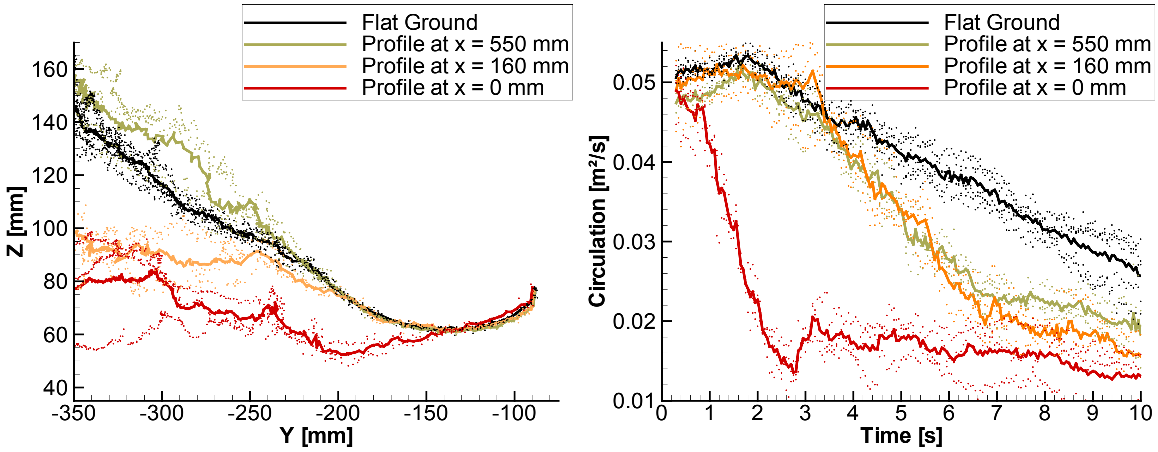

Figure 9. Vortex core trajectories (left) and time-dependent circulation (right) derived from PIV for different distances from a 30 x 30 mm² square profile. Depicted are individual runs (dotted) and their averages (lines). Model velocity U = 2.44 m/s, ground distance h = 80 mm, ground at Z = 0 mm.

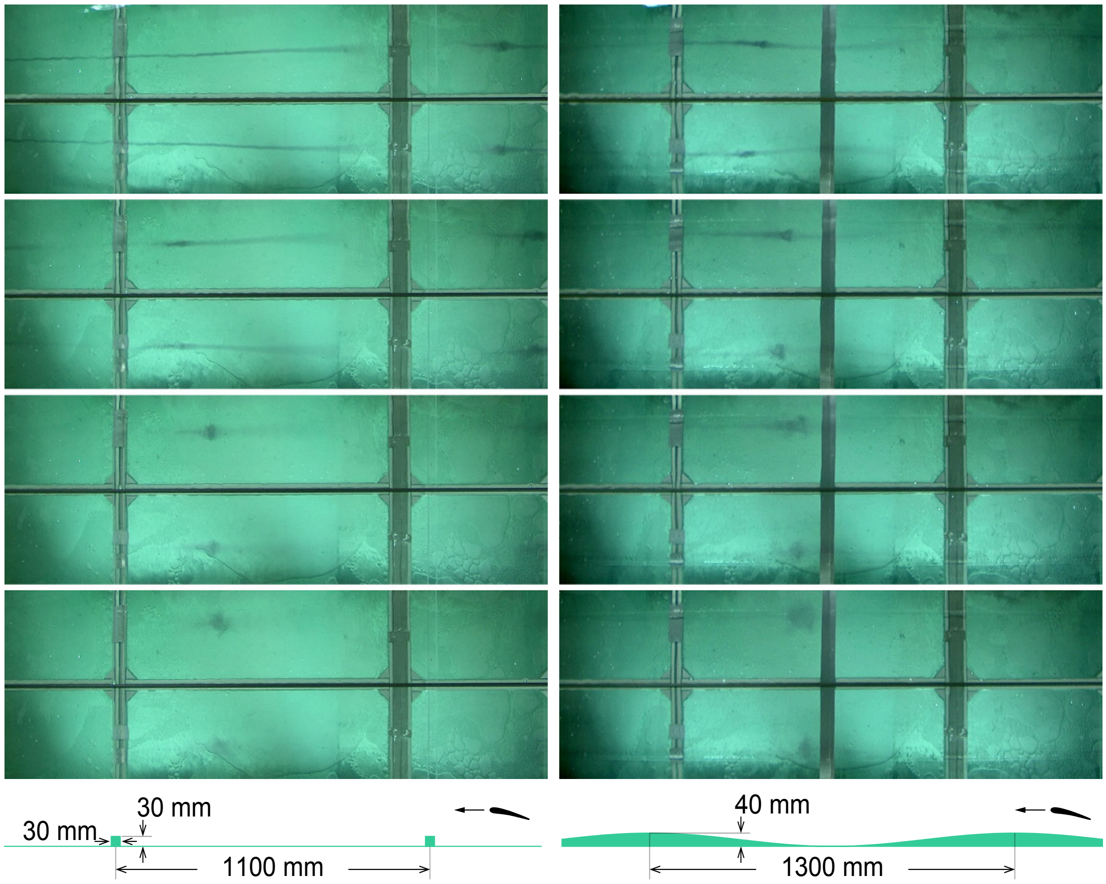

Figure 10. Vortex core visualization of the interaction with two 30 mm square profiles (left) and a 4π sine wave (right). Upper images 1.6 s after model passage, consecutive images with 0.4 s interframe time. Model velocity U = 2.44 m/s from right to left, ground distance h = 80 mm, image width approx. 2 m.

PIV recordings are taken at different distances from the hump. From the gained time-resolved 3-component velocity vector fields properties like vorticity and vortex circulation as well as vortex core traces are evaluated. Compared to the reference case with the plain flat ground, the hump forces the path of the vortex core downwards and reduces circulation (Figure 8, Figure 9). Far from the hump, however, the vortex rises higher than in the reference case (Figure 9, x = 550 mm).

The disturbances moving upstream and downstream look significantly different (Figure 7, right). However, the respective instability types seem to be somehow fundamental: The shapes emerging from sine profiles look similar to the ones caused by square profiles (Figure 10). Of course, due to the size of the sine wave profile, time and location differ. This spatiotemporal delay is also visible in the vortex core traces derived from PIV (Figure 11, left), where the traces at the end of a 1300 mm (2π) sine wave are located between the traces for square profiles at x = 160 mm and x = 550 mm, respectively. The circulation at sufficiently large distances (Figure 11, right) shows an almost identical behaviour.

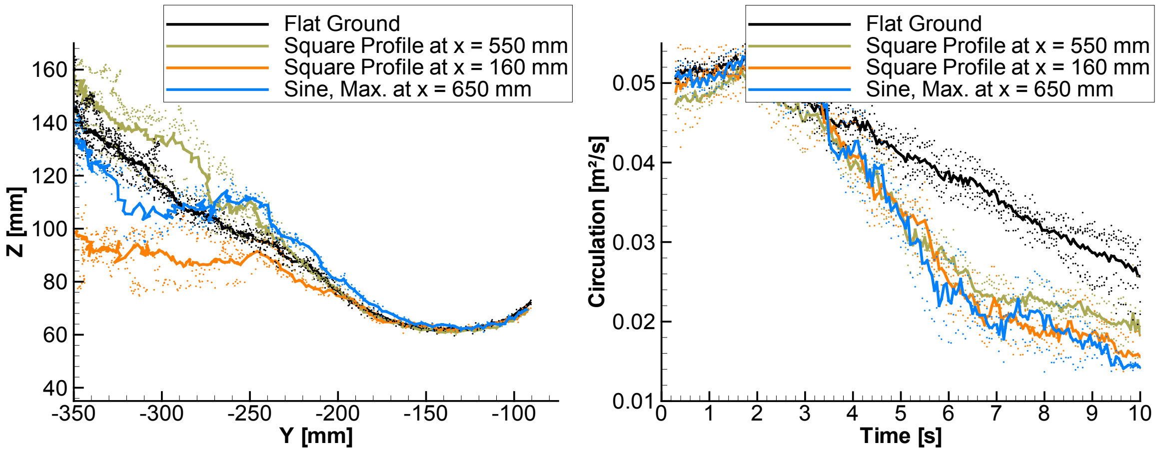

Figure 11. Vortex core trajectories (left) and time-dependent circulation (right) derived from PIV for single square profile and 2π (1300 mm) sine wave. Depicted are individual runs (dotted) and their averages (lines). Model velocity U = 2.44 m/s, ground distance h = 80 mm, ground at Z = 0 mm.

Conclusion

A generic aircraft wing model has been used to investigate the development of 2-vortex wake systems in a water towing tank. The experimental study has been focused on the influence of ambient turbulence and the impact of ground topologies on the decay of the wake. Time resolved stereo PIV has been used to determine the velocity vector fields. Vortex core traces have been visualized by contrast agents released from the wing tips.

Time-resolved images of the vortex core evolution in environments with different intensities of ambient turbulence have been taken in order to get both a first qualitative overview as well as a global quantitative characterization. The observed decay features include Crow instability, vortex-linking and the formation of vortex rings. Velocity vector fields are recorded by time-resolved stereo PIV for quantitative analysis. A vortex tracking evaluation is performed allowing the determination of the vortex core trajectories in selected cross planes as well as vortex parameters like circulation strength and core radius.

The interaction of the wake with different ground topologies, i.e. a plain flat plate, a flat plate including a rectangular hump and a sinusoidal shaped ground plate, is observed by vortex core visualization. Both ground irregularities cause an early breakdown of the vortices which travels up- and downstream of the maximum ground elevation. The quantitative analyses of the flow field measured with time-resolved PIV reveal that the circulation is reduced significantly by both ground irregularities. For the rectangular hump, the circulation strength is reduced dramatically directly above the hump, which is mainly caused by the production of opposite signed vorticity at the surfaces of the hump. At some distances up- and downstream of the hump, a remarkable reduction of about 50 percent with respect to the plain ground case still exists. The towing tank results show that ground irregularities have a positive effect on the decay of wake vortices in ground proximity, which is important for the starting and landing procedure of aircraft at airports. It is suggested that further investigations also consider higher Reynolds numbers.

References

[1] R.L. Bristol, J.M. Ortega, P.S. Marcus, O. Savas. On cooperative instabilities of parallel vortex pairs. J. Fluid Mech. 517:331–358, 2004.

[2] C.F.v. Carmer, R. Konrath, A. Schröder, J.-C. Monnier. Identification of vortex pairs in aircraft wakes from sectional velocity data, Exp. Fluids 44: 367-380, 2008.

[3] J.D. Crouch. Airplane trailing vortices and their control. C. R. Phys. 6(4–5):487–499, 2005.

[4] S.C. Crow. Stability Theory for a Pair of Trailing Vortices, AIAA Journal, Vol. 8, No. 12, pp. 2172–2179, 1970.

[5] D.P. Delisi and G.C. Greene. Experimental Measurements of the Evolution of a Vortex Pair in a Nonstratified Fluid Part 1: Migration and Persistence, AIAA Paper 2009-345, 2009.

[6] D.P. Delisi and G.C. Greene. Experimental Measurements of the Evolution of a Vortex Pair in a Nonstratified Fluid Part 2: Low Reynolds Number Wings and Vortex Wake Characterization, AIAA Paper 2009-345, 2009.

[7] D.P. Delisi. Laboratory Measurements of the Effect of Ambient Turbulence on Trailing Vortex Evolution, AIAA Paper 2006-1078, 2006.

[8] L. Dufresne and G. Winckelmans. Previous work and present knowledge on wake vortices near the ground, FAR-Wake EU-Project Deliverable D3.0, 2005.

[9] T. Gerz, F. Holzäpfel, D. Darracq. Commercial aircraft wake vortices. Prog. Aerosp. Sci. 38(3):181–208, 2002.

[10] T. Gerz, F. Holzäpfel, W. Bryant, F. Köpp, M. Frech, A. Tafferner, G. Winckelmans. Research towards a wake-vortex advisory system for optimal aircraft spacing. C. R. Phys. 6(4–5):501–523, 2005.

[11] J. Han, Y-L. Lin, D.G. Schowalter, S.P. Arya and F.H. Proctor. Large eddy simulation of aircraft wake vortices within homogenous turbulence: Crow instability, AIAA Journal 38, No. 2, 2000.

[12] J. K. Harvey and F.J. Perry. Flowfield produced by trailing vortices in the vicinity of the ground. AIAA Journal 9, No. 8, 1971.

[13] F. Holzäpfel, T. Hofbauer, D. Darracq, H. Moet, F. Garnier and C. Ferreira Gago. Analysis of Wake Vortex Decay Mechanisms in the Atmosphere, Aerospace Science and Technology 7, No. 4, pp. 263-275, 2003.

[14] L. Jacquin, D. Fabre, D. Sipp, E. Coustols. Unsteadiness, instability and turbulence in trailing vortices. C. R. Phys. 6(4–5):399–414, 2005.

[15] L. Jacquin, D. Fabre, D. Sipp, V. Theofilis, H. Vollmers. Instability and unsteadiness of aircraft wake vortices. Aerosp. Sci. Technol. 7(8):577–593, 2003.

[16] R. Konrath, D. Pallek, H. Mattner, C.F.v. Carmer. Analysis of flow field measurements obtained in a large tow tank regarding the decay of wake vortices in the far-field for two- and four-vortex systems, AIAA Paper 2009-342, 2009.

[17] R. Konrath, C.F.v. Carmer, G. Schrauf, K. Schmidt, G. Winckelmans, C. Cottin, O. Desenfans, G. Daeninck, R. Cocle, Dynamics and decay of spatially-evolving two- and four-vortex wakes near the ground, FAR-Wake project deliverable D 3.1.2, 2008.

[18] F.H. Proctor and D.W. Hamilton. Wake Vortex Transport and Decay in Ground Effect: Vortex Linking with the Ground, AIAA Paper 2000-0757.

[19] S.C. Rennich, S. K. Lele. Method for accelerating the destruction of aircraft wake vortices. J. Aircraft 36(2):398–404, 1999.

[20] R.E. Robins and D.P. Delisi. Potential hazard of aircraft wake vortices in ground effect with crosswind. Journal of Aircraft 30, No. 2, pp.201-206, 1993.

[21] P.R. Spalart. Airplane trailing vortices. Annual Rev. Fluid Mech. 30(1):107–138, 1998.

[22] T. Sarpkaya and J.J. Daly. Effect of Ambient Turbulence on Trailing Vortices. Journal of Aircraft, 24, pp. 399-404, 1987.

[23] P.R. Spalart, M.K. Strelets, A.K. Travin and M.L. Shur. Modelling the Interaction of a vortex Pair with the Ground, Fluid Dynamics 36(6), 2001.

[24] L. Turk, D. Coors and D. Jacob. Behaviour of wake vortices near the ground over a large range of Reynolds numbers, Aerospace Science and Technology, 1999.

[25] G. Winckelmans, R. Cocle, L. Dufresne, R.Capart. Vortex methods and their application to trailing wake vortex simulations. C. R. Phys. 6(4–5):467–486, 2005.

6.4 Large-Eddy Simulations of Wake Vortices in Ground Proximity and Crosswind

Anton Stephan, Takashi Misaka, Frank Holzäpfel
Institute of Atmospheric Physics

Results from large eddy simulations of the wake vortex behaviour in ground effect with turbulent cross-winds are presented. We have conducted wall-resolved and wall-modelled simulations at different Reynolds numbers to investigate the Reynolds-number dependency. Vortex displacement and decay has been validated with experimental data. In order to understand wake vortex decay mechanisms in ground proximity the interaction of primary and secondary vortices is thoroughly investigated. Obstacles at the ground surface are introduced to trigger rapid vortex decay.

Introduction

The interaction of a two-vortex system with the ground using numerical simulations has been investigated so far with different approaches. Either wall-resolved direct numerical simulations (DNS) [2], or large eddy simulations (LES) [4] have been employed. For wall resolved simulations not only DNS but also LES is limited by the Reynolds Number, $\mathrm{Re} = \Gamma_0/\nu$, and has been realized for a maximum Re of 20000. Another possibility is to use wall-modelling functions [18], which allows considering realistic Reynolds numbers up to 10^7. Similar as [4] we have conducted wall-resolved LES at a Reynolds number of $\mathrm{Re} =$ 23130. Using a wall model we have further performed wall-modelled LES with $\mathrm{Re} = 231300$.

In contrast to vortices at higher altitude vortex decay in ground effect is not only influenced by ambient turbulence but also by the interaction of secondary vortices detaching from the ground with the primary vortices. Here instabilities of secondary vortices play a significant roll. In contrast to the short-wavelength instability, reported in [4], we find that vortex decay is driven by the formation of omega-shaped secondary vorticity structures which themselves are triggered by the longitudinal streaks developing in the boundary layer flow close to the ground surface. Even more efficient vortex decay can be achieved by imposing dedicated obstacles at the ground plane that trigger the formation of powerful secondary vorticity structures.

In order to provide a realistic environmental flow, we first establish a three-dimensional unsteady cross-wind. This way we introduce time dependent velocity fluctuations modelling the atmosphere physically. The time-averaged stream-wise velocity of the wind at the initial vortex height is set to the initial vortex descent velocity $V_0 = \Gamma_0 / 2\pi b_0$.

The presence of the ambient wind induces a boundary layer with negative vorticity. In contrast to classical considerations without wind this causes an asymmetric situation. The sudden eruption of wall vorticity is faster and more intense for the downwind vortex where the wind shear and the secondary vorticity have the same sign, but is attenuated for the upwind vortex. In the simulations temperature effects are not taken into account.

Theoretical Background

As the crosswind tends to be three-dimensional, unsteady and turbulent pre-simulations are required to generate it. Prescribing a vertical profile following the universal logarithmic law and imposing a stream-wise pressure gradient the wind flow is driven through the computational domain. In this setting the flow can be considered as a turbulent half-channel flow with the domain truncated in the middle of the channel, where a slip condition is applied. Here we shortly repeat basic properties of the channel-flow (e.g. [3], [13]). Let δ denote the channel half height and consider the following quantities as averaged in time.

For the boundary layer approximation the Navier-Stokes equations yield $\tau_w = -\delta \cdot dp/dx$, with constant pressure in wall-normal direction. The wall friction velocity is defined by $u_\tau = (\tau_w/\rho)^{1/2}$. This gives us the normalized values $u^+ = u/u_\tau$ $z^+ = zu_\tau/\nu$ and an intrinsic Reynolds number $\mathrm{Re}_\tau = u_\tau\delta/\nu$. The boundary layer of a turbulent flow has now three characteristic parts:

	region	velocity law
viscous sublayer	$z^+ < 10$	$u^+(z^+) = z^+$
transition layer	$10 < z^+ < 35$	
logarithmic layer	$35 < z^+$	$u^+(z^+) = \frac{1}{\kappa}\log(z^+) + B$,

with experimentally determined constants $\kappa = 0.41$ and $B = 5.5$. In a fully developed flow each region has its own flow field characteristics. The viscous sublayer is shaped by coherent structures, so-called near-wall streaks (e.g. [10]). For Reynolds numbers $\mathrm{Re}_\tau < 1000$ this near-wall streaks are proven to have a spanwise spacing of $\lambda^+ \approx 100$. To resolve the viscous sublayer wall-resolved LES requires a stretched mesh in wall-normal direction, with $z^+{}_{\min} < 1$. For realistic Reynolds numbers this is not feasible, therefore a wall model is needed. We employ a wall model based on the logarithmic law, to establish realistic velocity profiles, also known as the Grötzbach model (e.g. [5]).

Obstacles are simulated by adding a drag force source term, $\partial u_i / \partial t = -C_D |u| u_i$, to the Navier-Stokes equations with a high drag coefficient in the region of the obstacle.

Numerical Set-up

Initial Vortex Pair

The fully rolled-up wake vortex is initialized by a pair of counter rotating Lamb-Oseen vortices. It is characterized by a circulation of $\Gamma_0 = 530$ m^2/s, a vortex core radius of $r_c = 3.0$ m and a vortex separation $b_0 = 47.1$ m. The Reynolds number is set to $\mathrm{Re} = \Gamma_0/\nu = 23130$, with $\nu = 2.29 \cdot 10^{-2}$ m^2/s in the wall-resolved cases and $\mathrm{Re} = \Gamma_0/\nu = 231300$, $\nu = 2.29 \cdot 10^{-3}$ m^2/s in the wall-modelled case. The velocity scale is based on the initial descent velocity of the vortex pair $V_0 = \Gamma_0 / 2\pi b_0 = 1.79$ m/s. This defines the non-dimensional time $t^* = t\frac{V_0}{b_0}$ with b_0/V_0 = 26.3 s. For computing the initial vortex induced velocity at each point of the domain, six image vortex pairs in spanwise direction and two mirror vortices in the direction perpendicular to the ground are taken into account.

Computational Domain and Numerical Method

The dimensions of the computational domain are L_x =192 m in axial or longitudinal, L_y = 384 m in spanwise or lateral, and L_z = 144 m in vertical directions, respectively, see Figure 1. The initial height of vortex pair is set to $h_0 = b_0$. We impose periodic boundary conditions in the x and y directions. A no-slip condition is set at the ground at $z = 0$ and a slip condition at the top at $z = 3b_0$.

The number of grid points are N_x = 256, N_y = 512 and N_z = 256, resulting in 33.5 million of grid points. In the vertical direction the mesh is stretched geometrically from ground to the initial height of the vortices and remains equidistant further up.

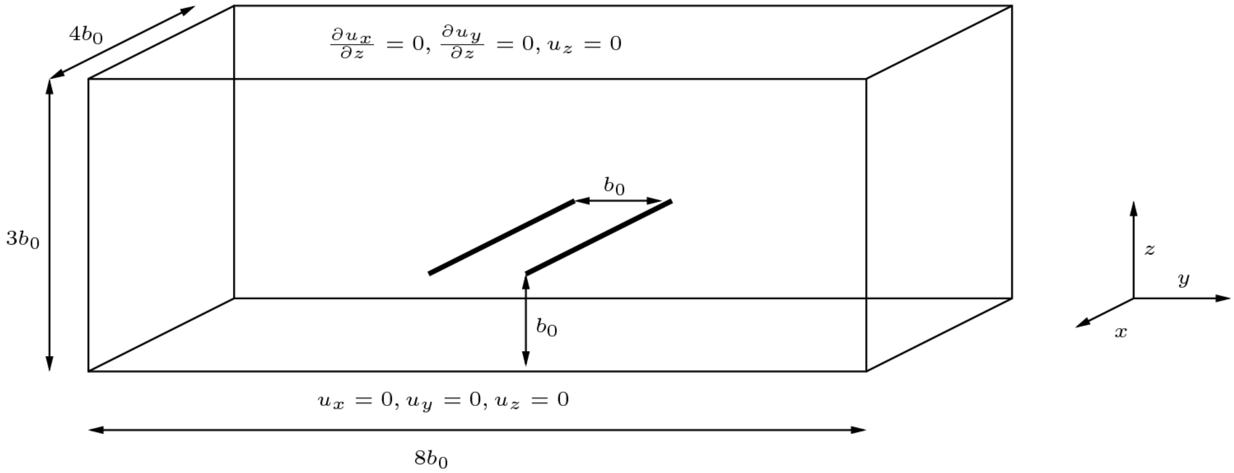

Figure 1. Sketch of the computational domain with boundary conditions and the initial vortex pair.

The mean cross-wind $u_y(z)$ is driven by a pressure gradient of dp/dy = $5.9 \cdot 10^{-5}$ N/m^3. With a friction velocity $u_\tau = 8.414 \cdot 10^{-2}$ m/s as reference we obtain z^+_{min} = 0.55, hence, the the first layer above ground is at z_{min} = 0.15 m and we can guarantee to resolve the wall in the LES, at least for the cross-wind driven boundary layer.

We impose three different types of obstacles at the ground surface which are all oriented in the y-direction. The first case employs a barrier with a quadratic cross section of 9 m x 9 m; followed by a case with 3 barriers with reduced heights of 6 m and widths of 9 m separated in x-direction by b_0. Finally, we impose 3 sinusoidally shaped barriers (along x) with a height difference (two times the amplitude) of 9 m and a wave length of $b_{0.}$

The LES is performed by using the incompressible Navier-Stokes code MGLET developed at Technische Universität München [14]. The momentum equation is solved by a finite-volume approach with the fourth-order finite-volume compact scheme [12, 6]. A Lagrangian dynamical subgrid-scale model is employed [15]. The simulation is performed in parallel using 1024 processors dividing the domain into 8x16x8 parts.

Results

Flow phenomenology

When the vortex pair descends it induces a vorticity layer at the ground (see Figure 2). Crosswind also induces vorticity close to the ground, which has the opposite sign as the boundary vorticity layer of the upwind vortex and the same sign as the vorticity layer of the downwind vortex (cf. Figure 7 below). As a consequence vorticity layers generated by the wake vortices become unequally strong and the upwind and downwind vortices behave asymmetrically. The magnitude of the wake-vortex induced vorticity layer is growing leading eventually to separation and the generation of counter-rotating vortices, first at the downwind and then at the upwind vortex. Then the secondary vortices rebound and start to interact with the primary vortices, which we will discuss later in detail. We also observe a roll-up process of the turbulent structures of the wind boundary layer while these disappear at the ground between the vortices.

Trajectories and Decay

The primary and secondary vortex centres are tracked detecting local pressure minima and extreme values of vorticity. The averaged vortex core trajectories can be seen in Figure 3 together with predictions of the deterministic and probabilistic two-phase wake vortex decay and transport model (D2P, P2P) [7].

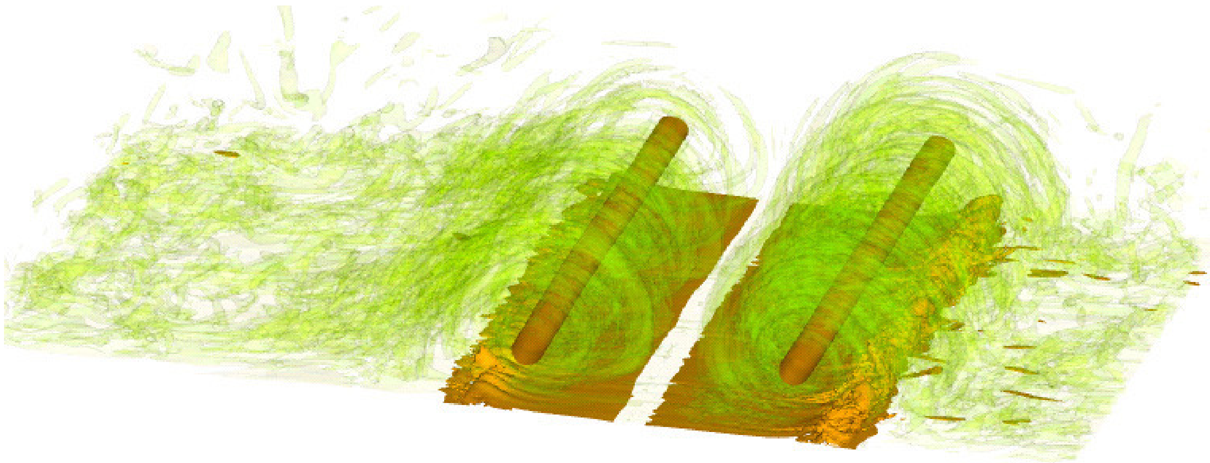

Figure 2. Visualisation of the flow field using iso-surfaces of $\|\omega\| b_0^2 / \Gamma_0 = 5$ and 0.5 at $t^* = 1.24$ s.

The averaged normalized closest distance to the ground of the primary vortices is 0.49 for the upwind and 0.57 for downwind vortex. Lidar measurements at Frankfurt airport [9] indicate average altitudes of 0.525 and 0.62, respectively, in corresponding situations [9]. Lateral displacement of the primary vortex trajectories has been analysed in [19], it scatters around a median of 3.2 at average vortex ages of t* = 3. The LES provides exactly a lateral displacement of 3.2 at a time of t* = 3.

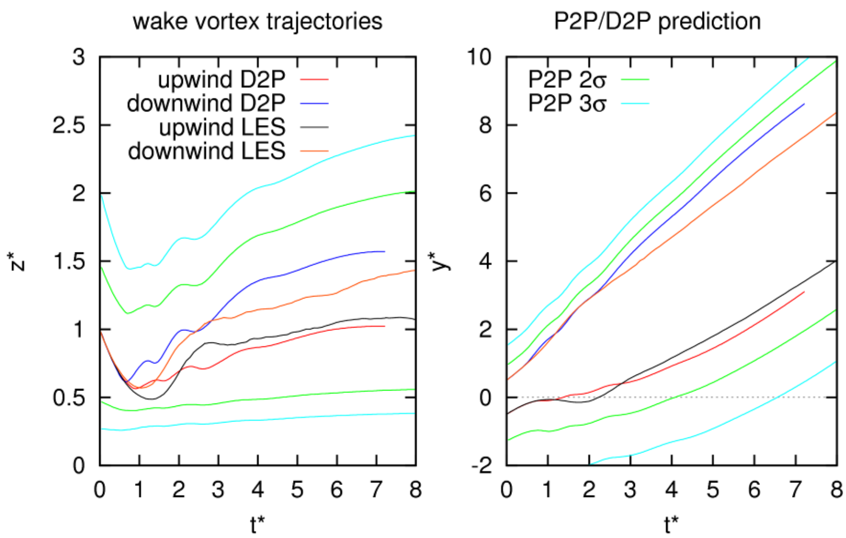

Figure 3. Evolution of normalized vertical and lateral positions. Results from simulations (black and orange) compared with predictions from D2P and P2P wake vortex model.

As a common measure of the vortex intensity for aircraft with a wingspan around 60 m we first consider $\Gamma_{5\text{-}15} = 0.1 \int_5^{15} \Gamma(r)dr$ for primary and Γ_5 for the secondary vortices, where $\Gamma(r)$ denotes the circulation distribution in a disk of radius r centred in the vortex core. The evolution of these quantities is shown in Figure 4. It is worth mentioning, that in spite of the rapid decay between t^* = 1.5 and 3 the core radius of the primary vortices is shrinking temporarily, see Figure 4, right.

Wake Vortex Decay Mechanism

In contrast to the decay mechanisms away from ground, which are driven by atmospheric turbulence and thermal stratification [16], [8], the origin of turbulence in our case is the no-slip condition at the ground, i.e. the strong shear established between the free crosswind flow and the zero velocity directly at the ground surface. The counter-rotating secondary vortices finally develop into relatively strong turbulent structures causing rapid decay. Figure 5 shows how those secondary vorticity structures (SVS) develop from the ground effect vortices on both upwind and downwind vortices at different times. To our knowledge, the origin of this kind of instabilities was not well documented and explained so far.

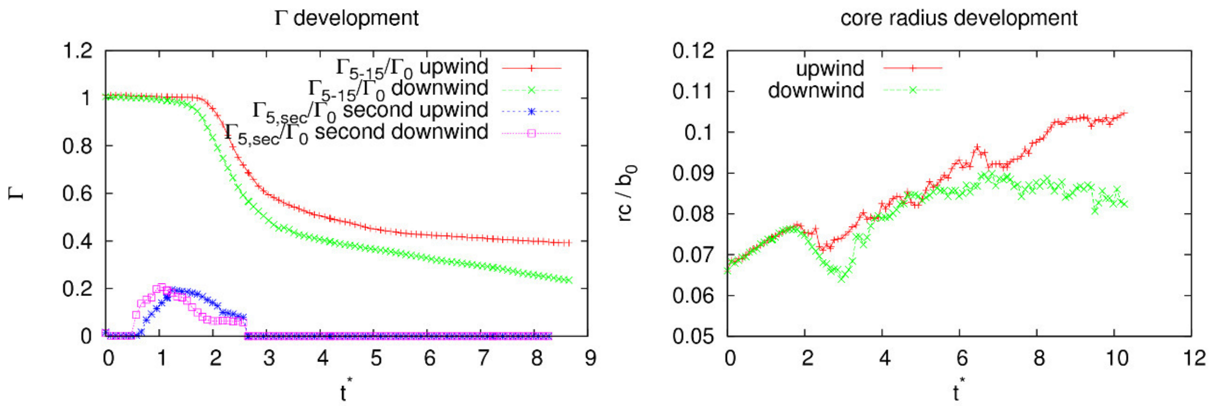

Figure 4. Evolution of vortex circulation for primary and secondary vortices (left) and core radius (right)

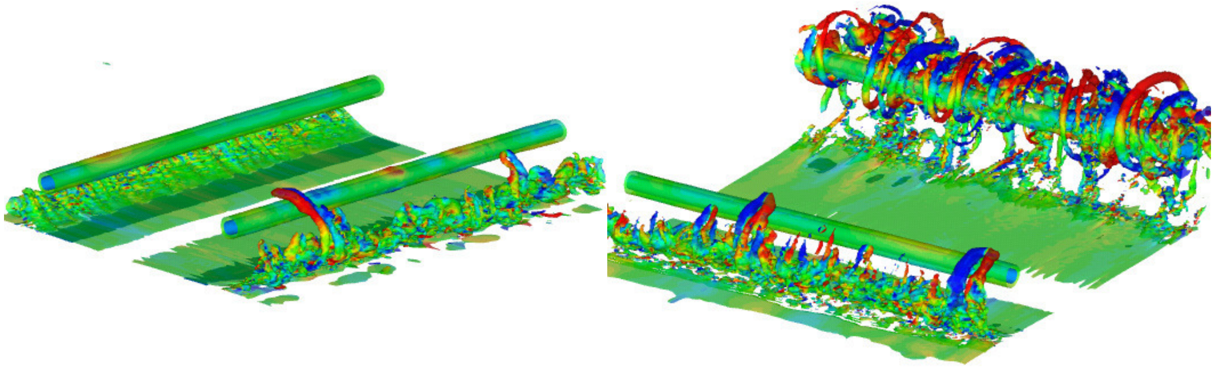

Figure 5. Iso-surfaces of vorticity magnitude $\|\omega\| = 1.5/s$, coloured by vorticity in span direction at t^* = 1.43 viewed upstream (left) and at t^* = 1.81 viewed downstream (right)

The unstable SVS wind around the primary vortex and form so-called omega loops that induce themselves a propagation speed towards the primary vortex. This self-induced approach speeds up and intensifies the interaction with the primary vortices. The prominent role of secondary vorticity structures for wake vortex decay is well known and has been analysed in detail in [8]. The formation of omega loops from secondary vortices has been studied in [17]. Here we want to focus on the origin of these instabilities.

A closer look at the velocity distribution at the ground, before imposing the vortex system reveals a wave-shaped pattern of highly elongated structures, the so-called streaks seen in Figure 6, left. These streaks correspond to regions of high velocities oriented in span direction (along u_y) in immediate ground proximity. Regions of high crosswind velocity (gradients) and low crosswind velocity (gradients) at the ground strengthen or weaken the roll-up process of the secondary vortices, respectively.

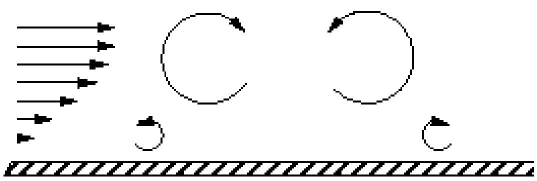

Figure 7. Sketch of flow

Crosswind velocity gradients induce vorticity of opposite sign as the secondary upwind vortex and of the same sign as the secondary downwind vortex (see Figure 7). So a region of small vertical wind gradients at the upwind secondary vortex and a region of high wind gradients at the downwind secondary vortex both enforce the secondary vortices to detach earlier, as shown in Figure 6. The shape and development of the omega loops is best visible in Figure 6 left below at the downwind vortex, whereas the correlation of the boundary layer streaks and the omega loops is even more obvious for the upwind vortex (see the red arrows in Figure 6, right).

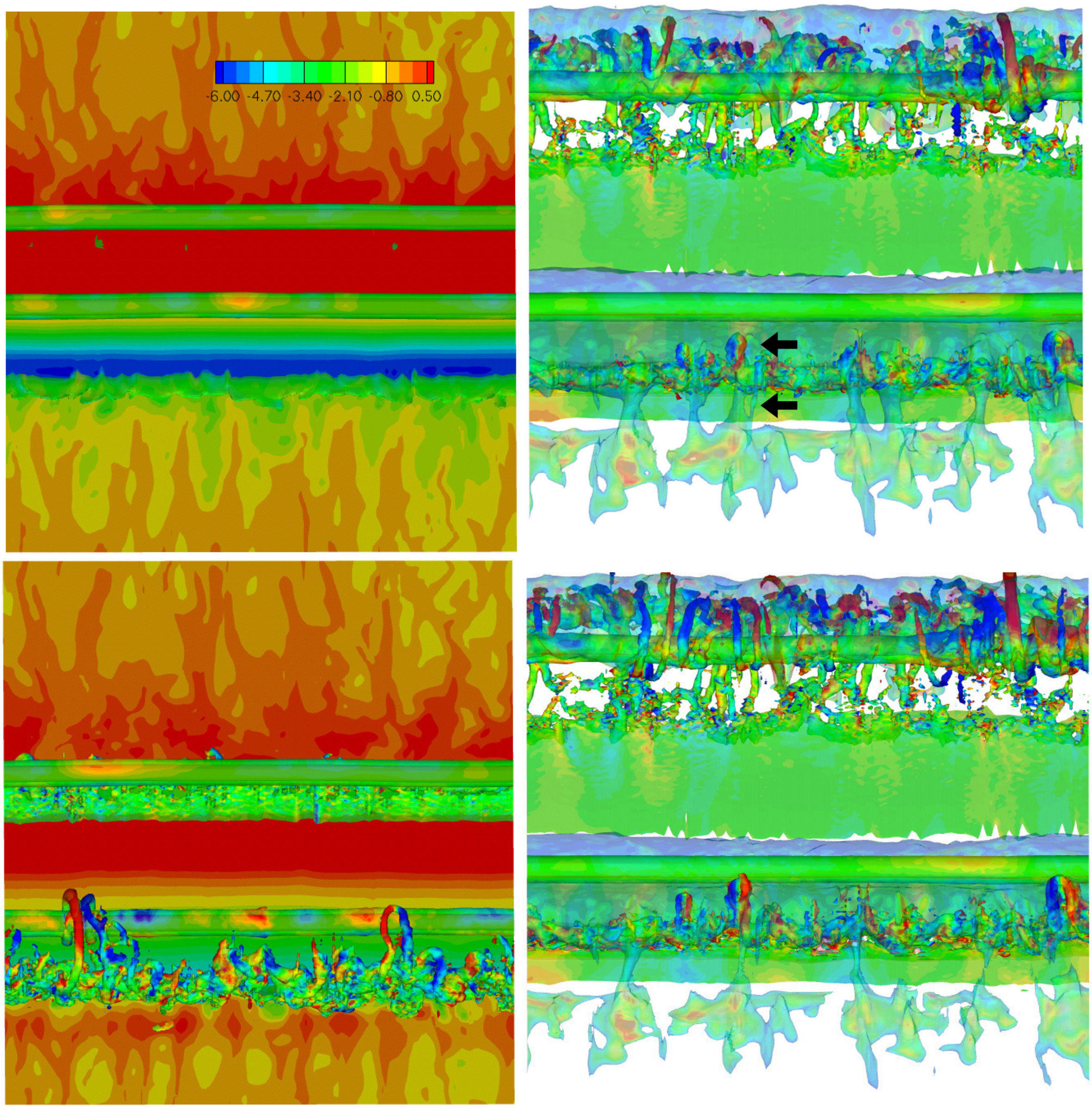

Figure 6. Iso-surface of vorticity magnitude $\|\omega\| = 1.5/s$ combined with (left) velocity at the ground at t^* = 0 (top) and 1.53 (bottom) and (right) with iso-surface of velocity v=0.1 m/s (transluscent) at t^* = 1.53 (top) and 1.81 (bottom); the lower vortex is the downwind (left) and the upwind (right) vortex.

As a consequence we may expect a one to one correspondence of the streak spacing of the crosswind flow and instability wave length of the secondary vortices. The streak spacing has found to be $\lambda^+ = 100$ in experiments ([1]) as well as in numerical simulations ([10]) for relatively small Reynolds numbers. Reference [11] gives some mathematical evidence that $\lambda^+ = 100$ may also hold for high Reynolds numbers. Consequently, the wave length of the secondary vortices is highly dependent on the Reynolds number, or in other words it is proportional to the molecular viscosity. This motivates us to perform some LES with higher Reynolds number.

Higher Reynolds Number Flows

In a simulation with $\mathrm{Re} = 231300$ and $\nu = 2.29 \cdot 10^{-3}$ m^2/s we investigate how Reynolds number affects the vortex decay. We impose a wall model based on the logarithmic wall law, to achieve the characteristic velocity profile in the pre-simulation. Again we use a pressure driven flow with the same pressure gradient dp/dy = 5.9·10^{-5} N/m^3 as before. As expected the turbulent SVS become much smaller and are actually not too well resolved anymore, see Figure 8, left. The vortex decay at the 10 times larger Re number appears to follow the same physics but is somewhat delayed and stabilises at a slightly higher value, see Figure 8, right. This might be considered as a Re number effect but possibly could also be explained with the insufficient resolution of the turbulent structures close to the ground.

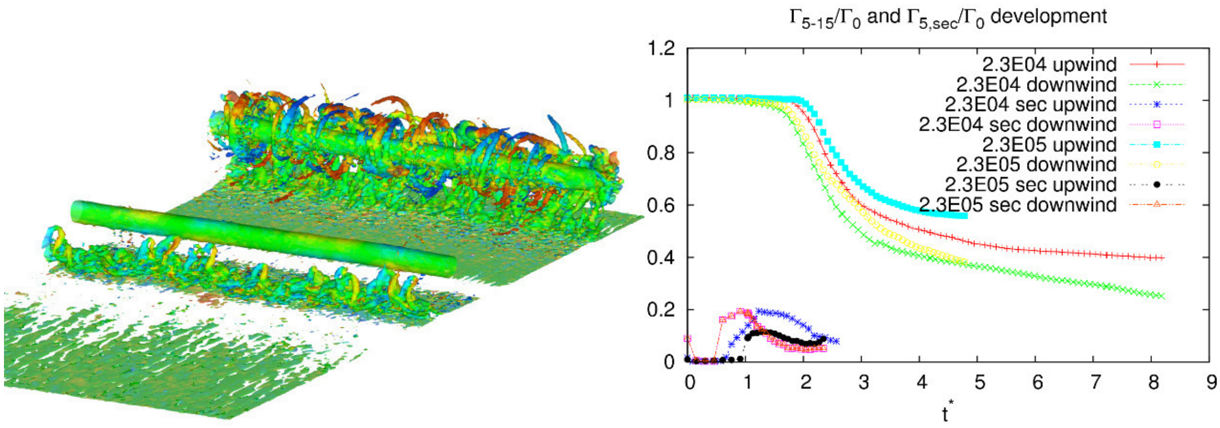

Figure 8. Left: iso-surface of vorticity magnitude $\|\omega\| = 1.5/s$, coloured by vorticity in span direction, at t^* = 1.66; right: evolution of vortex circulation for primary and secondary vortices for different values of *Re*.

Ground Obstacles

Different types of obstacles at the ground surface are introduced in order to trigger the formation of SVS and to achieve premature vortex decay. All initial parameters of the cross-wind and the wake vortices are taken from the wall-resolved LES at Re = 23130.

One barrier with quadratic cross section

After vortex initialisation secondary vorticity is generated rapidly at the top of the barrier, which subsequently detaches and develops a distinct loop, see Figure 9. The loop is stretched and winds around the primary vortex forming an omega loop, approaching and immersing into the primary vortex. The process follows the vortex stretching and tilting mechanisms explained in [8]. The geometrically induced SVS travel along the primary vortices by self-induced velocity while they weaken the primary vortices efficiently.

This simulation can be considered as a very clear illustration of the development of an SVS in the crosswind situation. While in the turbulent cross-wind situation several smaller SVS develop from the boundary layer streaks competing with less coherent turbulent structures, the obstacle (running parallel to the cross-wind direction) triggers a very distinct large single unadulterated secondary vorticity loop. Consequently, the different phases of its development can more clearly be distinguished in Figure 9.

Three barriers with different cross sections

Here we compare the influence of barriers with sinusoidal and squared cross sections. Three obstacles are imposed separated by b_0 along x. Figure 10 reveals that the flow characteristics are very similar for smooth and polygonal barriers. Both simulations show similar results concerning the evolution of the vortex intensity. All cases have in common that the geometrically induced instabilities weaken the primary vortices. In Figure11 the development of $\Gamma_{5\text{-}15}$ is plotted for all three cases with obstacles compared to the simulation with flat ground. The downwind vortices are fully decayed already between t^* = 3 and 4 compared to the pure cross-wind case where the downwind vortex survives beyond simulation time. Until t^* = 3 the upwind vortices in all three cases with obstacles show similar decay characteristics, multiple obstacles, obviously, result in lower final circulations.

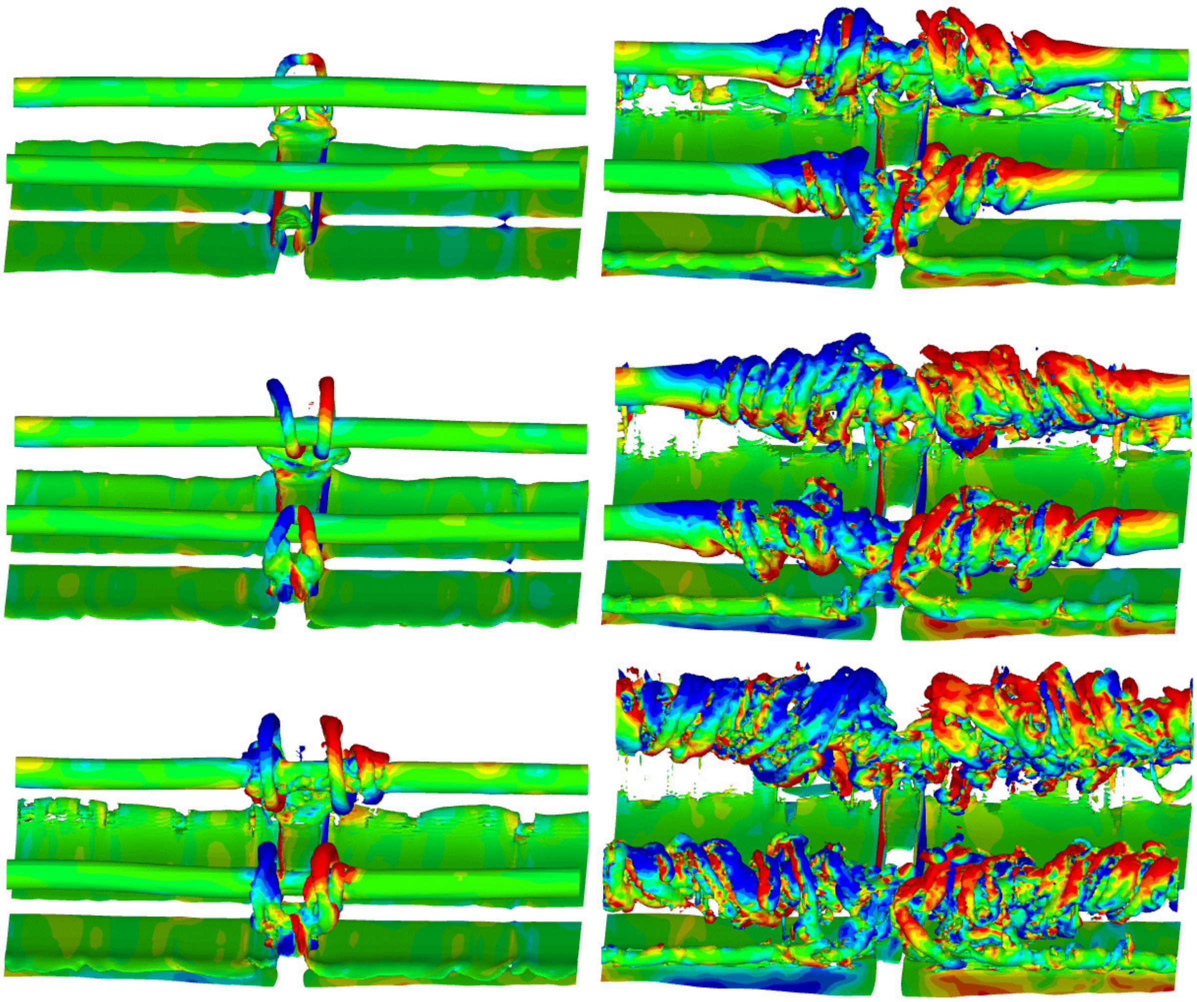

Figure 9. Iso-surface of vorticity magnitude $\|\omega\| = 1.5/s$, coloured by vorticity in span direction at t^* = 0.76, 0.91, 1.06, 1.21, 1.37, and 1.52, from top to bottom and left to right.

Conclusions

We conducted several LES to study the evolution of a counter-rotating vortex pair in ground effect with cross-wind. The investigation of the decay mechanism reveals that the strongly deforming and unstable secondary vortex structures trigger the rapid decay of the primary vortices. This motivated us to study the origin of the instabilities, which can be either initiated dynamically by coherent structures of the crosswind flow or geometrically by obstacles installed at the ground.

In the case with a flat lower boundary we found that the velocity streaks in the cross-wind flow close to the surface support the formation of secondary vorticity and thus accelerate the detachment of secondary vortices from the ground which subsequently causes the generation of omega loops. These omega loops approach the primary vortices driven by self-induced velocity and initiate the rapid decay in ground proximity.

Because the wall-resolving LES limits the Reynolds number of the flow, we further have conducted a simulation with a Re larger by a factor of 10. This forced us to model the near wall effects. The results show that the described instabilities of the secondary vortices are more filigree leading to a somewhat delayed vortex decay. Possibly, the employed wall model does not allow representing coherent small turbulent structures close to the ground with sufficient resolution.

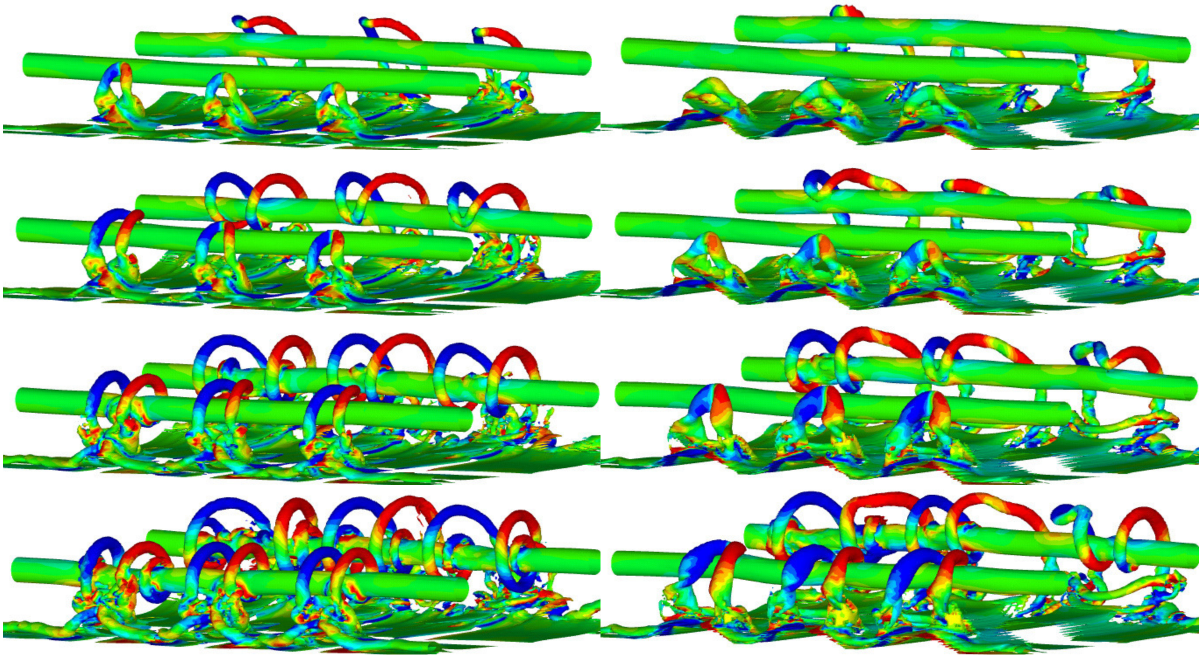

Figure 10. Iso-surface of vorticity magnitude $\|\omega\| = 1.5/s$, coloured by vorticity in span direction at t^* = 0.98, 1.06, 1.14, and 1.21. Left: square shaped barriers. Right: sinusoidal barriers.

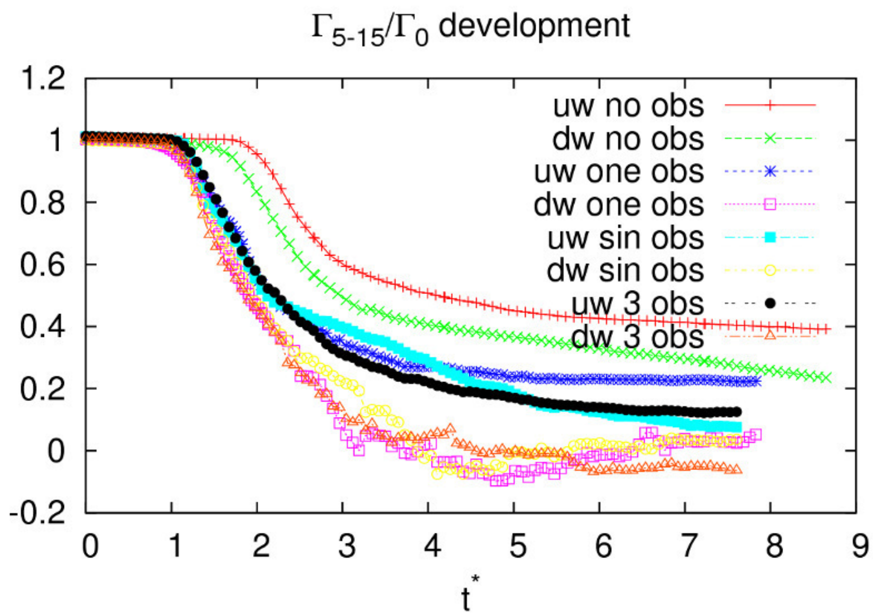

Figure 11. Evolution of vortex circulation, LES with / without obstacles; uw/dw = up-/downwind vortex.

Finally, we imposed obstacles of different type and shape. This setup allowed the dedicated use of properties of vortex dynamics to accelerate wake vortex decay in ground proximity with the following characteristics:

- early detachment of strong omega-shaped secondary vortices
- omega shape causes self-induced fast approach of the primary vortex
- after the secondary vortex has looped around the primary vortex it separates and travels along the primary vortex again driven by self induction

- the dedicated secondary vortex connects to the regular ground effect vortex and thus obtains continued supply of energy
- the highly intense interaction of primary and secondary vortices leads to rapid wake vortex decay independent from natural external disturbances

In summary the introduction of obstacles at the ground supports the selective generation of secondary vortices and smart utilisation of vortex properties in order to generate fast approaching and rapid spreading of disturbances along the primary vortex leading to premature vortex decay in ground proximity. Optimal obstacle shape and assembly with regard to vortex decay and feasibility is still to be investigated.

Acknowledgements

The simulations have been performed at DKRZ (Deutsches Klimarechenzentrum), Juropa (Forschungszentrum Jülich) and LRZ (Leibniz-Rechenzentrum). We would like to thank Andreas Dörnbrack for providing computation time at DKRZ as well as Prof. Dr. M. Manhart for providing the original version of the LES code MGLET. The work was funded by DLR project Wetter & Fliegen.

References

[1] Cantwell B., Coles D., Dimotakis P. (1978) Structure and Entrainment in the Plane of Symmetry of a Turbulent Spot, Vol. 87, 641-672.

[2] Duponcheel M., Lonfils T., Bricteux L., Winckelmans G. (2006) Simulations of three dimensional wake vortices in ground effect using a fourth-order incompressible code. 7th Nat.Congress on Theoretical and Applied Mechanics, Mons.

[3] Fröhlich J. (2006) Large Eddy Simulation turbulenter Strömungen. B.G. Teubner Verlag.

[4] Georges L., Geuzaine P., Duponchel M., Bricteux L., Lonfils T., Winckelmans G., Giovannini A. (2005) Technical Report 3.1.1-3, LES of two-vortex system in ground effect with and without wind. Techn. Ber., Université catholique de Louvain, Institut de Mécanique des Fluides de Toulouse.

[5] Grötzbach G. (1987) Direct numerical and large eddy simulation of turbulent channel flows. Encyclopedia of Fluid Mechanics (ed. N. Cheremisinoff). West Orange, NJ.

[6] Hokpunna A., Manhart M. (2010) Compact Fourth-order Finite Volume Method for Numerical Solutions of Navier-Stokes Equations on Staggered Grids. Journal of Computational Physics, Vol. 229, Nr. 20, pp. 7545-7570.

[7] Holzäpfel F. (2003) Probabilistic Two-Phase Wake Vortex Decay and Transport Model. Journal of Aircraft, Vol. 40, Nr. 2, pp. 323-331.

[8] Holzäpfel F., Hofbauer T., Darracq D., Moet H., Garnier F., Ferreira Gago C. 2003: Analysis of wake vortex decay mechanisms in the atmosphere. Aerospace Science and Technology. Vol.7, 263-275.

[9] Holzäpfel F., Steen M. (2007) Aircraft Wake-Vortex Evolution in Ground Proximity: Analysis and Parameterization. AIAA Journal, Vol. 45, 218-227.

[10] Jimenez J., Moin P. (1991) The minimal flow unit in near-wall turbulence. Journal of Fluid Mechanics Vol. 225, 213-240.

[11] Kathryn M. Butler and Brian F. Farrell 1993: Optimal perturbations and streak spacing in wall-bounded turbulent shear flow, Physics of Fluids Vol.5, 774-777.

[12] Kobayashi, M. H. (1999) On a Class of Páde Finite Volume Methods. Journal of Computational Physics, Vol. 156, Nr. 1, 137-180.

[13] Kundu P. (1990) Fluid Mechanics. Academic Press.

[14] Manhart M. (2004) A Zonal Grid Algorithm for DNS of Turbulent Boundary Layer. Computer and Fluids, Vol. 33, Nr. 3, 435-461.

[15] Meneveau C., Lund T.S., Cabot W.H. 1996: A Lagrangian dynamic subgrid-scale model of turbulence. Journal of Fluid Mechanics Vol 319, 353-385.

[16] Misaka T., Holzäpfel F., Hennemann I. Gerz T., Manhart M., Schwertfirm F. 2012: Vortex bursting and tracer transport of a counter-rotating vortex pair, Physics of Fluids, in press.

[17] Ortega J.M., Bristol R.L., Savas Ö. 2003: Experimental study of the instability of unequal strength counter-rotating vortex pairs. J. Fluid Mech., 474, 35-84.

[18] Proctor F.H., Han J.: 1999: Numerical Study of Wake Vortex Interaction with the Ground using the Terminal Area Simulation System. AIAA, 99-0754, 37th Aerospace Sciences Meeting & Exhibit, Reno.

[19] Steen M. (2005) Analyse und Parametrisierung des Wirbelschleppenverhaltens in Bodennähe. Diplomarbeit, Technische Universitaet Braunschweig.

6.5 Wake Characterisation by Encounter Flight Tests

Dietrich Fischenberg, Carsten Schwarz
Institute of Flight Systems

A wake encounter flight test campaign was conducted with the DLR Falcon 20 test aircraft. Applying a DLR developed evaluation method, wake characterising parameters such as wake strength (vortex circulation), wake descent, and lateral vortex spacing are assessed for each single encounter of a distinct aircraft type. The wake evolution is derived showing the encounter results as a function of wake age, or distance behind the aircraft. All results for a distinct aircraft type are summarized in a proposed "Wake Characterization Sheet", which may be a basis for wake severity discussions of (new) aircraft.

Wake Encounter Flight Tests

Several wake encounter in-situ flight tests were accomplished within the DLR project Weather & Flying. The objectives of these tests were:

(a) to gather in-situ wake encounter flight test data in different flight phases and at different distances behind several wake generator aircraft

(b) to evaluate the flight test data and derive wake characterizing parameters like wake strength, wake descent, and lateral wake spacing as a function of wake age (wake evolution)

(c) to measure the flight dynamic reaction of the wake encounter aircraft for validation of aerodynamic interaction models (AIM) of a swept wing aircraft configuration (not treated here).

The DLR Falcon 20 D-CMET (Figure 1) was used as encountering and measuring aircraft. 60 wake encounters in two flights were accomplished behind DLR's VFW-614 ATTAS aircraft in approach configuration (September 2010), and 202 wake encounters behind 12 different airliners in cruise (March 2011). Table 1 lists the airliner types, speeds, altitudes and number of encounters gathered during the cruising tests. Figure 2 shows a typical cruising scenario seen from the Falcon cockpit in this campaign.

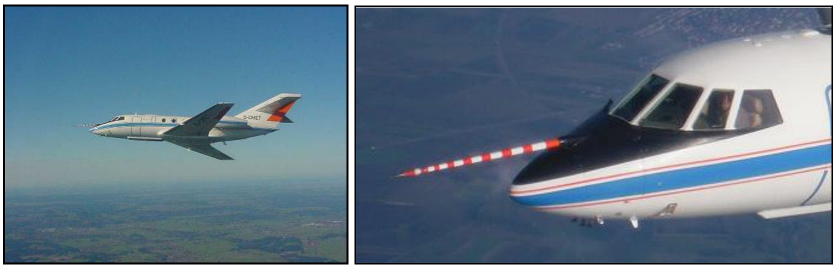

Figure 1: left: DLR's Falcon 20 D-CMET wake encounter and measuring aircraft;
right: Falcon noseboom with 5-hole probe for 100 Hz flow measurement

Figure 2: Falcon cockpit view during the cruise encounter flight tests

Table 1: Statistics of Falcon 20 D-CMET wake encounter flight tests in cruise

	airliner type	airliner mass [t]	Flight Level [FL]	true airspeed [kt]	# of encounters
1	CRJ-900	32	350	446	10
2	CRJ-900	30	370	460	9
3	Fokker 70	31	330	423	13
4	Fokker 100	36	350	424	8
5	B737-500	45	350	446	11
6	B737-400	50	360	433	9
7	B737-700	48	350	429	32
8	MD-82	58	340	430	20
9	B737-700	49	370	409	39
10	A319	58	370	439	15
11	B737-300	49	350	415	24
12	A320	62	360	440	12
total					**202**

Wake Characterisation Evaluation Model

The evaluation method used here was developed by DLR and is described in detail in [1] and [4]. It is capable to derive wake characterizing parameters from measured wake encounter flight test data. The key element of the method is the combination of a classical high precision flight path reconstruction [5] and the identification of the parameters of an analytical wake vortex model, see Figure 3.

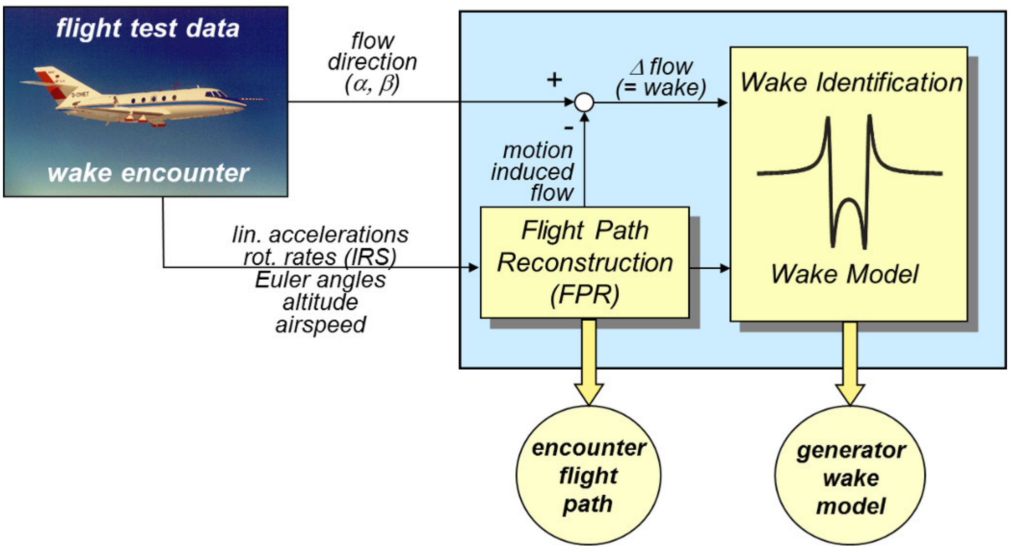

Figure 3: Evaluation method for wake characterization: combination of wake identification and flight path reconstruction [10]

The flight path reconstruction (FPR) inputs are: linear accelerations, rotational rates, Euler angles, altitude, and airspeed, all as measured on the encounter aircraft. With this information, the encounter aircraft flight path can be reconstructed in the geodetic axis system (and, knowing the wake orientation, also in the wake axis system). The FPR method also identifies the biases of the inertial sensors. The reconstructed translational and rotational motion of the aircraft allows computing the resulting flow angles α_i (AoA) and β_i (AoS) at all sensor locations assuming an undisturbed constant wind field (aircraft motion induced flow angles, cf. Figure 3). More details are documented in [1].

The measurement of the flow angles AoA and AoS is calibrated in an a-priori step [10]. The differences between these calibrated AoA and AoS and the reconstructed motion based ones are due to the local flow field of the encountered wake. These differences are clearly visible in Figure 4 (Falcon measurements in the ATTAS wake, approach speed) and in Figure 5 (Falcon measurements in a B737 wake, cruising speed) in the middle of the time sections when the encounters occur, respectively. Both encounters last about 2 s, and left and right vortex are clearly visible. At a measurement rate of 100 Hz, about 200 measurement samples are gathered in the wakes, respectively. Due to the higher airspeed, the wake induced flow angles are generally smaller in cruise: maximum about ±3° at cruising speed (Figure 5), and about ±8° at approach speed (Figure 4).

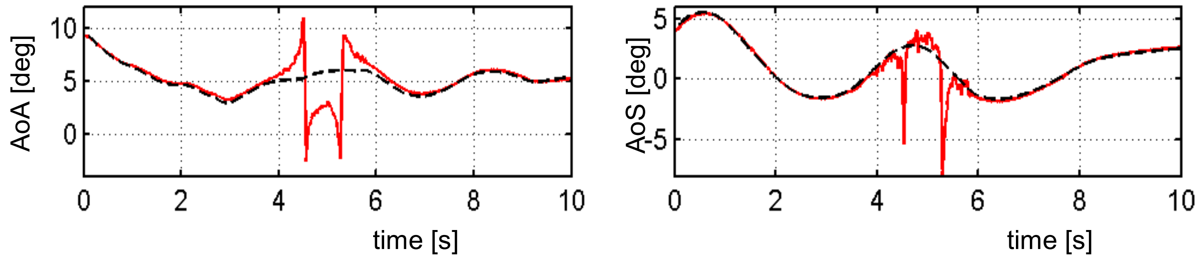

Figure 4: Falcon angle of attack (AoA) and sideslip (AoS) during a lateral wake encounter at approach speed: noseboom measured (———), reconstructed motion induced (- - -); wake generator: ATTAS

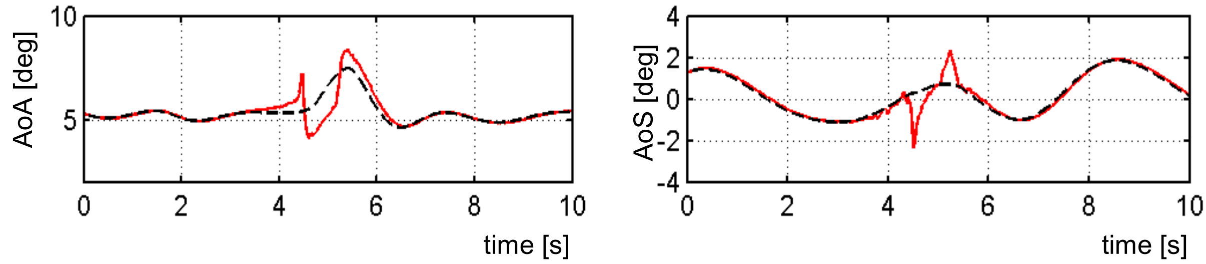

Figure 5: Falcon angle of attack (AoA) and sideslip (AoS) during a lateral wake encounter at cruising speed: noseboom measured (———), reconstructed motion induced (- - -); wake generator: B737

Using parameter identification methods [5], the differences between measured local flow and the motion induced flow can be minimized by tuning the parameters of an analytical wake model [1], from which the corresponding local wake flow angles are computed and added to the reconstructed ones. Figure 6 presents the result of the encounter example of Figure 4 after optimization convergence is achieved, and shows a high quality model fit to the measured data.

The analytical wake model used in the evaluation procedure applies the Burnham-Hallock velocity distribution [3]. The model parameters are

(1) vortex strength (circulation), core radius was set fixed to 4% wing span
(2-3) lateral position of left and right vortex in the wake system
(4-5) vertical position of left and right vortex in the wake system
(6-7) wake orientation in the geodetic reference frame.

In addition to the model parameters, the distance behind the corresponding wake generator was determined for each Falcon encounter, using GPS data in the approach speed tests and ATC radar data for the cruise tests [8]. The wake age was determined considering the horizontal wind. Gathering all information, wake evolution plots were generated.

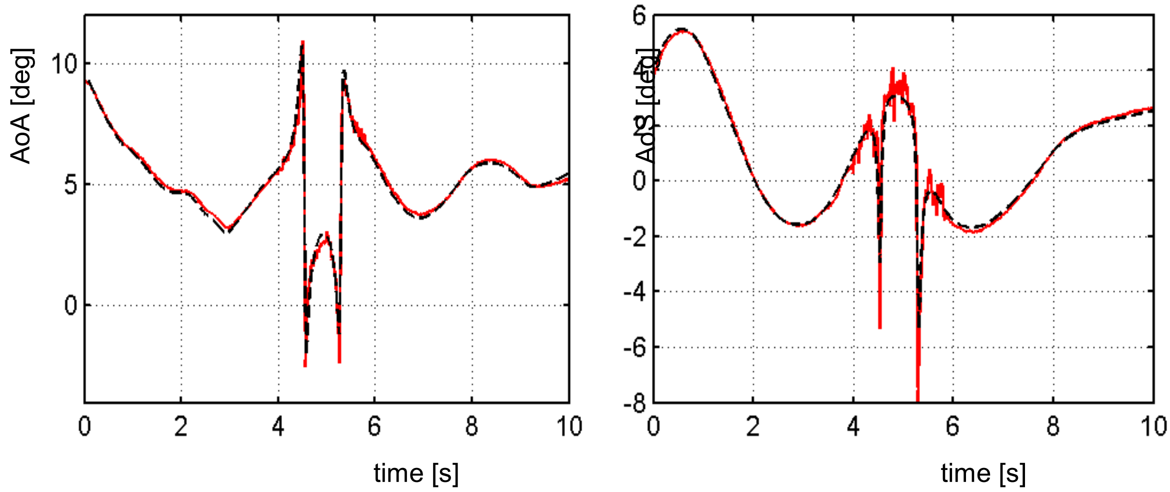

Figure 6: Falcon angle of attack (AoA) and sideslip (AoS) during a lateral wake encounter at approach speed: noseboom measured (———), and sum of reconstructed motion induced and wake model AoA/AoS (- - -); wake generator: ATTAS

Results

Figure 7 shows the ATTAS circulation (from tests at approach speed) as a function of wake age determined from the Falcon encounter measurements (flight 1 green, flight 2 red circles). The computed initial circulation according to Kutta-Joukowsky [10] is shown (blue diamond), as well as the worst case wake decay (only diffusion) from the DLR P2P model [6], [7].

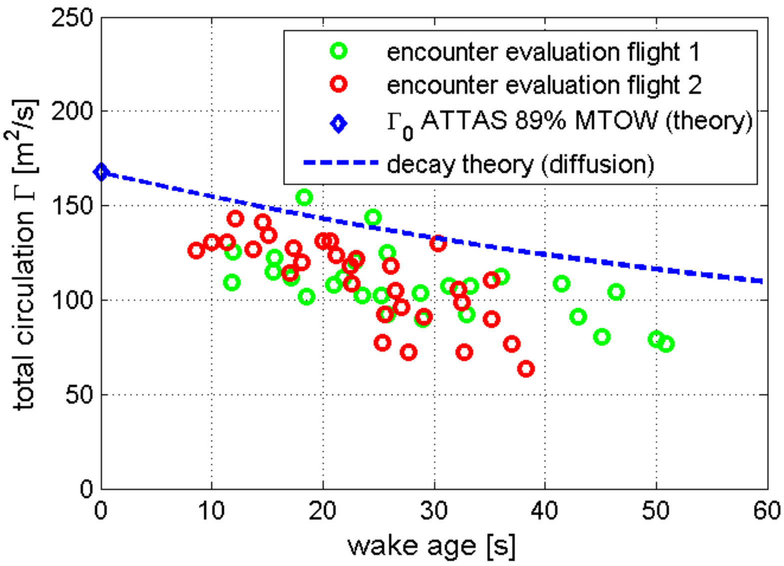

Figure 7: ATTAS circulation determined from Falcon wake encounter measurements

A detailed discussion of the results is available in [10]. The measurements of all 60 encounters at approach speed were sufficiently close to both vortex cores to apply the evaluation procedure of Figure 3. Generally, the identified wake decay results compare well to theory, Figure 7. The results have some scatter: the standard deviation with respect to a linear regression curve is about 15% of the averaged identified circulation. The scatter of the flight 1 results is somewhat smaller than that of flight 2, and maybe an outcome of a lower turbulence level. The flight 1 results show a 1-phase decay, and the determined circulation is a little below the theoretic diffusion decay. The wake decay in flight 2 seems to be somewhat faster, and indications of a 2-phase decay can be interpreted.

Also, the cruise flight evaluation results behind 12 different airliners are presented and discussed in detail in [10]. Selected results are shown in Figures 8-10 and compared to theory: circulation decay, lateral vortex separation, and wake descent of six airliners in cruise (B737-700 (2), MD-82, A319, B737-300, and A320). The results are determined from the Falcon encounter flight tests in March 2012.

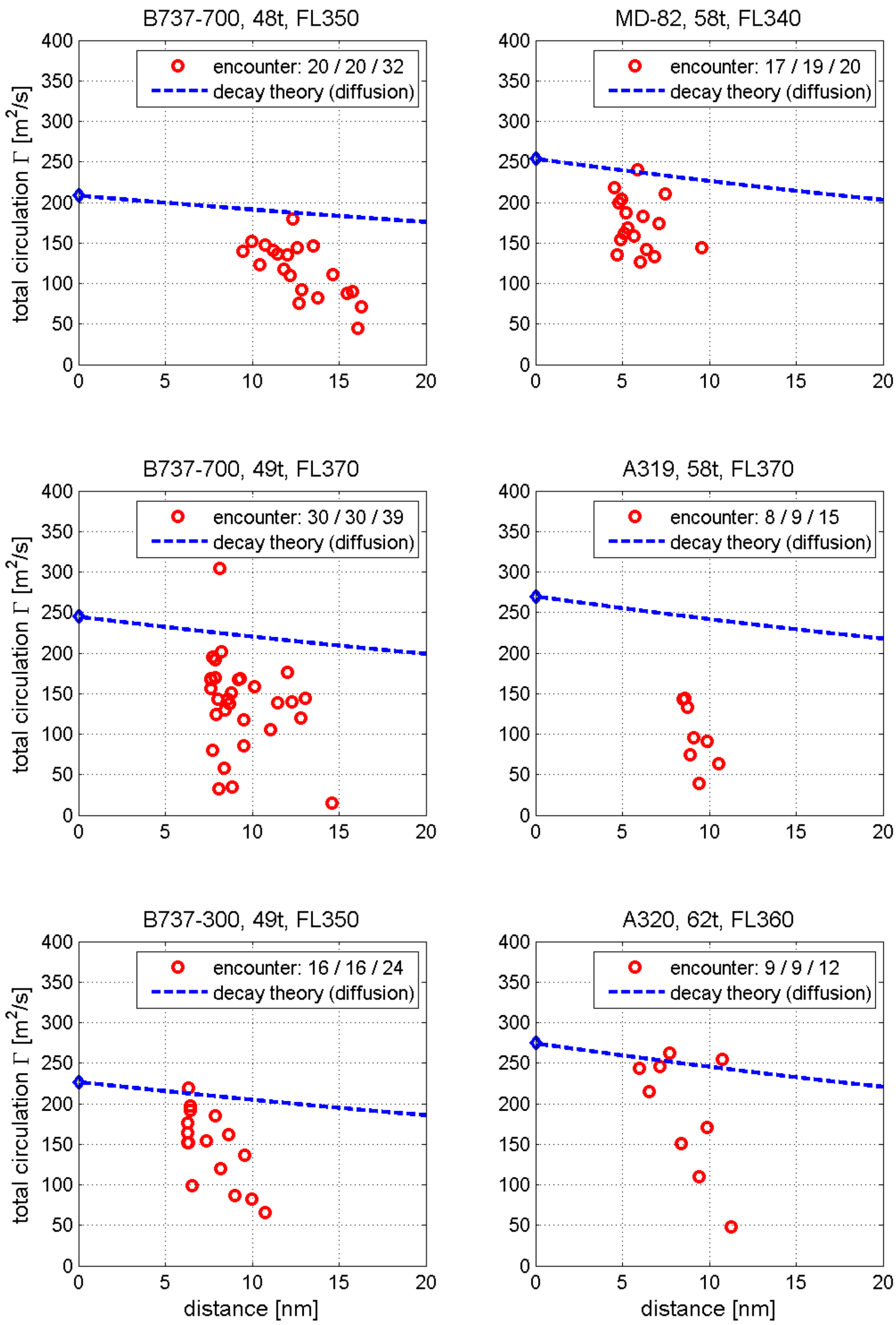

Figure 8: Identified circulation decay in cruise for B737-700 (2), MD-82, A319, B737-300, and A320 compared to theory; nomenclature behind 'o encounter' indicate: number of plotted / evaluable / flown encounters.

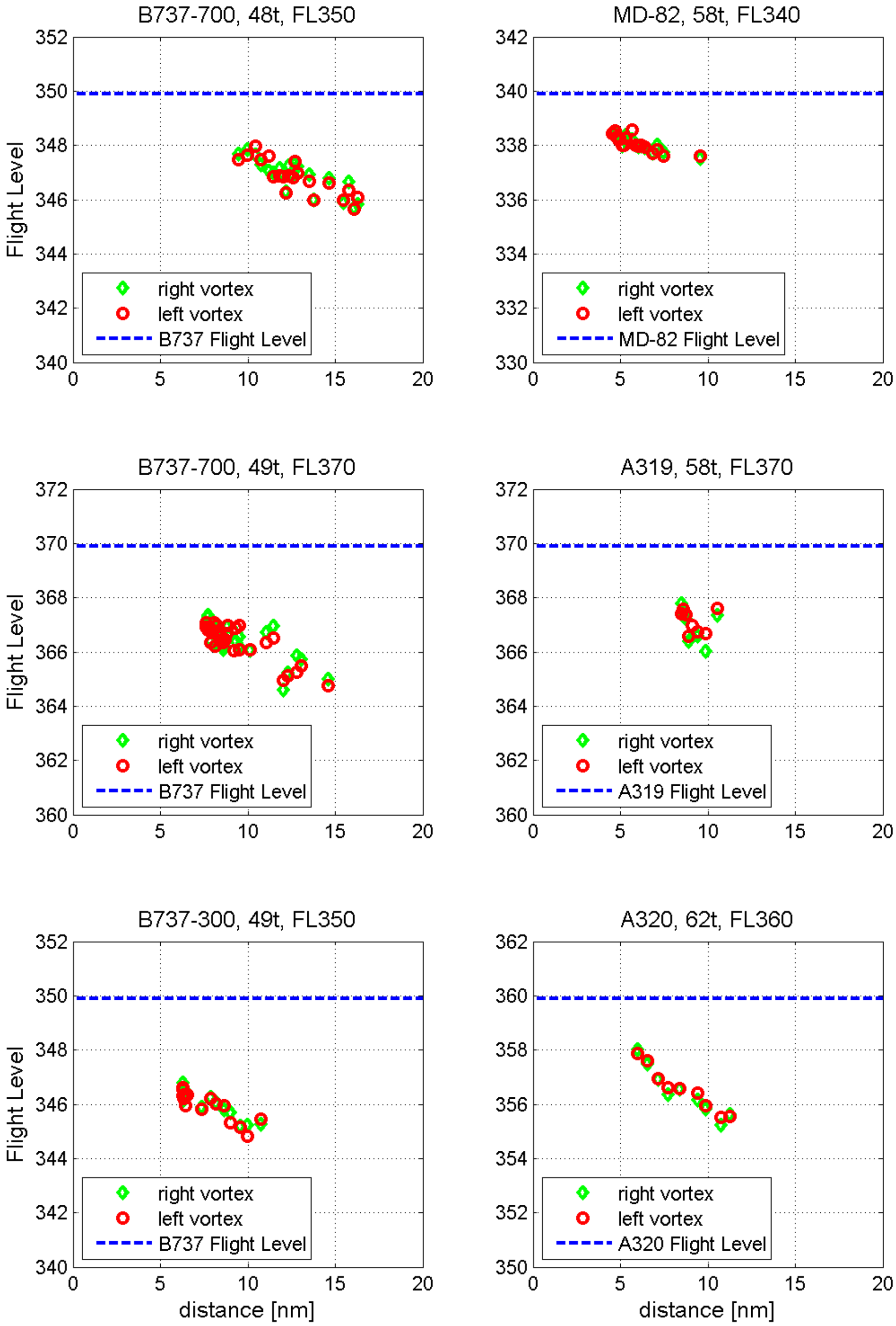

Figure 9: Identified wake decent in cruise for B737-700 (2), MD-82, A319, B737-300, and A320

In contrast to the approach tests behind ATTAS, in cruise only a limited number of encounters could be evaluated. Several reasons are relevant for this. Due to the higher airspeed, not all vortices could be hit with sufficient accuracy. The flight path should be close to both vortex cores, with a minimum distance of not more than 15 r_c (vortex core radius) [10]. After some pilot familiarization, about two-thirds of the cruise encounters were flown with that accuracy needed for evaluation. Secondly, wake deformation must not be too strong to apply the evaluation procedure.

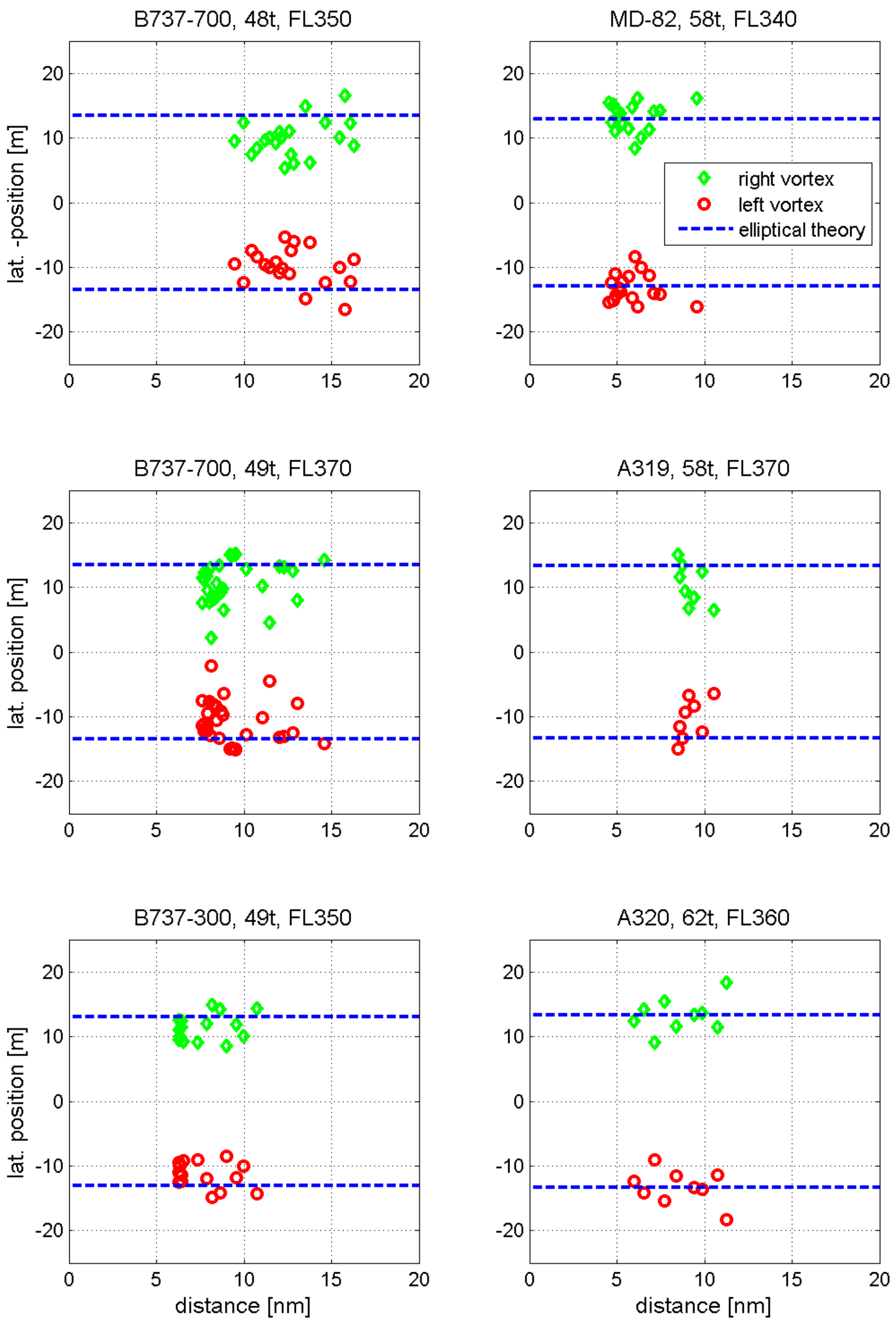

Figure 10: Identified lateral vortex spacing in cruise for B737-700 (2), MD-82, A319, B737-300, and A320 compared to theory

Wake deformation increases for wakes growing older due to Crow instability and atmospheric influences. The wake model used here assumes a straight vortex line without wake deformation. The typical, but sufficient measurement time interval is 1-3 seconds within the wake. For this duration, the assumption of an approximately straight wake may be acceptable in many cases, but only for a limited degree of deformation. Finally, the wake velocity distribution in the *y*-/*z*-plane should be such as to be properly described by the applied analytical wake model; in the present evaluation the Burnham-Hallock velocity distribution [3] is used. So, the method may not be applicable to measurements of very old wake vortices.

Overall, the determined circulation also in the cruise evaluation is in good accordance to theory (Figure 8). Due to ATC restrictions and/or contrail visibility, not the full range of wake ages of interest could be covered behind all airliners. A certain amount of scatter is seen in the results. A good result is the determined wake evolution for the B737-700 flying at FL 350: 20 evaluable encounters (from 32 flown) give a clear impression of the wake evolution between 9 nm and 17 nm. At 17 nm the wake strength is reduced to about a fourth of the initial circulation. The circulation results for the other B737-700 flying at FL 370 show more scatter: some encounters have 75% wake strength decay at 10 nm behind the generator, others only 40% at 13 nm. The wakes of an A319 at FL 370 as well as that of an A320 at FL 360 seem to have relatively rapid decay within a distance of 10-12 nm.

The large scatter of circulation at given wake ages is not necessarily only due to measurement uncertainties but can also be attributed to the evolving Crow instability of the vortex pair with subsequent linking. In such flow states the circulation of the vortex evaluated in flight direction will vary between zero (where linking occured) and still very high values (where the vortex is still much unperturbed) as LES have revealed [11, 12].

Wake descent plots (Figure 9) give a clear impression of descent characteristics. Left and right vortices differ in altitude up to 50 ft. A clear result is seen for A320, MD-82, and B737-300. Maximum descent of about 500 ft is observed for A320, B737-300, and the second B737-700. All values are well within the 1000 ft reduced vertical separation distance typically applied by ATC.

Lateral vortex spacing (Figure 10) is near to elliptical theory of $\pi/4$ wing span for A319, A320, and MD-82. The results of the Boeing types B737-700 and B737-300 show a moderate inboard loading: lateral spacing seems to be somewhat smaller than in theory. More details and the influence of the evaluation method and the specifics of the Falcon measurement equipment on these results are discussed in [10].

As a general result, a *Wake Characterization Sheet* is proposed. Figure 11 shows an example, derived from 20 single encounters within an 11 minute measurement period behind a Boeing B737-700 aircraft cruising at FL 350 with a weight of 48 t and an airspeed (TAS) of 429 kt. Wind speed was about 31 kt. The presented example shows clear results with relatively small scatter. The *Wake Characterization Sheet* summarizes the evaluations from real wake encounter flight tests and could be a valuable basis for discussions about the wake evolution of a distinct airliner type. To generalize the results, circulation and wake descent may be linearly extrapolated according to the relation of the actual mass during the flight test measurements to the maximum takeoff weight (MTOW) of the aircraft type under consideration.

Resumee and Outlook

A flight campaign was conducted with the DLR Falcon 20 test aircraft in 2010/2011 to gather wake encounter flight test data: (a) 60 encounters at approach speed behind the VFW-614 ATTAS aircraft, and (b) 202 encounters behind 12 different airliners in cruise. Maximum airliner weight was 62 t. The test data were evaluated applying a DLR developed evaluation method, determining wake characterizing parameters such as wake strength (circulation), wake descent, and lateral vortex spacing for each single encounter. Wake evolution was derived showing all encounter results of one aircraft type as a function of wake age, or distance behind the aircraft. Despite several constraints (e.g limitations of the flow measurement equipment, flight path inaccuracy relative to the vortex cores), all encounters flown at approach speed and about two-thirds of the encounters at cruising speed could be evaluated.

An outcome of the presented evaluation is the proposal of a “*Wake Characterization Sheet*”. In this sheet, all relevant information derived from the encounter flight test data is gathered to show the wake evolution of a distinct aircraft type. This may be a basis for wake severity discussions of (new) aircraft.

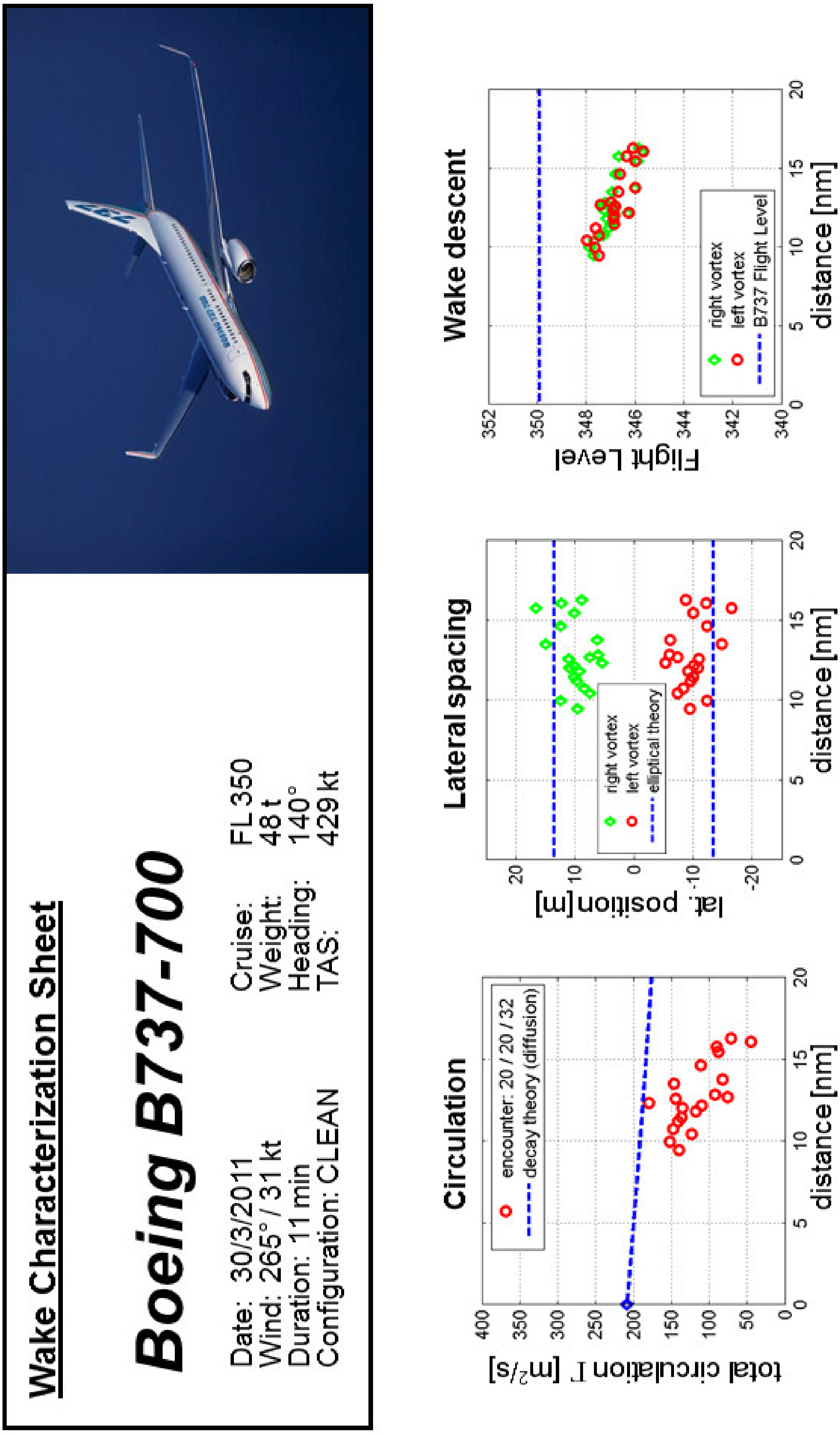

Figure 11: Proposal for a *Wake Characterization Sheet* [photo source: Boeing]

During some encounters behind MEDIUM category airliners in cruise, the limit loads of the relatively small test aircraft Falcon 20 (MTOW = 13 t) were nearly reached. So, it was decided for safety reasons not to gather encounter data behind heavier airliner types. To apply the test technique for airliners in the HEAVY category, a larger test aircraft (e.g. A320) should be used.

The gathered flight test data will also be used to validate flight mechanic wake encounter models (or aerodynamic interaction models) for a swept wing aircraft configuration (Falcon). For this, the reconstructed wake characteristics from the present evaluation will be used.

References

[1] Fischenberg, D. *Bestimmung der Wirbelschleppencharakteristik aus Flugmessdaten* DGLR-Jahrestagung Stuttgart, 23.-26. September 2002, DGLR-JT2002-170, Jahrbuch. Bonn: Deutsche Gesellschaft für Luft- und Raumfahrt (2002)

[2] de Bruin, A. *S-WAKE Assessment of Wake Vortex Safety – Publishable Summary Report* NLR-TP-2003-243 (2003)

[3] Burnham, D. C.; Hallock, J. N. *Chicago Monoacoustic Vortex Sensing System* Vol. 4, Wake Vortex Decay, Springfield, VA, National Information Service (1982)

[4] Fischenberg, D. *S-WAKE Results of Flight Test Data Analysis* DLR IB 111-2002/11 (2002)

[5] Jategaonkar, R. V. *Flight Vehicle System Identification: A Time Domain Methodology* Progress in Astronautics and Aeronautics Series, Vol. 216 Published by AIAA, ISBN-10: 1-56347-836-6 (2006)

[6] Holzäpfel, F. *Probabilistic Two-Phase Wake Vortex Decay and Transport Model* Journal of Aircraft Vol. 40, No.2 March-April 2003

[7] Holzäpfel, F., Robins, R. E. *Probabilistic Two-Phase Wake Vortex Model: Application and Assessment* Journal of Aircraft Vol. 41, No.5 September-October 2003

[8] Lorscheid, M. Radar Data of Selected Aircraft on 3/3/2010 & 30/3/2010 Deutsche Flugsicherung DFS

[9] McCormick, B. *Aerodynamics, Aeronautics and Flight Mechanics* John Wiley & Sons, Inc. (1995)

[10] Fischenberg, D. *Charakterisierung von Wirbelschleppen aus In-Situ-Flugmessdaten der Falcon D-CMET* DLR IB 111-2011/17 (2011)

[11] Gerz, T., Baumann, R., “Decay characteristics of single and double wake-vortex pairs in different atmospheric flow realisations”, ICAS 2006, 25th Int. Congress of the Aeronautical Sciences, Hamburg, ICAS 2006-3.8.1., Sept. 2006, pp. 13.

[12] Hennemann I., Holzäpfel F. 2011: Large-Eddy Simulation of Aircraft Wake Vortex Deformation and Topology, Proc. IMechE Vol. 225 Part G: J. Aerospace Engineering, pp. 1336-1350, DOI: 10.1177/0954410011402257.

6.6 On the Influence of Vortex Curvature on Wake Encounter Hazard

Dennis Vechtel
Institute of Flight Systems

This report summarises the achievements of research on the influence of vortex curvature on wake encounter hazard. The investigations described in this report were performed in the framework of the DLR Project "Wetter & Fliegen". Various simulations were carried out to quantify the differences between encounters with idealised straight vortices and realistically shaped curved vortices and to find metrics for a hazard assessment based on more realistic wake encounters. For these investigations offline simulations were performed with and without dynamic aircraft simulations as well as piloted simulator studies and in-flight simulations with the DLR research aircraft ATTAS. The investigation described here indeed outlines considerable results but unfortunately cannot give final quantitative values concerning hazard assessment. To finally quantify the influence of vortex curvature on encounter hazard further research will be undertaken.

Introduction

Present wake vortex related separation distances have proven over the last decades to sufficiently prevent from hazardous wake encounters. But in a world with daily increasing air traffic it might be necessary in the future to revise these separation distances as they limit airspace and airport capacities [1] without affecting the safety of flight operation. For this reason it is evident to understand the hazard posed by wake vortices.

Vortex Deformation and Atmospheric Conditions

For research and simulation purposes wake vortices are often assumed to consist of two straight, parallel, and infinite counter rotating vortices. In reality wake vortices can only be regarded as straight shortly after their generation. During the vortex decay the so-called Crow-instability leads to a sinusoidal deformation of the vortices with increasing amplitude. Eventually both vortices link at intervals and form ring structures. An image of the possible deformation during the vortex decay is shown in Figure 1. In this picture the vortices pass through the following stages: 1) nearly straight and parallel, 2) onset of Crow-instability, 3) sinusoidal deformation and 4) first linking and ring formation.

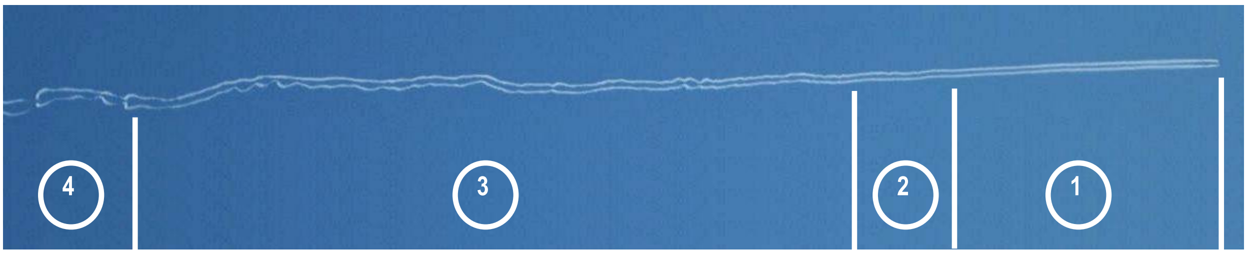

Figure 1. Deformation of wake vortices during decay [photo: DLR]

After the linking which can already be observed in Figure 1, ring vortices form out. These vortex rings are firstly formed out in the flight direction of the vortex generator with timely increasing lateral spread. After the formation of vortex rings the circulation decreases significantly in flight direction whereas the circulation in those areas of the vortex rings perpendicular to the flight direction show only a slowly decreasing circulation. This can be seen in Figure 2 as a result of large-eddy-simulations (LES). A real photography of vortex rings is also shown in Figure 2. Here one can clearly observe the similar shape of the vortex rings in comparison the numerical results. Especially in the stage of vortex ring formation it is clearly obvious that the assumption of wake vortices being straight is not sufficient. At the latest after the onset of the Crow-instability the vortex shape alters significantly during the further decay.

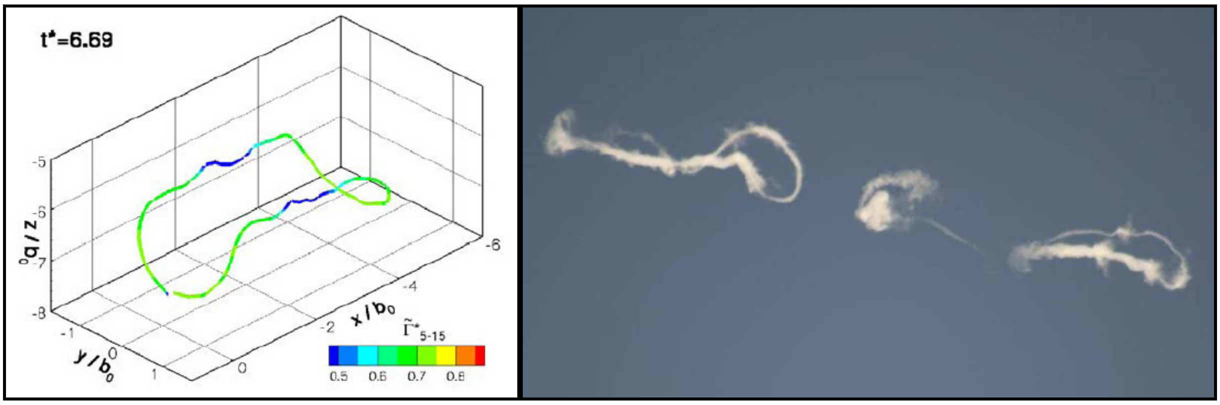

Figure 2. Vortex rings in numerical simulations [2] and in reality [photo: DLR]

The vortex bending has indeed an influence on the encounter characteristics as the deformation of the vortex line also results in a deformation of the whole flow field of the wake. Thus it can be expected that vortex curvature also influences the encounter hazard. On the one hand one can suppose that a strong vortex deformation decreases the impact of an encountering aircraft due to the much shorter duration of induced forces and moments acting on the encountering aircraft. On the other hand the encounter characteristics are more inhomogeneous in comparison to straight vortices which might lead to higher demands on the pilots of the encountering aircraft.

The vortex decay and deformation is strongly influenced by the atmospheric conditions. Especially the atmospheric turbulence and temperature stratification influence the vortex decay [2]. The energy of atmospheric turbulence is able to increase the vortex decay. The stronger the atmospheric turbulence the faster the vortex circulation decreases. The eddy-dissipation-rate is one important measure for the energy dissipation and thus for the vortex decay and deformation. The temperature stratification of the atmosphere affects all vertical motion of the air. In general it can be differentiated between stable, neutral an unstable stratification. In the project "Weather & Flying" only atmospheric conditions with neutral and stable temperature stratification were analysed. Unstable stratification produces turbulence and is to some degree already represented in the cases considered. A measure for the temperature stratification is the square of the Brunt-Väisälä-frequency N^2. Stable temperature stratification leads to a massive disruption of the vortex structure during the decay so that the vortices are being strongly deformed.

Large-Eddy Simulations (LES)

The investigations in the area of vortex curvature were based on flow-fields of deformed wake vortices of different vortex ages derived from large-eddy-simulations. LES are able to represent the shape and flow-field of wake vortices very realistically like shown on Figure 3 for three different vortex ages. The large-eddy-simulations were performed at the DLR Institut für Physik der Atmosphäre [3].

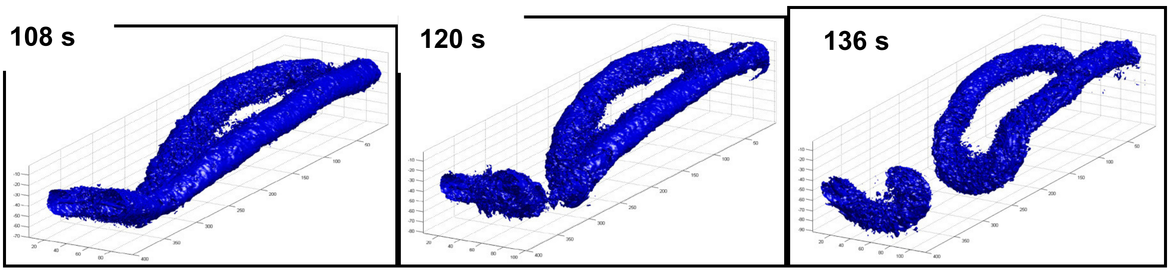

Figure 3. Velocity fields (magnitude of 5 m/s) from simulated vortices at t_{age} = 108 s, 120 s and 136 s

The LES were conducted with the numerical code LESTUF which is a 2nd order space and time finite differences code using a staggered grid with a modified Smagorinsky closure scheme. In advance to the actual large-eddy-simulations simulation runs are performed to adjust the ambient turbulence. When the actual vortex simulation is started the turbulence field is fully developed with a constant dissipation rate and a spectral inertia range following the $k^{-5/3}$-distribution after Kolmogorov. The curved vortices were initialised with a Lamb-Oseen vortex model [7] which comprises the following equation for the tangential velocity

$$V_T = \frac{\Gamma}{2\pi r}\left(1 - e^{-1.2544\frac{r^2}{r_c^2}}\right). \quad (1)$$

Results of the LES like they were applied in the presented analyses were 4-D flow fields for different vortex ages covering the whole decay process. For nine different atmospheric conditions the three velocity components [u,v,w] are given as a function of the spatial position [x,y,z] and the vortex age. The dependence on the atmospheric conditions is hereby represented by the normalised eddy-dissipation-rate ε^* as a measure of the atmospheric turbulence and the normalised Brunt-Väisälä-frequency N* as a measure of the temperature stratification. Thus the outputs of the LES are:

$$[u,v,w]_{flowfield} = f\left(x,y,z,t_{age},\varepsilon^*,N^*\right). \quad (2)$$

The generator aircraft in these LES was a heavy aircraft in landing configuration with a wing span of 60.3 m and a gross weight of 190 t. Due to numerical reasons the flow field matrices have a length of 400 m in flight direction with periodic boundaries in all three dimensions. This length is sufficient for the large-eddy-simulations as it covers one wavelength of the Crow-instability. The Crow-instability represents one of the dominant mechanisms for vortex decay. However, this length is not sufficient for wake encounter flight simulations. Therefore, for the simulation studies the flow field of one vortex age was connected in series so that in flight direction of the generator aircraft an infinitely long flow field was formed with the repeated shape of the oscillating LES vortices.

Offline Simulations

Besides the simulator campaign and the real flight tests described below, various offline studies were accomplished. These analyses should form a basic understanding of the influence of vortex curvature on the encounter hazard. This chapter will give a brief introduction to the outcome of the performed offline studies exemplarily by a Roll Control Ratio (RCR) analysis. RCR is the ratio of the rolling moment induced by the wake vortices and the maximum rolling control power (maximum rolling moment due to maximum deflection of all roll control motivators) [11].

This analysis was performed without any dynamic aircraft simulation and purely on the basis of the wake vortex induced forces and moments which theoretically act on an encountering aircraft moving along a pre-defined flight trajectory without responding to the flow field variations it is exposed to. Thus the results of this analysis cannot directly serve as metrics concerning aircraft response or encounter hazard. Nevertheless these simulations outline some interesting results especially regarding vortex rings. For the analysis on RCR level an aerodynamic interaction model using the strip method [4] for a medium aircraft was used with vortex flow fields derived from LES for three different vortex ages of t_{age} = 108 s (prior to linking), t_{age} = 120 s (at Linking) und t_{age} = 136 s (vortex rings) like depicted in Figure 3. The regarded encounter scenario was a vertical encounter with a 3° different flight path angle and the same azimuth between vortex and encountering aircraft (s. Figure 4).

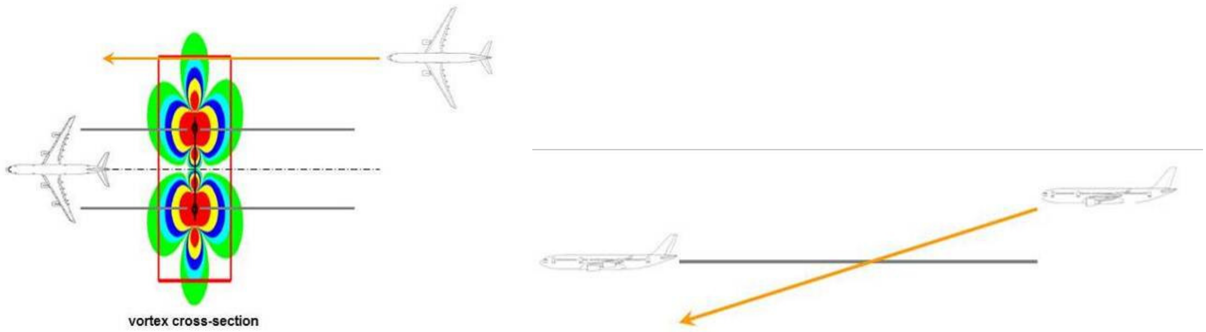

Figure 4. Analysed encounter scenario; coloured contours indicate RCR levels.

As for encounters with the curved LES-vortices the RCR distribution not only depends on the lateral distance from the vortex cores (like for straight vortices) but also on the x-position of the encounter, simulations were performed with a variation of the lateral y-position of the encounter in 2 m steps and a variation of the longitudinal x-position in 10 m steps. For reasons of comparison the same encounters have also been simulated with straight vortices (with a comparable circulation) applying a tangential velocity distribution after Burnham-Hallock [12]. In these simulations only the y-position of the encounter has been varied as the straight vortices are invariant in x-direction.

Wavy Vortices (t_{age} = 108 s)

With a true airspeed of the generator aircraft of 72 m/s (typical approach speed) this vortex age represents a separation distance between generator and follower aircraft of approximately 4.2 nm. With a required separation distance of 5 nm for medium behind heavy aircraft this scenario is very unlikely under IFR but possible during approaches under VFR. Figure 5 depicts the maximum RCR that occurred during the encounters with straight and curved vortices. As mentioned above the maximum RCR differs with the x-position of the encounter. Thus the figure shows the highest and the lowest maximum RCR values for encounters with curved vortices.

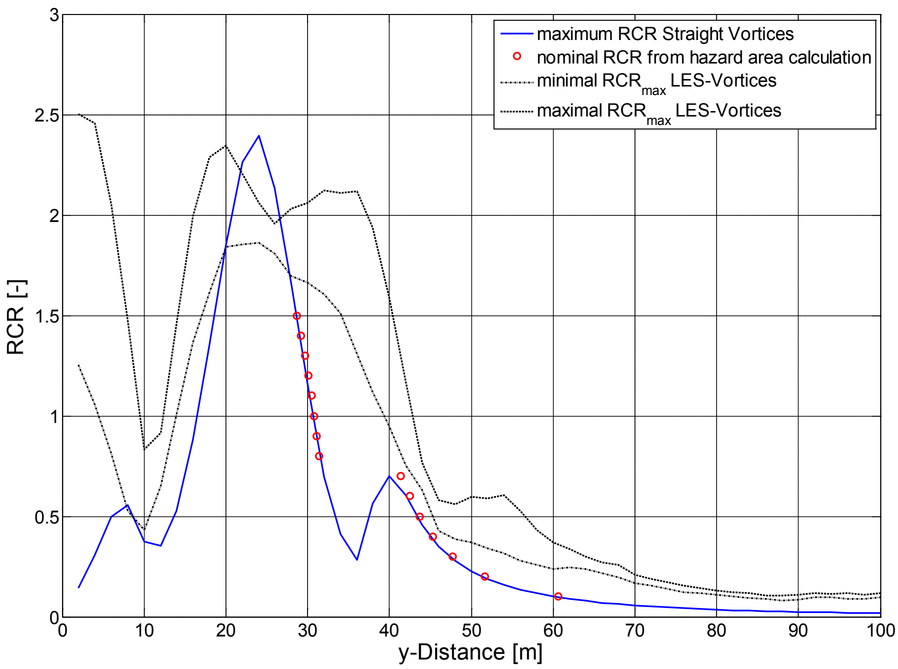

Figure 5. Maximum radial RCR-distribution at t_{age} = 108 s;
at y=0 is the centerline of the wake generating aircraft.

In addition Figure 5 shows the nominal RCR values from the hazard area calculation using straight vortices [13]. One can clearly observe that the nominal RCR values from the hazard area calculation match the RCR values from the encounter simulations with straight vortices quite well. Differences between these values only occur as for the hazard area calculation an aerodynamic interaction model was used which only takes the wings into account (contrary to the AIM used in the aircraft simulation which also takes into account the horizontal and vertical stabilisers as well as the fuselage).

For the curved vortices the lateral region where the maximum RCR value occurs during the encounter is much wider and shifted towards greater y-values in comparison to the straight vortices. The absolute value of the maximum RCR is in the same range for straight and curved vortices. Over the whole outer area the RCR values of the curved vortices are slightly above those of the straight vortices.

Linking Vortices (t_{age} = 120 s)

With a true airspeed of the generator aircraft of 72 m/s this vortex age represents a separation distance between generator and follower aircraft of 4.7 nm. So this scenario again is not allowed for medium behind heavy IFR separations but with today's air traffic density it is not impossible to happen. Under VFR this scenario is indeed not unlikely. Also for this vortex age the maximum RCR values which occurred during the encounters with the LES vortex (Figure 6) show a shift towards greater y-positions compared to the encounters with straight vortices. But the difference is larger compared to the vortices before linking. The absolute maximum is also in the same region for straight and curved vortices but with an RCR of about 1.6 to 1.9 smaller for curved vortices. Also over the whole outer region the RCR values of curved vortices are above those of straight vortices.

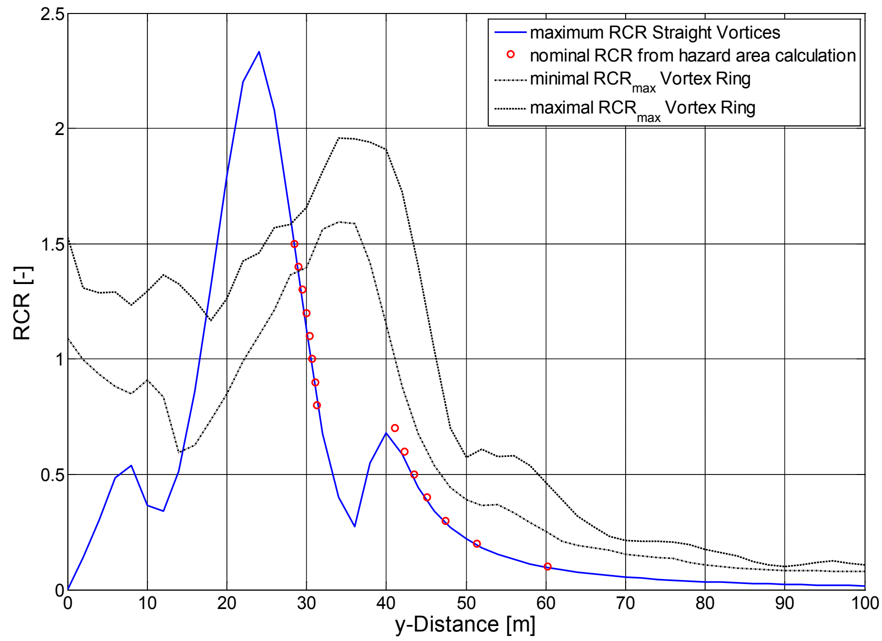

Figure 6. Maximum radial RCR-distribution at t_{age} = 120 s

Vortex Rings (t_{age} = 136 s)

With a true airspeed of the generator aircraft of 72 m/s this vortex age represents a separation distance of approximately 5.3 nm. So this scenario is indeed realistic for medium behind heavy aircraft even for IFR operations. Here the maximum RCR values of encounters with curved vortices (Figure 7) are again shifted further towards greater y-positions but with a furthermore decreased absolute maximum.

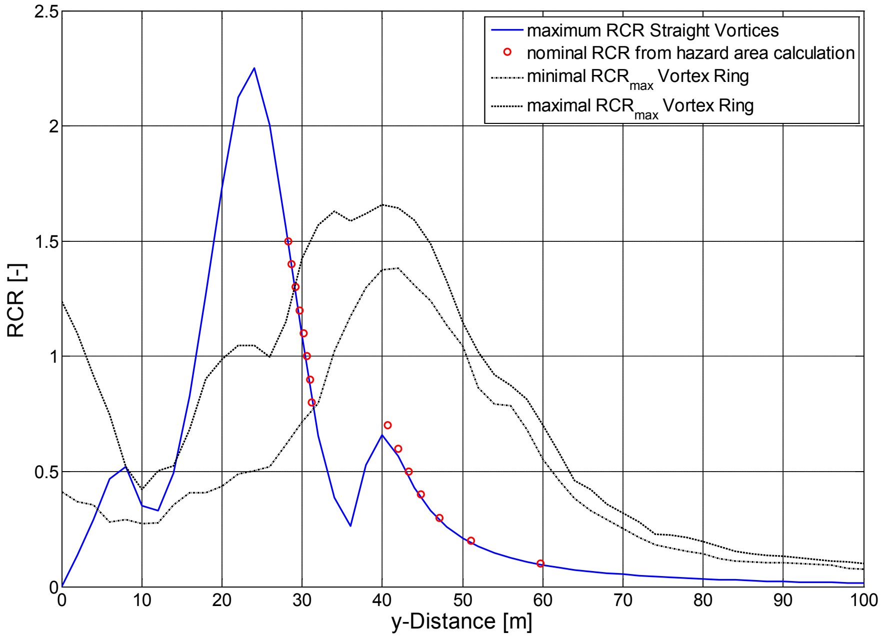

Figure 7. Maximum radial RCR-distribution at t_{age} = 136 s

Conclusions from the RCR Analysis

The RCR analysis showed that for a medium aircraft encountering the wake of a heavy aircraft vortex rings cannot be neglected regarding the respective hazard. The induced forces and moments are still considerable in the stage of vortex rings. Indeed the analysis of the roll control ratio does not directly allow conclusions concerning the aircraft response and the resulting hazard due to the wake impact. But the results show that even vortex rings may still contain a considerable hazard. Also the lateral distribution of RCR is different at any vortex age with increasing spread during the vortex decay. Thus the wider lateral spread of matured and deformed vortices must be considered for hazard assessment.

A330-Simulator Campaign at ZFB

A comprehensive simulator campaign was conducted in the convertible A330/A340-simulator of the Zentrum für Flugsimulation Berlin (ZFB, see Figure 8). The chosen aircraft for simulation was the A330 for this campaign. One great advantage of the simulator is the ability to implement external simulation modules or data into the simulator due to a separate scientific simulation host computer independently from the very training simulation. A detailed description of the campaign and the results are given in [5] and [6].

In the campaign so-called time-fixed encounters were simulated with both straight and curved vortices. “Time-fixed” means that pre-recorded force and moment histories were applied to the simulation in contrast to so-called space-fixed encounters where the vortex induced forces and moments are calculated online depending on the actual position of the encountering aircraft. Applying the “time-fixed” method is especially useful for piloted simulations as the impact of the vortex on the encountering aircraft is accurately repeatable. For the calculation of force and moment time histories different vortex flow-fields were used generated by a heavy aircraft with a mass of m = 190 t. The straight vortices where calculated with a radial velocity distribution after Burnham-Hallock whereas those encounters with curved vortices were based on the LES-flow-fields. The vortex age of the LES derived vortices was 108 s which represents a separation distance of approximately 4.2 nm for typical approach speeds. So the analysed aircraft pairing corresponds to the ICAO wake vortex separation for heavy behind heavy aircraft which is 4 nm. The calculation of induced forces and moments was performed with an aerodynamic interaction model based on the strip method [4].

Figure 8. Cockpit and external view of the A330/A340-simulator of the ZFB

The simulator tests were accomplished with 5 airline pilots and 1 test pilot. The pilot's task was to perform an ILS-approach under VFR until touchdown. To get a full idea of the influence of vortex curvature on the flight dynamics the approaches were performed with both, manual control and with autopilot engaged. The playback of the vortex force and moment data was initialised depending on a specific but differing playback height to avoid pilot adaptation to the investigated scenarios. After each approach the pilots had to rate the encounter by means of the following encounter rating scale (Figure 9).

The campaign showed that the A330 flight control system is well able to compensate the vortex induced forces and moments. Under manual control the A330 normal law compensated light and moderate disturbances that well that no impact on the aircraft was noticeable. Also the autopilot was well able to handle the wake impact. The pilots stated unanimously that the curved vortices feel a lot more realistic than the straight.

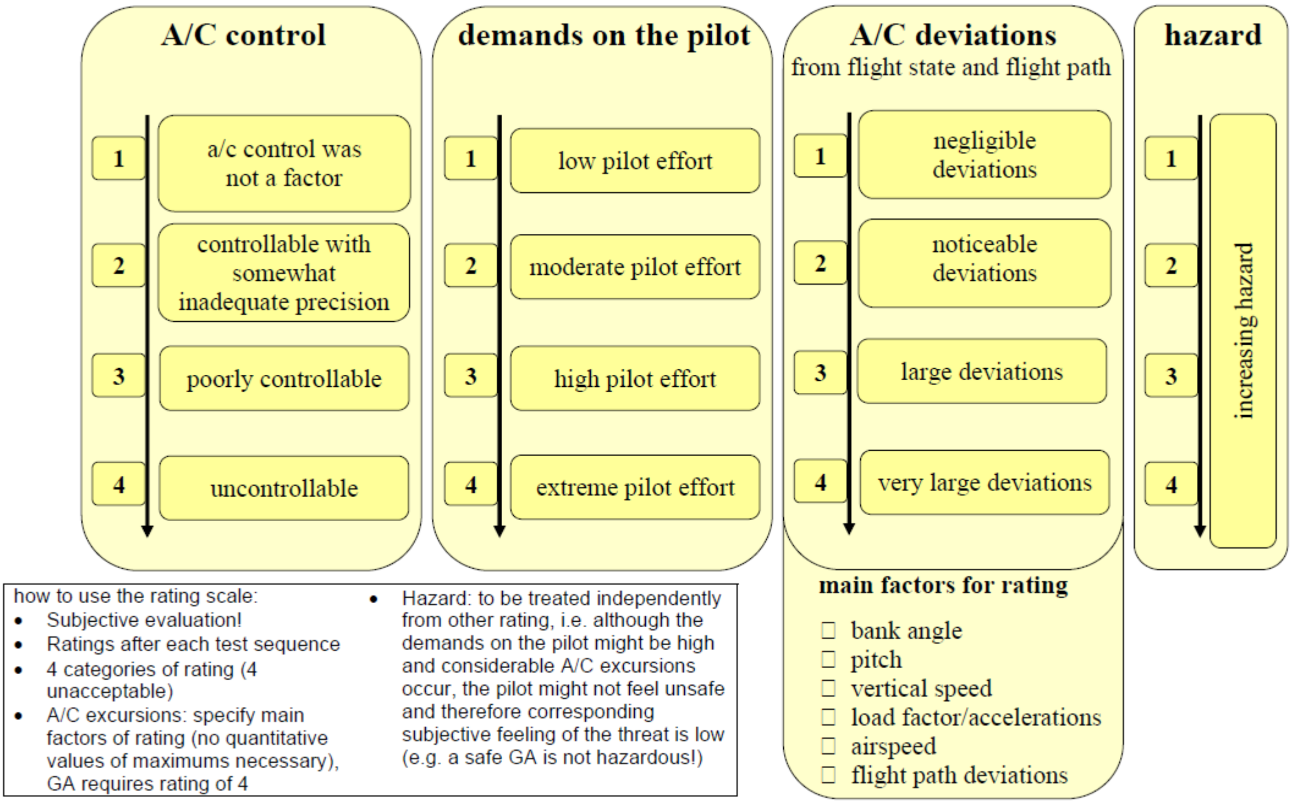

Figure 9. Wake vortex encounter rating scale [14]

The difference between encounters with curved and straight vortices are outlined exemplarily on Figure 10. One can observe that even though the induced rolling moments have similar amplitudes, the bank angle in case of manual control is significantly larger than with autopilot engaged. In this specific case the encounter characteristics resulted in a go-around under manual control.

The analysis of the different encounters showed that on average the pilot ratings and aircraft reaction respectively was in the same magnitude for straight and curved vortices. Nevertheless the evolution of induced forces and moments during the encounter is significantly different as can be seen in Figure 10. This could be the reason why under manual control the encounters were rated slightly worse with curved vortices. With autopilot engaged no significant differences could be noticed between curved and straight vortices.

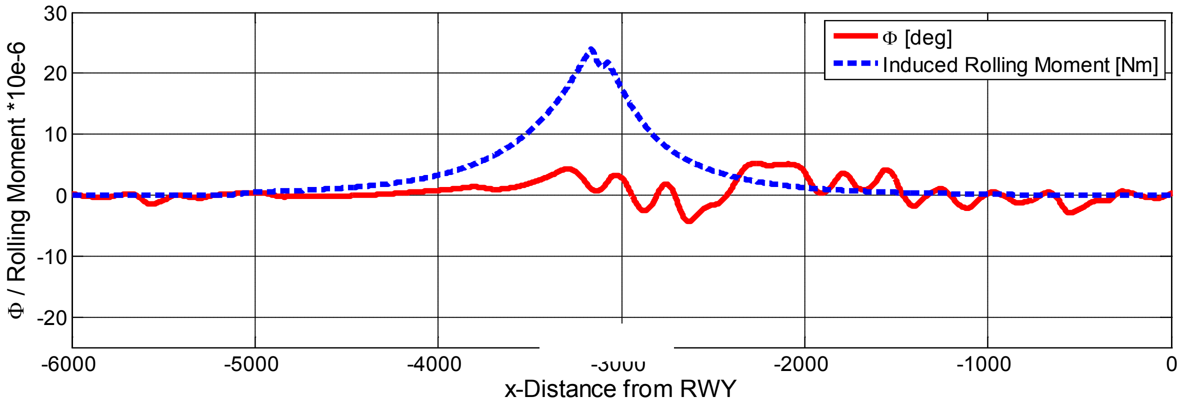

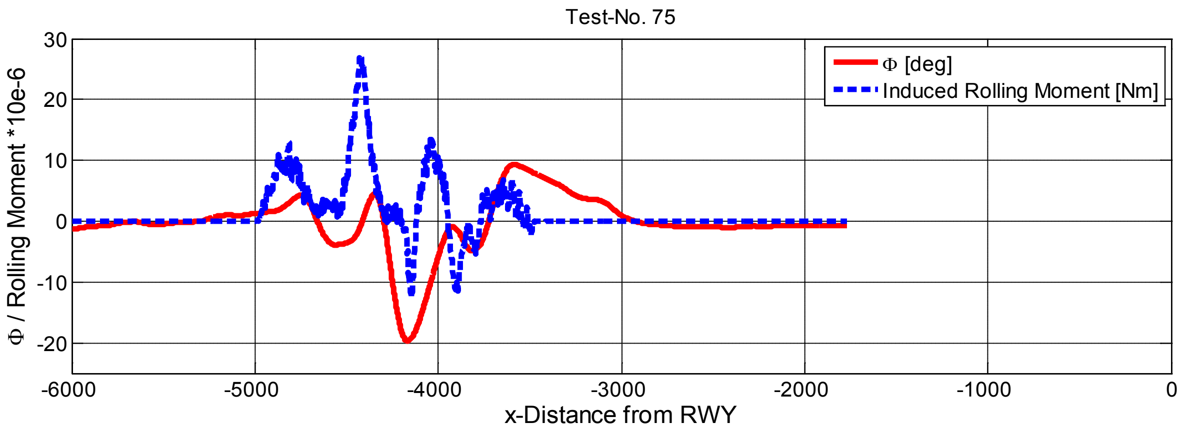

Figure 10: Comparison of curved (lower diagram) and straight vortices (upper diagram) under manual control

Regarding the encounter acceptance of the pilots as a function of the maximum RCR peak value one can observe differences between straight and curved vortices (s. Figure 11). The figure includes encounters under manual control and with autopilot engaged as well which explains the huge amount of accepted encounters with relatively high maximum RCR values.

The figure clearly outlines that with straight vortices all encounters below an RCR value of 0.58 were accepted. Contrary to this the acceptance threshold for curved vortices is at an RCR value of about 0.35. Although, without a sound statistical relevance this might give some indication that the aircraft response with curved and straight vortices is in the same magnitude but that the characteristics of encounters with curved vortices seem to decrease the acceptance threshold.

Even if the small amount of participating pilots is not a reliable base for statistics concerning the pilot's behaviour the characteristics of encounters with curved vortices seem to increase the risk of pilot-induced-oscillations (PIO). Indeed the worse rating under manual control with curved vortices seems to be directly related to PIO. The PIO are clearly triggered by the wake vortices and give an indication of a possible potential of hazardous interaction between the pilot and the normal law of the flight control system. One possible solution could be to take the pilot out of the loop in case of a wake encounter. This is what Airbus recommends to pilots not to command any control inputs in case of a wake encounter. During the simulator campaign an inverse correlation between the pilot's experience and his PIO tendency was observed. Also an inverse correlation between the pilot's experience in terms of flight hours and their average ratings was observed. This correlation implies that it could be helpful to include wake encounters into the airline pilot training. A training effect was observed during the simulator campaign. After many wake encounters the pilots ability to handle the encounter seemed to improve in the simulator.

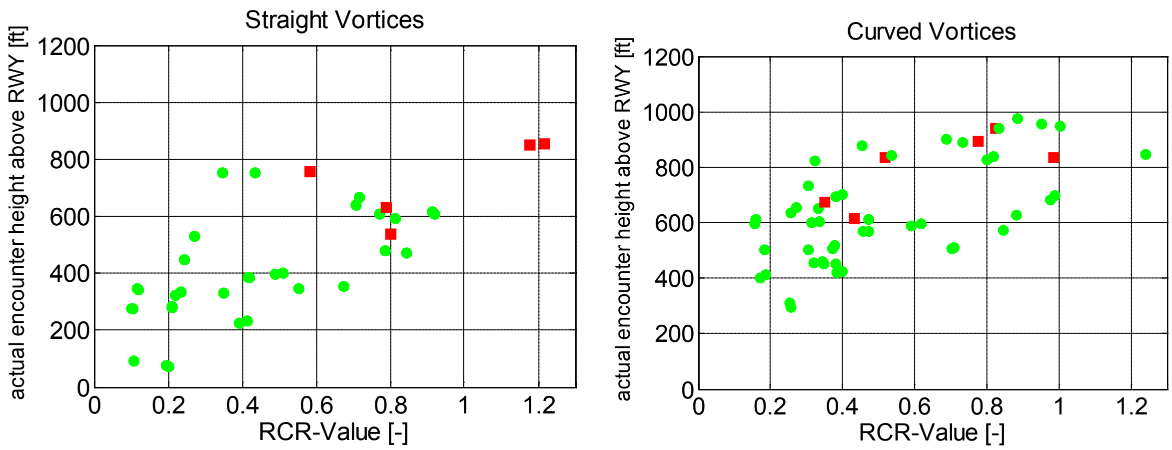

Figure 11. Encounter acceptance with straight and curved vortices; green/red colours mark acceptable/non-acceptable encounters.

Flight Test with ATTAS

Besides the simulator campaign, also various flight tests were performed with the VFW614 ATTAS (s. Figure 12) for hazard assessment of deformed vortices. In these flight tests the ATTAS in-flight-simulation capability was used. This means that no real vortices were encountered but that the wake encounters were simulated in-flight. Due to cost restrictions only a limited number of flight tests could be conducted. But this kind of test executed in the real environment of flying represents the most realistic way to analyse wake vortex encounters and the related hazard (besides flight tests with real wake vortices). Thus, the flight tests can be used to verify results gained in simulator test or offline simulations. To the author's knowledge these flight tests are the worldwide first flight tests of realistically shaped and deformed vortices derived from LES.

In-Flight Simulation of Wake Vortices with ATTAS

The aim of in-flight simulation is to match the behaviour of a model-based virtual aircraft and a specific host aircraft to provide nearly unconstrained motion and visual cues for the pilot under real flight conditions [8]. Due to additional control surfaces – like the direct lift control flaps - ATTAS is able to directly control five of six degrees of freedom. The in-flight-simulation is based on an aircraft simulation running on-board the ATTAS which is initialised and trimmed with the current aircraft state when the simulation is switched on. Downstream of this aircraft simulation is an inverted simulation model of the ATTAS host aircraft which calculates the necessary control surface deflections to make the real VFW-614 ATTAS follow the motion of the simulated aircraft. The simulated aircraft can be arbitrary (but within the envelope of dynamics of the host aircraft) but in case of the flight tests described here the simulated aircraft was also the VFW614 itself. Once the in-flight-simulation is started the experimental pilot does no longer control directly the real aircraft but his control inputs are fed into the simulated aircraft. Via the model following controller based on the inverted model the real ATTAS host aircraft is forced to follow the simulated aircraft. The safety pilot at the right seat is able all the time to stop the in-flight-simulation by a safety button or by commanding inputs to the conventional flight control system. A more detailed description of the ATTAS in-flight-simulation can be found in [9] and [10].

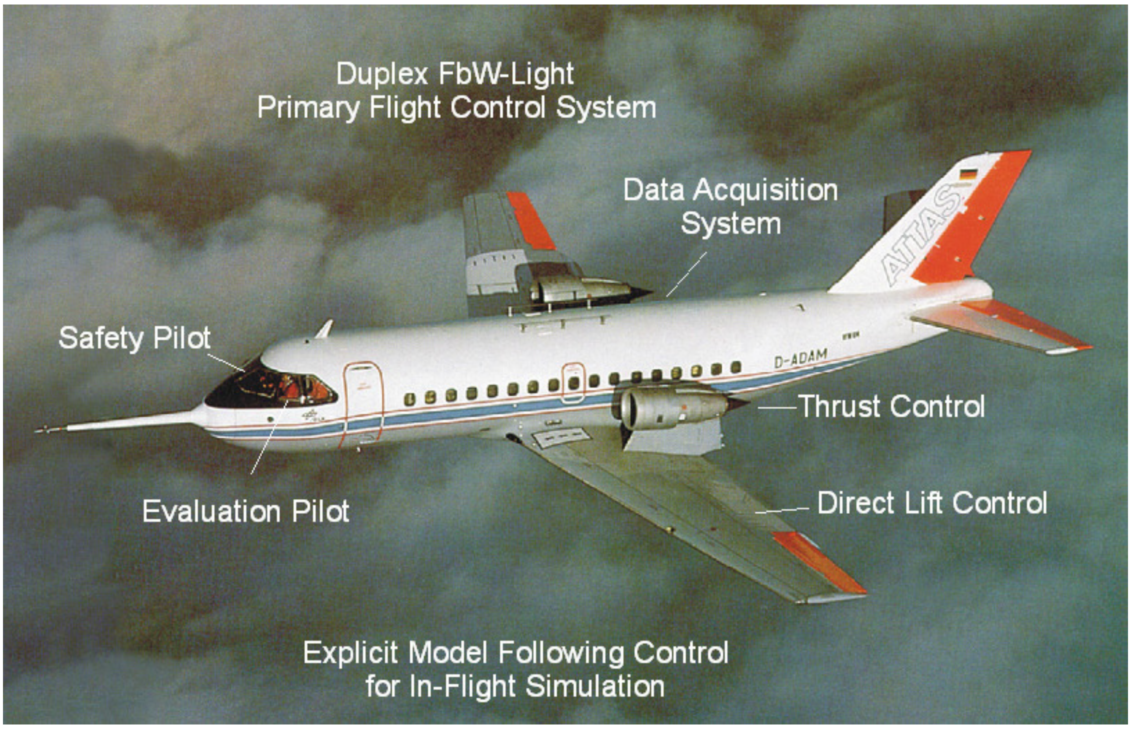

Figure 12. The DLR research aircraft ATTAS

This way it is possible to let the real aircraft encounter a simulated wake. Without any wake vortices the experimental pilot controls the real aircraft via the simulated aircraft and the model following controller. Similar to the simulator campaign in the A330 simulator (see above) the encounters were time-fixed. During the encounter the real ATTAS follows the motion of the simulated ATTAS if no control inputs were commanded by the experimental pilot. Thus the experimental pilot has to counteract the simulated wake impact on the aircraft like during a real encounter. A schematic description of the wake encounter in-flight-simulation with ATTAS is depicted in Figure 13. The analysis of the recorded data shows a good conformity of the motion of the simulated and the real aircraft. It can be stated that the real ATTAS represented the encounter simulation very realistically which was also confirmed by the test pilots.

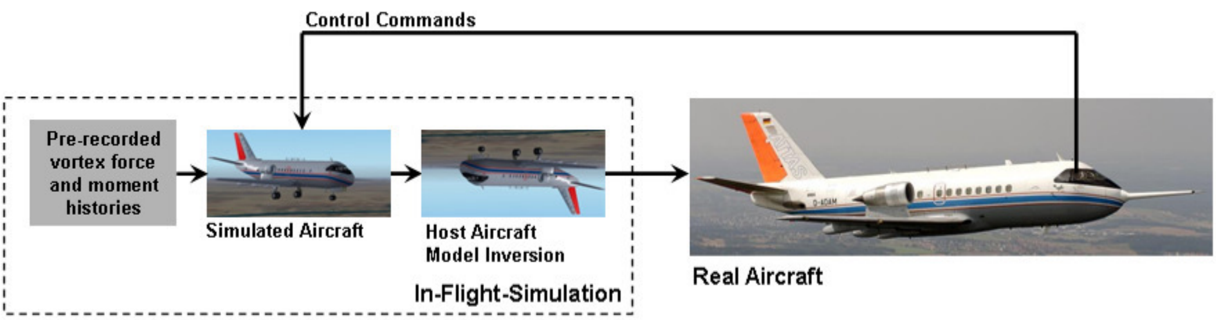

Figure 13. Schematic description of the ATTAS in-flight-simulation of wake vortices

Accomplishment

All wake encounters simulated with ATTAS were performed at final approach. The pilot's task was to perform an ILS-approach under VMC with the aim to land the aircraft. Landing was not intended during the tests but instead each approach was finished after the wake encounter with a go-around a few hundred feet above ground.

Depending on the pre-defined but differing playback height the vortex induced forces and moments were played back time-fixed after reaching this height. The induced forces and moments of each encounter were recorded prior to the flight tests. The playback height varied between 650 ft and 1050 ft above ground depending on the vortex strength. The flight tests comprised simulated encounters of vortices of two different ages. Those vortex ages correspond to deformed vortices prior to linking and vortex rings. In the flight tests solely those encounters with LES generated vortices have been simulated.

During and after the encounter the pilots should stabilise the aircraft and pursue the ILS-approach. The go-around was initiated after the encounter either if the pilot was sure that he could safely continue the landing or if he was not able to stabilise the approach due to the impact of the wake vortices. After each go-around the pilots had to rate the encounter by means of the encounter rating scale as depicted in Figure 9.

All in all 31 encounters were simulated in-flight during six flights with three different experimental pilots.

Results

As mentioned above the results from flight tests cannot serve as a base for statistics due to the small amount of conducted encounters. Nevertheless, the flight test results reveal additional findings and in general support the results from offline simulations and simulator test.

Figure 14 depicts the results from flight tests in terms of roll control ratio RCR, actual encounter height and pilot rating. The figure shows those encounters with wavy vortices (squares) and those with vortex rings (circles) as well. The colour coding depicts the pilot rating. Green marks mean that the average rating is below a value of 2. The experience made during the flight tests showed that those encounters are doubtless harmless. Those encounter still acceptable but with an average rating greater than 2 are marked yellow. Those encounters are indeed still accepted by the pilots but result in an increased pilot workload and noticeable flight state deviations. Those encounters with one or more issues rated with 4 are unacceptable by definition. In the figure below they are marked in red ("Single Rating = 4").

One can clearly observe hat the boundary between green and yellow marked encounters is in a similar range for wavy vortices and vortex rings (RCR ≈ 0.25…0.3). On the other side the boundary between yellow and red marked encounters – which is the actual acceptance threshold – is widely different for wavy vortices and vortex rings. The lowest unaccepted encounter (in terms of RCR) with wavy vortices is at an RCR of approximately 0.5 whereas encounters with vortex rings have all been accepted below an RCR value of about 1.

The qualitative impression experienced during the flight tests is that the impact of vortex rings acts on all axis whereas the wavy vortices impact is dominated by rolling motion. The data recorded during the flight tests support this impression quantitatively. Apparently pilots rated roll dominant encounters worse in the flight tests than those encounters with impact on each axis.

Pilot-induced-oscillations (PIO) as they occurred in the study in the A330 simulator have not been observed in the flight tests with ATTAS. This fact might indicate that PIO result on the interference between a controller-augmented flight control system and the pilot. With a conventional flight control system like in the VFW614 the risk of PIO during a wake encounter might not be an issue.

It is planned to conduct more inflight simulated encounters with ATTAS for a more comprehensive hazard analysis in the future.

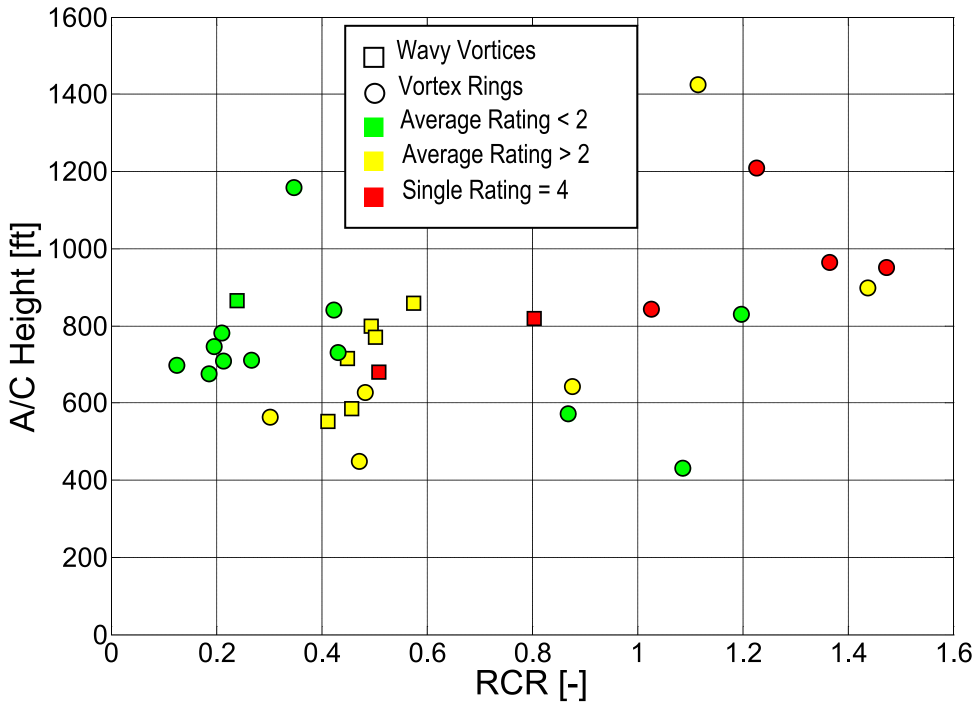

Figure 14. Encounter ratings of the ATTAS flight tests

Conclusions

In the frame of the DLR Project "Wetter & Fliegen" the DLR Institute of Flight Systems investigated on the influence of wake vortex curvature on the encounter hazard. Various offline simulations, simulator studies and flight tests were performed for hazard assessment regarding vortex deformation.

At the present state of investigation no final statement can be drawn concerning the overall hazard of deformed vortices. Nevertheless many remarkable results have been achieved during the project, which show some considerable facts.

The investigations showed that modern controller-augmented flight control systems are well able to cope with the wake impact up to a certain level no matter whether the vortices are straight or deformed. Under manual control pilots seem to tend to trigger pilot-induced-oscillations during and after the encounter as a consequence of interference between controller-augmented flight control system and pilot's control input. With a conventional flight control system like on the VFW614 these PIO tendency could not be observed. This tendency seems to decrease with increasing pilot's experience. Also some kind of training effect was observed in simulator and flight tests where pilots encountered wake vortices one after another. This tendency supports the suggestion that it could be useful to include wake vortex training into airline pilot training.

The hazard ratings of curved and straight vortices were at the same magnitude for encounters of comparable strength. But their encounter characteristics were totally different. The much higher frequencies of flow field variation during encounters with curved vortices seem to increase the pilot workload although the duration of the wake impact is mostly shorter. Both effects seem to counterbalance each other. After the ring formation of the vortices the pilot's acceptance threshold seems to increase towards greater roll control ratios. Encounters with vortex rings are often less roll dominated than encounters with wavy vortices although in some cases also vortex rings still have a considerable roll impact. Apparently, pilots rate roll dominant encounters worse than those with lesser roll impact but more considerable impact in all other axis.

Acknowledgement

The author gratefully acknowledges the contribution from Frank Holzäpfel and Ingo Hennemann of DLR Insitute of Atmosperic Physics for the supply and support of the LES data, the flight crews from DLR Flight Facilities Braunschweig, my colleague Dirk Leißling from DLR Institute of Flight Systems who did the software integration into the ATTAS experimental systems as well as many airline pilots from Lufthansa who participated the simulator campaigns enthusiastically.

References

[1] Hahn, K.-U., Schwarz, C. W., Wake Vortex Avoidance versus Landing Capacity, AIAA-2006-6322, AIAA Guidance, Navigation, and Control Conference, Keystone, Colorado, 2006

[2] Holzäpfel, F., Misaka, T., Hennemann, I., Wake-Vortex Topology, Circulation, and Turbulent Exchange Processes, AIAA-2010-7992, AIAA Atmospheric and Space Environments Conference, Toronto, Cananda, 2010

[3] Hennemann, I., 2010: “Deformation und Zerfall von Flugzeugwirbelschleppen in turbulenter und stabil geschichteter Atmosphäre”, PhD Thesis, Technische Universität München, DLR-FB 2010-21, 145 pp.

[4] Fischenberg, D., A Method to Validate Wake Vortex Encounter Models From Flight Test Data, ICAS, 27th International Congress of the Aeronautical Sciences, 2010

[5] Vechtel, D., Amelsberg, S., Full flight simulator study for evaluation of aircraft dynamics while encountering curved wake vortices, DLR Internal report IB 111-2009/17, Braunschweig, 2009

[6] Vechtel, D., Fezans, N., Full flight simulator study for evaluation of aircraft dynamics while encountering curved wake vortices (part II – result evaluation), DLR Internal Report IB 111-2010/18, Braunschweig, 2010

[7] Lamb, H., Hydrodynamics, Cambridge University Press, pp. 590-592, Cambridge, 1932

[8] Leißling, D., Gestwa, M., Bauschat, J.-M., In-Flight Simulation in Support of an Aircraft Certification Process, AIAA Modeling and Simulation Technologies Conference and Exhibit, Paper No. AIAA 2003-5532, Austin, Texas, August 11-14, 2003.

[9] Hanke, D., Bauschat, J.-M., Lange, H.-H., Heutger, H., In-Flight Simulator ATTAS – System Design and Capabilities, International Symposium “In-Flight Simulation for the 90’s”, Braunschweig, Germany, July 1-3, 1991, Conference Proceedings DGLR-91-05, Paper No. 91-05-02

[10] Bauschat, J.-M., Long-Term Flight Test Experience: A Nonlinear In-Flight Simulation Approach, AIAA Modeling and Simulation Technologies Conference and Exhibit, Paper No. AIAA 2002-4600, Monterey, California, August 5-8, 2002.

[11] Schwarz, C. W., Hahn, K.-U., Fischenberg, D., Wake Encounter Severity Assessment Based on Validated Aerodynamic Interaction Models, AIAA ASE Conference 2010, Paper No. AIAA 2010-7679, Toronto, Canada, August 2-5, 2010.

[12] Burnham, D., Hallock, J., Chicago Monoacoustic Vortex Sensing System Vol. 4, Wake Vortex Decay,Springfield, VA, National Information Service, 1982.

[13] Schwarz, C. W., Hahn, K.-U., Simplified Hazard Areas for Wake Vortex Avoidance, AIAA Paper No. AIAA 2007-6871, AIAA Atmospheric Flight Mechanics Conference and Exhibit, San Francisco, California, 2005.

[14] Schwarz, C. W., Subjective Wake Vortex Encounter Evaluation, DLR Internal report IB 111-2011/46, Braunschweig, 2011.

7. Concluding Remarks and Future Activities

The DLR project “Weather & Flying” (“Wetter & Fliegen”) 2008 – 2011 achieved many valuable results. Deeper insights were gained into wake vortex physics, the consequences for encountering aircraft and separation prediction, as well as weather monitoring and forecasting. Know-how was increased about operational concepts for air traffic control and flight systems, as well as technological and economical assessments. Prototype systems have been matured towards different levels of technology readiness and have been tested and evaluated with human-in-the-loop simulations and in field campaigns in real environment.

Many of the activities show promising progress and will be continued e.g. in the follow-on DLR activity “Weather Optimised Air Traffic” (“Wetteroptimierter Luftverkehr” - WOLV) starting 2012. The main goals comprise improving local weather forecasting by combining nowcasting and forecasting techniques, providing tailored weather information and possible effects on air traffic management, and improving and extending wake vortex simulation and prediction tools for air traffic management and aircraft applications.

For the wake vortex topic the activities will be embedded in the context of SESAR, partnering with industry, authorities, airports, universities, research organisations and Eurocontrol, for example to build industry-driven wake vortex advisory systems. Our reseach will also be linked to activities at NASA and FAA in the USA, for example in the urgent search of new aircraft separation criteria, in the development of multi-model techniques to obtain ensemble predictions of wake vortex transport and decay, and in the computation and assessment of wake encounter probabilities and severities over the airspaces of USA, the Atlantic ocean and Europe.

The WxFUSION system will further be developed aiming at a smart combination of data from observation networks, nowcasting tools, and numerical forecast models in order to detect, track, nowcast and forecast hazardous weather phenomena as thunderstorms and wintry weather for aviation purposes as precisely and as consistent as possible. In a campaign at Munich airport in summer 2012 the system will be demonstrated and validated at the ground and in the air in close cooperation with the decision makers. The aim is to bring the system to an international standard that makes it possible to apply the system European wide as a MET tool serving aviation needs in a Single European Sky.

In conclusion it can be stated that the conducted activities contributed significantly to the progress in research and development on meteorological and atmospheric phenomena with regard to aviation. A substantial basis is provided and will be extended subsequently for improving operations and systems in order to increase capacity, punctuality and reach safety goals for air traffic.

List of Publications and Reports of the Team

Bauer, T., Vechtel, D., Design of a Wake Encounter Avoidance and Advisory System (WEAA) – Part I – Conceptual Design, DLR internal report IB 111-2010/23, Braunschweig, 2010

Bauer, T., Vechtel, D., Towards a Wake Encounter Avoidance and Advisory System (WEAA) – Conceptual Design and First Implementations, 3rd CEAS Air&Space Conference, 24th -28th October 2011, Venice (Italy), 2011

Bertsch L., Looye G., Anton E., Schwanke S.: 2011: Flyover Noise Measurements of a Spiraling Noise Abatement Approach Procedure. Journal of Aircraft, 48 (2), Seiten 436-448. DOI: 10.2514/1.C001005.

Bitar, F., Ermittlung der Gefährdung durch Wirbelschleppen bei unterscheidlichen Staffelungsabständen mit WakeScene, DLR internal report IB 111-2012/03, Braunschweig, 2012

Bretl, S., 2010: Untersuchung des Lebenszyklus von Gewittern in Mitteleuropa mit Hilfe von Fernerkundungs- und Modelldaten. Diplomarbeit. Ludwig-Maximilians-Universität München, März 2010

Brüser P. 2010: Beobachtung, Verfolgung und Kurzfristvorhersage von Starkniederschlag mit Hilfe des hochaufgelösten Deutschland Radar-Komposits, Diplomarbeit in Meteorologie, Ludwig-Maximilians Universität München, 30. September 2010.

Dengler K., Keil C., Frech M., Gerz T., Kober, K. 2009: Comparison and validation of two high-resolution weather forecast models at Frankfurt Airport. Meteorologische Zeitschrift, 18, Nr. 5, 531-542.

Dengler K., Holzäpfel F., Gerz T., Wiegele A., De Visscher I., Winckelmans G., Bricteux L., Fischer H., Konopka J. 2011: Crosswind thresholds supporting wake-vortex-free corridors for departing aircraft. Meteorol. Appl. DOI: 10.1002/met.261

Dengler K., J. Anger, C. KEIL, 2011: Validation of high-resolution time-lagged ensemble wind forecasts. Meteorol. Z. 20, 625-634

Diebel S. 2011: Gewittervorhersage über dem nördlichen Mittelmeerraum mit Hilfe von Satellitendaten, Diplomarbeit in Meteorologie, Ludwig-Maximilians Universität München, 2. Dezember 2011.

Diekmann, J., H., Entwicklung eines Softwaremoduls zur Generierung von Trajektorien zum kleinräumigen Ausweichen vor Wirbelschleppen, DLR internal report IB 111-2010/59, Braunschweig, 2010

Dotzek, N., and C. Forster , Application of the European Severe Weather Database (ESWD) to the Verification of satellite-based nowcasting, EUMETSAT Meteorological Satellite Conference, Darmstadt, Germany, 8 - 12 September 2008.

Dotzek, N., and C. Forster, 2010: Quantitative comparison of METEOSAT thunderstorm detection and nowcasting with in situ reports in the European Severe Weather Database (ESWD), Atmos. Res., 100 (2011), 511-522, doi:10.1016/j.atmosres. 2010.12.013.

Dotzek N., Sander J., Gerz T., Groenemeijer P. 2010: Severe thunderstorms in a changing climate: Assessing their impact on European transport, in particular aviation. 8th European Conference on Applied Climatology, 13.–17. Sep. 2010, Zürich, Switzerland.

Fischenberg D. 2008: Auswertung von ATTAS Wirbelschleppeneinflügen. DLR-internal report. DLR-IB 111-2008/15.

Fischenberg D. 2010: Verfahren zur Bestimmung der Stärke und Position von Wirbelschleppen aus line-of-sight (LoS)-Messungen. DLR-Interner Bericht. DLR-IB 111-2010/04.

Fischenberg D.: A Method to Validate Wake Vortex Encounter Models from Flight Test Data 27th International Congress of the Aeronautical Sciences (ICAS), Nizza, France (2010)

Fischenberg D.: Verfahren zur Bestimmung der Stärke und Position von Wirbelschleppen aus line-of-sight (LOS)-Messungen DLR IB 111-2010/04 (2010)

Fischenberg D.: Charakterisierung von Wirbelschleppen aus In-Situ-Flugmessdaten der Falcon D-CMET DLR IB 111-2011/17 (2011)

Forster, C., A. Tafferner, C. Keil, T. Zinner, 2008, Validation of severe weather forecasts based on synthetic satellite data as part of an integrated thunderstorm forecast system for air traffic, Proceedings of the EUMETSAT Meteorological Satellite Conference, Darmstadt, Germany 8 - 12 September 2008, EUMETSAT P. 52, ISBN 978-92-9110-082-8, ISSN 1011-3932, 8 pages.

Forster, C., and A. Tafferner, An integrated user-oriented weather forecast system for air traffic using real-time observations and model data, 26th International Congress of the Aeronautical Sciences (ICAS), Anchorage, Alaska, 14 -19 September 2008, International Council of the Aeronautical Sciences Conf. Proc. (8.6.2), Optimage Ltd., Edinburgh, UK, ISBN 0-9533991-9-2, 2008.

Forster, C., and T. Zinner, Synthetic satellite images based on COSMO, invited presentation at the EUMETRAIN convection week 3 June 2009.

Forster, C., and A. Tafferner, 2009: Nowcasting and forecasting thunderstorms for air traffic with an integrated forecast system based on observations and model data, WMO Symposium on Nowcasting, Whistler, B.C., Canada, 30 August - 4 September 2009.

Forster, C. and N. Dotzek, Quantitative comparison of METEOSAT-based thunderstorm detektion and nowcastin with in-situ reports in the European Severe Weather Database (ESWD), Proceedings of the EUMETSAT Meteorological Satellite Conference, Bath, United Kingdom, 21 - 25 September 2009.

Forster, C., A. Tafferner, T. Zinner, H. Mannstein, S. Sénési, Y. Guillou, The use of remote sensing data for the nowcasting of thunderstorms within a weather information and management system for flight safety, Proceedings of the EUMETSAT Meteorological Satellite Conference, Bath, United Kingdom, 21 - 25 September 2009.

Forster, C., and A. Tafferner, 2009: An integrated user-oriented weather forecast system for air traffic using real-time observations and model data, Proceedings of the European Air and Space Conference (CEAS), Manchester, UK

Forster C., de Coning E., Zinner T. 2010; Satellite-based thunderstorm tracking, monitoring and nowcasting over South Africa, EUMETSAT Meteorological Satellite Conference, Cordoba, Spain, 20 - 24 September 2010.

Gall, Christian: „Entwicklung und Systembetrachtung eines Assistenzsystems zur Durchführung von Ausweichmanövern“, Diplomarbeit, DLR-Interner Bericht, DLR-IB 111-2011/10, DLR Institut für Flugsystemtechnik, Braunschweig, 2011

Gerz T., Holzäpfel F. 2008: WSVBS - An Advisory System for Aircraft Wake Vortices. 5th. European Congress on Computational Methods in Applied Sciences and Engineering (ECCOMAS 2008), June 30 – July 5, 2008, Venice, 2 pp.

Gerz T., Holzäpfel F. 2008: The wake vortex prediction and monitoring system WSVBS - Design and performance at Frankfurt airport. In: Proceedings of 9th ONERA-DLR Aerospace Symposium. ONERA-DLR Aerospace Symposium, 22. -24. Oct. 2008, Chatillon, France.

Gerz T., Hahn K.-U. 2008: The DLR project "Weather and Flying" - A contribution to cope with increasing demand in air transport. In: Proceedings of 9th ONERA-DLR Aerospace Symposium. ONERA-DLR Aerospace Symposium, 22. -24. Oct. 2008, Chatillon, France.

Gerz T., Schwarz C. 2009: The DLR Project "Weather and Flying" - A contribution to cope with increasing demand in air transport. Eighth USA/Europe Air Traffic Management Research and Development Seminar (ATM2009)

Gerz T., Holzäpfel F., Gerling W., Scharnweber A., Frech M., Kober K., Dengler K., Rahm S.: The Wake Vortex Prediction and Monitoring System WSVBS Part II: Performance and ATC Integration at Frankfurt Airport, Air Traffic Control Quarterly, Vol. 17, No. 4, 2009, pp. 323-346.

Gerz T., Keis F., Park S.: 2012: Tailored and On-time Weather Information for Road Traffic Management. 16th International Road Weather Confernce, 23-25 May 2012 in Helsinki, Finland

Hahn K.-U., Schwarz C. 2008: Alleviation of Atmospheric Flow Disturbance Effects on Aircraft Response. In: ICAS 2008 Proceedings. Optimage Ltd., Edingburgh, UK and ICAS. 26. Congress of International Council of Aeronautical Sciences (ICAS), 2008-09-14 - 2008-09-19, Anchorage, Alaska, USA. ISBN 0-9533991-9-2.

Hahn K.-U., Fischenberg D., Niedermeier D., Horn C. 2010: Wake Encounter Flight Control Assistance Based on Forward-Looking Measurement Processing. AIAA ASE 2010, 02.-05. Aug. 2010, Toronto, Kanada

Hennemann I., Holzäpfel F.: Effects of Turbulence Characteristics on Aircraft Wake Vortex Deformation and Decay, Int. Conf. on Jets, Wakes and Separated Flows, ICJWSF 2008, Technical University of Berlin, Berlin, 16 - 19 September 2008, 8 pages.

Hennemann I., Holzäpfel F.: Aircraft Wake Vortex Curvature and Resulting Risk Potential for Following Aircraft, CEAS 2009 European Air and Space Conference, Manchester, UK, 26-29 October 2009, 9 pages.

Hennemann I., Holzäpfel F.: Large-eddy simulation of aircraft wake vortex deformation and topology, Proceedings of the Institution of Mechanical Engineers, Part G: Journal of Aerospace Engineering, Volume 225, Issue 12, December 2011, pp. 1336-1350, published online on September 23, 2011, DOI: 10.1177/0954410011402257 (Proc. IMechE Vol. 225 Part G: J. Aerospace Engineering)

Hennemann, I., 2010: Deformation und Zerfall von Flugzeugwirbelschleppen in turbulenter und stabil geschichteter Atmosphäre, PhD Thesis, Technische Universität München, DLR-FB 2010-21, 145 pp.

Hirschberger M.C., Ehret G. 2011: Simulation and high-precision wavelength determination of noisy 2D Fabry-Pérot interferometric rings for direct-detection Doppler lidar and laser spectroscopy, Appl. Phys. B 103, pp. 207-222.

Holzäpfel F., Kladetzke J., Amelsberg S., Lenz H., Schwarz C., de Visscher I.: Aircraft Wake Vortex Scenarios Simulation for Take-Off and Departure, ICAS 2008, 26th Congress of the International Council of the Aeronautical Sciences and 8th AIAA Aviation Technology, Integration, and Operations (ATIO) Conference, ICAS 2008-11.8.3, AIAA 2008-8921, ISBN 0-9533991-9-2, Anchorage, Alaska, USA, 14 - 19 September 2008, 14 pages.

Holzäpfel F., Gerz T.: Performance of the Wake Vortex Prediction and Monitoring System WSVBS at Frankfurt Airport, ICAS 2008, 26th Congress of the International Council of the Aeronautical Sciences, ICAS 2008-8.11.2, ISBN 0-9533991-9-2, Anchorage, Alaska, USA, 14 - 19 September 2008, 12 pages.

Holzäpfel F., Frech M., Gerz T., Tafferner A., Hahn K.-U., Schwarz C., Joos H.-D., Korn B., Lenz H., Luckner R., Höhne G. 2009: Aircraft Wake Vortex Scenarios Simulation Package - WakeScene. Aerospace Science and Technology, 13, pp. 1-11. DOI: 10.1016/j.ast.2007.09.008.

Holzäpfel F., Kladetzke J., Amelsberg S., Lenz H., Schwarz C., de Visscher I.: Aircraft Wake Vortex Scenarios Simulation for Takeoff and Departure, Journal of Aircraft, Volume 46, Number 2, March-April 2009, pp. 713-717. doi:10.2514/1.39346

Holzäpfel F., Kladetzke J., Amelsberg S., de Visscher I., Winckelmans G.: Operational scenarios for wake vortex encounter safety assessment with WakeScene-D, CREDOS D3-8, March 2009, 25 pages.

Holzäpfel F., Kladetzke J.: Assessment of Wake Vortex Encounter Probabilities for Crosswind Departure Scenarios, CEAS 2009 European Air and Space Conference, Manchester, UK, 26-29 October 2009, 14 pages.

Holzäpfel F., Gerz T.: Performance of the Wake Vortex Prediction and Monitoring System WSVBS at Frankfurt Airport, CEAS 2009 European Air and Space Conference, Manchester, UK, 26-29 October 2009, 12 pages.

Holzäpfel F., Kladetzke J.: Wake vortex encounters during take-off & departure: Sensitivity analysis and worst case search, CREDOS D3-9, 5 November 2009, 94 pages.

Holzäpfel F., Gerz T., Frech M., Tafferner A., Köpp F., Smalikho I., Rahm S., Hahn K.-U., Schwarz C.: The Wake Vortex Prediction and Monitoring System WSVBS - Part I: Design, Air Traffic Control Quarterly, Vol. 17, No. 4, 2009, pp. 301-322.

Holzäpfel F., Misaka T., Hennemann I.: Wake-Vortex Topology, Circulation, and Turbulent Exchange Processes, AIAA Paper 2010-7992, AIAA Atmospheric and Space Environments Conference, 2-5 August 2010, Toronto, Ontario, Canada, 16 pages.

Holzäpfel F., Kladetzke J.: Assessment of Wake Vortex Encounter Probabilities for Crosswind Departure Scenarios, Journal of Aircraft, Volume 48, Number 3, May-June 2011, pp. 812-822. DOI 10.2514/1.C000236

Holzäpfel F., Dengler K., Gerz T., Schwarz C.: Prediction of Dynamic Pairwise Wake Vortex Separations for Approach and Landing, AIAA Paper 2011-3037, 3rd AIAA Atmospheric Space Environments Conference, 27-30 June 2011, Honolulu, Hawaii, 15 pages.

Holzäpfel F., Gerz T., Schwarz C.: The Wake Vortex Prediction and Monitoring System WSVBS - Design and Performance at Frankfurt and Munich Airport, Ninth USA/Europe Air Traffic Management Research and Development Seminar (ATM2011), June 14th - 17th 2011, Berlin, Germany, 10 pages.

Holzäpfel F., Misaka T., Stephan A.: Aircraft Wake Vortex Evolution in Ground Proximity and at Cruise Altitude, inSiDE, Innovatives Supercomputing in Deutschland, Vol. 9, No. 2, Autumn 2011, pp. 32-34

Kauertz S., Holzäpfel F., Kladetzke J.: Wake Vortex Encounter Risk Assessment for Crosswind Departures, Journal of Aircraft, proof 11/11, 11 pages.

Keis, F., 2012: Nowcasting von Winterwetter am Münchner Flughafen und Umgebung durch Verbindung von Beobachtungs-, Fernerkundungs- und Modelldaten. Ph.D. work in progress at Institut für Physik der Atmosphäre, DLR

Kier T. 2011: An Integrated Loads Analysis Model Including Unsteady Aerodynamic Effects for Position and Attitude Dependent Gust Fields. IFASD 2011 - 15th International Forum on Aeroelasticity and Structural Dynamics, 26.-30. Jun. 2011, Paris.

Klötzke T. 2011: Signaturen von Gewitterzugbahnen in SYNOP-Beobachtungen, Bachelorarbeit in Meteorologie, Freie Universität Berlin, 28. September 2011.

Kober K., Tafferner T. 2008: Tracking and nowcasting of convective cells using remote sensing data from radar and satellite, Meteorol. Zeitschrift, 1 (18), 75 - 84.

Köhler M. 2011: Untersuchung der Auslösung von Gewittern während der „Wetter & Fliegen“ Sommerkampagne 2010, Masterarbeit in Meteorologie, Ludwig-Maximilians Universität München, 6. Oktober 2011..

Köhler, M., 2012: Kombination von Nowcast- und Forecastverfahren zur optimalen Kurzfrist-vorhersage von Gewittern bis zu einem Zeitraum von 6 Stunden. Doktorarbeit at IPA, in progress

Lau A., C. Forster , A. Tafferner, N. Dzikus and V. Gollnick, Assessment of a Convective Weather Nowcasting and Tracking Algorithm Based on Delay Reduction Potential at Munich Airport (Part I), 11th AIAA Aviation Technology, Integration and Operations (ATIO) Conference, Virginia Beach, Virginia, USA, 20-22 September 2011.

Lombaerts T., Looye G. 2011: Design and Flight Testing of Manual Nonlinear Flight Control Laws. In: Proceedings of the AIAA 2011 GNC Conference and Exhibit. AIAA 2011 Guidance, Navigation and Control Conference and Exhibit, 7.-11. Aug. 2011, Portland, Oregon, USA.

Lombaerts T., Looye G. 2012: Design and Flight Testing of Automatic Nonlinear Flight Control Laws. Submitted to the AIAA 2012 GNC Conference and Exhibit. AIAA 2012 Guidance, Navigation and Control Conference and Exhibit, 13.-16. Aug. 2012, Minneapolis, Minnesota, USA.

Looye G. 2009: Flight Testing of Autopilot Control Laws: Fly the HELIX! Deutscher Luft- und Raumfahrtkongress 2009.

Looye G. 2011: Helical Flight Path Trajectories for Autopilot Evaluation. In: Selected Papers of the First CEAS Specialist Conference on Guidance, Navigation and Control Advances in Aerospace, Guidance, Navigation and Control. Springer. Seiten 79-90. ISBN 978-3-642-19816-8.

Meyer, V., 2010: Thunderstorm Tracking and Monitoring on the Basis of Three Dimensional Lightning Data and Conventional and Polarimetric Radar Data. Dissertation, Ludwig-Maximilians-Universität München, Mai 2010

Miedler S. 2011: Vorschriftsgemäßer Einbau eines Bordrechners in ein Experimentalflugzeug. Bachelors. DLR-internal report. DLR-IB 111-2011/21

Misaka T., Holzäpfel F., Gerz T., Manhart M., Schwertfirm F.: Large-Eddy Simulation of Wake Vortex Evolution from Roll-Up to Vortex Decay, AIAA Paper 2011-1003, 49th AIAA Aerospace Sciences Meeting including the New Horizons Forum and Aerospace Exposition, 4-7 January 2011, Orlando, Florida, 11 pages.

Misaka T., Holzäpfel F., Gerz T.: Large-Eddy Simulation of Spatially Developing Aircraft Wake, Eighth International Conference on Flow Dynamics, 9-11 November 2011, Sendai, Miyagi, Japan, 2 pages.

Misaka T., Holzäpfel F., Gerz T.: Wake Evolution of Wing-Body Configuration from Roll-Up to Vortex Decay, AIAA Paper 2012-0428, 50th AIAA Aerospace Sciences Meeting including the New Horizons Forum and Aerospace Exposition, 9-12 January 2012, Nashville, Tennessee, 15 pages.

Misaka T., Holzäpfel F., Gerz T., Manhart M., Schwertfirm F.: Vortex bursting and tracer transport of a counter-rotating vortex pair, Physics of Fluids, accepted.

Münster C., Modellierung, Identifizierung und Bewertung eines analytischen Modells für gekrümmte Wirbelschleppen, DLR internal report IB 2011/09, Braunschweig, 2011

Münster C., Schwarz C. 2010: Auswertung von Wirbelschleppenmeldungen im US Aviation Safety Reporting System (ASRS). DLR-IB 111-2010/33, 17 S.

Pradier, S., C. Forster, W. W. M. Heesbeen, C. Pagé, S. Sénési, A.Tafferner, I. Bernard-Bouissières, O. Caumont, A. Drouin, V. Ducroq, Y. Guillou, P. Josse, 2009: Description of convective-scale numerical weather simulation use in a flight simulator within the Flysafe project, Meteorology and Atmospheric Physics, doi:10.1007/s00703-008-0317-4

Raab C.: "DLR Projekt Wetter und Fliegen Wake Impact Attenuation and Avoidance Systems - Conceptual Design for Operation and Human Machine Interface", DLR-Interner Bericht, DLR-IB 111-2010/21, DLR Institut für Flugsystemtechnik, Braunschweig, 2010

Schwarz C. W., Hahn K.-U., Simplified Hazard Areas for Wake Vortex Avoidance, AIAA Paper No. AIAA 2007-6871, AIAA Atmospheric Flight Mechanics Conference and Exhibit, San Francisco, California, 2005.

Schwarz C., Holzäpfel F., Gerz T., Hahn K.-U. 2009: Wake vortex severity assessment – a core element of the safety case. First WakeNet3-Workshop on Wake Turbulence Safety in Future Aircraft Operations, 06 - 07 Jan 2009, Thales University, Jouy En Josas, France.

Schwarz, C. W., Hahn, K.-U., Fischenberg, D., Wake Encounter Severity Assessment Based on Validated Aerodynamic Interaction Models, AIAA ASE Conference 2010, Paper No. AIAA 2010-7679, Toronto, Canada, August 2-5, 2010.

Schwarz C., Fischenberg D. 2010: Analysis of two 2005 Wake Vortex Encounter Incidents. ICAS 2010, 19.- 24. Sept. 2010, Nizza, Frankreich.

Schwarz C., Hahn K.-U., Holzäpfel F., Gerz T. 2010: DLR Wake Solutions in Development. WakeNet USA Meeting October 2010, 20.-21. Okt. 2010, Cambridge, Massachusetts, USA.

Schwarz C., Hahn K.-U., Fischenberg D., Niedermeier D., Bauer T., Holzäpfel F., Gerz T. 2010: Wake Vortex Modeling and Applications - Wake Vortex Advisory and Pilot Assistance. Global Wake Vortex Conference II, 1.-2. 12. 2010, San Diego, CA, USA.

Schwarz C., Hahn K.-U. 2011: Subjective wake vortex encounter evaluation. DLR-IB 111-2011/46, 20 S.

Schwarz C., Hahn K.-U. 2011: Simplified Hazard Area Prediction Method - SHAPe. DLR-IB 111-2011/31, 34 S.

Schwarz C., Hahn K.-U. 2011: Automated pilot assistance for wake vortex encounters. Aerospace Science and Technology, Volume 15, Issue 5, 416–421.

Sénési, S., Y. Guillou, A. Tafferner, C. Forster , Cb Nowcasting in FLYSAFE : Improving flight safety regarding thunderstorm hazards, WMO Symposium on Nowcasting, Whistler, B.C., Canada, 30 August - 4 September 2009.

Stich, D., C. Forster , T. Zinner, A. Tafferner, 2011: Convection Initiation - Nowcasting by data fusion and its Verification, European Conferences on Severe Storms (ECSS 2011) Palma de Mallorca, Balearic Islands, Spain, 3 - 7 October 2011

Tafferner A., Forster C., Sénési S., Guillou Y., Tabary P., Laroche P., Delannoy A., Lunnon B., Turp D., Hauf T., Markovic D. 2008: Nowcasting thunderstorm hazards for flight operations: The CB WIMS approach in FLYSAFE. 26th International Congress of the Aeronautical Sciences (ICAS), Anchorage, September 2008, 10 pp.

Tafferner, A., C. Forster, M. Hagen, C. Keil, T. Zinner, H. Volkert, 2008: Development and propagation of severe thunderstorms in the Upper Danube catchment area: Towards an integrated nowcasting and forecasting system using real-time data and high-resolution simulations. Meteorol. Atmos. Phys. 101, 211-227, DOI 10.1007/s00703-008-0322-7.

Tafferner, A., C. Forster , S. Sénési, Y. Guillou, Improvement of thunderstorm hazard information for pilots through a ground based weather information and management system, The CB WIMS approach in FLYSAFE, Eighth USA/EUROPE Air Traffic Management Research and Development Seminar, Napa, California, 29 June - 2 July 2009.

Tafferner, A., C. Forster , Y. Guillou, S. Sénési, Nowcasting thunderstorm hazards for flight operations: the CB WIMS approach in FLYSAFE, Prodeedings of the European Air and Space Conference (CEAS), Manchester, UK, 26 - 29 October 2009.

Tafferner A., Forster C., Hagen M., Hauf T., Lunnon B., Mirza M., Guillou Y., Zinner T. 2010: Improved thunderstorm weather information for pilots through ground and satellite based observing systems, 14th conference on Aviation, Range, and Aerospace Meteorology (ARAM), 90th AMS Annual Meeting, Atlanta, 17-21 January 2010.

Tafferner A., Forster F., Gerz T., Hagen M. 2010: Improved Safety for Air Traffic through Ground and Satellite Based Observing Systems, International Air Safety and Climate Change Conference (IASCC), Cologne, 8-9 September 2010.

Tafferner A., Forster C., Hauf T., Lunnon B. 2010: Improved thunderstorm weather information for pilots through ground and satellite based observing systems, EUMETSAT Meteorological Satellite Conference, Cordoba, Spain, 20 - 24 September 2010.

Tafferner A., Forster C. 2011: WxFUSION, solicited presentation, EGU General Assembly, Vienna, Austria, 3 - 8 April 2011.

Tafferner A., Forster C., Mannstein H., Zinner T. 2011: Cb-TRAM - Tracking and monitoring severe convection over the Mediterranean from onset over rapid development to mature phase using multi-channel Meteosat SEVIRI data, 13th Plinius Conference on Mediterranean Storms, Savona, Italy, 7 - 9 September 2011

Tafferner A., Forster C., Zinner T. 2011: Improved thunderstorm information for pilots through satellite and ground based nowcasting systems, EMS Annual Meeting, 11th EMS and 10th ECAM, Vol. 8, EMS2011, Berlin, Germany, 12 - 16 September 2011

Vechtel, D., Flight Simulator Study on the influence of Vortex Curvature on Wake Encounter Hazard using LES Wind Fields, The Aeronautical Journal, Volume 116, No. 1177, March 2012.

Vechtel, D., DLR-Projekt “Wetter & Fliegen” AP W1.2 Wirbelkrümmung – Tätigkeiten von DLR-FT, DLR internal report IB 111-2011/47, Braunschweig, 2011

Vechtel, D., Amelsberg, S., Full Flight Simulator Study for Evaluation of Aircraft Dynamics while Encountering Curved Wake Vortices, DLR internal report IB 111-2009/17, Braunschweig, 2009

Vechtel, D., Fezans, N., Full Flight Simulator Study for Evaluation of Aircraft Dynamics while Encountering Curved Wake Vortices (Part II – Result Evaluation), DLR internal report IB 111-2010/18, Braunschweig, 2010

Vechtel, D., Entwicklung eines analytischen Modells zur Berechnung gekrümmter Wirbelschleppen, DLR internal report IB 111-2010/14, Braunschweig, 2010

Voigt C., Schumann U., Jurkat T., Schäuble D., Schlager H., Lichtenstern M., Scheibe M., Hamburger T., Petzold A., Dörnbrack A., Holzäpfel F., Gayet J.-F., Gourbeyre C., Krämer M., Kübbeler M., Meyer J., Schneider J., Schmale J., Eichler H., Frey W., Molleker S., Borrmann S.: Detection of young contrails - selected results from the CONCERT (CONtrail and Cirrus ExpeRimenT) campaign, Proceedings of the 2nd International Conference on Transport, Atmosphere and Climate TAC-2, 22-25 June 2009, Aachen, DE, and Maastricht, NL, DLR Forschungsbericht 2010-10, ISSN 1434-8454, ISRN DLR-FB--2010-10, pp. 57-62 pages.

Voigt C., Schumann U., Jurkat T., Schäuble D., Schlager H., Petzold A., Gayet J.-F., Krämer M., Schneider J., Borrmann S., Schmale J., Jessberger P., Hamburger T., Lichtenstern M., Scheibe M., Gourbeyre C., Meyer J., Kübbeler M., Frey W., Kalesse H., Butler T., Lawrence M.G., Holzäpfel F., Arnold F., Wendisch M., Döpelheuer A., Gottschaldt K., Baumann R., Zöger M., Sölch I., Rautenhaus M., Dörnbrack A.:, In-situ observations of young contrails - overview and selected results from the CONCERT campaign, Atmospheric Chemistry and Physics, 10, 9039-9056, 2010, doi:10.5194/acp-10-9039-2010.

Voss G., Gerz T., Baumann R., Stumpf E., Press M. 2009: Wake Vortex Alleviation by Differential and Oscillating Flap Setting: A flight test. 27th Applied Aerodynamics Conference, 22-25 Jun 2009, San Antonio, Texas.

Westermayer, A., 2012: Detektion und Verlagerung von Gewitter-Fallwinden und Böen aus POLDIRAD-, LLWAS- und COSMOairport –Daten. Masterarbeit at Institut für Physik der Atmosphäre, in progress

Zinner, T., H. Mannstein, A. Tafferner, 2008: Cb-TRAM: Tracking and monitoring severe convection from onset over rapid development to mature phase using multichannel Meteosat-8 SEVIRI data. – Meteor. Atmos. Phys. 101, 191–210, DOI 10.1007/s00703-008-0290-y.

Zinner, T., Betz, H.D., 2009. Validation of Meteosat storm detection and nowcasting based on lightning network data. Proc. 2009 EUMETSAT Meteorological Satellite Conference, Bath, 21–25 September 2009. 9 pp. Available at http://www.eumetsat.int/Home/Main/AboutEUMETSAT/Publications/ConferenceandWorkshopProceedings/SP_201001515267179.

Zinner, T., C. Forster, E. de Coning, and H.-D. Betz, 2011: Validation of the METEOSAT storm detection and nowcasting system Cb-TRAM with lightning network data, in preparation for Atmos. Chem. Phys.

Glossary

AIM	aerodynamic interaction model
AMAN	arrival manager of aircraft on an airport
AMDAR	aircraft meteorological data relay
AOC	airline operating centre
ATC/ATM	air traffic control / management
ATRA	advanced technology research aircraft
ATTAS	advanced technologies testing aircraft system
BL	backscatter lidar
Cb-TRAM	cumulonimbus tracking and monitoring based on satellite data
CCD	charge-coupled device
CFD	computational fluid dynamics
COSMO	consortium for small-scale modelling
COSMO DE	weather forecast model for Germany of DWD
COSMO EU	weather forecast model for Europe of DWD
COSMO*FRA*	limited area version of COSMO DE for Frankfurt airport area
COSMO*MUC*	limited area version of COSMO DE for München airport area
D2P	deterministic two-phase wake vortex model
DFS	Deutsche Flugsicherung GmbH
DLH	Deutsche Lufthansa
DLH-HCC	Deutsche Lufthansa Hub Control Center
DWD	Deutscher Wetterdienst
DWL	Doppler wind lidar
ESA	European Space Agency
FAA	Federal Aviation Administration of the USA
FI	fringe-imaging
FMG	Flughafen München Gesellschaft
FMS	flight management system
FPI	Fabry-Pérot-interferometer
GPWS	ground proximity warning system
HMI	human machine interface
ICAO	International Civil Aviation Organisation
IFALPA	International Federation of Air Line Pilots' Associations
IFR	instrumented flight rules
ILS	instrumented landing system
IMC	instrumented meteorological conditions
IRLIS	integrated ride and loads improvement system
ITWS	integrated terminal weather system and components
LES	large-eddy simulation
LESTUF	CFD code for LES of turbulence
LIDAR	light detection and ranging
LINET	lightning detection system, lightning network by nowcast GmbH
LLWAS	low-level wind shear alert system
LOS	line-of-sight
MET	meteorological data and information for the aviation community
MTOW	maximum take-off weight
MUC	airport of Munich

NASA	National Aeronautics and Space Administration of the USA
ND	navigation display
NDI	Nonlinear Dynamic Inversion
NLR	Nationaal Lucht- en Ruimtevaartlaboratorium of the Netherlands
NOWVIV	nowcasting wake vortex impact variables
ONERA	Office National d'Etudes et de Recherches Aérospatiale of France
P2P	probabilistic 2-phase model
PFD	primary flight display
PIV	particle image velocimetry
RADAR	radio-wave detection and ranging
Rad-TRAM	Radar tracking and monitoring of convective cells (Cb's) with weather radar
RANS	Reynolds-averaged Navier-Stokes
RASS	radio acoustic sounding system
RCR	roll control ratio
SHA	simplified hazard area
SHAPe	simplified hazard area prediction model
SODAR	sound detection and ranging
SYNOP	meteorological surface synoptic observations
TCAS	traffic alert and collision avoidance system
TLE	time-lagged ensemble
TMA	terminal manoeuvring area of an airport
UTC	universal time coordinated (Greenwich time)
VFR	visual flight rules
VMC	visual meteorological conditions
WakeScene	wake vortex scenarios simulation package
WEAA	wake encounter Avoidance and advisory system
WIMS	weather information management system
WV	wake vortex
WSVBS	Wirbelschleppen-Vorhersage- und Beobachtungssystem des DLR, wake vortex advisory
WxFUSION	weather forecast user-oriented system including object nowcasting

European Research Projects and Programmes

ALICIA	All Condition Operations and Innovative Cockpit Infrastructure, Large-scale integrating project in the 7th EU-FP, co-funded by the European Commission from 2009 to 2013
ATC-Wake	Project on Integrated Air Traffic Control Wake Vortex Safety and Capacity System, co-funded by the European Commission under Project Number IST-2001-34729 from 2002 to 2005
AWIATOR	Aircraft Wing With Advanced Technology Operation, co-funded by the European Commission under Project Number G4RD-CT-2002-00836 from 2002 to 2006
CREDOS	Crosswind - Reduced Separations for Departure Operations, co-funded by the European Commission under Project Number AST5-CT-2006-030837 from 2006 to 2009
C-Wake	Project on Wake Vortex Characterisation and Control, co-funded by the European Commission under Project Number GRD1-1999-10332 from 2000 to 2002

DELICAT	Demonstration of Lidar based Clear Air Turbulence Detection, Collaborative Project in the 7th EU-FP, co-funded by the European Commission from 2009 to 2012
FAR-Wake	Fundamental Research on Aircraft Wake Phenomena, co-funded by the European Commission under Project Number AST4-CT-2005-012238 from 2005 to 2008
FIDELIO	Fibre Laser Development for Next Generation LIDAR Onboard Detection System
Greenwake	Demonstration of Lidar based Wake-Vortex Detection System incorporating an Atmospheric Hazard Map, co-funded by the European Commission from 2008 to 2011
I-Wake	Project on Instrumentation Systems for on-board Wake--Vortex and other Hazards Detection Warning and Avoidance, co-funded by the European Commission under Project Number GRD1-2001-40176 from 2002 to 2005
FLYSAFE	Airborne Integrated System for Safety Improvements, Flight Hazard Protection and All Weather Operations, Integrated Project in the 6th EU-FP, co-funded by the European Commission under Project Number AIP4-CT-2005-516167 from 2005 to 2009
JTI Clean Sky	Joint Technology Initiative for Aeronautics and Air Transport
JU SESAR	Joint Undertaking for Single European Sky ATM Research
MFLAME	Project on Multi-Function Future Laser Atmospheric Measurement Equipment, co-funded by the European Commission under Contract Number BRPR-CT96-182 from 1996 to 2000
NextGen	Next Generation Air Transportation System in the USA
SESAR	Single European Sky ATM Research
S-Wake	Project on Assessment of Wake--Vortex Safety, co-funded by the European Commission under Project Number GRD1-1999-10695 from 2000 to 2002
WakeNet	Thematic Network on Aircraft Wake Vortices, funded by the European Commission under Contract Number BRRT-CT98-5050 from 1998 to 2002
WakeNet2-Europe	Thematic Network on Aircraft Wake Vortices II, funded by the European Commission from 2003 to 2005
WakeNet3-Europe	European Coordination Action for Aircraft Wake Turbulence, funded by the European Commission from 2008 to 2011
WAVENC	Project on Wake-Vortex Evolution and Encounter, co-funded by the European Commission under Contract Number BRP

ISSN 1434-8454

ISRN DLR-FB--2012-02